ACTA UNIVERSITATIS CAROLINAE

AUC GEOGRAPHICA

62
2/2026

CHARLES UNIVERSITY • KAROLINUM PRESS

AUC Geographica is licensed under a Creative Commons Attribution License
(https://creativecommons.org/licenses/by/4.0), which permits unrestricted use, distribution,
and reproduction in any medium, provided the original author and source are credited.

© Charles University, 2026
ISSN 0300-5402 (Print)
ISSN 2336-1980 (Online)

Suicidal ideation among older adults in Europe: The role of migration, loneliness, and regional contexts

Kristina Gundersen*, Tereza Chmelarova

Charles University, Faculty of Science, Social Geography and Regional Development, Czechia
* Corresponding author: gundersk@natur.cuni.cz

ABSTRACT
This article explores suicidal ideation among people aged 50+ in Central European (Czechia, Hungary, Poland, Slovakia), Nordic (Sweden, Finland, Denmark), and Baltic (Estonia, Latvia, Lithuania) countries, using SHARE Wave 9 data (N = 20,996, including 1,356 migrants). Migrants reported higher rates of suicidal thoughts (6.9%) than non-migrants (4.8%). Using logistic regression, factors such as age, education, loneliness, and depression explained most of the variance in suicidal ideation. The overall difference between migrants and non-migrants was small once these factors were controlled. Within the migrant subsample, those residing in Baltic countries had lower odds of suicidal ideation compared to those residing in Nordic countries. These findings underscore the importance of socio-geographical context and psychosocial factors, highlighting the need for targeted support strategies. As aging and migration reshape Europe, emotional well-being must remain central to suicide prevention efforts.

KEYWORDS
late-life suicide; migration; Baltic countries, Nordic countries; Central European countries

Received: 19 April 2025
Accepted: 20 January 2026
Published online: 2 February 2026

Gundersen, K., Chmelarova, T. (2026): Suicidal ideation among older adults in Europe: The role of migration, loneliness, and regional contexts. AUC Geographica 61(2), 161–174
https://doi.org/10.14712/23361980.2026.2
© 2026 The Authors. This is an open-access article distributed under the terms of the Creative Commons Attribution License (https://creativecommons.org/licenses/by/4.0).

1. Introduction

Suicide represents a pressing global public health issue, with over 700,000 deaths annually (WHO 2024). This figure likely underestimates the true scale of the problem due to the hidden and complex nature of suicidal behaviour. While awareness has increased, particularly after the COVID-19 pandemic (Pathirathna et al. 2022; Yan et al. 2023), older adults remain underrepresented in research and prevention strategies, despite their heightened vulnerability.

This study addresses this gap by investigating suicidal ideation among people aged 50 and older, focusing on migrants and regional differences within Europe. Our objective is to assess how individual-level factors and contextual factors interact to influence late-life suicidal ideation, a topic that has received limited cross-national comparative attention. We aim to identify risk patterns across different European contexts to inform targeted mental health strategies.

The motivation for this study stems from concerns about the unique challenges faced by older adults, who are often overlooked in mental health discussions. Unlike younger populations, late-life suicidal behaviour is frequently dismissed or misunderstood as inevitable (Simon 1989). Many older people experience anxiety over losing autonomy, identity, and self-care capacity (Kjølseth et al. 2010; Crocker et al. 2006). For migrants, such struggles are compounded by cultural dissonance, language barriers, social isolation, and limited healthcare access.

Migration has increased significantly due to global mobility and political, economic, and social unrest. In 2024, over 304 million international migrants were recorded, with Europe experiencing the largest increase, where they now comprise 12.6% of the population (UN 2024). Migration is a heterogeneous process, and pre-, during-, and post-migration stressors can elevate the risk of mental health disorders, including suicidal ideation (Norredam et al. 2013).

The Nordic, Baltic, and Central European (also referred to as the Visegrad group) regions offer a valuable comparative framework due to their differing welfare systems, migration histories, and healthcare infrastructures (Fenger 2007; Borevi 2017; Szikra 2014). Although all three face aging populations and rising mental health concerns (OECD 2021), their institutional responses vary. Our analysis deliberately focuses on these regions to maintain conceptual coherence and comparability across institutional, demographic, and historical contexts. Previous research shows clear contrasts in how welfare regimes affect health, with Scandinavian welfare system typically linked to more favourable health outcomes compared to Eastern European region (Eikemo et al. 2008; Widding-Havneraas and Pedersen 2020).

To our knowledge, no prior study has systematically examined the intersection of aging, migration, and suicidal ideation while addressing regional differences across the Nordic, Baltic, and Central European regions. Using SHARE data for multivariate regression analysis, we analyse both individual and contextual factors to assess the prevalence of suicidal ideation among older migrants and non-migrants while controlling for gender, age, and regional background, and examine how demographic, socioeconomic, regional, and mental health factors shape suicidal ideation in both groups.

2. Suicidal ideation in the context of migration and aging

Suicide is generally defined as self-harm intended to end one's life, encompassing completed suicides, attempts, and suicidal ideation, thoughts or plans of self-harm (Kuntz and Moutier 2021). Terms like "successful" or "failed" suicide are considered misleading (Klonsky et al. 2016).

Loneliness is a key correlate of suicidal ideation (McClelland et al. 2020) and tends to increase with age-related changes such as declining physical health, loss of mobility, retirement, and the reductions in social interactions. Based on the analysis of the Albanian elderly population, Nesturi and Nasufi (2025) concluded that these age-related factors, combined with deterioration of traditional family structures and ongoing migration trends, significantly deepen loneliness. By comparing the Nordic and Baltic regions, Reine et al. (2024) found significant regional differences in loneliness among individuals aged 67 and older, with heightened loneliness among respondents from Baltic countries. The authors highlight the role of both individual and societal factors in influencing late-life social isolation.

According to the International Organization for Migration, a migrant is anyone who moves from their usual residence, domestically or internationally, for various reasons (Sironi et al. 2019). Berry's (1980) acculturation model, though developed for recent migrants, also applies to older adults who continue to navigate cultural identity. Acculturative stress may build over time, especially without social support or inclusion (Cohen et al. 2018), guiding our focus on social integration, discrimination, and loneliness as key predictors of suicidal ideation.

Globally, suicide prevalence among migrants and refugees is about 2%, with suicidal ideation reaching 16% (Amiri 2020). While overall suicide risk is lower than among natives, non-fatal suicidal behaviour is more common, particularly among forcibly displaced individuals (Cogo et al. 2022). Older migrants often report poorer health, greater loneliness, and more stigma than younger migrants (Wu and Penning 2015; Reus-Pons et al. 2018). In Norway, immigrants report mental health issues at twice the rate of the general population (Kan et al. 2019). In Finland, migrants access psychotherapy less often than natives despite

similar needs (Lehti et al. 2025). Norwegian studies show first- and second-generation immigrants are less likely to receive mental health care before or after self-harm with generally lower suicide rates (Qin et al. 2022).

Migrants generally report lower subjective well-being than natives, with larger gaps in countries with restrictive family reunion policies (Sand and Gruber 2018). Bersani and Morabito (2020) highlight the "immigrant paradox", where foreign-born individuals often have better health, but suicidality varies across generations. They found that the effect of migration age on suicidality varies based on gender and nativity, underscoring the need for nuanced analyses.

Although previous research has illuminated the complexity of suicidal behaviour among older adults (Kjølseth et al. 2010), older migrants remain underexamined as a distinct group in suicide research. Much of the existing literature either focuses on younger or newly arrived populations, or it does not explore how migration history intersects with suicidal ideation in late life. While healthcare access, social isolation, and acculturation challenges are well-documented, their interaction with mental health in older age, especially across different European contexts, remains insufficiently understood.

3. Data and methods

Data from the Survey of Health, Ageing and Retirement in Europe (SHARE) were used, specifically wave 9 from 2022, which was the most recent wave available at the start of our research. Additionally, we incorporated demographic variables from participants' first interview (baseline data from waves 1–7).

3.1 Study sample

A sample of individuals aged 50 and above from 10 European countries: Czechia, Denmark, Estonia, Finland, Hungary, Poland, Slovakia, Sweden, Latvia, Lithuania was analysed for the paper. These countries were selected due to their geographical belonging to the Nordic, Central European, Baltic regions and EU. Norway and Iceland, although part of the Nordic region, are not members of the European Union and are therefore not included in the SHARE project, which is why they are not part of our sample.

The initial sample consisted of 69,447 respondents from SHARE Wave 9. As the focus of this study was on individuals residing in Central European, Nordic, and Baltic countries, those living outside these regions were excluded. Additionally, to maintain a focus on older adults, individuals younger than 50 or older than 94 were removed, reducing the sample to 24,902 respondents. Excluding the oldest-old is justified due to their likely mental and physical decline. According to a study by Lee et al. (2016), there is a sharp increase in the proportion of frail elderly when at the age of 95. The states of physical and mental decline increase the odds of incoherent responses, which, in turn, are likely to add unexplained variability in the dependent variable, thus obscuring the underlying relationships.

Next, respondents with missing migration status were excluded (n = 1,881), resulting in a sample of 21,439 non-migrants and 1,582 migrants. Further exclusions were made for respondents with missing data on suicidal thoughts (n = 390), leaving 21,081 non-migrants and 1,550 migrants. Finally, individuals with missing data on any predictor variables were removed (n = 1,635), yielding a final study population of 20,996 observations, including 19,640 non-migrants and 1,356 migrants. This final sample was used in the subsequent statistical analyses (Fig. 1).

3.1.1 Analysed variables

All "Refusal" and "Don't know" responses in the analysed variables were coded as missing and excluded from the analysis, which was conducted on complete cases only.

Dependent variable. The dependent variable in this study measures suicidal ideation or a wish to be dead, based on the question: "In the last month, have you felt that you would rather be dead?" Responses include refusal (−2), don't know (−1), any mention of suicidal feelings (1), and no such feelings (2). For this analysis, we focus on those who reported suicidal ideation (coded as 1) to examine prevalence and associated factors.

Independent variables

Demographics. Age at the time of the interview (age_int) was recoded into three categories: 50–64, 65–80, and 81–94 years to capture distinct life stages.

Gender was coded as 1 representing female respondents and 0 representing male respondents.

Education is grouped into Low (0–10 years of schooling), Middle (10–14 years of schooling), and High (15–25 years of schooling) based on socioeconomic outcomes. Cross-national findings indicate that both lower and higher levels of educational attainment are linked to higher elderly suicide rates (Shah 2012). At the same time, registry-based Norwegian data show that lower education consistently increases suicide risk, whereas higher education may be protective, particularly among men (Øien-Ødegaard et al. 2021). These categories allow for a clearer analysis of education's role in mental health and suicidal ideation.

Mental health indicators. The Three-Item Loneliness Scale (Hughes et al. 2004) assesses loneliness through three components: lack of companionship, feeling left out, and isolation. Responses range from "hardly ever"

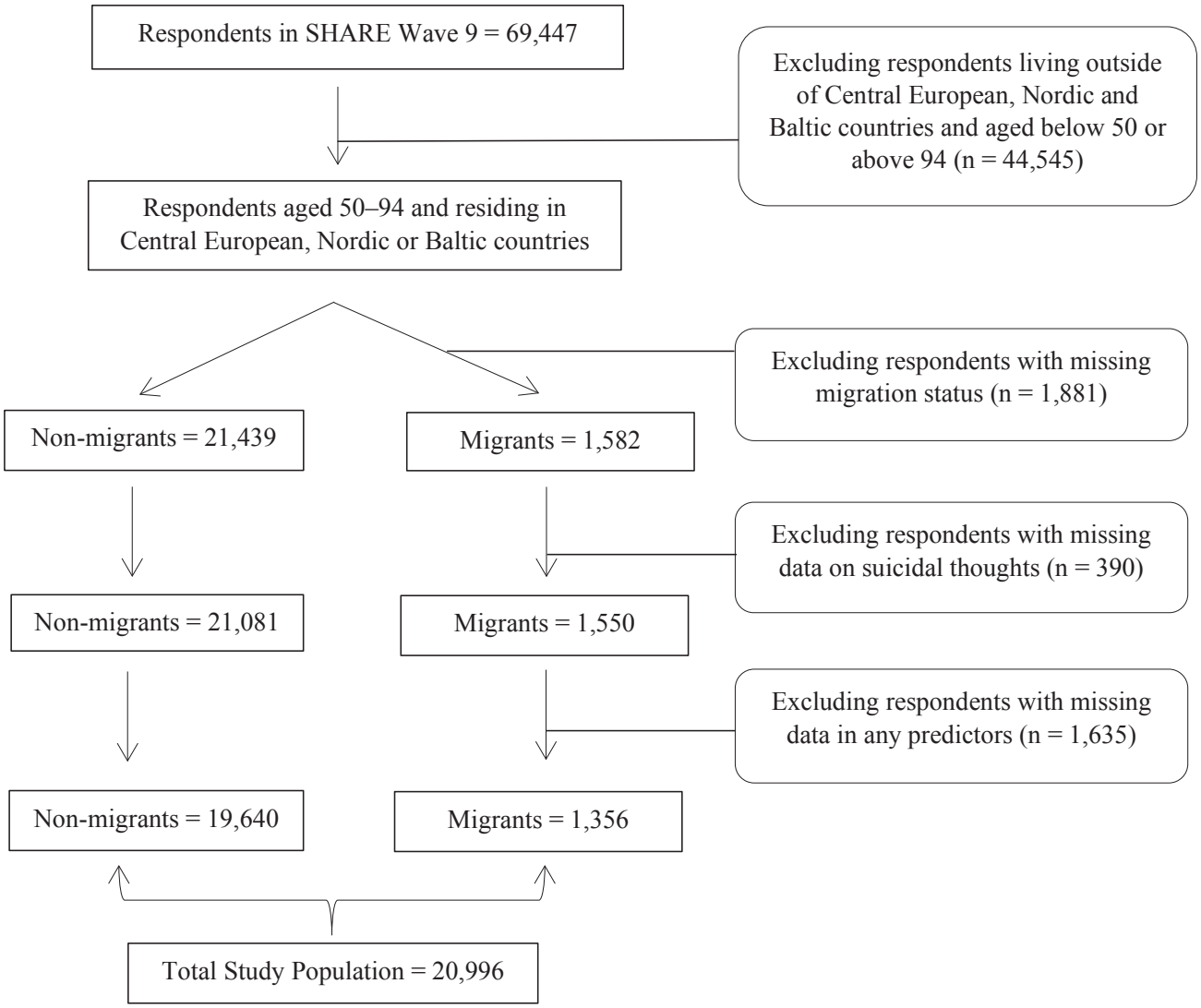

Fig. 1 Steps of the Sample Selection and Refinement Process.

to "often" (score 3–9). We categorize loneliness as Not lonely (3), Somewhat lonely (4–6), and Very lonely (7–9) to provide a nuanced understanding. Recent feelings of sadness were assessed using the original SHARE variable mh002, in which respondents reported whether they had felt sad or depressed in the past month. This variable was recoded into a binary indicator, with 1 for Yes and 0 for No.

Migration. Respondents were identified as migrants if they were not born in the country where the interview took place (dn004 "Born in the country of interview"). This was coded as 1 for migrants and 0 for non-migrants. Finally, for migrants, years in the country were calculated as the difference between the year of the interview (int_year) and the year the respondent arrived in the country (dn006). The variable dn005c ("Foreign Country of Birth") was recoded into three categories to reflect the region of birth for migrants: European Union (EU), Former Soviet Union (FSU), and Other Countries. EU countries include member states of the EU at the time of the data collection, regardless of their prior affiliations. Countries that belong to both the EU and the former Soviet Union, were categorized under the EU group. This decision was made to reflect their current institutional context, which shapes migrant integration policies, healthcare access, and overall societal structure more directly than historical affiliations. It also aligns with other literature that classifies countries primarily based on current political-economic alignment (e.g., Eurostat, OECD frameworks).

Geographical. The country of residence variable identified the ten countries included in the analysis. The region of residence was classified based on the country variable. Respondents were categorized into one of three regions: Nordic (Sweden, Denmark, Finland), Central European (Czechia, Poland, Hungary, Slovakia), and Baltic (Estonia, Latvia, Lithuania). The type of residence was recorded based on the "Area of building" variable to indicate whether respondents lived in a rural area. A score of 1 was assigned for rural areas, and a score of 0 for non-rural areas.

3.2 Methods

First, descriptive statistics along with Pearson's Chi-Square test of independence were calculated to examine the relationship between independent variables and suicidal ideation. To gain deeper insight we first assessed the pairwise associations among all analysed variables using the Phi coefficient. Based on the pairwise relationships, we selected informative predictors – focal and controls – to include in the logistic models.

Second, to examine the relationship between suicidal ideation and key predictors, we estimated a series of logistic regression models in a stepwise manner. We began by including control variables only, to assess their direct associations with suicidal ideation. In the next step, we added key predictors – the indicators of loneliness and depression and regional indicators of Central European, Nordic and Baltic countries. The models were initially calculated for all 20,996 respondents together and then separately for the sub-samples of migrants (1,356 respondents) and non-migrants (19,640 respondents). Finally, for the migrant subsample, we estimated one additional model: that further incorporated migrant-specific characteristics, namely years spent in the host

Tab. 1 Descriptive Statistics of the total study sample, migrants and non-migrants and prevalence of suicidal ideation across the Central European, Baltic, and Nordic regions.

	Total study sample			Migrants			Non-migrants		
Variable / Category	N	Preval. of suicide ideation (%)	P values*	N	Preval. of suicide ideation (%)	P values*	N	Preval. of suicide ideation (%)	P values*
Age groups (years)									
50–64	6,357	3.4	<0.001	301	4.3	<0.001	6,056	3.3	<0.001
65–80	11,727	4.5		754	5.7		10,973	4.4	
81–94	2,912	10.5		301	12.3		2,611	10.3	
Gender									
Female	12,336	5.8	<0.001	880	8.2	<0.001	11,456	5.6	<0.001
Male	8,660	3.8		476	4.4		8,184	3.8	
Educational groups									
Low	3,840	8.3	<0.001	244	13.1	<0.001	3,596	7.9	<0.001
Middle	12,201	4.7		749	5.9		11,452	4.7	
High	4,955	3.0		363	4.7		4,592	2.9	
Region of residence									
Central European	9,067	5.4	<0.001	193	9.3	0.058	8,874	5.3	<0.001
Baltic	5,696	5.2		937	5.8		5,470	5.1	
Nordic	6,233	4.1		226	9.3		5,296	3.9	
Type of residence – rural									
Yes	7,292	4.9	0.638	239	10.0	0.032	7,053	4.9	0.775
No	13,704	5.1		1,117	6.2		12,587	4.8	
Feelings of loneliness									
Not lonely	11,455	2.3	<0.001	711	3.7	<0.001	10,744	2.2	<0.001
Somewhat lonely	8,226	5.5		526	6.7		7,700	5.4	
Very lonely	1,315	24.7		119	26.9		1,196	24.6	
Recently sad or depressed									
Yes	8,591	9.7	<0.001	673	11.0	<0.001	7,908	9.6	<0.001
No	12,405	1.7		683	2.7		11,732	1.7	
Years in the country (for migrants)									
20 years or less				25	8.0	0.083			
21 to 50 years				480	4.8				
Over 50 years				851	8.0				
Region of birth (for migrants)									
Former Soviet Union				926	5.6	0.022			
European Union				317	10.1				
Other				113	8.0				
Total	20,996	5.0		1,356	6.9		19,640	4.8	

* The p-values come from Pearson's Chi-Square test of independence.

Tab. 2 Pairwise associations (Phi coefficients) for all analysed variables in the total study sample (n = 20,996), Central European, Baltic, and Nordic regions.

	Age: 50–64	Age: 65–80	Age: 81–94	Female	Education: Low	Education: Middle	Education: High	Migrant	Baltic	Central European	Nordic	Rural Area	Not lonely	Somewhat lonely	Very lonely	Recently sad or depressed
Suicidal thoughts	−0.049**	−0.025**	0.101**	0.045**	0.071**	−0.013	−0.050**	0.023**	0.006	0.017*	−0.025**	0.003	−0.133**	0.020**	0.235**	0.180**
Age (years): 50–64		−0.741**	−0.264**	−0.010	−0.177**	0.112**	0.030**	−0.046**	0.044**	0.021*	−0.069**	0.051**	0.121**	−0.095**	−0.057**	−0.057**
Age (years): 65–80			−0.451**	−0.019*	0.005	−0.005	0.001	−0.001	−0.093**	0.046**	0.045**	−0.020*	−0.026**	0.041**	−0.028**	−0.005
Age (years): 81–94				0.040**	0.227**	−0.142**	−0.042**	0.063**	0.076**	−0.094**	0.027**	−0.039**	−0.124**	0.069**	0.116**	0.083**
Female					0.041**	−0.021*	−0.013	0.033**	0.056**	−0.004	−0.053**	−0.042**	−0.065**	0.044**	0.045**	0.159**
Education: Low						−0.557**	−0.263**	−0.002	−0.036**	0.020*	0.014*	0.137**	−0.080**	0.045**	0.072**	0.045**
Education: Middle							−0.655**	−0.015*	0.011	0.135**	−0.162**	−0.005	0.018**	−0.012	−0.012	−0.029**
Education: High								0.020*	0.020*	−0.175**	0.175**	−0.119**	0.052**	−0.027**	−0.052**	−0.008
Migrant									0.227**	−0.154**	−0.062**	−0.094**	−0.011	−0.002	0.027**	0.051**
Baltic										−0.566**	−0.396**	−0.046**	−0.09	0.001	0.016*	0.085**
Central European											−0.532**	0.061**	−0.069**	0.051**	0.037**	−0.020*
Nordic												−0.021*	0.085**	−0.058**	−0.058**	−0.065**
Rural Area													−0.007	0.012	−0.011	−0.005
Not lonely														−0.879**	−0.283**	−0.266**
Somewhat lonely															−0.207**	0.169**
Very lonely																0.205**

** Pairwise relationship is significant at the 0.01 level (2-tailed), * Pairwise relationship is significant at the 0.05 level (2-tailed).

country and the region of birth. This modelling sequence allows for a clearer understanding of how psychosocial, geographical, and migration-related factors independently and jointly shape suicidal ideation in later life. Analyses were conducted using IBM SPSS Statistics 28.0.

4. Results

4.1 Descriptive statistics and matrix of pairwise relationships

Tab. 1 presents descriptive statistics for the study samples, which include 20,996 older adults, with 1,356 migrants and 19,640 non-migrants. Suicidal ideation is more prevalent among migrants (6.9%) than non-migrants (4.8%) and is higher among older age groups, those with lower education, loneliness, and recent sadness or depression. Women report higher suicidal ideation (5.8%) than men (3.8%), particularly among migrant women (8.2%). For the total study sample, regional differences show higher prevalence in the Central European (5.4%) and Baltic (5.2%) regions, while the Nordic countries have the lowest (4.1%). Among migrants, those from the European Union (10.1%) report more suicidal ideation than those from the Former Soviet Union (5.6%) or other regions (8.0%).

As suggested by the descriptive statistics and pairwise relationship matrix, having a migration background is associated with a higher probability of experiencing suicidal thoughts compared to the native population. Migrant status is also linked to greater reported loneliness and a higher likelihood of recent sadness or a depressive episode. Moreover, migration background shows significant associations with nearly all predictor variables, suggesting systematic differences between migrants and non-migrants. These preliminary differences suggest that the relationships between the independent variables and suicidal ideation may vary systematically between the two groups. Therefore, in the subsequent analysis, we estimate models separately for migrants and non-migrants.

The pairwise association table suggests that the relationship between middle education and suicidal ideation was very weak. However, the remaining two education categories showed somewhat stronger associations. Given the conceptual importance, education was retained in the further analysis.

The pairwise relationship matrix showed no relationship between residing in a rural area and reporting suicidal thoughts. Thus, this predictor was dropped from further analysis (Tab. 2).

Similarly, the pairwise association between residing in a Baltic country and suicidal ideation was minimal. Nevertheless, this variable is retained in the

Tab. 3 The sensitivity analysis comparing model estimates with and without Slovakia.

	Slovakia included		Slovakia excluded	
Sample size	n = 20,996		n = 20,064	
−2 Log Likelihood	7044.696		6850.379	
Nagelkerke R-square	0.179		0.180	
Cox & Snell R^2	0.058		0.060	
Variable / category	Adj. OR	95% CI	Adj. OR	95% CI
Migrant (Reference: No)				
	1.13	0.90–1.44	1.11	0.87–1.41
Rural area (Reference: No)				
Yes	1.02	0.88–1.18	1.04	0.90–1.20
Feelings of loneliness (Reference: Not lonely)				
Somewhat lonely	1.67	1.43–1.94	1.68	1.43–1.98
Very lonely	6.43	5.35–7.76	6.60	5.46–7.98
Recently sad or depressed (Reference: No)				
Yes	4.01	3.40–4.73	3.95	3.35–4.65
Age groups (Reference: 50–64)				
65–80	1.12	0.95–1.33	1.12	0.94–1.33
81–94	1.87	1.53–2.30	1.88	1.53–2.30
Gender (Reference: Male)				
Female	1.11	0.97–1.28	1.13	0.98–1.31
Educational groups (Reference: Low)				
Middle	0.77	0.66–0.91	0.79	0.67–0.93
High	0.51	0.42–0.63	0.52	0.42–0.65

analysis to assess whether the relationship between residing in the Baltic region – one of our studied predictors – and suicidal ideation also appears insignificant after adjusting for other covariates (Tab. 2).

According to Tab. 2, all pairwise relationships between analysed variables were low to moderate at most. Therefore, multicollinearity was not identified as a concern in the data. The highest absolute associations occur between mutually exclusive categorical dummies (e.g. Education: Low, Middle, High), where such strong negative relationships are expected due to coding.

Due to the small sample of migrants present within data for Slovakia, Slovakia was excluded from further analysis to account for this issue. To understand whether excluding Slovakia is justified, sensitivity analysis was performed by comparing parameter estimates and their confidence intervals with and without Slovakia. The sensitivity analysis was carried out for the key logistic models in this study, and the results suggest that excluding Slovakia did not significantly alter model parameters. The results of the sensitivity analysis can be found in Tab. 3.

4.2 Logistic regressions of suicidal ideation

We analysed associations between suicidal ideation and key predictors using a stepwise set of logistic regression models. First, the controls were included in the model to assess their direct associations with suicidal ideation (Tab. 4). Second, the models were expanded by adding the core predictors of interest: the region of residence, feelings of loneliness and depression (Tab. 5). This approach allowed an evaluation of whether the effects of the main predictors were independent of demographic composition. Finally, Tab. 6 shows the results of a model for the migrant subsample only. This model included the variables of interest and demographic controls and additionally controlled for migrant-specific variables (years spent in the host country and region of birth) to examine whether these factors further explained variation in suicidal ideation among older migrants.

Tab. 4 presents the results of logistic regressions examining the association between suicidal ideation and the control variables: age groups, gender, and education, providing an initial overview of how basic demographic factors are related to the likelihood of reporting suicidal thoughts before introducing additional covariates in later models.

Across all models, older age was associated with higher odds of experiencing suicidal thoughts. Compared with individuals aged 50–64, those aged 65–80 had higher odds of suicidal ideation in the total sample and among non-migrants. Among migrants, a similar pattern was observed, with further increase in odds among the oldest age group suggesting that the increase in risk with age may manifest later in life for this group.

For the oldest age group (81–94), the odds of suicidal ideation were markedly higher across all samples. Individuals aged 81–94 had almost three times higher odds of reporting suicidal thoughts in the total population and among non-migrants, and more than twice as high among migrants. These results indicate that the risk of suicidal thoughts escalates sharply in advanced old age, particularly beyond 80 years.

Gender was associated with suicidal ideation across all groups. Women were about 1.5 times more likely than men to report suicidal thoughts in the total population and among non-migrants. Among migrants, this gender difference was also evident, indicating that women more frequently experience such thoughts regardless of migration background.

Education showed a clear protective pattern in all three samples. Compared with individuals with

Tab. 4 Results of logistic regression models for suicidal ideation with control variables.

	Total study population		Migrants		Non-migrants	
−2 Log Likelihood	7795.320		646.962		7142.209	
Nagelkerke R-square	0.014		0.022		0.013	
Cox & Snell R^2	0.043		0.056		0.041	
Variable / category	Adj. OR	95% CI	Adj. OR	95% CI	Adj. OR	95% CI
Age groups (Reference: 50–64)						
65–80	1.28**	1.08–1.52	1.22	0.65–2.32	1.28**	1.08–1.52
81–94	2.84**	2.34–3.44	2.27*	1.15–4.50	2.85**	2.33–3.49
Gender (Reference: Male)						
Female	1.51**	1.32–1.73	1.73*	1.04–2.87	1.49**	1.29–1.71
Educational groups (Reference: Low education)						
Middle education	0.73**	0.63–0.85	0.536*	0.32–0.89	0.75**	0.64–0.88
High education	0.45**	0.37–0.55	0.416**	0.22–0.78	0.45**	0.36–0.56
Intercept	0.04**		0.06**		0.04**	

** Odds ratio is significant at the 0.01 level (2-tailed), * Odds ratio is significant at the 0.05 level (2-tailed).

low education, both middle and high education were associated with significantly lower odds of suicidal ideation across all groups. In the total population and among non-migrants, higher education reduced the odds of suicidal ideation by more than 50%. Among migrants, the protective effect was also significant. These results suggest that higher educational attainment reduces vulnerability to suicidal thoughts for both migrants and non-migrants.

The extended models including loneliness, recent sadness or depression, and regional context substantially improved the explanatory power of the model compared to controls-only. These results highlight the strong psychological correlates of suicidal ideation, while demographic and contextual effects remain more modest.

Loneliness emerged as one of the strongest and most consistent predictors of suicidal thoughts. Compared to those who reported not feeling lonely, individuals who described themselves as somewhat lonely had roughly 1.7 times higher odds of suicidal ideation in both the total population and among non-migrants. The effect was particularly pronounced for those who felt very lonely: the odds of suicidal thoughts were over six times higher in the total sample and among non-migrants. Among migrants, the association was also strong, confirming that intense loneliness is a powerful risk factor regardless of migration background.

Experiencing recent sadness or depression was another key determinant of suicidal ideation. Those who reported feeling sad or depressed had roughly four times higher odds of suicidal thoughts in the total sample and among non-migrants, and more than three times higher odds among migrants. This indicates that even after adjusting for loneliness and other factors, depressive feelings independently and strongly increase vulnerability to suicidal thinking.

Older age continued to be associated with higher odds of suicidal ideation, even after accounting for loneliness and sadness. Individuals aged 81–94 had approximately twice the odds of suicidal thoughts relative to those aged 50–64 in all groups. The persistence of this effect suggests that old age remains a structural risk factor for suicidal ideation, not fully explained by concurrent emotional distress. In the migrant sample, the effect was similar in size but not statistically significant, which can be explained by the smaller size of migrant sample.

Regional context generally did not play a major role, except for a notable protective effect among migrants residing in the Baltic countries, whose odds of suicidal thoughts were roughly two-thirds lower than their Nordic counterparts. This finding may point to contextual or cultural factors in Baltic societies that buffer against suicidal ideation among older migrants, though the pattern was not observed in the non-migrant population.

Tab. 5 Results of logistic regression models for suicidal ideation with key predictors and control variables.

	Total study population		Migrants		Non-migrants	
−2 Log Likelihood	6845.860		575.545		6255.469	
Nagelkerke R-square	0.060		0.072		0.059	
Cox & Snell R^2	0.180		0.184		0.181	
Variable / category	Adj. OR	95% CI	Adj. OR	95% CI	Adj. OR	95% CI
Region of residence (Reference: Nordics)						
Baltic	0.92	0.76–1.10	0.37**	0.21–0.66	0.98	0.81–1.19
Central European	1.10	0.93–1.31	0.56	0.27–1.16	1.15	0.97–1.38
Feelings of loneliness (Reference: Not lonely)						
Somewhat lonely	1.67**	1.42–1.96	1.41	0.82–2.43	1.70**	1.43–2.01
Very lonely	6.55**	5.41–7.92	5.29**	2.86–9.75	6.66**	5.45–8.15
Recently sad or depressed (Reference: No)						
Yes	3.99**	3.38–4.70	3.27**	1.86–5.76	4.05**	3.41–4.81
Age groups (Reference: 50–64)						
65–80	1.11	0.94–1.33	1.17	0.60–2.26	1.11	0.93–1.33
81–94	1.92**	1.57–2.35	1.86	0.90–3.84	1.93**	1.56–2.40
Gender (Reference: Male)						
Female	1.15	0.99–1.32	1.33	0.78–2.27	1.13	0.97–1.31
Educational groups (Reference: Low education)						
Middle education	0.80**	0.68–0.94	0.63	0.36–1.09	0.82*	0.70–0.97
High education	0.54**	0.43–0.66	0.44*	0.22–0.85	0.54**	0.43–0.68
Intercept	0.01		0.04		0.01**	

** Odds ratio is significant at the 0.01 level (2-tailed), * Odds ratio is significant at the 0.05 level (2-tailed).

Tab. 6 Results of a logistic regression model for migrants estimating suicidal ideation with key predictors, control variables, and migrant specific variables.

−2 Log Likelihood	572.646	
Nagelkerke R-square	0.074	
Cox & Snell R^2	0.189	
Variable / category	Adj. OR	95% CI
Region of residence (Reference: Nordics)		
Baltic	0.61	0.24–1.56
Central European	0.62	0.28–1.36
Feelings of loneliness (Reference: Not lonely)		
Somewhat lonely	1.37	0.79–2.36
Very lonely	5.25**	2.83–9.72
Recently sad or depressed (Reference: No)		
Yes	3.31**	1.88–5.84
Age groups (Reference: 50–64)		
65–80	1.14	0.56–2.30
81–94	1.81	0.81–4.07
Gender (Reference: Male)		
Female	1.33	0.78–2.29
Educational groups (Reference: Low education)		
Middle education	0.65	0.37–1.12
High education	0.45*	0.23–0.89
Years in the country (Reference: More than 50 years)		
20 years or less	1.32	0.27–6.42
21 to 50 years	0.87	0.48–1.57
Region of birth (Reference: EU)		
Former Soviet Union	0.54	0.25–1.18
Other	0.90	0.37–2.18
Intercept	0.05**	

** Odds ratio is significant at the 0.01 level (2-tailed), * Odds ratio is significant at the 0.05 level (2-tailed).

Once psychological predictors were included, gender differences in suicidal ideation largely disappeared. Education showed a protective effect, especially at higher levels, a trend that can be observed across all study samples. This suggests that the relationship between gender, education, and suicidal ideation may operate indirectly through psychological pathways such as loneliness and depressive symptoms. These factors may mediate or moderate the influence of sociodemographic variables, although confirming this would require additional analyses.

Adding migrant-specific variables (years in the country and region of birth) did not substantially improve the model fit or change the main conclusions. Neither years spent in the destination country nor region of birth showed significant associations with suicidal ideation.

The previously observed protective effect of residing in the Baltic countries disappeared once these variables were included, suggesting that the earlier pattern was partly compositional. Overall, emotional distress rather than migration background remains the key driver of suicidal ideation among older migrants.

5. Discussion

This study focuses on suicidal ideation among older adults in the Central European, Baltic, and Nordic (EU-member only) countries. Drawing comparisons between migrants and non-migrants, this study explores the prevalence and predictors of suicidal ideation while controlling for individual and contextual factors. Suicidal ideation was slightly more prevalent among migrants (6.9%) compared to non-migrants (4.8%), with separate models indicating subtle variations in the associations between risk factors and suicidal ideation across the two subgroups.

Feelings of loneliness, sadness, and depression were important predictors of suicidal ideation in all study samples. Suicidal ideation is often linked with mental health disorders, but it can also arise in response to situational stressors (Rizvi et al. 2024).

Our findings align with evidence identifying feelings of loneliness as a risk factor for suicidal ideation in both migrant and non-migrant population (Antonelli-Salgado et al. 2021; Gomboc et al. 2022; Shoib et al. 2023; McClelland et al. 2020). To fully understand suicidality in late life, physical health as well as social factors need to be considered. Loneliness has been shown to mediate the association between physical pain and suicidal ideation (Wiktorsson et al. 2010; Lutzman et al. 2021).

Among older immigrants, loneliness is associated with both social and personal factors, including absence of a spouse, lower financial status, and poor health. Additionally, poor psychological well-being, limited social connections, language difficulties, and weak sense of belonging further contribute to feelings of loneliness (Ruan and Cheung 2024; Alvi and Zaidi 2017). Social disconnection was found to be an important determinant of mental health and suicidal ideation among immigrants in anglosphere countries (Aran et al. 2023).

Depression is another potential risk factor for suicidal ideation among older adults (Jang and Kim 2005). In the context of migration, Bhatia et al. (2024) highlighted key social determinants of mental health in older adults aged 50 years and older. Among protective factors of mental health, warm family relationship, employment, and social support were included. Conversely, risk factors consist of high age, lack of partner, no support from children, language barriers, and limited access to healthcare services. These findings, along with our results, underscore the importance of psychosocial support for older adults, regardless of migration status.

Age is a key factor in this research, as it is related to many barriers that emerge later in life. Older immigrants are a vulnerable group, as increasing age often leads to deterioration in physical health, loss of social networks and loss of independence. All of these can be compounded by the stress of migration, language difficulties, cultural differences, feelings of isolation and other related challenges (Caidi et al. 2020; Anantapong et al. 2024). In this study, individuals aged 81–94 years exhibited the highest odds of suicidal thoughts.

Protective role of higher education was evident across all three samples. These results are consistent with previous research that identified lower socioeconomic status of older adults as a risk factor for suicidal behaviour (Ju et al. 2016; Kim et al. 2016).

In migrant sample, lower odds of suicidal ideation were found in respondents residing in the Baltic region as compared to those living in the Nordic countries, although this association was only statistically significant before including migrant-specific variables. One possible explanation is the socioeconomic background and migration patterns of these migrant populations. According to Włodarska-Frykowska (2017), Baltic societies are strongly influenced by historical ties to the post-Soviet space, which also affect the number of older immigrants from Soviet countries. Even though the research by Galstyan et al. (2021) focuses on emigration and identifying its main causes, the authors emphasize that since joining EU, the Baltic states have been making efforts to prevent emigration and to encourage return migration. Vorotnkov and Habarta (2021) highlight the efforts of Lithuania and, to somewhat more conservative extent, Latvia and Estonia to support long-term skilled and unskilled labour migrants and their integration into society. Furthermore, it is also worth highlighting the situation in Lithuania, where in 2024 more than half of the new long-term immigrants were family members who come to the country based on family ties (OECD 2025). On the other hand, the Nordic countries, which share similar welfare systems with active labour market policies and universal access to the provision of social benefits, differ in the structure of migrants and the reasons for migration (Greve 2016; Dahl et al. 2021). According to Dahl et al. (2021), the largest migrant structure in Denmark and Norway is represented by immigrants from other European countries, while in Sweden and Finland, the largest groups are immigrants from Syria and Iraq, with residence permits granted for family reasons, work, study, or asylum. In the context of Central European countries, the work-related motivations are often emphasized as predominant factor influencing migration (Drbohlav 2011; Bite et al. 2020; Papp et al. 2019; Schneider 2022).

Migrants in the Baltic region may have different migration trajectories and socioeconomic profiles, which could contribute to their lower risk of suicidal ideation. To confirm this relationship, further research with a larger sample would be needed.

Limitations. This study has several limitations. It is important to acknowledge that migrants are a heterogeneous group, with their health outcomes and suicidal ideation shaped by numerous interacting factors. The data were collected based on self-report measures, which may introduce bias. For example, mental health-related measures may be influenced by cultural factors, including the willingness to disclose suicidal ideation. Categorising continuous variables, while aiding interpretability, may involve some information loss and introduces a degree of subjectivity in how categories are defined. In particular, the small size of the reference group for "Years in the country" warrants cautious interpretation. Additionally, the cross-sectional design of the study does not allow for the confirmation of causal relationships. A longitudinal approach would provide valuable insights into the long-term effects and their potential impact on suicidal behaviour. Although many potential determinants were included in the analysis, the list was not exhaustive, and there may still be confounding variables that could influence suicidal ideation. Finally, the exclusive use of quantitative methods limits exploration of individual experiences.

6. Conclusion

This study examines the prevalence and predictors of suicidal ideation among older adults, with a particular focus on migration status and socio-geographical factors. Our findings indicate that individual factors such as age, loneliness, and mental health conditions, particularly depression, were the most important predictors of suicidal ideation among both migrants and non-migrants.

This research aligns with the UNs' Sustainable Development Goals (SDGs), particularly target 3.4, which prioritizes mental health improvement and suicide prevention. With the global population is aging rapidly, projecting to reach 16% aged 65 or older by 2050 (UN 2019), the need to address late-life mental health challenges has become increasingly urgent. As the proportion of older adults grows, so does their suicide risk. By incorporating a sociological perspective, this study aims to contribute to evidence-based strategies for mitigating suicidal ideation among older adults, with a particular focus on migration, gender, and socio-geographical disparities.

Acknowledgments

This work was supported by the NPO "Systemic Risk Institute" number LX22NPO5101, funded by the European Union – Next Generation EU (Ministry of Education, Youth and Sports, NPO: EXCELES). This work was also supported by GA UK project No 469025.

References

Alvi, S., Zaidi, A. U. (2017): Invisible Voices: An Intersectional Exploration of Quality of Life for Elderly South Asian Immigrant Women in a Canadian Sample. Journal of Cross-Cultural Gerontology 32(2), 147–170, https://doi.org/10.1007/s10823-017-9315-7.

Amiri, S. (2020): Prevalence of Suicide in Immigrants/Refugees: A Systematic Review and Meta-Analysis. Archives of Suicide Research 26(2), 370–405, https://doi.org/10.1080/13811118.2020.1802379.

Anantapong, K., Udomratn, P., Ventriglio, A., Pemberton, M., Poulter, D., Bhugra, D. (2024): Migration and mental health problems of older adults: Challenges and proposed solutions. Industrial Psychiatry Journal 33(1), 236–241, https://doi.org/10.4103/ipj.ipj_29_24.

Antonelli-Salgado, T., Monteiro, G. M. C., Marcon, G., Roza, T. H., Zimerman, A., Hoffmann, M. S., Cao, B., Hauck, S., Brunoni, A. R., Passos, I. C. (2021): Loneliness, but not social distancing, is associated with the incidence of suicidal ideation during the COVID-19 outbreak: a longitudinal study. Journal of affective disorders 290, 52–60, https://doi.org/10.1016/j.jad.2021.04.044.

Aran, N., Card, K. G., Lee, K. (2023): Patterns of Suicide and Suicidal Ideation in Relation to Social Isolation and Loneliness in Newcomer Populations: A Review. Journal of Immigrant and Minority Health 25(2), 415–426, https://doi.org/10.1007/s10903-022-01422-9.

Berry, J. W. (1980): Acculturation as varieties of adaptation. In: Padilla, A. (Ed.), Acculturation: Theory, Models and Findings; Westview: Boulder, pp. 9–25.

Bersani, B. E., Morabito, M. S. (2020): Immigrant Disparities in Suicide Ideation: Variation Across Age of Migration, Gender, and Nativity. Journal of Immigrant and Minority Health 22(5), 881–887, https://doi.org/10.1007/s10903-020-00993-9.

Bhatia, P., McLaren, H., Huang, Y. (2024): Exploring Social Determinants of Mental Health of Older Unforced Migrants: A Systematic Review. The Gerontologist 64(6): gnae003, https://doi.org/10.1093/geront/gnae003.

Bite, P., Konczos Szombathelyi, M., Vasa, L. (2020): The concept of labour migration from the perspective of Central and Eastern Europe. Economics and Sociology 13(1), 197–216, https://doi.org/10.14254/2071-789X.2020/13-1/13.

Borevi, K. (2017): Diversity and Solidarity in Denmark and Sweden. In: Banting, K., Kymlicka, W. (Eds.), The Strains of Commitment; Oxford University Press: Oxford, UK, pp. 364–388, https://doi.org/10.1093/acprof:oso/9780198795452.003.0013.

Caidi, N., Du, J. T., Li, L., Shen, J. M., Sun, Q. (2020): Immigrating after 60: Information experiences of older Chinese migrants to Australia and Canada. Information Processing & Management 57(3): 102111, https://doi.org/10.1016/j.ipm.2019.102111.

Cogo, E., Murray, M., Villanueva, G., Hamel, C., Garner, P., Senior, SL., Henschke, N. (2022): Suicide rates and suicidal behaviour in displaced people: A systematic review. PLoS ONE 17(3): e0263797, https://doi.org/10.1371/journal.pone.0263797.

Cohen, C. I., Lo, P., Nzodom, C., Sahlu, S. (2018): Migration, Acculturation, and Mental Health. In: Llorente, M. D. (Ed.), Culture, Heritage, and Diversity in Older Adult Mental Health Care; American Psychiatric Association Publishing: Washington, DC, USA, pp. 53–80, https://doi.org/10.1176/appi.books.9781615372119.lg03.

Crocker, L., Clare, L., Evans, K. (2006): Giving up or finding a solution? The experience of attempted suicide in later life. Aging & Mental Health 10(4), 364–374, https://doi.org/10.1080/13607860600640905.

Dahl, B. M., Buch Mejsner, S., Eklund Karlsson, L., Kostenius, C., Laverack, G., Andersen, H. M., Warne, M., Lidmark, J. (2021): The Nordic perspective on migration and empowerment. Health Promotion International 36(1), 216–222, https://doi.org/10.1093/heapro/daaa021.

Drbohlav, D. (2011): Immigration and Integration of Foreigners in Czechia: Some Thoughts on the Country's Migration Transition from a David to a Near Goliath. Geografie 116(4), 401–421, https://doi.org/10.37040/geografie2011116040401.

Eikemo, T. A., Bambra, C., Judge, K., Ringdal, K. (2008): Welfare state regimes and differences in self-perceived health in Europe: A multilevel analysis. Social Science & Medicine 66(11), 2281–2295, https://doi.org/10.1016/j.socscimed.2008.01.022.

Fenger, H. J. M. (2007): Welfare regimes in Central and Eastern Europe: Incorporating post-communist countries in a welfare regime typology. Contemporary Issues and Ideas in Social Sciences 3(2), 1–30, http://hdl.handle.net/1765/34876.

Galstyan, A., Grabowska, M., Bačiulienė, V. (2021): Economic development and migration after EU accession: the case of Baltic states. Pressburg Economic Review 1(1), 47–55, https://review.pressburgcentre.org/per/article/view/6.

Gomboc, V., Krohne, N., Lavrič, M., Podlogar, T., Poštuvan, V., Zadravec Šedivy, N., de Leo, D. (2022): Emotional and Social Loneliness as Predictors of Suicidal Ideation in Different Age Groups. Community Mental Health Journal 58(2), 311–320, https://doi.org/10.1007/s10597-021-00823-8.

Greve, B. (2016): Migrants and health in the Nordic welfare states. Public Health Reviews 37: 9, https://doi.org/10.1186/s40985-016-0023-6.

Rizvi, A., Harmer, B., Saadabadi, A. (2024): Suicidal Ideation. In StatPearls. StatPearls Publishing. Available online: https://pubmed.ncbi.nlm.nih.gov/33351435/ (accessed on 5 February 2025).

Hughes, M. E., Waite, L. J., Hawkley, L. C., Cacioppo, J. T. (2004): A Short Scale for Measuring Loneliness in Large Surveys: Results from Two Population-Based Studies. Research on Aging 26(6), 655–672, https://doi.org/10.1177/0164027504268574.

Jang, M.-H., Kim, Y.-H. (2005): The Relationship of Stress, Depression and Suicidal Ideation in the Elderly. Journal of Korean Academy of Psychiatric and Mental Health Nursing 14(1), 33–42, https://doi.org/10.12934/jkpmhn.2005.14.1.33.

Ju, Y. J., Park, E.-C., Han, K. T., Choi, J. W., Kim, J. L., Cho, K. H., Park, S. (2016): Low socioeconomic status and suicidal ideation among elderly individuals. International psychogeriatrics 28(12), 2055–2066, https://doi.org/10.1017/S1041610216001149.

Kan, Z., Søegaard, E. G. I., Thapa, S. B. (2019): Selvmord blant innvandrere i Norge. Suicidologi 24(1), 33–35. Available online: https://journals.uio.no/plugins/generic/pdfJsViewer/pdf.js/web/viewer.html?file=https%3A%2F%2Fjournals.uio.no%2Fsuicidologi%2Farticle%2Fdownload%2F7030%2F6000%2F21712 (accessed on 10 February 2025).

Kim, J. L., Kim, J. M., Choi, Y., Lee, T.-H., Park, E.-C. (2016): Effect of Socioeconomic Status on the Linkage Between Suicidal Ideation and Suicide Attempts. Suicide and Life-Threatening Behavior 46(5), 588–597, https://doi.org/10.1111/sltb.12242.

Kjølseth, I., Ekeberg, Ø., Steihaug, S. (2010): Why suicide? Elderly people who committed suicide and their experience of life in the period before their death. International Psychogeriatrics 22(2), 209–218, https://doi.org/10.1017/S1041610209990949.

Klonsky, E. D., May, A. M., Saffer, B. Y. (2016): Suicide, suicide attempts, and suicidal ideation. Annual Review of Clinical Psychology 12(1), 307–330, https://doi.org/10.1146/annurev-clinpsy-021815-093204.

Kuntz, L., Moutier C. Y. (2021): Suicide: Myths, media, and difficult discussions. Psychiatric Times. Available online: https://www.psychiatrictimes.com/view/suicide-myths-media-and-difficult-discussions (accessed on 20 September 2024).

Lee, D. R., Kawas, C. H., Gibbs, L., Corrada, M. M. (2016): Prevalence of frailty and factors associated with frailty in individuals aged 90 and older: The 90+ Study. Journal of the American Geriatrics Society 64(11), 2257–2262, https://doi.org/10.1111/jgs.14317.

Lehti, V., Kieseppä, V., Gissler, M., Suvisaari, J., Markkula, N. (2025): Psychotherapy use among migrants: a register-based longitudinal study. J Epidemiol Community Health 79(1), 49–55, https://doi.org/10.1136/jech-2024-222330.

Lutzman, M., Sommerfeld, E., Ben-David, S. (2021): Loneliness and social integration as mediators between physical pain and suicidal ideation among elderly men. International Psychogeriatrics 33(5), 453–459, https://doi.org/10.1017/S104161022000112X.

McClelland, H., Evans, J. J., Nowland, R., Ferguson, E., O'Connor, R. C. (2020): Loneliness as a predictor of suicidal ideation and behavior: A systematic review and meta-analysis of prospective studies. Journal of Affective Disorders 274, 880–896, https://doi.org/10.1016/j.jad.2020.05.004.

Nesturi, M., Nasufi, I. A. (2025): Loneliness and the changing care landscape for the elderly in Albania. AUC Geographica 60(1), 105–114, https://doi.org/10.14712/23361980.2025.3.

Norredam, M., Olsbjerg, M., Petersen, J. H., Laursen, B., Krasnik, A. (2013): Are there differences in injury mortality among refugees and immigrants compared with native-born? Injury Prevention 19(2), 100–105, https://doi.org/10.1136/injuryprev-2012-040336.

OECD (2021): Pensions at a Glance 2021: OECD and G20 Indicators; OECD Publishing: Paris, https://doi.org/10.1787/ca401ebd-en.

OECD (2025): International Migration Outlook 2025; OECD Publishing: Paris, https://doi.org/10.1787/ae26c893-en.

Øien-Ødegaard, C., Hauge, L. J., Reneflot, A. (2021): Marital status, educational attainment, and suicide risk: A Norwegian register-based population study. Population Health Metrics 19(1): 33, https://doi.org/10.1186/s12963-021-00263-2.

Papp, I. C., Bilan, S., Dajnoki, K. (2019): Globalization of the labour market – circular migration in Hungary. Journal of International Studies 12(2), 182–200, https://doi.org/10.14254/2071-8330.2019/12-2/11.

Pathirathna, M. L., Geethani Nandasena, H., Atapattu, A., Weerasekara, I. (2022): Impact of the COVID-19 pandemic on suicidal attempts and death rates: A systematic review. BMC Psychiatry 22(1): 506, https://bmcpsychiatry.biomedcentral.com/articles/10.1186/s12888-022-04158-w.

Qin, P., Syeda, S., Mehlum, L. (2022): Selvmord og villet egenskade blant innvandrerbefolk ningen i Norge: innsikt basert på norske registre. Arbeids- og inkluderingsdepartementet (AID), Prosjektrapport: 28-04-2022. Available online: https://www.med.uio.no/klinmed/forskning/sentre/nssf/forskning/nssf-prosjekter/selvmord-villetegenskade-minoriteter/sluttrapport-til-aid_nssf.pdf (accessed on 15 February 2025).

Reine, I., Miķelsone, M., Tomsone, S., Guðmundsson, H., Ivanovs, A., Guðmundsson, H. S., Koroļeva, I. (2024): Unraveling the dynamics of loneliness in the Baltic-Nordic region: A comparative analysis in the wake of COVID-19. Frontiers in Public Health 12, 1–12, https://doi.org/10.3389/fpubh.2024.1360285.

Reus-Pons, M., Mulder, C. H., Kibele, E. U. B., Janssen, F. (2018): Differences in the health transition patterns of migrants and non-migrants aged 50 and

older in southern and western Europe (2004–2015). BMC medicine 16: 57, https://doi.org/10.1186/s12916-018-1044-4.

Ruan, Y., Cheung, M. (2024): Systematic review of factors influencing loneliness in older-adult migrants. Aging & Mental Health 28(8), 1129–1141, https://doi.org/10.1080/13607863.2024.2340736.

Sand, G., Gruber, S. (2018): Differences in subjective well-being between older migrants and natives in Europe. Journal of Immigrant and Minority Health 20, 83–90, https://doi.org/10.1007/s10903-016-0537-5.

Schneider, O. (2022): Labour migration in the European Union: The case of Central and Eastern Europe. Economic Annals 67(233), 7–38, https://doi.org/10.2298/EKA2233007S.

Shah, A. (2012): The relationship between elderly suicide rates and different components of education: A cross-national study. Journal of Injury & Violence Research 4(2), 52–57, https://doi.org/10.5249/jivr.v4i2.75.

Shoib, S., Amanda, T. W., Saeed, F., Ransing, R., Bhandari, S. S., Armiya'u, A. Y., Gürcan, A., Chandradasa, M. (2023): Association Between Loneliness and Suicidal Behaviour: A Scoping Review. Turkish journal of psychiatry 34(2), 125–132, https://doi.org/10.5080/u27080.

Simon, R. (1989): Silent suicide in the elderly. The Bulletin of the American Academy of Psychiatry and the Law 17(1), 83–95.

Sironi, A., Bauloz, C., Emmanuel, M. (2019): Glossary on Migration. International Migration Law, No. 34; International Organization for Migration (IOM): Geneva. Available online: https://publications.iom.int/system/files/pdf/iml_34_glossary.pdf (accessed on 12 February 2025).

Szikra, D. (2014): Democracy and welfare in hard times: The social policy of the Orbán Government in Hungary between 2010 and 2014. Journal of European Social Policy 24(5), 486–500, https://doi.org/10.1177/0958928714545446.

United Nations (2024): International Migrant Stock 2024: Key facts and figures. United Nations. Available online: https://www.un.org/development/desa/pd/sites/www.un.org.development.desa.pd/files/undesa_pd_2025_intlmigstock_2024_key_facts_and_figures_advance-unedited.pdf (accessed on 8 January 2025).

United Nations, Department of Economic and Social Affairs, Population Division (2019): World Population Prospects 2019: Highlights. United Nations. Available online: https://population.un.org/wpp/Publications/Files/WPP2019_Highlights.pdf (accessed on 11 February 2025).

Vorotnkov, V. V., Habarta, A. (2021): Migration from Post-Soviet countries to Poland and the Baltic States: trends and features. Baltic Region 13(4), 79–94, https://doi.org/10.5922/2079-8555-2021-4-5.

Widding-Havneraas, T., Pedersen, S. H. (2020): The role of welfare regimes in the relationship between childhood economic stress and adult health: A multilevel study of 20 European countries. SSM – Population Health 12, https://doi.org/10.1016/j.ssmph.2020.100674.

Wiktorsson, S., Runeson, B., Skoog, I., Östling, S., Waern, M. (2010): Attempted suicide in the elderly: characteristics of suicide attempters 70 years and older and a general population comparison group. The American Journal of Geriatric Psychiatry 18(1), 57–67, https://doi.org/10.1097/JGP.0b013e3181bd1c13.

Włodarska-Frykowska, A. (2017): Migration processes in the Baltic States – the dynamic of change. Eastern Review 6, 143–158, https://doi.org/10.18778/1427-9657.06.10.

World Health Organization (2024): Suicide. World Health Organization. Available online: https://www.who.int/news-room/fact-sheets/detail/suicide (accessed on 11 February 2025).

Wu, Z., Penning, M. (2015): Immigration and loneliness in later life. Ageing & Society 35(1), 64–95, https://doi.org/10.1017/S0144686X13000470.

Yan, Y., Hou, J., Li, Q., Yu, N. X. (2023): Suicide before and during the COVID-19 pandemic: A systematic review with meta-analysis. International Journal of Environmental Research and Public Health 20(4): 3346, https://doi.org/10.3390/ijerph20043346.

Perceived intra-urban centrality in Kyiv: The student perspective

Oleksiy Gnatiuk*, Olena Kononenko

Taras Shevchenko National University of Kyiv, Faculty of Geography, Department of Economic and Social Geography, Ukraine
* Corresponding author: oleksii.gnatiuk@knu.ua

ABSTRACT
This article explores intra-urban perceived centrality in Kyiv, Ukraine's capital, investigating its relationships with the selected non-perceptual measures of centrality. Using a three-stage survey of 141 students, the study examines how respondents delineate the city center's boundaries, which locations they perceive as central, and how they use and experience the space of the city center. The findings reveal both overlaps and discrepancies between contour-derived and location-based intra-urban centrality. The Dnieper River, railways, and major highways serve as strong spatial referents of the center's boundary, while the main city street and square together with certain traditional historic neighborhoods anchor the perceived city center. At the same time, functional load, landmark value, and personal experiential factors significantly shape perceptions, creating local spikes and dips of centrality. Respondents emphasize not so much individual monuments as the broader historic environment and atmosphere of the city center, with walking and flânerie as dominant practices. The results highlight tensions between heritage preservation and aggressive commercialization, as well as the underutilized potential of the Dnieper waterfront in the Ukrainian capital. The main contribution of the study lies in underscoring perceived intra-urban centrality as a multidimensional and fluid social construct, shaped by history, functions, symbolism, and everyday social practices, which can be operationalized by urban planners.

KEYWORDS
city center perception; intra-urban centrality; post-socialist urban transformation; perception-based mapping; Kyiv

Received: 16 September 2025
Accepted: 26 January 2026
Published online: 9 February 2026

Gnatiuk, O., Kononenko, O. (2026): Perceived intra-urban centrality in Kyiv: The student perspective.
AUC Geographica 61(2), 175–194
https://doi.org/10.14712/23361980.2026.3
© 2026 The Authors. This is an open-access article distributed under the terms of the Creative Commons Attribution License (https://creativecommons.org/licenses/by/4.0).

1. Introduction

The concept of centrality is one of the key notions in human geography. The study of center-periphery relations contributes to a deeper understanding of the historical development of countries, regions, and cities. Classical geographical theories revealed the essence of the dichotomous notions of center and periphery (Christaller 1966; Friedmann 1966). Cities represent a vivid manifestation and the quintessence of the concept of centrality (Bird 1977; Lefebvre 2003), yet within cities there are also central areas with their own unique characteristics and functions: political, economic, transport, social, and symbolic (Batty 2008; Thurstain-Goodwin and Unwin 2000). Accelerated urbanization, city expansion, the development of information technologies, and urban digitalization call for a rethinking of both the essence and significance of the center for the city and its inhabitants, as well as approaches to its study, the identification of new meanings, and its delineation (Helbrecht and Dirksmeier 2012; Sun et al. 2016; Wurm et al. 2021). The functions performed by the city center are rapidly changing and acquiring new, specific features. For instance, scholars have focused on its residential (Tallon and Bromley 2004), commercial (Karayalcin and Yilmazkuday 2015), and transport (Simpson 2021) functions.

The centers of post-Soviet cities were for a long time controlled by the central authorities and primarily served as the location for buildings of local administrations, government, parliament, and other power structures, as well as the venue for parades, demonstrations, and other mass events (Mezentsev et al. 2023). The planning structure of cities, especially those with capital status, was subordinated to this function, while historical monuments were often demolished (Kostiuchok 2013). The current state of the central parts of post-Soviet cities is debated both in academic literature, particularly in architectural and urban planning studies (Oliinyk 2021), and in public discussions led by civic activists and local historians who criticize urban development and reconstruction plans.

Kyiv, the capital of Ukraine, offers a promising case for studying the contemporary city center. First, it lacks a single coherent architectural ensemble of a city center, leaving its spatial form, morphology and functions open to debate and reconstruction. Second, as the national capital, Kyiv hosts numerous functions that, to varying degrees, gravitate toward the center. This increases the concentration of economic and social activity within a rather large area around the city's key central streets and squares. The commercialization and uncontrolled character of changes heighten the need for research (Cybrivskyi 2014; Mezentseva 2017; Dronova and Maruniak 2019). Third, the Revolution of Dignity and Russia's full-scale invasion since 2022 have significantly reshaped the center through new memorials, commemorative sites, and exhibitions (Gentile 2025).

Thus, the aim of this study was to identify the perceived city center of Kyiv and delineate it according to aggregated individual perceptions based on the survey results. The research questions were the following:

1. In what ways does the perceived city center relate to various forms and indicators of centrality, and what are the reasons behind the coincidences and mismatches?
2. Does the definition of the perceived city center differ when it is understood as a continuous territory (an urban district) versus as a set of individual locations with their own characteristics, such as historicity, functions, etc., and why does this happen?
3. What kinds of places, social practices and functions are associated with the city center?

Various factors may shape how residents and visitors perceive the city center. Our hypothesis is that, despite the multifunctionality and ambiguity, a shared image emerges in people's perceptions, much like the image of the city as a whole (Lynch 1960). This perceived center should reflect local knowledge, personal experience, expectations and emotions (Deng et al. 2021). At the same time, it should be anchored in material structures that mark boundaries, such as old city walls, in landmarks of historical or symbolic, and in places performing specific functions, including commercial, recreational, entertainment sites, etc.

2. Theoretical aspects of intra-urban centrality

When studying the spatial development of a city, it is impossible to avoid analyzing center-periphery relationships, with particular attention given to the central part with its undeniable advantages. However, definition of a certain urban area as a central or peripheral often is ambiguous: intra-urban centrality may be associated with a variety of specific urban functions, morphological and topological features (Bird 1977; Sun et al. 2016; Wurm et al. 2021). When determining the spatial limits of the center from the perspective of a researcher, urban planner or ordinary city resident, one or several approaches or criteria for evaluating the degree of centrality of a given urban area may be used, either consciously or, in case of ordinary people, subconsciously.

First, the city center may be understood either geometrically or in terms of networks. Geometrically, it corresponds to the city's centroid or the barycenter of a specific distribution, such as population or built environment. In network terms, it is the most central node of the transport graph, the point of best accessibility, measured by centrality indices (Crucitti et al. 2006). Both are abstract models of centrality (van

Meeteren 2021), and their variety leads to multiple possible centers. Depending on criteria such as density, diversity, design, destinations, distance, demand management, or urban planning concept, different areas of the same city may be defined as central (Natalia and Heinrichs 2019). Nevertheless, better accessibility is considered to be the key advantage of the central position, which facilitates business activities, urban development management, and contributes to the formation of urban identity and city branding (Sun et al. 2016; Li et al. 2017; Simpson 2021). The corresponding economic and social effects of locating in the center are thoroughly described in classical geographic theories, primarily Central Place Theory (Christaller 1966), the center-periphery theory (Friedmann 1966), and related works (van Meeteren 2021).

Second, the city center can be considered as a historical category (Deng et al. 2021), which in turn reinforces the importance of historic city centers as spaces of aesthetic and cultural consumption (Henriques 2022). Centrality may function as a synonym for antiquity, historicity, a place "from which everything began". From this perspective, the center can be viewed as either a specific point location or a significant spatial core from which the city's development chronologically originated: a territory formerly protected by city walls, a central market square, a palace, a church, or another landmark (Bird 1977). Identifying a city's historical center depends on the presence of material evidence in the urban landscape that reflects antiquity and cultural value, such as monuments and historic buildings. Throughout different historical stages of development, older cities may face challenges in expanding their core in line with new technological conditions, which can lead to the emergence of new centers corresponding to the development of new urban functions (Bird 1977; Miranda et al. 2020). Thus, a city may have multiple historical centers.

Third, centrality can also serve as a synonym for power, governance, or authority, primarily political power. Associating the city center with a power core is one of the oldest concepts, since the administrative function has been one of the key city-shaping functions since antiquity (Nooraddin 2016). Accordingly, the city center can be identified with hubs of concentrated administrative and religious institutions at the urban level, and if the city holds the status of a regional administrative center or national capital, then also at the regional or national level.

Fourth, centrality has traditionally been associated with a business function as well. From this perspective, the center serves as a source of the city's economic growth – a locus of office complexes, including the headquarters of leading companies, banking and financial institutions that exert significant influence on financial and economic policy, as well as major establishments of commerce and entertainment, particularly shopping malls. In North American cities, business centers are known as Central Business Districts (CBDs). Such business districts function as symbols of urban economic growth, associated with ideas of progress, modernity, and prosperity. Their delimitation typically takes into account criteria such as the magnitude of land rent, building height, and traffic flows (Murphy and Vance 1954).

Fifth, the city center can also be understood as a locus of events and communication (Mitković and Brankovic 2004). Centrality can be associated with a place of high social activity, where "something is always happening" or where "something important" for the urban community takes place. Centers are the sites of mass gatherings – celebrations, concerts, presentations, civil and military parades and demonstrations, but also contestations, protests and revolutions. These moments, whether festive or tragic, strongly shape the emotional perception of centrality. Participation fosters communication and exchange of ideas, reinforcing the center as a space of interaction. Cultural events may even temporarily shift centrality to peripheral areas (Michel 2024).

Sixth, symbolic landmarks, streets, and squares often define and embody the city center, shaping city identity, image, and branding. Iconic examples include the Statue of Liberty, Fifth Avenue, Wall Street, and Broadway in New York. Most cities worldwide have a historically established and widely recognized "main" street or square, often though not always hosting city administration. Such status may not be formally designated but is firmly embedded in public consciousness, sometimes even in the street's name. In some cases, central districts are formally defined (for example, Śródmieście in Warsaw or Mitte in Berlin), reinforcing symbolic centrality.

Ultimately, city center may be perceived not as a place of concentration or dominance of a single function, but rather as a multifunctional hub, a space where multiple functions intersect (Burgess 1925/1967). From this perspective, centrality is defined primarily through multifunctionality, while mono-functional urban districts cannot claim the role of a center. Due to the highest possible concentration of diverse functions, the center is characterized by the most intensive use of urban space. In historical and touristic cities, this often manifests as the geographical proximity of administrative and historical centers, where key symbolic landmarks, as well as "main" streets and squares are typically located (Sun et al. 2016). A generalized model of intra-urban centrality includes religious and administrative buildings, the inner/historic city, transport hubs, the business district, workplaces around it, and commercial establishments (Bird 1977), thereby ensuring the political, economic, administrative, and social functions of the center.

Under the influence of industrialization, accelerated urbanization, and globalization, city centers and the mere essence of urban centrality began to change rapidly (Helbrecht and Dirksmeier 2012). The set of functions inherent to the city center has shifted; in

some cities it has remained singular, while in others the phenomenon of polycentricity can be observed (Harris and Ullman 1945; Zhu et al. 2024). The increased concentration of human activity leads to a reassessment of the advantages and disadvantages of centrality. Many city centers are noisy, polluted, and face problems such as congestion and excessive touristification (Gusman et al. 2019; Foronda Robles et al. 2025). In historic towns, subcenters are emerging as a town grows and the historic center co-evolving with the entire urban area and surrounding urban centralities; the rise of centralities testifies to the vitality of the town (Miranda et al. 2020). On the other hand, deindustrialization and revitalization of central urban areas create a new form of centrality (Helbrecht and Dirksmeier 2012), which imposes new demands on architecture and the organization of public spaces.

Thus, centrality, which for many centuries was based on economic rationale and could be described using geometric models, is increasingly imbued with social meaning. A unique social space is produced in the city center (Lefebvre, 1974/1991, 2003). Cities seek a balance between designating the center for tourists or for residents, combining historical value with modern design and architecture (Gusman et al. 2019). These processes underscore the importance of involving residents in identifying and delineating the spatial boundaries of the city center and shaping its future development trajectories.

The spatially-referenced image of intra-urban perceived centrality and, more specifically, perceived city centre embodies via cognitive or mental maps – selective mental representations of spatial physical structures of a city center and meanings (emotions, senses, values, activities, etc.) associated with them (Gould 1966; Gould and White 1974; Nasar 1990). Visualizing such maps, people typically emphasize symbolic landmarks, key streets and squares, familiar routes, and areas of concentrated everyday practices, while omitting or simplifying less meaningful spaces. Boundaries of the center, similar to the other vernacular urban districts, may appear as blurred, irregular, or fragmented rather than fixed, reflecting personal experience, cultural narratives, and functional use of space (Lynch 1960; Appleyard 1970). In this way, mental maps reveal both the spatial structure and the subjective, experiential dimension of how the city center is understood and lived.

3. Characteristics of Kyiv in the context of the city center perception

In this section, we briefly describe key features and landmarks in Kyiv that are important for understanding the geographical context of the study and its results (Fig. 1).

From a historical perspective, the city center can be seen as either the city's oldest neighborhoods or the location of its historic built environment. Until the early 19th century, Kyiv lacked a single center and consisted of three distinct parts (Diomin and Oliinyk 2022): (1) Verkhnie Misto / Staryi Kyiv [Upper City / Old Kyiv], the political and religious core since Kyivan Rus, home to princely palaces, the Church of the Tithes, Saint Sophia Cathedral, and St. Michael's Monastery; (2) Podil, which developed as a crafts-and-trade district, later industrializing around the Dnieper port; (3) Pechersk, centered on the princely settlement of Berestove and the Kyiv-Pechersk Lavra, later a fortified and administrative city hearth. These areas are most often described in scholarship (Vecherskyi 2012; Oliinyk 2021) and media as Kyiv's historical neighborhoods. Yet their combined boundaries do not fully coincide with the limits of the "historical" built environment (up to 1918): historic buildings also exist beyond them, while some of their parts contain modern development (LUN Misto n.d.b; Sliudikova 2009).

Kyiv's Khreshchatyk and Maidan Nezalezhnosti are widely recognized as the city's main street and square, respectively, symbolizing the highest concentration of centrality, which also extends to adjacent areas (Bondar 2018). Considering Khreshchatyk and Maidan Nezalezhnosti as the absolute center of Kyiv, the centrality of other locations can be assessed based on their distance from them. Yet this was not always so: in the late 18th century Khreshchatyk remained undeveloped. Architect Andriy Melenskyi foresaw its potential to connect Kyiv's three main historic neighborhoods – Verkhnie Misto, Podil, and Pechersk – and during the 19th century it gradually became prestigious and well-accessible (Stebletska 2014). By the mid-19th century, with the relocation of the city council and other administrative and commercial institutions, Khreshchatyk was firmly established as Kyiv's main street. The same considerations apply to the gradual rise of the present-day Maidan Nezalezhnosti, one of the key focal points along the Khreshchatyk linear axis, as the main square of Kyiv and a nation. The role of Khreshchatyk and, especially, Maidan Nezalezhnosti as the symbolic center was further strengthened after the events of the Orange Revolution in 2004 and the Revolution of Dignity in 2013–2014.

If the city center is viewed as a concentration of specific functions, three main aspects emerge: tourist, administrative, and commercial-business. Tourist activity largely aligns with Kyiv's historical built-up area, mainly on the high right-bank plateau, where tall landmarks shape the city's panorama, including Kyiv-Pechersk Lavra, St. Michael's Monastery, St. Andrew's Church, Vydubychi Monastery, and the River Station. The Motherland Monument (1981) and Independence Monument (2001) further define the cityscape. Administratively, Khreshchatyk hosts the city council, while the Government Quarter in Pechersk concentrates national authorities, giving

the area a "power center" status; the journalistic expression "Pechersk Hills" is used as a synonym for national political authorities. Commercially, shopping malls and offices have developed primarily in the historical center, key urban nodes near metro stations, and revitalized former industrial areas, but are scarce in poorly connected districts, especially on the left bank (Dronova and Polieshko 2017; Mezentsev and Mezentseva 2017; Mezentseva 2017; Bykova and Shchabelska 2022). Consequently, Kyiv's commercial-business center overlaps largely with the historical center but extends beyond it, forming a diffuse network of hubs potentially perceived as having elevated centrality.

The Dnieper River also shapes Kyiv's intra-urban centrality. While historically a vital factor in the city's development, it also functions as its main internal barrier due to limited bridges and rapid transit connections. The right bank, where Kyiv originated, concentrates historical landmarks, business districts, and state institutions, reinforcing its image as the prestigious and "central" side. By contrast, the left bank, developed intensively only from the mid-20th century, is dominated by large housing estates and industrial zones. Often perceived as a "bedroom community" with poor accessibility, it remains widely regarded as peripheral rather than central (Gnatiuk et al. 2023).

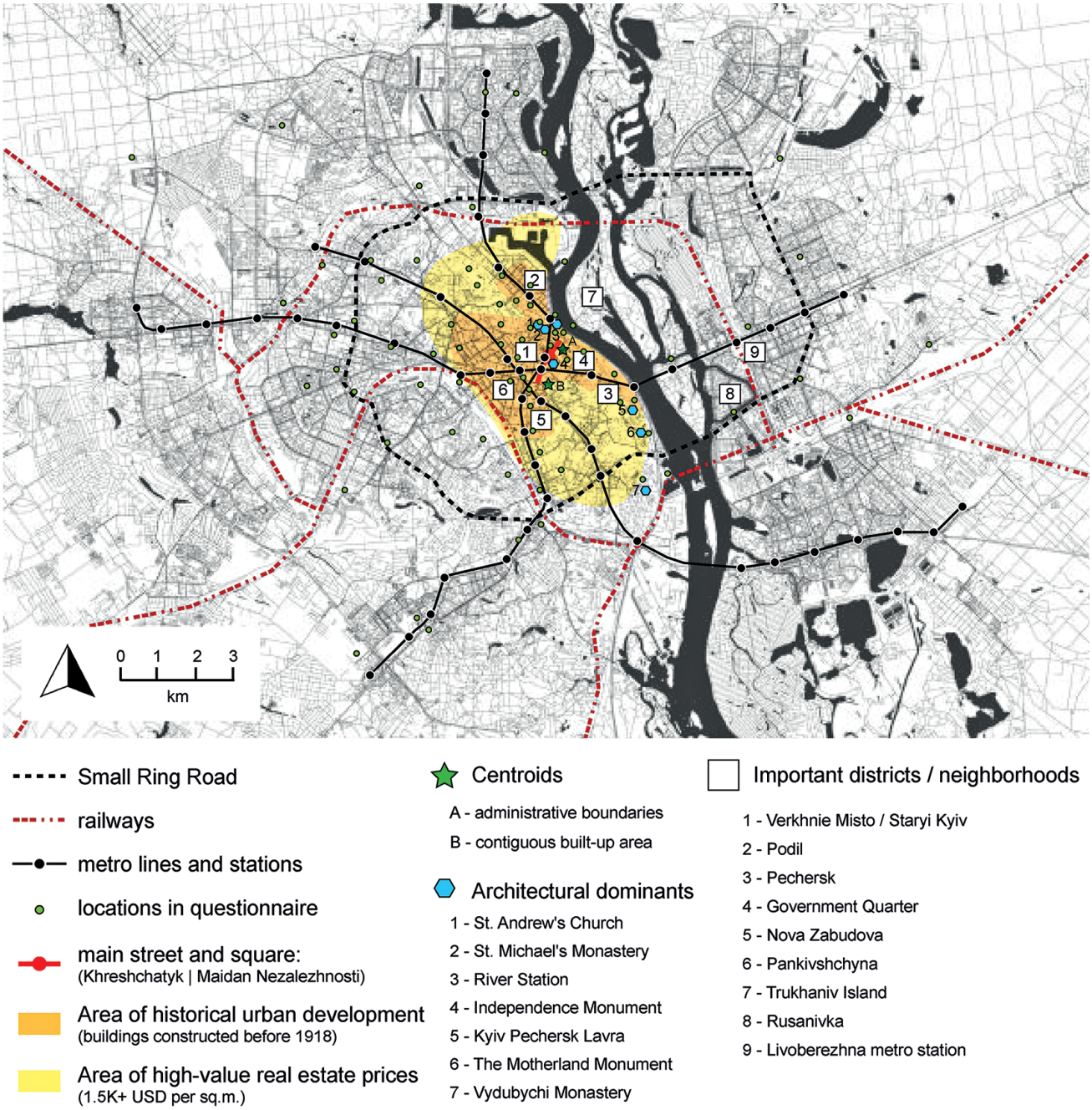

Fig. 1 Kyiv as a study area: key features and landmarks.
Source: authors' elaboration; data on the area of historical urban development and real estate prices from LUN Misto.

Geometrically, Kyiv's centroid varies depending on the area considered. Within the city administrative boundaries, the centroid lies near the north end of Khreshchatyk. Considering only the contiguous built-up area, excluding forests and wastelands, the centroid shifts slightly southwards and locates south to Maidan Nezalezhnosti. In both cases, centroid aligns closely with the city's symbolic center and fits into the area of historical urban development.

4. Data and methods

The study surveyed 141 bachelor 17–22 year old students studying in Kyiv. Among the respondents, men accounted for 74 (52.5%) and women for 67 (47.5%). All students were from Ukraine; 42 (29.8%) were native residents of Kyiv, while the remaining majority of 98 (69.5%) came to study from other regions of Ukraine. Of the latter group, 17 had lived in Kyiv for less than one year, 24 for 1–2 years, 32 for 2–3 years, and 25 for more than three years; the vast majority resided in a university dormitory located on the south-western periphery of Kyiv. The respondents were students of economic geography and urban studies and planning.

The anonymous survey was conducted from March to May 2025, yielding 141 completed paper-based questionnaires. The questionnaire was pilot-tested with a small group of students (n = 10), whose answers have not been included into the research sample. The survey consisted of three stages, combining drawing sketch maps of a city and answering the interview questions (Nasar 1990). In the first stage, respondents evaluated 84 specific locations in Kyiv using their names and photographs, indicating whether each location belonged to the city center ("Yes", "No", or "I don't know the location"). All participants completed this stage. In the second stage, which employed adopted Lynch-type mental map research technique (Lynch 1960; Montello et.al. 2003; Nawrocki 2017), respondents drew their perceived boundaries of Kyiv's city center on a contour map showing key spatial landmarks (city boundary, Dnieper River, main streets, railways); 136 maps were usable, as five were incomplete or spoiled. The third stage involved three open-ended questions: (1) frequency of visiting the city center, (2) purposes of visiting, and (3) specific places visited. All respondents completed this stage. This design allowed the study to capture both individual perceptions of centrality and patterns of spatial interaction with Kyiv's center.

The key concepts employed in the subsequent analysis of the questionnaires were "perceived center" and "perceived centrality". A perceived center refers to an individual respondent's view of the city center, including its spatial boundaries, features, functions, and purposes. Perceived centrality refers to the degree to which a specific location is perceived as central, measured as the percentage of respondents identifying a location as part of the city center.

To map contour-derived perceived centrality, all respondent maps were digitized in Adobe Illustrator creating a filled polygon corresponding to the drawn contour of the city center. After that, specifically elaborated Python script (employing NumPy, Pandas and Pillow libraries) sequentially processed the rasterized image of each map, determined, for every pixel, the percentage of maps on which that pixel was marked by respondents as part of the city center, and draw a final isoline map of the integral contour-derived perceived centrality. To map location-based perceived centrality, for each location a percentage of "Yes [, it is a city center]" answers was calculated excluding "I don't know" responses, and then isoline map of perceived centrality was generated using kriging interpolation (utilizing Surfer software) of points representing locations. Additionally, an isoline map showing differences between location-based and contour-derived centralities was produced. A heat map of locations "in the city center", visited by the respondents, was created using a 500 × 500 m grid, with shading intensity proportional to the frequency of mentions per cell. The rest of the answers (on the frequency and aim of visiting the city center, and the functional categories of the visited places) were processed using simple percentages from the total number of questionnaires.

It is important to note the limitations of the study. We engaged university students as respondents because the views of young people are particularly valuable for understanding how the city center is perceived by a generation that has grown up entirely in the post-socialist period and within a globalised society; these are people who will most actively use and shape the city center in the future decades (cf. Osóch and Czaplińska 2019; Gnatiuk et al. 2023). At the same time, since university students are predominantly young people with quite specific everyday practices, values, and worldviews, it is likely that perceptions of the city center and centrality among other social groups, as well as among residents of different parts of the city, may differ. Therefore, we do not claim that the identified characteristics of Kyiv's perceived center are representative of all its residents. The other limitation is the specific temporality of the research. As it is discussed below, condition of war and the presence of the memory about the Revolution of Dignity in the urban environment may affect perceived centrality, especially in such symbolically important place as a present-day Ukrainian capital. The involvement of students as research subjects together with a specific historic settings restrain the generalizability of the findings. One more methodological limitation lies in the use of kriging interpolation to construct the map of location-based perceived centrality. This procedure was applied (1) to obtain an integral visualization of the perceived city

center and (2) to compare location-based and contour-derived centralities. However, location-based centrality, in a strict sense, can only be defined for specific locations. Therefore, first, its approximation between locations may not correspond to actual values; the real spatial pattern may be more fragmented and indented. Second, the interpolation depends on the specific set of employed locations, their number, and spatial distribution. Third, the result depends on the particular interpolation method used. All these considerations indicate the possibility of inaccurate interpretation, although this risk can be minimized through a reasonable selection of the most representative locations (which we sought to ensure), as uniform a spatial distribution of locations across the city as possible (in our case, location density by necessity is higher in the geometric city center and lower in the periphery), and the use of an appropriate interpolation method (kriging is widely regarded as a golden standard in geostatistics).

5. Results

5.1 Contour-derived centrality

When delineating the city center on the map (Fig. 2), respondents often rely on criteria of geometric and network symmetry. They also tend to configure the center as compactly as possible, avoiding sharp indentations or protrusions along its boundaries.

The Dnieper River is the clearest spatial referent. Its right bank forms a sharp eastern boundary of Kyiv's perceived center, with centrality sharply dropping from 80% to 30%, reflecting the historical built-up area and main administrative and business hubs. At the same time, up to 30% of respondents include the Dnieper islands and up to 20% the adjacent left-bank areas near Livoberezhna metro station and Rusanivka residential area. The railway delineates the center from the west and south: centrality drops sharply from 70% to 40–50% across the tracks,

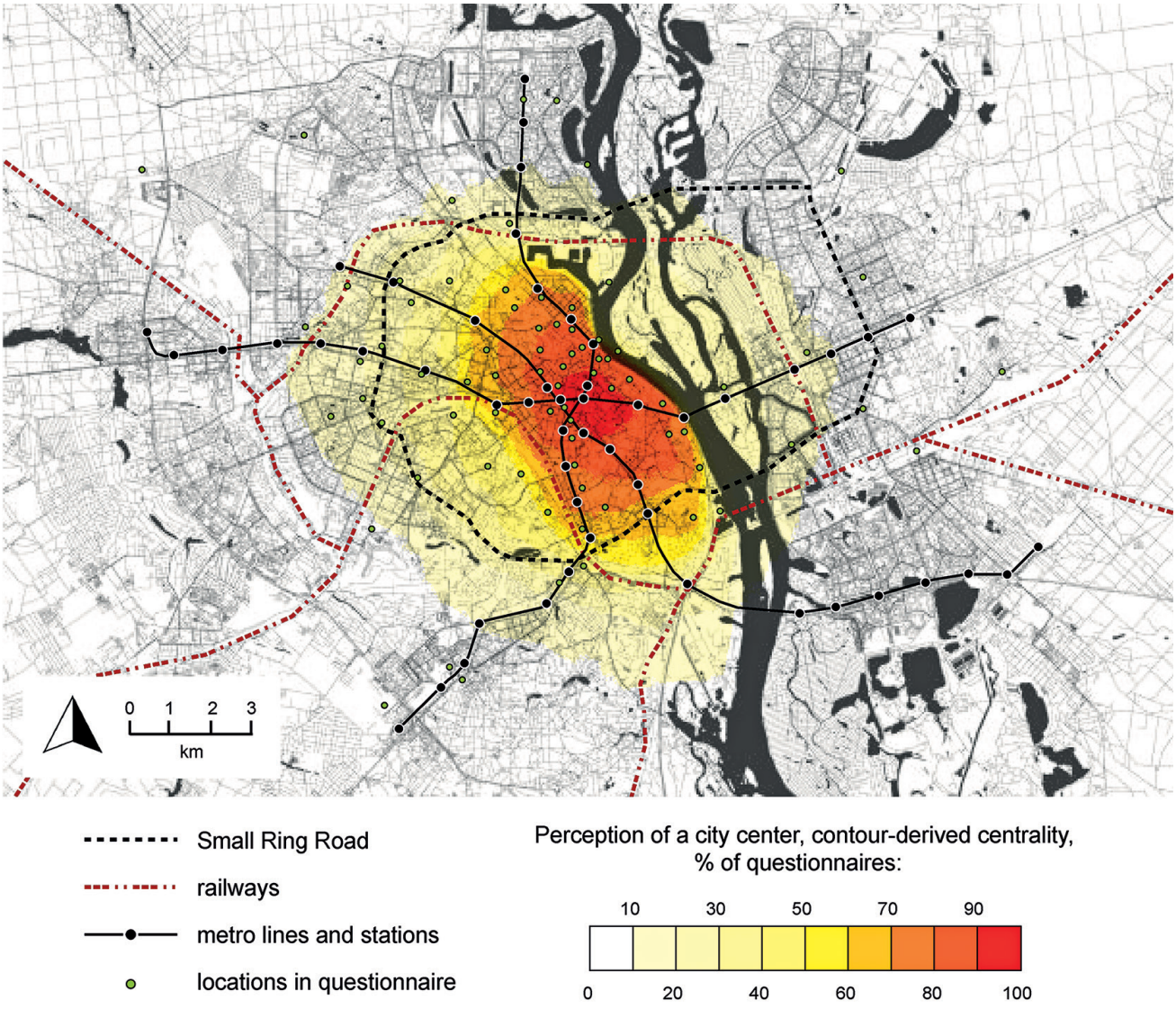

Fig. 2 Contour-derived intra-urban centrality in Kyiv. Source: authors' elaboration.

particularly where the railway follows the Lybid River valley. The Small Ring Road (a circular highway running within the city), together with the northern semicircle of the railway, acts as a third, although weaker spatial referent: centrality isolines of 20–30% on the right bank and 10–20% on the left bank closely follow these transport arteries. Areas beyond these boundaries are almost universally perceived as peripheral.

Overall, Kyiv's contour-derived perceived center has an oval-like shape, elongated from northwest to southeast along the Dnieper River. The transition zone from the center to the periphery is narrower where aforementioned spatial referents are present, and broader and more diffuse where such referents are absent (for example, in the northeast direction).

It is noteworthy that the area delineated by the 60% perceived centrality isoline closely corresponds to the continuous area of elevated housing values in central part of Kyiv (Fig. 1; LUN Misto n.d.a) with Jaccard index of polygon overlap as high as 0.8 (Fig. 3). Outside this zone, which is clearly associated with the city's core, high prices are observed only in the immediate vicinity of metro stations (LUN Misto n.d.a). Real estate values can thus serve as an indirect indicator of centrality, as "central" is often synonymous with "prestigious" and therefore more valuable. Overall, the perceived center defined by the contour maps much better corresponds with the high-value real estate area than with the historical built-up core.

The frequency diagram of Kyiv's center relative area (measured as the percentage ratio of perceived center's area to the city's total administrative area) reveals distinct peaks, reflecting most common perceptions of the city center's size. The prominent peak occurs at 3% (frequency 0.19), 7% (0.12) and 9% (0.07). Although these peaks cannot be directly linked to specific contour configurations, they show parallels with patterns identified for individual locations (see the next subsection). For most respondents, Kyiv's center occupies no more than one-fifth of the city's total area. If the city were imagined as a circle, a circle five times smaller would have a radius roughly two (more precisely 2.2) times smaller – a ratio that may intriguingly reflect common geometric perceptions of centrality and peripherality in geometric sense.

5.2 Location-based centrality

When assessing the centrality of specific locations (Fig. 4), the perceived center's shape becomes more complex, extending beyond linear referents in some

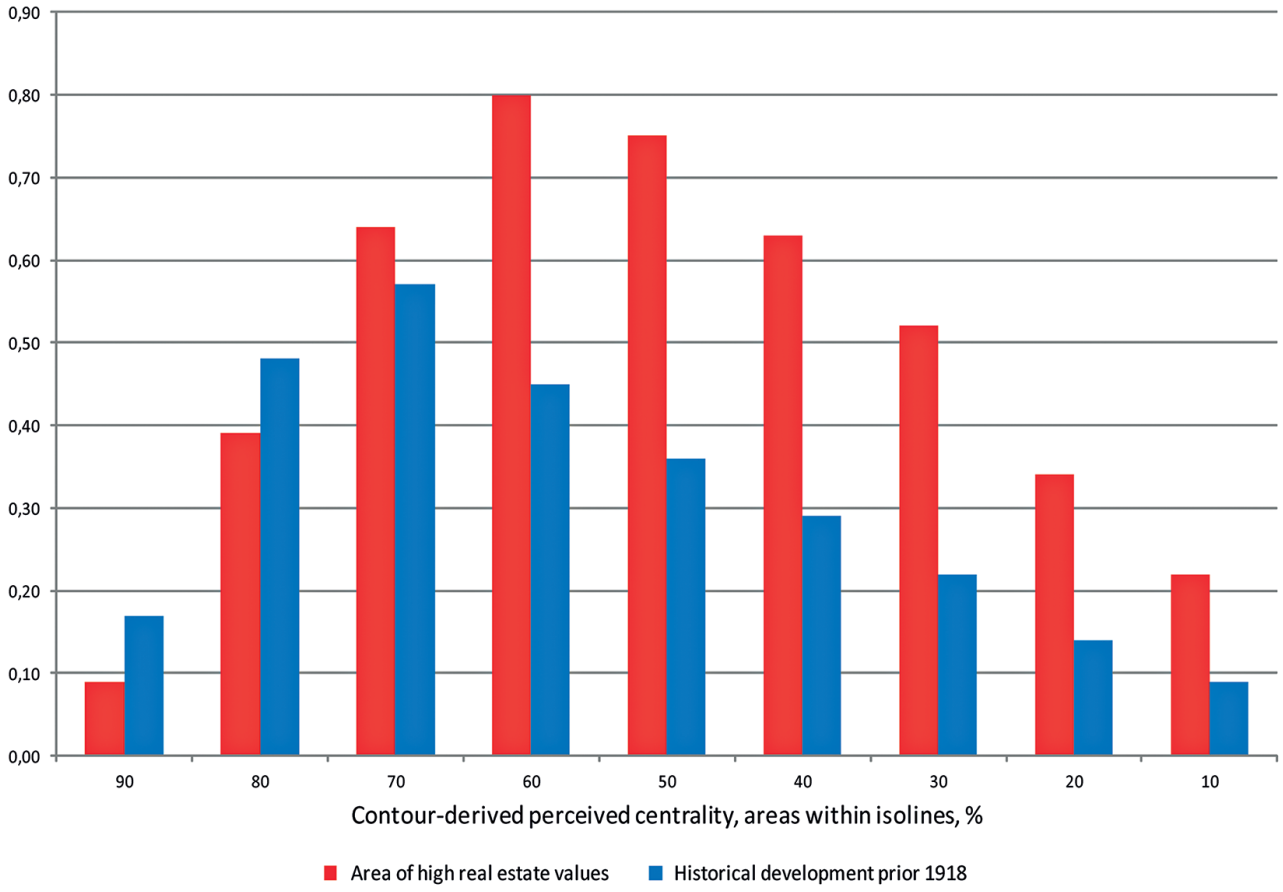

Fig. 3 Jaccard indices for the overlap of the contour-derived intra-urban centrality in Kyiv with the area of the high real estate prices and the historical built-up area before 1918.
Source: calculations by the authors.

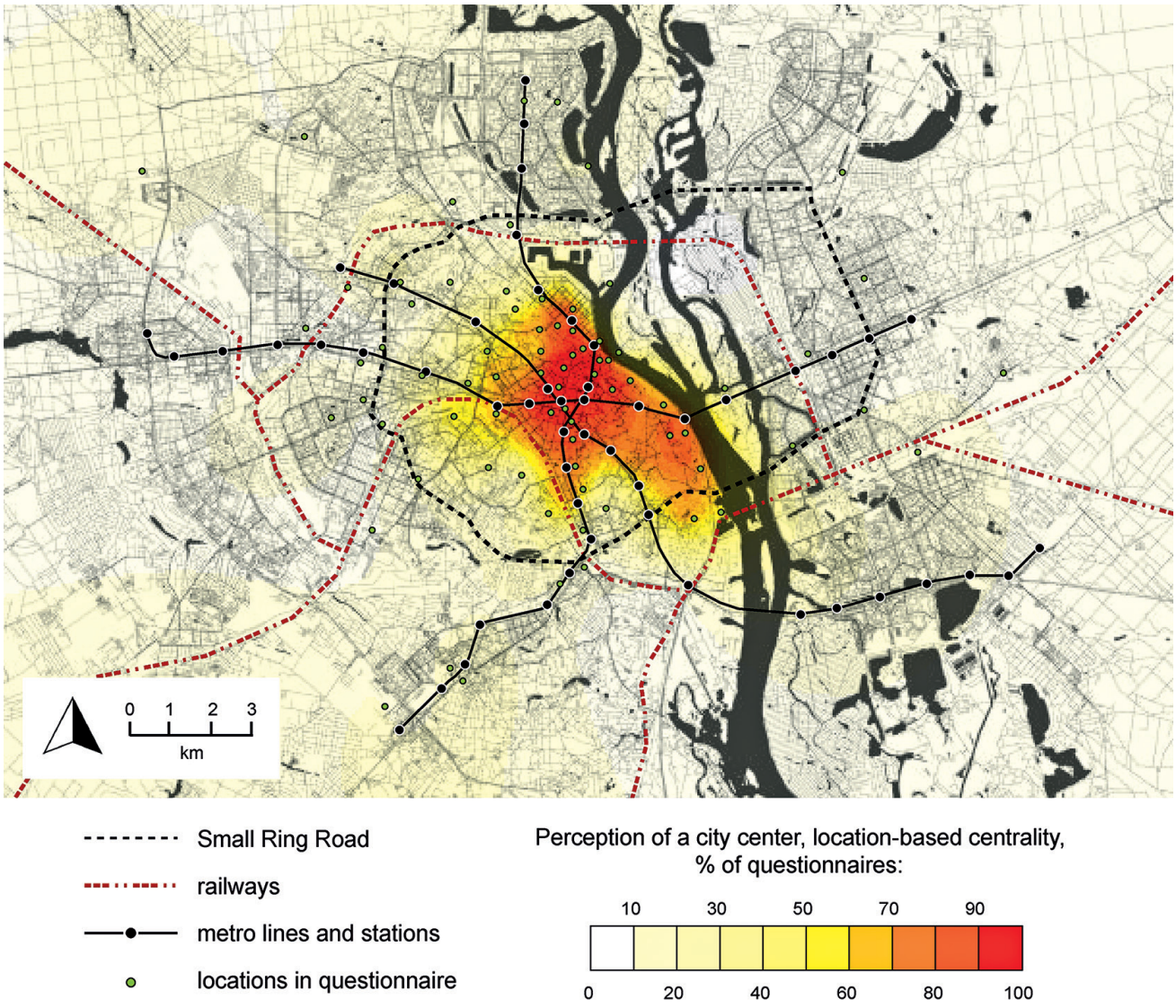

Fig. 4 Location-based intra-urban centrality in Kyiv.
Source: authors' elaboration.

areas and curving inward in others. Consequently, the influence of most spatial referents weakens, except for the Dnieper River, which remains a key boundary: perceived centrality drops sharply from 80% on the right bank to 10% on the left. The left bank's centrality is lower when measured by specific locations than by contour. The railway in the Lybid River valley still marks the western limit, with centrality falling from 70–80% to 30–50%, but in south its role diminishes, as the factual decline in centrality occurs north of the railway. The Small Ring Road's influence is minor, visible only on the right bank near the 10% isoline, while the northern railway semi-ring has no noticeable effect.

The role of personal familiarity in shaping perceptions of centrality is evident in locations such as Podil, the Central Railway Station, and the areas around Khreshchatyk, Velyka Vasylkivska Street, and Andriivskyi Descent, being also the most frequently mentioned by respondents as visited in Kyiv's center (see next subsection). A similar effect is seen with landmarks like the Kyiv-Pechersk Lavra and the Motherland Monument, which, though not cited as personally visited, are well-known architectural dominants. This suggests a tendency to perceive as central both locations familiar through personal experience and those embedded in the stereotypical image of the city.

The impact of historical or landmark status on perceived centrality is evident in sites such as the Kyiv-Pechersk Lavra, the Motherland Monument, the Monument to the Founders of Kyiv, the National Museum of the Holodomor, St. Nicholas Cathedral, Babyn Yar massacre site, and the Ministry of Defense, housed in a classicist building. These places demonstrate higher perceived centrality than nearby locations. In contrast, Vozdvyzhenka, a 21st-century neighborhood built in pseudo-historic style, lacks this effect. Similarly, Baikove Cemetery, a genuine historical site, is considered central by 30% of respondents, compared with only 13% for the Protasiv Yar ski

complex, despite its closer proximity to the geometric and symbolic city centers.

The 70% isoline on the perceived map of individual locations almost perfectly coincides with buildings constructed before 1918 (Fig. 1; LUN Misto n.d.b), while, for instance, structures from 1918–1956 show virtually no correlation with perceived centrality (LUN Misto n.d.b). The diagram of Jaccard indices demonstrates an outstanding peak at 70% isoline for the historical development area (Fig. 5). This suggests that respondents strongly associate urban centrality with historicity, particularly with the built environment shaped before the socialist era in 20 century. Centrality is also linked to power and governance: locations such as the Verkhovna Rada (Ukrainian Parliament), Ministry of Defense, and Kyiv Court of Appeal illustrate how central government institutions are expected to be located in, or to define, the city center. In some cases, green spaces are perceived as more central than surrounding areas. For instance, Natalka Park, despite its peripheral location in the modernist Obolon mass housing area, is slightly more often identified as central compared to the surrounding locations, and Hryshko National Botanical Garden demonstrates noticeably higher perceived centrality compared to nearby sites.

And conversely, certain locations may be perceived as less central than their surroundings when they are little known, lack historical or tourist value, feature modern architecture, or serve "non-central" functions such as housing, retail, or public health. The combined effect of pro- and contra-factors is often hard to predict. A clear example is the Central Election Commission building, which also houses the Kyiv Regional State Administration. Despite its governmental role and location in Pechersk, traditionally viewed as central city neighborhood, it shows unusually low perceived centrality compared to surrounding sites. This likely reflects its modernist architecture and infrequent interaction of respondents with this part of the city. Thus, location-based centrality allows to identify the "undisputed center" as well as objects perceived as central. These objects are not necessarily geographically close to the historical core of the city. Rather, they have characteristics or functions that are perceived as central, or they are familiar and located in frequently visited areas of the city. The results of the study showed that functions indicating location-based centrality include political, historical, tourist, and entertainment.

Theoretically, the histogram of perceived centrality of locations could show two extreme scenarios: a uniform decline from the center to the periphery in the case of random perception, or two plateaus (high and low) with a sharp slope between them if perceptions were consistent. In reality, the histogram exhibits several steps, reflecting homogeneous areas in terms of centrality and zones of rapid perceptual

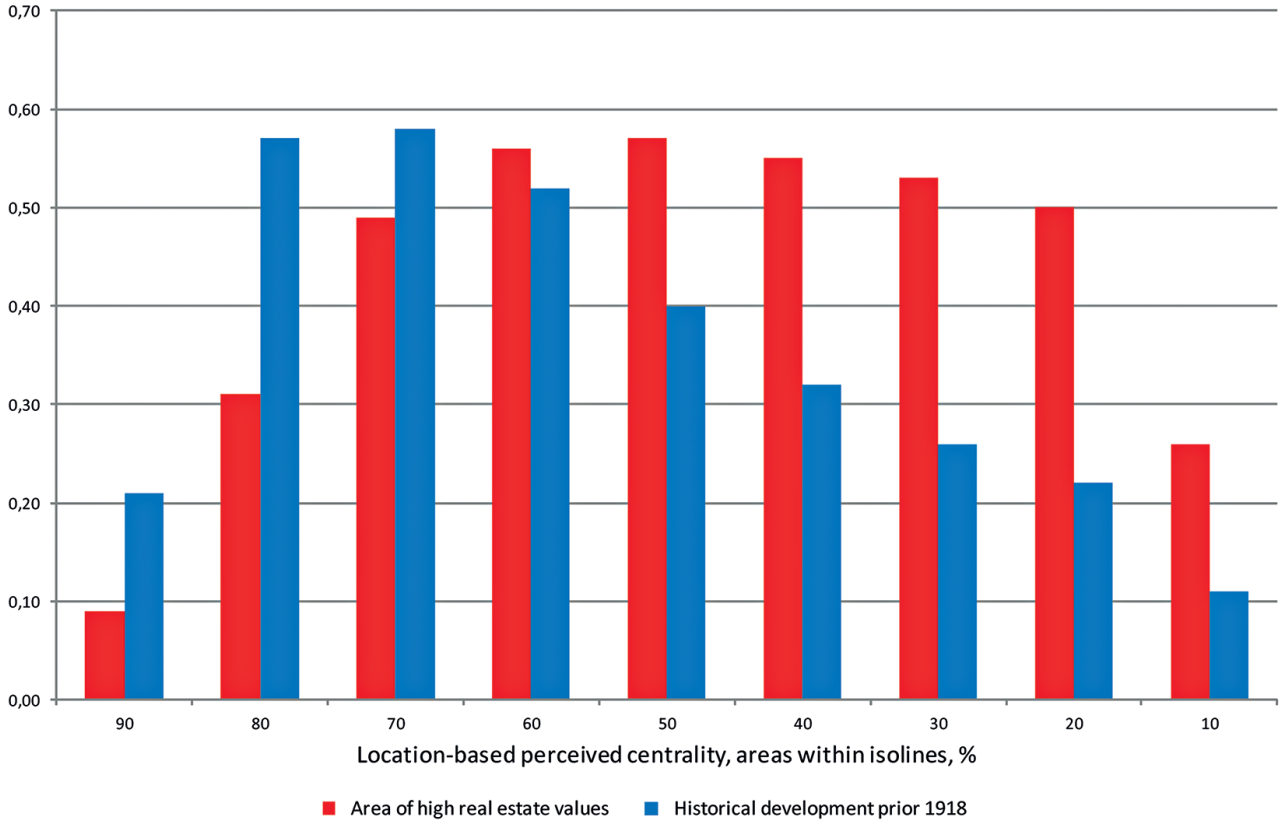

Fig. 5 Jaccard indices for the overlap of the location-based intra-urban centrality in Kyiv with the area of the high real estate prices and the historical built-up area before 1918.
Source: calculations by the authors.

change. The first plateau (87–100%) corresponds to two "undisputed center" clusters: the larger encompassing Khreshchatyk, the government quarter, part of Verkhnie Misto, and the proximal part of Podil, and the smaller represented by the Kyiv-Pechersk Lavra. The second plateau (70–73%) – the "center for the majority" – includes areas surrounding these clusters (Pechersk, Verkhnie Misto, Nova Zabudova, Pankivshchyna), bounded by the Dnieper River to the east and the railway to the west, roughly matching the pre-1918 built-up area. This is followed by a sharp decline – a transitional zone ending with the third plateau (29–34%) – the "semi-center", a zone of "uncertain centrality", where respondents' opinions about whether locations belong to the center extremely vary, and perception is strongly influenced by function, age, historical significance, spatial context, and personal experience. The fourth plateau (18–21%) represents the "mostly periphery", although a small portion of respondents still consider these locations part of the center. Beyond this, perceived centrality gradually declines to the "definitely not center" or "absolute periphery".

5.3 Comparison of the contour-derived and location-based centralities

The perceived center defined by specific locations is smaller than that defined by the contour, particularly below the 70% isoline. The same isoline demonstrates the highest level of overlap between the two types of centrality (Fig. 6).

As already mentioned, in the case of individual locations the perception of the city center is more fragmented than when respondents think of the center as an integral space. As a result, when drawing sketches, respondents often treated as central certain

Contour-derived centrality, isolines, % \ Location-based centrality, isolines, %	90	80	70	60	50	40	30	20	10
90	0,44	0,30	0,18	0,12	0,09	0,07	0,06	0,05	0,02
80	0,23	0,58	0,65	0,48	0,38	0,30	0,25	0,21	0,10
70	0,14	0,47	0,71	0,68	0,59	0,48	0,41	0,35	0,17
60	0,10	0,33	0,55	0,66	0,68	0,62	0,56	0,50	0,24
50	0,08	0,27	0,46	0,60	0,66	0,66	0,62	0,58	0,30
40	0,06	0,21	0,36	0,49	0,58	0,62	0,65	0,65	0,38
30	0,05	0,17	0,28	0,40	0,50	0,59	0,65	0,68	0,48
20	0,03	0,11	0,18	0,26	0,35	0,44	0,52	0,59	0,59
10	0,02	0,07	0,11	0,17	0,22	0,28	0,34	0,40	0,50

Fig. 6 Jaccard indices for the overlap of the contour-derived and location-based intra-urban centralities in Kyiv. Source: calculations by the authors.

locations that are not perceived as such when focusing on them specifically. This applies both to individual locations and to entire areas (Fig. 7). Such locations include those that, in the respondents' perception, lack historical or cultural significance, do not correspond to their idea of "centrality" in terms of function (for example, residential or industrial functions are not associated with the city center), or are simply personally unfamiliar to most respondents. Examples include the Frantsuzkyi Kvartal residential complex, the Central Election Commission building, Ar-Rahma Mosque, and Zvirynetska and Tarasa Shevchenka metro stations.

At the same time, some locations in themselves were much more frequently identified as central than when they were included within the city center contour on the map. Three such clusters are clearly visible in Fig. 7: the first is associated with the main railway station and the main building of Taras Shevchenko National University of Kyiv, the second with a part of Podil, and the third with a part of Pechersk. These locations are either well known to respondents through everyday experience (railway station, university building, Poshtova Square), or are widely recognized historical and cultural landmarks and city symbols, including strong visual dominants (Kyiv-Pechersk Lavra, Motherland Monument, St. Andrew's Church, Vydubychi Monastery, Freedom of the Ukrainian People Arch, the Pedestrian Bridge, the Monument to the Founders of Kyiv), or they represent popular public spaces that offer opportunities for walking and various leisure activities (Poshtova Square, Hryshko National Botanical Garden).

Overall, the spatial configuration of the Kyiv's perceived center is resembling Haggett's (1965) field distributions, comprising "theoretically continuous [spatial] distributions with a very rapid fall-off near their centre and a very slow, al-most asymptotic fall-off at their outer ranges", which are often observed in another social spatial structures (e.g. Poorthuis and van Meeteren 2021).

5.4 Activities in the city center: How often, where, what, and why?

The frequencies of visiting the city center by the respondents distributed in the following way: 19% visit Kyiv's center "almost daily", usually because they live or work there, while a similar share (20%) do so "less than once per month"; 40% visit city center "at least one time per week", and the rest 21% do that "several times per month". These figures mean that the majority of the respondents visit the city center on a regular (daily or weekly) basis.

The most frequently visited specific places are Khreshchatyk (main street), Maidan Nezalezhnosti (main square), and adjacent Verkhnie Misto sites such as the Golden Gate, Andriivskyi Descent, Ukrainian Heroes Square, the Palace of Sports, Volodymyr

Hill Park, and Shevchenko Park. Podil also features prominently, especially its principal open public spaces such as Poshtova and Kontraktova Squares. Other visited locations include scattered sites in Verkhnie Misto and Pechersk, parts of Pankivshchyna and Nova Zabudova, Trukhaniv Island, the Livoberezhna metro station area, and de-facto peripheral places near the university campus in the city's south-western sector (Fig. 8).

Among the categories of locations visited by respondents in Kyiv's center, open public spaces – streets and squares without further specification – are mentioned most frequently. This category accounts for 29% of all mentioned specific locations and 47% of all answers. The second tier includes specific city neighborhoods or localities (most common: Podil, Pechersk, Verkhnie Misto, Lypky) (16% and 11%), metro stations and transport hubs (14% and 9%), tourist and cultural sites (museums, exhibitions, monuments, architectural landmarks) (11% and 14%), and open green spaces (parks, squares, botanical gardens) (10% and 8%, respectively). Less frequent mentions include cultural and entertainment venues (theatres, cinemas, sports arenas, concert halls) (6% and 4%), commercial establishments, specifically large malls (5% and 2%), educational and scientific institutions (3% and 2%), cafés and restaurants (3% and 1%), and waterfronts (Dnieper embankments) (2% and 1%, respectively).

Walking and strolling were the most common purposes for visiting the city center (40%). The next popular reasons were visits to historical landmarks and various cultural institutions (20%), as well as visits to the entertainment and leisure facilities (20%), visiting restaurants and cafés (17%), and socializing with relatives, friends, and colleagues (17%). Less common motives involve shopping (13%), work (11%), errands (administrative, medical, or beauty services) (9%), attending public events, such as celebrations, (6%), using the center for transit (3%), or residing there (1.5%). Worth noting that 12% of the respondents visited the city center to enjoy the local urban

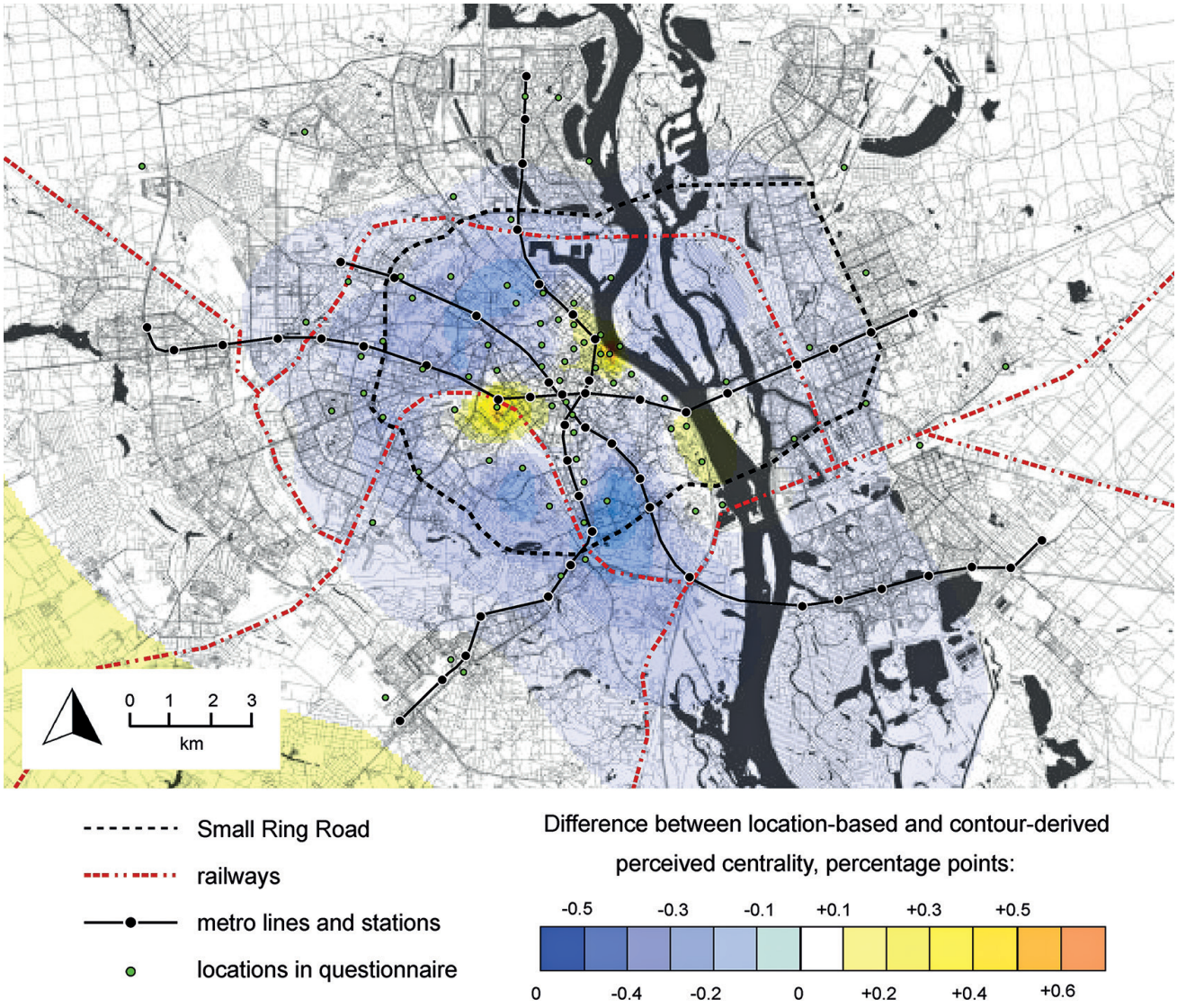

Fig. 7 Difference between location-based and contour-derived intra-urban centrality in Kyiv.
Source: authors' elaboration.

atmosphere regardless of specific locations or particular purposes: to "gain new impressions", "change the environment", "draw inspiration from history and architecture", "appreciate the scenery", "feel the atmosphere, urban vibe and pace of life", "take photos or record videos for social media", and even "cringing at people".

6. Discussion

The study results show that contour-derived and location-based centrality in Kyiv are broadly similar yet differ markedly in detail. Tab 1 presents the summarizing overview of the causal relationship between perceived centrality and other centralities in Kyiv.

On the one hand, respondents imagine the city center primarily as a compact and coherent spatial structure whose boundaries are defined by key natural and man-made spatial referents with a barrier effect (Lynch 1960), such as rivers, railways, and roads, and simultaneously correlate with the city's morphological layout, where the historical character of the built environment plays a crucial role. In addition, the perceived center is structured by topographical symbols embedded in local tradition and media over decades and centuries – most notably the city's main street (Khreshchatyk) and square (Maidan Nezalezhnosti), seen as the quintessence of centrality and among the most visited sites, as well as neighborhoods such as Verkhnie Misto, Podil, Pechersk, rarely Nova Zabudova and Pankivshchyna, which maintain a stable central image. On the other hand, at the level of individual locations, spatial pattern of perceived centrality becomes more diffuse, and the influence of aforementioned spatial referents weakens. This suggests that perception of centrality depends not only on spatial position and traditional images of the center, but also on function, appearance, and frequency of personal interaction, underscoring the importance of experiential and functional factors in shaping urban centrality.

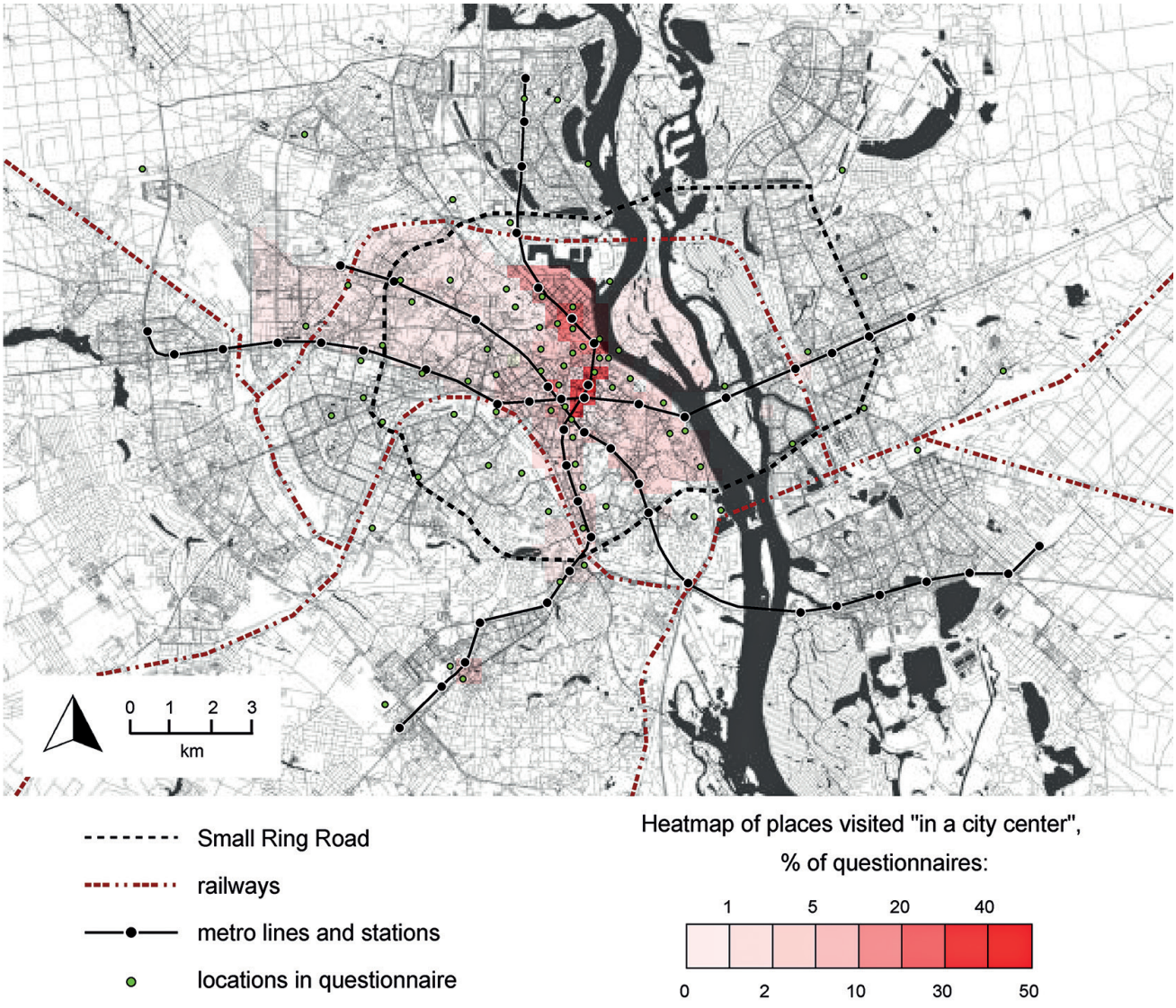

Fig. 8 Heatmap of places visited "in a city center" of Kyiv. Source: authors' elaboration.

Tab. 1 Relationships between perceived centrality and other centralities in Kyiv.

Type of centrality	Description of the relationship
Geometrical centrality	**Strong but ambiguous:** Both centroids (calculated for the total area and the continuous built environment) situate within the area of the maximal (>80%) perceived centrality. However, due to the possible interference with historical or symbolic centrality, their direct influence on perceived centrality is vague.
Network / accessibility centrality	**Strong:** Since the metro system forms the backbone of Kyiv's public transport network (Gnatiuk et al. 2022), public transport accessibility can be fairly well approximated by accessibility to metro stations. Pearson's pairwise correlation coefficients for the locations are as follows: between perceptual centrality (PC) and the distance to the nearest metro station (D, m): −0.40; between perceptual centrality (PC) and the relative accessibility index of the nearest metro station (RA): +0.84. The results of multiple linear regression in Statistica software: PC = −1.064 − 0.00001*D + 1.98726*RA ($R = 0.84$, $R^2 = 0.70$, Adjusted $R^2 = 0.70$, $F(2,81) = 94,2$, $p < 0.0000$). The bubble chart (Fig. 9) further illustrates the identified patterns. A strong relationship between perceptual centrality and the relative accessibility of metro stations and a moderate relationship with the distance to the nearest station have been identified. Other studies of Kyiv indicate a positive relationship between poor public transport accessibility and the perception of an urban area as peripheral (e.g. Gnatiuk et al. 2023 on mass housing estates).
Historical centrality	**Very strong:** Area with perceived centrality more than 70% corresponds well with the area built up before 1918. This suggests that respondents strongly associate urban centrality with the historical urban environment shaped before the socialist era. Important historical and cultural landmarks usually exhibit higher perceived centrality than the surrounding places that do not possess such value. Exploring historical and cultural landmarks, as well as the overall historic atmosphere was among the most popular aims of visiting the center.
Administrative centrality (power, governance)	**Moderate:** Principal national- and city-level centers of power and governance are strongly associated with the concept of centrality and are therefore perceived as inherent parts of the city center. However, this may not apply to less important administrative institutions, where the factor of historical and cultural significance may play a more important role. Administrative institutions were rarely mentioned by the respondents as their destinations in the city center.
Economic centrality (business, trade)	**Moderate:** According to the sketches drawn by the respondents, the area with high perceived centrality (>60%) roughly coincides with the continuous zone of elevated housing values in the central part of Kyiv. The same area concentrates the majority of the top-class business centers in the city. Some apparently peripheral areas with concentrations of business activity and large-scale retail probably appear to correspond to secondary peaks of perceived centrality, for example near the Livoberezhna metro station on the left bank. Nevertheless, to make stronger claims, this relationship requires further investigation.
Social centrality (public events, personal communication)	**Moderate to strong:** Socializing, often in combination with other activities, was among the top ways of spending time in the city center according to the questionnaires. Specific locations for such interactions include both open public spaces (notably, well-maintained green areas are perceived as more central than the surrounding spaces) and a wide range of restaurants and cafés. Participation in public events such as political gatherings, festivals, fairs, and concerts was indicated only rarely; however, this should be viewed in the context of martial law, under which such events are relatively infrequent.
Symbolic centrality	**Very strong:** Kyiv's main street (Khreshchatyk) and main square (Maidan Nezalezhnosti) form the spatial backbone of the perceived city center. Moreover, they are among the most visited sites within it according to the respondents. Certain neighborhoods are strongly referenced as the central ones. Major architectural landmarks that function as key city symbols demonstrate very high levels of perceived centrality compared to their surroundings, even despite their large distance from the symbolical city center.

Thus, while the city center remains closely tied in perception to the historic environment and to specific places and districts traditionally recognized as central, in a contemporary globalized society its boundaries may blur and shift. The center is not a fixed entity but rather a process and the outcome of struggles among social, cultural, and economic forces (Helbrecht and Dirksmeier 2012). Centrality becomes mobile: location itself loses importance, while greater attention is directed to what actually occupies urban space (Harvey 1990; Lefebvre 2003), including the growing significance of architecture and the physical settings of centrality (Helbrecht and Dirksmeier 2012). It is unlikely that respondents equated Kyiv's center directly with areas of high-value real estate extending beyond the historic core; however, they may well have envisioned gentrified districts of the Ukrainian capital, particularly in southern Pechersk and Nova Zabudova, densely developed over recent decades with skyscrapers, luxury housing, and business centers, embodying the ideas of new centrality (Helbrecht and Dirksmeier 2012). However, spatial boundaries of Kyiv's perceived center remain closely tied to the historic built environment. This may illustrate how crucial the presence of a historical setting is for perceived centrality in most large post-Soviet cities, whose relatively modest historic cores tend to be overshadowed by the mass residential development of the 20th century.

For the most respondents, the center of Kyiv is a fairly attractive and frequently visited part of the city. Given that, historical and cultural value is perceived by respondents as a primary characteristic of the city center and centrality in general. The presence of historical and cultural landmarks has the strongest impact on the perceived centrality of a specific location. However, based on places visited and, no less importantly, the activities performed by the respondents in the city center, we argue that historical urban space serves as an arena for other social activities rather than an attractor for students as such. To draw people in, the historical and cultural arena needs to be combined with other attractions, such as retail and entertainment venues (from little shops to large malls

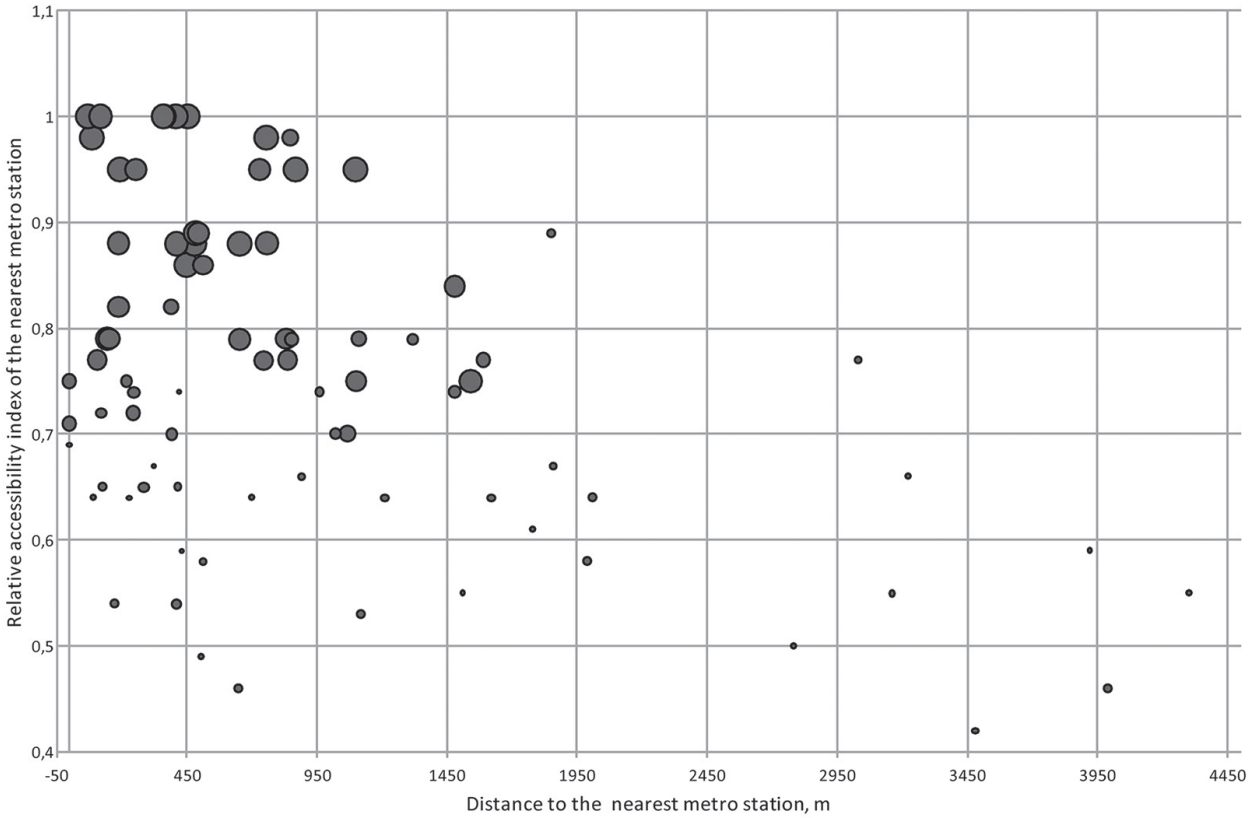

Fig. 9 Relationship between location-based perceived centrality (bubble size) and distance to the nearest metro station and its relative accessibility index.
Source: authors' elaboration.

and entertainment centers), dining establishments (restaurants, cafés), and interesting and comfortable public spaces (squares, parks, gardens) (cf. Deng et al. 2021). At the same time, without historical scenery and cultural senses embedded in the urban landscape, such service venues and public spaces alone do not create a sense of centrality. This aligns with Mezentseva's (2017) observation: although the role of malls in Kyiv has significantly increased over the past decades, they cannot be said to have assumed the role of primary public spaces. The "malling" of a city center is not a good way of inner-city development (Goss 1993; Popp 2004). The results support the idea of a multifunctional and multidimensional center: new functions and forms are layered onto a pre-existing historical and cultural foundation, and together they create a unique and diverse urban environment (Bird 1977).

Another important finding is that respondents value not so much individual famous monuments or architectural dominants but rather the overall atmosphere of the historic built environment, the layout of public spaces, and the activity of people within them. This explains why walking was identified as the primary purpose of visiting the center and why "ordinary" historic streets are often mentioned, even without major landmarks or tourist attractions. The city center thus functions as a space for flânerie – a relaxed, seemingly aimless stroll centered on observing urban life and enjoying the city's atmosphere, allowing people to discover the city, watch others, and observe events unfold. Unlike classical sightseeing, this practice represents a more personal, intimate interaction with urban space that requires no mediators such as guides (Matos Wunderlich 2008; Kramer and Short 2011). This underscores the importance of preserving not only individual monuments but also the broader historic and cultural environment of the city center, which provides the essential setting for such experiences (Deng et al. 2021).

Another important point concerns the perception of the city center as a place for social interaction. First, it provides a convenient meeting point for residents from different parts of the city due to its optimal transport accessibility. Second, it offers a comfortable environment for gatherings, thanks to its unique atmosphere and the presence of interesting, unconventional places and establishments. As a result, the city center functions as a venue for various types of meetings – with close and distant relatives, friends, colleagues, and business partners. Specific locations for such interactions include both open public spaces and a wide range of restaurants and cafés, both mainstream and niche. The center also hosts various events, which create opportunities for different forms of social interaction among participants. Thus, although public spaces in contemporary cities increasingly serve as places for observing rather than interacting (Sennett 1992) – for instance,

in Kyiv, people can be seen sitting silently for hours in large café windows, restaurants, or on benches in parks and squares (Mezentseva 2017) – the public spaces of Ukraine's capital remain actively used by young people not only for observing the surrounding urban environment and life, but for active socializing as well.

In light of the above, the threat of aggressive commercialization and chaotic, unregulated development in Kyiv's historic center is increasingly evident (Dronova and Polieshko 2017; Dronova and Maruniak 2019; Mezentsev and Mezentseva 2017). Massive glass-and-concrete "monsters" (Cybriwsky 2014), disconnected from the authentic historic environment, undermine the city center's atmosphere, aesthetic value, and architectural integrity. They erode its role as a space for flânerie, observation, and social interaction, especially among youth. While the new functions offered by these structures (shops, restaurants, malls, clubs) may attract visitors, their appeal is not unique to the center and could easily be found in peripheral districts. The key challenge for Kyiv lies in finding a recipe of harmonious integration of traditional and new urban elements, balancing between heritage preservation and continuous renewal (Mezentsev and Mezentseva 2017). This may require specific actions from Kyiv's city administration to integrate memory politics and cultural landscape sensitivity into planning decisions and to protect views, landmarks, and symbolic spaces central to Kyiv's historical narrative from large-format retail and speculative commercial development. At the same time, the administration may encourage cultural, educational, and community-oriented functions, expand pedestrianization and calm private motor traffic (Oliynyk 2022), as well as provide affordable cafés, social spaces, and non-commercial recreational opportunities in order to avoid a luxury monoculture and make the city center more comfortable and affordable for young people with different social backgrounds.

The case of Kyiv highlights the role of major rivers in structuring intra-urban centrality. Kyiv's waterfronts were almost never mentioned as visited places in the city center, underscoring the limited openness of the existing centre to its natural waterfront – the Dnieper River. A busy thoroughfare runs along the river, while the embankment remains poorly landscaped and weakly connected to pedestrian zones of the historic core. At the same time, although the Dnieper clearly divides the city into a more central right bank and a more peripheral left bank, up to 30% of respondents still consider the river section adjacent to the historic centre, as well as some Dnieper islands, to be part of the city center. Global experience shows that most new downtowns integrate large water bodies (Jones 2016; Maciukenaite and Povilaitienė 2013). These observations suggest considerable potential for expanding Kyiv's center or developing new forms of downtown along the river – on the right bank through regenerated industrial and warehouse areas, on the left bank as a counterbalance to right-bank dominance, or on the islands (the latter scenario would endanger natural landscapes and is therefore undesirable from a sustainable development perspective). In terms of the city's spatial planning policy, it is recommended to develop the Dnieper waterfront as a continuous, truly accessible, and multifunctional urban space that combines a variety of activities, with priority given to cultural and educational venues, public event spaces, and sports and recreation, while ensuring moderate commercialization and limiting commercial monoculture and gated development. The Dnieper waterfront should be physically and symbolically integrated into the city's historical center by enhancing pedestrian transit connections and supporting visual and spatial continuity. Also, the city may benefit from the revitalization of the Lybid River, a tributary of the Dnieper, whose valley accommodates the railway and currently forms a clear south-western boundary of Kyiv's perceived center.

The impact of the Revolution of Dignity and Russia's military invasion of Ukraine on perceived centrality in the Ukrainian capital cannot be overlooked. It has at least two dimensions, some of which are traceable in the empirical findings. First, since 2014, Maidan Nezalezhnosti and the surrounding streets have transformed into a de-facto open-air museum and a place of commemoration for the Heavenly Hundred. Since 2022, several commemorative sites for Ukrainian soldiers killed in the war have been functioning within the historical center, including Maidan Nezalezhnosti, parts of Khreshchatyk Street, as well as Mykhailivska and Sofiivska Squares. In 2022, Mykhailivska Square also hosted an exhibition of Russian military equipment destroyed by Ukrainian forces during the defense of Kyiv. The National Museum of the History of Ukraine in the Second World War also organized a special exhibition dedicated to the actual Russo-Ukrainian war. Such memorials and exhibitions may accentuate the importance of certain locations and emphasize the role of the city center as a place of memory and commemoration. Indeed, these places were among the most frequently mentioned by respondents in the present study, although there were no explicit references to the commemorative function of the city center. On the other hand, following the onset of the full-scale Russian invasion, certain parts of the traditional historical center became inaccessible to the general public for security reasons. This primarily concerns the so-called Government Quarter, which hosts the key institutions of state authority, including the Office of the President, the Parliament, and the Cabinet of Ministers. Consequently, some areas of Pechersk and Lypky have been inaccessible since 2022 to people who do not live or work there. This may contribute to the exclusion of this part of the city (despite being a place concentrating "central" functions and attributes like power, governance, as well as

historical and cultural landmarks) from the perceived image of the center (which is indeed observed in our results), particularly among students, many of whom are not native Kyiv residents and actively experience and explore the city exactly during their university studies.

We have not found academic publications that directly examine the issue of intra-urban perceived centrality in large post-Soviet or post-socialist cities, while the existing studies related to this topic differ significantly in their conceptualization, methodology, and the period of data collection. Nevertheless, certain parallels can be identified with previous research conducted in cities in Poland and Ukraine. As in Kyiv, in Kharkiv the perception of the spatial boundaries of the city center varies considerably among respondents due to the presence of multiple possible criteria of centrality: some rely on historical boundaries (within the former fortress walls), while others refer to a broader area of historical development. Thus, when various criteria coexist, a single spatial image of the city center may not necessarily form among residents (Miroshnychenko 2013). The Kharkiv case also revealed a moderate relationship between centrality and prestige defined through housing prices (Miroshnychenko 2014). It was also shown that in perceiving the external boundary of the central areas of Kharkiv, Katowice and Rybnik, as in the case of Kyiv, certain key locations, so-called anchor points, play an important role (Bierwiaczonek and Nawrocki 2009; Miroshnychenko 2013). The delimitation of the central vernacular district of Lviv indicates a clear and strong association with the historical and symbolic center – the area around the main square within the former medieval city walls, characterized by UNESCO-protected historical heritage and pronounced tourist functions; the influence of transport network centrality also appears to be evident (Sosnova 2022). The importance of the symbolic city center – the main square – is likewise confirmed for four Silesian cities (Bierwiaczonek and Nawrocki 2009). Similar to Kyiv, studies of the spatial images of the Katowice city center demonstrated a complete absence of religious buildings and sites in respondents' mental representations, despite their physical presence, which may indicate a desacralization of the city center image, at least among younger people (Bierwiaczonek and Nawrocki 2009). In Szczecin, surveyed students seem to perceive urban space in only two categories: as the city center, where (in their opinion) the most important facilities are concentrated, and as residential areas, perceived as peripheral; within the city center, they pay particular attention to recreational green spaces and shopping malls (Osóch and Czaplińska 2019). Also, in Szczecin, central district (Centrum) is clearly separated from the oldest historical part of the city (Stare Miasto) (Osóch and Czaplińska 2019). However, most of these studies did not focus specifically on city centers, and therefore any comparison should be treated with caution. For a proper systematic assessment of the generalizability of the obtained results, further comparative research based on a unified methodology is needed.

7. Conclusions

The study explores the perceived center of Kyiv, employing the concept of intra-urban perceived centrality and applying a mixed-method approach that combined cartographic tasks, location-based assessments, and open-ended survey questions. The results highlight both the persistence of traditional centrality patterns and the influence of contemporary socio-cultural dynamics.

On the one hand, Kyiv's perceived center demonstrates a strong attachment to the historic built environment, with its boundaries closely aligned with long-established neighborhoods such as Verkhnie Misto, Podil, and Pechersk. The centrality of these areas is further reinforced by symbolic landmarks like Khreshchatyk Street and Maidan Nezalezhnosti, which embody the essence of "the center" in public consciousness. At the same time, the Dnieper River, railways, and major highways act as significant spatial referents, sharply defining transitions from central to peripheral zones.

On the other hand, the findings indicate that perceived centrality depends not only on spatial position or historic tradition but also on the functional profile and personal familiarity of locations. Respondents more frequently associated centrality with places they visit regularly or that serve as well-known urban symbols. Conversely, modernist residential estates or sites lacking cultural and historic significance often showed lower perceived centrality despite their high centrality in terms of accessibility or location within the historical city neighborhood. The research supports the idea of a city center as a multifunctional urban space rather than a concentration of a certain specific function.

Furthermore, the results reveal the importance of atmosphere and experience. Respondents emphasized walking, flânerie, and enjoying the urban environment as key motivations for visiting the center, suggesting that centrality is as much about lived experience as about formal functions. This reinforces the need to preserve Kyiv's historic fabric and human-scale public spaces in the face of aggressive commercialization and uncoordinated development.

Finally, the study underscores both the resilience and fluidity of centrality within the city. While Kyiv's perceived center remains firmly tied to its historic core, processes of globalization, gentrification, and socio-political transformation are reshaping its boundaries and meanings. Centrality emerges not as a fixed point but as a dynamic construct shaped by social, cultural, and economic forces.

Future research should address the limitations of this study by including broader population groups, longitudinal and comparative perspectives, to better capture how perceptions of intra-urban centrality evolve over space and time.

Acknowledgments

The authors express their gratitude to the students who participated in the survey. Also, they are thankful to the two anonymous reviewers for their rigorous scrutiny of the manuscript and constructive comments.

References

Appleyard, D. (1970): Styles and methods of structuring a city. Environment and Behavior 2(1), 100–117, https://doi.org/10.1177/001391657000200106.

Batty, M. (2008): The size, scale, and shape of cities. Science 319(5864), 769–771, https://doi.org/10.1126/science.1151419.

Bierwiaczonek, K., Nawrocki, T. (2009): Społecznapercepcja przestrzeni centralnej miast śląskich. In: Dymnicka, M., Majer, A. (Eds.), Współczesne miasta. Szkice socjologi czne; Łódź, pp. 114–121.

Bird, J. (1977): Centrality and Cities; Routledge and Kegan Paul Ltd: Oxon – Boston, Mass.

Bondar, V. (2018): Historical aspects of the formation of the city center of the capital metropolis. In: Lisovskyi, S. A. et al. (Eds.), Geographical Science and Education: From Statement to Constructivism; Institute of Geography of the NAS of Ukraine: Kyiv, Ukraine, pp. 131–133.

Burgess, E. W. (1925/1967): The Growth of the City. An Introduction to a Research Project. In: Burgess, E. W., McKenzie, R. D., Park, R. E. (Eds.), The City; University of Chicago Press: Chicago, US – London, UK, pp. 47–62.

Bykova, M., Shchabelska, V. (2022): Spatial organisation of Kyiv's office buildings. Odesa National University Herald. Geography and Geology 26(39), 94–107, https://doi.org/10.18524/2303-9914.2021.2(39).246197.

Christaller, W. (1966 [1933]): Central Places in Southern Germany; Prentice Hall: Eaglewood Cliffs, New Jersey, US.

Crucitti, P., Latora, V., Porta, S. (2006): Centrality measures in spatial networks of urban streets. Physical Review E 73(3): 036125, https://doi.org/10.1103/PhysRevE.73.036125.

Cybriwsky, R. (2014): Kyiv, Ukraine: The City of Domes and Demons from the Collapse of Socialism to the Mass Uprising of 2013–2014, revised edition; Amsterdam.

Deng, Z., Chen, D., Qin, X., Wang, S. (2021): Comprehensive assessment to residents' perceptions to historic urban center in megacity: a case study of Yuexiu District, Guangzhou, China. Journal of Asian Architecture and Building Engineering 20(5), 566–580, https://doi.org/10.1080/13467581.2021.1942000.

Diomin, M., Oliynyk, O. (2022): Analysis of the Kyiv public space network on the basis of configuration models. Urban Development and Spatial Planning 79, 148–163 (in Ukrainian), https://doi.org/10.32347/2076-815x.2022.79.

Dronova, O., Maruniak, E. (2019): Changing the Symbolic Language of the Urban Landscape: Post-Socialist Transformation in Kyiv. In: Brunn, S., Kehrein, R. (Eds.), Handbook of the Changing World Language Map; Springer: Cham, Switzerland, pp. 2941–2972, https://doi.org/10.1007/978-3-030-02438-3_117.

Dronova, O., Polieshko, D. (2017): Functional and spatial changes of Kyiv's nodal areas. In: Mezentsev, K., Oliynyk, Y., Mezentseva, N. (Eds.), Urban Ukraine: In the Epicenter of Spatial Changes; Fenix: Kyiv, pp. 211–226 (in Ukrainian).

Friedmann, J. (1966): Regional Development Policy: A Case Study of Venezuela; MIT Press: Cambridge, MA, US – London, UK.

Foronda-Robles, C., Galindo-Pérez-de-Azpillaga, L., Armario-Pérez, P. (2025): The sustainable management of overtourism via user content. Annals of Tourism Research Empirical Insights 6(2): 100184, https://doi.org/10.1016/j.annale.2025.100184.

Gentile, M. (2025): War memorialization and nation-building in Ukraine. Eurasian Geography and Economics 66(7), 765–792, https://doi.org/10.1080/15387216.2025.2498159.

Gnatiuk, O., Kononenko, O., Mezentsev, K. (2022): Kyiv metro and urban imageability: a student youth vision. Acta Universitatis Carolinae Geographica 57(1), 255–268, https://doi.org/10.14712/23361980.2022.2.

Gnatiuk, O., Kononenko, O., Slavnova, H. (2023): Perception of the (post-)socialist mass housing in Kyiv by the student youth. Geographia Polonica 96(2), 199–220, https://doi.org/10.7163/GPol.0253.

Goss, J. (1993): The "magic of the mall": An analysis of form, function, and meaning in the contemporary retail built environment. Annals of the Association of American Geographers 83(1), 18–47, https://doi.org/10.1111/j.1467-8306.1993.tb01921.x.

Gould, P. (1966): On Mental Maps; University of Michigan: Ann Arbour.

Gould, P., White, R. (1974): Mental Maps; Penguin Books: Harmondsworth.

Gusman, I., Chamusca, P., Fernandes, J., Pinto, J. (2019): Culture and tourism in Porto city centre: Conflicts and (im)possible solutions. Sustainability 11(20): 5701, https://doi.org/10.3390/su11205701.

Harris, C., Ullman, E. (1945): The nature of cities. Annals of the American Academy of Political and Social Science 242, 7–17, https://doi.org/10.1177/000271624524200103.

Haggett, P. (1965): Locational Analysis in Human Geography; Edward Arnold: London.

Harvey, D. (1990): The Condition of Postmodernity: An Enquiry into the Origins of Cultural Change; Blackwell: Cambridge, UK.

Helbrecht, I., Dirksmeier, P. (2012): New downtowns: A new form of centrality and urbanity in world society. In: Helbrecht, I., Dirksmeier, P. (Eds.), New Urbanism: Life, Work, and Space in the New Downtown; Ashgate Publishing Limited: Farnham, UK, pp. 1–21.

Henriques, R. (2022): The right to the city centre: Urban culturalization strategies as modelers of the uses of historic city centres. Visual Review 9(1), 69–82, https://doi.org/10.37467/gkarevvisual.v9.3090.

Jones, A. L. (2016): Regenerating urban waterfronts – creating better futures – from commercial and leisure market places to cultural quarters and innovation

districts. Planning Practice & Research 32(3), 333–344, https://doi.org/10.1080/02697459.2016.1222146.
Karayalcin, C., Yilmazkuday, H. (2015): Trade and cities. The World Bank Economic Review 29(3), 523–549, https://doi.org/10.2139/ssrn.2149567.
Kostiuchok, O. (2013): The Government Centre in Kyiv (1934–1937): A history of construction. Studii Mystetetstvoznavchi (1–2), 103–113 (in Ukrainian).
Kramer, K., Short, J. R. (2011): Flânerie and the globalizing city. City 15(3–4), 322–342, https://doi.org/10.1080/13604813.2011.595100.
Lefebvre, H. (1991/1974): The Production of Space; Blackwell Publishing: Oxford, UK – Cambridge, MA, US.
Lefebvre, H. (2003): The Urban Revolution. The University of Minnesota Press: Minneapolis, US.
Li, J., Qian, J., Liu, Y. (2017): A novel analysis method of geographical centrality based on space of flows. ISPRS International Journal of Geo-Information 6(5), 153, https://doi.org/10.3390/ijgi6050153.
LUN Misto (n.d.a): 3D Map of New-Building Prices: Data for Kyiv and the Suburbs. Available online: https://lun.ua/misto/3d-price-map (accessed on 20 August 2025).
LUN Misto (n.d.b): Map of Years of Multi-Apartment Residential Development in Kyiv. Available online: https://lun.ua/misto/buildings-age (accessed on 20 August 2025).
Lynch, K. (1960): The Image of the City; MIT Press: Cambridge, US.
Maciukenaite, J., Povilaitienė, I. (2013): The role of the river in the city centre and its identity. Journal of Sustainable Architecture and Civil Engineering, 4(5), 33–41, https://doi.org/10.5755/j01.sace.4.5.4820.
Matos Wunderlich, F. (2008): Walking and rhythmicity: Sensing urban space. Journal of Urban Design 13(1), 125–139, https://doi.org/10.1080/13574800701803472.
Mezentsev, K., Provotar, N., Gnatiuk, O. (2023): Courtyards, parks and squares of power in Ukrainian cities: planning and reality of everyday life under socialism. In: Mariotti, J., Leetmaa, K. (Eds.), Urban Planning during Socialism: Views from the Periphery; Routledge: London, UK, pp. 153–175, https://doi.org/10.4324/9781003327592-13.
Mezentsev, K., Mezentseva, N. (2017): Changes in the urban space of the capital city. In: Mezentsev, K., Oliynyk, Y., Mezentseva, N. (Eds.), Urban Ukraine: In the Epicenter of Spatial Changes; Fenix: Kyiv, Ukraine, pp. 181–184 (in Ukrainian).
Mezentseva, N. (2017): Public spaces of Kyiv: model and contemporary transformations. In: Mezentsev, K., Oliynyk, Y., Mezentseva, N. (Eds.), Urban Ukraine: In the Epicenter of Spatial Changes; Fenix: Kyiv, Ukraine, pp. 185–210 (in Ukrainian).
Michel, B. (2024): Arts and culture in the city: Peripheral centrality, cultural vitality, and urban change in inner suburbs. Cities 150, 104983, https://doi.org/10.1016/j.cities.2024.104983.
Miranda, E., Batista e Silva, J., Ricardo da Costa, A. (2020): Emergence and structure of urban centralities in a medium-sized historic city. Sage Open 10(3), https://doi.org/10.1177/2158244020930002.
Miroshnychenko, V. V. (2013): Vernacular districts of Kharkiv. Pskov Journal of Regional Science 16, 61–69 (in Russian).
Miroshnychenko, V. V. (2014): Estimation of degree of prestige of vernacular districts of Kharkiv. Visnyk of V. N. Karazin Kharkiv National University. Ecology Series 10(1104), 118–125 (in Ukrainian).
Mitković, P., Dinić, M. (2004): City center organization and its influence on the city structure. Facta universitatis – series: Architecture and Civil Engineering 3(1), 41–56, https://doi.org/10.2298/FUACE0401041M.
Montello, D. R., Goodchild, M. F., Gottsegen, J., Fohl, P. (2003): Wheres downtown?: Behavioral methods for determining referents of vague spatial queries. Spatial Cognition & Computation 3(2–3), 185–204, https://doi.org/10.1080/13875868.2003.9683761.
Murphy, R. E., Vance Jr., J. E. (1954): A comparative study of nine central business districts. Economic Geography 30(4), 301–336, https://doi.org/10.2307/142117.
Natalia, V. V., Heinrichs, D. (2019): How to define urban centres: Concepts overview and propose indicators. Transportation Research Procedia 41, 150–154, https://doi.org/10.1016/j.trpro.2019.09.027.
Nasar, J. L. (1990): The valuative image of the city. Journal of the American Planning Association 56(1), 41–53, https://doi.org/10.1080/01944369008975742.
Nawrocki, T. (2017): The usefulness of mental maps for sociological research of the city. Architecture, Civil Engineering, Environment 10(3), 19–31, https://doi.org/10.21307/acee-2017-031.
Nooraddin, H. (2016): City centers as urban growth cores. Journal of Economics and Sustainable Development 7(16), 17–26.
Oliynyk, O. (2021): Features of spatial organization of the system of pedestrian zones in the historical center of Kyiv. Architectural Bulletin of KNUCA 22–23, 53–63 (in Ukrainian), https://doi.org/10.32347/2519-8661.2021.22-23.53-63.
Oliynyk, O. (2022): Issues of the organization of systems of pedestrian zones in the historical center of Kyiv. Transportation Research Procedia 63, 1681–1689, https://doi.org/10.1016/j.trpro.2022.06.182.
Osóch, B., Czaplińska, A. (2019): City image based on mental maps – the case study of Szczecin (Poland). Miscellanea Geographica 23(2), 111–119, https://doi.org/110.2478/mgrsd-2019-0016.
Popp, M. (2004): Developing shopping centres in inner-city locations: Opportunity or danger for town centres? Die Erde 135(1), 107–124.
Poorthuis, A., van Meeteren, M. (2021): Containment and connectivity in Dutch urban systems: A network-analytical operationalisation of the three-systems model. Tijdschrift voor Economische en Sociale Geografie 112(4), 387–403, https://doi.org/10.1111/tesg.12391.
Sennett, R. (1992): The Fall of Public Man; W. W. Norton Press: London, UK.
Simpson, B. J. (2021): City Centre Planning and Public Transport: Case Studies from Britain, West Germany and France; Routledge: Abingdon, UK – New York, NY, US.
Sosnova, N. (2022): Tasks in forming the pedestrian network of the city. Current Problems of Architecture and Urban Planning 63, 154–163 (in Ukrainian), https://doi.org/10.32347/2077-3455.2022.63.154-163.
Sliudikova, T. (2009): Urban development and improvement of Kyiv in the 19th–20th centuries (based on the documents of Kyiv State Archives). Archives of Ukraine 1–2, 61–78 (in Ukrainian).

Stebletska, Yu. (2014): Planning of Kyiv development: historical-geographical aspects. Bulletin of Taras Shevchenko National University of Kyiv, Geography 1(62), 70–73 (in Ukrainian), https://doi.org/10.17721/1728-2721.2014.62.17.

Sun, Y., Fan, H., Li, M., Zipf, A. (2016): Identifying the city center using human travel flows generated from location-based social networking data. Environment and Planning B: Planning and Design 43(3), 480–498, https://doi.org/10.1177/0265813515617642.

Tallon, A. R., Bromley, R. D. (2004): Exploring the attractions of city centre living: evidence and policy implications in British cities. Geoforum 35(6), 771–787, https://doi.org/10.1016/j.geoforum.2004.05.004.

Thurstain-Goodwin, M., Unwin, D. (2000): Defining and delineating the central areas of towns for statistical monitoring using continuous surface representations. Transactions in GIS 4(4), 305–317.

van Meeteren, M. (2021): About being in the middle: conceptions, models and theories of centrality in urban studies. In: Rozenblat, C., Neal, Z. P. (Eds.), Handbook of Cities and Networks; Edward Elgar: Northampton, MA, US, pp. 252–271.

Vecherskyi, V. (Ed.) (2012): Historical and Urban Planning Studies of Kyiv; Fenix: Kyiv, Ukraine (in Ukrainian).

Wurm, M., Goebel, J., Wagner, G. G., Weigand, M., Dech, S., Taubenböck, H. (2021): Inferring floor area ratio thresholds for the delineation of city centers based on cognitive perception. Environment and Planning B: Urban Analytics and City Science 48(2), 265–279, https://doi.org/10.1177/2399808319869341.

Zhu, J., Niu, X., Wang, Y. (2024): Polycentric urban spatial structure identification based on morphological and functional dimensions: Evidence from three Chinese cities. Sustainability 16(6): 2584, https://doi.org/10.3390/su16062584.

The variation in groundwater level and groundwater recharge based on the rainfall received in four semi-arid districts of West Bengal, India

Sujatha Chakraborty, Thendiyath Roshni*

National Institute of Technology Patna, Department of Civil Engineering, India
* Corresponding author: roshni@nitp.ac.in

ABSTRACT
This article investigates the fluctuations in groundwater level (GWL) and groundwater recharge in response to rainfall variability using 2001–2021 rainfall data from four districts in West Bengal, India: Purulia, Bankura, West Midnapore, and East Midnapore. Purulia and Bankura have a tropical semi-arid to sub-humid type of climate, while West Midnapore and East Midnapore have a tropical wet-dry monsoon climate. The GWL analysis was performed using the Mann-Kendall Test (M-K Test) and Sen's Slope Estimator, while groundwater recharge was estimated using empirical expressions, including the Chaturvedi and Modified Chaturvedi formulas, and the Maxey-Eakin and Krishna Rao methods. We used pre-monsoon and post-monsoon GWL data for the GWL trend analysis and monthly rainfall data for groundwater recharge estimation. To assess the impact of climate change on GWL variation for the 2022–2050 period, the global climatic model (GCM) CanESM5-SSP126 rainfall data was used. The trend analysis of groundwater level at East Midnapore and West Midnapore shows a higher rate of decline (GWL beyond 15 m bgl) compared to Purulia and Bankura during both the pre- and post-monsoon periods. Groundwater recharge estimates increased linearly with rainfall and the results show the Modified Chaturvedi formula as the most suitable in the selected districts. Additionally, new empirical expressions developed between rainfall and groundwater levels showed a better fit for Bankura and Purulia stations. These expressions suggest that rainfall will increase in Purulia toward 2050, leading to a subsequent rise in groundwater levels.

KEYWORDS
groundwater level; recharge; Mann-Kendall; climatic model; Chaturvedi Formula; West Benga; India

Received: 7 May 2025
Accepted: 11 February 2026
Published online: 25 February 2026

Chakraborty, S., Roshni, T. (2026): The variation in groundwater level and groundwater recharge based on the rainfall received in four semi-arid districts of West Bengal, India. AUC Geographica 61(2), 195–209
https://doi.org/10.14712/23361980.2026.4
© 2026 The Authors. This is an open-access article distributed under the terms of the Creative Commons Attribution License (https://creativecommons.org/licenses/by/4.0).

1. Introduction

Groundwater (GW) represents approximately 30% of the global freshwater supply and serves as a crucial resource for over two billion people across the world (Ajami 2021). The growing population, multiple environmental issues, extended periods of drought, and ineffective water system management pose significant challenges on a global scale. These concerns necessitate immediate intervention from authorities overseeing groundwater resources. Jasechko et al. (2024) highlights that unsustainable pumping and reduced precipitation are the key drivers of depletion, leading to risks like land subsidence, streamflow loss, and wells running dry. Groundwater plays a vital role in ensuring both food and freshwater security, especially in water-scarce countries like India (Yazdian et al. 2021). In India, groundwater supports over 60% of irrigation needs and provides nearly 80% of the drinking water supply. Similar to many other water-stressed areas worldwide, India has also seen immense groundwater depletion in the recent years (Asoka et al. 2017; Wada et al. 2010). The pronounced decline in groundwater reserves has been predominantly attributed to unsustainable extraction practices for irrigation and alterations in the spatiotemporal distribution of monsoonal precipitation (Asoka et al. 2017). A substantial body of literature has documented with marked reductions in groundwater storage and water levels, primarily linking these trends to intensive groundwater withdrawal for irrigation purposes (Macdonald et al. 2016; Shah 2017; Mukherjee et al. 2015). Despite this, the influence of precipitation dynamics on groundwater recharge is a critical component for assessing long-term groundwater sustainability and that remains insufficiently explored in the Indian context. Over recent decades, notable changes have occurred in both the intensity and structural attributes of the Indian southwest monsoon rainfall (Mishra et al. 2016; Singh et al. 2014). A notable hydrological shift identified in recent decades is the decline in monsoonal precipitation over the Indo-Gangetic Plain (Mishra et al. 2016; Roxy et al. 2017). As a result, ensuring sustained groundwater recharge has become critical for maintaining long-term water security. The eastern segment of the Indian subcontinent, which embodies these geoclimatic constraints, offers a unique context for investigating the multifaceted drivers of groundwater recharge.

The fluctuation of groundwater levels is governed by a range of factors, including precipitation patterns, recharge rates, subsurface flow dynamics, soil characteristics, and groundwater extraction capacities, among other variables (Maliva 2020; Osborn and Hardy 1999; Stempvoort et al. 1993). Beyond these hydrogeological and anthropogenic parameters, climate variability serves as a critical determinant influencing groundwater systems. Studies have demonstrated that climate change exerts direct effects on soil properties, land cover, and hydrological processes, primarily through increased temperatures, altered precipitation regimes, shifts in evapotranspiration, and a heightened frequency of extreme weather events such as cyclones, floods, and droughts (Hamed et al. 2018; Mokadem et al. 2018).

This study presents an investigation into the variations of groundwater level and groundwater recharge in the districts of Purulia, Bankura, East Midnapore, and West Midnapore of West Bengal. This work also projected the groundwater levels for changing climatic scenarios in future period using CanESM5 model for SSP-126 scenario. The groundwater hydrology of the selected regions transit from hard rock terrain to coastal alluvial plains. By examining the relationship between rainfall patterns and groundwater level fluctuations, the study captures the heterogeneity in recharge potential influenced by rainfall variability. Unlike previous localized studies, this research offers a comparative regional analysis that integrates historical groundwater and rainfall data to identify recharge trends and stress zones. By establishing empirical correlations and recharge response patterns across physiographical distinct districts, the study addresses a critical data and knowledge gap in regional aquifer behavior, particularly under the stress of seasonal rainfall variability and increasing extraction pressures. The findings have significant implications for sustainable groundwater management, especially in areas facing agricultural water stress, and contribute to bridging the gap between climate variability and groundwater resource planning in eastern India.

2. Study area and data collection

The study area encompasses four major districts of West Bengal, namely Purulia, Bankura, West Midnapore and East Midnapore (Bhattacharya et al. 2020), which span an area of 9,658 km^2 (Fig. 1). All the four selected districts is a part of Kangsabati river basin, in which the aquifer system of the entire basin is more of diversified characteristic. This aquifer has arranged of upper and lower aquifers under unconfined and confined condition, where upper aquifer has 40 m bgl water level depth under unconfined condition whereas lower aquifer has <50 m water depth under confined condition (Bhattacharya et al. 2020). In this study, all selected wells are tapping the upper aquifer. Within the four districts of the study area, Purulia and Bankura have tropical semi-arid to sub-humid (dry type) of climate (Goswami et al. 2022) while West Midnapore and East Midnapore have tropical wet-dry monsoon climate (Ghosh et al. 2015; CGWB 2022). Block wise (administrative sub-district) 2 data sets per year i.e pre-monsoon and post-monsoon depth to groundwater level (GWL) of

the four districts of the study area Purulia, Bankura, West and East Midnapore from Government of West Bengal collected for a period of 21 years (from 2001 to 2021) has been used for the analysis. This data was collected from 5 stations of East Midnapore, 8 stations of West Midnapore, 8 stations of Bankura and 13 stations of Purulia district and is marked in Fig. 1. In this, only one well data is considered as the representative well among each district, as the variation of data is minimum and hence it is used for further groundwater level analysis (Bharti et al. 2024). Henceforth, the analysis of the selected representative well represents the entire district in this study. Monthly rainfall data was collected for each district from the India Meteorological Department (IMD), during the period 2001 to 2021. The climatic model data for the future period (2022–2050) is downloaded for CanESM5-SSP126 climatic model from WCRP CMIP6. Compared to CMIP5, the latest CMIP6 modelling framework incorporates updated specifications for greenhouse gas concentrations, emissions trajectories, and land-use change, along with a revised baseline year for future scenario simulations. A key advancement in CMIP6 is the integration of Shared Socioeconomic Pathways (SSPs) with the Representative Concentration Pathways (RCPs) previously used in CMIP5. The SSP framework comprises five distinct socioeconomic narratives that describe alternative global development patterns (Riahi et al. 2017): sustainable development (SSP1), middle-of-the-road development (SSP2), regional rivalry (SSP3), inequality (SSP4), and fossil fuel-driven development (SSP5). Detailed descriptions of the SSPs are available in O'Neill et al. (2016). In the present study, only one emission scenario SSP1-2.6 from the CanESM5 global climate model, which was found to most appropriate for this region in the previous literature (Chakraborty and Roshni 2025), is applied for projection of the groundwater levels under changing climate. SSP1-2.6 represents a low-emission, sustainability-oriented pathway characterized by reduced greenhouse gas emissions, improved resource efficiency, and strong environmental stewardship.

The selected districts form a major part of the Kangsabati river basin. The Kangsabati river flows generally in the south easterly direction and after traversing through the district of Purulia, it flows through Bankura and Midnapore for the remaining course before it falls into the river Hooghly. It originates from Jabarbund (641 m altitude) in the hilly areas of Chotanagpur Plateau in Jharkhand, which gradually flows down the lateritic/old alluvium areas of Purulia, Bankura and Midnapur districts and then extends to the interfluvial region between the Rupnarayan and Kheliaghai basins in the lower Gangetic Plain of West Bengal (Chakraborty and Roshni

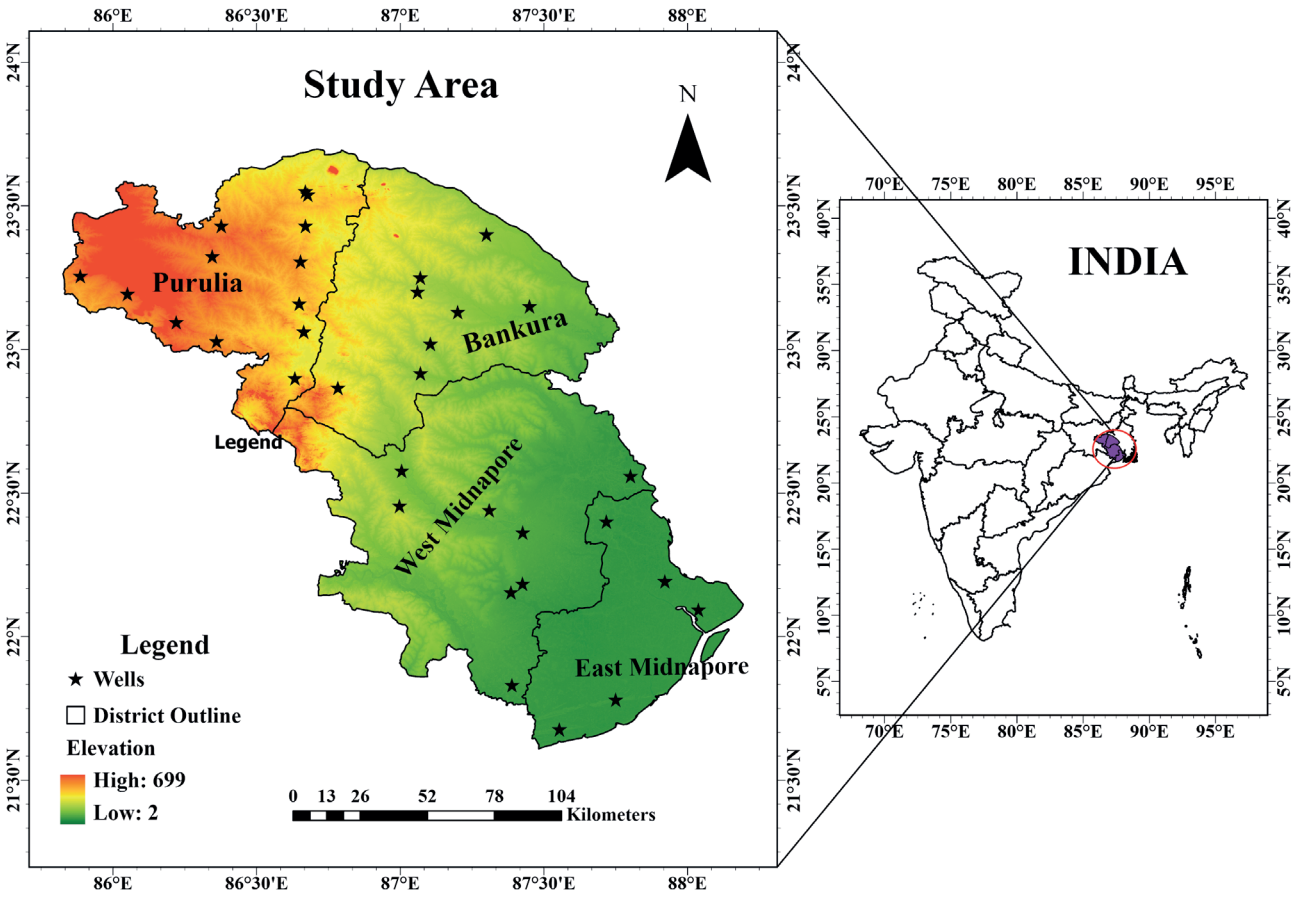

Fig. 1 Location of study area in semi-arid region of eastern India.

2025). River Kangsabati, is tropically rain-fed (Ghosh et al. 2022) and remains almost dry for most parts of the year, except the monsoon season. During the rainy season, sometimes this catchment area experiences heavy rainfall, and the river carries too much water in a short period of time with a high velocity, which frequently results in sudden and violent floods heavily loaded with rolling sand and suspended silt (Chakraborty et al. 2022).

The hydro-meteorological characteristics of this study area exhibit a predominantly subtropical humid climate. However, the majority of rainfall is concentrated during the monsoon season, ranging between 2360mm/year to 1170 mm/year. The data has been collected from India Meteorological Department, Pune, India. The diverse geological formations of the study area influence its aquifer zones which primarily consist of granite, granite gneiss, and mica schist in the upper reaches, laterite and metavolcanic rocks in the middle sections, and alluvial deposits in the lower regions. Weathered and fractured aquifers in the upper reaches, having limited storage capacity due to the hard rock terrain. The middle regions of the study area with geomorphic units offer moderate groundwater potential while extensive alluvial plains and floodplains with unconsolidated sediments are seen in the lower basin, making it for groundwater extraction (Ghosh et al. 2022).

The study area encompasses a wide range of stratigraphic formations, extending from the Precambrian Archean basement – characterized by fractured crystalline hard rock – to the more recent Tertiary-Quaternary sequences, which include both the older porous alluvium and younger alluvial plains (Mukhopadhyay 1992). During the pre-monsoon season, the depth to the water table in shallow phreatic aquifers typically ranges from 4 to 10 meters below ground level (m bgl), primarily influence by the presence of substantial layers of sand, silt, and clay in the upland lateritic terrain. In contrast, the deeper aquifer systems, which occur beneath semi-confined to confined conditions, exhibit water table and piezometric surface levels between 5 and 9 m bgl.

The Purulia district is geologically characterized by a Precambrian and Archean lithological framework that includes granite, gneiss, calgranulite, ultrabasic, and other metamorphic rocks. Groundwater is predominantly confined to the weathered zone within a depth of 10 meters below ground level. The water table fluctuates, with pre-monsoon levels ranging between 3.63 and 9.76 meters below ground level, and post-monsoon levels ranging from 1.32 to 7.3 meters below ground level (Shah 2017). Bankura is predominantly composed of crystalline rock, with groundwater residing in a weathered mantle whose thickness ranges between 6 and 15 meters. In the eastern alluvial region, groundwater is confined beneath a clay layer approximately 10 meters thick. Seasonal variations include a water table decline of about 2.5 to 3 meters during peak summer, followed by a rise of around 1 meter in the post-monsoon period. (Chatterjee 2018).

In West Midnapore, the phreatic aquifer is encountered at depths ranging from 12 to 30 m bgl. During the summer season, the water table fluctuates between 2 and 21 m bgl, whereas in the post-monsoon period it ranges from 1.5 to 9 m bgl. Overall, the groundwater level exhibits a fluctuation of 6 to 19 m, which is consistent with the reported findings (Bhunia et al. 2012). In East Midnapore, hydrological data from Public Health Engineering Department (PHED), West Bengal indicate that the groundwater level generally remains 15–20 meters below the surface throughout most of the year. However, coastal regions such as Contai, Egra, and Digha are experiencing saltwater intrusion, which complicates the water quality and reduces the volume of usable water.

Furthermore, reduced precipitation in the East Medinipur (Midnapore) in recent years has resulted in significant saline contamination of surface water, leading to groundwater extraction rates that exceed natural recharge (Chakraborty et al. 2020).

3. Methodology

Mann-Kendall (M-K) test for GWL and rainfall trend detection was used in this study. The MK test (Mann 1945; Kendall 1955) has been frequently employed in water resources and climatic research to measure the trend in a time series of data (Patle et al. 2015, Himayoun and Roshni 2019). Monotonic trends in a given time series can be identified using the Mann-Kendall (M-K) test (Mann 1945; Kendall 1975). This is a statistical method, which involves in comparing the Groundwater data. This in turn leads to the formulation of two hypotheses:

a) Null hypothesis (H_0): It shows that the data is independent and shows no trend.
b) Alternative hypothesis (H_a): It shows that the data has the possible existence of a monotonic trend over time.

3.1 The M-K statistic

The Mann-Kendall test is a non-parametric statistical test used to detect monotonic trends in time-series data (like rainfall, temperature, groundwater levels, etc).

$$S = \sum_{i=1}^{n-1} \sum_{j=i+1}^{n} \mathrm{sgn}(x_j - x_i)$$

where n is the number of data points, x_i is the rank for i_{th} observations ($i = 1,2 \ldots n-1$), x_j is the rank for j_{th} observations ($j = i + 1,2 \ldots n$).

The variance σ^2 for the S-statistic is defined by:

$$\sigma^2 = \frac{[n(n-1)(2n+5)]}{18}$$

The standard test statistic Z_S is calculated as follows:

$$Z_s = \begin{cases} \frac{S-1}{\sigma}; \text{ for } S > 0 \\ 0; \text{ for } S = 0 \\ \frac{S+1}{\sigma}; \text{ for } S < 0 \end{cases}$$

If |Z| >Zα/2, reject null hypothesis (no trend), Z > 0 → increasing trend, Z < 0 → decreasing trend.

- In the Mann-Kendall (M-K) test, the p-value is the probability of observing the test statistic (or a more extreme value) if the null hypothesis is true. If p < α (commonly α = 0.05), reject null hypothesis → there is a significant trend.
- If p ≥ α, fail to reject null hypothesis → no significant trend.

Utilizing the computed values of S and σ, the standard test statistic (Z_8) is derived and subsequently employed to calculate the p-value. The null hypothesis is rejected when the absolute value $|Z_8|$ exceeds the critical value Z(α/2), with α denoting the significance level, thereby indicating a significant trend. A lower p-value provides compelling evidence against the null hypothesis, confirming the statistical significance of the observed trend. Specifically, a p-value below 0.05 signifies the presence of a monotonic trend.

3.2 Sen's Slope test

Sen's Slope represents the magnitude and direction of the trend, where a positive value indicates an increasing trend and a negative value indicates a decreasing trend (Sen 1968). The equation for Sen's slope is expressed as follows:

$$\text{Sen's slope} = \text{median}\left[\frac{Y_i - Y_j}{(i-j)}\right]; j < i,$$

where Y_i and Y_j are the rainfall data values at time periods i and j.

3.3 Empirical formula for groundwater recharge estimation

For effective groundwater modeling, development, and sustainability, accurate estimation of the recharge rate is very important. A fraction of the precipitation reaching the surface does not contribute to groundwater recharge, as portions are lost via evaporation, transpiration, and surface runoff. The infiltrated rainwater mitigates soil moisture deficits and percolates to recharge aquifers. Quantitative assessments of rainfall-induced recharge were conducted using several empirical correlations between recharge and precipitation, developed from regions with comparable climatic conditions (i.e., similar rainfall and temperature profiles) and is shown in Tab. 1.

Maxey and Eakin (1949) developed the empirical relationship between mean annual precipitation of the subbasin and Recharge from precipitation by considering evapotranspiration, surface water runoff, and recharge coefficient values between 0–25%. Chaturvedi formulated an empirical model that quantifies recharge as a function of annual precipitation, based on observed fluctuations in water levels and recorded rainfall in the Ganga-Yamuna doab (Chaturvedi 1973). Later, this formula was modified at the UP-Irrigation Research Institute, Roorkee as Modified Chaturvedi Formula. The Chaturvedi formula is extensively employed for the initial estimation of groundwater recharge resulting from rainfall. It is important to note that there exists a rainfall threshold below which no recharge occurs. This lower rainfall limit within the formula likely incorporates losses attributable to runoff, soil moisture deficits, interception, and evaporation. Krishna Rao developed an empirical relationship to determine the groundwater recharge in a limited climatological homogeneous area (Chaturvedi 1973). The factors of each of the above specified empirical correlations are inherently site-specific; therefore, a single generalized formula may not be applicable to all alluvial regions.

3.4 Rainfall variation within the study area

Fluctuations in groundwater levels are directly influenced by rainfall, which serves as the primary source of recharge for aquifers. The response of groundwater levels to rainfall events is governed by the hydrogeological characteristics of the region. The Fig. 2 depicts the annual rainfall variability (2001–2021) across four districts of West Bengal: East Midnapore, West Midnapore, Bankura, and Purulia. Rainfall fluctuated between ~1,000–2,500 mm, with coastal districts (East and West Midnapore) consistently receiving higher precipitation compared to the drought-prone districts of Bankura and Purulia. Distinct peaks are observed in 2005, 2007, 2013, 2017, and 2021,

Tab. 1 Empirical correlations for recharge estimation from rainfall.

Sl. No.	Formula name	Equation(s)	Definition of parameter and coefficient value range
1	The Maxey-Eakin (1949) method	R = P*a	P = Yearly rainfall, a–20%, R = Net Recharge (mm)
2	Chaturvedi Formula (Chaturvedi 1973)	$R = 2.0(P-15)^{0.4}$	P = Yearly rainfall (inch), R = Net Recharge (inch)
3	Modified Chaturvedi Formula (Kumar and Seethapathi 2002)	$R = 1.35(P-14)^{0.5}$	P = Yearly rainfall (inch), R = Net Recharge (inch)
4	Relationship of Krishna Rao (Krishna Rao 1970)	R = 0.30(P–500)	P = Yearly rainfall (mm), R = Net Recharge (mm)

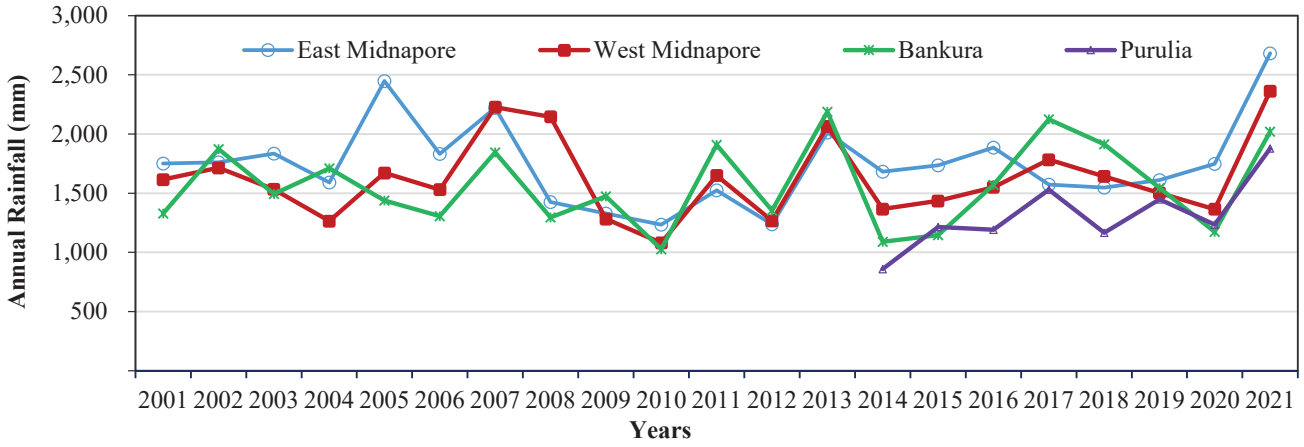

Fig. 2 District-wise annual rainfall plots during the period 2001 to 2021.

with 2021 recording exceptionally high rainfall (>2,800 mm in East Midnapore). Post-2016 rainfall shows a rising tendency, culminating in a sharp increase in 2021, likely linked to anomalous monsoonal activity and cyclonic events. Overall, the data reflect the spatial heterogeneity and temporal fluctuations of monsoonal rainfall in the Red and Lateritic Zone, with coastal districts being wetter and western plateau districts experiencing greater variability (Ghosh et al. 2015; Das et al. 2015). Similar finding has been observed in the study of Roy et al. 2024, in which the authors have analysed rainfall trends in eastern India, covering 23 districts of West Bengal, based on data from 1993 to 2022, reveals a significant increase of nearly 34% in post-monsoon rainfall and an overall 3% rise in annual rainfall.

4. Results and discussion

4.1 Groundwater level trend analysis

Tab. 2 shows the outcomes of the Mann-Kendall (M-K) trend test and Sen's Slope for groundwater levels across different locations of the study area. The primary parameter here is the p-value, which indicates the significance of the trend. East and west Midnapore, demonstrates a significant downward trend, implying reduced groundwater recharge as well as excessive groundwater pumping for agriculture, industry or domestic use. Bankura and Purulia shows insignificant trends, suggesting that GWL changes are not consistent enough to establish a clear pattern. With the study area experiencing very hot and dry to humid summers, erratic monsoon to heavy monsoons with cyclones and storms, combined with over-extraction of groundwater, geological factors for reduced retention capacity and human interventions, the groundwater level is declining. This decline was quantified using Sen's slope estimator, which reveals that most locations are undergoing a significant reduction in groundwater levels with East Midnapore exhibiting the highest negative values with Sen's slope of 0.50873 m/year in the pre-monsoon season and 0.50742 m/year in the post-monsoon season, as shown in Table 2.

4.2 Groundwater level variations of pre-monsoon and post-monsoon period

Based on the collected data, preliminary GW analysis (Bharti et al. 2024) has been carried out for pre-monsoon and post monsoon period for the study area i.e. four selected districts of West Bengal. In regions

Tab. 2 District-wise GWL trend analysis by using M-K and Sen's slope estimation during pre-monsoon and post-monsoon (2001–2021).

Location	Period	p-value	Sen's slope	Test interpretation
East Midnapore	pre-monsoon	0.0005	−0.509	significant decreasing trend
	post-monsoon	0.00001	−0.507	significant decreasing trend
West Midnapore	pre-monsoon	0.043	−0.181	significant decreasing trend
	post-monsoon	0.003	−0.201	significant decreasing trend
Bankura	pre-monsoon	0.608	0.019	no trend
	post-monsoon	0.194	−0.040	no trend
Purulia	pre-monsoon	0.415	0.020	no trend
	post-monsoon	0.880	0.004	no trend

influenced by monsoonal rainfall, groundwater levels exhibit seasonal fluctuations. During the pre-monsoon period, the groundwater table is situated at greater depths, whereas in the post-monsoon phase, the water table rises to shallower depths due to enhanced rainwater infiltration during the monsoon season. The GW level data for pre- and post-monsoon from 2001 to 2021 for the four districts has been analysed from total 34 (East Midnapur-5, West Midnapore-8, Bankura-8, Purulia-13) monitoring wells (as obtained from State Water Investigation Directorate, Government of West Bengal, India).

Variation of GWL from <5m to >15m below ground level has been studied for a period of 20 years from a number of monitoring wells within the study area. Data shows that the GWL varies from a minimum of 1.96m to a maximum level of 20.39m. The percentage (%) of the wells (monitoring wells) lying within this ranges have been categorized into 4 divisions below ground level, such as i) <5m, ii) >=5 to <10m, iii) 10 to 15m and iv) >15m depth.

In East Midnapore, the GWL in 100% of the wells were found to be at a depth >15m since 2015 in the pre-monsoon period while in the post-monsoon period, the GWL was between 10–15m depth in most of the region. West Midnapore showed a major percentage of the wells within >=5m to <10m and 10m-15m range while in the post-monsoon period, this GWL

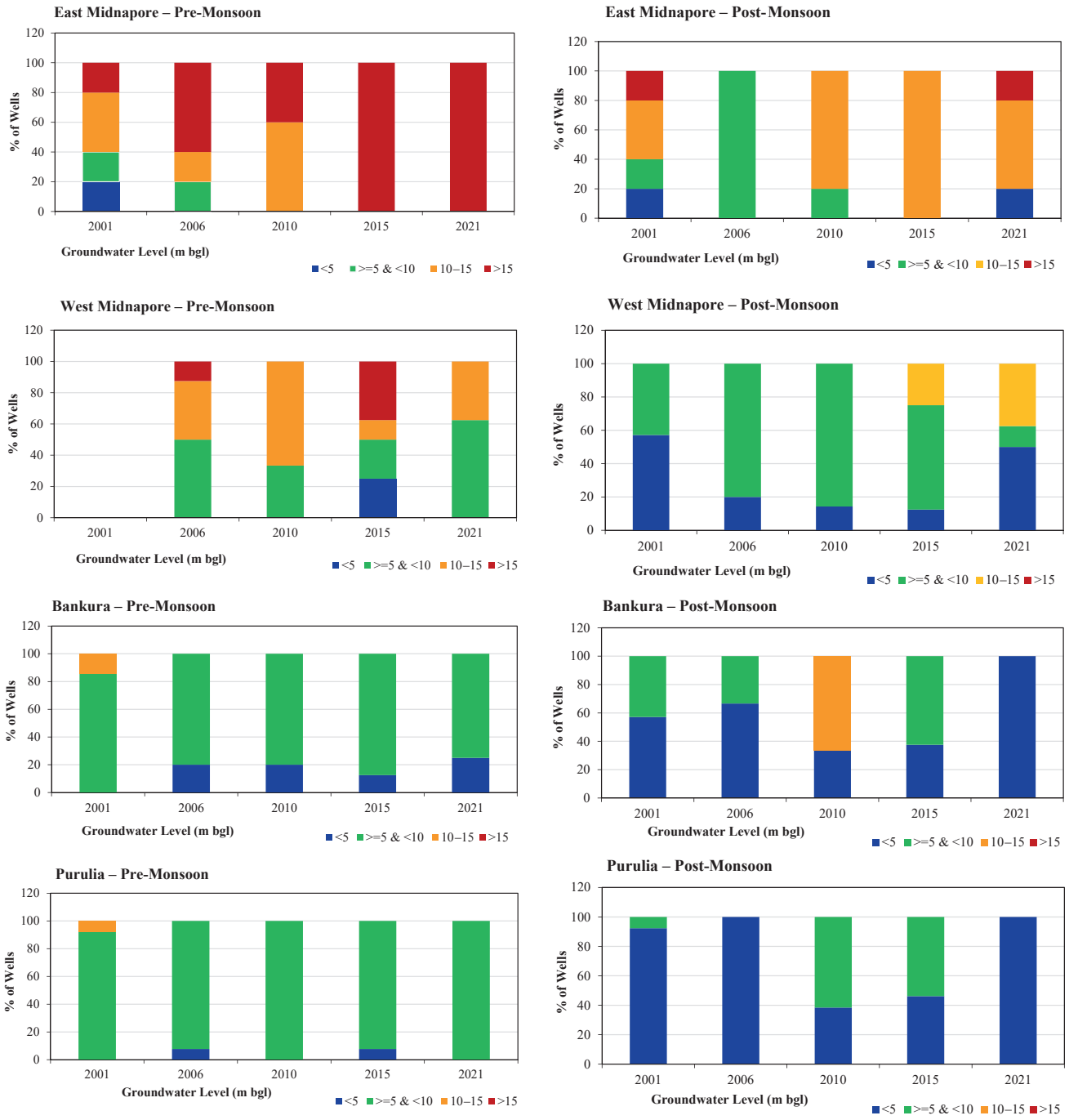

Fig. 3 District-wise plots for groundwater level (m bgl) data with % of wells (2001–2021).

increased to 5 to 10m in most of the wells. In Bankura more than 80% of the wells were found with a GWL <10m depth in pre-monsoon which increased to <5m depth in the post-monsoon period. In Purulia, GWL in 90–100% of the wells were within >=5 to <10m depth in pre-monsoon while <5m in post monsoon period. On an average it can be stated that, there is a difference of more or less 5m between the pre- and post-monsoon GWL within the study area.

The pre-monsoon period of East Midnapore shows 100% of the wells to have the GWL more than 15m since 2015 while post-monsoon shows a rise of at least 5m in the GWL. In case of West Midnapore, pre-monsoon period shows a major % of the wells to have a GWL within 10–15m throughout the period with few variations while post monsoon shows a rise of at least 5m in the GWL. In Bankura and Purulia, 80 to 90% of the wells showed the GWL to be within 5–10m range in pre-monsoon which later had a rise of at least 5m in the post-monsoon period. Overall, it can be stated that, there is a difference of more or less 5m between the pre- and post-monsoon GWL within the study area (DSR 2022; Bhattacharya et al. 2020).

4.3 Plot of GWL variation in pre-monsoon and post-monsoon period

GWL variation plotted for pre-monsoon and post-monsoon data from 2001 to 2021, for the four districts are shown in Fig. 3 and Fig. 4. From Fig. 3, it is evident that pre-monsoon GWL is decreasing from 2001 to 2021(Bera et al. 2022). The rate of decline in Bankura and Purulia is much less than East and West Midnapore. In Bankura and Purulia, there is no significant fluctuation throughout the study period except one or two instances.

The pre-monsoon groundwater level trends across the four districts of the western part of West Bengal (East Midnapore, West Midnapore, Bankura, and Purulia) were analyzed using linear regression (Fig. 4). The regression equations and coefficients of determination (R^2) reveal significant spatial differences in groundwater dynamics.

In East Midnapore, the regression slope is positive ($y = 0.3973x - 784.76$, $R^2 = 0.4886$), indicating a clear groundwater decline before monsoon, with a moderately strong trend. The trend reflects a clear long-term declining nature in pre-monsoon groundwater availability, likely due to intensive pumping and increased anthropogenic demand. West Midnapore, (equation: $y = 0.0543x - 98.986$, $R^2 = 0.0266$) shows a very small positive slope which implies a slight groundwater decline and the R^2 value indicates an extremely weak fit i.e. No strong trend; year-to-year variations dominate. In contrast, Bankura and Purulia, exhibit very low R^2 values (<0.05) and slightly negative slopes implies a marginal rise in the water table. These changes are statistically insignificant due to the extremely weak fit of the regression models. Similarly, West Midnapore shows a marginal decline, but the trend is unreliable given the negligible R^2.

Overall, the regression analysis highlights East Midnapore as the only district with a statistically meaningful declining trend in pre-monsoon groundwater levels, whereas the other districts show no significant temporal trends, with fluctuations likely driven by short-term hydroclimatic variability and localized pumping stresses rather than long-term depletion.

Post-monsoon groundwater levels in East Midnapore, West Midnapore, Bankura, and Purulia show distinct spatial variability (Fig. 5). The post-monsoon groundwater levels across four districts of West Bengal display spatial variability in depletion trends. East Midnapore exhibits the steepest decline, indicating severe groundwater depletion (~12–20 m bgl over time). With a regression slope of 0.4977 m/year

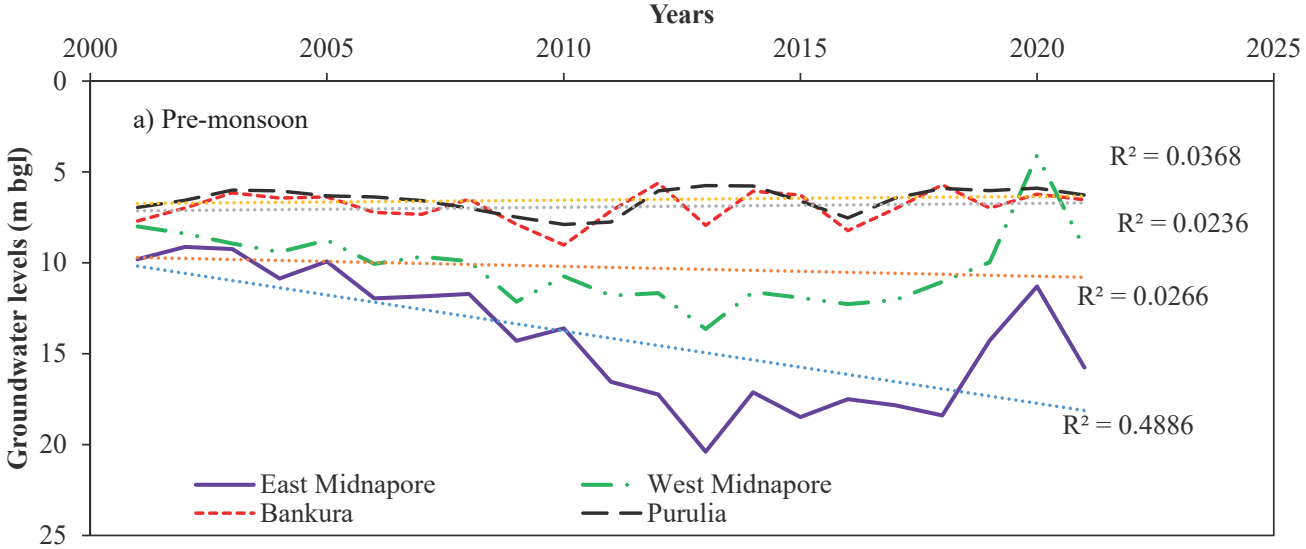

Fig. 4 District-wise temporal groundwater levels (2001–2021) plot for pre-monsoon season in the study regions of West Bengal.

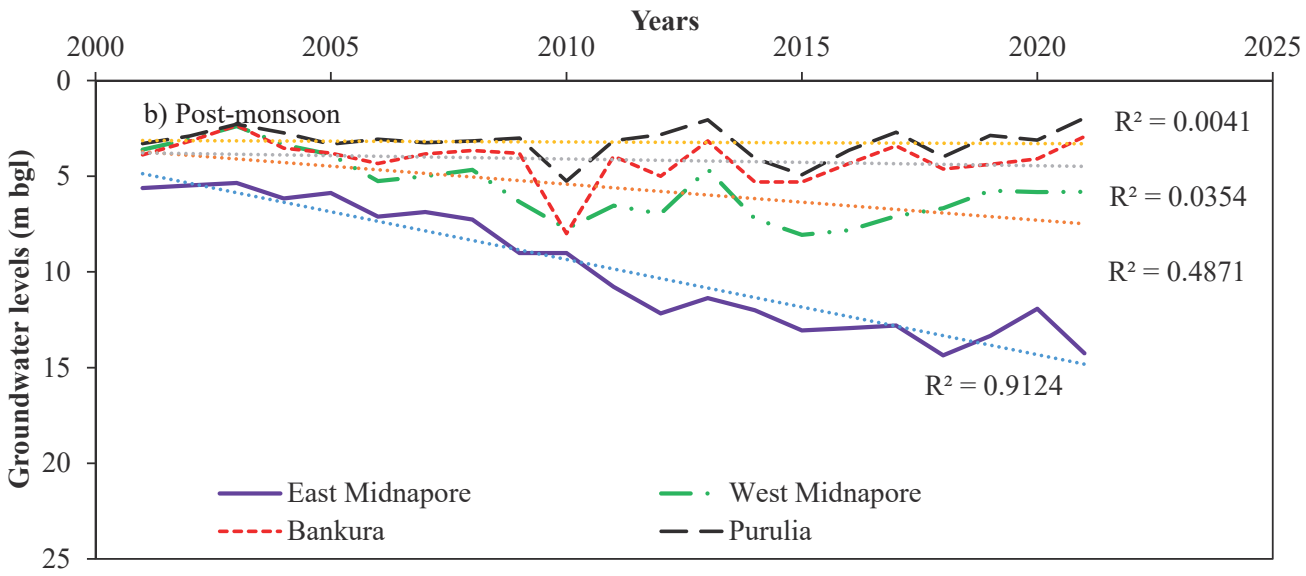

Fig. 5 District-wise temporal groundwater levels (2001–2021) plot for post-monsoon season in the study regions of West Bengal.

(R^2 = 0.9124), indicating a consistent and significant groundwater depletion over the study period. West Midnapore shows a moderate declining trend (0.1882 m/year, R^2 = 0.4871), suggesting localized stress. In contrast, Bankura (0.0351 m/year, R^2 = 0.0354) and Purulia (0.0084 m/year, R^2 = 0.0041) exhibit negligible long-term trends, with very low coefficients of determination, implying largely stable groundwater conditions.

In East and West Midnapore, according to groundwater bulletins by the Central Ground Water Board (CGWB 2022), parts of West and East Midnapore have experienced a post-monsoon water level fall of less than 2 m, reflecting moderate depletion trends in these regions. Further, district-level water management reports indicate that East Midnapore has substantial groundwater reserves (71,090.4 ha-m), of which irrigation accounts for 17,103.2 ha-m and domestic use for 4,751.4 ha-m highlighting intense extraction pressures, especially for agriculture. Bankura and Purulia show negligible long-term trends; however, both experience episodic recharge limitations and drought-induced stress in hard-rock aquifers especially Purulia, where deep aquifers show low resilience and groundwater levels during lean periods can reach upto 8–10 m bgl (Bera et al. 2022).

4.4 Groundwater recharge estimation with different empirical methods

Groundwater recharge was estimated using the four empirical methods namely, the Chaturvedi method, the Modified Chaturvedi method, Krishna Rao method and the Maxey and Eakin method, and is shown in Fig. 6. These methods were applied to the same study area, to evaluate their respective estimates and understand the variability introduced by methodological differences. The recharge estimates (in inch/year), primarily based on rainfall, when plotted against the post monsoon groundwater level, for the period 2000 to 2021, shows a similar trend in all the four districts of the study area (Fig. 6).

Recharge estimates in East Midnapore, range between ~5–25 mm/year, with major peaks in 2006–2008 and 2021. Groundwater levels, however, show a steady decline from ~6–8 m bgl in the early 2000s to ~12–15 m bgl after 2010, despite high recharge events. This mismatch suggests that over-extraction outweighs natural replenishment, consistent with coastal aquifer stress (Ghosh et al. 2022).

In West Midnapore, recharge varied from ~8–20 mm/year, with peaks in 2004–2007, 2011–2013 and 2021. Groundwater levels declined sharply from ~2–3 m bgl in 2000 to ~8 m bgl in 2014–2015, before partially recovering (~5–6 m bgl) post-2016. The data suggest initial shallow aquifers subjected to progressive depletion but with partial resilience during high rainfall years. Recharge estimates in Bankura fluctuates between ~8–18 mm/year, with episodic peaks above 20 mm/year (2004, 2012, 2016, 2019). Groundwater levels showed high sensitivity to recharge fluctuations, ranging from ~2 m bgl (shallow, wet years) to ~9 m bgl (2010 drought year). This indicates a direct climate-driven recharge–storage linkage in Bankura, where rainfall variability governs aquifer conditions more strongly than extraction.

While Recharge estimates (2014–2021) remained comparatively low, with recharge values (8.21–10.36 mm/year), lowest among the four districts. These results confirm Purulia's semi-arid, water-stressed environment, where limited rainfall and low-yielding lateritic aquifers restrict recharge capacity.

The suitability of the groundwater recharge estimation methods for different types of soil is detailed

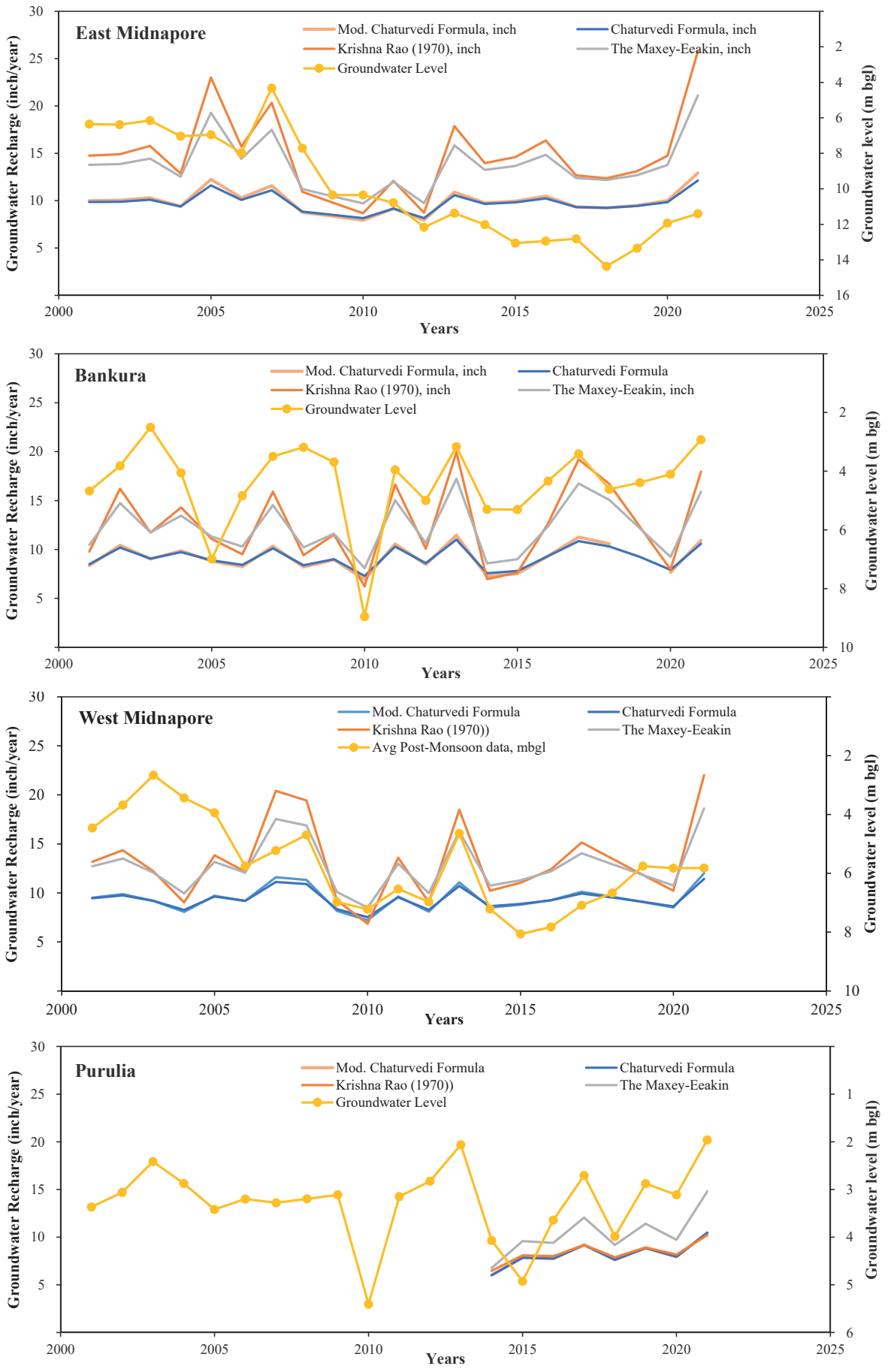

Fig. 6 Districtwise plot of groundwater recharge estimates using four empirical methods against post monsoon groundwater level for the period 2000 to 2021.

Tab. 3 Suitability of Empirical recharge estimation methods in the Red and Lateritic Zone of West Bengal.

East Midnapore	Coastal alluvial aquifers, high abstraction	Chaturvedi method (1936) / Modified Chaturvedi	Better suited to alluvial systems; Modified Chaturvedi can supplement.
West Midnapore	Lateritic uplands, semi-humid	Krishna Rao (1970) / Modified Chaturvedi	Krishna Rao captures variability; Modified Chaturvedi provides stable conservative values.
Bankura	lateritic, hard-rock terrain	Krishna Rao (1970)	Captures monsoon-driven recharge; aligns with hard-rock aquifers.
Purulia	low-rainfall, lateritic hard-rock	Krishna Rao (1970)	Best reflects episodic recharge in fractured aquifers

in Tab. 3. It is evident from the Table that the most appropriate empirical formula that can be applied consistently across Bankura, Purulia, West Midnapore, and East Midnapore, is the Modified Chaturvedi formula because, it is widely used across India for both alluvial and hard-rock settings and provides realistic, conservative estimates that avoid overestimation (Barik and Ghosh 2024).

4.5 Correlation between groundwater level and groundwater recharge by modified Chaturvedi formula

The correlation analysis between groundwater recharge (estimated using the Modified Chaturvedi formula) and groundwater levels (Fig. 7) reveals marked spatial contrasts across the four districts. Purulia shows a moderately strong positive correlation which indicates that groundwater levels in Purulia are relatively sensitive to recharge variations. This may be due to its shallow, fractured lateritic aquifers and semi-arid climate (Chakraborty and Roshni 2025). Bankura represents a moderate correlation. Groundwater levels respond to rainfall-driven recharge, but the relationship is partly obscured by abstraction for irrigation. Aquifers are slightly more buffered than in Purulia, hence weaker correlation. By contrast, East Midnapore (R^2 = 0.0076) and West Midnapore (R^2 = 0.0113) display very weak correlations, reflecting the dominance of anthropogenic abstraction and aquifer storage effects over natural recharge in coastal and lateritic upland settings (Ghosh et al. 2022). These results underscore that while the Modified Chaturvedi formula provides a consistent basis for recharge estimation across diverse hydrogeological contexts, the degree of correlation with observed groundwater levels is strongly mediated by local aquifer characteristics and abstraction pressures.

4.6 Correlation between rainfall and groundwater level

The regression analysis (Fig. 8) provides insights into the spatial variability of GWL in four districts of West Bengal against the variability in average annual rainfall. Purulia exhibits the strongest correlation (R^2 = 0.6392), suggesting that groundwater levels here are highly sensitive to rainfall variability. This is expected in, lateritic hard-rock aquifers with limited storage, where recharge events directly translate into water-level fluctuations (Chakraborty and Roshni 2025). Bankura displays a moderate correlation (R^2 = 0.3295), reflecting that there is some dependence of groundwater levels on rainfall recharge. These findings also suggest that rainfall contributes to recharge processes, but it is not the sole or dominant driver of groundwater fluctuations in these areas. Instead, the

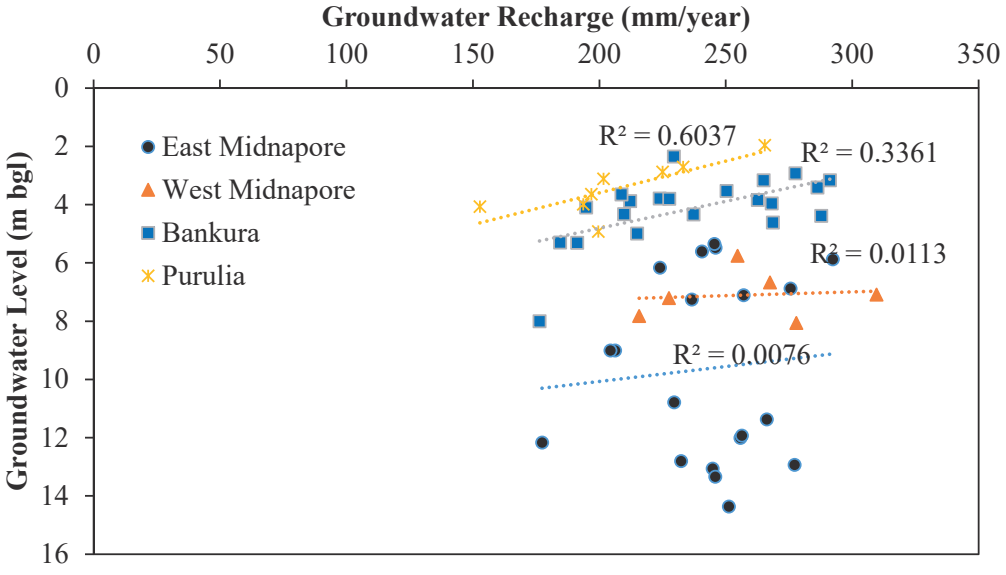

Fig. 7 Groundwater level (2001–2021) plot in relation with groundwater recharge in the study area.

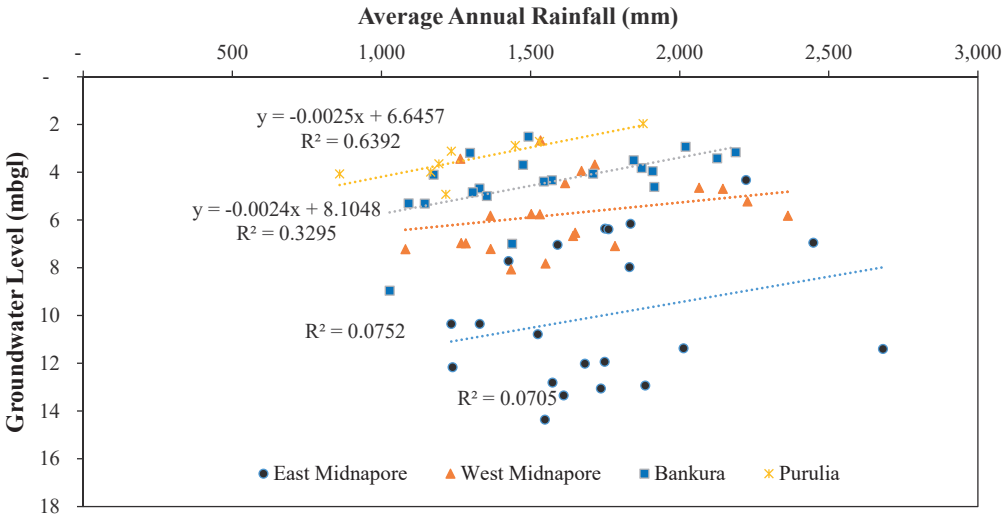

Fig. 8 Groundwater level (2001–2021) plot in relation with average annual rainfall in the study area.

moderate correlations indicate the presence of additional controlling factors. East and West Midnapore show a weak correlation indicating that groundwater levels are only marginally influenced by rainfall. Persistent abstraction and larger aquifer storage reduce the observable rainfall and GWL linkage (Ghosh et al. 2022) and intensive pumping for agriculture and domestic water supply outweighs the contribution of rainfall recharge. Hence, an in-depth study related to surface water-groundwater interaction is required in this study area to find the additional controlling factors affecting groundwater fluctuations. Hence, for projection of groundwater level in future time periods, only the relation for Purulia and Bankura has been considered.

4.7 Projection of groundwater levels under changing climate

Based on the previous literature (Chakraborty and Roshni 2025), the rainfall data from CanESM5 climatic model with SSP-126 scenario (Fig. 9a) is highly suitable for the present study area. Hence, the rainfall data of this climatic model (Fig. 9a) has been utilized for the projection of groundwater levels in the selected study region. With the empirical expressions developed for the observation period (Fig. 8) for the stations Bankura ($y = -0.0024x + 8.1048$) and Purulia ($y = -0.0025x + 6.6457$), the future groundwater levels have been projected and are shown in Fig. 9 (b). It is observed from the figure (Fig. 9a) that there appears to be a slight increase in the annual rainfall for the time period 2022–2050. As average annual rainfall increases, groundwater levels tend to become shallower across all districts. This is reflected in the negative slopes of all regression lines, i.e. higher rainfall generally enhances groundwater recharge, allowing the water table to rise closer to the surface. However, the strength of this trend differs significantly between districts. Areas like Purulia show a strong and clear response of groundwater levels to variations in rainfall ($R^2 \approx 0.64$), which implies as rainfall increases, groundwater levels become shallower.

5. Conclusions

This study examined the variability of groundwater levels and recharge in four semi-arid to sub-humid districts of West Bengal (Purulia, Bankura, West Midnapore, and East Midnapore) using long-term rainfall records, groundwater observations, empirical recharge models, and future climate projections.

The Mann-Kendall and Sen's slope analyses revealed a significant declining trend in groundwater levels in East and West Midnapore, while Bankura and Purulia exhibited insignificant trends, consistent with their comparatively lower abstraction pressures and hard-rock aquifer buffering.

Recharge estimation demonstrated that rainfall-driven variability is primary in Bankura and Purulia, where correlations between rainfall/recharge and groundwater levels were moderate to strong ($R^2 = 0.3295–0.6392$), reflecting the limited storage and direct rainfall dependency of lateritic aquifers. In contrast, East and West Midnapore displayed very weak correlations, emphasizing the dominance of anthropogenic abstraction and aquifer storage effects in alluvial and coastal settings.

Recharge assessments indicate that rainfall-driven variability is the dominant control in Purulia, where rainfall/recharge–groundwater level relationships exhibit moderate coefficients of determination in Bankura. Conversely, East and West Midnapore show very weak correlations, suggesting that groundwater dynamics in these alluvial and coastal aquifers are governed primarily by pumping stresses and subsurface storage characteristics rather than direct rainfall inputs.

Among the Empirical recharge estimation methods, Krishna Rao's formulation was most compatible

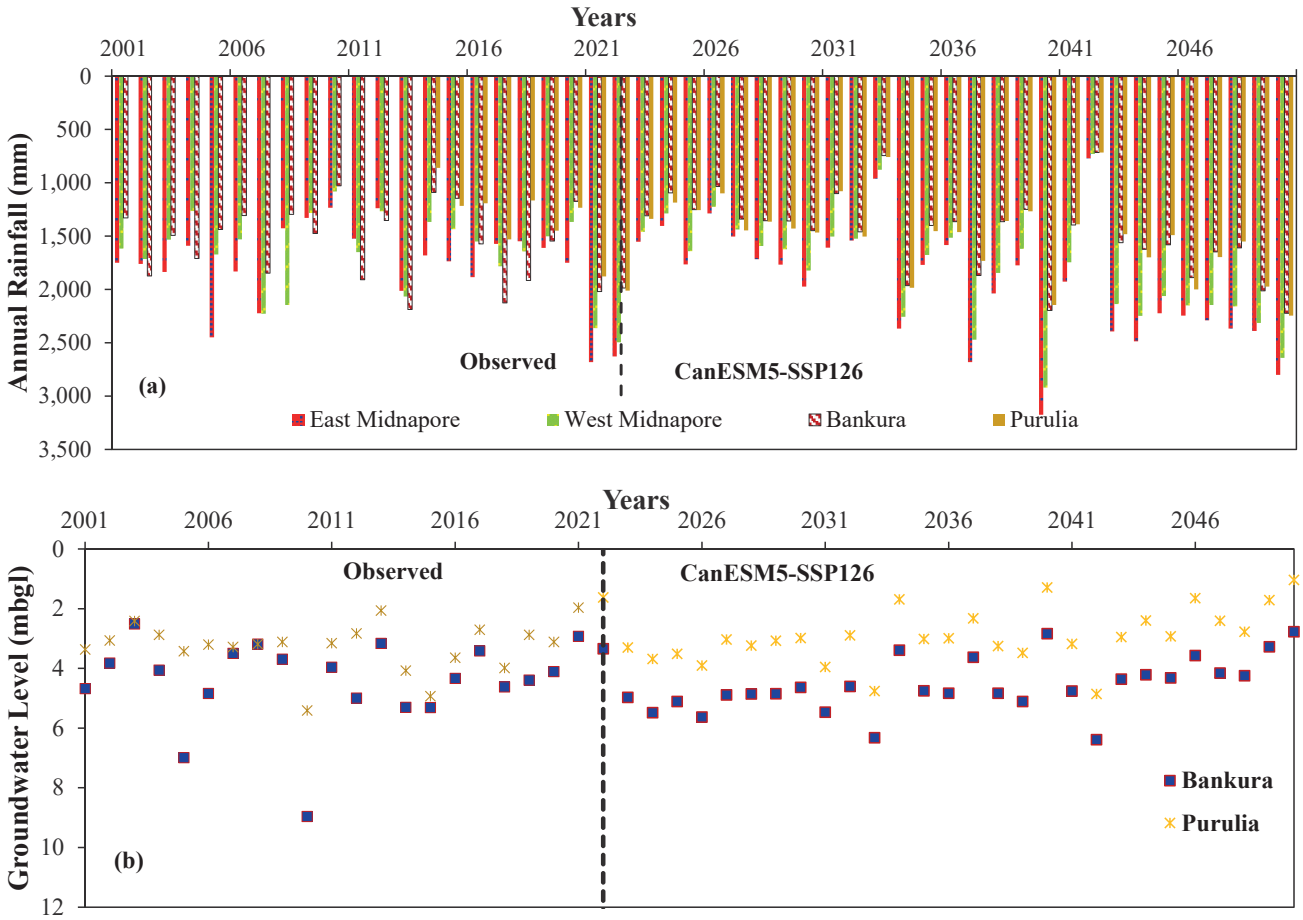

Fig. 9 Temporal variation. (a) Rainfall data of selected districts for the observed time period and the projected time period. (b) Observed groundwater levels (2001–2021) and the projected groundwater levels for the time period (2022–2050).

with hard-rock settings, whereas the Chaturvedi method showed better agreement with recharge behaviour in alluvial aquifers. Nevertheless, the Modified Chaturvedi equation provided the most robust and consistent performance across all four districts, owing to its applicability in both hard-rock and alluvial terrains and its conservative recharge estimates that minimize the risk of overestimation.

Future projections using the CanESM5 GCM under the SSP1-2.6 scenario indicated marginal increases in rainfall through 2050. The results suggest that even if rainfall increases, it will not be enough to balance the heavy stress caused by groundwater extraction, which is also a major cause of groundwater decline across India.

Future simulations based on the CanESM5 GCM under the SSP1–2.6 pathway indicate only marginal increases in rainfall by 2050. Correspondingly, groundwater levels are expected to remain broadly stable in Bankura and Purulia. However, the projections also underscore that any rainfall-induced recharge increases are unlikely to offset the substantial groundwater stress imposed by sustained extraction – an established driver of groundwater depletion across India.

The correlation of groundwater level and rainfall in East and West Midnapore is very poor. Hence, further in-depth analysis may be required for finding other potential factors for groundwater level decline. Overall, the study emphasizes the urgent need for sustainable groundwater governance, particularly in East and West Midnapore where declining trends are acute. Incorporating climate variability into water resource planning, adopting efficient irrigation practices, and strengthening aquifer recharge interventions are critical to ensure long-term water security in the Red and Lateritic Zone of West Bengal.

Acknowledgement

Authors would like to thank IMD and CGWB for providing data for the present analysis.

References

Ajami, H. (2021): Geohydrology: Groundwater. In: Alderton, D., Elias, S. A. (Eds.), Encyclopedia of Geology (Reference Module in Earth Systems and Environmental Sciences); Elsevier, pp. 408–415, https://doi.org/10.1016/B978-0-12-409548-9.12388-7.

Asoka, A., Gleeson, T., Wada, Y., Mishra, V. (2017): Relative contribution of monsoon precipitation and pumping

to changes in groundwater storage in India. Nature Geoscience 10(2), 109–117, https://doi.org/10.1038/ngeo2869.

Barik, B., Ghosh, K. (2024): Evaluating groundwater potential in water-deficit laterite zones of Eastern India using RS and GIS techniques, combining an analytical hierarchical process for sustainable water resources management. Groundwater for Sustainable Development 27: 101344, https://doi.org/10.1016/j.gsd.2024.101344.

Bera, B., Shit, P. K., Sengupta, N., Saha, S., Bhattacharjee, S. (2022): Steady declining trend of groundwater table and severe water crisis in unconfined hard rock aquifers in extended part of Chota Nagpur Plateau, India. Applied Water Science 12: 31, https://doi.org/10.1007/s13201-021-01550-x.

Bharti, V., Roshni, T., Jha, M. K., Ghorbani, M. A., Ibrahim, O. R. A. (2024): Complex network analysis of groundwater level in Sina Basin, Maharashtra, India. Environment, Development and Sustainability 26, 18017–18032, https://doi.org/10.1007/s10668-023-03375-x.

Bhattacharya, R. K., Chatterjee, N. D., Das, K. (2020): Land use and land cover change and its resultant erosion susceptibility: An appraisal using RUSLE and logistic regression in a tropical plateau basin of West Bengal, India. Environment, Development and Sustainability 23, 1411–1446, https://doi.org/10.1007/s10668-020-00628-x.

Bhunia, G. S., Samanta, S., Pal, D. K., Pal, B. (2012): Assessment of groundwater potential zone in Paschim Medinipur District, West Bengal: A meso-scale study using GIS and remote sensing. Approach. Journal of Environment and Earth Science 2(5), 41–59.

CGWB (2022). Ground Water Yearbook of West Bengal & Andaman & Nicobar Islands (2021–2022) (Technical Report Series D No. 287). Eastern Region, Kolkata: Ministry of Jal Shakti, Department of Water Resources, River Development & Ganga Rejuvenation, Government of India. Available online: https://cgwb.gov.in/cgwbpnm/public/download/692 (accessed on 2 February 2025).

Chakraborty, M., Mukherjee, A., Ahmed, K. M. (2022): Regional-scale hydrogeochemical evolution across the arsenic-enriched transboundary aquifers of the Ganges River Delta system, India and Bangladesh. Science of the Total Environment 823: 153490, https://doi.org/10.1016/j.scitotenv.2022.153490.

Chakraborty, S., Roshni, T. (2025): Analysis of rainfall epochs in changing climate of Kangsabati River Basin, India. AUC Geographica 61(1), 16–32, https://doi.org/10.14712/23361980.2025.7.

Chakraborty, S., Maity, P. K., Das, S. (2020): Investigation, simulation, identification, and prediction of groundwater levels in coastal areas of Purba Midnapur, India, using MODFLOW. Environment, Development and Sustainability 22(4), 3805–3837, https://doi.org/10.1007/s10668-019-00344-1.

Chatterjee, U. (2018): Water scarcity in semi-arid regions of Bankura District, West Bengal, India: Problems and prospects. Khoj: An International Peer Reviewed Journal of Geography 5(1), 87–96, https://doi.org/10.5958/2455-6963.2018.00007.3.

Chaturvedi, R. S. (1973): A note on the investigation of groundwater resources in western districts of Uttar Pradesh. Annual Report, UP Irrigation Research Institute, 86–122.

Das, S., Chatterjee, M., Bhattacharya, S. (2015): Climatic classification and variability in the dry tracts of Purulia and Bankura districts, West Bengal, India. Asian Journal of Environmental Research 7(1), 45–60.

DSR (2022): District Survey Report of Paschim Medinipur District, West Bengal (Report). Government of West Bengal, India. Available online: https://www.dmm.gov.in/pdfs/DSR/DSR_of_Paschim_Medinipur.pdf (accessed on 8 February 2025).

Ghosh, K., Singh, P., Kumar, L. (2015): Monsoon dynamics and climatic classification in the coastal districts of West Bengal. Climate Research Letters 8(4), 77–91.

Ghosh, S., Sarkar, B., Islam, A., Shit, P. K., Quesada-Román, A., Gazi, H. A. R. (2022): Surface Water and Groundwater Suitability for Irrigation Based on Hydrochemical Analysis in the Lower Mayurakshi River Basin, India. Geosciences 12(11): 415, https://doi.org/10.3390/geosciences12110415.

Goswami, A., Banerjee, R., Dutta, T. (2022): Spatio-temporal climate dynamics of the western Rarh region, West Bengal. International Journal of Climatology and Weather Science 14(3), 201–219.

Hamed, Y., Hadji, R., Redhaounia, B., Zighmi, K., Bâali, F., El Gayar, A. (2018): Climate impact on surface and groundwater in North Africa: a global synthesis of findings and recommendations. Euro-Mediterranean Journal for Environmental Integration 3: 25, https://doi.org/10.1007/s41207-018-0067-8.

Himayoun, D., Roshni, T. (2019): Spatio-temporal variation of drought characteristics, water resource availability and the relation of drought with large scale climate indices: A case study of Jhelum basin, India. Quaternary International 525, 140–150, https://doi.org/10.1016/j.quaint.2019.07.018.

Jasechko, S., Seybold, H., Perrone, D., Fan, Y., Shamsudduha, M., Taylor, R. G., Fallatah, O., Kirchner, J. W. (2024): Rapid groundwater decline and some cases of recovery in aquifers globally. Nature 625, 715–721, https://doi.org/10.1038/s41586-023-06879-8.

Kendall, M. G. (1955): Rank correlation methods. 2nd ed.; Charles Griffin & Co. Ltd.: London, 196 pp.

Kendall, M. G. (1975): Rank Correlation Methods. 4th ed.; Charles Griffin & Co. Ltd.: London, 202 pp.

Kumar, C. P., Seethapathi, P. V. (2002): Assessment of natural groundwater recharge in Upper Ganga Canal command area. Journal of Applied Hydrology 15(4), 13–20.

MacDonald, A. M., Bonsor, H. C., Ahmed, K. M., Burgess, W. G., Basharat, M., Calow, R. C., Dixit, A., Foster, S. S. D., Gopal, K., Lapworth, D. J., Lark, R. M., Moench, M., Mukherjee, A., Rao, M. S., Shamsudduha, M., Smith, L., Taylor, R. G., Tucker, J., van Steenbergen, F., Yadav, S. K. (2016): Groundwater quality and depletion in the Indo-Gangetic Basin mapped from *in situ* observations. Nature Geoscience 9, 762–766, https://doi.org/10.1038/ngeo2791.

Maliva, R. G. (2020): Vadose Zone Hydrology Basics. In: Anthropogenic Aquifer Recharge. Springer Hydrogeology; Springer: Cham, https://doi.org/10.1007/978-3-030-11084-0_3.

Mann, H. B. (1945): Nonparametric Tests Against Trend. Econometrica 13(3), 245–259, https://doi.org/10.2307/1907187.

Maxey, G. B., Eakin, T. E. (1949): Ground Water in White River Valley, White Pine, Nye, and Lincoln Counties, Nevada. Water Resources Bulletin No. 8, Nevada State Engineer, 59 pp.

Mishra, V., Aadhar, S., Asoka, A., Pai, S., Kumar, R. (2016): Frequency of the 2015 monsoon-season drought in the Indo-Gangetic Plain. Geophysical Research Letters 43(23), 12,102–12,112, https://doi.org/10.1002/2016GL071407.

Mokadem, N., Boughariou, E., Mudarra, M., Ben Brahim, F., Andreo, B., Hamed, Y., Bouri, S. (2018): Mapping potential zones for groundwater recharge and its evaluation in arid environments using a GIS approach: Case study of North Gafsa Basin (Central Tunisia). Journal of African Earth Sciences 141, 107–117, https://doi.org/10.1016/j.jafrearsci.2018.02.007.

Mukherjee, A., Saha, D., Harvey, C. F., Taylor, R. G., Ahmed, K. M., Bhanja, S. N. (2015): Groundwater systems of the Indian Sub-Continent. Journal of Hydrology: Regional Studies 4, part A, 1–14, https://doi.org/10.1016/j.ejrh.2015.03.005.

Mukhopadhyay, S. (1992): Terrain analysis and its impact on land use, Kangsabati River Basin; Vohra Publications, 309 pp.

O'Neill, B. C., Tebaldi, C., van Vuuren, D. P., Eyring, V., Friedlingstein, P., Hurtt, G., Knutti, R., Kriegler, E., Lamarque, J.-F., Lowe, J., Meehl, G. A., Moss, R., Riahi, K., Sanderson, B. M. (2016): The Scenario Model Intercomparison Project (ScenarioMIP) for CMIP6. Geoscientific Model Development 9(9), 3461–3482, https://doi.org/10.5194/gmd-9-3461-2016.

Osborn, N. I., Hardy, R. H. (1999): Statewide groundwater vulnerability map of Oklahoma. Oklahoma Water Resources Board Technical Report 99-1. Available online: https://oklahoma.gov/content/dam/ok/en/owrb/documents/science-and-research/hydrologic-investigations/statewide-groundwater-vulnerability-map-1999.pdf (accessed on 5 January 2025).

Patle, G. T., Singh, D. K., Sarangi, A., Rai, A., Khanna, M., Sahoo, R. N. (2015): Time Series Analysis of Groundwater Levels and Projection of Future Trend. Journal of the Geological Society of India 85(2), 232–242, https://doi.org/10.1007/s12594-015-0209-4.

Riahi, K., van Vuuren, D. P., Kriegler, E., Edmonds, J., O'Neill, B. C., Fujimori, S., Bauer, N., Calvin, K., Dellink, R., Fricko, O., Lutz, W., Popp, A., Crespo Cuaresma, J., KC, S., Leimbach, M., Jiang, L., Kram, T., Rao, S., Emmerling, J., Ebi, K., Tavoni, M. (2017): The Shared Socioeconomic Pathways and their energy, land use, and greenhouse gas emissions implications: An overview. Global Environmental Change 42, 153–168, https://doi.org/10.1016/j.gloenvcha.2016.05.009.

Roxy, M. K., Ghosh, S., Pathak, A., Athulya, R., Mujumdar, M., Murtugudde, R., Terray, P., Rajeevan, M. (2017): A threefold rise in widespread extreme rain events over central India. Nature Communications 8: 708, https://doi.org/10.1038/s41467-017-00744-9.

Roy, P. K., Sarkar, A., Saha, S., Ray, P., Roy, M. B. (2024): Spatio-temporal analysis of precipitation in eastern India over three decades. Spatial Information Research 32, 727–738, https://doi.org/10.1007/s41324-024-00591-z.

Sen, P. K. (1968): Estimates of the Regression Coefficient Based on Kendall's Tau. Journal of the American Statistical Association 63(324), 1379–1389, https://doi.org/10.1080/01621459.1968.10480934.

Shah, T. (2017): Sustainable groundwater governance: India's challenge and response. The Journal of Governance 14, 23–45.

Singh, D., Tsiang, M., Rajaratnam, B., Diffenbaugh, N. S. (2014): Observed changes in extreme wet and dry spells during the South Asian summer monsoon season. Nature Climate Change 4, 456–461, https://doi.org/10.1038/nclimate2208.

Stempvoort, D. V., Ewert, L., Wassenaar, L. (1993): Aquifer vulnerability index: A GIS-compatible method for groundwater vulnerability mapping. Canadian Water Resources Journal / Revue Canadienne Des Ressources Hydriques 18(1), 25–37, https://doi.org/10.4296/cwrj1801025.

Wada, Y., van Beek, L. P. H., van Kempen, C. M., Reckman, J. W. T. M., Vasak, S., Bierkens, M. F. P. (2010): Global depletion of groundwater resources. Geophysical Research Letters 37(20): L20402, https://doi.org/10.1029/2010GL044571.

Yazdian, M., Rakhshandehroo, G., Nikoo, M. R., Mooselu, M. G., Gandomi, A. H., Honar, T. (2021): Groundwater sustainability: Developing a non-cooperative optimal management scenario in shared groundwater resources under water bankruptcy conditions. Journal of Environmental Management 292: 112807, https://doi.org/10.1016/j.jenvman.2021.112807.

Geomorphological estimates of orogenic uplift based on fluvial relief types in the Bohemian Massif

†Břetislav Balatka, Jan Kalvoda*, Tereza Steklá

Charles University, Faculty of Science, Department of Physical Geography and Geoecology, Prague, Czechia
* Corresponding author: kalvoda@natur.cuni.cz

ABSTRACT

This article presents research results regarding geomorphological topics investigated by the late RNDr. Břetislav Balatka, CSc. (1931–2025) and his colleagues in recent years. It primarily focuses on the classification of fluvial relief types and their relationship to the extent and rate of tectonic uplift of morphostructural units in the Bohemian Massif, Czechia.

The morphogenetic diversity of fluvial relief types of the Bohemian Massif is a consequence of the synergy between differential tectonic uplift induced by the ongoing Alpine orogeny and the variability of exogenous processes caused by pronounced climatic changes during the Cenozoic. The extent of vertical tectonic movements of morphostructural units in the Bohemian Massif, determined based on types of fluvial relief, reaches values on the order of 10^1–10^3 m over the Late Cenozoic. These represent minimum values for tectonic uplift in the Bohemian Massif. This approximate estimation is based on the substantial erosion and denudation of its landforms, including planation surfaces of various origins and age, and fluvial sediments of river terrace systems, under the influence of intensive climate-morphogenetic processes. Moreover, significant epigenetic and antecedent deepening of river valleys took place only from the late Middle Pleistocene. The fluvial sediments of river terraces I and II of the main streams were deposited during the Cromerian Complex period, while river terrace III was deposited during the Elsterian glaciation.

KEYWORDS

landform evolution; fluvial relief types; orogenic uplift; the Bohemian Massif; Late Cenozoic

Received: 10 October 2025
Accepted: 5 March 2026
Published: 7 April 2026

Balatka, B., Kalvoda, J., Steklá, T. (2026): Geomorphological estimates of orogenic uplift based on fluvial relief types in the Bohemian Massif. AUC Geographica 61(2), 210–240
https://doi.org/10.14712/23361980.2026.5
© 2026 The Authors. This is an open-access article distributed under the terms of the Creative Commons Attribution License (https://creativecommons.org/licenses/by/4.0).

1. Introduction

1.1 Aims of the study

The study focuses on the results of research into one of the geomorphological topics that RNDr. Břetislav Balatka, CSc. (*11. 1. 1931 – †15. 2. 2025) and his colleagues have been working on in recent years. It mainly concerns determining the types of fluvial relief and their relationship to the extent of tectonic uplift of the morphostructural units in the Bohemian Massif. The solution consists in a combination of the created geomorphological division of the Bohemian Massif, the historical-genetic classification of its fluvial relief types, and research into the evolution of landforms in selected regions in Czechia. A comprehensive interpretation of the above-mentioned data sets and findings then enabled the preparation of a map showing the extent of tectonic uplift of morphostructural units in the Bohemian Massif in regions with fluvial relief types from the Upper Miocene to the present. By presenting this research work, we commemorate the creative spirit of Břetislav Balatka on the occasion of the 95th anniversary of his birth.

1.2 A brief reminder of the scientific work of Břetislav Balatka

The diverse trajectories of Břetislav Balatka's professional and personal life were closely connected with the Czech landscape. The results of his natural science research are a classic part of the intellectual wealth of Central European geography (Přibyl 2001; Kalvoda 2011, 2016 and Appendix 1). In the last period of his active work at the Department of Physical Geography and Geoecology of the Faculty of Science, Charles University, Břetislav Balatka focused primarily on the further development of selected thematic areas that are currently relevant in the international context of the development of geomorphology and physical geography.

He continued research on river terraces and the evolution of fluvial valleys in Czechia, as well as the study of methodological and morphogenetic aspects of regional geomorphological mapping. He also focused on the morphostructural and climate-morphogenetic evolution of specific types of georelief in the Bohemian Massi in the late Cenozoic. Břetislav Balatka contributed decisively to the conceptual framework and elaboration of the morphostructural regionalisation of the Czech part of the Bohemian Massif (according to the geomorphological terminology the Česká vysočina Highland; Balatka 2003; Balatka and Kalvoda 2006a), as well as to physical-geographical research in the central part of the Sázava River drainage basin and in the Prague area (Balatka 2007; Kalvoda and Balatka 2016). Furthermore, he continued the comprehensive interpretation of long-term geomorphological research in the Ohře (Eger) River drainage basin (Balatka and Kalvoda 2018; Balatka et al. 2019). These regional studies were carried out with the aim of identifying signatures of the late Quaternary tectonic activity, slope movements, and related types of natural hazards.

Břetislav Balatka's fundamental achievement was the completion of a detailed classification of the georelief of the Bohemian Massif, presented in both text and cartographic form at a scale of 1:500,000 (Balatka and Kalvoda 2006a, 2006b), including the determination of morphographical and morphogenetic types of georelief. The catastrophic floods in the Czechia were, for Břetislav Balatka, one of the impulses for further extensive research of river accumulation terraces in Central Europe. Regional river terrace systems and the evolution of the Sázava and Želivka valleys were studied (e.g., Balatka and Štěpančíková 2006; Balatka 2007; Balatka and Kalvoda 2010a, 2010b), including their parallelisation with the river terrace systems of the Vltava and Labe rivers (Balatka and Kalvoda 2008, 2010c).

Břetislav Balatka devoted considerable attention to the current topic of the correlation between the morphostratigraphy of river accumulation terraces in the Bohemian Massif and the European sequence of the chronostratigraphic division of the Quaternary (Balatka et al. 2010a, 2010b, 2015, 2019). The original results of his research also testify to the fact that the Bohemian Massif is one of the key regions for understanding the interplay between orogenetic activity and climate-morphogenetic processes during the evolution of the natural environment of Europe.

1.3 Motivation for the topic

In physical-geographical and geological publications, there is broad consensus and tradition that the current morphostructures of the Bohemian Massif were formed by neotectonic processes during the Cenozoic (e.g., Balatka et al. 1983; Chlupáč et al. 2002; Demek et al. 2007, 2009; Grygar 2016), predominantly during the Neogene phases of the Alpine orogeny and partly also in the Quaternary. The fundament of the current georelief of the Bohemian Massif was the Paleogene planation surface (Balatka 1968; Malkovský 1975, 1979; Král 1985; Kovanda et al. 2001), which was progresively broken up by differential tectonic movements, including subhorizontal displacements. uplift and subsidence. The long-term trend of differentiated tectonic uplift of the morphostructural units of the Bohemian Massif, whose boundaries are often defined by pronounced fault scarps, continues to prevail over relative subsidence even at present.

The geomorphology of the Czech lands is highly diverse, which is mainly caused by their location on the northern edge of the Alpine-Carpathian orogenic zone between the African and European continental plates (Pharaoh 1999; Chlupáč et al. 2002; Cháb et al. 2007, 2008). Morphostructural analyses of the

Hercynian crystalline rocks of the Bohemian Massif have shown (cf. Balatka and Kalvoda 2006a, 2010a; Demek et al. 2009; Pánek and Hradecký Eds. 2016) that its individual parts responded to Alpine orogenetic processes in varied ways. Several phases of tectonic activity during the Tertiary led to the formation of the ridge and graben structure of the Bohemian Massif and to the uplift of its marginal mountain ranges (Ivan 1999; Ivan et al. 2000; Pánek and Kapustová 2016). Older planation surfaces were reshaped by neotectonic processes, uplifted to various elevations and simultaneously subjected to deep erosion and denudation. Substantial paleoclimatic changes during the Cenozoic (e.g., Přibyl 1972; Ložek 1973; Kopecký and Cílek 1998; Ložek et al. 2003; Hradecký and Brázdil 2016) further controlled the variability of exogenous geomorphological processes in Central Europe.

The Paleogene planation surface was mainly of an etchplain character (Král 1966, 1968; Demek 2004) with variously strong weathering of crystalline rocks, deep igneous rocks, and Mesozoic sediments of the Česká tabule Table. The fragmentation of the Paleogene planation surface probably increased from the area of today's central part of the Česká tabule Table toward the south and southwest. Collisional stresses associated with the Alpine orogeny on the Hercynian block of the Bohemian Massif caused undulation and flexural deformation of its originally flat surface, including the reactivation of older fault zones. As a result, neotectonic structures of the Bohemian Massif developed in the form of anticlines, synclines, escarpments, faults and tectonic trenches.

It should be noted that the morphostructural principles of the development of the Bohemian Massif had been already studied by Daneš (1913), Dědina (1914) and Moschelesová (1923, 1930), including the identification of fundamental tectonic zones trending NW–SE, SW–NE, and N–S. A more detailed arrangement of geomorphological units was subsequently established on these primary megastructures, usually in combinations of the above-mentioned main tectonic zones (Hrádek and Ivan 1972, 1974; Coubal 1989; Coubal and Adamovič 2000). Examples include the mosaic pattern of geomorphological units in the Šumava subprovince (Fig. 1), the alternation of anticlines and synclines within the Česká tabule Table and in the Brněnská vrchovina Hill Country, where horsts and grabens were formed.

The Sudeten direction of tectonic zones (NW–SE) (Cymerman 1999; Danišík et al. 2010, 2012) is particularly evident in the arrangement of morphostructural units of the Krkonoše-Jizera subprovince, the Šumava subprovince, in the northern part of the Českomoravská vrchovina Highland (e.g., Železné hory Mountains, Hornosvratecká vrchovina Hill Country), in the area of the so-called Central Bohemian Threshold and in the distinctive concave units of the Labe (Elbe) basins and South Bohemian basins (Fig. 1; Balatka and Kalvoda 2006a). The Krušné hory Mountains direction of tectonic zones (SW–NE) prevails in the morphostructures of the Krušnohorská subprovince (Balatka and Sládek 1975; Vilímek 1993, 1997; Stolínová and Vilímek 2003), the Poberounská subprovince and in the Brněnská vrchovina Hill Country. The Jizera direction of tectonic lines (N–S) (Balatka 1958, 1966; Balatka and Sládek 1973; Zeman 1978; Balatka et al. 2000) is striking in the patterns of morphostructural units along the southeastern edge of the Česká tabule Table and in the southern part of the Českomoravská vrchovina Highland.

During the late Cenozoic, differential tectonic uplift and changes in climatic conditions significantly affected the development of the river network of the Bohemian Massif Gradually, substantial changes of drainage pattern occurred, accompanied by intensive epigenetic and antecedent development of river valleys, as well as by the reworking of large areas of fluvial deposition (Kunský 1929, 1966; Balatka and Sládek 1962a, 1963, 1970, 1974; Balatka et al. 1964, 1966; Ložek et al. 2004). The grain-size characteristics of Pliocene fluvial sediments in the Bohemian Massif is similar to those of Lower Pleistocene deposits (cf. Kunský 1929, 1966; Záruba 1942; Záruba and Rybář 1961; Kovanda et al. 2001). This similarity suggests that the Bohemian Massif already had a similar orographic arrangement as it has today.

The synergistic action of climate-morphogenetic processes and tectonic uplift have created Quaternary systems of river accumulation terraces in the valleys of the main streams of the Bohemian Massifd (e.g., Balatka and Sládek 1964, 1976; Balatka and Loučková 1992; Balatka et al. 2015, 2019). These fluvial sediments, together with other signatures of the antecedent development of river valleys (e.g., Mazáčová et al. 1963; Přibylová et al. 1967; Přibyl and Votýpka 1970; Balatka and Přibyl 1996, 1997), presents an important source of data on the history of the georelief of the Bohemian Massif. The briefly described paleogeographic aspects of the formation of morphostructural units are significantly reflected in the present-day orography of the Bohemian Massif. Consequently, they have traditionally provided a key impetus for development of geomorphological regionalisation schemes of landforms across the broader Central European region at the collisional contact of the Hercynian, Alpine and Carpathian orogens.

2. Methodology

2.1 Concept and types of geomorphological regionalisation

Geomorphological regionalisation involves the separation and delimitation of objectively existing territorial units of the Earth's surface relief according to defined criteria. In this analytical process, two

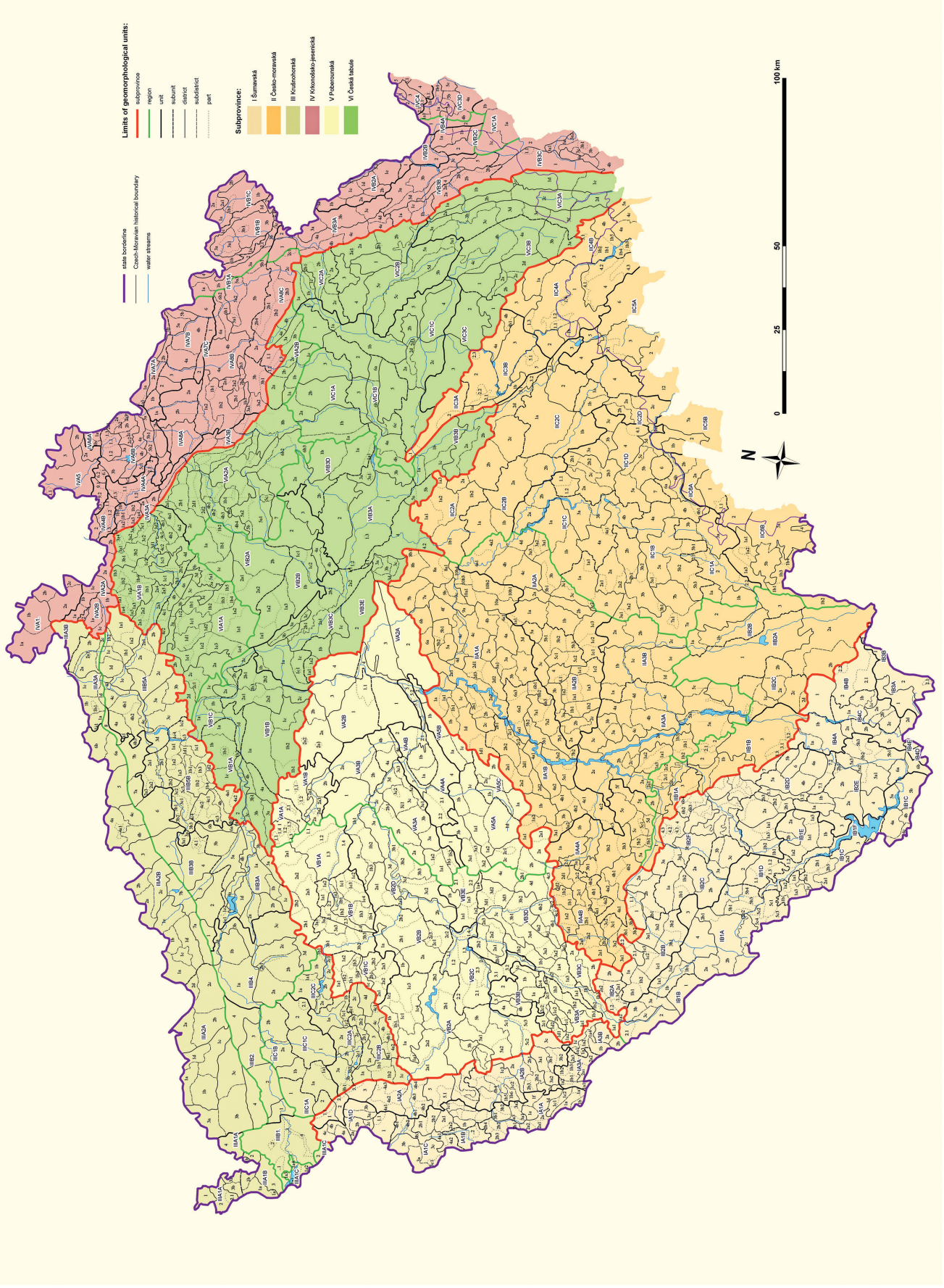

Fig. 1 Geomorphological units in the territory of Bohemian (Czech) part of the Bohemian Massif (the Česká vysočina Highland) ranging from subprovinces to subunits (adapted according to detailed maps and tables in Balatka and Kalvoda 2006a). Basic data on these geomorphological units are given in Tab. 1. Created by Břetislav Balatka, Jan Kalvoda and Tereza Steklá.

Tab. 1 Geomorphological regionalisation of the relief of Bohemia in the range from subprovince to subunit (modified after Balatka and Kalvoda 2006a).

Subprovince	Region	Unit	Subunit	Name of the geomorphological unit	Highest point [m a.s.l.]	Lowest point [m a.s.l.]	Amplitude span [m]
I				Šumavská subprovincie	1378	370	1008
I	A			Českoleská oblast	1042	370	672
I	A	1		Český les	1042	425	617
I	A	1	A	Čerchovský les	1042	425	617
I	A	1	B	Kateřinská kotlina	546	496	50
I	A	1	C	Přimdský les	894	450	444
I	A	1	D	Dyleňský les	940	470	470
I	A	2		Podčeskoleská pahorkatina	679	370	309
I	A	2	A	Tachovská brázda	679	420	259
I	A	2	B	Chodská pahorkatina	662	370	292
I	A	3		Všerubská vrchovina	751	405	346
I	A	3	A	Českokubická vrchovina	668	420	248
I	A	3	B	Jezvinecká vrchovina	751	405	346
I	B			Šumavská hornatina	1378	400	978
I	B	1		Šumava	1378	465	913
I	B	1	A	Šumavské pláně	1370	565	805
I	B	1	B	Železnorudská hornatina	1343	465	878
I	B	1	C	Trojmezenská hornatina	1378	560	818
I	B	1	D	Boubínská hornatina	1362	600	762
I	B	1	E	Želnavská hornatina	1228	693	535
I	B	1	F	Vltavická brázda	845	711	134
I	B	2		Šumavské podhůří	1096	385	711
I	B	2	A	Strážovská vrchovina	770	415	355
I	B	2	B	Svatoborská vrchovina	989	450	539
I	B	2	C	Vimperská vrchovina	922	455	467
I	B	2	D	Prachatická hornatina	1096	430	666
I	B	2	E	Českokrumlovská vrchovina	1066	485	581
I	B	2	F	Bavorovská vrchovina	700	385	315
I	B	3		Novohradské hory	1072	485	587
I	B	3	A	Pohořská hornatina	1072	570	502
I	B	3	B	Jedlická vrchovina	832	485	347
I	B	4		Novohradské podhůří	870	400	470
I	B	4	A	Kaplická brázda	753	400	353
I	B	4	B	Stropnická pahorkatina	696	400	296
I	B	4	C	Soběnovská vrchovina	870	430	440
I	B	4	D	Hornodvořišťská sníženina	721	555	166
I	B	4	E	Klopanovská vrchovina	824	648	176
II				Česko-moravská subprovincie	836	189	647
II	A			Středočeská pahorkatina	729	195	534
II	A	1		Benešovská pahorkatina	638	195	443
II	A	1	A	Dobříšská pahorkatina	546	195	351
II	A	1	B	Březnická pahorkatina	638	250	388
II	A	2		Vlašimská pahorkatina	723	285	438
II	A	2	A	Mladovožická pahorkatina	635	285	350
II	A	2	B	Votická vrchovina	723	350	373
II	A	3		Táborská pahorkatina	633	295	338
II	A	3	A	Písecká pahorkatina	633	295	338
II	A	3	B	Soběslavská pahorkatina	545	370	175

Subprovince	Region	Unit	Subunit	Name of the geomorphological unit	Highest point [m a.s.l.]	Lowest point [m a.s.l.]	Amplitude span [m]
II	A	4		Blatenská pahorkatina	729	380	349
II	A	4	A	Horažďovická pahorkatina	596	380	216
II	A	4	B	Nepomucká vrchovina	729	405	324
II	B			Jihočeské pánve	583	360	223
II	B	1		Českobudějovická pánev	480	360	120
II	B	1	A	Putimská pánev	466	360	106
II	B	1	B	Blatská pánev	480	375	105
II	B	2		Třeboňská pánev	583	370	213
II	B	2	A	Lomnická pánev	525	405	120
II	B	2	B	Kardašořečická pahorkatina	514	400	114
II	B	2	C	Lišovský práh	583	370	213
II	C			Českomoravská vrchovina	836	198	638
II	C	1		Křemešnická vrchovina	765	325	440
II	C	1	A	Jindřichohradecká pahorkatina	665	440	225
II	C	1	B	Pacovská pahorkatina	760	410	350
II	C	1	C	Želivská pahorkatina	633	325	308
II	C	1	D	Humpolecká vrchovina	765	355	410
II	C	2		Hornosázavská pahorkatina	650	210	440
II	C	2	A	Kutnohorská plošina	525	210	315
II	C	2	B	Světelská pahorkatina	601	320	281
II	C	2	C	Havlíčkobrodská pahorkatina	650	390	260
II	C	2	D	Jihlavsko-sázavská brázda	567	410	157
II	C	3		Železné hory	668	200	468
II	C	3	A	Chvaletická pahorkatina	450	200	250
II	C	3	B	Sečská vrchovina	668	270	398
II	C	4		Hornosvratecká vrchovina	836	340	496
II	C	4	A	Žďárské vrchy	836	340	496
II	C	4	B	Nedvědická vrchovina	774	350	424
II	C	5		Křižanovská vrchovina	706	375	331
II	C	5	A	Bítešská vrchovina	706	375	331
II	C	5	B	Brtnická vrchovina	683	455	228
II	C	6		Javořická vrchovina	836	455	381
II	C	6	A	Jihlavské vrchy	836	515	321
II	C	6	B	Novobystřická vrchovina	738	455	283
III				Krušnohorská subprovincie	1244	116	1128
III	A			Krušnohorská hornatina	1244	116	1128
III	A	1		Smrčiny	758	430	328
III	A	1	A	Ašská vrchovina	758	490	268
III	A	1	B	Hazlovská vrchovina	744	443	301
III	A	1	C	Chebská pahorkatina	656	430	226
III	A	2		Krušné hory	1244	270	974
III	A	2	A	Klínovecká hornatina	1244	420	824
III	A	2	B	Loučenská hornatina	994	270	724
III	A	3		Děčínská vrchovina	723	116	607
III	A	3	A	Děčínské stěny	723	116	607
III	A	3	B	Jetřichovické stěny	495	120	375
III	B			Podkrušnohorská oblast	934	140	794
III	B	1		Chebská pánev	534	413	121
III	B	2		Sokolovská pánev	573	355	218
III	B	3		Mostecká pánev	460	140	320

Subprovince	Region	Unit	Subunit	Name of the geomorphological unit	Highest point [m a.s.l.]	Lowest point [m a.s.l.]	Amplitude span [m]
III	B	3	A	Žatecká pánev	395	185	210
III	B	3	B	Chomutovsko-teplická pánev	460	140	320
III	B	4		Doupovské hory	934	275	659
III	B	5		České středohoří	837	125	712
III	B	5	A	Verneřické středohoří	726	125	601
III	B	5	B	Milešovské středohoří	837	142	695
III	C			Karlovarská vrchovina	983	360	623
III	C	1		Slavkovský les	983	360	623
III	C	1	A	Kynžvartská vrchovina	983	420	563
III	C	1	B	Hornoslavkovská vrchovina	883	360	523
III	C	1	C	Bečovská vrchovina	817	450	367
III	C	2		Tepelská vrchovina	847	415	432
III	C	2	A	Toužimská plošina	847	555	292
III	C	2	B	Bezdružická vrchovina	762	415	347
III	C	2	C	Žlutická vrchovina	734	445	289
IV				Krkonošsko-jesenická subprovincie	1602	208	1394
IV	A			Krkonošská oblast	1602	208	1394
IV	A	1		Šluknovská pahorkatina	610	294	316
IV	A	2		Lužické hory	793	290	503
IV	A	2	A	Lužický hřbet	793	300	493
IV	A	2	B	Kytlická hornatina	760	290	470
IV	A	3		Ještědsko-kozákovský hřbet	1012	263	749
IV	A	3	A	Ještědský hřbet	1012	263	749
IV	A	3	B	Kozákovský hřbet	744	263	481
IV	A	4		Žitavská pánev	593	235	358
IV	A	4	A	Liberecká kotlina	593	312	281
IV	A	4	B	Hrádecká pánev	445	235	210
IV	A	5		Frýdlantská pahorkatina	572	209	363
IV	A	6		Jizerské hory	1124	280	844
IV	A	6	A	Smrčská hornatina	1124	400	724
IV	A	6	B	Jizerská hornatina	1122	280	842
IV	A	7		Krkonoše	1602	440	1162
IV	A	7	A	Krkonošské hřbety	1602	620	982
IV	A	7	B	Krkonošské rozsochy	1423	470	953
IV	A	7	C	Vrchlabská vrchovina	809	440	369
IV	A	8		Krkonošské podhůří	835	265	570
IV	A	8	A	Železnobrodská vrchovina	835	265	570
IV	A	8	B	Podkrkonošská pahorkatina	673	305	368
IV	A	8	C	Zvičinsko-kocléřovský hřbet	671	285	386
IV	B			Orlická oblast	1115	285	830
IV	B	1		Broumovská vrchovina	880	351	529
IV	B	1	A	Žacléřská vrchovina	880	365	515
IV	B	1	B	Polická vrchovina	828	375	453
IV	B	1	C	Meziměstská vrchovina	880	351	529
IV	B	2		Orlické hory	1115	419	696
IV	B	2	A	Deštenská hornatina	1115	546	569
IV	B	2	B	Mladkovská vrchovina	765	419	346
IV	B	2	C	Bukovohorská hornatina	995	440	555
IV	B	3		Podorlická pahorkatina	835	285	550
IV	B	3	A	Náchodská vrchovina	835	285	550

Subprovince	Region	Unit	Subunit	Name of the geomorphological unit	Highest point [m a.s.l.]	Lowest point [m a.s.l.]	Amplitude span [m]
IV	B	3	B	Žamberská pahorkatina	658	310	348
IV	B	3	C	Moravskotřebovská pahorkatina	626	305	321
IV	B	4		Kladská kotlina	610	434	176
IV	B	4	A	Králická brázda	610	434	176
IV	C			Jesenická oblast	1491	208	1283
IV	C	1		Zábřežská vrchovina	714	228	486
IV	C	1	A	Drozdovská vrchovina	714	287	427
IV	C	3		Hanušovická vrchovina	1003	236	767
IV	C	3	D	Branenská vrchovina	1003	320	683
IV	C	4		Králický Sněžník	1423	520	903
V				Poberounská subprovincie	865	170	695
V	A			Brdská oblast	865	170	695
V	A	1		Džbán	537	255	282
V	A	1	A	Ročovská vrchovina	536	255	281
V	A	1	B	Řevničovská pahorkatina	537	285	252
V	A	2		Pražská plošina	434	170	264
V	A	2	A	Říčanská plošina	410	180	230
V	A	2	B	Kladenská tabule	434	170	264
V	A	3		Křivoklátská vrchovina	721	220	501
V	A	3	A	Zbirožská vrchovina	721	220	501
V	A	3	B	Lánská pahorkatina	488	223	265
V	A	4		Hořovická pahorkatina	499	190	309
V	A	4	A	Hořovická brázda	490	190	300
V	A	4	B	Karlštejnská vrchovina	499	210	289
V	A	5		Brdská vrchovina	865	192	673
V	A	5	A	Brdy	865	330	535
V	A	5	B	Hřebeny	660	192	468
V	A	5	C	Příbramská pahorkatina	667	390	277
V	B			Plzeňská pahorkatina	773	230	543
V	B	1		Rakovnická pahorkatina	677	230	447
V	B	1	A	Kněževeská pahorkatina	462	230	232
V	B	1	B	Žihelská pahorkatina	633	340	293
V	B	1	C	Manětínská vrchovina	677	395	282
V	B	2		Plaská pahorkatina	704	240	464
V	B	2	A	Stříbrská pahorkatina	704	330	374
V	B	2	B	Kaznějovská pahorkatina	597	300	297
V	B	2	C	Plzeňská kotlina	430	300	130
V	B	2	D	Kralovická pahorkatina	537	240	297
V	B	3		Švihovská vrchovina	773	300	473
V	B	3	A	Chudenická vrchovina	773	360	413
V	B	3	B	Merklínská pahorkatina	536	335	201
V	B	3	C	Klatovská kotlina	590	385	205
V	B	3	D	Radyňská pahorkatina	673	310	363
V	B	3	E	Rokycanská pahorkatina	575	300	275
VI				Česká tabule	696	141	555
VI	A			Severočeská tabule	696	150	546
VI	A	1		Ralská pahorkatina	696	150	546
VI	A	1	A	Dokeská pahorkatina	614	150	464
VI	A	1	B	Zákupská pahorkatina	696	238	458
VI	A	2		Jičínská pahorkatina	562	205	357

Subprovince	Region	Unit	Subunit	Name of the geomorphological unit	Highest point [m a.s.l.]	Lowest point [m a.s.l.]	Amplitude span [m]
VI	A	2	A	Turnovská pahorkatina	562	205	357
VI	A	2	B	Bělohradská pahorkatina	525	260	265
VI	B			Středočeská tabule	461	141	320
VI	B	1		Dolnooharská tabule	461	141	320
VI	B	1	A	Hazmburská tabule	418	150	268
VI	B	1	B	Řipská tabule	461	150	311
VI	B	1	C	Terezínská kotlina	211	141	70
VI	B	2		Jizerská tabule	410	155	255
VI	B	2	A	Středojizerská tabule	410	195	215
VI	B	2	B	Dolnojizerská tabule	320	155	165
VI	B	3		Středolabská tabule	400	156	244
VI	B	3	A	Nymburská kotlina	285	175	110
VI	B	3	B	Čáslavská kotlina	340	195	145
VI	B	3	C	Mělnická kotlina	247	156	91
VI	B	3	D	Mrlinská tabule	278	190	88
VI	B	3	E	Českobrodská tabule	400	168	232
VI	C			Východočeská tabule	692	199	493
VI	C	1		Východolabská tabule	351	199	152
VI	C	1	A	Cidlinská tabule	329	219	110
VI	C	1	B	Chlumecká tabule	351	202	149
VI	C	1	C	Pardubická kotlina	294	199	95
VI	C	2		Orlická tabule	451	230	221
VI	C	2	A	Úpsko-metujská tabule	360	235	125
VI	C	2	B	Třebechovická tabule	451	230	221
VI	C	3		Svitavská pahorkatina	692	208	484
VI	C	3	A	Českotřebovská vrchovina	692	270	422
VI	C	3	B	Loučenská tabule	657	248	409
VI	C	3	C	Chrudimská tabule	453	208	245

approaches are applied and combined, namely individual and typological regionalisation (see Balatka and Sládek 1989a, 1989b; Balatka and Kalvoda 2006a). Individual regionalisation represents a methodological approach that results in the determination of geomorphological units. Each unit has its individual characteristics, expressed, for example, by a name and code, which apply to a single territorial entity. In contrast, typological regionalisation applies a selected criterion to a larger number of units delimited on a map. The previously used orographic criteria considered only certain features of the Earth's surface, especially its topography and external appearance. A cartographic approach to the delimitation of orographical units was used especially by Kořistka (1885) and Kuchař (1955). By comparison, the geomorphological approach allows for the development of a comprehensive regionalisation of the georelief within the natural environment (Balatka and Sládek 1989a, 1989b).

The creation of geomorphological regionalisation of the Czech lands represents one of the traditional topics of Czech physical geography and cartography (e.g., Kořistka 1885; Kuchař 1955; Hromádka 1956; Balatka and Sládek 1989a, 1989b). In this regard, several important map series were published during the second half of the 20th century, by Balatka et al. (1971a, 1971b, 1973, 1975), Kudrnovská 1975, Kudrnovská and Kousal (1971, 1975a, 1975b), Czudek et al. (1972) and Demek et al. (1987). Based on the publications of the above-mentioned expert teams, a map of the Higher Geomorphological Units of the Czech Republic (1996) was subsequently compiled.

The aim of the geomorphological regionalisation of the georelief of the Bohemian Massif in the 1990s and early 21st century at the Department of Physical Geography and Geoecology of the Faculty of Science, Charles University, was to develop a taxonomy system of geomorphological classification and its cartographic representation on the base map of the Czech Republic at a scale of 1:500,000 (Balatka and Kalvoda 2006a; Fig. 1). In addressing this topic, Břetislav Balatka's expert team followed up on the results of previous geomorphological and cartographic works by Hromádka (1956), Czudek et al. (1972), Balatka et al. (1973, 1975) and Demek et al. (1987). Methodological

inspiration was also taken from maps and related text summaries of conceptual papers on individual and typological regionalisation of the georelief of Slovakia prepared by Mazúr and Lukniš (1978, 1979) and Mazúr (1979).

This comprehensive geomorphological approach enabled the detailed individual regionalisation of the georelief of Bohemia into a ten-level classification system, comprising the following taxonomic levels (Balatka and Kalvoda 2006a): system, subsystem, province, subprovince, region, unit, subunit, district, subdistrict, and part. However, only one province (the Česká vysočina Highland) is represented in the territory of Bohemia, which is part of a single subsystem (the Hercynian Mountains) and therefore also of a single system (the Hercynian system). Given the role of georelief as the main factor among the components of the natural environment (e.g., Ložek 1973; Czudek 1997, 2005; Demek et al. 2009), geomorphological regionalisation represents the fundamental framework for the regionalisation of other components of the landscape and also for the possibility of the development of comprehensive physical-geographic regionalisation.

Typological classification of relief, as another basic form of geomorphological regionalisation, consists of the determination and cartographical delimitation of main relief types according to certain classification principles. A relief type is a territory with a homogenous complex of landforms sharing the same morphographic features and similar genesis depending on the morphostructure with a similar paleogeographical history (Czudek et al. 1972; Balatka et al. 1975; Demek and Mackovčin Eds. 2006; Demek et al. 2007). The types of the georelief in the Bohemian Massif are primarily determined by the varying intensity of neotectonic movements as well as climate-morphogenetic processes during the Cenozoic. In orographic terms, these include mountains, highlands, hill countries, hills, plains in the form of plateaus or tables, and basins.

Higher mountains, characterised by stronger neotectonic uplift, reach altitudes of over 1,200 m a.s.l. in the Bohemian Massif, while the lower mountains mostly reach 900–1,200 m a.s.l. Mountains form a distinct border of the Česká vysočina Highland province in the Šumava, Krušnohorská and Krkonoše-Jizera subprovinces (Fig. 1), which is interrupted in the intermountain areas by the georelief of hill countries to hilly lands. The hill countries are characterised by a rugged relief with remnants of Neogene planation surfaces at altitudes of mostly 500–900 m (e.g., Král 1971, 1985; Votýpka 1975, 1997; Křížek 2001, 2006; Demek 2004). They were formed as relatively extensive foothills of mountains and occupy large areas in the central and upper parts of the Česká vysočina Highland province. Hilly lands are characterised by less undulation and more extensive Neogene planation surfaces at altitudes of up to 600 m a.s.l. (Balatka and Přibyl 1996, 1997; Kuncová 2005; Bláhová and Křížek 2007). Plains, plateaus and tables occur mainly in the territory of the Česká tabule Table and surround the tectonically conditioned basins of the Česká vysočina Highland province (Balatka et al. 1959, 2019; Lochman 1971; Lipský 1980; Balatka and Přibyl 1997; Steklá and Kalvoda 2024). Morphostructurally controlled basins represent a specific type of relief at various elevations. These basins in the Bohemian Massif are characterised by relative tectonic subsidence and are usually filled with predominantly Tertiary sediments.

The course of the boundaries of the geomorphological units of the Czech part of the Bohemian Massif largely reflects the varying morphographic character of their georelief (Fig. 1; Tab. 1). In mountainous areas and most hill countries and basins, these boundaries follow the course of more or less distinct foothill lines. Morphographic boundaries can also be defined by river valleys, e.g., in the case of asymmetric valleys in terms of height and/or slope; however, the breakthrough river valleys should not be used as boundary lines (Balatka et al. 1975; Balatka and Sládek 1989b). In flat and poorly dissected units (hilly lands, tables and plains), morphographic boundary is often defined as median line within transition zones of variable width, where landforms of adjacent units gradually merge. In such cases, the boundary separates genetically different types of georelief without clear topographic differences.

2.2 The strategy and course of research work

The dynamics of geomorphological evolution of a certain area can only be assessed and stratigraphically interpreted through broader regional correlations. We therefore started to compare the geomorphological findings from different parts of the relatively large Bohemian Massif only after several decades of gaining experience in physical-geographical research, both in Europe and in orogenetically active regions of the High Asian mountains (e.g., Kalvoda 1992a, 1993, 1998b, 2020). Conceptually and methodologically, our work also benefited from geomorphological studies in the Alpine zone of Europe from the Pyrenees to the Caucasus, especially in the Alps, Vosges, Western Carpathians, and the mountains of the Balkan Peninsula.

The morphostructural development of the Czech part of the Bohemian Massif was briefly described in the study by Kalvoda and Balatka (2006) as a part of Břetislav Balatka's map and tabular work on the geomorphological regionalisation (Balatka and Kalvoda 2006a). A contribution to understanding the evolution of river terrace systems of the Bohemian Massif are provided by studies that followed the fundamental works of Balatka and Sládek (1962a, 1962b, 1962c, 1965, 1975), Záruba et al. (1977), Tyráček (2001a, 2001b, 2010), Tyráček et al. (2004), Tyráček and Havlíček (2009). These further developed in publications

by Kalvoda and Balatka (1995), Přibyl (1999), Balatka and Přibyl (2003), Balatka and Kalvoda (2008, 2010a, 2010b, 2018) and Balatka et al. (2010b, 2015, 2019).

Together with a number of colleagues, we also studied the evolution of landforms in the contact area of the Stříbrská pahorkatina Hills, Tepelská vrchovina Hill Country and Tachovská brázda Furrow (Kalvoda 1966, 1980), then especially in the High Tatras (Kalvoda 1970, 1974, 1994, 1998a), the Moravian-Silesian Beskydy Mountains (Prášek 1985, 1993; Kalvoda and Prášek 1987, 1996), the Děčínská vrchovina Hill Country (Balatka and Kalvoda 1995), the Krkonoše Mountains (Mercier et al. 2000, 2002; Carr et al. 2002, 2007; Engel and Kalvoda 2002a, 2002b; Mercier et al. 2003; Bourlés et al. 2004; Braucher et al. 2006), the Orlické hory Mountains (Vaníčková 2004; Vaníčková and Kalvoda 2006a, 2006b), the Česká tabule Table (Engel and Kalvoda 2002a; Steklá and Kalvoda 2024) and in the Sázava River area (Štěpančíková 2003; Kalvoda 2005, 2007a; Balatka 2007; Balatka and Kalvoda 2010a, 2010b; Balatka et al. 2010a).

We have continuously applied the above geomorphological studies during engineering geological research of landslides and other types of slope movements (e.g., Kalvoda and Zvelebil 1983a, 1983b, 1989; Kalvoda et al. 1997; Rybář et al. 2000; Hartvich and Vilímek 2008; Vilímek et al. 2010) and with interpretation of geodetic and geophysical measurements of the Earth's surface movements. Geomorphological procedures could be used to address several topics: a) determination of the causes of movements of the Earth's surface detected by repeated geodetic measurements (e.g., Kalvoda and Pašek 1975; Kalvoda and Zeman 1979, 1982, 1983; Kalvoda 1995a, 1995b,1996a, 1996b; Kalvoda et al. 1990, 1994; Vilímek 1995; Vilímek et al. 2021); b) monitoring of movements in fault zones of the near-surface part of the rock massif, including seismic activity (Kalvoda and Košťák 1984; Kalvoda Ed. 1995a, 1995b; Košťák et al. 2000; Stemberk et al. 2000, 2010; Štěpančíková et al. 2008, 2010, 2018, 2019; Štěpančíková and Stemberk 2016); c) geomorphological aspects of Earth dynamics monitored by methods of space geodesy and geophysics (Kalvoda et al. 2004, 2013; Kostelecký et al. 2005; Klokočník et al. 2014).

We also gained valuable experience and knowledge during our teaching activities and geographical research in selected localities of the Bohemian Massif and the Western Carpathians, which we conducted with students and doctoral candidates of the Faculty of Science, Charles University. With regard to the topics of this paper, we refer, for example, to regional geomorphological studies by Šust (1981), Pánková (1995), Tomeček (2007), Hasenkopfová (2002), Soukupová (2008), Steklá (2012) and Halžová (2017) and studies on the development of fluvial landforms by Průša (1993), Čtyroký (1996), Lachmanová (1996), Novotná (1998), Hartvich (2002, 2008) and Mikisková (2009). References to other (published) research results by graduates in physical geography are provided throughout the present paper.

3. Results concerning orogenic uplift of the Česká vysočina Highland

3.1 The determination of the types of fluvial relief

An important geomorphological record of fluvial processes in the Bohemian Massif is provided by the extent and structure of river accumulation terraces. Therefore, alongside his research work on the historical-genetic geomorphological regionalisation of the Bohemian Massif (Balatka and Kalvoda 2006a), Břetislav Balatka prepared graphic manuscripts of two additional maps of this type, focused on the fluvial landforms. These original maps of fluvial relief types, river terraces, and erosion in relation to the morphostructures of the Bohemian Massif at a scale of 1:500,000 (Balatka 2006) represent a pilot solution to the current geomorphological topic. They depict varied regions classified by structure of fluvial sediments, their position in the longitudinal river profiles and the areal distribution of river accumulation terraces.

The main criterion is the extent of the river terrace system in the georelief of the Bohemian Massif, which provides a basis for understanding relationships to other landforms (Balatka and Kalvoda 2006b for details) and shows the intensity of erosion and denudation. From the above-mentioned manuscript maps by Břetislav Balatka, we have prepared the resulting map of fluvial relief types in relation to the morphostructures of the Bohemian Massif (Fig. 2). This thematic map also served as one of the key foundations for the subsequent stage of research, namely in creating a primary map of the extent of differential tectonic uplift of morphostructural units in the Bohemian Massif in the Late Cenozoic (Chapter 3.2).

The basis for the typification of the fluvial relief of the Bohemian Massif was the regional division into lower geomorphological units, down to the level of subunits (Fig. 1; Tab. 1). These units are morphostructurally and, to a certain extent, morphogenetically homogeneous areas that have been classified according to a defined typological legend. The classification criteria for fluvial relief types include ten morphogenetically specific regions, which are shown in Fig. 2 as coloured areas with Roman numerals. From a morphostructural point of view, the specified regions of fluvial relief types can be considered homogeneous units (Balatka 2006). These regions include both areas where river accumulation terraces are the dominant landforms, and erosion-denudation areas in which river terraces are limited to small localities or, except for valley floodplains, are completely absent. When evaluating the georelief of the Bohemian Massif according to the types of river terraces, their complete

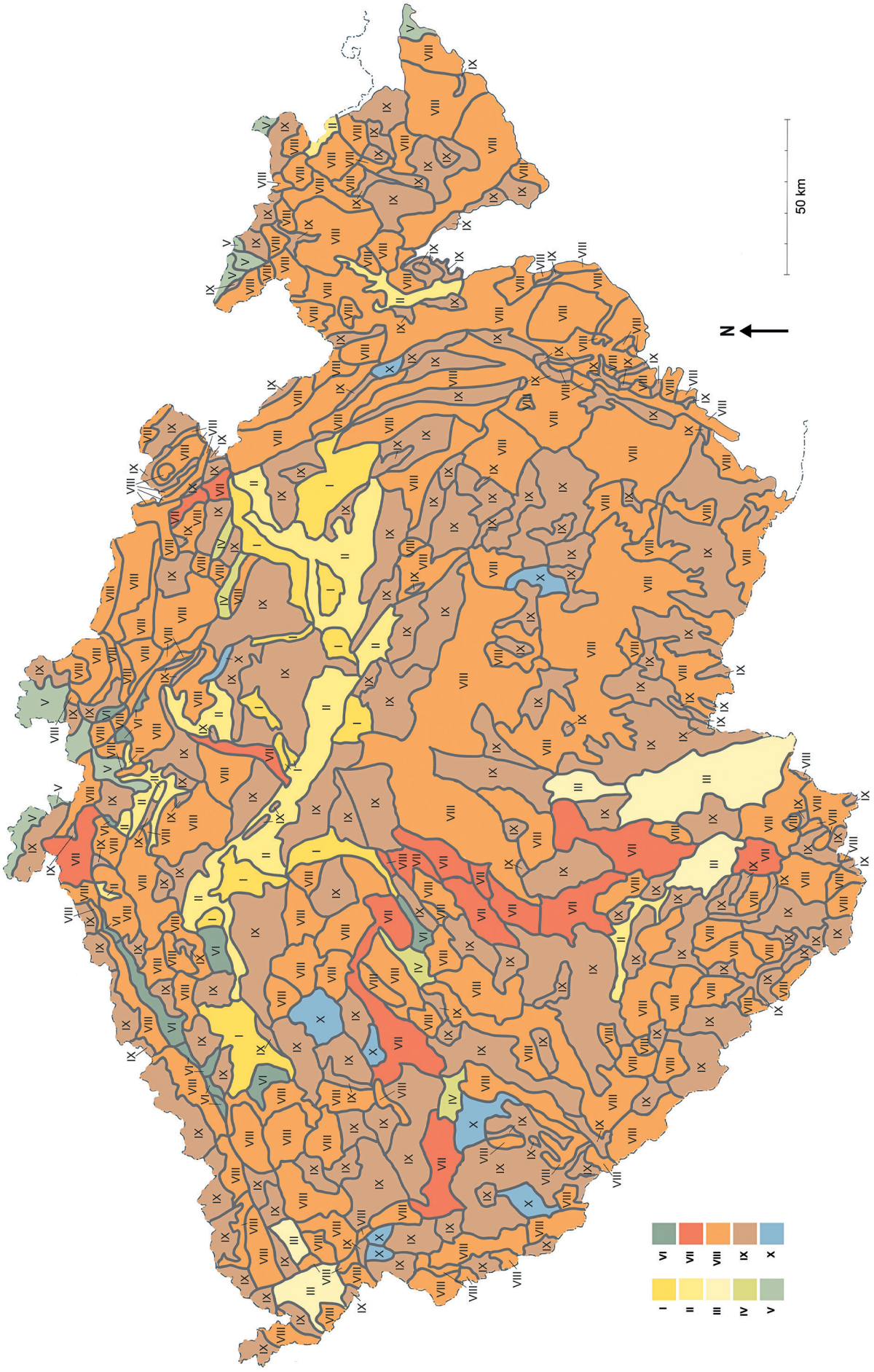
50 km
N
V VI VII IX X
I II III IV V

Fig. 3 Neovolcanic hill of Říp (461 m) is formed by a selectively denuded nephelinitic diatreme. The hill is surrounded by the Quaternary system of river accumulation terraces near the confluence area of the Labe (Elbe) and Vltava rivers. Photo Břetislav Balatka.

system was considered including relics of the oldest levels developed during the Lower Pleistocene.

The determination of the types of fluvial relief of the Bohemian Massif could be clearly represented cartographically (in the original scale of 1:500,000) only based on detailed research by Břetislav Balatka and his collaborators (Chapters 1.2 and 2.2). From a conceptual point of view, the papers of Balatka (1960, 1961, 2003), Balatka and Sládek (1962a, 1962b, 1975), Balatka et al. (1964, 1966), Balatka and Loučková (1992), Balatka and Kalvoda (1995, 2006a) should be mentioned. Morphogenetically, the most significant is Region I of the fluvial relief (Fig. 2), which includes an area with extensive Quaternary river terraces, with relative heights of their highest levels of 90–110 m above the present-day valley floors. The territories classified as Region I have a fluvial relief with the best-developed (and preserved) river accumulation terraces in the lower tabular and basin morpho-structural units of the northern part of the Bohemian Massif (e.g., Fig. 3). These are mainly the Východolabská, Středolabská, Dolnooherská, Orlická tabule Tables, as well as the Mostecká pánev Basin, the southern part of the Pražská plošina Plateau and the adjacent area of the Hořovická brázda Furrow (Balatka 2006; Balatka and Kalvoda 2006a).

Region II corresponds to the distribution of lower river terraces of predominantly Middle Pleistocene and Upper Pleistocene age (mostly up to a relative height of 20–25 m) and extensive valley floodplains. These ladnforms are preserved mainly in the basins of the Česká tabule Table (Terezínská,

Fig. 2 Types of fluvial relief in relation to morphostructures of the Bohemian Massif. The working scale of this thematic map is 1:500,000. According to the original manuscript maps and documentation of Břetislav Balatka (2006) adapted and drawn by Jan Kalvoda and Tereza Steklá. Regions of fluvial erosion and accumulation relief: Region I (deep yellow colour): Lowlands, lower plateaus and hilly lands with accumulation-erosion relief of extensive river terraces of a complete system with relative heights of up to 90–110 m. Region II (yellow): Lowlands with accumulation-erosion relief of mainly Middle and Upper Pleistocene river terraces up to a relative height of 20–25 m and extensive valley floodplains. Region III (orange): Higher-lying basins with accumulation-erosion to erosion-accumulation relief of river terraces up to a relative height of mostly 30–40 m and extensive valley floodplains. Region IV (light green): Basins with denudation and erosion-accumulation relief of less extensive river terraces up to a relative height of mostly 30–40 m. Region V (light blue): Lower hilly lands and basins influenced by continental glaciation with erosion-denudation relief including Middle and Upper Pleistocene river terraces to a relative height of mainly 30 m. Region VI (green): Basins with accumulation relief of extensive proluvial and fluvial cones, commonly incorporated into river terraces. Region VII (orange): Hills and hilly lands with erosion-denudation relief, with deeply incised valleys, and spatially limited river terraces up to a relative height of 50–90 m, diverging downstream. Region VIII (light orange): Erosion-denudation relief of tables, hilly lands, hill countries and mountains with deeply incised valleys without river terraces, or only with small relics of fluvial sediments. Region IX (brown): Erosion-denudation relief of tables, hilly lands, hill countries and mountains with shallow or widely open valleys, without river terraces or with only limited remnants of low-level terraces. Region X (deep blue): Lowlands and hilly lands with erosion-denudation relief and extensive occurrences of Neogene fluvial or limnic-fluvial sediments.

Mělnická, Nymburská, Čáslavská, Pardubická, Českolipská, Jestřebská, Mnichovo-hradišťská and Mladoboleslavská pánev Basins). Region II is occasionally represented in some other depressions, e.g., in the north-western headland of the Českobudějovická pánev Basin, the Děčínská pánev Basin, the Mohelnická brázda Furrow, and in the Opavická niva Floodplain and the Albrechtická kotlina Basin in the Jindřichovická pahorkatina Hills in Silesia (Balatka 2006).

Region III consists of fluvial relief with Pleistocene river terraces reaching a relative height of mostly 30–40 m and extensive valley floodplains in Tertiary and Cretaceous basins (with the exception of the Mostecká pánev Basin), namely in the Chebská and Sokolovská pánev Basins (Svatavská pánev Basin), in the central part of the Českobudějovická pánev Basin (Blatská pánev Basin) and in the Třeboňská pánev Basin. The Pleistocene river terraces of Region IV are in a similar position in the territory of some other depressions of structural origin. These are the northern part of the Plzeňská pánev Basin (Touškovská pánev Basin), the central part of the Hořovická brázda Furrow (Zdická brázda Furrow) and the Miletínský úval Graben and the Královédvorská pánev Basin (Balatka and Kalvoda 2006a, 2006b).

Region V corresponds to areas affected by or influenced by continental glaciation during the Quaternary. River accumulation terraces of Pleistocene age are developed here at lower relative heights, in two stages: a) up to 40 m (mainly from the Elsterian glaciation), b) up to 10–20 m (from the Saalian glaciation). These include the Šluknovská and Frýdlantská pahorkatina Hilly Land, the Hrádecká pánev Basin, the central part of the Zákupská pahorkatina Hilly Land, the Vidnavská nížina Lowland, part of the Žulovská nížina Lowland and the Osoblažská nížina Lowland.

Region VI includes areas with extensive Pleistocene proluvial and fluvial cones of various ages (Balatka 2006), which in places transition into river terraces at relative heights from several meters to several tens of meters. These are mainly the areas of the Chomutovsko-Teplická pánev Basin at the foot of the Krušné hory Mountains, the Pětipeská pánev Basin, the western part of the Liberecká pánev Basin, the Hostimická pánev Basin at the northern foot of the Hřebeny Hill Country, parts of the Podještědská and Českodubská pahorkatina Hilly Land at the foot of the Ještědský hřbet Ridge and the Klapská tabule Table between the České středohoří Mountains and the Ohře (Eger) River valley.

Region VII is characterised by the limited occurrence of river accumulation terraces of Pleistocene age at various relative heights, in places up to 90 m, often well expressed morphologically in deeply incised valleys of the hilly lands and hill countries. This region occupies striking strips along larger streams, namely along the Vltava in the Středočeská pahorkatina Hilly Land and in the southern parts of the Pražská plošina Plateau, as well as along the Mže River in the Stříbrská pahorkatina Hilly Land, along the Berounka River between Pilsen and Řevnice, along the lower Lužnice, Otava and Sázava rivers in the Středočeská pahorkatina Hilly Land, along the Jizera River in the Jizera tabule Table and along the Úpa River in the Krkonoše Mts. foothills (Balatka 2006; Balatka and Kalvoda 2006b).

Region VIII is represented by tectonically more strongly uplifted areas without river terraces or with sporadic relics of fluvial sediments. These are mainly geomorphological units with deeply incised valleys in the mountains, highlands and hilly lands, including the sandstone areas of the Česká tabule Table. Region IX represents tectonically less uplifted area with sporadic occurrence of fluvial sediments in shallow and widely open valleys of hilly lands, tables and basins or in hill countries and mountains with extensive relics of Tertiary planation surfaces (Fig. 4).

Region X is characterised by areas with substantial relics of Neogene fluvial and limnic sediments, located

Fig. 4 Part of an abandoned valley of the Sázava river near Chabeřice, infilled by fluvial sediments of the III. river terrace up to 25 m thick. Photo Břetislav Balatka.

in shallow valleys with low levels of river accumulation terraces. These include, for example, parts of the Podčeskoleská and Plzeňská pahorkatina Hilly Lands, as well as the Jihlavsko-sázavská brázda Furrow, the Čeremenská pahorkatina Hilly Land near Lanškroun, and the Velišský hřbet Ridge in the Turnovská pahorkatina Hilly Land.

A specific aspect of determining the types of fluvial relief of the Bohemian Massif, as expressed in the maps of Balatka (2006), is the possibility of deriving the approximate intensity of erosion and denudation during the Late Cenozoic. Balatka (2006) classified the extent of this reduction of the georelief on a scale from very strong intensity (exceeding 200 m) to very weak intensity (below 50 m) of the effects of erosion-denudation processes. However, the values given should be considered indicative only (Balatka and Kalvoda 2006b), because the maximum intensity of erosion and denudation in the defined morphostructural units of the Bohemian Massif is often restricted to narrow strips of territory along larger watercourses and to the lower reaches of their tributaries. On the contrary, in neighbouring areas (e.g., watershed zones), the values of erosion and denudation of the georelief estimated using this approach are significantly lower.

3.2 The extent of the vertical component of tectonic movements

The evaluation of the pattern of fluvial relief types in the Bohemian Massif (Fig. 2) and the relevant professional literature show that, mainly due to the influence of neotectonic movements, significant changes occurred in the structure of the river network, the courses of watersheds of various orders, and the deepening of valleys during the Late Cenozoic. Therefore, we focused on comparing the river terrace systems of the main streams (especially) in the central part of the Bohemian Massif and specifying their stratigraphical position in the current Quaternary subdivision (International Commission on Stratigraphy 2007; Gibbard et al. 2008, 2010). The results of these regional research efforts are collected in a series of studies by Balatka and Kalvoda (2008, 2010a, 2010b, 2010c, 2018), Balatka et al. (2010a, 2010b, 2015, 2019) and Steklá and Kalvoda (2024). The gradually acquired palaeogeographical knowledge was the basis for identifying the geomorphological record of differential tectonic uplift and (relative) subsidence of the main morphostructural units in the Bohemian Massif. In the subsequent stage of research, following up on the determination of fluvial relief types within the morphostructures of the Bohemian Massif (Fig. 2), we focused on identifying and graphically expressing the extent of the vertical component of tectonic movements during the Late Cenozoic.

When classifying the morphostructural units of the Bohemian Massi (to the level of subunits; Tab. 1) into the categories by the extent of tectonic uplift, we evaluated the geomorphological conditions of these areas, including the current elevation of planation surfaces of various types and ages (cf. Fig. 5 and Fig. 6). Their gradual development and long-term transformation by weathering and denudation processes represent a period of relative tectonic stability in the paleogeographical history of the Bohemian Massif (e.g., Král 1985; Demek 2004; Kalvoda and Balatka 2006a). Morphometrical data were obtained from topographical maps mostly of the scale 1:50 000. The approximate extent of the reduction in the thickness of the weathered material and rock assemblages was derived from data on the relative height of the relics of the oldest river terraces (e.g., Fig. 5), as well as from the elevation of the Upper Miocene planation surface and the surface of Neogene sediments.

It should be noted that the process of exhumation of crystalline rocks of the deeper part of the Earth's crust and the planation surfaces of the Bohemian Massif of various origins and ages has received considerable attention in the geomorphological and geological literature (e.g., Demek et al. 1965; Král 1968, 1971, 1985; Migoň 1999; Danišík et al. 2010, 2012). The current valley network of Bohemian rivers is incised into the Upper Miocene planation surface to an extent that largely corresponds to differential neotectonic movements (Balatka and Kalvoda 2006b). This tectonic activity, with a predominance of spatially and temporally varied uplift (Fig. 6), together with the regimen of the streams, amount of transported material and the lithology of the bedrock, controlled the intensity of erosion and denudation processes during the Late Cenozoic.

We illustrated the extent of tectonic uplift of morphostructural units of the Bohemian Massif in regions of fluvial relief types from the Upper Miocene to the present on a thematic map (Fig. 7). The interpretation of the above-defined geomorphological data and the described methodological procedures for determining the extent of the vertical component of tectonic movements in the last ca. 10^7 years of the palaeogeographical history of the Bohemian Massif can, however, provide only an approximate quantitative estimate of the phenomenon under investigation. For this reason, we have distinguished only five classification levels on the thematic map (Fig. 7), representing areas with different intensities of neotectonic uplift. The extent of very strong tectonic uplift in the demarcated territories during the indicated period is approximately 900–1,200 m, while in areas with minor tectonic uplift it is only 50–150 m.

When determining the extent of tectonic uplift of morphostructural units of the Bohemian Massif, we relied on the depth of the Quaternary incision of river valleys (which is mostly 30–60 m, but often exceeds these values; Fig. 8) relative to the current elevation level of the originally Upper Miocene planation surface. However, we also assumed a certain

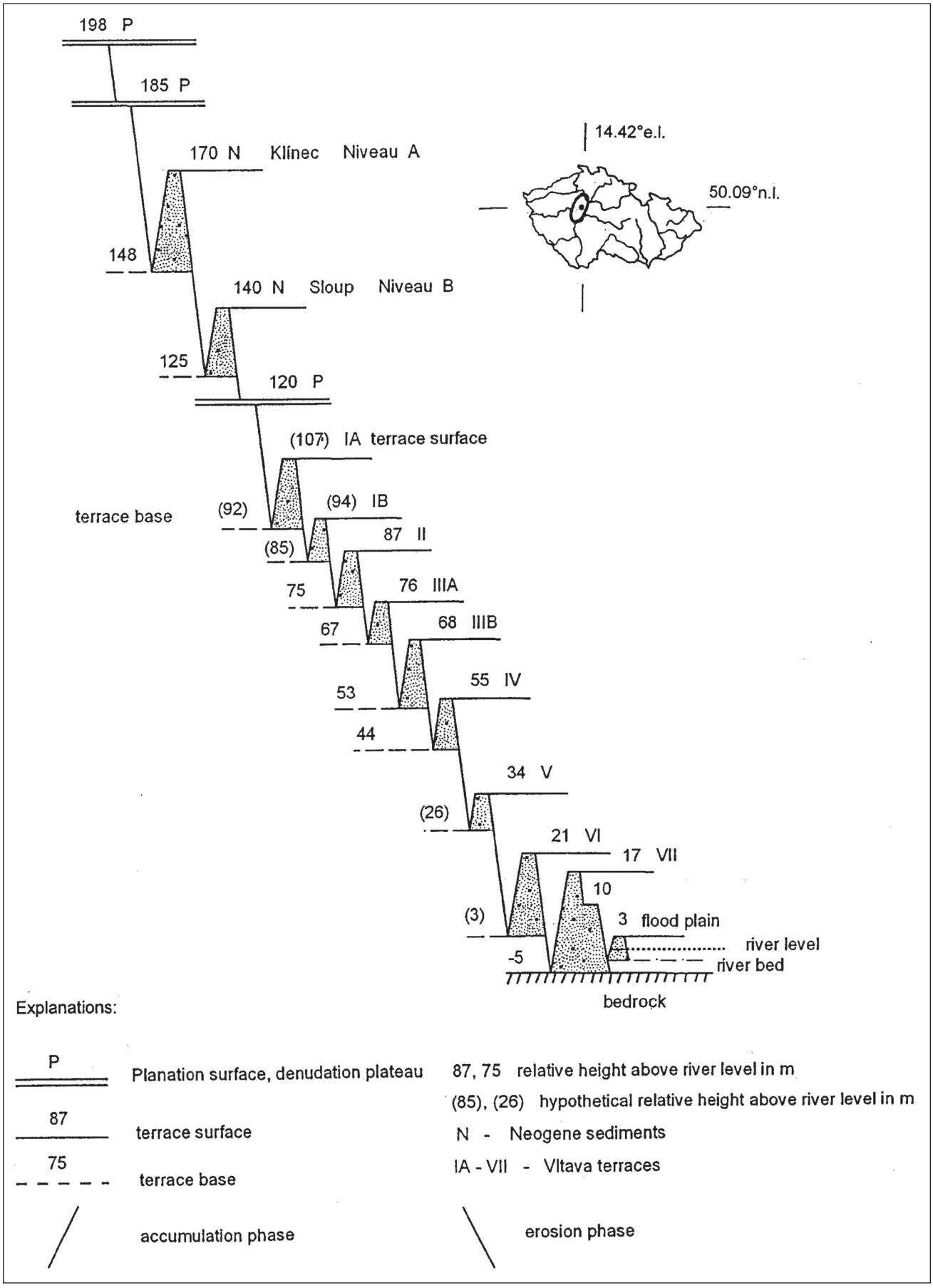

Fig. 5 River accumulation terraces in the Vltava valley between the mouths of the Sázava and Berounka rivers (modified after Balatka and Štěpančíková 2006; Balatka and Kalvoda 2010a). The morphostratigraphical correlation of river terraces is presented in Tab. 2.

reduction of this planation surface, by up to several tens of metres, which was preserved in a less disturbed form especially in the watershed areas. Regions with the highest intensity of tectonic uplift during the Late Cenozoic (red and brown colours in Fig. 7) should, under the above assumptions, correspond to both some of the most elevated areas (mountains and highlands) and areas with deeply incised valleys of larger watercourses in hill countries. Regions with less intense and weak tectonic uplift (green and yellow colours in Fig. 7) are typically lower-lying basins and furrows, structural tables and hilly lands. We emphasise that areas classified especially within categories characterised by weaker tectonic uplift may, in fact, have the character of relative subsidence due to the stronger uplift of adjacent morphostructural units.

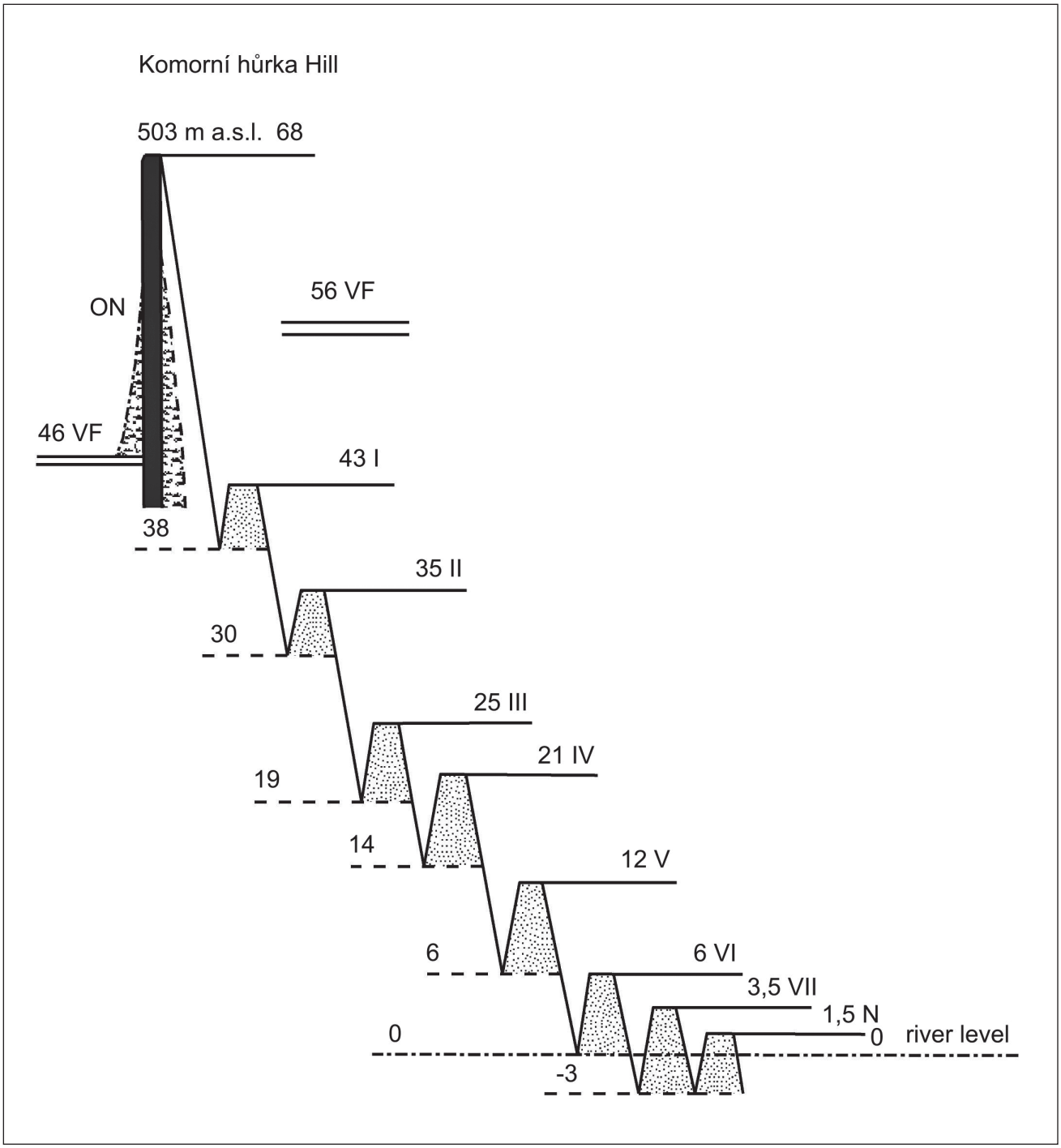

Fig. 6 Graphical scheme of successive incision of the river during the Ohře (Eger) valley evolution in the western part of the Chebská pánev Basin, river km 245–237 (Balatka and Kalvoda 2018; Balatka et al. 2019). Explanations: ON – olivine nephelinite and pyroclastic rocks of the Komorní hůrka Hill (with dated activity between 0.85 up to 0.26 Ma; Wagner et al. 1998); VF – the Vildštejn Formation: quartz micaschists, clay sand and gravel of the Upper Pliocene – Lower Pleistocene age; I–VII – Pleistocene river accumulation terraces; N – alluvium (floodplain); 8, 13, … – relative height above river level in metres. Graphical explanations are presented in Fig. 5.

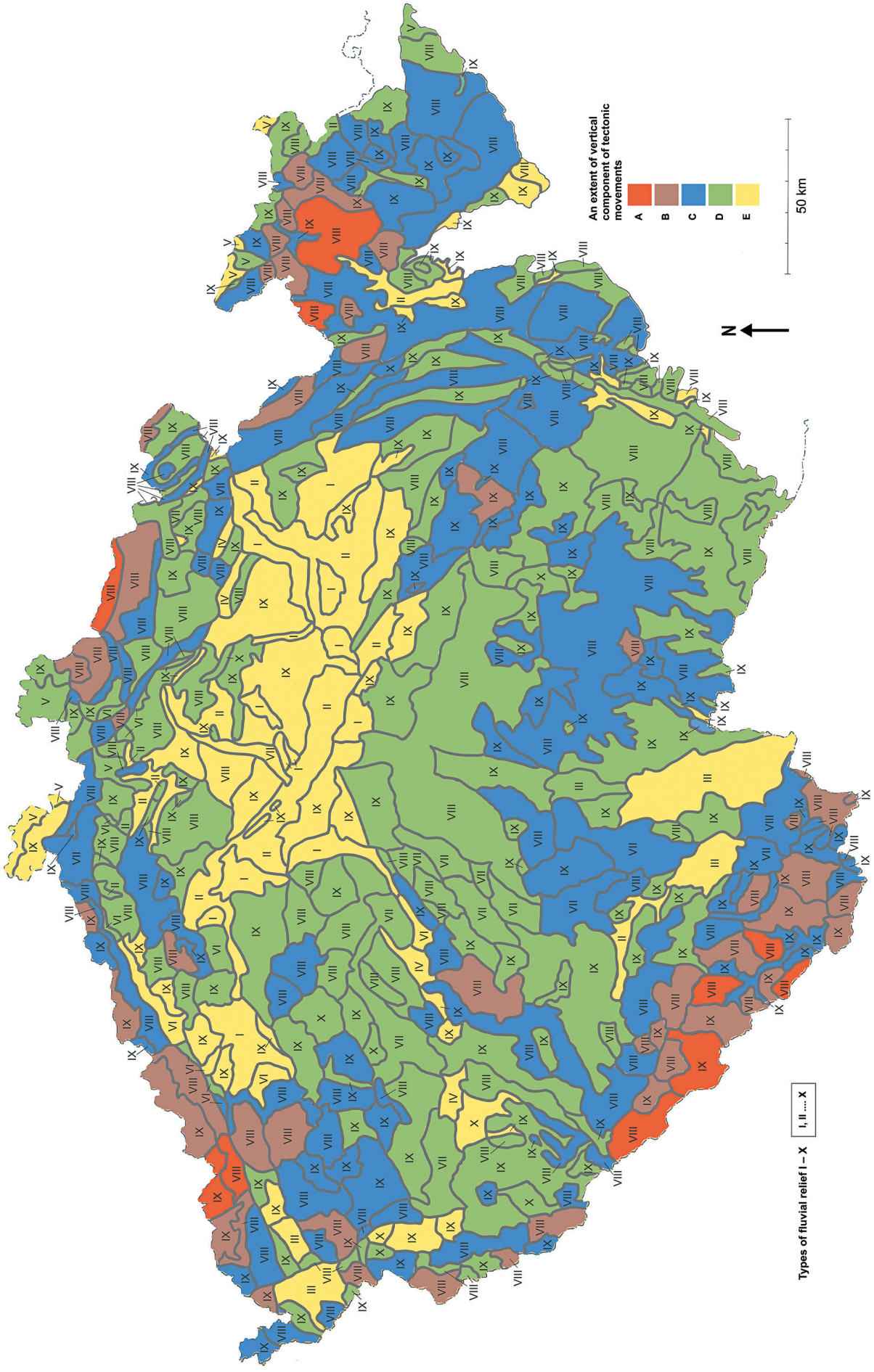
An extent of vertical component of tectonic movements
A
B
C
D
E
50 km
N
Types of fluvial relief I – X
I, II X

Fig. 8 The Labe (Elbe) River canyon developed in the Upper Cretaceus sandstones of the Děčínská vrchovina Highland during the Quaternary. Photo Jan Kalvoda.

The long-term trend of tectonic uplift of the Bohemian Massif is primarily a manifestation of the youngest Alpine collisional orogeny in Central Europe. The differentiation of morphostructural units of the Bohemian Massif took place in several phases, which significantly influenced the evolution of river valleys (Balatka and Kalvoda 2008; Balatka et al. 2015, 2019). For example, a comparison of the terrace systems of the Sázava, Vltava, Berounka and Labe (Elbe) rivers in the central part of Bohemia shows (Tab. 2) that significant epigenetic and antecedent deepening of the valleys took place as late as in the younger Middle Pleistocene (Balatka and Kalvoda 2008, 2010a; Tyráček and Havlíček 2009; Balatka et al. 2015). The fluvial sediments of river terraces I and II were formed during the Cromerian Complex, while terrace III was deposited during the Elsterian glaciation (Tab. 2).

It is important to note that the rate of tectonic uplift is not directly related to the conform rate of river incision. Deep erosion processes and the related bedrock valley development are determined by varied environmental changes of valley gradient, bed erodibility, catchment sediment production and discharge conditions. These factors include, in particular, valley slope, the resistance of bedrock to erosion, the quantity and lithological properties of weathered material and the nature of its transport, the hydrological regime, and precipitation-runoff conditions throughout the catchment area. Of these environmental factors, only an increased valley gradient may occur directly as a consequence of tectonic activity through regional uplift, flexuring, and faulting. As an example, the repeatedly increased incision of rivers can also be attributed to the increased intensity of periglacial processes during glacial stages in the Quaternary, namely frost weathering of rocks, regelation, solifluction phenomena, and related coarse detrital sediment supply. These climate-induced changes in the natural environment led to a significantly higher amount of material being carried by rivers and to a higher rate of subsequent fluvial sediment deposition. Given the combined effects of valley gradient, flow regime, bed

Fig. 7 The extent of tectonic uplift from the Upper Miocene to the present in regions of fluvial relief types of the Bohemian Massif. The working scale of the thematic map, till this time unpublished, is 1:500,000. Created by Břetislav Balatka, Jan Kalvoda and Tereza Steklá. Explanations: The extent of the vertical component of tectonic movements: A – area with very strong tectonic uplift (900–1,200 m); B – area with strong tectonic uplift (500–900 m); C – area with medium tectonic uplift (300–500 m); D – area with weak tectonic uplift (150–300 m); E – area with minor tectonic uplift (up to 150 m), or with relative tectonic subsidence. The types of fluvial relief in regions I–X are described in the explanations to Fig. 2.

Tab. 2 Chronostratigraphical correlation of river terrace deposits in the central part of the Česká vysočina Highland related to North-West European stratigraphical stages of the Quaternary (modified after Balatka et al. 2015).

Regional stratigraphical stage/substage divisions of the Quaternary (Gibbard et al. 2004, 2008, 2010)	SÁZAVA Balatka (2007), Balatka and Kalvoda (2010a)	BEROUNKA Balatka and Loučková (1992)	VLTAVA – LABE confluence area Balatka and Sládek (1962b)	VLTAVA Záruba et al. (1977)	VLTAVA and LABE system Tyráček (2001a, 2001b); Tyráček et al. (2004); Tyráček and Havlíček (2009)
Late Pleistocene Weichselian	Pikovice Terrace (VII)	Lipence Terrace (VIIa) Dobřichovice Terrace (VIIb)	Hostín Terrace (VIIa, b, c, d)	Maniny Terrace (VII)	Maniny Terrace (Weichselian) Hostín 1 Terrace
Middle Pleistocene Saalian (Warthe Stadial)	Poříčí Terrace (VI)	Kazín Terrace (VI)	Mlčechvosty Terrace (VIa, b, c)	Veltrusy Terrace (VI)	Veltrusy Terrace (Warthe)
Middle Pleistocene Saalian (Drenthe Sadial)	Městečko Terrace (V)	Liblín Terrace (Va) Poučník Terrace (Vb)	Cítov Terrace (a, Vb)	Dejvice Terrace (V)	Dejvice 1 and 2 Terrace (Drenthe)
Middle Pleistocene Saalian (Fuhne Stadial)	Týnec Terrace (IV)	Zbraslav Terrace (IVa) Hýskov Terrace (IVb)	Hněvice Hill Terrace (IV)	Letná Terrace (IV)	Letná Terrace (Fuhne)
Middle Pleistocene Elsterian	Buda Terrace (IIIb)	Srbsko Terrace (IIIb)	Straškov Terrace (IIIb)	Vinohrady Terrace (IIIB)	Vinohrady Terrace (Elster)
Middle Pleistocene Cromerian Complex (glacial c)	Chabeřice Terrace (IIIa)	Tetín Terrace (IIIa)	(IIIa)	Kralupy Terrace (IIIA)	Kralupy Terrace (Cromerian C)
Middle Peistocene Cromerian Complex (Glacial c)	Český Šternberk Terrace (II)	Pohořelec Terrace (IIa) Hlince Terrace (IIb)	Ledčice Terrace (II)	Pankrác Terrace (II)	Pankrác Terrace (Cromerian C)
Middle Pleistocene Cromerian Complex (Glacial b)	Hvězdonice Terrace (Ib)	Řevnice Terrace (Ib)		Suchdol Terrace (IB)	Suchdol Terrace (Cromerian B)
Middle Pleistocene Cromerian Complex (Glacial a)	Střechov Terrace (Ia)	Skryje Terrace (Ia)	Krabčice Terrace (I)	Lysolaje Terrace (IA)	Lysolaje Terrace (Cromerian A)
Early Pleistocene Bavelian (Dorst) Menapian			Rovné Terrace		Rovné Terrace (Dorst) Vráž Terrace (Menapian)
Early Pleistocene Eburonian – Menapian	Niveau B Radvanice	Niveau B		Zdiby Stadial (Pliocene)	Zdiby Terrace (Eburonian – Menapian)
Early Pleistocene Tiglian					Stříbrníky Terrace (upper Tiglian)
Neogene	Niveau A Bojiště	Niveau A		Klínec Stadial	

material load, bedrock exposure and erodibility, the formation and structure of river terrace systems give evidence to the evolutionary complexity and diversity of the natural environment.

The comparison of river terrace systems from different parts of the Bohemian Massif shows that the major rivers respond sensitively and therefore diversely to the local character and changes in morphostructural and climate-morphogenetic conditions (Balatka et al. 1964, 2010a, 2010b, 2015, 2019; Balatka and Sládek 1976; Balatka and Kalvoda 1995, 2008, 2018; Bridgland 2000; Tyráček et al. 2004; Tyráček and Havlíček 2009). However, stratigraphically significant indicators of large-scale (possibly global) changes in the environment during the Quaternary are very similar in their palaeogeographical record.

4. Discussion

The main current approaches to research into the geomorphological record of tectonic movements and related phenomena in the Bohemian Massif, carried out by several generations of physical geographers

and Quaternary geologists, can be described in the methodological context as follows:

Morphostructural, morphographical and morphogenetic analysis of planation surfaces of various genesis and age, their typological classification, determination of age and distribution, assessment of the effects of tectonic movements in their present-day elevation, and their relationship to the development of the valley system and palaeohydrological changes in the Late Cenozoic.

Geomorphological research of terrace systems of major Bohemian rivers, especially using the reconstruction method, and their integration into the continuously evolving international stratigraphical system of the Quaternary. This research includes, for example, geomorphological analysis of anomalies in the course of river accumulation terraces along longitudinal and transverse profiles, aimed at identifying the extent of discontinuities of the near-surface part of the Earth's crust caused by tectonic movements, and the influence of the bedrock lithology. It is also essential to address the relationship of fluvial relief to the relics of landforms of Quaternary continental and mountain glaciation. These topics have already been addressed in the Czech Republic by Šibrava (1972, 1979), Macoun and Králík (1975), Macoun (1985), Králík (1987), Engel (1996, 2004), Nývlt (1998, 1999, 2003, 2008), Růžička (2004), Engel et al. (2010) and Štor et al. (2019).

A comprehensive study of morphostructural signatures of neotectonic activity through the delineation of typologically homogeneous regions and the determination of historical-genetic relationships of planation surfaces and fluvial landforms in the Bohemian Massif. The described and presented geomorphological procedures can mainly detect tectonic uplift and subsidence. However, tectonic differentiation of morphostructural units in Central Europe, which gradually evolved from the Miocene up to the Quaternary, is one of manifestations of the latest phase of alpine orogeny. Geological structure of the Eastern Alps and the Western Carpathian systems gives evidence that subhorizontal tectonic movements prevailed during main phases of the collisional orogeny in the Cenozoic. The extension and course of related horizontal tectonic movements in the Bohemian Massif was studied, e.g., by Coubal (1989), Kopecký (1996), Coubal and Adamovič (2000), Štěpančíková and Stemberk (2004), Stemberk et al. (2010) and Štěpančíková et al. (2018, 2019).

Geomorphological analysis and monitoring of selected geodynamic processes and phenomena are significant trends in research on global changes in geographical systems. Special attention is paid to recent tectonic movements of the near-surface part of the Earth's crust and to the dynamics of current climate-morphogenetic processes, including natural hazards and risks. The nature of research in Earth sciences and the current needs of society suggest that these investigations in the Central Europe should be evaluated in relation to current knowledge about: 1) the state and development of European landscape and society, and 2) trends in global environmental changes (Kalvoda Ed. 2003; Drbohlav et al. 2004a, 2004b). Geomorphological research aims both at understanding the principles of dynamic behaviour of natural systems (Goudie and Kalvoda 1997, 2007a, 2007b), and at the necessary diagnosis of natural hazards, the prediction of catastrophic events, and the mitigation of risk situations such as rapid soil erosion, landslides, floods, and seismic phenomena (Kalvoda and Rosenfeld Eds. 1998; Demek et al. 2006; Langhammer Ed. 2008; Kalvoda and Novotná 2024).

The multidisciplinary study of tectonic movements in the Bohemian Massif during the Quaternary, including current tectonic activity (e.g., Hejl et al. 1997; Štěpančíková et al. 2008, 2010, 2018, 2019, 2022; Steklá et al. 2017; Stemberk Jb. 2021), is a very topical theme of geodynamic research of orogenetic processes and phenomena in Central Europe. Various approaches to assessing the extent of tectonic movements in the Bohemian Massif were described, e.g., in earlier studies by Kopecký (1970a, 1970b, 1972, 1973, 1983, 1986, 1989a, 1989b, 1996), Vyskočil (1975, 1984, 1988), Kalvoda and Pašek (1975), Kalvoda and Prášek (1987), Kalvoda and Zeman (1979, 1982, 1983), Kalvoda et al. (1990, 1994). Recent comprehensive approaches to the topic can be demonstrated, for example, by papers of Mrlina (2000), Bankwitz et al. (2003), Schenk et al. (2003), Hartvich (2005), Balatka and Kalvoda (2006, 2008), Stemberk et al. (2010, 2017) or Balatka et al. (2015, 2019).

The systematic efforts of expert teams to link research on the long-term development of landforms with current geomorphological processes and phenomena is continuously applied in the identification of geomorphological hazards and risks during the construction and operation of large engineering works (Kalvoda 1978, 1996a, 1996b, 1998a, 2007b; Zvelebil 1989; Stemberk 1994; Kalvoda and Mercier Eds. 1996; Demek et al. 2006; Kalvoda and Balatka 2016). In this regard, geomorphological studies focused on selected nuclear power plant sites in Central Europe have become again highly relevant (e.g., Kalvoda and Demek 1991; Demek and Kalvoda 1991, 1992; Kalvoda 1992b; Kalvoda and Stemberk 1993).

Currently, thematic emphases in projects focused on natural hazards are shifting from primary research into risk processes, their detection, monitoring and predicting (e.g., Štěpančíková and Stemberk 2004; Štěpančíková et al. 2008; Raška and Emmer 2014) toward efforts aimed at the controlled reduction or even elimination of environmental hazards and risks. This primarily involves prevention and development of resilient society, creating expert early-warning systems and the rapid deployment of rescue capacities when required. Furthermore, emphasis is placed on the essential importance of controlled mitigation of

cascading effects and understanding the variability of long-term impacts of catastrophic events on society.

5. Conclusions

The morphogenetic diversity of fluvial relief types in the Bohemian Massif (Fig. 2) is a consequence of the synergy between differential tectonic uplift induced by the continuing Alpine orogeny and the variability of exogenous processes caused by pronounced climatic changes during the Cenozoic. The extent of the vertical component of tectonic movements of morphostructural units of the Bohemian Massif, determined by means of fluvial relief types, reaches values in the order of 10^1–10^3 m (Fig. 7). We consider these values to be the lower limit of the extent of differential tectonic uplift in the Bohemian Massif. The reason why this estimation is only approximate is incomplete geomorphological record of the substantial erosion and denudation of its georelief, including planation surfaces of different origin and age as well as fluvial sediments of river terrace systems, under the influence of intensive climate-morphogenetic processes.

Geomorphological research in the central part of the Bohemian Massif indicates that significant epigenetic and antecedent deepening of river valleys took place only from the late part of the Middle Pleistocene (Table 2). The fluvial sediments of river terraces I and II of the main streams were deposited during the Cromerian Complex period and river terrace III during the Elsterian glaciation.

Substantial progress in methods of geomorphological analysis, numerical and physical dating of landform evolution, and monitoring of the intensity and causes of recent movements of the Earth's surface provides a comprehensive knowledge for morphostratigraphical interpretations of the dynamic evolution of the georelief in the Bohemian Massif. These regional geomorphological investigations also offer effective applications in determining serious natural hazards and risks, including their link to ongoing changes in the European landscape environment.

Acknowledgements

The work is dedicated to RNDr. Břetislav Balatka, CSc. on the occasion of what would have been his 95th birthday. The presented study was prepared as part of the Charles University project "Cooperatio Geography".

References

Balatka, B. (1958): Bočná koryta v údolí Jizery u Mnichova Hradiště. Sborník Československé společnosti zeměpisné 63, 10–18.

Balatka, B. (1960): Terasy Jizery. Doctoral thesis, Charles University, Prague.

Balatka, B. (1961): Podélný profil a poznámky ke genezi spodních a údolních teras středního Labe. Sborník Československé společnosti zeměpisné 66, 6–22, https://doi.org/10.37040/geografie1961066010006.

Balatka, B. (1966): K středopleistocénnímu a mladopleistocénnímu vývoji údolí nejdolejší Jizery. Sborník Československé společnosti zeměpisné 71(3), 217–230, https://doi.org/10.37040/geografie1966071030217.

Balatka, B. (1968): Vývoj říční sítě (Geomorfologie České vysočiny). Československá vlastivěda. Díl 1. Příroda. Vývoj povrchových tvarů 1–4; Orbis: Prague, pp. 354–375.

Balatka, B. (2003): Podrobné geomorfologické členění reliéfu Čech. Map Collection, Faculty of Science, Charles University, Prague, 3 maps 1:500 000.

Balatka, B. (2006): Fluviální reliéf morfostruktur Čech. Výzkumná zpráva, 2 tematické mapy a text komentáře 8 p. Autorské podklady. Map Collection, Faculty of Science, Charles University, Prague. Available online: https://cuni.primo.exlibrisgroup.com/permalink/420CKIS_INST/1ustijj/alma9925963010906986 (accessed on 5 May 2025).

Balatka, B. (2007): River terraces and the Sázava Valley evolution. In: Goudie, A. S., Kalvoda, J. (Eds.), Geomorphological variations; P3K Publishers: Prague, pp. 361–386.

Balatka, B., Czudek, I., Demek, J., Ivan, A., Sládek, J. (1975): Typologické třídění reliéfu ČSR. Sborník Československé společnosti zeměpisné 80(3), 177–183, https://doi.org/10.37040/geografie1975080030177.

Balatka, B., Gibbard, P., Kalvoda, J. (2010a): Evolution of the Sázava valley in the Bohemian Massif. Geomorphologia Slovaca et Bohemica AV SR 10(1), 55–76.

Balatka, B., Gibbard, P., Kalvoda, J. (2010b): Morphostratigraphy of the Sázava river terraces in the Bohemian Massif. AUC Geographica 45(1–2), 3–34.

Balatka, B., Kalvoda, J. (1995): Vývoj údolí Labe v Děčínské vrchovině. Sborník České společnosti zeměpisné 100(3), 173–192.

Balatka, B., Kalvoda, J. (2006a): Geomorfologické členění reliéfu Čech; Kartografia: Prague.

Balatka, B., Kalvoda, J. (2006b): Metodologický komentář a vysvětlivky k mapám typů fluviálního reliéfu, říčních teras a eroze ve vztahu k morfostrukturám České vysočiny v měřítku 1:500 000. In: Balatka, B., Fluviální reliéf morfostruktur Čech. Výzkumná zpráva, 2 tematické mapy a text komentáře 8 p. Autorské podklady. Map Collection, Faculty of Science, Charles University. Available online: https://cuni.primo.exlibrisgroup.com/permalink/420CKIS_INST/1ustijj/alma9925963010906986 (accessed on 5 May 2025).

Balatka, B., Kalvoda, J. (2008): Evolution of the Quaternary river terraces related to the uplift of the central part of the Bohemian Massif. Geografie – Sborník České geografické společnosti 113(3), 205–222.

Balatka, B., Kalvoda, J. (2010a): Vývoj údolí Sázavy v mladším kenozoiku; Česká geografická společnost: Prague.

Balatka, B., Kalvoda, J. (2010b): Kvartérní terasy řeky Želivky. Geografie – Sborník České geografické společnosti 115(2), 113–131.

Balatka, B., Kalvoda, J. (2010c): Vývoj akumulačních teras řeky Želivky v kvartéru. Sborník příspěvků XXII. sjezdu České geografické společnosti Geografie pro život v 21. století; Ostrava, pp. 49–54.

Balatka, B., Kalvoda, J. (2018): Terasový systém řeky Ohře mezi Smrčinami a západní částí Sokolovské pánve. Informace České geografické společnosti 37(2), 1–15.

Balatka, B., Loučková, J. (1992): Terasový systém a vývoj údolí Berounky. Studia geographica 96; Geografický ústav ČSAV: Brno, 1–53.

Balatka, B., Přibyl, V. (1996): Synthesis of the geomorphological development in the northern part of the Písecká pahorkatina Hillyland. AUC Geographica 31(2), 97–113.

Balatka, B., Přibyl, V. (1997): Geomorfologické poměry západní části Líšovského prahu a přilehlé části Blatské pánve. AUC Geographica 32(2), 15–30.

Balatka, B., Přibyl, V. (2003): Morphostructural analysis and geomorphological development of the Nedvědička River valley near Pernštejn. AUC Geographica 35, Supplementum 2000, 211–224.

Balatka, B., Sládek, J. (1962a): Říční terasy v českých zemích; Nakladatelství Československé akademie věd: Prague, 578 p.

Balatka, B., Sládek, J. (1962b): Terasový systém Vltavy a Labe mezi Kralupy a Českým středohořím. Rozpravy Československé akademie věd 72(11); Academia: Prague, 1–64.

Balatka, B., Sládek, J. (1962c): O vývoji českých řek. Lidé a země 3, 103–110.

Balatka, B., Sládek, J. (1963): K problematice terasového systému českých řek. Sborník Československé společnosti zeměpisné 68(1), 67–71, https://doi.org/10.37040/geografie1963068010067.

Balatka, B., Sládek, J. (1964): The geomorphology of Prague. Journal of the Geological Society, Supplementum for the XXst International Geographical Congress in London, 22–30.

Balatka, B., Sládek, J. (1965): Pleistocénní vývoj údolí Jizery a Orlice. Rozpravy Československé akademie věd 75(11); Academia: Prague.

Balatka, B., Sládek, J. (1970): Ke geomorfologickému pojetí říčních teras (diskuse). Sborník Československé společnosti zeměpisné 75(1), 71–74.

Balatka, B., Sládek, J. (1973): K vývoji Mělnického úvalu. Sborník Československé společnosti zeměpisné 78(2), 130–133, https://doi.org/10.37040/geografie1973078020081.

Balatka, B., Sládek, J. (1974): Poznámky ke genezi a systému říčních teras v Čechách. Geografický časopis 26(2), 175–182.

Balatka, B., Sládek, J. (1975): Geomorfologický vývoj dolního Poohří. Rozpravy Československé akademie věd 85(5); Academia: Prague.

Balatka, B., Sládek, J. (1976): Terasový systém střední a dolní Ohře. AUC Geographica 11(2), 3–26.

Balatka, B., Sládek, J. (1989a): Typizace reliéfu kvádrových pískovců české křídové pánve. Rozpravy Československé akademie věd 94(6); Academia: Prague, 1–80.

Balatka, B., Sládek, J. (1989b): Geomorfologické či orografické členění reliéfu? Sborník Československé společnosti zeměpisné 94, 274–279, https://doi.org/10.37040/geografie1989094040274.

Balatka, B., Sládek, J., Loučková, J. (1966): Vývoj hlavní erozní báze českých řek. Rozpravy Československé akademie věd 76(9); Academia: Prague, 74 p.

Balatka, B., Štěpančíková, P. (2006): Terrace system of the middle and lower Sázava River. Geomorphologia Slovaca 6(1), 69–81.

Balatka, B., Michovská, J., Sládek, J. (1959): Podrobná geomorfologická mapa území na sever od Prahy. Sborník Československé společnosti zeměpisné 64, 289–302.

Balatka, B., Loučková, J., Sládek, J. (1964): The terrace system of the Bohemian Labe. Journal of the Czechoslovak Geographical Society. Supplement for the 20th International Geographical Congress in London, 31–36, https://doi.org/10.37040/geografie1964069050031.

Balatka, B., Chrastina, J., Elznicová, J., Heřmanová, M., Hradecký, J., Hudeček, J., Janák, M., Karel, W., Kožíšek, J., Kročil, P., Krásný, J., Krňoul, Z., Kundrát, J., Kučera, J., Mrkvička, J., Nedvědický, M., Opravil, Z., Pánek, J., Pešek, J., Plášil, L., Plešinger, J., Pokorný, P., Rabušic, L., Řepa, V., Schmidt, J., Štěpánek, J., Tolasz, R., Tomášek, J., Valenta, J., Velebil, J., Volf, F. (1971a): Regionální členění reliéfu ČSR. Soubor map fyzicko-geografické regionalizace ČSR 1:500 000; Geografický ústav ČSAV: Brno.

Balatka, B., Chrastina, J., Elznicová, J., Heřmanová, M., Hradecký, J., Hudeček, J., Janák, M., Karel, W., Kožíšek, J., Kročil, P., Krásný, J., Krňoul, Z., Kundrát, J., Kučera, J., Mrkvička, J., Nedvědický, M., Opravil, Z., Pánek, J., Pešek, J., Plášil, L., Plešinger, J., Pokorný, P., Rabušic, L., Řepa, V., Schmidt, J., Štěpánek, J., Tolasz, R., Tomášek, J., Valenta, J., Velebil, J., Volf, F. (1971b): Typologické členění reliéfu ČSR. Soubor map fyzicko-geografické regionalizace ČSR 1:500 000; Geografický ústav ČSAV: Brno.

Balatka, B., Demek, J., Loučková, J., Sládek, J., Zapletal, L. (1973): Regionální členění reliéfu ČSR. Sborník Československé společnosti zeměpisné 78(2), 81–96, https://doi.org/10.37040/geografie1973078020081.

Balatka, B., Roth, Z., Sládek, J., Zeman, A. (1983): Český masiv: diskuse o jeho vymezování a tektonickém členění. Věstník Ústředního ústavu geologického 58, 369–376.

Balatka, B., Přibyl, V., Vilímek, V. (2000): Morfologické rysy reliéfu povodí horní Jihlavy. Geografie – Sborník České geografické společnosti 105(3), 276–285, https://doi.org/10.37040/geografie2000105030276.

Balatka, B., Kalvoda, J., Gibbard, P. (2015): Morphostratigraphical correlation of river terraces in the central part of the Bohemian Massif with the European stratigraphical classification of the Quaternary. AUC Geographica 50(1), 63–73, https://doi.org/10.14712/23361980.2015.87.

Balatka, B., Kalvoda, J., Steklá, T., Štěpančíková, P. (2019): Morphostratigraphy of river terraces in the Eger valley (Czechia) focused on the Smrčiny Mountains, the Chebská pánev basin and the Sokolovská pánev basin. AUC Geographica 54(2), 240–259, https://doi.org/10.14712/23361980.2019.21.

Bankwitz, P., Bankwitz, E., Bräuer, K., Kämpf, H., Störr, M. (2003): Deformation structures in Plio- and Pleistocene sediments (NW Bohemia, Central Europe). In: Van Rensbergen, P., Hillis, R. R., Maltman, A. J., Morley, C. K. (Eds.), Subsurface sediment mobilization; Geological Society: London, pp. 73–93, https://doi.org/10.1144/GSL.SP.2003.216.01.06.

Bláhová, Š., Křížek, M. (2007): Spatial distribution of potential planation surfaces in the Bohemian Forest (the Šumava Mts.). Silva Gabreta 13(3), 217–224.

Braucher, R., Kalvoda, J., Bourlès, D., Brown, E., Engel, Z., Mercier, J.-L. (2006): Late Pleistocene deglaciation in the Vosges and the Krkonoše Mountains: correlation of cosmogenic 10Be exposure ages. Geografický časopis 58(1), 3–14.

Bridgland, D. R. (2000): River terrace systems in north-west Europe: an archive of environmental change, uplift and early human occupation. Quaternary Science Reviews 19(13), 1293–1303, https://doi.org/10.1016/S0277-3791(99)00095-5.

Carr, S. J., Engel, Z., Kalvoda, J., Parker, A. (2002): Sedimentary evidence to suggest extensive glaciation of the Úpa valley, Krkonoše Mountains, Czech Republic. Zeitschrift für Geomorphologie, N. F. 46(4), 523–537, https://doi.org/10.1127/zfg/46/2002/523.

Carr, S., Engel, Z., Kalvoda, J., Parker, A. (2007): Towards a revised model of Quaternary mountain glaciation in the Krkonoše Mountains, Czech Republic. In: Goudie, A. S., Kalvoda, J. (Eds.), Geomorphological variations; P3K Publishers: Prague, pp. 253–268.

Coubal, M. (1989): Projevy saxonské tektogeneze v centrální části české křídové pánve (Effects of Saxonian tectogeny in the central part of the Bohemian Cretaceous Basin). Doctoral thesis, Charles University, Prague.

Coubal, M., Adamovič, J. (2000): Youngest tectonic activity on faults in the SW part of the Most Basin. Geolines 10, 15–17.

Cymerman, Z. (1999): Terranes and Terrane Boundaries in the Sudetes. Geolines 8, 15–16.

Czudek, T. (1997): Reliéf Moravy a Slezska v kvartéru; Sursum: Tišnov, 213 p.

Czudek, T. (2005): Vývoj reliéfu krajiny České republiky v kvartéru; Moravské zemské muzeum: Brno, 238 p.

Czudek, T. (Ed.) (1972): Geomorfologické členění ČSR. Studia geographica 23; Geografický ústav ČSAV: Brno, 137 p.

Čtyroký, J. (1996): Vývoj údolí Ohře ve Slavkovském lese. Master thesis, Faculty of Science, Charles University, Prague.

Daneš, J. V. (1913): Morfologický vývoj středních Čech. Sborník České společnosti zeměpisné 19, 1–18, 94–108, 168–176.

Danišík, M., Migoń, P., Kuhlemann, J., Evans, N. J., Dunkl, I., Frisch, W. (2010): Thermochronological constraints on the long-term erosional history of the Krkonosze Mts., Central Europe. Geomorphology 117(1–2), 78–89, https://doi.org/10.1016/j.geomorph.2009.11.010.

Danišík, M., Štěpančíková, P., Evans, N. J. (2012): Constraining long-term denudation and faulting history in intraplate regions by multisystem thermochronology: An example of the Sudetic Marginal Fault (Bohemian Massif, central Europe). Tectonics 31: TC2003, https://doi.org/10.1029/2011TC003012.

Demek, J. (2004): Etchplain, rock pediments and morphostructural analysis of the Bohemian Massif tectonic uplift, fluvial erosion (Czech Republic). In: Drbohlav, D., Kalvoda, J., Voženílek, V. (Eds.), Czech Geography at the Dawn of the Millennium. (IGU, Glasgow 2004); Palacký University Press: Olomouc, pp. 69–81.

Demek, J., Kalvoda, J. (1991): Kriteria geomorfologického hodnocení lokalit výstavby a provozu jaderně energetických zařízení. Životné prostredie 25(6), 313–315.

Demek, J., Kalvoda, J. (1992): Geomorphology and the Location of Nuclear Power Plant Sites: the Czechoslovakian Experience. GeoJournal 28(4), 395–402, https://doi.org/10.1007/BF00273108.

Demek, J., Mackovčin, P. (Eds.) (2006): Zeměpisný lexikon ČR. Hory a nížiny; Agentura ochrany přírody a krajiny ČR: Brno, 531 p., mapa geomorfologického členění 1:500 000.

Demek, J., Mackovčinová, V., Price, J., Vacková, J. (1965): Geomorfologie Českých zemí; Nakladatelství ČSAV: Prague, 335 p.

Demek, J., Mackovčin, P., Balatka, B., Buček, A., Čermák, P., Dobiáš, D., Havlíček, M., Hradek, M., Kirchner, K., Lacina, J., Pánek, T., Slavík, P., Vašatko, J. (1987): Zeměpisný lexikon ČSR. Hory a nížiny; Academia: Prague, 584 p.

Demek, J., Kalvoda, J., Kirchner, K., Vilímek, V. (2006): Geomorphological aspects of natural hazards and risks in the Czech Republic. Studia Geomorphologica Carpatho-Balcanica 40, 79–92.

Demek, J., Kirchner, K., Mackovčin, P., Slavík, P. (2007): The Map of morphostructures of the Czech Republic. Geomorphologia Slovaca et Bohemica 7(1), 5–14.

Demek, J., Kirchner, K., Mackovčin, P., Slavík, P. (2009): Morphostructures on the Territory of the Czech Republic (Europe). Zeitschrift für Geomorphologie 53(3), 135–144, https://doi.org/10.1127/0372-8854/2009/0053S3-0001.

Dědina, V. (1914): Morfologický vývoj severních Čech. Sborník České společnosti zemněvědné 20, 145–168.

Drbohlav, D., Kalvoda, J., Voženílek, V. (Eds.) (2004a): Czech Geography at the Dawn of the Millennium. (IGU, Glasgow 2004); Nakladatelství Univerzity Palackého: Olomouc, 428 p.

Drbohlav, D., Kalvoda, J., Voženílek, V. (2004b): Frontiers of Czech geography. In: Drbohlav, D., Kalvoda, J., Voženílek, V. (Eds.), Czech Geography at the Dawn of the Millennium. (IGU, Glasgow 2004); Nakladatelství Univerzity Palackého: Olomouc, pp. 413–421.

Engel, Z. (1996): Geomorfologie Labského dolu v Krkonoších. Master thesis, Charles University, Prague.

Engel, Z. (2004): Vývoj pleistocenního zalednění v české části Krkonoš. Doctoral thesis, Charles University, Prague.

Engel, Z., Kalvoda, J. (2002a): Morphostructural development of the sandstone relief in the Bohemian Cretaceous Basin. In: Přikryl, R., Viles, H. (Eds.), Understanding and managing stone decay; SWAPNET, Karolinum: Prague, pp. 225–231.

Engel, Z., Kalvoda, J. (2002b): Review on current research of the Pleistocene glaciation in the Krkonoše Mountains. In: Schenk, V., Schenková, Z. (Eds.), Recent geodynamics of the Sudety Mts. and adjacent areas. Acta Montana 20(124), Serie A, Geodynamics: Prague, 67–74.

Engel, Z., Nývlt, D., Křížek, M., Treml, V., Jankovská, V., Lisá, L. (2010): Sedimentary evidence of landscape and climate history since the end of MIS 3 in the Krkonoše Mountains, Czech Republic. Quaternary Science Reviews 29, 913–927, https://doi.org/10.1016/j.quascirev.2009.12.008.

Gibbard, P. L., Cohen, K. M. (2008): Global chronostratigraphical correlation table for the last 2.7 million years. Episodes 31(2), 243–247, https://doi.org/10.18814/epiiugs/2008/v31i2/011.

Gibbard, P. L., Boreham, S., Cohen, K. M., Moscariello, A. (2004): Global chronostratigraphical correlation table for the last 2.7 million years; Quaternary Palaeoenvironment Group, University of Cambridge: Cambridge, 2 p., 1 plate.

Gibbard, P. L., Head, M. J., Walker, M. J. C. and the Subcommission on Quaternary Stratigraphy (2010): Formal ratification of the Quaternary System/Period and the Pleistocene Series/Epoch with a base at 2.58 Ma. Journal of Quaternary Science 25(2), 96–102, https://doi.org/10.1002/jqs.1338.

Goudie, A., Kalvoda, J. (1997): The study of environmental hazards in extreme environments as a frontier of physical geography. AUC Geographica 32(2), 11–14.

Goudie, A. S., Kalvoda, J. (Eds.) (2007a): Geomorphological variations; P3K Publishers: Prague, 407 p.

Goudie, A. S., Kalvoda, J. (2007b): Variable faces of present-day geomorphology. In: Goudie, A. S., Kalvoda, J. (Eds.), Geomorphological variations; P3K Publishers: Prague, pp. 11–17.

Grygar, R. (2016): Geology and Tectonic Development of the Czech Republic. In: Pánek, T., Hradecký, J. (Eds.), Landscapes and Landforms of the Czech Republic. World Geomorphological Landscapes; Springer International Publishing: Cham, pp. 7–18, https://doi.org/10.1007/978-3-319-27537-6_2.

Halžová, D. (2017): Geomorfologické aspekty výskytu vltavínov v strednej Europe. Master thesis, Charles University, Prague.

Hartvich, F. (2002): Geomorfologický výzkum a využití digitálních geomorfologických dat na příkladu lokality Městiště. Master thesis, Charles University, Prague.

Hartvich, F. (2005): Research of geodynamic activity in the vicinity of Obří Hrad, Šumava Mts. Acta Geodynamica et Geomaterialia 2(1), 29–35.

Hartvich, F. (2008): Geodynamický vývoj údolí Losenice na severovýchodním okrajovém svahu Šumavy. Doctoral thesis, Charles University, Prague.

Hartvich, F., Vilímek, V. (2008): Selected landforms and their significance in the analysis of the slope origin in the Losenice river valley, Šumava Mts. Acta Geodynamica et Geomaterialia 5(151), 1–22.

Hasenkopfová, S. (2002): Geomorfologie a vegetace povodí Bubovického potoka v Českém krasu. Master thesis, Charles University, Prague.

Hejl, E., Coyle, D., Nand, L., Van den Haute, P., Wagner, G. A. (1997): Fission-track dating of the western border of the Bohemian Massif: thermochronology and tectonic implications. Geologische Rundschau 86, 210–219, https://doi.org/10.1007/s005310050133.

Hradecký, J., Brázdil, R. (2016): Climate in the Past and Present in the Czech Lands in the Central European Context. In: Pánek, T., Hradecký, J. (Eds.), Landscapes and Landforms of the Czech Republic. World Geomorphological Landscapes; Springer: Cham, https://doi.org/10.1007/978-3-319-27537-6_3.

Hrádek, M., Ivan, A. (1972): Study of the block structure and neotectonic movements in the Česká vysočina (Bohemian Highland) by methods of morphostructural analysis. Sborník Československé společnosti zeměpisné 77(2), 135–144, https://doi.org/10.37040/geografie1972077020135.

Hrádek, M., Ivan, A. (1974): Neotektonické vrásno-zlomové struktury v širším okolí Brna. Sborník Československé společnosti zeměpisné 79(4), 245–257, https://doi.org/10.37040/geografie1974079040249.

Hromádka, J. (1956): Orografické třídění Československé republiky. Sborník Československé společnosti zeměpisné 61(3), 161–180; 61(4), 265–299.

Cháb, J., Stráník, Z., Eliáš, M. (2007): Geologická mapa České republiky 1:500 000; Česká geologická služba: Prague.

Cháb, J., Breiter, K., Fatka, O., Hladil, J., Kalvoda, J., Šimůnek, Z., Štorch, P., Vašíček, Z., Zajíc, J., Zapletal, J. (2008): Stručná geologie základu Českého masivu a jeho karbonského a permského pokryvu; Česká geologická služba: Prague, 283 p.

Chlupáč, I., Brzobohatý, R., Kovanda, J., Stráník, Z. (2002): Geologická minulost České republiky; Academia: Prague.

International Commission on Stratigraphy (2007): Stratigraphical table of the Quaternary. Available online: http://www.quaternary.stratigraphy.org.uk/correlation/chart.html (accessed on 10 February 2025).

Ivan, A. (1999): Geomorphological aspects of late Saxonian epiplatform orogeny of the Bohemian Massif. Moravian Geographical Reports 7(1), 18–33; 7(2), 12–31.

Ivan, A., Kirchner, K., Krejčí, O. (2000): K poznání morfostrukturních rysů reliéfu moravské části Západních Karpat a Panonské pánve. Geografický časopis 52(4), 221–230.

Kalvoda, J. (1966): Geomorfologická mapa a mapa základových půd Stříbro – list mapy 1:25 000, M-33-74-D-a (Damnov). Master thesis, Charles University, Prague.

Kalvoda, J. (1970): Geomorfologie hřebenové části Vysokých Tater. Doctoral thesis, Geografický Ústav ČSAV, Brno, 166 p.

Kalvoda, J. (1974): Geomorfologický vývoj hřebenové části Vysokých Tater. Rozpravy Československé akademie věd 84(6); Academia: Prague, 65 p.

Kalvoda, J. (1978): Antropogénne narušenie reliéfu Vysokých Tatier. Zborník prací oTANAPu 20, 115–126.

Kalvoda, J. (1980): Náčrt geomorfologie styčného území Stříbrské pahorkatiny, Tepelské vrchoviny a Tachovské brázdy. Sborník Československé společnosti zeměpisné 85(4), 320–324.

Kalvoda, J. (1992a): Geomorphological Record of the Quaternary Orogeny in the Himalaya and the Karakoram; Elsevier: Amsterdam, 315 p.

Kalvoda, J. (1992b): Geomorphological hazards and risks of selected nuclear power plants in the ČSFR. AUC Geographica 27(1), 111–113.

Kalvoda, J. (1993): Some observations on the morphotectonic activity in the Pamirs and the Tian-Shan. AUC Geographica 28(2), 3–20.

Kalvoda, J. (1994): Rock Slopes of the High Tatras Mountains. AUC Geographica 29(2), 13–33.

Kalvoda, J. (Ed.) (1995a): Dynamic geomorphology of tectonic active zones. AUC Geographica 30, Supplementum, 167 p.

Kalvoda, J. (1995b): Geomorphological analysis of levelling measurements between Mikulovice village and Jezeří castle in the Krušné hory Mountains. AUC Geographica 30, Supplementum, 139–160.

Kalvoda, J. (1996a): The geodynamics of landforms hazard processes. AUC Geographica 31(2), 7–32.

Kalvoda, J. (1996b): Geomorphological aspects of levelling measurements of the Earth's surface movements in the Czech Republic. Acta Universitatis Palackiensis Olomouc, Geographica 34, 7–16.

Kalvoda, J. (1998a): Geomorphological hazards and risks in the High Tatra Mountains. In: Kalvoda, J., Rosenfeld, Ch. (Eds.), Geomorphological Hazards in High Mountain Areas. The GeoJournal Library 46; Springer: Dordrecht, https://doi.org/10.1007/978-94-011-5228-0_15.

Kalvoda, J. (1998b): Geomorphological hazards on stratovolcanos in Southeast Asia. AUC Geographica 33(1), 31–49.

Kalvoda, J. (Ed.) (2003): Global change in geomorphology. AUC Geographica 35, Supplementum, 262 p.

Kalvoda, J. (2005): Morfostrukturní vývoj reliéfu locality GOPE v Ondřejovské vrchovině. Geomorfologický sborník 4, 33–36.

Kalvoda, J. (2007a): Morphostructural evolution of the relief in the locality of the Geodynamic Observatory at Pecný, the Ondřejovská vrchovina Highland, Czech Republic. In: Goudie, A. S., Kalvoda, J. (Eds.), Geomorphological variations; P3K Publishers: Prague, pp. 387–407.

Kalvoda, J. (2007b): Rapid fluvial processes in the Late Quaternary. In: Langhammer, J. (Ed.), Změny v krajině a povodňové riziko. Sborník příspěvků semináře Povodně a změny v krajině, 5. 6. 2007; Přírodovědecká fakulta Univerzity Karlovy: Prague, pp. 17–28.

Kalvoda, J. (2011): Životní jubileum Břetislava Balatky. Informace České geografické společnosti 30(2), 85–88.

Kalvoda, J. (2016): 85. výročí dr. Břetislava Balatky. Informace České geografické společnosti 35(2), 91–94.

Kalvoda, J. (2020): The Dynamics of Geomorphic Evolution in the Makalu Barun Area of the Nepal Himalaya; P3K publishers: Prague, 378 p.

Kalvoda, J., Balatka, B. (1995): Chronodynamics of the Labe river antecedence in the Děčínská vrchovina Highland, Czech Republic. Acta Montana, Ser. A, Geodynamics 8(97), 43–60.

Kalvoda, J., Balatka, B. (2006): Morfostrukturní vývoj reliéfu české části Českého masivu. Morphostructural evolution of the relief of the Bohemian part of the Český masiv Massif. In: Balatka, B., Kalvoda, J. (2006): Geomorfologické členění reliéfu Čech; Kartografie Praha: Prague, pp. 5–12.

Kalvoda, J., Balatka, B. (2016): The Geomorphological Evolution and Environmental Hazards of the Prague Area. In: Pánek, T., Hradecký, J. (Eds.), Landscapes and Landforms of the Czech Republic. World Geomorphological Landscapes; Springer: Cham, https://doi.org/10.1007/978-3-319-27537-6_5.

Kalvoda, J., Demek, J. (1991): Geomorfologická specifika vybraných lokalit jaderných elektráren v ČSFR. Životné prostredie 25(6), 300–305.

Kalvoda, J., Košťák, B. (1984): Geomorfologická analýza měření dilatací pískovcových bloků v údolí Liběchovky, Polomené hory. Sborník Československé geografické Společnosti 89(3), 199–210, https://doi.org/10.37040/geografie1984089030199.

Kalvoda, J., Mercier, J.-L. (Eds.) (1996): The geodynamics of landforms hazard processes. AUC Geographica 31(2), 113 p.

Kalvoda, J., Novotná, E. (Eds.) (2024): The nature of geomorphological hazards in the Nepal Himalaya; Springer: Cham, https://doi.org/10.1007/978-3-031-58421-3.

Kalvoda, J., Pašek, J. (1975): Revize využití opakované nivelace v geologii. Geologický průzkum 17(6), 165–166.

Kalvoda, J., Prášek, J. (1987): Tektonické aspekty vývoje reliéfu Moravskoslezských Beskyd v oblasti geodynamického polygonu Horní Bečva. Sborník referátů k XVII. sjezdu Československé geografické společnosti v Ostravě, svazek 1; Brno, pp. 120–124.

Kalvoda, J., Prášek, J. (1996): Geomorphological observation in the area of the Bečva geodynamic polygon (the Moravskoslezské Beskydy Mountains). Studia Geomorphologica Carpatho-Balcanica 30, 63–72.

Kalvoda, J., Rosenfeld, Ch. (Eds.) (1998): Geomorphological Hazards in High Mountain Areas. The GeoJournal Library 46; Springer: Dordrecht, https://doi.org/10.1007/978-94-011-5228-0.

Kalvoda, J., Stemberk, J. (1993): Morphotectonic evidences of the Quaternary geodynamics in selected localities of nuclear power plants. Acta Montana, Ústav geologie a geotechniky AV ČR, Serie A, Geodynamics 4(90), 63–80.

Kalvoda, J., Zeman, A. (1979): Sledování pohybů zemského povrchu na geodynamickém polygonu Horní Bečva v Moravskoslezských Beskydech. Věstník Ústředního ústavu geologického 54(6), 349–360.

Kalvoda, J., Zeman, A. (1982): Geological interpretation of the measurement in 1952–1981 on the test levelling circuit in Prague – Podbaba. Sborník výzkumných zpráv VÚGTK 14, 89–124, https://doi.org/10.1017/S0016756800067467.

Kalvoda, J., Zeman, A. (1983): Interpretace měření recentních pohybů zemského povrchu. Sborník prací Geografického ústavu ČSAV 1, 81–90.

Kalvoda, J., Zvelebil, J. (1983a): Porušování skalních svahů údolí Labe v Děčínské vrchovině. Sborník prací Geografického ústavu ČSAV 1, 163–173.

Kalvoda, J., Zvelebil, J. (1983b): Dynamika a typy porušování svahů při vývoji údolí Labe v Děčínské vrchovině. Acta Montana 63, 5–74.

Kalvoda, J., Zvelebil, J. (1989): Vývoj skalních svahů a pseudokrasových jeskyní údolí Labe v Děčínské vrchovině. Sbor. Sympozium o krasu sudetské soustavy. Knihovna České speleologické společnosti, sv. 10; Prague, 112–126.

Kalvoda, J., Stemberk, J., Vilímek, V., Zeman, A. (1990): Analysis of levelling measurements of the Earth's surface movements on the geodynamical polygon Mikulovice – Jezeří in the Krušné hory Mts. Proceedings of the 6th Congress of the International Association of Engineering Geology 3, 1631–1637, https://doi.org/10.1201/9781003762805-18.

Kalvoda, J., Vilímek, V., Zeman, A. (1994): Earth's Surface Movements in the Hazardeous Area of Jezeří Castle, Krušné hory Mountains. GeoJournal 32(3), 247–252, https://doi.org/10.1007/BF01122116.

Kalvoda, J., Zvelebil, J., Vilímek V. (1997): Geomorphological history and monitoring of selected rapid mass movements in north-western Bohemia. Paläoklimaforschung 19, Special Issue: ESF Project European Paleoclimate and Man, Matthews, J. A. et al. (Eds.), Rapid mass movement as a source of climatic evidence for the Holocene; Mainz, Stuttgart, pp. 137–146.

Kalvoda, J., Kostelecký, J. jr., Kostelecký, J. (2004): A pilot morphotectonic interpretation of position changes of the permanent GPS stations in Central Europe. In: Drbohlav, D., Kalvoda, J., Voženílek, V. (Eds.), Czech Geography at the Dawn of the Millenium. (IGU, Glasgow

2004); Nakladatelství Univerzity Palackého: Olomouc, pp. 113–123.
Kalvoda, J., Klokočník, J., Kostelecký, J., Bezděk, A. (2013): Mass distribution of Earth landforms determined by aspects of the geopotential as computed from the global gravity field model EGM 2008. AUC Geographica 48(2), 17–25, https://doi.org/10.14712/23361980.2015.1.
Klokočník, J., Kostelecký, J., Kalvoda, J., Eppelbaum, L. V., Bezděk, A. (2014): Gravity Disturbances, Marussi Tensor, Invariants and Other Functions of the Geopotential Represented by EGM 2008. Journal of Earth Science Research 2(3), 88–101, https://doi.org/10.18005/JESR0203003.
Kopecký, A. (1970a): Úloha kvartérní tektoniky při dotváření současné struktury a geomorfologie Českého masivu. Časopis pro mineralogii a geologii 15(4), 347–357.
Kopecký, A. (1970b): Neotektonický vývoj severních a severovýchodních Čech. (Neotectonic development in northern and north-eastern Bohemia). Věstník Ústředního ústavu geologického 45, 339–346.
Kopecký, A. (1972): Hlavní rysy neotektoniky Československa (Main features of the neotectonics of Czechoslovakia). Sborník geologických věd, Antropozoikum 6, 77–155.
Kopecký, A. (1973): Neotektonická mapa ČSSR. 1:1 000 000; Ústřední ústav geologický a Kartografie: Prague.
Kopecký, A. (1983): Neotektonický vývoj a stavba šumavské horské soustavy (Neotectonic structural history of the Šumava Mts. System). Sborník geologických věd, Antropozoikum 15, 71–159.
Kopecký, A. (1986): Neotektonika Hrubého Jeseníku a východní části Orlických hor (Neotectonics of the Hrubý Jeseník Mountains and eastern part of Orlické hory Mountains). Časopis Slezského Muzea, Serie A 35, 117–141.
Kopecký, A. (1989a): Neotektonika severočeské hnědouhelné pánve a Krušných hor (Neotectonics of the North Bohemian Brown Coal Basin and Krušné hory Mountains). Sborník geologických věd, Geologie 44, 155–170.
Kopecký, A. (1989b): Mapa mladších tektonických struktur Českého masivu 1:500 000; Ústřední ústav geologický: Prague.
Kopecký, A. (1996): Some General Problems of the Neotectonics of the Bohemian Massif; Seismicity, Neotectonics and Recent Dynamics with Special Regard to the Territory of Czech Republic. VÚGTK 42 (15), 55–76.
Kopecký, J., Cílek, V. (1998): Pískovcový fenomén: klima, život a reliéf; Česká speleologická společnost, Geologický ústav AV ČR: Prague.
Kořistka, K. (1885): Přirozené krajiny Čech, jejich půda a podnebí; Ministerstvo zemědělství: Prague.
Kostelecký, J., Vondrák, J., Zeman, A., Kalvoda, J., Schenk, V. (2005): Center for Earth's dynamic research (CEDR) – results of five years activity. Reports on Geodesy, Special No. EGU G9, Warsaw University of Technology 73(2), 67–83.
Košťák, B., Kalvoda, J., Stemberk, J., Rybář, J., Vilímek, V., Zvelebil, J. (2000): Deformational function of tectonic structures in massifs. Acta Montana, Ústav struktury a mechaniky hornin AV ČR, Serie AB 8(115), 17–22.
Kovanda, J., Balatka, B., Bernard, J. H., Brunnerova, Z., Březinová, D., Bukanovská, M., Cílek, V., Fridrichová, M., Havlíček, V., Holub, V., Hrdlička, L., Chlupáč, I., Kadlecová, R., Kachlík, V., Kaprasová, E., Kleček, M., Král, J., Kříž, J., Lochmann, Z., Lysenko, V., Mašek, J., Šalanský, K., Tomášek, M., Zelenka, P. (2001): Neživá příroda Prahy a jejího okolí; Academia: Prague.
Král, V. (1966): Geomorfologie střední části Českého středohoří. Rozpravy Československé akademie věd 76(5); Academia: Prague, 1–64.
Král, V. (1968): Geomorfologie vrcholové oblasti Krušných hor a problém paroviny. Rozpravy Československé akademie věd 78(9); Academia: Prague, 1–64.
Král, V. (1971): Zarovnané povrchy v jižním předpolí Doupovských hor. AUC Geographica 1(2), 39–47.
Král, V. (1985): Zarovnané povrchy České vysočiny. Studie ČSAV 10, 1–72.
Králík, F. (1987): Nové poznatky o kontinentálních zaledněních severních Čech. Sborník geologických věd, Antropozoikum 19, 9–74.
Křížek, M. (2001): The Quaternary sculpturing of sandstones in the Rusavská hornatina Mts. AUC Geographica 36(2), 99–109.
Křížek, M. (2006): Morfostrukturní ovlivnění údolní sítě Rusavské hornatiny. In: Smolová, I. (Ed.), Geomorfologické výzkumy v roce 2006; Česká asociace geomorfologů: Olomouc, pp. 123–128.
Kudrnovská, O. (1975): Morfometrické metody a jejich aplikace při fyzickogeografické regionalizaci. Studia geographica 45; Geografický ústav ČSAV: Brno, 182 p.
Kudrnovská, O., Kousal, J. (1971): Výšková členitost reliéfu ČSR. Soubor map fyzickogeografické regionalizace ČSR 1:500 000; Geografický ústav ČSAV: Brno.
Kudrnovská, O., Kousal, J. (1975a): Střední sklony reliéfu ČSR. Soubor map fyzickogeografické regionalizace ČSR 1:500 000; Geografický ústav ČSAV: Brno.
Kudrnovská, O., Kousal, J. (1975b): Střední výšky reliéfu ČSR. Soubor map fyzickogeografické regionalizace ČSR 1:500 000; Geografický ústav ČSAV: Brno.
Kuchař, K. (1955): Novější snahy o vymezení orografických celků v ČSR. IV. Vymezení celků upínacími sedly. Kartografické přehledy 9, 58–64.
Kuncová, M. (2005): Geomorfologie středního toku Sázavy v okolí Senohrab. Master thesis, Charles University, Prague.
Kunský, J. (1929): Studie o třetihorních štěrcích ve středních Čechách. Sborník Státního geologického ústavu Československé republiky 8(1), 229–255.
Kunský, J. (1966): Terasový system labský a jeho vztah ke čtvrtohornímu zalednění kontinentálnímu a horskému. AUC Geographica 1(1–2), 21–22.
Lachmanová, M. (1996): Geologie mezi Loukovem a Novou Vsí u Bakova se zvláštním zřetelem na terasy Jizery. Master thesis, Charles University, Prague.
Langhammer, J. (Ed.) (2008): Údolní niva jako prostor ovlivňující průběh a následky povodní; Faculty of Science, Charles University: Prague, 276 p.
Lipský, Z. (1980): Geomorfologie Říčanska na styku Pražské plošiny a Benešovské pahorkatiny. Rigorous thesis, Charles University, Prague.
Lochmann, Z. (1971): K vývoji kotlin západního okraje České vysočiny. Rozpravy Československé akademie věd 81(5); Academia: Prague, 1–68.

Ložek, V. (1973): Příroda ve čtvrtohorách; Academia: Prague, 372 p.
Ložek, V., Cílek, V., Kubíková, J. (2003): Střední Čechy: příroda, člověk, Krajina; Nakladatelství Dokořán: Prague, 127 p.
Ložek, V., Žák, K., Cílek, V. (2004): Z minulosti českých řek. Vesmír 83(8), 447–454.
Macoun, J. (1985): Stratigrafie středního pleistocénu Moravy ve vztahu k evropskému kvartéru. Časopis Slezského Muzea, Série A 29, 219–237.
Macoun, J., Králík, F. (1995): Glacial history of the Czech Republic. In: Ehlers, J., Kozarski, S., Gibbard, P. (Eds.), Glacial Deposits in Northeast Europe (1st ed.); CRC Press, 17 p., https://doi.org/10.1201/9781003077695-51.
Malkovský, M. (1975): Paleogeography of the Miocene of the Bohemian Massif. Věstník ústředního ústavu geologického 50(1), 27–31.
Malkovský, M. (1979): Tektogeneze platformního pokryvu Českého masivu. Ústřední ústav geologický; Academia: Prague.
Mazáčová, K., Přibyl, V., Chrobok, J., Kepková, B., Král, V., Kunský, J. (1963): Geomorfologický vývoj oblasti Týna nad Vltavou. Sborník Československé společnosti zeměpisné 68(4), 317–327, https://doi.org/10.37040/geografie1963068040317.
Mazúr, E. (1979): Typologické členenie reliéfu. Mapa 12, IV. Povrch. 1:500 000. Atlas Slovenskej socialistickej republiky; Nakladatelství SAV: Bratislava.
Mazúr, E., Lukniš, M. (1978): Regionálne geomorfologické členenie SSR. Geografický časopis 30(2), 101–125.
Mazúr, E., Lukniš, M. (1979): Geomorfologické jednotky. Mapa 16, IV. Povrch 1:500 000. Atlas Slovenskej socialistickej republiky; Nakladatelství SAV: Bratislava.
Mercier, J.-L., Kalvoda, J., Bourlés, D. L., Braucher, R., Engel, Z. (2000): Preliminary results of 10Be dating of glacial landscape in the Giant Mountains. AUC Geographica 35, Supplementum, 157–170.
Mercier, J.-L., Bourlès, D. L., Kalvoda, J., Engel, Z., Braucher, R. (2002): Report on radiometric 10Be dating of glacial and periglacial landforms in the Giant Mountains. Opera corcontica 39, 169–174.
Mercier, J.-L., Bourlès, D. L., Kalvoda, J., Engel, Z., Braucher, R. (2003): Preliminary results of 10Be dating of glacial landscape in the Giant Mountains. AUC Geographica 35, Supplementum 2000, 157–170.
Migoń, P. (1999): The role of "preglacial" relief in the development of mountain glaciation in the Sudetes, with special reference to the Karkonosze Mountains. Zeitschrift für Geomorphologie 113, Supplementum, 33–44.
Mikisková, I. (2009): Paleokoryto řeky Jizery. Master thesis, Charles University, Prague.
Moschelesová, J. (1923): Morfologické důkazy nejmladších tektonických pohybů v severozápadních Čechách. Sborník Československé společnosti zeměpisné 29(1), 132–134.
Moschelesová, J. (1930): Vlnité pohyby o velké amplitudě v Jižních Čechách. Sborník Československé společnosti zeměpisné 36(1), 155–158.
Mrlina, J. (2000): Vertical displacements in the Novy Kostel seismoactive area. Studia geophysica et geodaetica 44(2), 336–345, https://doi.org/10.1023/A:1022179329713.
Novotná, R. (1998): Geomorfologická analýza a vývoj reliéfu opuštěného pleistocenního údolí Jizery v úseku Domousnice – Všejany. Master thesis, Charles University, Prague.
Nývlt, D. (1998): Kontinentální zalednění severních Čech. Geografie – Sborník České geografické společnosti 103(4), 445–457, https://doi.org/10.37040/geografie1998103040445.
Nývlt, D. (1999): Pevninské zalednění Oldřichovské vrchoviny. Master thesis, Charles University, Prague.
Nývlt, D. (2003): Geomorphological aspects of glaciation in the Oldřichov Highland, Northern Bohemia, Czechia. AUC Geographica 35, Supplementum 2000, 171–183.
Nývlt, D. (2008): Paleogeografická rekonstrukce kontinentálního zalednění Šluknovské pahorkatiny. Doctoral thesis, Charles University, Prague.
Pánek, T., Hradecký, J. (Eds.) (2016): Landscapes and Landforms of the Czech Republic. World Geomorphological Landscapes; Springer International Publishing: Berlin, 422 p., https://doi.org/10.1007/978-3-319-27537-6.
Pánek, T., Kapustová, V. (2016): Long-Term Geomorphological History of the Czech Republic. In: Pánek, T., Hradecký, J. (Eds.), Landscapes and Landforms of the Czech Republic. World Geomorphological Landscapes; Springer: Cham, https://doi.org/10.1007/978-3-319-27537-6_4.
Pánková, B. (1995): Reliéf Krušných hor mezi Českým Jiřetínem a Osekem. Master thesis, Charles University, Prague.
Pharaoh, T. C. (1999): Paleozoic terranes and their lithospheric boundaries within the TransEuropean Suture Zone (TESZ): a review. Tectonophysics 314(1–3), 17–41, https://doi.org/10.1016/S0040-1951(99)00235-8.
Prášek, J. (1985): Geomorfologická analýza a vývoj tvarů reliéfu povodí horní Rožnovské Bečvy. Master thesis, Charles University, Prague.
Prášek, J. (1993): Geomorfologie pramenné oblasti povodí Rožnovské Bečvy. Acta Facultatis Rerum Naturalium Universitas Ostraviensis 136(1), 21–32.
Průša, V. (1993): Geomorfologický vývoj reliéfu území soutoku Srbské a Chřibské Kamenice. Master thesis, Charles University, Prague.
Přibyl, V. (1972): Geomorfologie navátých písků v Čechách. Rozpravy Československé akademie věd 82(1); Academia: Prague, 70 p.
Přibyl, V. (1999): Vltava River Terrace System between Lipno and Rožumberk nad Vltavou. AUC Geographica 34(2), 157–171.
Přibyl, V. (2001): Břetislav Balatka, Seventy-Years Old. RNDr. Břetislav Balatka, CSc. sedmdesátiletý. AUC Geographica 36(2), 5–18.
Přibyl, V., Votýpka, J. (1970): Geomorfologické poměry okolí Českého Krumlova. Sborník Československé společnosti zeměpisné 75(4), 293–300, https://doi.org/10.37040/geografie1970075040293.
Přibylová, N., Viktorová, H., Vojna, L., Jeřábek, J. (1967): Geomorfologický vývoj oblasti Písku. Sborník Československé společnosti zeměpisné 72(1), 89–98, https://doi.org/10.37040/geografie1967072020089.
Raška, P., Emmer, A. (2014): The 1916 catastrophic flood following the Bílá Desná dam failure: the role of historical data sources in the reconstruction of its

geomorphologic and landscape effects. Geomorphology 226(1), 135–147, https://doi.org/10.1016/j.geomorph.2014.08.002.

Růžička, M. (2004): The Pleistocene glaciation of Czechia. Developments in Quaternary Sciences 2(Part 1), 27–34, https://doi.org/10.1016/S1571-0866(04)80054-X.

Rybář, J., Vilímek, V., Cílek, V., Košťák, B., Novotný, J., Stemberk, J., Suchý, J., Kalvoda, J., Cajz, V., Hlaváč, J. (2000): Rozbor vývoje hlubokého porušení svahů v neovulkanitech Českého středohoří. Acta Montana, Ústav struktury a mechaniky hornin AV ČR, Serie AB 8(115), 149–156.

Schenk, V., Schenková, Z., Cacoń, S., Koutný, B., Bosý, J., Kottnauer, P. (2003): To Geodynamic Interpretations of GPS Data Monitored on the EAST SUDETEN Network. Acta Montana, Series A 24(131), 87–97.

Soukupová, L. (2008): Geomorfologický vývoj Hřebenů v Brdech. Master thesis, Charles University, Prague.

Steklá, T. (2012): Recentní morfogenetické procesy v lokalitě Geodynamické observatoře Pecný. Master thesis, Charles University, Prague.

Steklá, T., Kalvoda, J. (2024): Morphostructural evolution of the Labe and Jizera rivers confluence area (the Bohemian Massif, Czechia). AUC Geographica 59(1), 35–59, https://doi.org/10.14712/23361980.2024.3.

Steklá, T., Kalvoda, J., Kostelecký, J. (2017): Landforms and morphogenetic processes in the locality of Geodetic Observatory Pecný, Ondřejovská vrchovina Highland. AUC Geographica 52(1), 5–17, https://doi.org/10.14712/23361980.2017.4.

Stemberk, J. (1994): Aktivita vybraných geodynamických procesů ve středním Poohří. Doctoral thesis, Ústav geologie a geotechniky ČSAV, Prague.

Stemberk, J., Vilímek, V., Kalvoda, J., Košťák, B., Rybář, J., Zvelebil, J. (2000): Analysis of manifestation of tectonic activity in seismically active regions of the Bohemian Massif. Acta Montana, ÚSMH AV ČR, Serie AB 8(115), 61–63.

Stemberk, J., Košťák, B., Cacoń, S. (2010): A tectonic pressure pulse and increased geodynamic activity recorded from the long-term monitoring of faults in Europe. Tectonophysics 487, 1–12, https://doi.org/10.1016/j.tecto.2010.03.001.

Stemberk, J., Hartvich, F., Blahůt, J., Rybář, J., Krejčí, O. (2017): Tectonic strain changes affecting the development of deep seated gravitational slope deformations in the Bohemian Massif and Outer Western Carpathians. Geomorphology 289, 3–17, https://doi.org/10.1016/j.geomorph.2016.07.004.

Stemberk, J. jr. (2021): Vývoj údolí Kladské Bělé. Doctoral thesis, Charles University, Prague.

Stolínová, E., Vilímek, V. (2003): Geomorfologická interpretace geodetických měření v Krušných horách. In: Mentlík, P. (Ed.), Geomorfologický sborník 2. Sborník příspěvků mezinárodního semináře Stav geomorfologických výzkumů v roce 2003, 22. 4. – 24. 4. 2003, Nečtiny; Západočeská univerzita v Plzni: Plzeň, pp. 247–252.

Šibrava, V. (1972): Zur Stellung der Tschechoslovakei in Korrelierungssystem des Pleistozäns in Europa. Sborník geologických věd, Antropozoikum; Academia: Prague, 218 p.

Šibrava, V. (1979): Erforschung der Pleistozänablagerungen auf dem Hügel Zlatý kopec bei Přezletice. Sborník geologických věd, Antropozoikum 12, 57–146.

Štěpančíková, P. (2003): Terasy dolní Sázavy v úseku od Vrabčího Brodu po Kamenný Přívoz. Geografie – Sborník České geografické společnosti 108(3), 216–226, https://doi.org/10.37040/geografie2003108030216.

Štěpančíková, P., Stemberk, J. (2004): Morphotectonic research of the East Czech Sudeten in the Czech Republic and monitoring of present-day tectonic movements. AUC Geographica 39(1), 173–180.

Štěpančíková, P., Stemberk, J., Vilímek, V., Košťák, B. (2008): Neotectonic development of drainage networks in the East Sudeten Mountains and monitoring of recent fault displacements (Czech Republic). Geomorphology 102(1), 68–80, https://doi.org/10.1016/j.geomorph.2007.06.016.

Štěpančíková, P., Hók, J., Nývlt, D., Dohnal, J., Sýkorová, I., Stemberk, J. (2010): Active tectonics research using trenching technique on the southeastern section of the Sudetic Marginal Fault (NE Bohemian Massif, central Europe). Tectonophysics 485(1–4), 269–282, https://doi.org/10.1016/j.tecto.2010.01.004.

Štěpančíková, P., Stemberk, J. jr. (2016): Region of the Rychlebské Hory Mountains – Tectonically Controlled Landforms and Unique Landscape of Granite Inselbergs (Sudetic Mountains). In: Pánek, T., Hradecký, J. (Eds.), Landscapes and Landforms of the Czech Republic. World Geomorphological Landscapes; Springer: Cham, https://doi.org/10.1007/978-3-319-27537-6_21.

Štěpančíková, P., Flašar, J., Stemberk, J., Balatka, B., Kalvoda, J., Sana, H. (2018): Neotectonic activity reflected in morphology along the Mariánské Lázně fault and in the adjacent Cheb Basin (Bohemian Massif, central Europe). In: Proceedings of the 9th International INQUA Meeting on Paleoseismology (PATA), 25–27th June, Possidi, Greece, pp. 275–278.

Štěpančíková, P., Fischer, T., Stemberk, J. jr., Nováková, L., Hartvich, F., Figuiredo, P. M. (2019): Active tectonics in the Cheb Basin: youngest documented Holocene surface faulting in Central Europe? Geomorphology 327, 472–488, https://doi.org/10.1016/j.geomorph.2018.11.007.

Štor, T., Schaller, M., Merchel, S., Martínek, K., Rittenour, T., Rugel, G., Scharf, A. (2019): Quaternary evolution of the Ploučnice River system (Bohemian Massif) based on fluvial deposits dated with optically stimulated luminescence and in situ produced cosmogenic nuclides. Geomorphology 329, 152–169, https://doi.org/10.1016/j.geomorph.2018.12.019.

Šust, P. (1981): Geomorfologická mapa území mezi Suchou Kamenicí a Studeným potokem v Děčínské vrchovině. Master thesis, Charles University, Prague.

Tomeček, J. (2007): Geomorfologie lokality Skalka v Ondřejovské vrchovině. Master thesis, Charles University, Prague.

Tyráček, J. (2001a): Upper Cenozoic fluvial history in the Bohemian Massif. Quaternary International 79(1), 37–53, https://doi.org/10.1016/S1040-6182(00)00121-X.

Tyráček, J. (2001b): Quaternary of the Mělník area: Excursion Guide; Czech Geological Survey: Prague.

Tyráček, J. (2010): Geologie kvartérních fluviálních sedimentů na soutoku Labe s Jizerou.

Geoscience Research Reports for 2011, 133–137, https://doi.org/10.1007/s00503-011-2127-x.

Tyráček, J., Havlíček, P. (2009): The fluvial record in the Czech Republic: A review in the context of IGCP 518. Global and Planetary Change 68(4), 311–325, https://doi.org/10.1016/j.gloplacha.2009.03.007.
Tyráček, J., Westaway, R., Bridgland, D. (2004): River terraces of the Vltava and Labe (Elbe) system, Czech Republic, and their implications for the uplift history of the Bohemian Massif. Proceedings of the Geologists' Association 115(2), 101–124, https://doi.org/10.1016/S0016-7878(04)80022-1.
Vaníčková, E. (2004): Geomorfologický vývoj údolí Divoké Orlice v oblasti Zemské brány. Master thesis, Charles University, Prague.
Vaníčková, E., Kalvoda, J. (2006a): Geomorphology of the Divoká Orlice valley in the Zemská brána Gate area, the Orlické hory Mountains, Czech Republic. Geomorphologia Slovaca 6(1), 36–44.
Vaníčková, E., Kalvoda, J. (2006b): Geomorfologický vývoj údolí Divoké Orlice v oblasti Zemské brány, Orlické hory. Geomorfologický sborník 5, 300–305.
Vilímek, V. (1993): Morfostrukturní vývoj reliéfu kateřinohorské klenby v Krušných horách. Doctoral thesis, Ústav geologie a geotechniky ČSAV, Prague.
Vilímek, V. (1995): Quaternary development of Kateřinohorská Vault relief in the Krušné hory Mountains. AUC Geographica 30, Supplementum, 115–137.
Vilímek, V. (1997): Morphostructural analysis of Kateřinohorská Vault in Krušné hory Mts. Acta Montana, Series AB 108(5), 7–59.
Vilímek, V., Kalvoda, J., Kroczek, T. (2021): Historie a výsledky nivelačních měření v okolí štoly Jezeří. Zpravodaj Hnědé uhlí 1, 24–28.
Vilímek, V., Zvelebil, J., Kalvoda, J., Šíma, J. (2010): Landslide field research and capacity building through international collaboration. Landslides 7(3), 375–380, https://doi.org/10.1007/s10346-010-0209-9.
Votýpka, J. (1975): Kvartérní modelace zarovnaných povrchů Plechého na Šumavě. AUC Geographica 10(1–2), 43–60.
Votýpka, J. (1997): Geomorphological analysis of the development of the south-eastern Šumava granite region. AUC Geographica 32(2), 133–148.
Vyskočil, P. (1975): Recent crustal movements in the Bohemian Massif. Tectonophysics 29, 269–282, https://doi.org/10.1016/0040-1951(75)90161-4.
Vyskočil, P. (1984): Results of recent crustal movements studies. Rozpravy Československé akademie věd 94(8); Academia: Prague, 104 p.
Vyskočil, P. (1988): The dynamics of the Bohemian Massif. Journal of Geodynamics 10(2–4), 157–165, https://doi.org/10.1016/0264-3707(88)90022-1.
Wagner, G. A., Gögen, K., Jonckheere, R., Kämpf, H., Wagner, I., Woda, C. (1998): The age of Quaternary volcanoes Železná hůrka and Komorní hůrka (western Eger Rift), Czech Republic: alpha-recoil track, TL, ESR and fission track chronometry. In: Magmatism and Rift Basin Evolution (IGCP Project No. 369): Excursion Guide and Abstracts of the Workshop, Liblice, 7–11 September 1998; Czech Geological Survey: Prague, pp. 95–96.
Záruba, Q. (1942): Podélný profil vltavskými terasami mezi Kamýkem a Veltrusy. Rozpravy Československé akademie věd 52(9); Academia: Prague, 39 p.
Záruba, Q., Rybář, J. (1961): Doklady pleistocenní agradace údolí Sázavy. Sborník Československé společnosti zeměpisné, 66(1), 23–30, https://doi.org/10.37040/geografie1961066010023.
Záruba, Q., Bucha, V., Ložek, V. (1977): Significance of the Vltava Terrace system for Quaternary chronostratigraphy. Rozpravy Československé akademie věd 87(4); Academia: Prague, 90 p.
Zeman, J. (1978): Deep-seated fault structures on the Bohemian Massif. Sborník geologických věd 31, 155–182.
Zvelebil, J. (1989): Inženýrskogeologické aspekty vývoje svahů v Děčínské vrchovině. Doctoral thesis, Ústav geologie a geotechniky ČSAV, Prague.

Appendix 1

In memory of RNDr. Břetislav Balatka, CSc. (*11. 1. 1931 – †15. 2. 2025) (Jan Kalvoda)

January 2026 marked 95 years since the birth of the prominent Czech geographer RNDr. Břetislav Balatka, CSc. He was born in Benešov near Semily on 11 January 1931, graduated with honours from the grammar school in Planá near Mariánské Lázně (1950) and completed his university studies at the Faculty of Geology and Geography (Natural Sciences) of Charles University in Prague in 1954. Břetislav Balatka then became a research assistant at the Geology and Geography Section of the Czechoslovak Academy of Sciences, where his supervisor was Professor RNDr. Josef Kunský, DrSc., a corresponding member of the Czechoslovak Academy of Sciences. From 1957, Břetislav Balatka worked at the Geomorphological Department of the Czechoslovak Academy of Sciences and in 1963 he became a researcher at the Institute of Geography of the Czechoslovak Academy of Sciences, where he worked for more than 30 years. He obtained his Candidate of Geographical Sciences (CSc.) degree (a PhD-equivalent academic research degree) in 1963 and in 1966 he received the title of Doctor of Natural Sciences (RNDr.) at Charles University in Prague. In 1993, Břetislav Balatka became a senior researcher and lecturer at the Department of Physical Geography and Geoecology, Faculty of Science, Charles University.

A detailed biography and professional focus of Břetislav Balatka was subject of an article by doc. RNDr. Václav Přibyl, CSc., published on the occasion of his seventieth birthday (Přibyl 2001). The article also includes a list of Břetislav Balatka's works from 1956–2001. A selection of his publications from the 21st century is then presented in articles by Kalvoda (2011, 2016). Lists of Břetislav Balatka's publications

include over 40 books, more than 80 original professional articles, around 25 thematic maps and 90 research reports, as well as over 100 popular papers and dozens of conference contributions and studies. Moreover, his teaching, editing and reviewing activities were also very extensive.

Břetislav Balatka and his main collaborators, PhDr. Jaroslav Sládek, CSc. and RNDr. Jaroslava Loučková, CSc., are prominent researchers in Czech physical geography and geomorphology. It was not possible to freely implement their excellent professional work in the international scientific context due to the unfortunate (or, more accurately, tragic) history of Czech society in the years 1948–1989. Therefore, they were unable to systematically participate in addressing and correlating geographical topics in the wider European region.

From Břetislav Balatka's extensive geographical work, it is particularly worth highlighting his geomorphological research focused on the development of the river network and fluvial relief in the Czech lands, as well as his physical-geographical work on selected regions of the Bohemian Massif. His professional experience in researching geomorphological, climatic, and hydrological processes and phenomena, as well as nature protection and natural hazards, allowed Břetislav Balatka to deepen and update the solutions to varied geomorphological problems in Czechia.

Břetislav Balatka's encyclopaedic knowledge in several Earth science disciplines and his extraordinary teaching skills were put to good use in university lectures, seminars, field excursions and during the education of undergraduate and postgraduate students. It should be noted that Břetislav Balatka, in addition to the fluvial geomorphology of the Czech lands, also investigated in detail the evolution of the landforms of the Czech Cretaceous Table, including its unique sandstone relief. He paid considerable attention to the evolution of the Ohře (Eger) valley, the main stages of which are associated with both substantial changes in climatic and morphogenetic processes and neotectonic activity in the Late Quaternary. His other favourite topics were pseudokarst phenomena on neovolcanic rocks and crystalline rocks, as well as the significant phenomenon of slope movements in the Czech landscape. Břetislav Balatka and Jaroslav Sládek also focused on the very current issue of precipitation and runoff conditions in relation to changes in the water content of Czech rivers, including extraordinary events of this kind.

For a long time, Břetislav Balatka, together with colleagues from the Institute of Geography of the Czechoslovak Academy of Sciences, worked on the concept of various methods of geomorphological mapping, including the creation of their legends, as well as updates to the orographic subdivisions and the characteristics of historical-genetic types of georelief of the Czech lands. In the first decade of the 21st century, this classic figure in Czech physical and regional geography significantly contributed to the successful work of the Center for Earth Dynamics Research. Břetislav Balatka was a key member of the expert team that dealt with dynamic and evolutionary geomorphology. Systematic measurements and monitoring of geodynamic processes and phenomena using geodetic, geological and geophysical methods, including remote sensing, must be consistently integrated with their geomorphological and physical-geographical interpretations. This methodologically and knowledge-intensive comprehensive approach allows to identify evolutionary features of Earth dynamics in the palaeogeographical and/or prognostic context of global and regional changes in the natural environment.

Břetislav Balatka's dedication to scientific and pedagogical work was combined with his refined intuition for capturing the essential features of the observed natural processes and phenomena and at the same time with his creative ability to combine analytical and comprehensive approaches to the geographical topics he addressed. For these rare qualities, as well as his admirable diligence, modesty and very kind approach to colleagues and students, Dr. Břetislav Balatka became a shining example of a noble person and researcher for the current and upcoming generation of Czech geographers.

Evaluation of SAR C-band radar vegetation indices for rice crop monitoring in Tamil Nadu, India

Haseeb Habeebulla[1], Sivasankar S[1], Arun Pratap Mishra[2,*], Sanjeevi Prasad[1], Mijing Gwra Basumatary[3], Vipin Chandra Lal[4]

[1] University of Madras, Department of Geography, India
[2] Ministry of Home Affairs, Government of India, Office of the Registrar General of India, India
[3] Gauhati University, B. Borooah College (Autonomous), Department of Geography, India
[4] University of Delhi, Dr. Bhim Rao Ambedkar College, Department of Geography, India
* Corresponding author: apmishra88.rgi@nic.in

ABSTRACT

Rice (Oryza sativa) cultivation plays a critical role in food security across Asia, where smallholder farmers depend heavily on timely information about crop development and field conditions. Monitoring these changes using optical remote sensing is constrained by persistent cloud cover during monsoon-driven growing seasons, underscoring the necessity of Synthetic Aperture Radar (SAR) for continuous observation. This study evaluates the capability of Sentinel-1 C-band SAR for tracking rice phenology in two smallholder fields in Mayiladuthurai District, Tamil Nadu, during the Late Samba season (September to January). Field-scale analysis of VV, VH, and NDVI time series for 2023–2024 captured key phenological transitions, with polarization showing a strong correlation with NDVI (Farm 1: r = 0.75; Farm 2: r = 0.73). Radar Vegetation Indices (RVI, mRVI, and RVI4S1) were computed from multi-year Sentinel-1 data (2018–2023) and compared with MODIS NDVI. Although the radar indices showed high inter-correlation (r > 0.90), their relationship with NDVI remained weak (0.15–0.30). Machine learning experiments over a 1.5 × 1.5 km region (2018–2022) demonstrated that a Linear Regression model (6.92×10^{-5}) outperformed Random Forest Regression (0.000258) in predicting RVI4S1 from VV and VH, indicating linear relationship between radar channels and the index. The study highlights the suitability of Sentinel-1 SAR-particularly VH polarization – for phenology tracking in smallholder contexts, especially where optical data are limited by cloud cover.

KEYWORDS

rice (Oryza sativa); remote sensing; Sentinel-1; radar vegetation indices; machine learning; small-scale farmers; India

Received: 30 July 2025
Accepted: 14 April 2026
Published online: 30 April 2026

Habeebulla, H., S, S., Mishra, A. P., Prasad, S., Basumatary, M. G., Lal, V. C. (2026): Evaluation of SAR C-band radar vegetation indices for rice crop monitoring in Tamil Nadu, India. AUC Geographica 61(2), 241–255
https://doi.org/10.14712/23361980.2026.6
© 2026 The Authors. This is an open-access article distributed under the terms of the Creative Commons Attribution License (https://creativecommons.org/licenses/by/4.0).

1. Introduction

Rice (Oryza sativa) is one of the most prominent staple foods that sustains food security around the world; it mainly grows in Asia (Muthayya et al. 2014). It is consumed by nearly half of the world's population and occupying more than 11% of cultivated land (Kumar et al. 2022). More than 90% of global rice production occurs in Asian countries, where it is primarily consumed. About 80% of the world's rice is grown by small-scale farmers with low incomes, mostly in developing countries, involving around 140 million rice-growing households (FAO 2017). Rice (Oryza sativa) is traditionally grown as an annual plant, but in tropical regions, it can survive as a perennial and produce a ratoon crop for up to 30 years. Biophysical parameters, such as biomass, yield estimation, leaf area index (LAI), and water content, are critical for farmers in rice cultivation. For instance, dry biomass can be used to estimate yield. Rice cultivation is predominantly practiced in regions with abundant rainfall and relatively low labor costs, as it is a labor-intensive crop with high water requirements. In this context, timely and accurate estimation of rice-growing areas and production in Tamil Nadu state of India is essential for effective agricultural planning, food security assessment, and environmental sustainability (Surendran et al. 2021; Udimal et al. 2017).

Traditional data on rice-growing regions, seasons, and yields are often sub-national, but current systems may not meet the data requirements for food security and policy formulation. Reliable monitoring of rice phenology and crop condition is essential (Wu et al. 2023). Rice farming is linked to various environmental aspects, from water use to climate change, due to its high methane emissions (Shen et al. 2024). Thus, long-term annual monitoring is required to study the impacts of changes in rice cultivation areas and farming practices, which are likely to evolve in the coming years to address economic and environmental challenges. The use of optical data for crop monitoring and management has been widely explored over the last two decades. Vegetation indices, such as NDVI, EVI, and LAI, from optical remote sensing observations, are majorly applied to assess crop growth stages (Omia et al. 2023). However, persistent cloud cover under monsoon-driven rice cultivation severely constrains passive optical remote sensing, leading to data gaps during critical phenological transitions. SAR is unaffected by these constraints by providing day-night, cloud-independent observations sensitive to the canopy structure, the accumulation of biomass, and conditions in field water. Moreover, the Sentinel-1 provides C-band SAR data with dual polarization (VV and VH), enabling systematic, all-weather monitoring of agricultural surfaces (ESA 2018). Various studies have proven that dual-polarimetric SAR backscatter efficiently characterizes soil and vegetation conditions over agricultural croplands (Bhogapurapu et al. 2022). These properties make Sentinel-1 especially suitable for monitoring transplanted rice systems (Atzberger 2013; Inoue et al. 2014; Wu et al. 2023).

Early studies have shown that C-band SAR backscatter is highly sensitive to rice phenological stages, especially in conditions related to flooding and canopy development (Le Toan et al. 1997). Time-series Sentinel-1 SAR data have proven effective for mapping rice extent and cropping patterns in cloud-prone deltaic environments (Nguyen et al. 2016). Temporal variation in Sentinel-1 VV and VH backscatter aligns with critical rice phenological stages, such as transplanting, vegetative growth, and maturity, supporting use of SAR for rice monitoring (Choudhury et al. 2022). Despite these advances relatively few studies have evaluated SAR performance in heterogeneous smallholder landscapes where field size, planting dates, irrigation schedules, and waterlogging vary greatly. Radar Vegetation Indices (RVIs) have been proposed to enhance crop monitoring; however, their long-term consistency and relationship to optical vegetation indices at the farm scale remain insufficiently investigated (Inoue et al. 2014; Veloso et al. 2017; Wu et al. 2023). To address these gaps, this study integrates multi-year Sentinel-1 C-band backscatter with both field-scale and multi-year NDVI time series to assess the potential of SAR for rice monitoring in two farm fields in Mayiladuthurai District, Tamil Nadu. It has been observed in previous studies that SAR times series are capable of providing complementary information to optical satellite data, such as NDVI, especially for crop structure and moisture (Blaes et al. 2005).

Random Forest regression models were employed to predict RVI4S1 using Sentinel-1 VV and VH polarization data. The effectiveness of machine learning approaches for analyzing multi-temporal Sentinel-1 SAR data in rice-growing regions has been reported in earlier studies (Onojeghuo et al. 2018). Comprehensive reviews have emphasized the importance of integrating optical and SAR data for reliable rice crop monitoring at regional and global scales (Kuenzer and Knauer 2013). A multi-year radar-optical correlations with phenological analyses at the field scale and offers an integrated evaluation of Sentinel-1 SAR data with respect to smallholder rice systems. The specific objectives of this study are to analyse field-scale phenological trajectories of rice during the 2023–2024 Late Samba season using Sentinel-1 VV and VH backscatter and Sentinel-2 NDVI, to evaluate multi-year (2018–2023) radar-optical relationships by examining correlations between MODIS NDVI and SAR-derived radar vegetation indices (RVI, mRVI, and RVI4S) and to compare machine learning models of Linear Regression and Random Forest Regression to predict RVI4S1 using VV and VH.

2. Study area

The study area is predominantly agricultural, with irrigated rice (Oryza sativa) forming the major crop and occupying most cultivated lands. The study was carried out in Arangakudi, Vadakarai village, located in Mayiladuthurai District of Tamil Nadu, India (Fig. 1). These two farmlands are cultivated with the rice (Oryza sativa) crop variety (ADT 45) on both lands. The farms have been cultivating this variety for nearly 10 years. The cultivation of rice (Oryza sativa) crops during the Late Samba period spans 135 days, from September to January. Investigation reveals that the rice (Oryza sativa) crop cultivation during the Late Samba season occurred from September 2023 to January 2024. Seedling transplantation took place on September 1, 2023, followed by transplanting on September 21, 2023. The crop matured by December 21, 2023, but harvesting was delayed until January 25, 2024, due to unexpected water logging. Originally, harvesting was planned for January 15, 2024.

3. Datasets

3.1 Google Earth Engine (GEE) datasets

3.1.1 Sentinel-2 optical data

Sentinel-2 multispectral data is accessed from European Space Agency (ESA) through GEE. The data is used for computing Normalized Difference Vegetation Index (NDVI) for vegetation monitoring during 2023–2024, 135 days cropping cycle with Band-4 (Red) and Band-8 (NIR) of 10m resolution (Drusch et al. 2012; Tucker 1979; Gorelick et al. 2017).

3.1.2 Sentinel-1 SAR C-band data

Sentinel-1 Ground Range Detected (GRD) C-band SAR data (VV and VH dual polarization) were utilized to

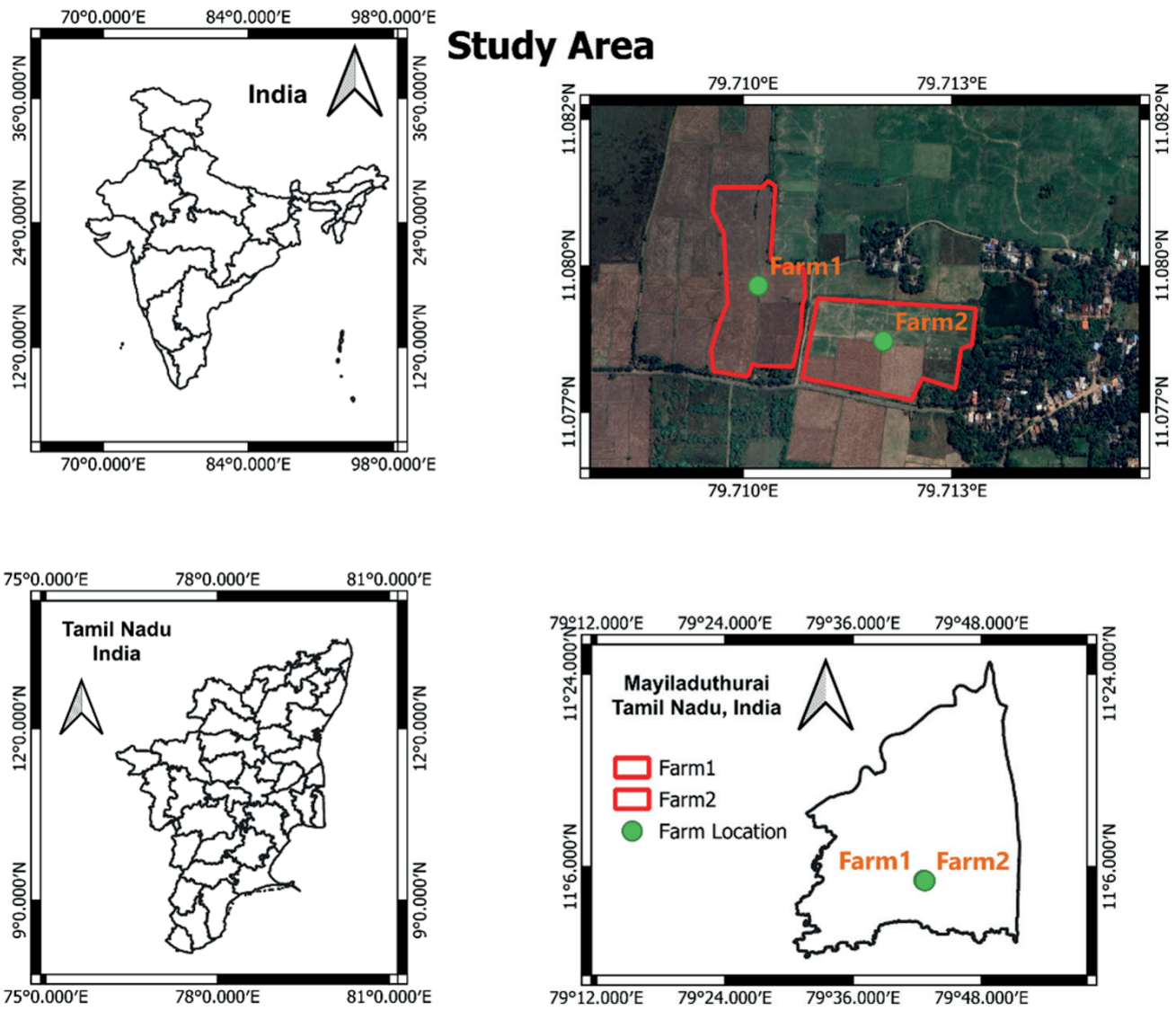

Fig. 1 Maps of locations. Farm 1: Area-Acre 7.71, Farm 2: Area-Acre 8.182.

monitor structural and moisture-related changes within irrigated rice (Oryza sativa) fields. Data were pre-processed using Sentinel-1 toolbox, thermal noise removal, radiometric calibration, terrain correction using SRTM 30 or ASTER DEM (ESA 2018; Small 2011). The terrain-corrected backscatter coefficients were converted to decibels using logarithmic scaling. VV and VH polarization channels were then extracted for further analysis. For this study, mosaic scenes corresponding to specific phenological stages of the crop 135 days growth cycle were generated, ensuring temporal alignment with optical NDVI observations. Dual-polarization of C-band SAR (VV and VH) is well suited for monitoring rice environments due to its sensitivity to surface water conditions, canopy structure, and biomass dynamics (Inoue et al. 2014; Bouvet and Le Toan 2011).

3.1.3 MODIS Terra daily NDVI

Seasonal NDVI time-series data have been widely used to map rice extent and phenological patterns in high-intensity cropping systems (Gumma et al. 2014). Multi-temporal MODIS imagery has been widely used to map paddy rice extent and seasonal dynamics across South and Southeast Asia (Xiao et al. 2006). MODIS Terra Daily NDVI product (2018–2022) was incorporated for historical vegetation trend analysis (Tab. 1). It has a coarser spatial resolution and its high temporal frequency enhances phenological assessment over multiple year (Li et al. 2024).

Tab.1 Specifications of GEE datasets.

	Dataset	Acquired
GEE	Sentinel-2A	2023–2024 (Sept, Oct, Nov, Dec, Jan)
	MODIS Terra (Daily) NDVI	2018–2023 (Sept, Oct, Nov, Dec, Jan)
	Sentinel-1 SAR GRD: C-Band	2023–2024 (Sept, Oct, Nov, Dec, Jan)

Source: ESA and NASA datasets accessed via Google Earth Engine (Gorelick et al. 2017).

4. Methodology

4.1 Phenological stages

The temporal changes in VV and VH backscatter were compared with NDVI to assess their relationship. Variations in backscatter corresponds closely changes to canopy structure and moisture content. By examining these parameters together, it is possible to identify phenological transitions, such as vegetation growth, reproductive stages, and maturity. Increases in NDVI typically align with rising VV and VH signals during biomass accumulation, while declines as the crop approaches senescence and harvest. This integrated analysis enables clearer interpretation of crop developmental stages across the 135-day growth cycle.

4.2 Correlation between different radar vegetation indices and NDVI

4.2.1 Normalized difference vegetation index (NDVI)

The NDVI used in this study was derived from the MODIS Terra Daily NDVI product (2018–2023). To enhance its suitability for Sentinel-1, the MODIS NDVI was resampled to a 10-m spatial resolution using the bilinear interpolation method. The resampled NDVI dataset was subsequently used to extract Normalized Difference Vegetation Index (NDVI) for specific dates corresponding to key stages of the 135 days crop growth cycle.

4.2.2 Radar vegetation indices

Sentinel-1 C-band VV and VH backscatter was speckle-filtered to produce Radar Vegetation Indices (RVIs). In order to ensure a physically meaningful representation of scattering intensities, the polarization values of VV and VH values were transformed from decibels (dB) to linear units using 10^ (dB/10).

- Radar Vegetation Index (RVI)
  Co- and cross-polarized backscatter intensities are used by the RVI to measure vegetation development:

$$\mathrm{RVI} = \frac{4 \cdot \mathrm{VH}}{\mathrm{VV} + \mathrm{VH}} \qquad \text{(Bhogapurapu et al.2022)}$$

  By normalizing the scattering response, this formulation produces values that ideally fall between 0 and 1. Higher values indicate more vegetation cover and larger canopy volume scattering.

- Radar vegetation index for Sentinel-1 (RVI4S1)
  The degree of polarization (DOP) is incorporated into the RVI4S1 metric to improve crop structural sensitivity:

$$q = \frac{VH}{VV}, DOP = \frac{1-q}{1+q}$$

$$\mathrm{RVI}_{4S1} = \sqrt{\mathrm{DOP}} \cdot \frac{4 \cdot \mathrm{VH}}{\mathrm{VV} + \mathrm{VH}} \quad \text{(Choudhury et al.2022)}$$

- Modified Radar Vegetation Index (mRVI)
  The mRVI is calculated as:

$$\mathrm{mRVI} = \left(\frac{\gamma^0_{\mathrm{VV}}}{\gamma^0_{\mathrm{VV}} + \gamma^0_{\mathrm{VH}}}\right)^{0.5} \left(\frac{4\,\gamma^0_{\mathrm{VH}}}{\gamma^0_{\mathrm{VV}} + \gamma^0_{\mathrm{VH}}}\right)$$

(Çolak et al. 2021)

The RVI, RVI4S1, and mRVI indices were all calculated using VV and VH. Their temporal profiles were then statistically compared with NDVI to identify which radar-based metric exhibits the strongest correspondence with vegetation crop growth dynamics.

4.3 Comparison of machine learning model of random forest Regression and linear regression

4.3.1 Random forest regression

Random Forest Regression was implemented to predict the RVI4S1 using VV and VH backscatter as input features.

$$\widehat{RVI4S1}(x) = \frac{1}{B}\sum_{b=1}^{B} \hat{y}_b\,(x)$$

This model is used for nonlinear relationships between SAR backscatter (VV, VH) and the vegetation index.

4.3.2 Linear regression

Linear Regression was used as a baseline model to quantify the linear dependency of RVI4S1 on VV and VH. A multiple linear regression model was fitted using:

$$RVI4S1 = \beta_0 + \beta_1 VV + \beta_2 VH,$$

where and represent the contribution of each polarization to the predicted vegetation index. This study-specific formulation evaluates how well simple linear combinations of VV and VH explain variability in RVI4S1, allowing direct comparison with the Random Forest model's nonlinear predictive capability.

5. Results and discussion

5.1 Phenological stages analysis

The Fig. 2 illustrates the temporal variation of VV backscatter for Farm 1 from September 2023 to January 2024. Spatial variations in backscatter intensity indicate changes in surface conditions and Oryza sativa growth stages, with marked responses at the selected field locations. The phenological graph illustrated in Fig. 3 shows seasonal variations in Oryza sativa growth for both Farm 1 and Farm 2. The decreases observed on 1 October 2023 for Farm 1 and 15 September 2023 for Farm 2 correspond to the transplanting stage, during which flooded conditions and a smooth soil-water surface reduce radar backscatter. According to farmer records, transplanting at Farm 2 occurred approximately one week later than Farm 1 due to temporary labour shortages; this temporal offset is clearly reflected in the respective backscatter profiles. Subsequent increases in signal intensity, around 30 October 2023 for Farm 1 and 15 November 2023 for Farm 2, are onset of the flowering stage, when canopy density and biomass begin to rise. For Farm 1, VV backscatter values ranging from approximately −11.147 dB to −8.788 dB between 15 November 2023 and 25 January 2024, indicating progressively stronger canopy scattering, characteristic of late reproductive to early maturity phases and approaching the harvest stage. Findings of the study align with previous research observation in the Asian context carried out by Dineshkumar and Satishkumar (2019) that demonstrated that Sentinel-1 C-band SAR data can effectively monitor rice crop growth, with volume scattering increasing and surface scattering decreasing as the crop progresses through its phenological stages. In a similar GEE-based analysis, Dineshkumar et.al (2019) showed that both scattering of VV and VH polarization were lowest during the transplanting stage and increase toward peak vegetation, demonstrating the sensitivity of SAR backscatter to rice phenological progression.

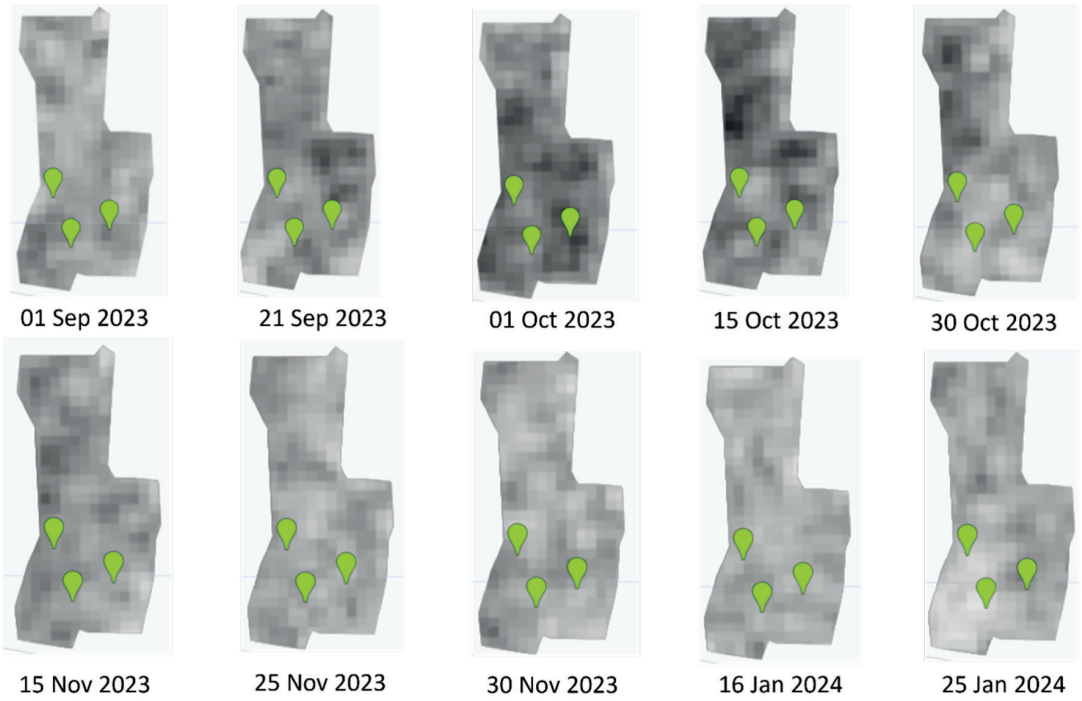

Fig. 2 VV backscatter from Farm 1 (Sep 2023–Jan 2024).

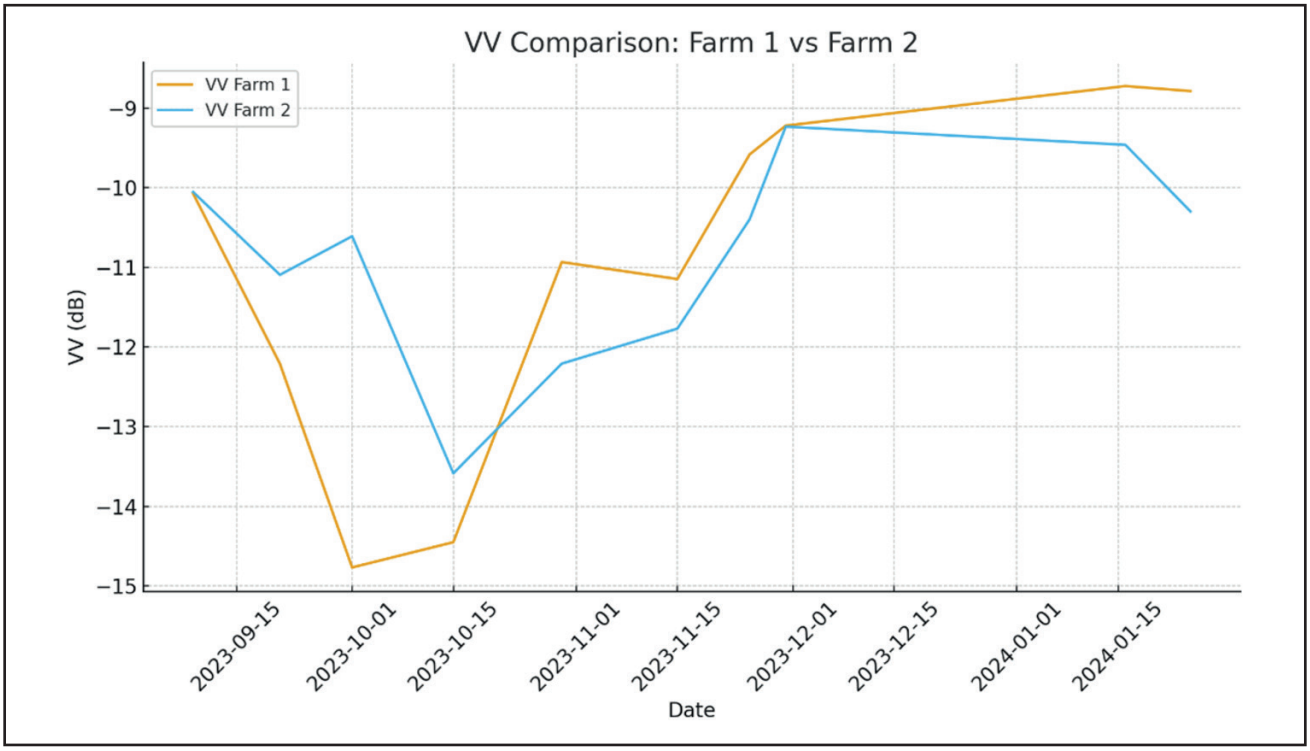

Fig. 3 VV backscatter graph from Farm 1 and Farm 2 (Sep 2023–Jan 2024).

5.2 Interpretation of VH polarization

The Fig. 4 shows multi-date VH-polarized SAR backscatter images of Farm 1 during the Oryza sativa cropping period. Variations in backscatter intensity across dates reflect changes in canopy structure and moisture conditions at the selected field locations VH backscatter for Farm 1 shows an increasing trend from −20.255 dB starting on 30 October 2023, corresponding to canopy development. The backscatter reaches a peak value of −13.51 dB on 25 January 2024, which coincides with the harvesting stage (Fig. 5). VH polarization is observed as dip associates with early growth stages characterized by low biomass and soil or surface water conditions; similarly, Mohit et al. (2022) found that VV and VH backscatter decreased during pearl millet's early growth phase and then increased as canopy development advanced. The interpretation of the observed October minimum as a transplanting and early establishment phase is supported by the increase in VH backscatter in the current study, which is consistent with increased volume scattering from the growing rice canopy.

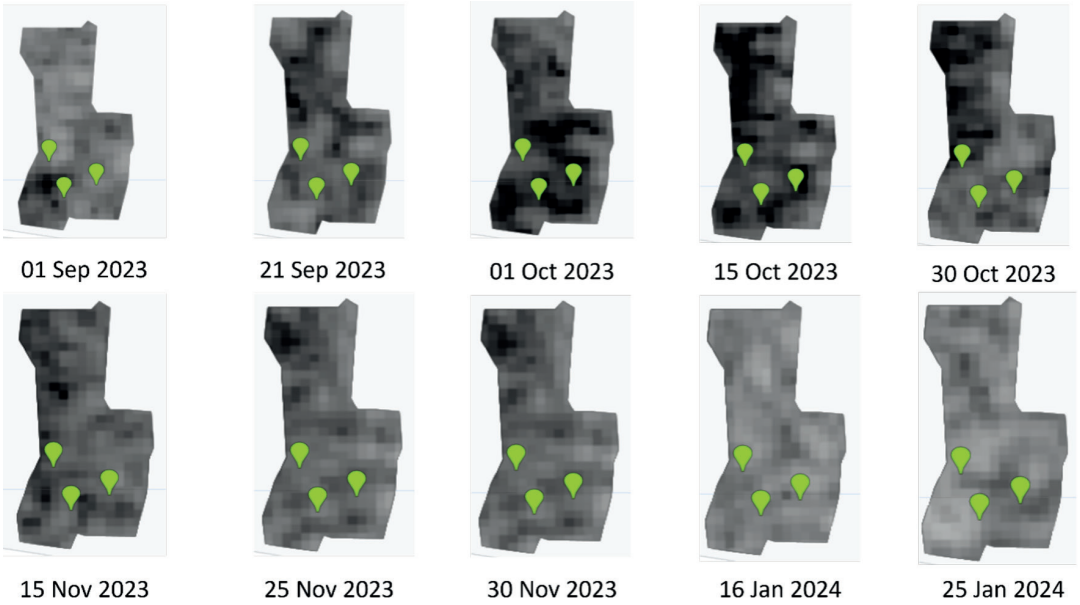

Fig. 4 VH backscatter from Farm 1 (Sep 2023–Jan 2024).

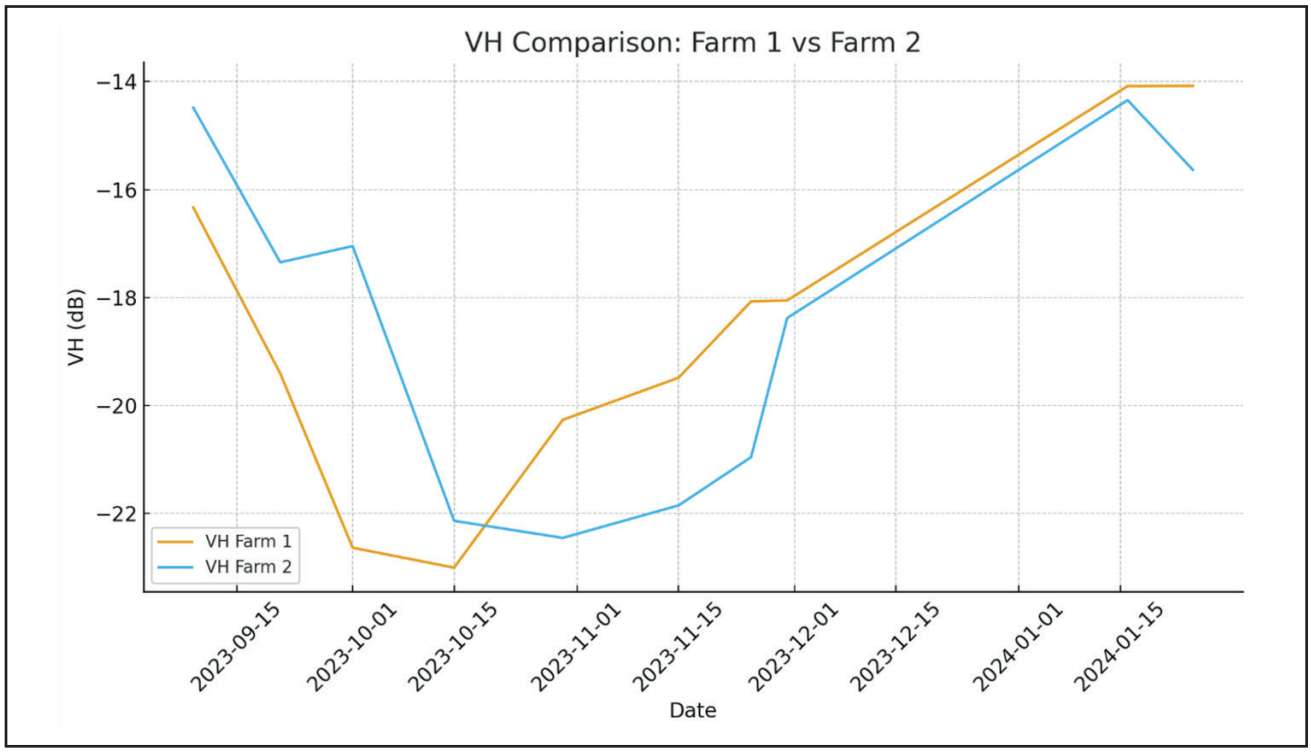

Fig. 5 VH backscatter graph from Farm 1 and Farm 2 (Sep 2023–Jan 2024).

5.3 Interpretation of NDVI

The Fig. 6 illustrates the spatial and temporal variation of SAR-based NDVI values over Farm 1 from September 2023 to January 2024. Progressive changes in NDVI intensity indicate Oryza sativa growth and canopy development at the sampled field locations. Comparing NDVI (Fig. 7) with VV (Fig. 5) and VH (Fig. 3) clearly shows the phenological transition of Farm 1 during late 2023. NDVI begins to rise after 15 November 2023 (−0.002 to 0.280 by 16 January 2024), corresponding with increasing VV backscatter (−11.147 to −8.725 dB) as canopy structure develops. In contrast, VH backscatter becomes progressively less negative (−19.487 to −14.081 dB), indicating a reduction in water-rich biomass as plants enter maturity. In correlation analysis, this shows strong associations between VH-NDVI (Pearson: 0.75; Spearman: 0.90)

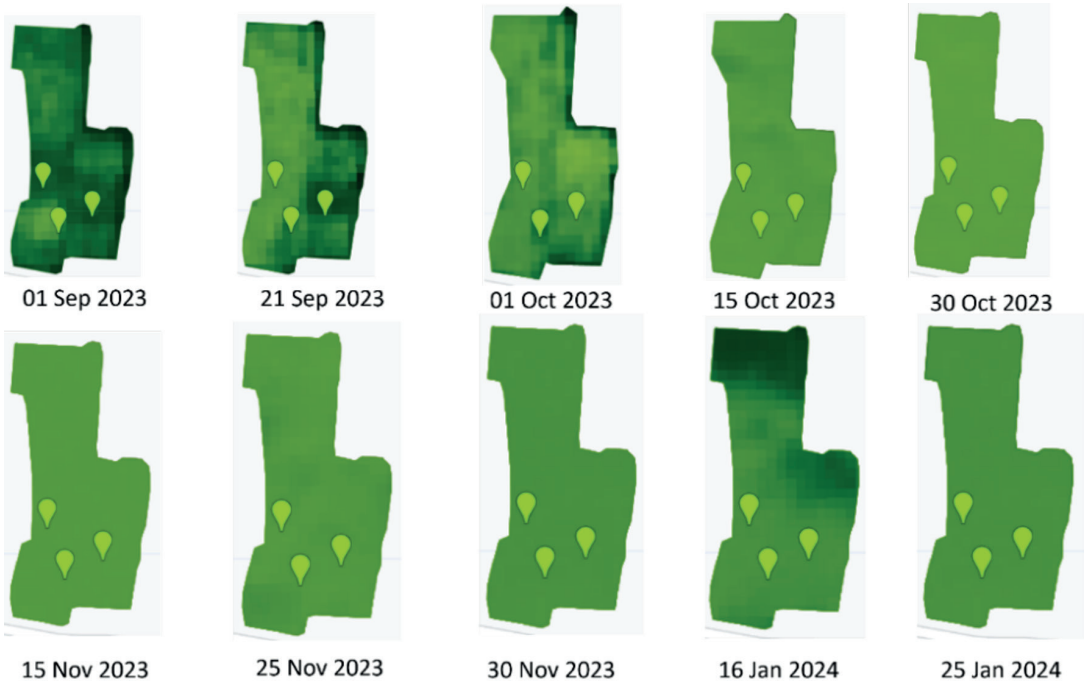

Fig. 6 NDVI from Farm 1 (Sep 2023–Jan 2024).

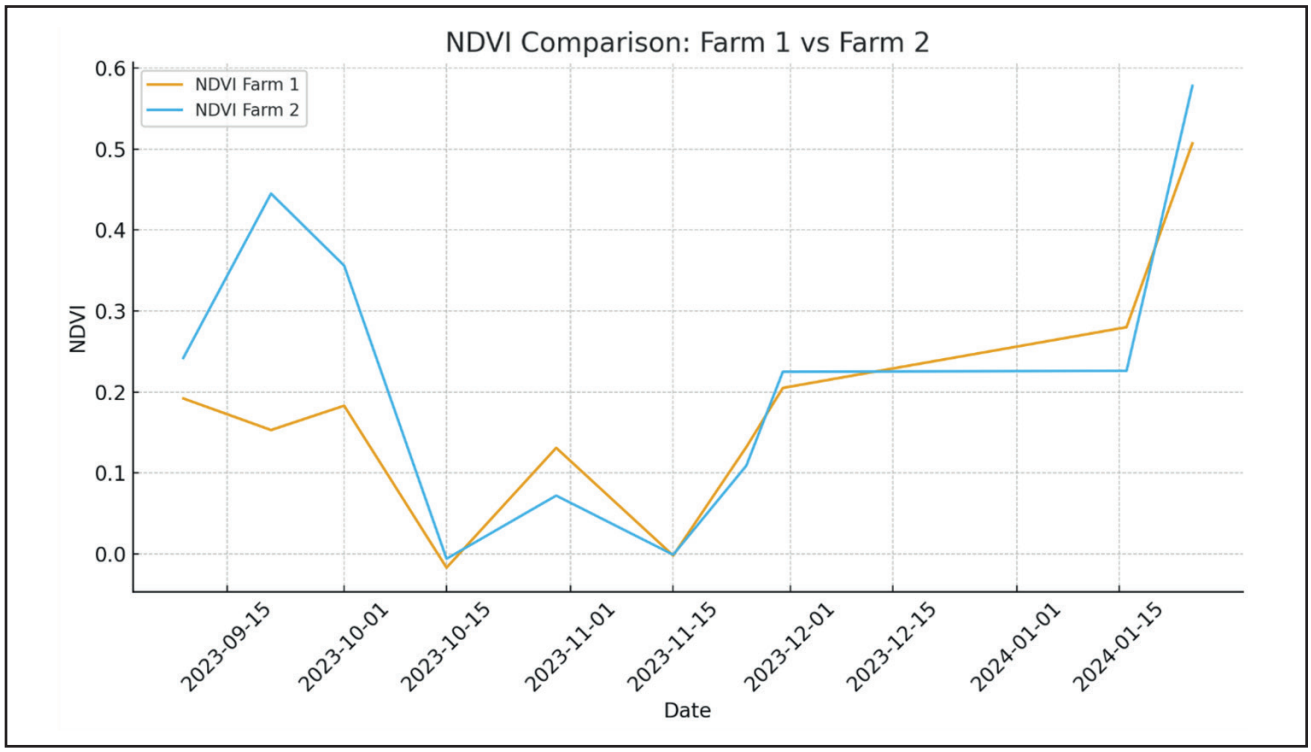

Fig. 7 NDVI graph from Farm 1 and Farm 2 (Sep 2023–Jan 2024).

Farm 1 and VH-NDVI (Pearson: 0.73; Spearman: 0.76) Farm 2, reflecting VH's sensitivity to biomass changes. The combined trends in NDVI, VV, and VH therefore confirm a decline in wet biomass after mid-November, marking the progression from reproductive growth toward harvest readiness.

5.4 Highly Correlated Radar Vegetation Index with NDVI

The Correlation Matrix data taken for the Farm 1 for the year 2018 (Sep, Oct, Nov, Dec, Jan), 2019 (Sep, Oct, Nov, Dec, Jan), 2020 (Sep, Oct, Nov, Dec, Jan), 2021 (Sep, Oct, Nov, Dec, Jan), 2022 (Sep, Oct, Nov, Dec, Jan), 2023 (Sep, Oct, Nov, Dec, Jan). The correlation matrix shows the correlation coefficients between different indices, including RVI, RVI4S1, mRVI, and NDVI (Fig. 8–10; Tab. 2). The correlation analysis reveals a strong relationship among the radar vegetation indices. RVI has a very strong positive correlation with both RVI4S1 (r = 0.95) and mRVI (r = 0.95). A slightly lower but still strong correlation exists between RVI4S1 and mRVI (r = 0.91). In contrast, the relationship between NDVI and radar-derived indices is weak. The correlation is about 0.15 for both RVI and mRVI, and 0.21 for RVI4S1. Of all the radar indices, RVI4S1 exhibits the strongest correlation with NDVI. This indicates that RVI4S1 is the most sensitive SAR-based index to vegetation variations recorded by optical NDVI.

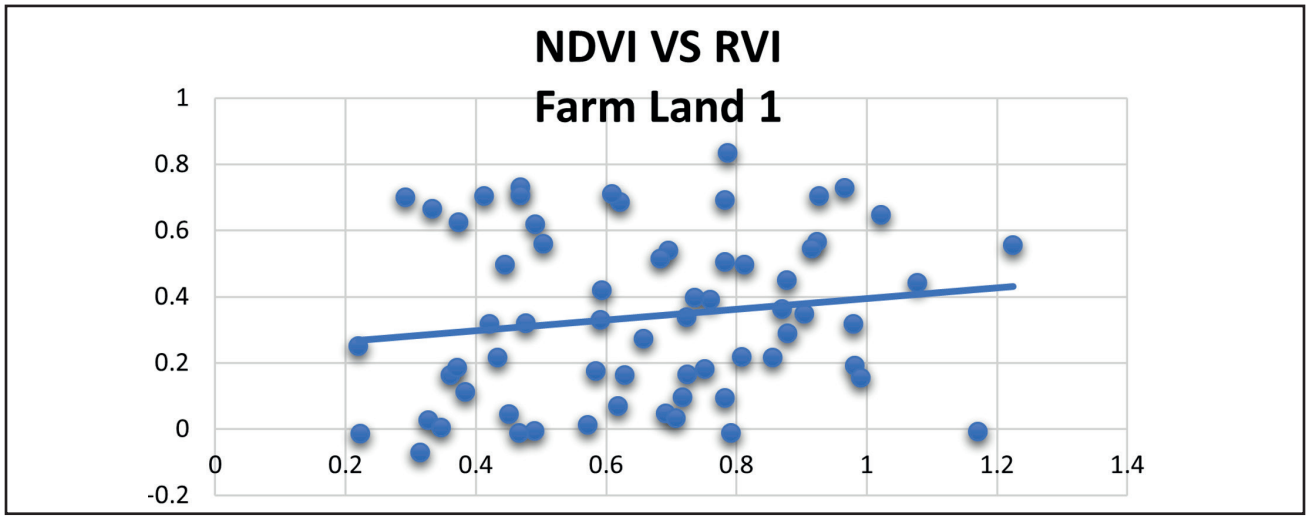

Fig. 8 Correlation between NDVI and RVI for Farm 1 (Sep 2018–Jan 2024).

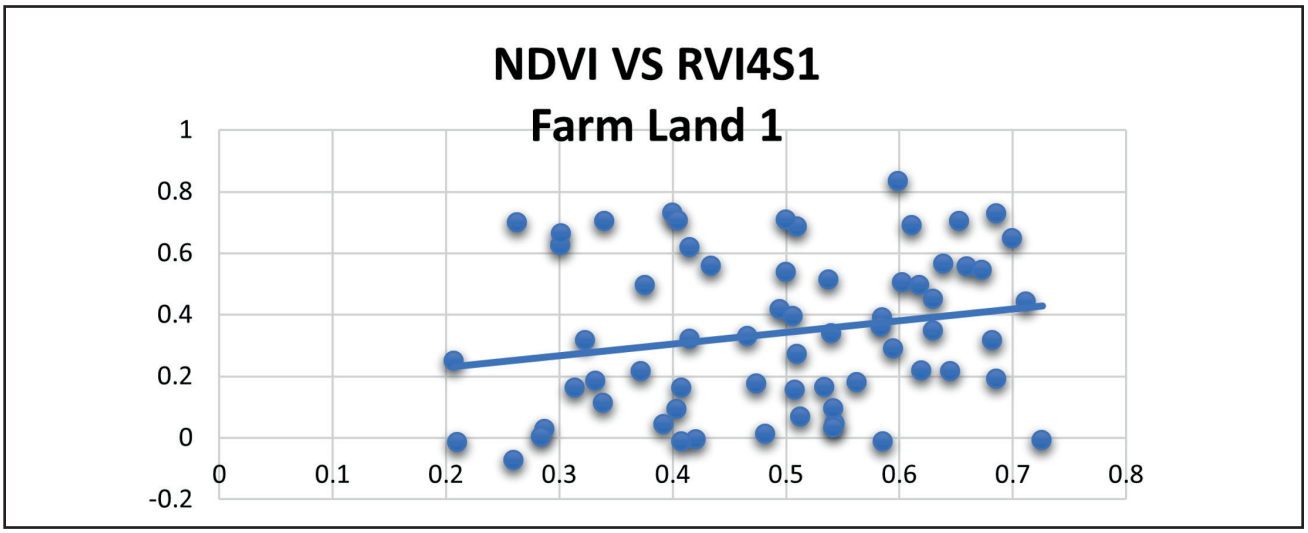

Fig. 9 Correlation between NDVI and RVI4S1 for Farm 1 (Sep 2018–Jan 2024).

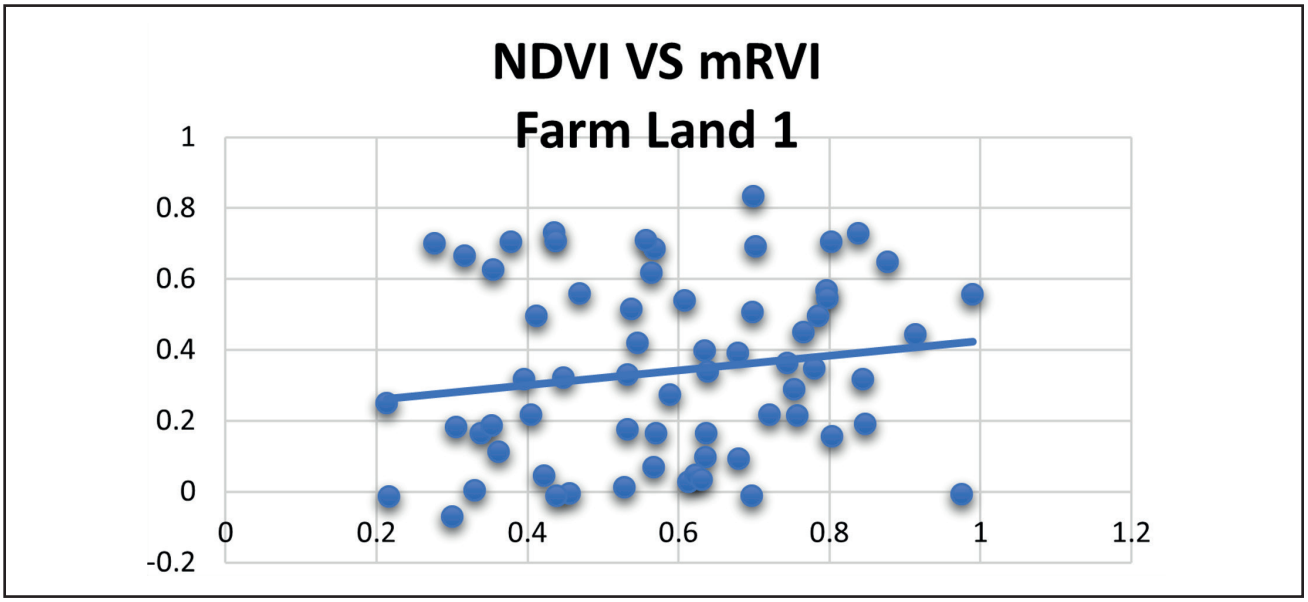

Fig. 10 Correlation between NDVI and mRVI for Farm 1 (Sep 2018–Jan 2024).

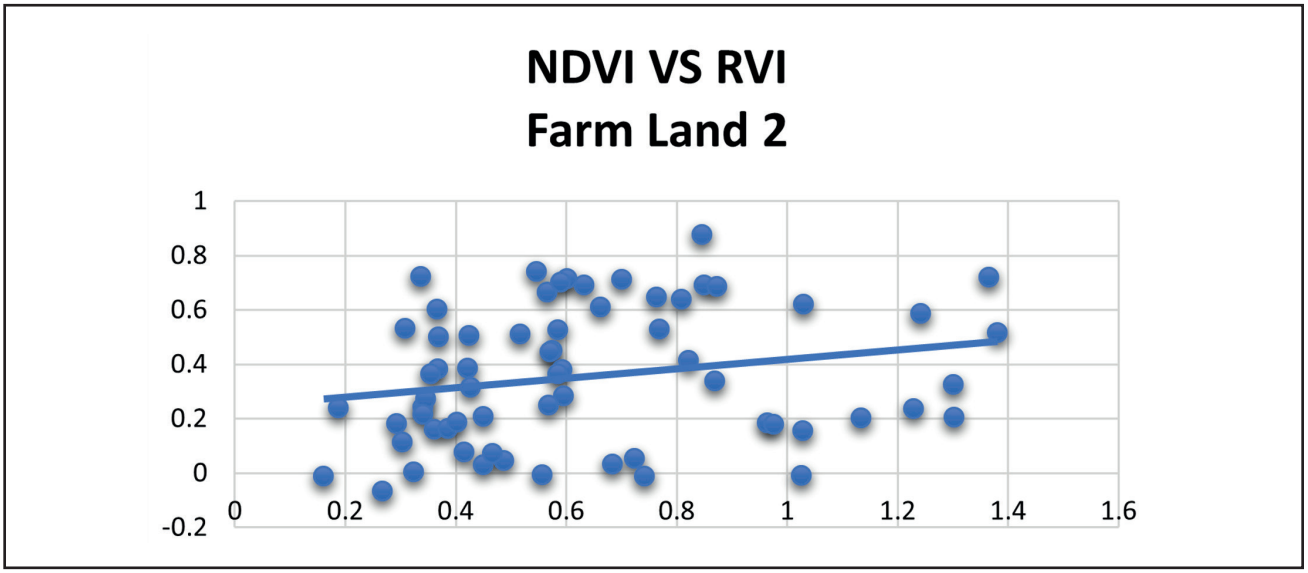

Fig. 11 Correlation between NDVI and RVI for Farm 2 (Sep 2018–Jan 2024).

Tab. 2 Farm 1 correlation matrix for year (2018–2024).

	RVI	RVI4S1	mRVI	NDVI
RVI	1			
RVI4S1	0.947171	1		
mRVI	0.948482	0.908005	1	
NDVI	0.145436	0.211982	0.149054	1

In this study, the correlation analysis in Farm 2 shows a high degree of relationship among the radar vegetation indices (Fig. 11–13; Tab. 3). There is a very high positive relationship between RVI and both RVI4S1 (r = 0.96) and mRVI (r = 0.97). This establishes a high degree of similarity among the above three SAR vegetation indices. There is also a high level of similarity between RVI4S1 and mRVI (r = 0.94). Conversely, the other three vegetation indices (RVI, mRVI, and RVI4S1) show a low degree of similarity with the optical vegetation index of NDVI. The correlation coefficient values are estimated to be about 0.22 in the case of RVI, 0.19 in the case of mRVI, and 0.31 in the case of RVI4S1. Out of the three radar vegetation indices, RVI4S1 shows the highest similarity with the vegetation index of NDVI. This explains that the above index has the highest similarity with vegetation activities.

Tab. 3 Farm 2 correlation matrix for year (2018–2024).

	RVI	RVI4S1	mRVI	NDVI
RVI	1			
RVI4S1	0.962686	1		
mRVI	0.969511	0.936074	1	
NDVI	0.216434	0.305704	0.193061	1

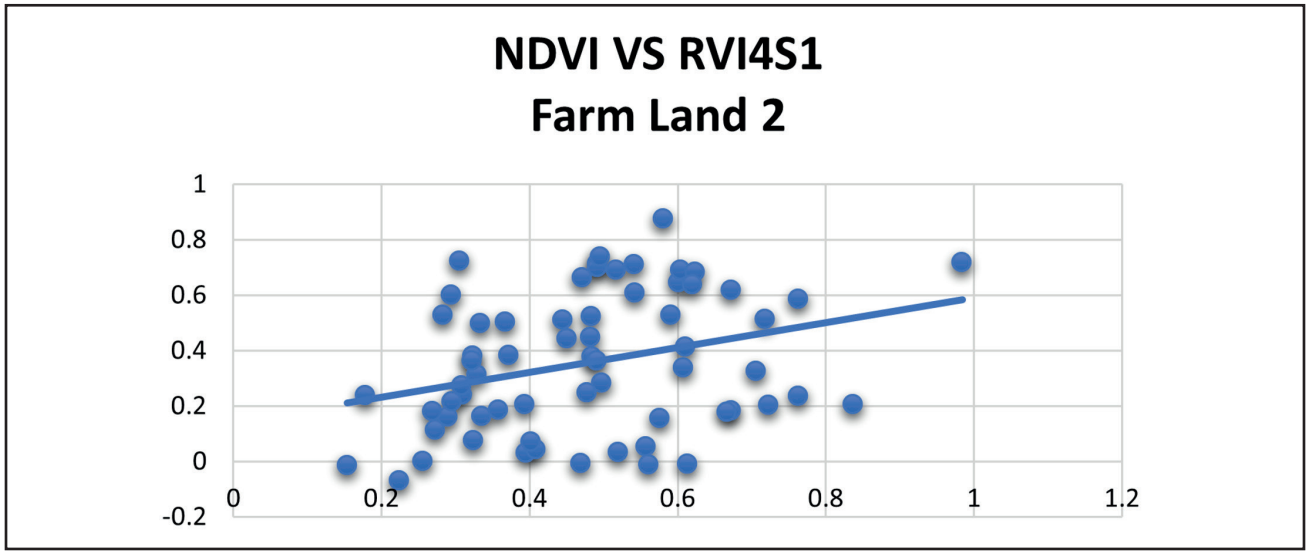

Fig. 12 Correlation between NDVI and RVI4S1 for Farm 2 (Sep 2018–Jan 2024).

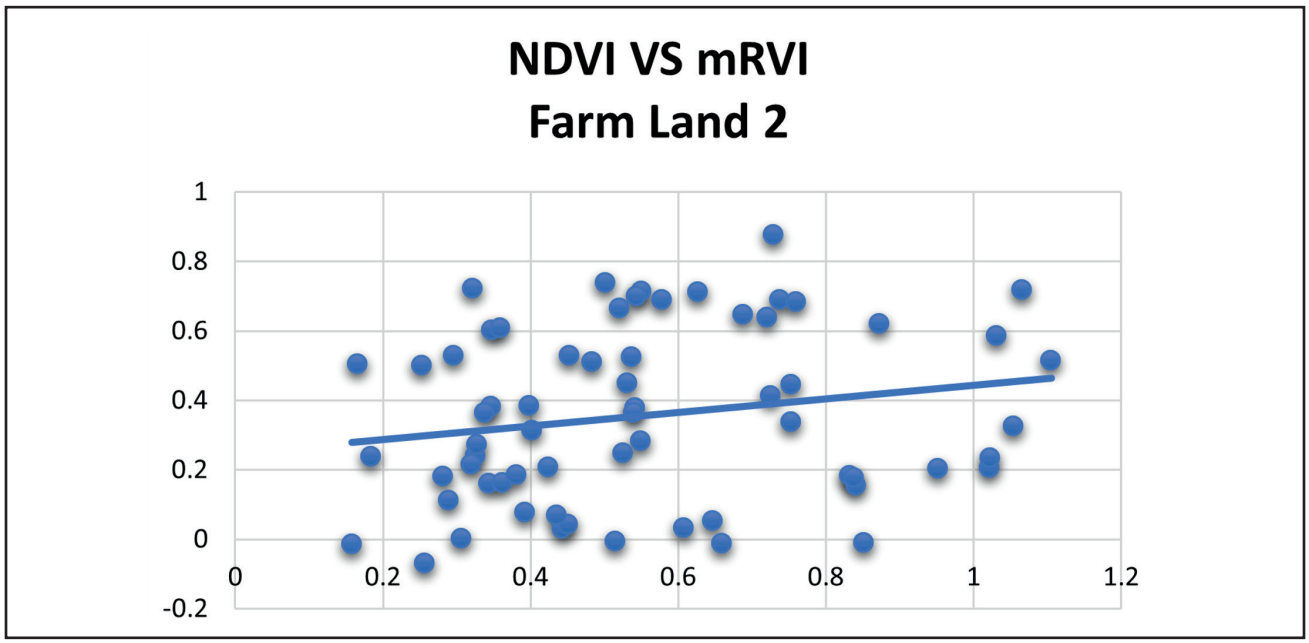

Fig. 13 Correlation between NDVI and mRVI for Farm 2 (Sep 2018–Jan 2024).

5.5 Machine learning-based analysis using random forest and linear regression on ROI mean VV, VH, and RVI4S1 data

The analysis has been performed using machine learning based on the mean backscatter values derived from a 1.5 × 1.5 km region of interest (ROI) (Fig. 14). The data involves average values of Sentinel 1, in VV, VH, as well as RV4S1, for the area of study, during 2018–2022, as illustrated in Tab. 4. Average values for every ROI, as well as every acquisition date, are one thing that is observable in the data. The latitude and longitude are retained since it is an important location parameter. The objective for the machine learning task entailed making predictions for RVI4S1, which would depend on the VV and VH values of backscatter using the Random Forest Regression (RFR) model, in addition to the Linear Regression model. The two models would operate on the same set of data. Fig. 15 shows the Plot of observed and predicted RVI4S1 values of RFR model. The mean squared error (MSE) obtained by the RFR model is 0.000258, which indicates that it works well, but it sometimes performs irregularly. The Linear Regression model outcome is represented by Fig. 16, which shows that there is good correlation between the actual and predicted values of RVI4S1. The mean squared error, 6.92×10^{-5}, is greatly reduced by the Linear Regression model, thereby proving that it is more accurate compared to the Random Forest model. The fact that the mean squared error is smaller in the Linear Regression model suggests that the linear correlation of RVI4S1 is mainly linear to VV and VH backscattering. Hence, it can be inferred that Linear Regression works better than Random Forest Regression in predicting RVI4S1.

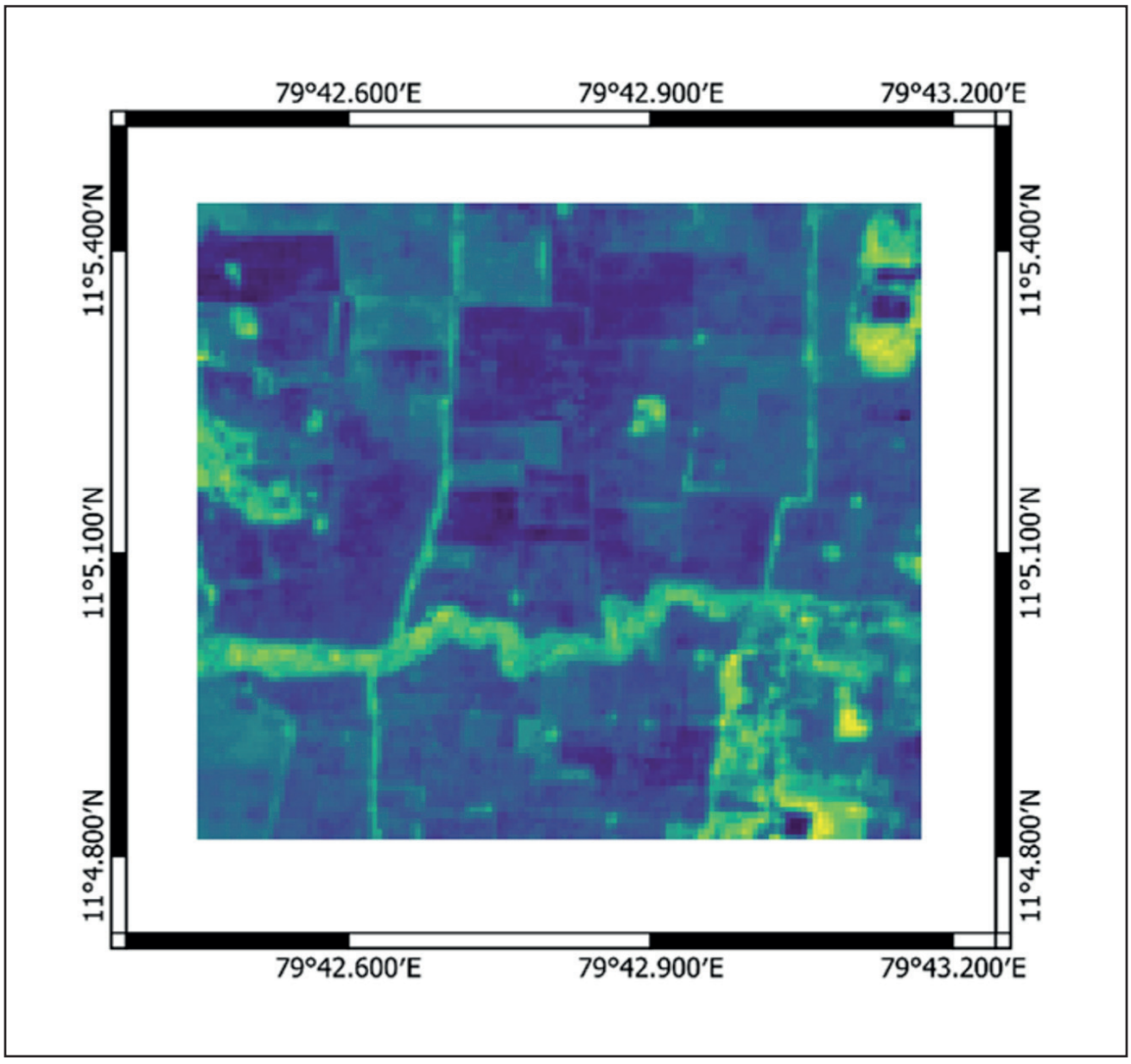

Fig. 14 Study area for ML 1.5 × 1.5 sq.km.

Tab. 4 Dataset of VV, VH, RVI4S1 (mean value study area).

Date	VH	VV	RVI4S1	Latitude	Longitude
09-09-2018	−17.3979	−9.37856	0.467578	11.0793	79.71018
21-09-2018	−23.3393	−15.0424	0.469467	11.0793	79.71018
03-10-2018	−22.937	−12.8425	0.360679	11.0793	79.71018
27-10-2018	−18.6237	−10.0553	0.447358	11.0793	79.71018
08-11-2018	−16.092	−9.59329	0.573938	11.0793	79.71018
20-11-2018	−15.555	−9.07016	0.578037	11.0793	79.71018
02-12-2018	−14.5366	−9.81567	0.661762	11.0793	79.71018
14-12-2018	−15.4968	−9.92271	0.617427	11.0793	79.71018
26-12-2018	−15.0288	−9.72776	0.650841	11.0793	79.71018
07-01-2019	−15.2461	−10.7951	0.676116	11.0793	79.71018
19-01-2019	−15.42	−9.66462	0.625057	11.0793	79.71018
31-01-2019	−14.6419	−9.51988	0.649853	11.0793	79.71018
12-02-2019	−16.4884	−10.2188	0.57928	11.0793	79.71018
24-02-2019	−16.3255	−11.302	0.659398	11.0793	79.71018

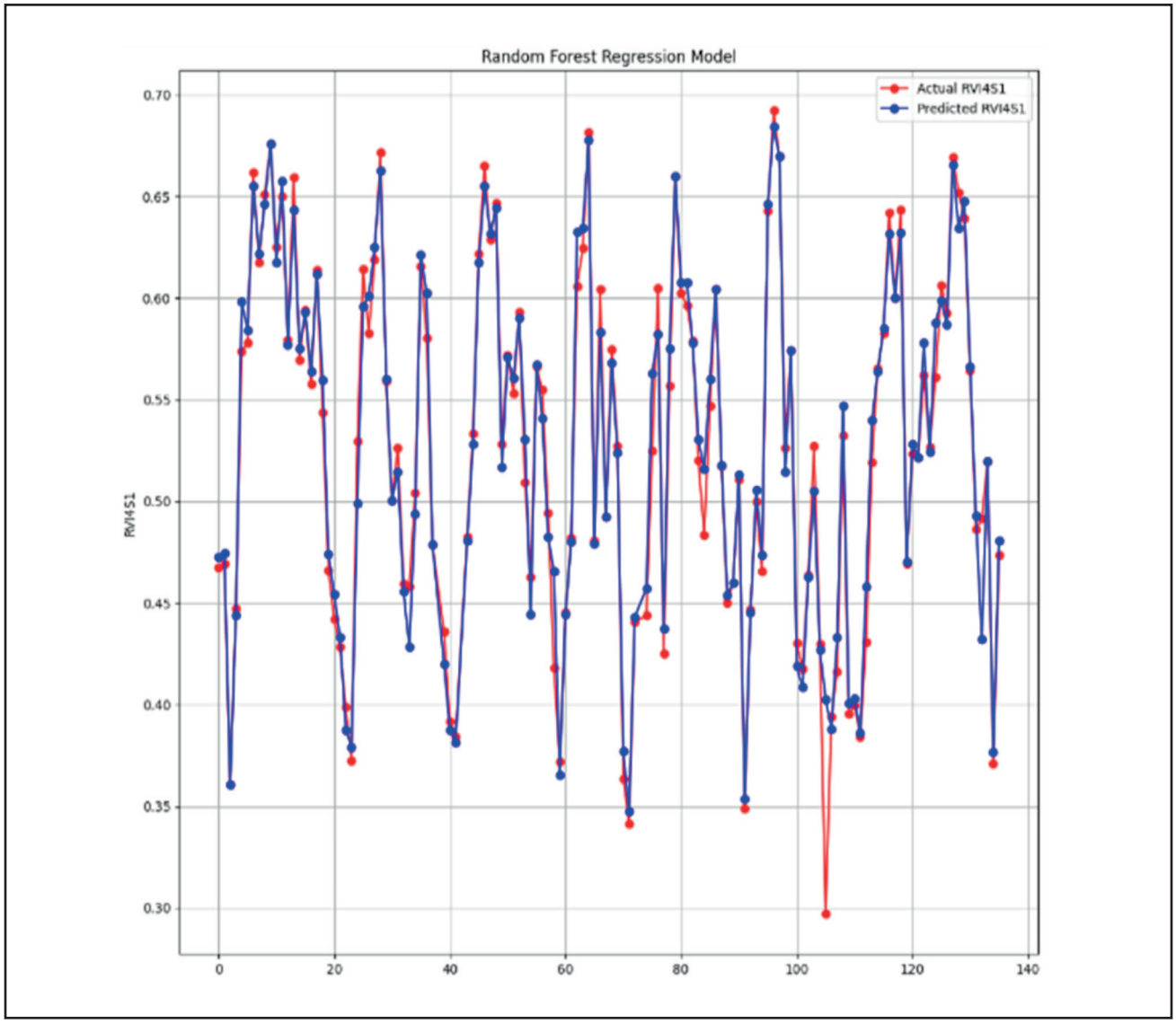

Fig. 15 Actual RVI4S1 and predicted RVI4S1 using random forest regression (Mean ROI).

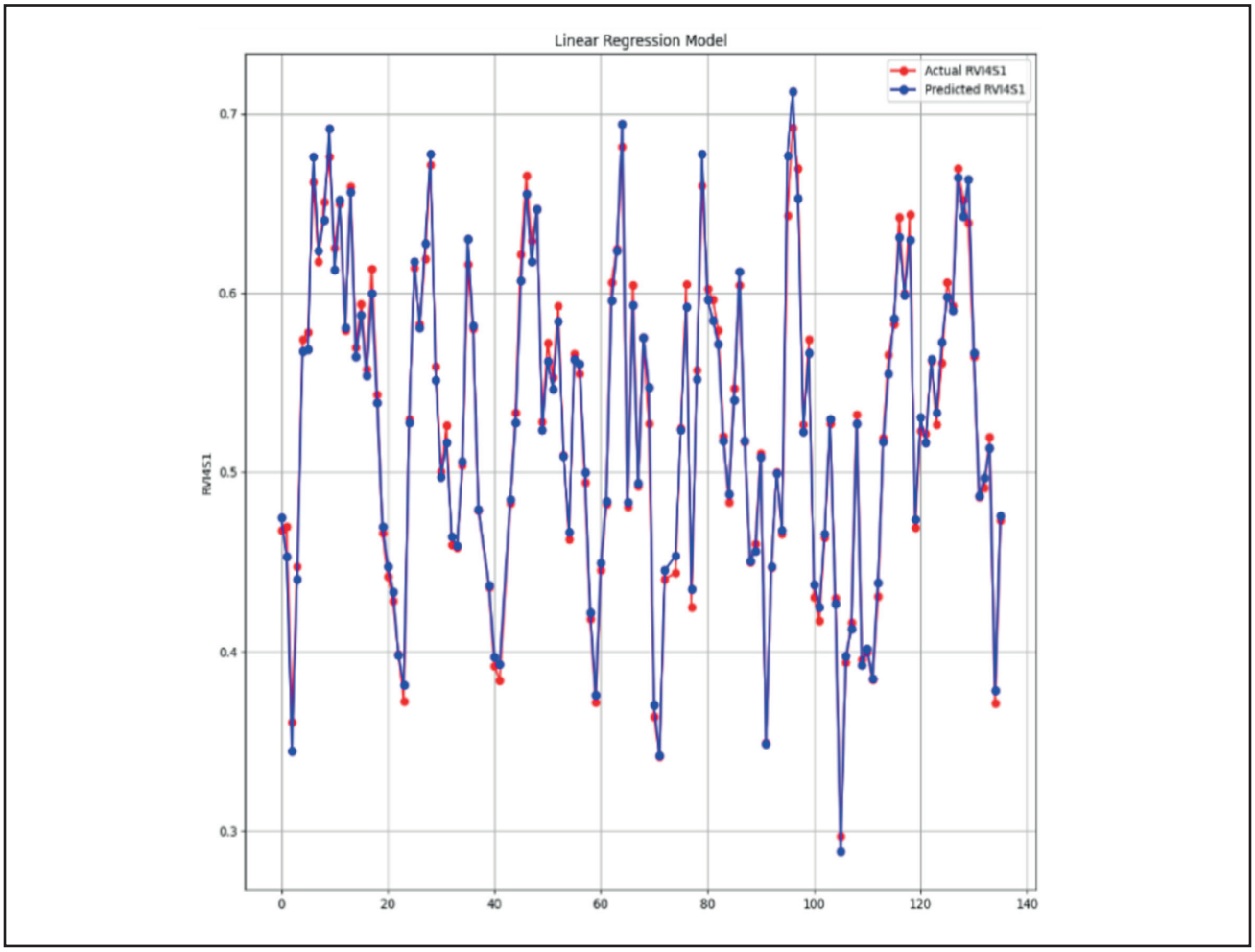

Fig. 16 Actual RVI4S1 and predicted RVI4S1 using linear regression (Mean ROI).

6. Conclusion

By combining multi-year radar backscatter, multi-year MODIS NDVI, optical and SAR measurements, this study assessed the feasibility of Sentinel-1 C-band SAR for tracking rice phenology and vegetation dynamics in two smallholder fields. VV and VH backscatter successfully capture important developmental stages, including transplanting, vegetative growth, flowering, and maturity, according to the phenological analysis for the 2023–2024 Late Samba season. VH showed especially great sensitivity to biomass and canopy moisture. Its dependability for identifying phenological transitions based on Pearson and Spearman correlations between VH and NDVI (up to 0.75 and 0.90 in Farm 1, 0.73 and 0.76 in Farm 2). Among the three Radar Vegetative Indices (RVI, mRVI, RVI4S1) exhibited strong internal correlation ($r > 0.90$) but only weak correlation with MODIS NDVI among three RVI4S1 has weak positive correlation (0.20–0.30). This indicates that radar indices primarily capture structural and moisture-related scattering, whereas NDVI represent optical greenness. The Machine Learning comparison showed that Linear Regression predicted with lower MSE than Random Forest Regression which indicates that VV, VH has Linear Relationship with RVI4S1. The result support the integration of SAR-based phenology tracking and simple linear modelling as effective, scalable tools for smallholder rice monitoring in monsoon-prone region.

Acknowledgment

This research was conducted with minimal external assistance. The authors are thankful to the editor and the anonymous learned reviewers for the insightful comments that were helpful in significantly improving the scientific quality of this research paper. The authors also acknowledge ESA and NASA for providing open-source data. We acknowledge the academic and professional resources that have contributed to shaping the understanding of the topic.

References

Atzberger, C. (2013): Advances in remote sensing of agriculture. Remote Sensing 5(2), 949–981, https://doi.org/10.3390/rs5020949.

Bhogapurapu, N., Dey, S., Mandal, D., Bhattacharya, A., Karthikeyan, L., McNairn, H., Rao, Y. S. (2022): Soil moisture retrieval over croplands using dual-pol L-band GRD SAR data. Remote Sensing of Environment 271: 112900, https://doi.org/10.1016/j.rse.2022.112900.

Blaes, X., Vanhalle, L., Defourny, P. (2005): Efficiency of Crop identification based on optical and SAR image time series. Remote Sensing of Environment 96 (3–4), 352–365, https://doi.org/10.1016/j.rse.2005.03.010.

Bouvet, A., Le Toan, T. (2011): Use of ENVISAT/ASAR wide-swath data for timely rice fields mapping in the Mekong River Delta. Remote Sensing of Environment 115(4), 1090–1101, https://doi.org/10.1016/j.rse.2010.12.014.

Choudhury, A., Mahammood, V., Rao, K. H. V. D. (2022): Rice mapping and various stages of rice growth using Sentinel-1 SAR Data-A case study of Mahabubnagar District, Telangana. International Journal of Recent Technology and Engineering 11(3), 97–100, https://doi.org/10.35940/ijrte.c7259.0911322.

Çolak, E., Chandra, M., Sunar, F. (2021): The Use of Sentinel 1/2 Vegetation Indexes with Gee Time Series Data in Detecting Land Cover Changes in the Sinop Nuclear Power Plant Construction Site. The International Archives of the Photogrammetry, Remote Sensing and Spatial Information Sciences, XLIII-B3-2021, 701–706, https://doi.org/10.5194/isprs-archives-XLIII-B3-2021-701-2021.

Dineshkumar, C., Satishkumar, J. (2019): Rice Crop Monitoring Using Sentinel-1 C-Band Data. The International Archives of the Photogrammetry, Remote Sensing and Spatial Information Sciences XLII-3/W6, 73–77, https://doi.org/10.5194/isprs-archives-XLII-3-W6-73-2019.

Dineshkumar, C., Kumar, J. S., Nitheshnirmal, S. (2019): Rice Monitoring Using Sentinel-1 Data in the Google Earth Engine Platform. Proceedings 24(1): 4, https://doi.org/10.3390/IECG2019-06206.

Drusch, M., Del Bello, U., Carlier, S., Colin, O., Fernandez, V., Gascon, F., Hoersch, B., Isola, C., Laberinti, P., Martimort, P., Meygret, A., Spoto, F., Sy, O., Marchese, F., Bargellini, P. (2012): Sentinel-2: ESA's Optical High-Resolution Mission for GMES Operational Services. Remote Sensing of Environment 120, 25–36, https://doi.org/10.1016/j.rse.2011.11.026.

European Space Agency (ESA) (2024): Sentinel-1: Radar vision for Copernicus. Available online: https://www.esa.int/Applications/Observing_the_Earth/Copernicus/Sentinel-1 (accessed on 15 December 2024).

Food and Agriculture Organization of the United Nations (FAO) (2017): Rice Market Monitor. Food and Agriculture Organization of the United Nations XX (4). Available online: https://reliefweb.int/report/world/fao-rice-market-monitor-december-2017-volume-xx-issue-no-4 (accessed on 20 March 2025).

Gorelick, N., Hancher, M., Dixon, M., Ilyushchenko, S., Thau, D., Moore, R. (2017): Google Earth Engine: Planetary-scale geospatial analysis for everyone. Remote Sensing of Environment 202, 18–27, https://doi.org/10.1016/j.rse.2017.06.03.

Gumma, M. K., Thenkabail, P. S., Maunahan, A., Islam, S., Nelson, A. (2014): Mapping seasonal rice cropland extent and area in the high cropping intensity environment of Bangladesh using MODIS 500m data for the year 2010. ISPRS Journal of Photogrammetry and Remote Sensing 91, 98–113, https://doi.org/10.1016/j.isprsjprs.2014.02.007.

Inoue, Y., Sakaiya, E., Wang, C. (2014): Capability of C band backscattering coefficients from high-resolution satellite SAR sensors to assess biophysical variables in paddy rice. Remote Sensing of Environment 140, 257–266, https://doi.org/10.1016/j.rse.2013.09.001.

Kuenzer, C., Knauer, K. (2013): Remote Sensing of Rice Crop Areas. International Journal of Remote Sensing 34(6), 2101–2139, https://doi.org/10.1080/01431161.2012.738946.

Kumar, D., Ramesh, K., Jinger, D., Rajpoot, S. K. (2022): Effect of potassium fertilization on water productivity, irrigation water use efficiency, and grain quality under direct seeded rice-wheat cropping system. Journal of Plant Nutrition 45(13), 2023–2038, https://doi.org/10.1080/01904167.2022.2046071.

Le Toan, T., Ribbes, F., Wang, L. F., Floury, N., Ding, K. H., Kong, J. A., Fujita, M., Kurosu, T. (1997): Rice crop mapping and monitoring using ERS-1 data based on experiment and modeling results. IEEE Transactions on Geoscience and Remote Sensing 35(1), 41–56, https://doi.org/10.1109/36.551933.

Li, H., Cao, Y., Xiao, J., Yuan, Z., Hao, Z., Bai, X., Wu, Y., Liu, Y. (2024): A daily gap-free normalized difference vegetation index dataset from 1981 to 2023 in China. Scientific Data 11: 527, https://doi.org/10.1038/s41597-024-03364-3.

Mohit, K., Akash, G., Neeti, N., Maity, S., Mukesh, K., Chowdary, V. M., Bimal, B., Jha, C. S., Kumar, R. (2022): Machine learning-based meta-classifier for Kharif Bajra (pearl millet) discrimination in mixed cropping environments using multi-temporal SAR data. Geocarto International 37(27), 16671–16686, https://doi.org/10.1080/10106049.2022.2113452.

Muthayya, S., Sugimoto, J. D., Montgomery, S., Maberly, G. F. (2014): An overview of global rice production, supply, trade, and consumption. Annals of the New York Academy of Sciences 1324 (1), 7–14, https://doi.org/10.1111/nyas.12540.

Nguyen, D. B., Gruber, A., Wagner, W. (2016): Mapping rice extent and cropping scheme in the Mekong Delta using Sentinel-1A data. Remote Sensing Letters 7(12), 1209–1218, https://doi.org/10.1080/2150704X.2016.1225172.

Omia, E., Bae, H., Park, E., Kim, M. S., Baek, I., Kabenge, I., Cho, B. K. (2023): Remote Sensing in Field Crop Monitoring: A Comprehensive Review of Sensor Systems, Data Analyses and Recent Advances. Remote Sensing 15(2): 354, https://doi.org/10.3390/rs15020354.

Onojeghuo, A. O., Blackburn, G. A., Wang, Q., Atkinson, P. M., Kindred, D., Miao, Y. (2018): Mapping paddy rice fields by applying machine learning algorithms to multi-temporal Sentinel-1A and Landsat data. International Journal of Remote Sensing 39(4), 1042–1067, https://doi.org/10.1080/01431161.2017.1395969.

Shen, N., Tan, J., Wang, W., Xue, W., Wang, Y., Huang, L., Gang, Y., Song, Y., Li, L. (2024): Long-term changes of methane emissions from rice cultivation during 2000–2060 in China: Trends, driving factors, predictions and policy implications. Environment International 191: 108958, https://doi.org/10.1016/j.envint.2024.108958.

Small, D. (2011): Flattening Gamma: Radiometric Terrain Correction for SAR Imagery. IEEE Transactions on

Geoscience and Remote Sensing 49(8), 3081–3093, https://doi.org/10.1109/TGRS.2011.2120616.

Surendran, U., Raja, P., Jayakumar, M., Subramoniam, S. R. (2021): Use of efficient water saving techniques for production of rice in India under climate change scenario: A critical review. Journal of Cleaner Production 309: 127272, https://doi.org/10.1016/j.jclepro.2021.127272.

Tucker, C. J. (1979): Red and photographic infrared linear combinations for monitoring vegetation. Remote Sensing of Environment 8(2), 127–150, https://doi.org/10.1016/0034-4257(79)90013-0.

Udimal, T. B., Jincai, Z., Ayamba, E. C., Owusu, S. M. (2017): China's water situation; the supply of water and the pattern of its usage. International Journal of Sustainable Built Environment 6(2), 491–500, https://doi.org/10.1016/j.ijsbe.2017.10.001.

Veloso, A., Mermoz, S., Bouvet, A., Le Toan, T., Planells, M., Dejoux, J. F., Ceschia, E. (2017): Understanding the temporal behavior of crops using Sentinel-1 and Sentinel-2-like data for agricultural applications. Remote Sensing of Environment 199, 415–426, https://doi.org/10.1016/j.rse.2017.07.015.

Wu, B., Zhang, M., Zeng, H., Tian, F., Potgieter, A. B., Qin, X., Yan, N., Chang, S., Zhao, Y., Dong, Q., Boken, V., Plotnikov, D., Guo, H., Wu, F., Zhao, H., Deronde, B., Tits, L., Loupian, E. (2023): Challenges and opportunities in remote sensing-based crop monitoring: a review. National Science Review 10(4): nwac290, https://doi.org/10.1093/nsr/nwac290.

Xiao, X., Boles, S., Frolking, S., Li, C., Babu, J. Y., Salas, W., Moore, B. (2006): Mapping paddy rice agriculture in South and Southeast Asia using multi-temporal MODIS images. Remote Sensing of Environment 100(1), 95–113, https://doi.org/10.1016/j.rse.2005.10.004.

Orographically induced flows contributing to convective storm initiation: A review

Robert Kvak[1,2,*], Marek Kašpar[2]

[1] Charles University, Faculty of Science, Department of Physical Geography and Geoecology, Czechia
[2] Czech Academy of Sciences, Institute of Atmospheric Physics, Department of Meteorology, Czechia
[*] Corresponding author: kvak@ufa.cas.cz

ABSTRACT

Mountainous regions worldwide are seasonal hotspots for convective storms. Orographic deep convection is integral to local hydrologic cycles yet poses distinctive natural hazards and remains difficult to forecast, with impacts often extending into adjacent lowlands and densely populated areas. This review synthesizes the current understanding of how terrain-atmosphere interactions and orographically influenced mesoscale flows affect convection initiation (CI) over inland midlatitude complex terrain. The discussion is organized around thermally and mechanically driven processes that control the regional distribution of the three basic CI ingredients, moisture, instability, and lift, with lift being the ingredient most directly modified by mountainous terrain. Under weak synoptic forcing, elevated terrain typically generates thermally driven circulations, whereas stronger background flow forces air to ascend over or divert around topographic barriers. In both regimes, orographic ascent can facilitate CI, especially when combined with terrain-induced modifications of the prestorm thermodynamic environment that enhance low-level moisture and instability. However, convection may be suppressed by shallow cool or stable near-surface layers, persistent intermountain inversions, leeside drying, and mixing by downslope winds, or large-scale warm, dry elevated layers. Orography also exerts a broader regional influence because sufficiently high ranges can modify surface-atmosphere exchange and flow regimes far from the terrain, increasing CI frequency, the propensity for severe weather, and forecast uncertainty. The paper highlights the need for future meso- and microscale research in mountain environments to improve the understanding of CI distributions and their associated societal impacts.

KEYWORDS

convection initiation; orographic processes; prestorm thermodynamics; mesoscale flows; mountain meteorology

Received: 15 December 2025
Accepted: 9 April 2026
Published online: 30 April 2026

Kvak, R., Kašpar, M. (2026): Orographically induced flows contributing to convective storm initiation: A review.
AUC Geographica 61(2), 256–278
https://doi.org/10.14712/23361980.2026.7
© 2026 The Authors. This is an open-access article distributed under the terms of the Creative Commons Attribution License (https://creativecommons.org/licenses/by/4.0).

1. Introduction

Convective storms are formally defined by the occurrence of deeply developed cumulonimbus clouds that produce precipitation (AMS 2025; CMeS 2025). In the literature, various terms are used to describe such phenomena, often referring to the same process of deep moist convection driven by buoyancy (Markowski and Richardson 2010). In this review, expressions including deep convection, thunderstorm, or simply storm are used synonymously, while recognizing that not every convective storm produces lightning and that such storms do not necessarily occur as part of a larger synoptic-scale storm system (Doswell 1987; Doswell 2001; Doswell and Bosart 2001). A similar principle of terminological flexibility, applied without strict distinction throughout this paper, extends to terrain-related features that may, according to their natural significance or origin, be referred to as mountains, hills, orography, topography or complex terrain, depending on regional or disciplinary conventions (e.g., Price et al. 2019).

All convective storms require three atmospheric preconditions for their initial growth: (1) a sufficient volume of moist air that is relatively warm, (2) an adequately decreasing temperature with height that allows this air to ascend, and (3) a mechanism that provides the initial lift for the air (Doswell et al. 1996). This fundamental set of ingredients applies to the initiation of every type of convective storm, including single cells, multicells, and supercells, but the persistence and organization of more complex storms or larger convective systems also depend on environmental wind shear (Weisman and Klemp 1982). Because storm organization is not the focus here, we refer readers to the relevant literature (e.g., Markowski and Dotzek 2011; Miglietta and Rotunno 2014; Soderholm et al. 2014; Mulholland et al. 2018; Ammon et al. 2025; Riggin et al. 2025).

The foregoing preconditions arise from surface-atmosphere exchanges of heat, moisture, mass, and momentum, so changes in surface properties inherently modify the prestorm environment (Kang and Ryu 2016; Kirshbaum et al. 2018; Schneider et al. 2018). For several decades, research has examined how mountainous terrain alters these environments and whether such influences promote or hinder convective storm development, an issue highlighted early by Banta (1990) in the textbook edited by Blumen (1990). By that time, it was already recognized that orography can provide crucial initial lift for moist air on scales smaller than synoptic ascent, which is typically too weak to initiate deep convection (Doswell 1987). It was also understood that basic processes over elevated terrain can modify temperature and dewpoint lapse rates and the wind field relative to lower elevations (e.g., Houze et al. 1993). However, a more integrated picture of how mountainous terrain modifies prestorm environments and influences deep convection initiation remained comparatively limited.

Some studies (e.g., Barthlott et al. 2010; Weckwerth et al. 2011; Khodayar et al. 2013; Davolio et al. 2016) confirmed and expanded earlier knowledge by showing that the primary and strongest sources of orographically induced environmental modification stem from two broader groups of mesoscale effects, described by De Wekker and Kossmann (2015) as active and passive. These effects comprise (1) differential heating of sloping terrain, which generates thermally driven temperature and pressure perturbations, and (2) interactions between elevated terrain and the larger-scale airflow, which produce mechanically forced pressure anomalies. Resulting mesoscale circulations and flow perturbations can cause coherent ascent or descent of air masses and transport heat and moisture, leading to localized anomalies in vertical motion, temperature, and moisture distribution (Kirshbaum et al. 2016; Kirshbaum and Schultz 2018; Reif and Bluestein 2018; Nelson et al. 2021, 2022).

This review focuses specifically on these mesoscale atmospheric processes, described by Doswell (2001) as forced and external during the initiation of convective storms (hereafter CI), and which range in scale from a few to several hundred kilometers (Markowski and Richardson 2010). Because they exist regardless of the various surface characteristics present (for example, bare rock or vegetation), they are collectively referred to as orographic (De Wekker et al. 2018). These processes operate across a wide range of terrain scales, from minor coastal asymmetries to high alpine peaks, and their spatial extent, magnitude, and regime vary considerably among different landforms (e.g., Hilel Goldshmid et al. 2018), climatic regions (e.g., Nicolas and Boos 2022), and synoptic patterns (e.g., Schultz et al. 2025). Some of these processes may also occur in winter (e.g., Afrifa et al. 2025), and over coastal areas, where additional mechanisms such as land-sea breezes can favor CI (e.g., Kirshbaum et al. 2016).

The coverage of this paper is limited to midlatitude inland regions and primarily to the warmer months, when deep convection is most frequent. During the European warm season, ten-year satellite analyses have shown that CI tends to intensify on the lee sides of major mountain ranges (Levizzani et al. 2010), including the Alps, Apennines, Atlas Mountains in North Africa, Carpathians, Pyrenees, and the mountains of the Balkan Peninsula. Less direct but complementary evidence from lightning observations confirms that these mountains experience the highest seasonal frequencies of lightning-producing storms (e.g., Battaglioli et al. 2023). Fig. 1 presents results from Taszarek et al. (2019), demonstrating that some of those areas exhibit, on average, up to about 40 thunderstorm days per warm season. Similar mountain-enhanced lightning activity is also evident in global data (e.g., Peterson et al. 2021). Within Europe, climatological studies

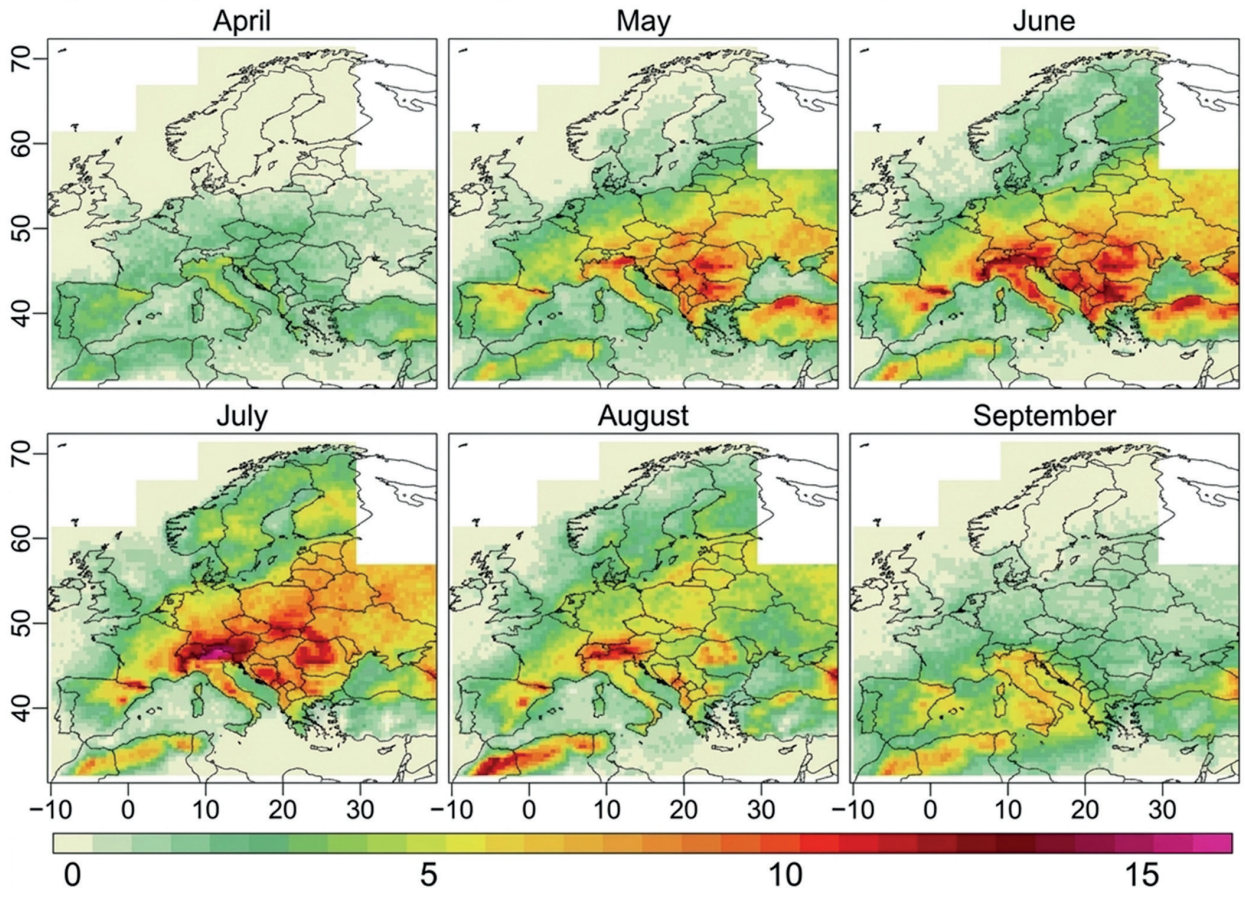

Fig. 1 Monthly (April–September) mean number of days with thunderstorms over Europe based on lightning data from the EUCLID and ZEUS networks. A thunderstorm day is defined as one with more than two lightning flashes within a 0.5° × 0.5° grid cell, which corresponds to roughly 55 km in the north-south direction and 25–45 km in the east-west direction. Figure reproduced from Taszarek et al. (2019, their Fig. 4) with permission.

of convective precipitation (e.g., Lombardo and Bitting 2024), hail (e.g., Punge and Kunz 2016), and other hazardous convective weather and associated environments (e.g., Taszarek et al. 2020a, b) are consistent with these findings.

Because higher storm frequency implies higher exposure, mountainous regions can be disproportionately vulnerable. Narrow valleys, especially in arid, sparsely vegetated mountains, can function as runoff channels, producing localized flash floods (e.g., Panziera et al. 2015), while heavy rainfall on steep terrain and saturated soils can initiate landslides and destructive debris flows (e.g., Bačová Mitková et al. 2018). An enhanced occurrence of large-hail events in the vicinity of mountains can result in frequent injuries to people and animals and severe damage to agriculture (e.g., Trefalt et al. 2018), whereas severe winds may break branches, uproot trees, or cause other impacts in terrain-induced exposure zones (e.g., Frame and Markowski 2006). Additionally, elevated lightning activity poses direct dangers to individuals engaged in recreational activities (e.g., Kühne et al. 2025) and can also trigger secondary hazards such as wildfires (e.g., Rorig and Ferguson 1999).

Public risk perception often underestimates the frequency of convective storms and their associated hazards, and not only in mountains (Doswell 2015; Brooks et al. 2019). Moreover, numerical weather prediction models continue to struggle with forecasting convective storms over complex terrain (e.g., Rotach et al. 2022; Fischer et al. 2025), and operational forecasters face even greater challenges when interpreting weather patterns in mountainous regions (e.g., Barrett et al. 2015; Groenemeijer et al. 2017). Consequently, the public may rely on vague forecasts, misunderstand the communicated information, or, in the worst cases, disregard the forecast altogether.

Motivated by these challenges, this review provides a process-based synthesis and conceptual framework for a broad Earth-science readership, including students and early-career researchers, focused on mesoscale orographic processes that shape the pre-storm environment and contribute to CI. This topic is often treated only briefly in broad Earth-science overviews, despite its relevance for warm-season hazards in some regions. In addition to summarizing the literature, the paper frames terrain-driven CI mechanisms through an ingredients lens and highlights key knowledge gaps. The manuscript is not intended as an operational forecasting guide and does not attempt a comprehensive synoptic classification or case-study approach.

The review is organized around thermally driven and mechanically forced mesoscale flows, interpreted through their impacts on the three CI ingredients (moisture, instability, and lift). Section 2 summarizes key characteristics of mountainous convective environments, emphasizing the vertical structure of instability. Sections 3 and 4 review CI mechanisms linked to thermally driven and mechanically forced flows, respectively. Section 5 summarizes the main findings and closes with directions for future work.

2. Overview of prestorm thermodynamics in mountain environments

In mountainous environments, mesoscale orographic processes modify the prestorm environment by redistributing boundary-layer moisture and heat and by generating mesoscale convergence and ascent, thereby contributing to CI. These processes can often be grouped into two dominant forcing pathways: (1) thermally driven circulations that promote buoyancy and convergence, and (2) mechanically forced ascent associated with terrain-flow interaction (Lareau et al. 2024). Although this split is a useful organizing framework, many real cases involve concurrent thermal and mechanical contributions that are difficult to separate observationally. For successful CI, both initiation pathways ultimately require conditional instability, meaning that the environmental temperature lapse rate (Γ) lies between the moist-adiabatic lapse rate ($\Gamma_s \approx 2$–9 K km^{-1}) and the dry-adiabatic lapse rate ($\Gamma_d \approx 9.8$ K km^{-1}), allowing saturated air parcels to accelerate upward and produce deep vertical motions (Doswell 2001; Kirshbaum et al. 2018).

Most environments with conditional instability are created by large-scale circulations (Doswell 1987; Doswell and Bosart 2001; Roe 2005), whereas orographic effects reshape how that instability is realized as CI (Houze 2012; Katona et al. 2016). While evidence for systematic terrain-driven changes in instability is robust, their translation into CI outcomes can vary widely with the depth of the moist layer, cloud-layer entrainment, and background forcing. Overall, sloped terrain exposed to solar radiation warms more rapidly and can steepen the near-surface Γ. This steepening may be limited by weaker surface heating over bright land cover, colder water bodies, vegetation, snow cover, or glaciers (e.g., De Wekker and Kossmann 2015; Ammon et al. 2025). In contrast, during nighttime, inversions of air temperature (T) commonly form in valleys and basins, leading to strong static stability (Whiteman 2000).

In addition to instability, sufficient low-level humidity is essential for the development of positively buoyant updrafts. This is challenging in mountainous regions, where specific humidity generally decreases with height and air masses at higher elevations are typically much drier than near the surface (Barry 2008). Nevertheless, Fig. 1 and several observational studies (e.g., Weckwerth et al. 2011; Lock and Houston 2015; Feldmann et al. 2021) show that CI occurs more frequently over hilly or mountainous terrain than over flat plains, implying that moisture is transported upslope by flows that enhance low-level convergence or is supplemented by local evaporation (e.g., Hassanzadeh et al. 2016). As a result, low-level air over mountains can become more humid, and correspondingly warmer, than the surrounding free atmosphere at the same elevation, promoting enhanced moist destabilization (Imamovic et al. 2019). The vertical depth and persistence of this moist anomaly remain uncertain and can differ substantially between enclosed basins, open valleys, and exposed ridgelines. This behavior was documented by Kelsey et al. (2018) in the northeastern United States, although they noted that humidity at the summit remained lower than within roughly the lowest 560 m above ground level (AGL) in the nearby valley.

Higher near-surface humidity, represented by the dewpoint T_d, together with soil moisture, vegetation, and nearby water bodies, can reduce the daytime Γ by enhancing evaporative cooling, which limits sensible heat fluxes, turbulent mixing, and moist convective circulations (Barthlott and Kalthoff 2011). Nonetheless, several studies (e.g., Laiti et al. 2014; Imamovic et al. 2017; Feldmann et al. 2024) show that increased water-vapor content can also strengthen local circulations and convective updrafts. Imamovic et al. (2017) found that the sensitivity of precipitation totals to soil moisture decreases with increasing mountain elevation and that soil-moisture effects are overwhelmed by thermally driven circulations once terrain exceeds roughly 500 m. In addition, localized heat sources such as wildfires can trigger deep convection in some settings, even without enhanced low-level moisture (e.g., Peterson et al. 2017).

Given sufficient instability and moisture, an air parcel lifted by orographic influence or other mechanisms cools dry adiabatically until it reaches the lifting condensation level (LCL), where it becomes saturated and further ascent produces condensation and cloud formation (Houze 1993). In more humid mountainous regions, such as central Europe, LCLs in both nonsevere and severe storm environments are typically near or below 1000 m AGL, whereas in drier regions such as central Argentina, they more often exceed 1000 m during CI (e.g., Púčik et al. 2015; Mulholland et al. 2018; Taszarek et al. 2020b; Lareau et al. 2024). Across studies, LCL height appears more influential for severe-storm character than for nonsevere convection. Mulholland et al. (2019) linked higher LCLs in high-terrain experiments to stronger supercell downdrafts, and Púčik et al. (2015) suggested that higher LCLs may support more persistent, broader updrafts conducive to large hail.

For moist air to accelerate upward and reach CI, it must be lifted from below the LCL to the level of

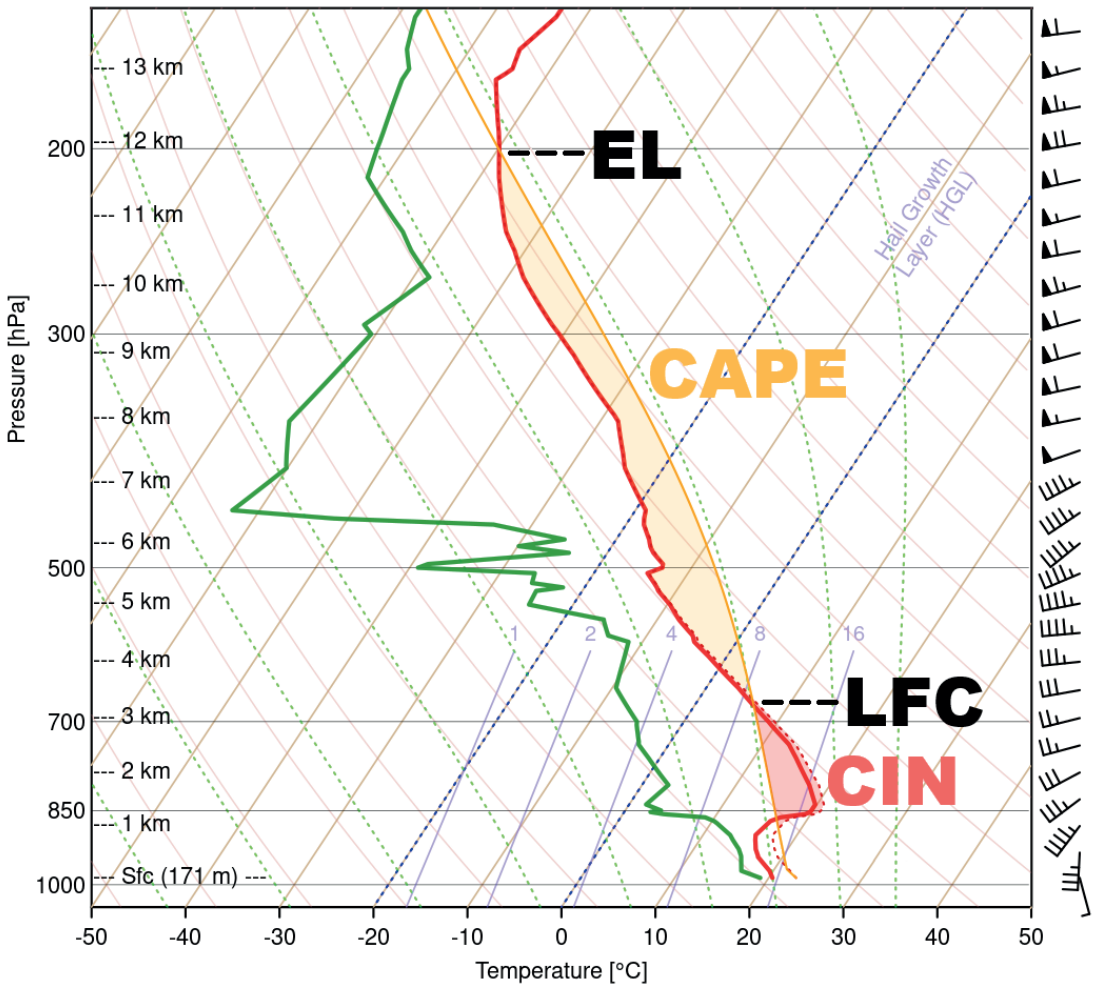

Fig. 2 Skew *T*-log *p* diagram from an atmospheric radiosonde launched at 1200 UTC 9 April 2015 from Fort Worth, Texas (USA). Environmental temperature (solid red) and dewpoint (solid green) profiles are shown with pressure and height AGL on the left vertical axis, and wind barbs on the right. The dashed red curve denotes the environmental virtual temperature profile, which is used together with the virtual temperature of the lifted air parcel (yellow curve) to compute LFC, equilibrium level (EL), CAPE, and CIN. The physically meaningful LFC above the temperature inversion (above 1 km AGL) and the EL are marked for a surface-based parcel. The yellow-shaded area represents CAPE, and the red-shaded area below the LFC represents CIN. For further details on the diagram, see, for example, Markowski and Richardson (2010, pp. 15 and 34). Figure generated using the *thundeR* software (Czernecki et al. 2025).

free convection (LFC), where it becomes warmer than the environment, and buoyancy becomes positive. Enhanced vertical motions provided by orographic lifting are often crucial for successful CI (e.g., Nelson et al. 2021; Marquis et al. 2023). Without sufficient lift, other mesoscale processes are unlikely to initiate convection, and CI frequently fails (e.g., Lock and Houston 2014; Smith et al. 2015). Observation-based studies in South America (Marquis et al. 2021; Feng et al. 2022; Nelson et al. 2022) further showed that free-tropospheric humidity strongly modulates CI, with entrainment of dry air limiting updraft depth, buoyancy and storm lifetime. In practice, near-cloud thermodynamics are rarely sampled well enough to attribute CI success or failure to the local moisture and stability field. Fig. 2 summarizes the thermodynamic controls on CI: convective available potential energy (CAPE) quantifies how strongly an updraft can accelerate once convection becomes buoyant, whereas convective inhibition (CIN) quantifies the cap that resists parcel ascent and can prevent initiation.

Steeper Γ combined with higher low-level T_d increases instability and CAPE while reducing CIN. Over higher terrain, however, CAPE and storm frequency are often lower because near-surface air is cooler and drier and the vertical depth available for ascent is reduced (e.g., Panosetti et al. 2016; Feldmann et al. 2021). Mountains can still enhance CAPE locally through stronger surface heating and modified low-level moisture flows (Chen and Lin 2005; Kirshbaum 2013; Panziera et al. 2015). For example, climatological studies such as Katona et al. (2016) and Taszarek et al. (2020b) show, in addition to a latitudinal dependence of prestorm CAPE, clear orographic signatures along major ranges. CIN decreases when enhanced heating on sunlit slopes steepens the low-level Γ and increases T_d locally (e.g., Scheffknecht et al. 2017). By contrast, CIN increases when stable layers develop in valleys at night, when cold-air pools or downslope flows strengthen near-surface stability, or when dry, warm air aloft overlies moist boundary-layer air and reinforces a capping inversion (Doswell and

Bosart 2001; Degiacomi et al. 2025). These contrasts underscore that the effective CAPE and CIN influencing CI in complex terrain can remain poorly constrained, because initiating parcels sample a highly heterogeneous near-surface thermodynamic field.

Although conditional instability provides the basic thermodynamic support for deep convection, other mesoscale instability types can also aid CI. Potential instability arises when equivalent potential temperature (θ_e) decreases with height and mechanical lift releases latent heat from moist lower layers beneath cooler, drier air aloft (Řezáčová et al. 2007; Afrifa et al. 2025). Some studies (e.g., Kaspar et al. 2009; Wulfmeyer et al. 2011; Tang et al. 2016; Kunz et al. 2018) have linked this instability to severe storm development near mountains, where it can be released by terrain-forced lifting. This configuration commonly occurs when daytime heating over mountains steepens Γ and advection of the destabilized air over more humid boundary-layer air forms an elevated mixed layer (EML; Reif and Bluestein 2018; Schultz et al. 2025). Fig. 2 illustrates such an environment in Texas, with an EML near 850 hPa characterized by higher T and lower T_d and southwesterly flow aloft from the central Mexican Plateau, while south-southeasterly low-level winds beneath the inversion transport moist air from the Gulf of Mexico.

To conclude this section, and paraphrasing Markowski and Richardson (2010, p. 188), in mountain environments, both CAPE and CIN can be modified on the mesoscale by three categories of processes that arise from surface-atmosphere interactions. They can be enhanced and reduced, respectively, by (1) thermally driven circulations resulting from warming on sunlit slopes, (2) mechanically forced ascent around terrain barriers, and (3) low-level moistening through moisture advection or evapotranspiration. These changes can arise from warming or moistening alone, without requiring large changes in Γ. The following sections emphasize the first two categories, consistent with the CI mechanisms summarized by Houze (1993, 2012), because they most directly generate mesoscale convergence and ascent while redistributing heat and moisture. This separation also reflects their contrasting controls: thermally driven circulations are most prominent under weak background flow and strong diurnal heating, whereas mechanically forced ascent is favored under stronger ambient flow and depends primarily on upstream stability and terrain geometry.

3. Thermally driven orographic circulations

Solar radiation drives the surface-atmosphere energy balance and the vertical temperature stratification that governs atmospheric stability and the potential for CI. Thermally induced orographic circulations contribute to CI by generating mesoscale convergence and ascent while also redistributing boundary-layer moisture and modifying CAPE and CIN. Their effectiveness therefore depends on the presence (or local enhancement) of sufficiently moist, conditionally unstable air. During the diurnal cycle, solar-driven surface turbulent heat fluxes generate buoyant thermals of various sizes and magnitudes that strongly depend on the intensity of solar insolation and thus on latitude and altitude, season, solar elevation angle, aspect and slope of terrain, and shading by clouds or nearby terrain, and also on land cover (e.g., Serafin and Zardi 2010; Kirshbaum 2017; De Wekker et al. 2018; Serafin et al. 2018; Ammon et al. 2025). Accordingly, thermally driven circulations are most effective under weak background flow, when diurnal heating can organize persistent convergence that lifts parcels toward their LFC. The east-west progression of diurnal heating in the Northern Hemisphere also shifts surface-based buoyancy and inhibition across opposing slopes and interacts with smaller-scale thermals (e.g., Kottmeier et al. 2008).

Sensible heat flux drives shallow convective boundary-layer (CBL) updrafts of 0.1–1 m s^{-1} and, over well-heated hilly terrain, can produce vertical velocities of several m s^{-1} (Kirshbaum and Wang 2014; Panosetti et al. 2016). Even vertical velocities near 10 cm s^{-1} can help lift air parcels toward saturation, reduce CIN, and promote CI in environments already close to instability (Doswell and Bosart 2001). These thermally driven motions shape the CBL and often initiate early convective clouds within low-level convergence zones and surface thermal hot spots, most prominent on cloudless summer days (e.g., Bianco et al. 2011; Imamovic et al. 2019). Nelson et al. (2022) showed that terrain-enhanced lift can allow CI to develop from boundary-layer thermals that are more than twice as narrow as those required without terrain forcing (~1–2 km versus ~5 km). A persistent challenge is that storm-scale convergence and near-CI updraft structure are highly localized and short-lived, and are therefore difficult to observe and attribute in complex terrain (e.g., Marquis et al. 2023).

Since complex elevated terrain typically undergoes stronger diabatic heating and cooling than surrounding lower elevations, the resulting solar- and terrain-driven temperature and pressure gradients (∇T and ∇p) generate persistent solenoidal and baroclinic circulations from local to mountain range scales once low-level stability is eroded (e.g., Doswell 2001; Barthlott et al. 2006; Wagner et al. 2015). Conceptual models (e.g., Barry 2008; Chow et al. 2013) typically categorize five such orographic circulations based on the size, landform, diurnal phasing, and flow strength: slope winds, valley winds, plateau winds, basin winds, and mountain-plain circulations. Fig. 3 shows that the diurnal cycle of each circulation reflects the local ∇T and ∇p, with two main phases: daytime flow from lower to higher elevations and nighttime flow from higher to lower elevations, separated by transition periods.

Crucially, each circulation occupies a different layer AGL, and its transition phases are shifted relative to the others, with the timing depending on the distance from the landform that generates it (e.g., Graf et al. 2016).

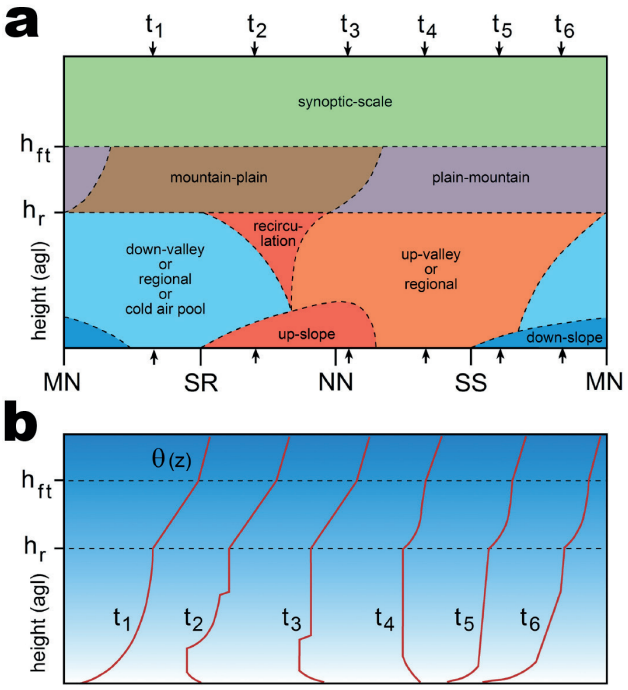

Fig. 3 Diurnal mountain circulations and boundary-layer structure over a slope. (a) The panel illustrates prevailing mountain circulations and their transition phases (dashed lines) as a function of time (MN for midnight, SR for sunrise, NN for noon, and SS for sunset) and height above the mountainside. The levels h_r and h_{ft} indicate the ridge-top height and the base of the free troposphere outside the mountain atmosphere. (b) The panel shows the diurnal evolution of potential-temperature profiles $\vartheta(z)$ above slopes (t_1 to t_6), with the timing of each profile marked by small arrows in panel (a). Figure reproduced from De Wekker and Kossmann (2015, their Fig. 3) with permission.

These mountain circulations are most efficient under clear skies, weak low-level stability, and mild synoptic background flows, although the threshold at which weak background flow transitions to a regime where thermal circulations are disrupted remains difficult to generalize (e.g., Hagen et al. 2011; Khodayar et al. 2013; Kirshbaum 2013; Bergmaier and Geerts 2015; Scheffknecht et al. 2017). Consequently, relatively dry and complex terrain enhances thermal circulations and increases the likelihood of CI (Banta 1990; Damiani et al. 2008; Imamovic et al. 2017). Despite this, very dry regions may lack adequate low-level moisture, limiting deep convection unless elevated mountains ventilate the CBL with additional moisture from the free troposphere, producing local θ_e maxima. Additionally, thermal circulations become weakened by vast reflective, cool or moistened surfaces, when ∇T and ∇p diminish, and the near-surface vertical gradient of potential temperature ($\partial\theta/\partial z$) becomes strongly positive (Imamovic et al. 2019). Under strong ambient winds, thermal circulations can be partly masked, yet they generally persist even if difficult to observe directly (e.g., De Wekker et al. 1998; Barthlott et al. 2010; Wagner et al. 2015; Kelsey et al. 2018).

3.1 Airflow over mountain slopes

Slope winds are the fundamental component of thermally driven circulations in mountainous terrain. Slope aspect, angle, and surface properties control the thermal forcing that drives local slope flows and, in turn, larger valley and mountain-plain circulations (Fig. 3a). During daytime, anabatic winds develop along heated slopes, accompanied by weak compensating return flows aloft, and can form paired opposing circulations when present on both sides of a valley (Fig. 4). These

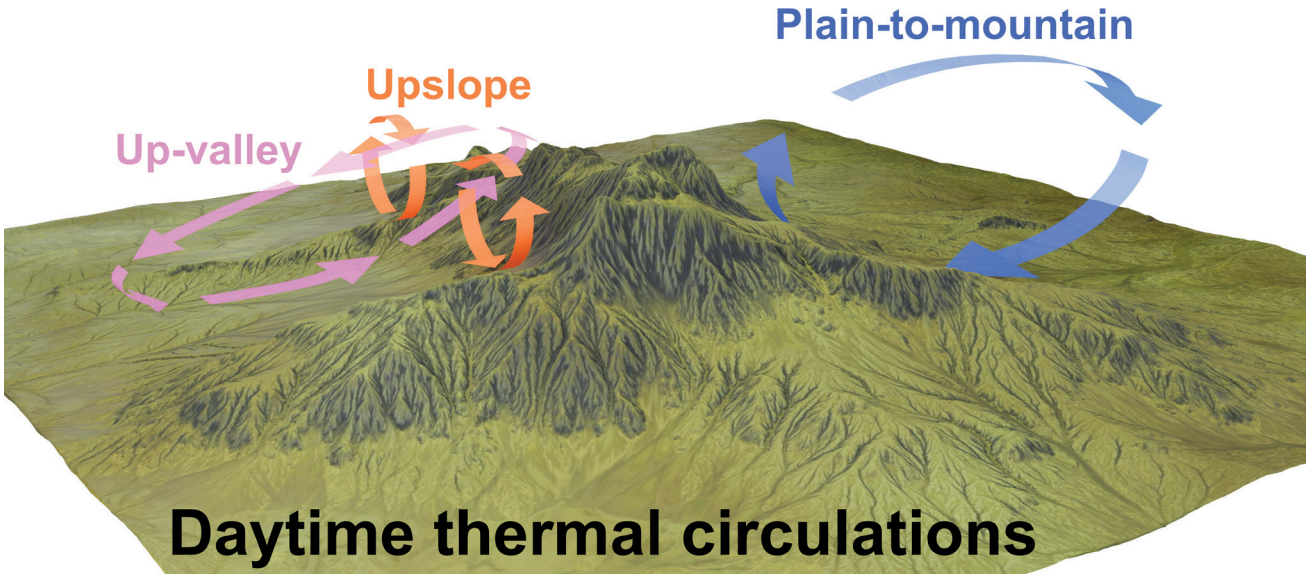

Fig. 4 Three interacting thermally driven wind systems over mountainous terrain during daytime. The upslope flows on the valley sidewalls oppose each other and are accompanied by subsidence over the valley center. Similar upslope flow also develops outside the valley along the surrounding foothills. The up-valley flow extends from the valley mouth toward the valley head and may be crossed by a cross-valley circulation that transports air from cooler to warmer sidewalls (not shown). The plain-to-mountain flow is the spatially largest system and transports air from the adjacent plain toward the mountain thermal low. Figure drafted by Miroslav Truben in collaboration with the authors.

buoyancy-driven flows typically reach 1–5 m s^{-1}, occupy roughly the lowest 200 m AGL, and are strongly damped by surface friction (e.g., Chow et al. 2013; Serafin and Zardi 2010). Daytime solar heating produces a near-surface superadiabatic layer with $\partial\theta/\partial z < 0$ (profiles t_2–t_4 in Fig. 3b), which promotes buoyant instability, strengthens upslope flow, and favors convergence zones along sun-exposed slopes where air is forced to ascend (Barthlott et al. 2006).

Under fair-weather conditions, the strongest surface heat fluxes, converging upslope flows, moistening, and resulting orographic ascent occur over the highest terrain and along ridge crests (e.g., Kottmeier et al. 2008). This forcing warms and deepens the CBL and destabilizes the air near ridge-top level (profiles t_4–t_6 in Fig. 3b), producing local CIN minima over elevated peaks (e.g., Kalthoff et al. 2011; Bergmaier and Geerts 2015). Fig. 5a illustrates the first initiation mechanism, in which thermally driven lift within these exposed thermal hot spots enhances the likelihood for CI. Strong contrasts in upslope wind strength, CAPE, and CIN often exist between sunlit and shaded slopes. In the Northern Hemisphere, south-facing slopes receive greater solar input and are therefore more favorable for thermal hot spot formation (e.g., Panziera et al. 2018). Idealized simulations by Hassanzadeh et al. (2016) indicate that CI may occur relatively early in the morning in the lee of a mountain when thermal upflow interacts and converges with the background wind.

Numerical simulations by Imamovic et al. (2019) showed that upslope winds are essential for transporting moist, conditionally unstable air toward thermal hot spots and, under even weak background flow oriented perpendicular to the main mountain range, can carry this air beyond complex ridge systems. Their results also demonstrated that mountain geometry strongly modulates moisture transport. Narrower, taller mountains produce stronger upslope winds but draw from a smaller CBL volume and therefore transport less total moisture, whereas wider, lower mountains generate weaker winds yet interact with a larger reservoir of near-surface air and convey more moisture. The taller mountains, however, tend to produce the strongest summit moisture anomalies. Such geometric contrasts may influence the location of CI. For example, Bergmaier and Geerts (2015) suggested that particularly high mountain ranges can act as natural barriers to mesoscale moist upslope flows and inhibit CI over adjacent terrain.

After sunset, radiative surface cooling generates a stable near-surface layer that initiates katabatic downslope winds that are slightly weaker than their daytime anabatic counterparts (Fig. 3a). In this regime, $\partial\theta/\partial z > 0$ dominates the vertical profile (Fig. 3b), producing a low-CAPE, high-CIN environment in which deep convection is usually suppressed, especially over mountain crests and higher slopes. Only later in the night may higher terrain protrude above the deepening nocturnal inversion over lower elevations, reducing its stabilizing influence. Downslope winds can nevertheless interact with background or locally moist low-level flows over adjacent plains, as observed along the Rockies and Andes (e.g., Friedrich et al. 2016; Mulholland et al. 2018; Reif and Bluestein 2018; Singh et al. 2022), where such interactions contributed to the evolution of convergence zones capable of providing sufficient lift for CI (Fig. 5b). This mechanism is favored when downslope winds strengthen under weak ambient flow and stability (e.g., Kirshbaum and Wang 2014).

Radar analysis by Kaltenboeck and Steinheimer (2015) showed that lightning activity often propagates off the mountains into the Alpine foreland during the evening and early night. Consistently, Taszarek et al. (2020a) found that mean annual nighttime lightning over land maximizes in relatively flat lowland regions, including the northern Great Plains and Columbia Plateau in the United States and the Pannonian Basin and North European Plain in Europe. Although environmental stability increases at night, secondary nocturnal CI can be as strong as daytime initiation, and mountain convection can act as a precursor to subsequent lowland CI (Chow et al. 2013). These patterns suggest organized lifting, but the mechanisms controlling the timing and preferred mountain-to-plain

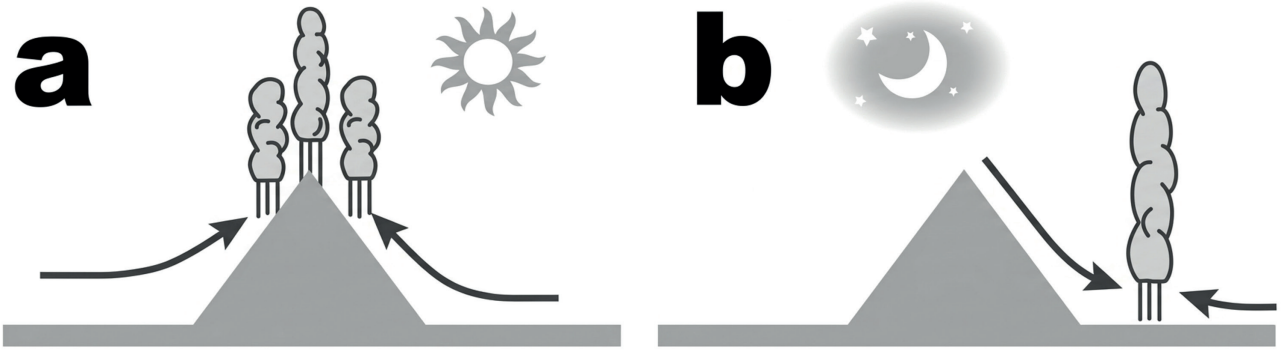

Fig. 5 Diurnal thermally induced initiation mechanisms that contribute to the formation of precipitating deep convection in the vicinity of mountains; (a) and (b) illustrate daytime and nighttime conditions, respectively, highlighting converging flows and forced ascent. Arrows indicate the direction of prevailing low-level airflows. Figure adapted from Houze (1993, his Fig. 12.24; 2012, his Fig. 3) with permission.

initiation corridors remain uncertain. Under strong low-level forcing or elevated thermodynamic anomalies, off-mountain nocturnal convection may evolve into large mesoscale convective systems that produce substantial nighttime precipitation across adjacent or even distant lowlands (e.g., Chu and Lin 2000; Damiani et al. 2008; Mulholland et al. 2020; Da Silva and Haerter 2023).

3.2 Airflow within valleys

Beyond slope flows, complex valley topography supports along- and cross-valley circulations that govern the mesoscale diurnal airflow (Markowski and Richardson 2010). These circulations are driven by ∇p arising from heating and cooling contrasts between higher elevations near the valley head and lower terrain at the valley mouth or adjacent plains (Fig. 4). Wagner et al. (2015) showed that valleys transport air from the surface to the free atmosphere three to four times more efficiently than flat terrain. Valley winds involve a larger air volume and typically higher velocities than slope winds and evolve on longer time scales (Serafin et al. 2018). When slope winds weaken or remain shallow, they are often overtaken by valley flows, although they still contribute to low-level cross-valley circulation (Figs. 3a, 4), which can at times exceed the along-valley component (e.g., Laiti et al. 2014).

The structure of valley airflow components and the associated air mass density changes depend strongly on valley geometry, including variations in width, depth, altitude, and orientation (e.g., Schmidli and Rotunno 2012). Blumen (1990) noted that differences in the air volume contained within valley sectors, or between a valley and an adjacent plain, strongly influence local flow behavior. This effect is quantified by the topographic amplification factor (TAF), a geometric measure of how efficiently a valley warms relative to a nearby plain based on the solar-exposed area and underlying air volume. Higher TAF values indicate more effective heating, which increases θ, lowers pressure up-valley, and strengthens the up-valley flow (e.g., De Wekker et al. 1998).

Daytime up-valley winds typically reach 1–8 m s^{-1} and often extend nearly to ridge height, with the deepening CBL focusing thermal hot spots and convergence near the valley head (e.g., Schmidli and Rotunno 2012; Bianco et al. 2011; Hagen et al. 2011). In deep, moist valleys, changes in $\partial\theta/\partial z$ and ∇p can persist all day, whereas in broader, drier valleys they develop within only a few hours, and particularly deep valleys may not generate flows strong enough to overcome CIN or capping inversions (e.g., Khodayar et al. 2013; Weckwerth et al. 2014). At night, the circulation reverses, becoming shallower and less intense (Serafin et al. 2018). Down-valley winds can develop a jet-like profile, with peak speeds near valley mouths up to 20 m s^{-1}, increasing low-level shear (e.g., Whiteman 2000). Although the cooler, stable air pool depresses the CBL and increases CIN (e.g., Kalthoff et al. 2011), CI can still occur where down-valley winds interact with circulations near the valley mouth or over the adjacent plain (Fig. 5b).

Temperature contrasts between the valley floor and opposing sidewalls generate weak cross-valley flows, producing a circulation that can favor stronger destabilization on one slope depending on time of day (De Wekker and Kossmann 2015). Combined with relatively strong slope winds, these contrasts create convergence and divergence zones over the valley floor, where ascending and descending motions compensate the paired slope flows (Fig. 4). In this context, valley channeling can superpose air masses of different origin and produce sharp gradients that are rarely resolved by coarse observations. Across studies (e.g., Laiti et al. 2014), valley-lake interactions can either suppress or enhance destabilization, depending on whether advection and subsidence dominate or whether moisture fluxes increase θ_e and CAPE locally. Feldmann et al. (2024) showed that in such cases large alpine lakes can amplify these thermodynamic anomalies and, together with channeling flows, enhance updraft strength in convective storms.

Under weak synoptic flow, the diurnal cycle of cross-valley winds often favors nocturnal CI in the valley center rather than along its margins, consistent with Fig. 5b. Although cold, stable air from surface cooling or precipitation-driven cold pools accumulates in the valley center, CI can still occur when these downslope-moving pools collide with residual upslope winds and enhance low-level convergence (e.g., Panosetti et al. 2016). Valley circulations also channel low-level flows, including warm and moist air from adjacent plains, through flanking slopes, tributary valleys, ridges, saddles, and gaps, where they interact with local thermals and background winds (e.g., Wang et al. 2016; Singh et al. 2022). In such cases, parcels may reach their LFC without needing to ascend to the mountain summit (e.g., Kottmeier et al. 2008; Weckwerth et al. 2011). An open question is when CI forms in the lee of mountains as valley flows from behind a ridge converge downstream, and whether modified low-level winds exert more control than ambient stratification (e.g., Barthlott et al. 2006; Hagen et al. 2011).

3.3 Airflow within basins

Basins are closed or semi-closed topographic depressions with wider floors than valleys and typically circular or oval shapes. Their circulation regimes resemble those of valleys, although classic up-valley winds are generally absent, and many valley-type circulations can still develop within basin atmosphere (Banta 1990). Basin geometry strongly influences thermally driven winds and vertical transport, and Barry (2008) identified three asymmetric basin-wind

regimes, of which shallow daytime upslope flow along the inner basin slopes is most relevant for CI (Fig. 5a). The strength of this upslope flow depends on slope steepness and the height of the basin floor relative to surrounding ridges. As in valleys, daytime upslope winds are compensated by subsidence and divergence in the basin center (e.g., Serafin and Zardi 2010). Because basin winds are often less affected by synoptic or mesoscale circulations, the primary limitation for daytime CI is the strong residual lid produced by nocturnal stable stratification, which likely varies across basin types and moisture regimes (e.g., Afrifa et al. 2025).

TAF enhances CBL growth in basins because the basin atmosphere warms more rapidly than the surrounding lowlands, while basin side slopes also supply substantial sensible heat fluxes that increase the diurnal temperature range (e.g., De Wekker et al. 1998). Resulting ∇T and ∇p drive winds into the basin atmosphere by late afternoon, allowing air to cross adjacent ridges with steeper $\partial\theta/\partial z > 0$ on their lee sides. These inflows may then collide with weakening inner-basin upslope flows, strengthening updrafts near the basin floor through added moisture and heat. De Wekker and Kossmann (2015) showed that the initial convergence zone forms on plain-side slopes and shifts toward basin slopes once the basin becomes warmer than the adjacent plains, although late-afternoon inflow surges from surrounding lowlands can abruptly shallow the CBL over nearby mountains and disrupt convergence around the basin.

3.4 Airflow over elevated plateaus

Elevated plateaus form a distinct type of thermally driven circulation, differing from basins primarily in that slope-wind forcing is shifted to the plateau margins rather than acting directly over the plateau interior. Thermally driven flows develop along the bordering hillsides and within the plain-to-plateau circulation, which directs low-level air toward the plateau with compensating return flow above the deep CBL. The height and horizontal extent of the plateau strongly determine the strength of this circulation, when the horizontal scale must exceed the typical CBL depth to generate meaningful mesoscale lifting (De Wekker and Kossmann 2015). Under strong solar heating and weak synoptic forcing, plateaus often develop a warm core (Chow et al. 2013). High-elevation plateaus exhibit less pronounced warm cores because vigorous convection enhances vertical heat loss, deepens the CBL, and strengthens horizontal ∇T across the plateau top (De Wekker et al. 1998).

Schmidli and Rotunno (2012) showed that plateau-induced warm cores elevate temperatures aloft over adjacent lowlands and valleys, intensifying along-valley ∇p and strengthening up-valley winds, often doubling their magnitude relative to valleys not bordered by a plateau. On a larger scale, the Spanish plume, a synoptic pattern associated with EMLs (Fig. 2; Ribeiro and Bosart 2018), has been viewed as analogous to such warm-core processes and predisposes western Europe to severe convection (e.g., Taszarek et al. 2020b). Schultz et al. (2025) argued that Spanish-plume EMLs need not originate over the Iberian Plateau and may instead develop over northern Africa or the Mediterranean Sea. Even when elevated terrain contributes, diurnal heating produces transient warm anomalies rather than a continuous plume. These anomalies do not always coincide with favored CI, with strong sensitivity to the low-level flow, and the controlling mechanisms remain poorly quantified.

Plateau circulations are often weak, so they may transport limited low-level moisture onto the plateau with reduced CAPE. They are also easily overwhelmed by synoptic flows, limiting the influence of TAF and reducing diurnal temperature amplitudes. On the other hand, morning instability and cold-air drainage can support large-scale plateau updrafts, and persistent afternoon convergence zones along the plateau edge may promote CI, further enhanced by peripheral upslope winds. Laboratory experiments by Goldshmid et al. (2018) showed that upslope thermals may detach from the surface under certain slope and plateau geometries, reducing their ability to feed the plateau-core updraft and the associated convergence, so additional horizontal entrainment is required to sustain CI-relevant lifting. In contrast, escarpment-like slopes maintain attached upslope flow that more effectively reinforces the plateau core. When turbulent convection over the plateau weakens, opposing density currents may collide and stabilize the environment or provide mechanical lifting that can bring moist low-level air to saturation. In this context, more generally, sustained low-level updrafts preceding CI may need to exceed a critical horizontal scale (approximately 3–5 km) to withstand midlevel dry-air entrainment, as suggested by Marquis et al. (2021).

Furthermore, findings from several idealized studies (e.g., Kirshbaum 2013; Hassanzadeh et al. 2016; Panosetti et al. 2016; Imamovic et al. 2019) suggest that both the volume and orientation of plateau-like terrain relative to ambient winds influence the preferred location of CI and associated precipitation patterns, although these sensitivities may not generalize across mountain heterogeneity and varying synoptic forcing. Imamovic et al. (2019) showed that convective precipitation scales linearly with mountain volume and increases for flows parallel to the major axis of the mountain, while stronger background winds tend to shift CI maxima downwind and reduce precipitation efficiency. Hassanzadeh et al. (2016) likewise found that precipitation intensity increases with mountain height until the terrain becomes tall enough for synoptic winds to deflect or split the flow around it.

3.5 Mountain-plain transition circulations

Although slope, valley, basin, and plateau winds can extend over broad areas, they rarely match the larger-scale thermally driven air exchange that develops between a substantial mountain massif and the surrounding lowlands (Fig. 4). Such circulations can reach the upper end of the mesoscale and may exhibit diurnally oscillating behavior (Barry 2008). A prominent example is the Alpine Pump, a thermally induced circulation in which low-level air is drawn from adjacent plains toward a thermal low over the Alps, with substantial effects on directional wind shear and storm organization near the range (e.g., Trefalt et al. 2018). Graf et al. (2016) found that this circulation occurs on roughly 62 days per year and influences lowland airflow up to 100 km away, with simulated up-mountain inflow depths reaching about 1.5 km. However, key uncertainties remain in how plain-to-mountain and valley circulations determine the source regions and thermodynamic properties of the inflow air that ultimately feeds cloud-base updrafts.

The plain-to-mountain circulation (and its nocturnal reverse) extends over the height of the mountain ridge and overlies smaller slope and valley flows but is generally too weak to dominate them (Fig. 3a). It acts mainly in the upper part of the mountain boundary layer. During the day, negative ∇p toward the mountains generates up-mountain winds from adjacent plains, with typical speeds up to about 2 m s^{-1} and a broad compensating return flow aloft. Although easily suppressed by stronger ambient winds (e.g., Lareau et al. 2024), these flows can still transport key thermodynamic ingredients over long distances or shift drylines that support deep CI downwind of higher mountains (e.g., Bergmaier and Geerts 2015). The nocturnal phase is shallower, weaker, and reversed. Plain-mountain circulations also adjust more slowly to ∇T and ∇p than other thermally driven flows, producing time-shifted transition periods (Fig. 3b).

Persistent up-mountain transport causes the CBL to bulge upward, forming a thermal hot spot that can encompass an entire range. Yet, the presence of a range-scale hot spot does not necessarily imply uniformly favorable thermodynamic conditions across all internal ranges and basins, because the resulting vertical profiles depend on tropospheric depth and because temperature and moisture generally decrease with elevation. Nevertheless, observational studies (e.g., Weckwerth et al. 2011; Lock and Houston 2015; Lombardo and Bitting 2024) showed that CI occurs far more frequently over mountain ranges than over adjacent lowlands, with CI densities over the mountains about twice those in valleys and plains. Mountain volume and the interaction of thermal and ambient winds govern where CI subsequently expands (e.g., Levizzani et al. 2010; Hassanzadeh et al. 2016; Imamovic et al. 2017, 2019).

The analysis of prestorm environments in the Western Carpathians provides an illustrative example of how these controls shape the buoyancy field under contrasting wind regimes (Fig. 6). In a weak-wind, weak-forcing regime associated with slow-moving supercells forming closer to the mountains (Fig. 6a), CAPE is comparatively uniform across ranges, valleys, and basins, with the dominant gradient primarily controlled by elevation and decreasing toward higher terrain. By contrast, under stronger synoptic forcing associated with faster-moving supercells forming predominantly farther from the major ranges (Fig. 6b), CAPE exhibits a markedly different pattern. It is substantially reduced over windward slopes during prevailing southwesterly to westerly mid- to upper-level flow and can be suppressed even over lower mountains which showed elevated buoyancy in a weaker regime. At the same time, larger air-mass contrasts emerge across the region, such that well-ventilated mountain areas embedded within cooler, drier air exhibit markedly lower CAPE, whereas leeside mountains that remain within warmer and moister air can retain appreciable buoyancy and thermally driven low-level winds that are maintained despite stronger synoptic flow. Under these strong-flow conditions, terrain-flow interaction can also generate leeside convergence zones and displace thermally favored initiation regions downwind (e.g., Kirshbaum 2017; Reif and Bluestein 2018).

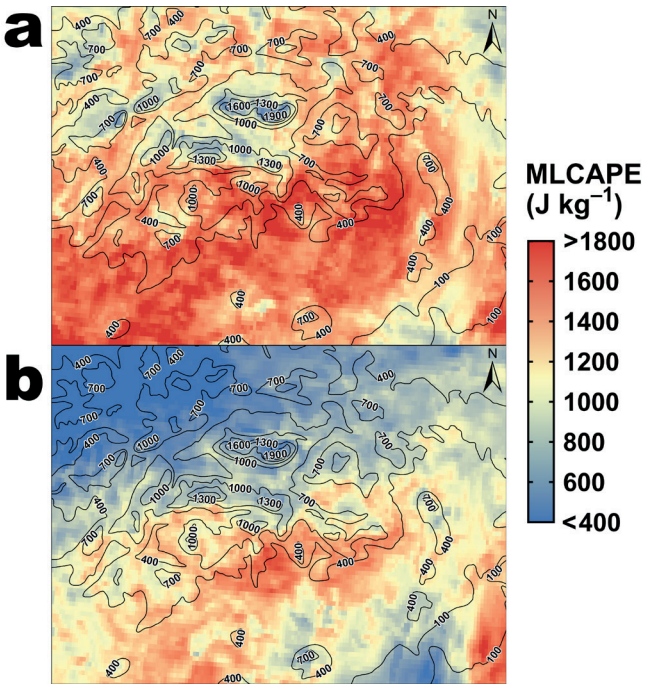

Fig. 6 Spatial distribution of median mixed-layer CAPE (0–500 m AGL parcel) from COSMO simulations over the Western Carpathians prior to supercell initiation. Panels show (a) slow-moving supercells in a weak-wind regime and (b) fast-moving supercells in a strong-wind regime, with predominant southwesterly-westerly mid- to upper-tropospheric flow. Smoothed elevation contours are shown every 300 m above mean sea level and topographic features with boundary lengths < 23 km are excluded.

Plain-to-mountain winds opposing the flow aloft can further modify leeside vertical shear and hodograph curvature, thereby influencing supercell initiation (e.g., Soderholm et al. 2014; Scheffknecht et al. 2017; Mulholland et al. 2019). Indeed, Kvak et al. (2023) found that 68% of the studied mesocyclones emerged over the leeward slopes of the Carpathians, although the first CI signatures may appear farther upstream. Yet larger samples and regime-based stratification are needed to separate robust signals from anomalous events. Moreover, although recent work has substantially expanded understanding of terrain effects on supercell environments (e.g., Purpura et al. 2023; Feldmann et al. 2024; McKeown et al. 2024; Riggin et al. 2025), it remains unclear under what combinations of terrain-forced convergence, buoyancy, and storm-relative flow supercells can form and persist when deep-layer shear is weak (e.g., Tang et al. 2016).

4. Mechanically forced orographic flow perturbations

Mechanically forced ascent occurs when a sufficiently strong large-scale flow impinges on terrain and undergoes terrain-flow interaction within the mountain environment (e.g., Kirshbaum et al. 2007; Barrett et al. 2015; Lareau et al. 2024). It is most prominent under moderate to strong ambient flow, when lift patterns are controlled mainly by flow direction, stability, and terrain geometry, and CI occurs where the resulting ascent is deep enough to lift moist air to its LFC while CIN is weak enough to be overcome by the available lift (e.g., Marquis et al. 2023). Terrain alters both the vertical and horizontal wind components, which can support CI by lifting parcels through forced ascent, by generating low-level convergence zones, and by producing upward acceleration in ducted orographic waves near mountains (e.g., Markowski and Richardson 2010; Nelson et al. 2021; Nicolas and Boos 2022) that locally modulate the vertical depth of moisture and parcel buoyancy.

Nonetheless, mechanically forced ascent alone is not sufficient for CI. Its effectiveness depends on whether sufficiently moist, conditionally unstable air is present (or becomes locally enhanced) and on how terrain-induced subsidence and mixing in adjacent lee regions modify moisture and CAPE, potentially strengthening CIN and suppressing CI (e.g., Marquis et al. 2023). Accordingly, CI tends to occur where terrain-modified convergence and moisture transport maintain or increase low-level moisture and reduce inhibition enough to permit ascent to the LFC. Resulting deformation of the wind field strongly affects low-level flow and can modify the magnitude of vertical wind shear (e.g., Mulholland et al. 2019). Because shear helps govern storm organization and longevity once CI occurs, terrain-driven shear modulation can either favor or inhibit both CI and subsequent storm organization in the vicinity of mountains (e.g., Houze et al. 1993; Markowski and Dotzek 2011; Mulholland et al. 2020; Feldmann et al. 2021; Da Silva and Haerter 2023).

Key factors that influence mechanically forced ascent and determine whether air ascends a mountain or becomes blocked include the upstream stability, the strength of the impinging flow, and the spatial extent of the barrier (e.g., Whiteman 2000; Reeves and Lin 2007; Miglietta and Rotunno 2014; Degiacomi et al. 2025). The terrain shape relative to the flow, its vertical and horizontal scales, surface roughness, and the arrangement of ridges and valleys further modulate the flow response and thereby the spatial distribution of low-level moisture and instability in the vicinity of mountains (Fig. 6; e.g., Roe 2005; Imamovic et al. 2019; Ammon et al. 2025). Less stable upstream flow, sufficiently strong incoming winds, and a narrow barrier favor ascent over the terrain and flow crossing the ridge, with CI often developing along windward slopes (e.g., Chen and Lin 2005). In contrast, more stable air with $\partial\theta_e/\partial z > 0$, weaker flow, and a broad barrier promotes partial or complete blocking. The flow then detours the obstacle, and CI is more likely upstream, downstream, or around the terrain rather than directly over it (e.g., Frame and Markowski 2006).

Both vertically and horizontally, terrain-modified wind effects are strongest near large mountains that interact with upper-level flow or lie within dynamically active regions (e.g., Barry 2008). Elevated terrain can slow synoptic low-level flow through increased surface friction, yet compression and channeling of the impinging airstream may locally accelerate mesoscale currents (e.g., Houze 2012; Tang et al. 2016). Strong background flow can also advect surface-based buoyancy anomalies, such as warm thermal wakes, into the lee, where they interact with mechanically induced CI (e.g., Bougeault et al. 2001; Kirshbaum and Wang 2014). These modified wind and buoyancy patterns are consistent with a foreland maximum in the overlap of lift, moisture, and weak inhibition, which can also favor environments supportive of hailstorms (e.g., Punge and Kunz 2016; Battaglioli et al. 2023). Although mountain-flow regime concepts are harder to apply in conditionally unstable environments or in elevated convection (e.g., Kirshbaum et al. 2018), the evolution of moist low-level air remains critical for CI (e.g., Weckwerth et al. 2014; Wang et al. 2016).

4.1 Vertical deformation of the background wind field

Orographic flow modification occurs regardless of how susceptible the low-level air is to blocking, since commonly used blocking diagnostics describe only whether near-surface flow tends to ascend over or detour around a barrier (e.g., Hagen et al. 2011; Kirshbaum et al. 2018). Even when the low-level flow would

ordinarily ascend the terrain, any vertically stacked air column that is not absolutely unstable experiences at least some degree of blocking or deflection as it encounters the mountain (Blumen 1990; Kirshbaum and Wang 2014; Kirshbaum 2017). Airflow approaching complex terrain is forced to compress and converge near the surface and within the lower troposphere. Density and cross-barrier velocity of the impinging air, together with terrain characteristics such as slope angle and horizontal extent, control the intensity of vertical deformation (Hilel Goldshmid et al. 2018). These momentum perturbations can extend vertically through much of the troposphere, and even hills only a few hundred meters high can disrupt an otherwise balanced wind field (e.g., Kirshbaum and Schultz 2018).

Moist, conditionally unstable air that is not blocked or diverted is mechanically forced to rise and cross part or all of the terrain (e.g., Miglietta and Rotunno 2014). Static destabilization associated with thermal circulations, together with reduced upstream blocking, further promotes terrain-forced ascent and lowers CIN within the windward CBL by deepening the mixed layer and increasing near-surface θ_e (e.g., Chu and Lin 2000; Riggin et al. 2025). Fig. 7a illustrates a CI mechanism in which a positive vertical-velocity anomaly and a convergence zone develop over windward slopes, allowing even modest ambient flow to provide sufficiently deep mechanically forced lift to raise moist conditionally unstable air to its LFC (Lock and Houston 2014). Windward ascent is a common mechanism for CI and convective precipitation enhancement (e.g., Hagen et al. 2011; Kirshbaum et al. 2016; Bačová Mitková et al. 2018). Even under stronger stability, a potentially unstable layer within a stratiform precipitating system may still be lifted to its LFC, producing embedded convection when sufficient midlevel moisture and lapse rates support elevated CAPE above a stable near-surface layer (e.g., Davolio et al. 2016; Friedrich et al. 2016; Kašpar et al. 2021).

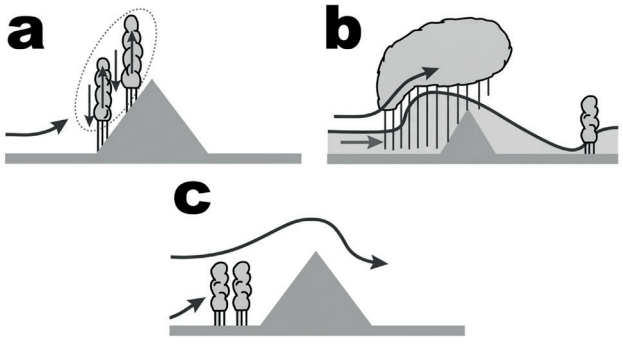

Fig. 7 Mechanically induced initiation mechanisms that contribute to the formation of precipitating deep convection in the vicinity of mountains. (a) Terrain-forced ascent along windward slopes, (b) downslope-propagating outflows from stratiform or convective precipitation, and (c) partially or fully blocked low-level flow. Arrows indicate the direction of prevailing airflows. Figure adapted from Houze (1993, his Fig. 12.24; 2012, his Fig. 3) with permission.

Once thunderstorms develop over mountains, or when stratiform precipitation is present, cold pools and outflows can propagate rapidly downstream and downslope, supporting distant CI (Fig. 7b) along convergence zones, thermal contrasts, or hydraulic-jump-like transitions, where CAPE is preserved by moisture pooling on the warm side of the boundary (e.g., Reeves and Lin 2007; Kirshbaum and Schultz 2018; Schneider et al. 2018; Nicolas and Boos 2022). In conditionally unstable environments, strong ascent along these jumps can initiate new convection or reinvigorate existing storms (e.g., Chu and Lin 2000; Frame and Markowski 2006; Smith et al. 2015). Under weaker background winds, outflows can interact with opposing upslope flow and regenerate CI upstream through new cell development (e.g., Chen and Lin 2005; Miglietta and Rotunno 2014; Panziera et al. 2015).

Apparent outflow-like signatures (Fig. 7b) in the lee of mountain ranges can also arise from non-precipitating processes, including downslope-wind descent and turbulent mixing that substantially dry the boundary layer and reduce surface-based CAPE during synoptic-scale cross-barrier flow (e.g., Kaspar et al. 2009). This mountain-induced mixing often does not suppress CI everywhere. Instead, it displaces the most favorable CI corridor to the edge of the lee-modified air mass, where a dryline-like moisture boundary and sharp instability gradient form along the foreland, focusing low-level convergence while preserving buoyancy on the moist side (e.g., Bergmaier and Geerts 2015). Downwind CI can therefore occur well away from the mountains when a downslope surge undercuts or abuts a moist boundary-layer reservoir, yielding a narrow corridor where CIN is locally reduced despite widespread drying nearby. Such complex interactions among local terrain-forced lift, leeside mixing, gust-front lifting, and free-tropospheric entrainment in sustaining convection after CI are not easily quantified even in high-resolution models, complicating CI diagnosis and forecasting (e.g., Kaltenboeck and Steinheimer 2015; Marquis et al. 2023).

Fig. 7c illustrates a CI mechanism in which the mountain height greatly exceeds the LFC and the upstream flow is partially or fully blocked and stable. In such cases, pulsing CI may develop where the airstream is forced to bend upward, and the conditionally unstable layer first reaches its LFC provided that sufficient moisture is retained to sustain CAPE and CIN is locally reduced by the convergence-driven ascent (Houze 1993). When blocking extends through a deep layer, wind speed can decrease sharply in front of the mountain, and the resulting convergence may produce a hydraulic-jump-like transition with enhanced upward motion (Řezáčová et al. 2007). This feature can shift CI well away from the barrier on the upstream side (e.g., Davolio et al. 2016). In upstream-blocking regimes, deep convective clouds are often lower because the upper troposphere is

more stable, the available CAPE is limited, and strong vertical shear tilts and weakens updrafts.

Mechanically forced ascent on the lee side can generate lee waves that initiate convective clouds downstream of hills or modest mountains when sufficient moisture and CAPE are present and CIN can be breached (e.g., Kirshbaum et al. 2007). Fig. 8a shows a CI mechanism in which lee waves arise as stable flow ($\partial\theta/\partial z > 0$) passes over a small mountain, producing oscillating pressure, wind, and buoyancy anomalies (e.g., Serafin et al. 2018). Leeside lifting and flow acceleration create a pressure trough that draws air inward and forms a convergence zone where moisture can pool and enhance parcel buoyancy (e.g., Kirshbaum et al. 2016). For strong-flow regimes, it is not fully resolved how terrain geometry and stratification control the evolution and persistence of leeside convergence and its effectiveness for CI. If the leeside terrain slopes upward or environmental conditions favor persistent ascent, these waves can initiate precipitating convective clouds that are advected downwind as narrow rainbands aligned with the flow (e.g., Barrett et al. 2015; Kirshbaum and Schultz 2018a; Degiacomi et al. 2025). Turbulence, separation eddies, and wakes near the surface or within the mountain CBL may further enhance ascent, especially in complex or forested terrain where surface roughness strengthens small-scale convergence and intermittently lifts parcels through the residual inhibition (e.g., Whiteman 2000; De Wekker et al. 2018).

Another CI mechanism (Fig. 8b) involves vertically propagating mountain waves that develop over higher and steeper terrain and tilt upstream, producing persistent wave-induced ascent and quasi-stationary CI near prominent crests (e.g., Chu and Lin 2000). These waves, sustained in stable environments, may amplify above the crest and interact with moist low-level inflow, yielding elevated CI downstream of the mountain (e.g., Reif and Bluestein 2018; Feng et al. 2022). Nevertheless, it is not yet clear how upstream surface fluxes precondition the inflow humidity and static stability that modulate mechanically forced CI through their control on CAPE and CIN in the inflow layer. Figs. 9i, j show simulations of Mulholland et al. (2019) when higher terrain generates stronger and deeper waves, evident from bent-back isentropes and enhanced upward motion. In these cases, standing waves with vertical velocities of 1–4 m s^{-1} formed near the ridgetop, while the mixed-layer LFC was lower over the crest. This combination of larger wave amplitude, stronger ascent, and reduced LFC height produced earlier CI by weakening the effective inhibition. By contrast, lower terrain yielded weak or absent mountain waves (Figs. 9f, g) and higher ridgetop LFCs, delaying CI.

4.2 Horizontal deformation of the background wind field

Orographically forced horizontal flow modifications are important for CI in complex terrain because they create convergence zones, shift initiation maxima away from peaks (e.g., Wang et al. 2016), transport heat and moisture, and displace unstable layers (e.g., Ribeiro and Bosart 2018). As with vertically forced motions, they occur regardless of blocking, although when low-level flow cannot surmount the barrier, a larger fraction is diverted laterally (Blumen 1990). Air more readily detours around tall, narrow, or isolated peaks than around broad or elongated ranges oriented perpendicular to the inflow. Surface characteristics, ridge orientation, and curvature strongly influence wind direction and speed along the flanks (e.g., Reif and Bluestein 2018; Ammon et al. 2025), with parallel or convex terrain promoting efficient lateral deflection and sharpening low-level moisture gradients between deflected inflow and adjacent mixed or subsident air (Whiteman 2000). Depending on the terrain shape, the flow may accelerate along one side or separate around the lateral edges (Houze 1993), and because these modifications act within the moist low-level layer, they can efficiently promote CI (Kirshbaum and Wang 2014).

When upstream blocking or stagnation occurs, and depending on the mountain geometry and the lower terrain downstream, the flow often diverts around the lower flanks rather than over the higher summits (e.g., Hagen et al. 2011). Under weaker

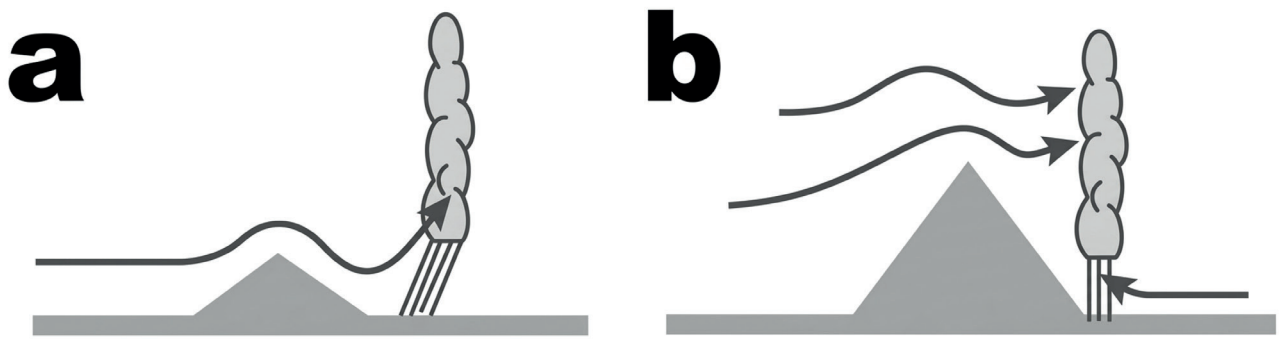

Fig. 8 As in Fig. 7, but showing: (a) downstream lee-wave convection initiated by ascent in the lee-wave crests downstream of hills or low mountains, and (b) upstream-tilted vertically propagating mountain waves over higher terrain. Figure adapted from Houze (1993, his Fig. 12.24; 2012, his Fig. 3) with permission.

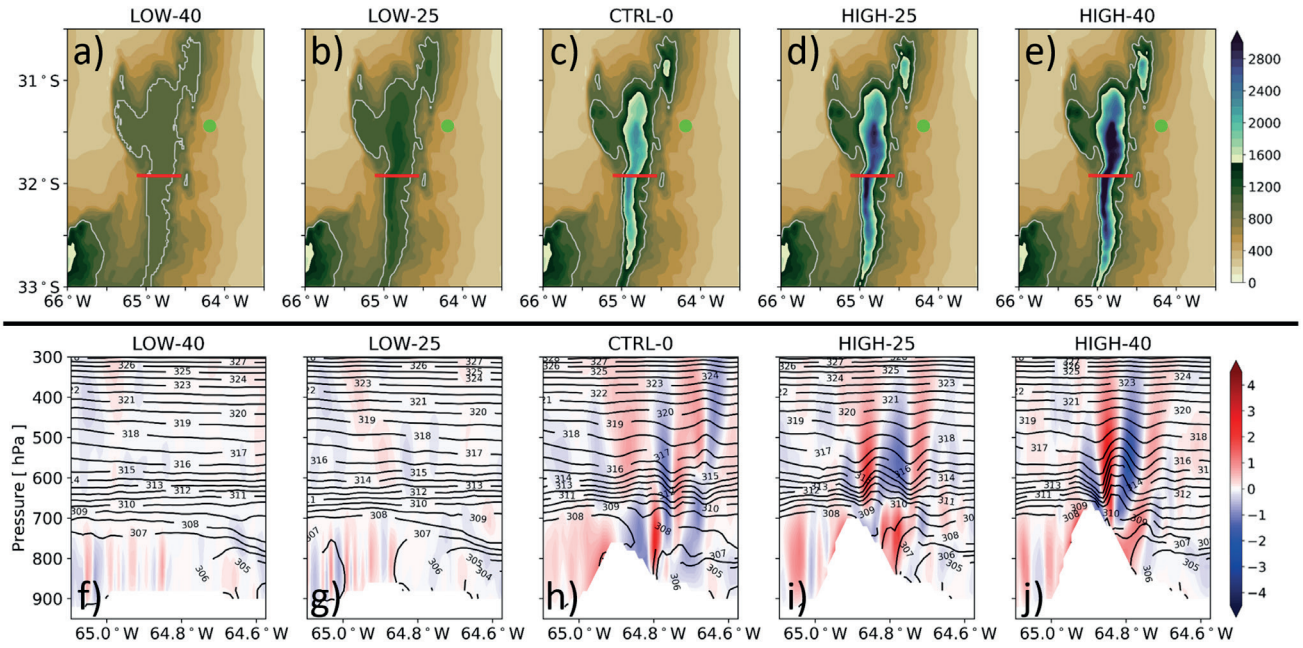

Fig. 9 Orographic model experiments illustrating vertically propagating mountain waves over the Sierras de Córdoba, Argentina, on 29 November 2017. Panels (a–e) display plan-view terrain height (shaded; m), the 1000-m elevation contour (gray), the location of Córdoba (lime dot), and the west-east cross-section transects (red lines) corresponding to the lower panels (f–j). In panel (h), CTRL-0 provides the baseline terrain configuration, whereas panels (f) LOW-40, (g) LOW-25, (i) HIGH-25, and (j) HIGH-40 depict terrain reductions or increases of 40%, 25%, 25%, and 40%, respectively. The vertical sections (f–j) show vertical velocity (shaded; m s^{-1}) and potential temperature (black contours at 1-K intervals) at 1500 UTC 29 November 2017. Figure reproduced from Mulholland et al. (2019, their Fig. 2) with permission.

winds, the separated flow commonly reassembles in a confluence zone with accumulated moisture and reduced CIN. Because these confluence zones shift between events, composite analyses may obscure the true placement and timing of the peak ascent (e.g., Bougeault et al. 2001; Schneider et al. 2018). Fig. 10a presents a CI mechanism in which the confluence of deflected and ambient flows generates ascent in the lee, with further upward acceleration possibly enhanced through interaction with vertically displaced flows (e.g., Kirshbaum and Schultz 2018a). CI may also develop under stronger background winds along the path of the diverted flow on extended mountain flanks, where stronger low-level winds allow the deflected branch to merge with the environmental flow and form a flanking convergence zone along one or both sides of the barrier (Banta 1990).

Diverted airflow may form an elevated barrier jet along windward slopes, blowing parallel to the mountain and strongest near the foothills (Chow et al. 2013). Although barrier jets are often associated with winter cold-air surges, they also occur in summer and can contribute to CI (e.g., Davolio et al. 2016; Nicolas and Boos 2022; Singh et al. 2022). Their characteristics depend on synoptic forcing, regional climate, and mountain geometry, which together determine the prevailing flow regime (Houze 2012; Ribeiro and Bosart 2018). Such low-level jets transport moisture over long distances, favor high-CAPE environments (e.g., Chu and Lin 2000; Feng et al. 2022), and, when acting as barrier jets, can exceed 15 m s^{-1} up to 500 m AGL (Whiteman 2000), thereby also increasing low-level shear (Reif and Bluestein 2018). However, strong shear within these jets can hinder CI by

Fig. 10 As in Fig. 7, but showing: (a) the deflection of low-level flows around the terrain and their confluence in the lee, and (b) an elevated mixed layer is horizontally advected off the horizontal advection of an elevated mixed layer from the mountains over adjacent plains, creating a capped but potentially unstable environment. Figure adapted from Houze (1993, his Fig. 12.24; 2012, his Fig. 3) with permission.

disrupting developing updrafts (Markowski and Richardson 2010).

Within valleys, gorges, gaps, and passes, airflow is laterally and vertically constricted and becomes channeled, enhancing low-level moisture transport (e.g., Wulfmeyer et al. 2011; Tang et al. 2016; Singh et al. 2022). The strength and depth of these gap flows depend on upstream-downstream differences in $\partial\theta/\partial z$ and on hydrostatically driven ∇p through the narrowed terrain (e.g., Schmidli and Rotunno 2012; Chow et al. 2013). Downstream, the flow commonly shows a wind-speed maximum, enhanced turbulent mixing beneath a stagnant cap, and sometimes a hydraulic-jump-like rebound (Markowski and Richardson 2010). Because the gap entrance is typically more stable, CI there is uncommon. Instead, outflowing air more often encounters more favorable conditions just downstream, where CIN is minimized and CAPE, though reduced, can still support CI along the exit flanks (e.g., Markowski and Dotzek 2011). When the outflow aligns with the along-gap axis, it may also enhance storm dynamics (Riggin et al. 2025), raising the question of how different terrain features interact with low-level winds and storm motion.

In another example of terrain-modified low-level flow, Wang et al. (2016) showed that CI along the Dabie Mountains ridge results from the interaction of thermally driven upslope winds, mechanically deflected around-peak flow, and valley-channeled upslope currents (Fig. 11). This configuration aligned convergence zones along the ridge, shifted them slightly downwind, and produced the strongest lifting

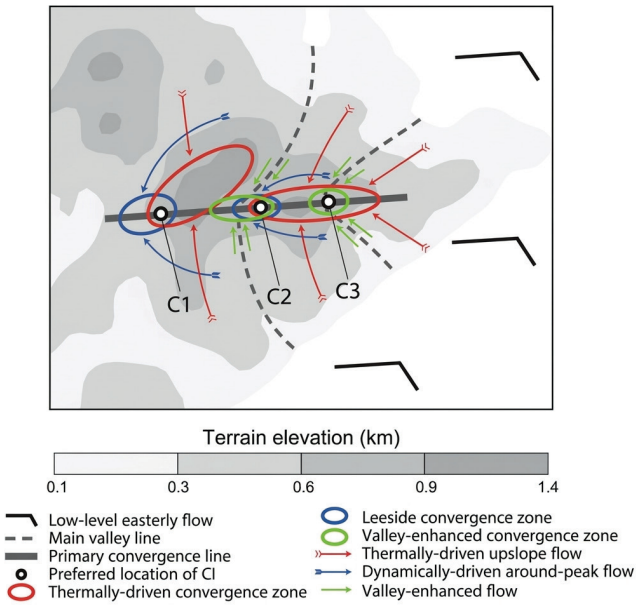

Fig. 11 Low-level convergence zones over the Dabie Mountains ridge, China, on 10 June 2010. Wind barbs depict the ambient low-level flow, while colored arrows show the main terrain-modified currents. The bold gray line marks the primary convergence zone above the ridge where these flows interact. White-filled black circles (C1, C2, C3) denote the three major deep convective cells initiated before 0600 UTC. Figure reproduced from Wang et al. (2016, their Fig. 13) with permission.

and earliest CI where two or more convergence mechanisms overlapped and where low-level moisture was deepest, allowing parcels to access buoyancy with minimal inhibition. Soderholm et al. (2014) similarly found that quasi-stationary storms are favored when low-level winds run parallel to a ridge, allowing outflows to propagate downwind without disrupting the upslope inflow that maintains elevated convergence, whereas cross-ridge flow suppresses repeated CI. The behavior of these outflows depends on terrain steepness and rain-induced momentum, as steeper mountains slow their lateral spread and modulate their interaction with elevated convergence zones (Imamovic et al. 2019).

The last orographically influenced CI process, illustrated in Fig. 10b, is more indirect because it does not generate ascent itself but instead involves horizontal displacement of a surface-based capping inversion from mountains toward adjacent lowlands. EMLs that form over mountains may be partially or fully advected off the terrain by terrain-modified ambient winds (Fig. 2). Such environments are common east of the Rockies and Andes (e.g., Ribeiro and Bosart 2018) and north-northwest of the Meseta Central (e.g., Schultz et al. 2025) and do not entirely prevent CI (e.g., Bergmaier and Geerts 2015; Taszarek et al. 2020b; Nelson et al. 2021). When sufficient mesoscale lift develops later in the day (e.g., Fig. 7b; Doswell 1987), the cap can be breached, and parcels can reach their LFCs. By modifying the thermodynamic profile and delaying early CAPE release, these elevated layers allow potential instability to accumulate far downstream from the EML source, making mountains a significant, albeit indirect, contributor to intense severe convection once lifting finally overcomes CIN (e.g., Doswell and Bosart 2001; Kaspar et al. 2009; Kunz et al. 2018).

5. Summary and perspectives

This review brings together current understanding of how orography influences convective storm initiation within a mesoscale framework. Houze (2012) emphasized that topography acts as a passive boundary condition in precipitation processes and does not itself provide the essential ingredients for convective storm formation. In many cases, the large-scale environment would still support thunderstorms over flat terrain, although their timing and location would differ without orographic effects. Orography modifies all three ingredients required for CI, namely moisture, instability, and lift, by redistributing heat and moisture, reorganizing low-level flow, and providing localized ascent (Doswell et al. 1996). These modifications arise through thermally driven circulations that are most prominent under weak background flow and strong diurnal heating, and through mechanically forced flow perturbations that become

more influential under moderate to strong ambient flow. Together, these terrain-atmosphere interactions create mesoscale convergence and ascent and can precondition the thermodynamic environment so that parcels reach the level of free convection, above which buoyant acceleration proceeds largely independent of the underlying terrain as cumulonimbus clouds develop.

Thermally driven circulations emerging from diurnal differential heating across slopes, valleys, basins, plateaus, and adjacent plains organize the mountain boundary layer and strongly influence CI. Upslope flows, the primary low-level response to daytime heating, create greater instability and convergence along sunlit slopes and ridges where CI often begins. Valley geometry modulates up-valley transport, boundary-layer growth, and erosion of convective inhibition, while basins, plateaus, and larger massifs support broader plain-to-mountain inflows that transport moist, unstable air and focus ascent along terrain edges. Upslope and up-valley transport can deepen the boundary layer and create convective hot spots. Under stronger background flow, terrain-flow interaction can displace these hot spots downwind and can also produce leeside convergence zones. At night, radiative cooling stabilizes higher terrain and nearby valleys, but downslope and down-valley flows can still support CI where they encounter moist air. Observations show that CI occurs more frequently over mountains than adjacent lowlands, with a late-morning to early-afternoon maximum that reflects the dominant role of diurnal thermal circulations in modulating buoyancy, moisture, and low-level convergence.

Mechanically based terrain effects profoundly modify low-level flow and redistribute thermodynamic properties through forced ascent, leeside subsidence and mixing, deflection, channeling, and splitting, and these adjustments often control when and where CI occurs. Whether air ascends a barrier or detours around it depends on static stability, wind speed and direction, and terrain geometry, which can shift CI to windward slopes, leeside convergence zones, flanks, or upstream regions. Thermally driven upslope winds, mechanically deflected cross-barrier flows, and valley-channeled currents frequently converge to form persistent lifting corridors, while cold-pool outflows, hydraulic-jump-like transitions, and dryline-like moisture boundaries can regenerate CI, shift it downstream, or locally suppress it. Mountain waves provide additional elevated ascent that can anchor quasi-stationary CI over and downstream of high terrain, and terrain-modified vertical shear further shapes storm organization. Mountains also influence CI indirectly by producing elevated mixed layers that are advected over adjacent plains, delaying convection while allowing substantial convective available potential energy accumulation until mesoscale ascent finally erodes the cap.

With increasing terrain height, the relative importance of mechanically forced processes generally increases during strong-flow situations, because windward ascent, blocking and deflection, lee convergence, and mountain-wave responses become more pronounced. In low mountain ranges and hilly terrain, thermally driven circulations often provide the dominant mesoscale mechanism during weak-flow warm-season conditions. In medium to high mountain ranges, thermally driven circulations still frequently precondition the boundary layer through moisture transport and erosion of convective inhibition, but mechanically forced lift and lee convergence more often determine where and when initiation occurs during periods of synoptic-scale forcing.

5.1 Open questions and research priorities

A central research need is to move from documenting where CI occurs in mountains to explaining why it occurs preferentially in certain terrain features and flow regimes, by tracing how terrain-driven processes modify the CI ingredients and interact across multiple scales (e.g., Imamovic et al. 2019; Rotach et al. 2022). For thermally driven regimes, key unknowns include how valley and plain-to-mountain circulations set the source regions and thermodynamic properties of rising parcels, and how boundary-layer heterogeneity controls effective convective inhibition and the width and depth of cloud-base updrafts as thermals transition through the capping layer into the free troposphere (e.g., Marquis et al. 2021; Nelson et al. 2022). For mechanically forced regimes, major gaps persist in quantifying transient and nonlinear processes such as the evolution of leeside convergence, cloud-diabatic feedbacks on mountain waves and blocking, and the role of upstream surface fluxes in preconditioning stability and humidity (e.g., Kirshbaum et al. 2018; Nicolas and Boos 2022). Across both regimes, the challenge is not only the mean forcing but also the organization of lift in space and time, including how terrain channeling can superpose air masses of different origin and create sharp gradients in moisture, convective inhibition, and low-level shear that are rarely resolved by coarse observations or compositing approaches (e.g., Markowski and Dotzek 2011; Lareau et al. 2024).

Progress on these questions will require coordinated strategies that link CI mechanisms to CI outcomes using complementary observations and modeling. Priorities include (i) dense, three-dimensional measurements of near-cloud thermodynamics, convergence, and turbulence across valleys, slopes, ridges, and adjacent plains, with scanning strategies designed to test explicit hypotheses about CI (e.g., Serafin et al. 2018; Marquis et al. 2023); (ii) systematic numerical experimentation spanning convection-permitting to large-eddy simulation scales to isolate sensitivities to terrain geometry, land-surface heterogeneity,

and background flow, while addressing marginally resolved terrain forcing in simulations of orographic CI (e.g., De Wekker and Kossmann 2015; Panosetti et al. 2016); and (iii) analysis frameworks that distinguish robust regimes from anomalies through larger samples, more sophisticated statistical tools, and alternative stratification by wind speed, shear, instability, and flow direction in different terrain settings (e.g., Katona et al. 2016; Kvak et al. 2023).

Supercells and other organized storms provide a useful test for these efforts because they amplify small terrain-driven changes in low-level flow and hodograph structure, yet are difficult to confirm observationally in complex terrain (e.g., Scheffknecht et al. 2017; Da Silva and Haerter 2023). Research priorities therefore include identifying when thermally driven circulations meaningfully enhance low-level shear and storm-relative inflow, how leeside convergence corridors modulate storm initiation likelihood, and under what conditions terrain-forced lifting and heterogeneity can compensate for weak deep-layer shear to support persistent rotating updrafts (e.g., Fischer et al. 2025).

In mountainous regions where convective storms occur at least seasonally, orographically induced flows create distinctive environments in which storm activity differs in several important ways from that over lower elevations. Of greatest societal relevance are a higher frequency of storm initiation, an increased likelihood of convection-related severe weather, and greater uncertainty in forecasts of both storm occurrence and intensity (e.g., Barrett et al. 2015; Kühne et al. 2025). Despite substantial progress, many processes remain difficult to quantify, limiting operational forecast accuracy and the ability to anticipate societal impacts (Brooks et al. 2019). Quantitative statistics comparing the prevalence of specific CI mechanisms across mountain settings and flow regimes within a given region also remain limited, highlighting a need for expanded observations and targeted modeling. Readers are encouraged to consult the references cited herein for more detailed discussion, as a comprehensive treatment of all issues lies beyond the scope of this condensed review, but the priorities outlined above provide a path toward improved understanding and predictability.

Acknowledgments

We thank Miloslav Müller and Petr Zacharov for their comments and encouragement and Miroslav Truben for assistance with the figure illustrating idealized thermally driven circulations over a mountain. We also thank the authors who granted permission to reproduce figures from their publications. We appreciate the constructive feedback from two anonymous reviewers for AUC Geographica, which helped shape the manuscript in its final form.

References

Afrifa, F. O. T., and Coauthors (2025): A Case Study of Cold-Season Emergent Orographic Convection and Its Impact on Precipitation. Part I: Mesoscale Analysis. Monthly Weather Review 153 (10), 2229–2250, https://doi.org/10.1175/MWR-D-24-0241.1.

American Meteorological Society (AMS) (2025): Cumulonimbus. Glossary of Meteorology. Available online: https://glossary.ametsoc.org/wiki/Cumulonimbus (accessed on 10 November 2025).

Ammon, M. B., Bell, T. M., Smith, E. N., Gebauer, J. G., Pardun, T. J. (2025): Relating the Effects of Heterogeneous Terrain on Boundary-Layer Flow to the Evolution of Preconvection Environments Using Remote Profiler Datasets from PERiLS. Monthly Weather Review 153(11), 2555–2569, https://doi.org/10.1175/MWR-D-24-0108.1.

Bačová Mitková, V., Pekárová, P., Halmová, D., Miklánek, P. (2018): Reconstruction and post-event analysis of a flash flood in a small ungauged basin: a case study in Slovak territory. Natural Hazards 92, 741–760, https://doi.org/10.1007/s11069-018-3222-2.

Banta, R. M. (1990): The Role of Mountain Flows in Making Clouds. In Blumen, W. (Eds.), Atmospheric Processes over Complex Terrain. Meteorological Monographs 23; American Meteorological Society: Boston, MA, https://doi.org/10.1007/978-1-935704-25-6_9.

Barrett, A. I., Gray, S. L., Kirshbaum, D. J., Roberts, N. M., Schultz, D. M., Fairman, J. G., Jr. (2015): Synoptic versus orographic control on stationary convective banding. Quarterly Journal of the Royal Meteorological Society 141(689), 1101–1113, https://doi.org/10.1002/qj.2409.

Barry, R. G. (2008): Mountain Weather and Climate. 3rd ed.; Cambridge University Press: Cambridge, UK, 532 pp., https://doi.org/10.1017/CBO9780511754753.

Barthlott, Ch., Corsmeier, U., Meißner, C., Braun, F., Kottmeier, Ch. (2006): The influence of mesoscale circulation systems on triggering convective cells over complex terrain. Atmospheric Research 81(2), 150–175, https://doi.org/10.1016/j.atmosres.2005.11.010.

Barthlott, Ch., Schipper, J. W., Kalthoff, N., Adler, B., Kottmeier, Ch., Blyth, A., Mobbs, S. (2010): Model representation of boundary-layer convergence triggering deep convection over complex terrain: A case study from COPS. Atmospheric Research 95(2–3), 172–185, https://doi.org/10.1016/j.atmosres.2009.09.010.

Barthlott, Ch., Kalthoff, N. (2011): A Numerical Sensitivity Study on the Impact of Soil Moisture on Convection-Related Parameters and Convective Precipitation over Complex Terrain. Journal of the Atmospheric Sciences 68(12), 2971–2987, https://doi.org/10.1175/JAS-D-11-027.1.

Battaglioli, F., Groenemeijer, P., Púčik, T., Taszarek, M., Ulbrich, U., Rust, H. (2023): Modeled Multidecadal Trends of Lightning and (Very) Large Hail in Europe and North America (1950–2021). Journal of Applied Meteorology and Climatology 62(11), 1627–1653, https://doi.org/10.1175/JAMC-D-22-0195.1.

Bergmaier, P. T., Geerts, B. (2015): Characteristics and Synoptic Environment of Drylines Occurring over the Higher Terrain of Southeastern Wyoming. Weather and Forecasting 30(6), 1733–1748, https://doi.org/10.1175/WAF-D-15-0061.1.

Bianco, L., Djalalova, I. V., King, C. W., Wilczak, J. M. (2011): Diurnal Evolution and Annual Variability of Boundary-Layer Height and Its Correlation to Other Meteorological Variables in California's Central Valley. Boundary-Layer Meteorology 140, 491–511, https://doi.org/10.1007/s10546-011-9622-4.

Blumen, W. (Ed.) (1990): Atmospheric Processes over Complex Terrain. 1st ed.; American Meteorological Society: Boston, MA, USA; 323 pp., https://doi.org/10.1007/978-1-935704-25-6.

Bougeault, P., and Coauthors (2001): The MAP Special Observing Period. Bulletin of the American Meteorological Society 82(3), 433–462, https://doi.org/10.1175/1520-0477(2001)082<0433:TMSOP>2.3.CO;2.

Czech meteorological society (CMeS) (2025): Convective storm (in Czech). Electronic Glossary of Meteorology (eMS). Available online: http://slovnik.cmes.cz/fulltext/317 (accessed on 10 November 2025).

Brooks, H. E., and Coauthors (2019): A Century of Progress in Severe Convective Storm Research and Forecasting. Meteorological Monographs 59(1), 18.1–18.41, https://doi.org/10.1175/AMSMONOGRAPHS-D-18-0026.1.

Czernecki, B., Taszarek, M., Szuster, P. (2025): thundeR: Computation and Visualisation of Atmospheric Convective Parameters. R package version 1.1.3. Available online: https://bczernecki.github.io/thundeR/ (accessed on 10 November 2025).

Da Silva, N. A., Haerter, J. O. (2023): The Precipitation Characteristics of Mesoscale Convective Systems Over Europe. Journal of Geophysical Research: Atmospheres 128(23): e2023JD039045, https://doi.org/10.1029/2023JD039045.

Damiani, R., Zehnder, J., Geerts, B., Demko, J., Haimov, S., Petti, J., Poulos, G. S., Razdan, A., Hu, J., Leuthold, M., French, J. (2008): The Cumulus, Photogrammetric, In Situ, and Doppler Observations Experiment of 2006. Bulletin of the American Meteorological Society 89(1), 57–74, https://doi.org/10.1175/BAMS-89-1-57.

Davolio, S., Volonté, A., Manzato, A., Pucillo, A., Sicogna, A., Ferrario, M. E. (2016): Mechanisms producing different precipitation patterns over north-eastern Italy: Insights from HyMeX-SOP1 and previous events. Quarterly Journal of the Royal Meteorological Society 142(S1), 188–205, https://doi.org/10.1002/qj.2731.

De Wekker, S. F. J., Zhong, S., Fast, D., Whiteman, C. D. (1998): A Numerical Study of the Thermally Driven Plain-to-Basin Wind over Idealized Basin Topographies. Journal of Applied Meteorology and Climatology 37(6), 602–622, https://doi.org/10.1175/1520-0450(1998)037<0606:ANSOTT>2.0.CO;2.

De Wekker, S. F. J., Kossmann, M. (2015): Convective Boundary Layer Heights Over Mountainous Terrain – A Review of Concepts. Frontiers in Earth Science 3: 77, https://doi.org/10.3389/feart.2015.00077.

De Wekker, S. F. J., Kossmann, M., Knievel, J. C., Giovannini, L., Gutmann, E. D., Zardi, D. (2018): Meteorological Applications Benefiting from an Improved Understanding of Atmospheric Exchange Processes over Mountains. Atmosphere 9(10): 371, https://doi.org/10.3390/atmos9100371.

Degiacomi, T., Zonato, A., Davolio, S., Miglietta, M. M., Giovannini, L. (2025): Deep Banded Orographic Convection over an Idealized Mountain Range: Influence of Upstream Atmospheric Conditions. Journal of the Atmospheric Sciences 82(6), 1033–1055, https://doi.org/10.1175/JAS-D-24-0056.1.

Doswell, C. A. (1987): The Distinction between Large-Scale and Mesoscale Contribution to Severe Convection: A Case Study Example. Weather and Forecasting 2(1), 3–16, https://doi.org/10.1175/1520-0434(1987)002<0003:TDBLSA>2.0.CO;2.

Doswell, C. A., Brooks, H. E., Maddox, R. A. (1996): Flash Flood Forecasting: An Ingredients-Based Methodology. Weather and Forecasting 11(4), 560–581, https://doi.org/10.1175/1520-0434(1996)011<0560:FFFAIB>2.0.CO;2.

Doswell, C. A. (2001): Severe Convective Storms – An Overview. Meteorological Monographs 28(50), 1–26, https://doi.org/10.1175/0065-9401-28.50.1.

Doswell, C. A., Bosart, L. F. (2001): Extratropical Synoptic-Scale Processes and Severe Convection. Meteorological Monographs 28(50), 27–70, https://doi.org/10.1175/0065-9401-28.50.27.

Doswell, C. A. (2015): Severe convective storms in the European societal context. Atmospheric Research 158–159, 210–215, https://doi.org/10.1016/j.atmosres.2014.08.007.

Feldmann, M., Germann, U., Gabella, M., Berne, A. (2021): A characterisation of Alpine mesocyclone occurrence. Weather Climate Dynamics 2(4), 1225–1244, https://doi.org/10.5194/wcd-2-1225-2021.

Feldmann, M., Rotunno, R., Germann, U., Berne, A. (2024): Supercell Thunderstorms in Complex Topography – How Mountain Valleys with Lakes Can Increase Occurrence Frequency. Monthly Weather Review 152(2), 471–489, https://doi.org/10.1175/MWR-D-22-0350.1.

Feng, Z., Varble, A., Hardin, J., Marquis, J., Hunzinger, A., Zhang, Z., Thieman, M. (2022): Deep Convection Initiation, Growth, and Environments in the Complex Terrain of Central Argentina during CACTI. Monthly Weather Review 150(5), 1135–1155, https://doi.org/10.1175/MWR-D-21-0237.1.

Fischer, J., Groenemeijer, P., Holzer, A., Feldmann, M., Schröer, K., Battaglioli, F., Schielicke, L., Púčik, T., Antonescu, B., Gatzen, C., TIM Partners (2025): Invited perspectives: Thunderstorm intensification from mountains to plains. Natural Hazards and Earth System Sciences 25(8), 2629–2656, https://doi.org/10.5194/nhess-25-2629-2025.

Frame, J., Markowski, P. (2006): The Interaction of Simulated Squall Lines with Idealized Mountain Ridges. Monthly Weather Review 134(7), 1919–1941, https://doi.org/10.1175/MWR3157.1.

Friedrich, K., Kalina, E. A., Aikins, J., Gochis, D., Rasmussen, R. (2016): Precipitation and Cloud Structures of Intense Rain during the 2013 Great Colorado Flood. Journal of Hydrometeorology 17(1), 27–52, https://doi.org/10.1175/JHM-D-14-0157.1.

Graf, M., Kossmann, M., Trusilova, K., Mühlbacher, G. (2016): Identification and Climatology of Alpine Pumping from a Regional Climate Simulation. Frontiers in Earth Science 4: 5, https://doi.org/10.3389/feart.2016.00005.

Groenemeijer, P., Púčik, T., Holzer, A. M., Antonescu, B., Riemann-Campe, K., Schultz, D. M., Kühne, T., Feuerstein, B., Brooks, H. E., Doswell, C. A., III, Koppert, H., Sausen, R. (2017): Severe Convective Storms in Europe: Ten

Years of Research and Education at the European Severe Storms Laboratory. Bulletin of the American Meteorological Society 98(12), 2641–2651, https://doi.org/10.1175/BAMS-D-16-0067.1.

Hagen, M., van Baelen, J., Richard, E. (2011): Influence of the wind profile on the initiation of convection in mountainous terrain. Quarterly Journal of the Royal Meteorological Society 137(S1), 224–235, https://doi.org/10.1002/qj.784.

Hassanzadeh, H., Schmidli, J., Langhans, W., Schlemmer, L., Schär, C. (2016): Impact of topography on the diurnal cycle of summertime moist convection in idealized simulations. Meteorologische Zeitschrift 25(2), 181–194, https://doi.org/10.1127/metz/2015/0653.

Hilel Goldshmid, R., Bardoel, S. L., Hocut, C. M., Zhong, Q., Liberzon, D., Fernando, H. J. S. (2018): Separation of Upslope Flow over a Plateau. Atmosphere 9(5): 165, https://doi.org/10.3390/atmos9050165.

Houze, R. A., Jr. (1993): Cloud Dynamics; Academic Press: San Diego, USA; 573 pp.

Houze, R. A., Jr., Schmid, W., Fovell, R. G., Schiesser, H.-H. (1993): Hailstorms in Switzerland: Left Movers, Right Movers, and False Hooks. Monthly Weather Review 121(12), 3345–3370, https://doi.org/10.1175/1520-0493(1993)121<3345:HISLMR>2.0.CO;2.

Houze, R. A., Jr. (2012): Orographic effects on precipitating clouds. Reviews of Geophysics 50 (1): RG1001, https://doi.org/10.1029/2011RG000365.

Chen, S., Lin, Y. (2005): Effects of Moist Froude Number and CAPE on a Conditionally Unstable Flow over a Mesoscale Mountain Ridge. Journal of the Atmospheric Sciences 62(2), 331–350, https://doi.org/10.1175/JAS-3380.1.

Chow, F. K., De Wekker, S. F. J., Snyder, B. J. (2013): Mountain Weather Research and Forecasting: Recent Progress and Current Challenges; Springer: Dordrecht, Netherlands; 750 pp., https://doi.org/10.1007/978-94-007-4098-3.

Chu, C., Lin, Y. (2000): Effects of orography on the generation and propagation of mesoscale convective systems in a two-dimensional conditionally unstable flow. Journal of the Atmospheric Sciences 57(23), 3817–3837, https://doi.org/10.1175/1520-0469(2001)057<3817:EOOOTG>2.0.CO;2.

Imamovic, A., Schlemmer, L., Schär, C. (2017): Collective Impacts of Orography and Soil Moisture on the Soil Moisture-Precipitation Feedback. Geophysical Research Letters 44(22), 11682–11691, https://doi.org/10.1002/2017GL075657.

Imamovic, A., Schlemmer, L., Schär, C. (2019): Mountain Volume Control on Deep-Convective Rain Amount during Episodes of Weak Synoptic Forcing. Journal of the Atmospheric Sciences 76(2), 605–626, https://doi.org/10.1175/JAS-D-18-0217.1.

Kaltenboeck, R., Steinheimer, M. (2015): Radar-based severe storm climatology for Austrian complex orography related to vertical wind shear and atmospheric instability. Atmospheric Research 158–159, 216–230, https://doi.org/10.1016/j.atmosres.2014.08.006.

Kalthoff, N., Kohler, M., Barthlott, C., Adler, B., Mobbs, S. D., Corsmeier, U., Traumner, K., Foken, T., Eigenmann, R., Krauss, L., and Coauthors (2011): The dependence of convection-related parameters on surface and boundary-layer conditions over complex terrain. Quarterly Journal of the Royal Meteorological Society 137(S1), 70–80, https://doi.org/10.1002/qj.686.

Kang, S.-L., Ryu, J.-H. (2016): Response of moist convection to multi-scale surface flux heterogeneity. Quarterly Journal of the Royal Meteorological Society 142(698), 2180–2193, https://doi.org/10.1002/qj.2811.

Kaspar, M., Müller, M., Kakos, V., Řezáčová, D., Sokol, Z. (2009): Severe storm in Bavaria, the Czech Republic and Poland on 12–13 July 1984: A statistic- and model-based analysis. Atmospheric Research 93(1–3), 99–110, https://doi.org/10.1016/j.atmosres.2008.10.004.

Kašpar, M., Bližňák, V., Hulec, F., Müller, M. (2021): High-resolution spatial analysis of the variability in the subdaily rainfall time structure. Atmospheric Research 248: 105202, https://doi.org/10.1016/j.atmosres.2020.105202.

Katona, B., Markowski, P., Alexander, C., Benjamin, S. (2016): The Influence of Topography on Convective Storm Environments in the Eastern United States as Deduced from the HRRR. Weather and Forecasting 31(5), 1481–1490, https://doi.org/10.1175/WAF-D-16-0038.1.

Kelsey, E., Bailey, A., Murray, G. (2018): The Impact of Mount Washington on the Height of the Boundary Layer and the Vertical Structure of Temperature and Moisture. Atmosphere 9(8): 293, https://doi.org/10.3390/atmos9080293.

Khodayar, S., Kalthoff, N., Wickert, J., Kottmeier, Ch., Dorninger, M. (2013): High-resolution representation of the mechanisms responsible for the initiation of isolated thunderstorms over flat and complex terrains: analysis of CSIP and COPS cases. Meteorology and Atmospheric Physics 119, 109–124, https://doi.org/10.1007/s00703-012-0232-6.

Kirshbaum, D. J., Bryan, G. H., Rotunno, R., Durran, D. R. (2007): The Triggering of Orographic Rainbands by Small-Scale Topography. Journal of the Atmospheric Sciences 64(5), 1530–1549, https://doi.org/10.1175/JAS3924.1.

Kirshbaum, D. J. (2013): On Thermally Forced Circulations over Heated Terrain. Journal of the Atmospheric Sciences 70(6), 1690–1709, https://doi.org/10.1175/JAS-D-12-0199.1.

Kirshbaum, D. J., Wang, C. (2014): Boundary Layer Updrafts Driven by Airflow over Heated Terrain. Journal of the Atmospheric Sciences 71(4), 1425–1442, https://doi.org/10.1175/JAS-D-13-0287.1.

Kirshbaum, D. J., Fabry, F. Cazenave, Q. (2016): The Mississippi Valley Convection Minimum on Summer Afternoons: Observations and Numerical Simulations. Monthly Weather Review 144(1), 263–272, https://doi.org/10.1175/MWR-D-15-0238.1.

Kirshbaum, D. J. (2017): On upstream blocking over heated mountain ridges. Quarterly Journal of the Royal Meteorological Society 143(702), 53–68, https://doi.org/10.1002/qj.2945.

Kirshbaum, D. J., Schultz, D. M. (2018): Convective Cloud Bands Downwind of Mesoscale Mountain Ridges. Journal of the Atmospheric Sciences 75(12), 4265–4286, https://doi.org/10.1175/JAS-D-18-0211.1.

Kirshbaum, D. J., Adler, B., Kalthoff, N., Barthlott, Ch., Serafin, S. (2018): Moist Orographic Convection: Physical Mechanisms and Links to Surface-Exchange Processes. Atmosphere 9(3): 80, https://doi.org/10.3390/atmos9030080.

Kottmeier, C., Kalthoff, N., Barthlott, C., Corsmeier, U., van Baelen, J., Behrendt, A., Behrendt, R., Adler, B., Blyth, A., Coulter, R., Crewell, S., di Girolamo, P., Dorninger, M., Flamant, C., Foken, T., Gorgas, T., Harnisch, F., Hauck, C., Höller, H., Konow, H., Kunz, M., Mahalek, H., Mobbs, S., Richard, E., Steinacker, R., Weckwerth, T., Wieser, A., Wulfmeyer, V. (2008): Mechanisms initiating deep convection over complex terrain during COPS. Meteorologische Zeitschrift 17(6), 931–948, https://doi.org/10.1127/0941-2948/2008/0348.

Kühne, T., Antonescu, B., Groenemeijer, P., Púčik, T. (2025): Lightning Fatalities in Europe (2001–20). Weather, Climate, and Society 17(2), 205–215, https://doi.org/10.1175/WCAS-D-24-0038.1.

Kunz, M., Blahak, U., Handwerker, J., Schmidberger, M., Punge, H. J., Mohr, S., Fluck, E., Bedka, K. M. (2018): The severe hailstorm in southwest Germany on 28 July 2013: characteristics, impacts and meteorological conditions. Quarterly Journal of the Royal Meteorological Society 144(710), 231–250, https://doi.org/10.1002/qj.3197.

Kvak, R., Okon, Ľ., Bližňák, V., Méri, L., Kašpar, M. (2023): Spatial distribution and precipitation intensity of supercells: Response to terrain asymmetry in the Western Carpathians, Central Europe. Atmospheric Research 292: 106885, https://doi.org/10.1016/j.atmosres.2023.106885.

Laiti, L., Zardi, D., de Franceschi, M., Rampanelli, G., Giovannini, L. (2014): Analysis of the diurnal development of a lake-valley circulation in the Alps based on airborne and surface measurements. Atmospheric Chemistry and Physics 14(18), 9771–9786, https://doi.org/10.5194/acp-14-9771-2014.

Lareau, N. P., Knopp, T., Kirshbaum, D. J. (2024): Mechanical and Thermal Forcing for Upslope Flows and Cumulus Convection over the Sierras de Córdoba. Monthly Weather Review 152(9), 2149–2167, https://doi.org/10.1175/MWR-D-23-0254.1.

Levizzani, V., Pinelli, F., Pasqui, M., Melani, S., Laing, A. G., Carbone, R. E. (2010): A 10-year climatology of warm-season cloud patterns over Europe and the Mediterranean from Meteosat IR observations. Atmospheric Research 97(4), 555–576, https://doi.org/10.1016/j.atmosres.2010.05.014.

Lock, N. A., Houston, A. L. (2014): Empirical Examination of the Factors Regulating Thunderstorm Initiation. Monthly Weather Review 142(1), 240–258, https://doi.org/10.1175/MWR-D-13-00082.1.

Lock, N. A., Houston, A. L. (2015): Spatiotemporal distribution of thunderstorm initiation in the US Great Plains from 2005 to 2007. International Journal of Climatology 35(13), 4047–4056, https://doi.org/10.1002/joc.4261.

Lombardo, K., Bitting, M. (2024): A Climatology of Convective Precipitation over Europe. Monthly Weather Review 152(7), 1555–1585, https://doi.org/10.1175/MWR-D-23-0156.1.

Marquis, J. N., Varble, A. C., Robinson, P., Nelson, T. C., Friedrich, K. (2021): Low-Level Mesoscale and Cloud-Scale Interactions Promoting Deep Convection Initiation. Monthly Weather Review 149(8), 2473–2495, https://doi.org/10.1175/MWR-D-20-0391.1.

Marquis, J. N., Feng, Z., Varble, A., Nelson, T. C., Houston, A., Peters, J. M., Mulholland, J. P., Hardin, J. (2023): Near-Cloud Atmospheric Ingredients for Deep Convection Initiation. Monthly Weather Review 151(5), 1247–1267, https://doi.org/10.1175/MWR-D-22-0243.1.

Markowski, P., Richardson, Y. (2010): Mesoscale Meteorology in Midlatitudes; Wiley-Blackwell: Chichester, UK, and Hoboken, NJ, USA; 407 pp., http://dx.doi.org/10.1002/9780470682104.

Markowski, P., Dotzek, N. (2011): A numerical study of the effects of orography on supercells. Atmospheric Research 100(4), 457–478, https://doi.org/10.1016/j.atmosres.2010.12.027.

McKeown, K. E., Davenport, C. E., Eastin, M. D., Purpura, S. M., Riggin, R. R. (2024): Radar Characteristics of Supercell Thunderstorms Traversing the Appalachian Mountains. Weather and Forecasting 39(4), 639–654, https://doi.org/10.1175/WAF-D-23-0110.1.

Miglietta, M. M., Rotunno, R. (2014): Numerical Simulations of Sheared Conditionally Unstable Flows over a Mountain Ridge. Journal of the Atmospheric Sciences 71(5), 1747–1762, https://doi.org/10.1175/JAS-D-13-0297.1.

Mulholland, J. P., Nesbitt, S. W., Trapp, R. J., Rasmussen, K. L., Salio, P. V. (2018): Convective Storm Life Cycle and Environments near the Sierras de Córdoba, Argentina. Monthly Weather Review 146(8), 2541–2557, https://doi.org/10.1175/MWR-D-18-0081.1.

Mulholland, J. P., Nesbitt, S. W., Trapp, R. J. (2019): A Case Study of Terrain Influences on Upscale Convective Growth of a Supercell. Monthly Weather Review 147(12), 4305–4324, https://doi.org/10.1175/MWR-D-19-0099.1.

Mulholland, J. P., Nesbitt, S. W., Trapp, R. J., Peters, J. M. (2020): The Influence of Terrain on the Convective Environment and Associated Convective Morphology from an Idealized Modeling Perspective. Journal of the Atmospheric Sciences 77(11), 3929–3949, https://doi.org/10.1175/JAS-D-19-0190.1.

Nelson, T. C., Marquis, J., Varble, A., Friedrich, K. (2021): Radiosonde Observations of Environments Supporting Deep Moist Convection Initiation during RELAMPAGO-CACTI. Monthly Weather Review 149(1), 289–309, https://doi.org/10.1175/MWR-D-20-0148.1.

Nelson, T. C., Marquis, J., Peters, J. M., Friedrich, K. (2022): Environmental Controls on Simulated Deep Moist Convection Initiation Occurring during RELAMPAGO-CACTI. Journal of the Atmospheric Sciences 79(7), 1941–1964, https://doi.org/10.1175/JAS-D-21-0226.1.

Nicolas, Q., Boos, W. R. (2022): A Theory for the Response of Tropical Moist Convection to Mechanical Orographic Forcing. Journal of the Atmospheric Sciences 79(7), 1761–1779, https://doi.org/10.1175/JAS-D-21-0218.1.

Panosetti, D., Boing, S., Schlemmer, L., Schmidli, J. (2016): Idealized Large-Eddy and Convection-Resolving Simulations of Moist Convection over Mountainous Terrain. Journal of the Atmospheric Sciences 73(10), 4021–4041, https://doi.org/10.1175/JAS-D-15-0341.1.

Panziera, L., James, C. N., Germann, U. (2015): Mesoscale Organization and Structure of Orographic Precipitation Producing Flash Floods in the Lago Maggiore Region. Quarterly Journal of the Royal Meteorological Society 141(686), 224–248, https://doi.org/10.1002/qj.2351.

Panziera, L., Gabella, M., Germann, U., Martius, O. (2018): A 12-year radar-based climatology of daily and sub-daily extreme precipitation over the Swiss Alps. International

Journal of Climatology 38(10), 3749–3769, https://doi.org/10.1002/joc.5528.

Peterson, D. A., Fromm, M. D., Solbrig, J. E., Hyer, E. J., Surratt, M. L., Campbell, J. R. (2017): Detection and Inventory of Intense Pyroconvection in Western North America using GOES-15 Daytime Infrared Data. Journal of Applied Meteorology and Climatology 56(2), 471–493, https://doi.org/10.1175/JAMC-D-16-0226.1.

Peterson, M., Mach, D., Buechler, D. (2021): A Global LIS/OTD Climatology of Lightning Flash Extent Density. Journal of Geophysical Research: Atmospheres 126(8): e2020JD033885, https://doi.org/10.1029/2020JD033885.

Price, M. F., Arnesen, T., Gløersen, E., Metzger, M. J. (2019): Mapping mountain areas: learning from Global, European and Norwegian perspectives. Journal of Mountain Science 16, 1–15, https://doi.org/10.1007/s11629-018-4916-3.

Punge, H. J., Kunz, M. (2016): Hail observations and hailstorm characteristics in Europe: A review. Atmospheric Research 176–177, 159–184, https://doi.org/10.1016/j.atmosres.2016.02.012.

Purpura, S. M., Davenport, C. E., Eastin, M. D., McKeown, K. E., Riggin, R. R. (2023): Environmental Evolution of Supercell Thunderstorms Interacting with the Appalachian Mountains. Weather and Forecasting 38(1), 179–198, https://doi.org/10.1175/WAF-D-22-0115.1.

Púčik, T., Groenemeijer, P., Rýva, D., Kolář, M. (2015): Proximity Soundings of Severe and Nonsevere Thunderstorms in Central Europe. Monthly Weather Review 143(12), 4805–4821, https://doi:10.1175/MWR-D-15-0104.1.

Reeves, H. D., Lin, Y.-L. (2007): The Effects of a Mountain on the Propagation of a Preexisting Convective System for Blocked and Unblocked Flow Regimes. Journal of the Atmospheric Sciences 64(7), 2401–2421, https://doi.org/10.1175/JAS3959.1.

Reif, D. W., Bluestein, H. B. (2018): Initiation Mechanisms of Nocturnal Convection without Nearby Surface Boundaries over the Central and Southern Great Plains during the Warm Season. Monthly Weather Review 146(9), 3053–3078, https://doi.org/10.1175/MWR-D-18-0040.1.

Řezáčová, D., Novák, P., Kašpar, M., Setvák, M. (2007): The Physics of Clouds and Precipitation (in Czech); Academia: Praha, Czech Republic, 574 pp.

Ribeiro, B. Z., Bosart, L. F. (2018): Elevated Mixed Layers and Associated Severe Thunderstorm Environments in South and North America. Monthly Weather Review 146(1), 3–28, https://doi.org/10.1175/MWR-D-17-0121.1.

Roe, G. H. (2005): Orographic precipitation. Annual Review of Earth and Planetary Sciences 33, 645–671, https://doi.org/10.1146/annurev.earth.33.092203.122541.

Rorig, M. L., Ferguson, S. A. (1999): Characteristics of Lightning and Wildland Fire Ignition in the Pacific Northwest. Journal of Applied Meteorology and Climatology 38(11), 1565–1575, https://doi.org/10.1175/1520-0450(1999)038<1565:COLAWF>2.0.CO;2.

Rotach, M. W., Serafin, S., Ward, H. C., Arpagaus, M., Colfescu, I., Cuxart, J., De Wekker, S. F. J., Grubišić, V., Kalthoff, N., Karl, T., Kirshbaum, D. J., Lehner, M., Mobbs, S., Paci, A., Palazzi, E., Bailey, A., Schmidli, J., Wittmann, C., Wohlfahrt, G., Zardi, D. (2022): A Collaborative Effort to Better Understand, Measure, and Model Atmospheric Exchange Processes over Mountains. Bulletin of the American Meteorological Society 103(5), E1282–E1295, https://doi.org/10.1175/BAMS-D-21-0232.1.

Scheffknecht, P., Serafin, S., Grubišić, V. (2017): A long-lived supercell over mountainous terrain. Quarterly Journal of the Royal Meteorological Society 143(709), 2973–2986, https://doi.org/10.1002/qj.3127.

Schmidli, J., Rotunno, R. (2012): Influence of the valley surroundings on valley wind dynamics. Journal of the Atmospheric Sciences 69(2), 561–577, https://doi.org/10.1175/JAS-D-11-0129.1.

Schneider, L., Barthlott, C., Barrett, A., Hoose, C. (2018): The precipitation response to variable terrain forcing over low-mountain ranges in different weather regimes. Quarterly Journal of the Royal Meteorological Society 144(713), 970–989, https://doi.org/10.1002/qj.3250.

Serafin, S., Zardi, D. (2010): Daytime Heat Transfer Processes Related to Slope Flows and Turbulent Convection in an Idealized Mountain Valley. Journal of the Atmospheric Sciences 67(11), 3739–3756, https://doi.org/10.1175/2010JAS3428.1.

Serafin, S., Adler, B., Cuxart, J., De Wekker, S. F. J., Gohm, A., Grisogono, B., Kalthoff, N., Kirshbaum, D. J., Rotach, M. W., Schmidli, J., Stiperski, I., Večenaj, Ž., Zardi, D. (2018): Exchange Processes in the Atmospheric Boundary Layer Over Mountainous Terrain. Atmosphere 9(3): 102, https://doi.org/10.3390/atmos9030102.

Singh, I., Nesbitt, S. W., Davis, C. A. (2022): Quasi-Idealized Numerical Simulations of Processes Involved in Orogenic Convection Initiation over the Sierras de Córdoba. Journal of the Atmospheric Sciences 79(4), 1127–1149, https://doi.org/10.1175/JAS-D-21-0007.1.

Schultz, D. M., Young, M. V., Kirshbaum, D. J. (2025): The Spanish Plume Elevated Mixed Layer: A Review of Its Use and Misuse within the Scientific Literature. Monthly Weather Review 153(5), 737–761, https://doi.org/10.1175/MWR-D-24-0139.1.

Smith, V. H., Mobbs, S. D., Burton, R. R., Hobby, M., Aoshima, F., Wulfmeyer, V., Di Girolamo, P. (2015): The role of orography in the regeneration of convection: A case study from the convective and orographically-induced precipitation study. Meteorologische Zeitschrift 24(1), 83–97, https://doi.org/10.1127/metz/2014/0418.

Soderholm, B., Ronalds, B., Kirshbaum, D. J. (2014): The Evolution of Convective Storms Initiated by an Isolated Mountain Ridge. Monthly Weather Review 142(4), 1430–1451, https://doi.org/10.1175/MWR-D-13-00280.1.

Tang, B., Vaughan, M., Lazear, R., Corbosiero, K., Bosart, L., Wasula, T., Lee, I., Lipton, K. (2016): Topographic and Boundary Influences on the 22 May 2014 Duanesburg, New York, Tornadic Supercell. Weather and Forecasting 31(1), 107–127, https://doi.org/10.1175/WAF-D-15-0101.1.

Taszarek, M., Allen, J. T., Púčik, T., Groenemeijer, P., Czernecki, B., Kolendowicz, L., Lagouvardos, K., Kotroni, V., Schulz, W. (2019): A Climatology of Thunderstorms across Europe from a Synthesis of Multiple Data Sources. Journal of Climate 32(6), 1813–1837, https://doi.org/10.1175/JCLI-D-18-0372.1.

Taszarek, M., Allen, J. T., Groenemeijer, P., Edwards, R., Brooks, H. E., Chmielewski, V., Enno, S.-E. (2020a): Severe

Convective Storms across Europe and the United States. Part I: Climatology of Lightning, Large Hail, Severe Wind, and Tornadoes. Journal of Climate 33(23), 10239–10261, https://doi.org/10.1175/JCLI-D-20-0345.1.

Taszarek, M., Allen, J. T., Púčik, T., Hoogewind, K. A., Brooks, H. E. (2020b): Severe Convective Storms across Europe and the United States. Part II: ERA5 Environments Associated with Lightning, Large Hail, Severe Wind, and Tornadoes. Journal of Climate 33(23), 10263–10286, https://doi.org/10.1175/JCLI-D-20-0346.1.

Trefalt, S., Martynov, A., Barras, H., Besic, N., Hering, A. M., Lenggenhager, S., Noti, P., Röthlisberger, M., Schemm, S., Germann, U., Martius, O. (2018): A severe hail storm in complex topography in Switzerland – observations and processes. Atmospheric Research 209, 76–94, https://doi.org/10.1016/j.atmosres.2018.03.007.

Wagner, J. S., Gohm, A., Rotach, M. W. (2015): The impact of valley geometry on daytime thermally driven flows and vertical transport processes. Quarterly Journal of the Royal Meteorological Society 141(690), 1780–1794, https://doi.org/10.1002/qj.2481.

Wang, Q. W., Xue, M., Tan, Z. M. (2016): Convective initiation by topographically induced convergence forcing over the Dabie Mountains on 24 June 2010. Advances in Atmospheric Sciences 33(10), 1120–1136, https://doi.org/10.1007/s00376-016-6024-z.

Weckwerth, T. M., Wilson, J. W., Hagen, M., Emerson, T. J., Pinto, J. O., Rife, D. L., Grebe, L. (2011): Radar climatology of the COPS region. Quarterly Journal of the Royal Meteorological Society 137(S1), 31–41, https://doi.org/10.1002/qj.747.

Weckwerth, T. M., Bennett, L. J., Jay Miller, L., Van Baelen, J., Di Girolamo, P., Blyth, A. M., Hertneky, T. J. (2014): An Observational and Modeling Study of the Processes Leading to Deep, Moist Convection in Complex Terrain. Monthly Weather Review 142(8), 2687–2708, https://doi.org/10.1175/MWR-D-13-00216.1.

Weisman, M. L., Klemp, J. B. (1982): The Dependence of Numerically Simulated Convective Storms on Vertical Wind Shear and Buoyancy. Monthly Weather Review 110(6), 504–520, https://doi.org/10.1175/1520-0493(1982)110<0504:TDONSC>2.0.CO;2.

Whiteman, C. D. (2000): Mountain Meteorology: Fundamentals and Applications; Oxford University Press: New York, NY, USA; 355 pp., https://doi.org/10.1093/oso/9780195132717.001.0001.

Wulfmeyer, V., and Coauthors (2011): The Convective and Orographically-induced Precipitation Study (COPS): the scientific strategy, the field phase, and research highlights. Quarterly Journal of the Royal Meteorological Society 137(S1), 3–30, https://doi.org/10.1002/qj.752.

Will the Soutok/Confluence protected area fit in with other Moravian lowland riverine protected areas? Comparing landscapes, values, pressures, and effective protection

Tomáš Janík[1,2,*], Vladimír Zýka[1], Marek Havlíček[3], Katarína Demková[4], Michal Andreas[1], Jaroslav Vojta[1], Barbora Mrkvová[1], Roman Borovec[3], Anna Lichová[3], Tomáš Veith[4], Jiří Dostálek[4], Ivo Dostál[5], Markéta Šantrůčková[4], Dušan Romportl[1]

[1] Landscape Research Institute, Department of Spatial Ecology, Czechia
[2] Charles University, Faculty of Science, Department of Physical Geography and Geoecology, Czechia
[3] Landscape Research Institute, Department of Landscape Ecology, Czechia
[4] Landscape Research Institute, Department of Cultural Landscape and Sites, Czechia
[5] Transport Research Centre, Department of Sustainable Transport, Czechia
* Corresponding author: tomas.janik@vuk.gov.cz

ABSTRACT

Lowland riverine protected areas in Czechia are relatively rare and threatened by anthropogenic pressure. In the Moravian region, two protected landscape areas (PLAs), Litovelské Pomoraví and Poodří, were established in the early 1990s. In 2025, the Soutok (Confluence) PLA was designated. This article compares these three areas based on landscape characteristics (land cover, watercourse length, landscape fragmentation and connectivity, anthropogenic pressure, and priorities for protection) to evaluate how Soutok compares to the established two. The analysis includes a 3km buffer area. A marked contrast exists between the PLAs and their buffers; while the PLAs are largely natural or semi-natural with an increasing proportion of forests (especially Litovelské Pomoraví and Soutok) or permanent grasslands, arable land and built-up areas dominate adjacent areas. This land-use intensification causes landscape fragmentation, creating a crucial limitation for landscape connectivity. Therefore, nature protection priorities are concentrated along the watercourses, which remain relatively natural in the PLAs (with a slight decrease in naturalness in Litovelské Pomoraví and Soutok, and an increase in Poodří), but channelized, regulated, and shortened in adjacent areas. Positive changes are evident within the two PLAs designated in the 1990s; Soutok shares similar traits with Litovelské Pomoraví, which may indicate a relatively positive future for this new PLA.

KEYWORDS

Soutok/Confluence of the Morava and Dyje Rivers; protected landscape area (PLA); landscape change; anthropogenic pressure; Czechia

Received: 17 September 2025
Accepted: 9 April 2026
Published online: 6 May 2026

Janík, T., Zýka, V., Havlíček, M., Demková, K., Andreas, M., Vojta, J., Mrkvová, B., Borovec, R., Lichová, A., Veith, T., Dostálek, J., Dostál, I., Šantrůčková, M., Romportl, D. (2026): Will the Soutok/Confluence protected area fit in with other Moravian lowland riverine protected areas? Comparing landscapes, values, pressures, and effective protection. AUC Geographica 61(2), 279–297
https://doi.org/10.14712/23361980.2026.8
© 2026 The Authors. This is an open-access article distributed under the terms of the Creative Commons Attribution License (https://creativecommons.org/licenses/by/4.0).

1. Introduction

Riverine landscapes are a vital part of natural processes. The landscape around rivers is connected to the water streams and fluvial processes transporting material and energy through the landscape (Montgomery and Wohl 2003). These parts of the landscape are dynamic and important for broader surroundings from a biological and ecological point of view because they are acknowledged as biodiversity hotspots (Tockner et al. 2000).

In Central Europe, there are few areas with a natural hydrological regime and a preserved, close-to-nature landscape. The rivers in Czechia have been negatively affected by channelization (Grygar et al. 2010) and by high anthropogenic impact, such as intensification of agriculture and construction (Kiliánová et al. 2017). Despite these changes, floodplain forests and close-to-nature habitats persist in some localities, making these localities highly naturally valuable (Miklín et al. 2014).

In the Morava region, three lowland protected areas of high merit in this regard can be found: Litovelské Pomoraví, Poodří, and Soutok.

Protected areas (PAs) are used as a key tool for preserving natural values. They are established to face biodiversity loss and enhance ecosystem conditions (Watson et al. 2014). Natura 2000 is a significant network of protected sites for selected species and habitats in the European Union (European Commission 2021). However, implementation of the Natura 2000 can be suboptimal in the case of Czechia (Křenová and Kindlmann 2015; Miklín and Čížek 2014). Moreover, Natura 2000 sites are more concentrated on protecting certain species and habitats, not ecosystems or landscape (European Commission 2015). On the other hand, Protected Landscape Areas (PLAs) have zonation, detailed management plans, and other tools for better fulfilment of their objectives (Czech National Council 1992).

Many studies have been published for specific sites (e.g. Mácha et al. 2023; Miklín and Čížek 2014; Miklín and Hradecký 2016; Połedniková et al. 2025); however, there is no comparison of three similar areas regarding landscape characteristics. This article, therefore, focused on comparing landscape development and the qualities of three areas to highlight their strengths, weaknesses, opportunities, and threats, as well as the similarities and differences between them. The aim was to analyze landscape changes, anthropogenic pressure on the landscape, landscape connectivity, fragmentation, and spatial natural conservation prioritization to detect key phenomena of the PLAs and their surroundings (Kubacka et al. 2022; Mingarro and Lobo 2023). Litovelské Pomoraví and Poodří have been protected as nationally designated PLAs since the early 1990s, but Soutok has been protected only as Natura 2000 sites since 2005 and became a PLA recently (2025).

We concentrated on comparing long-term nationally non-protected Soutok with the other two older PLAs to evaluate whether Soutok has similar landscape features as the others.

Generally, we hypothesized that:

- the PLAs have similar landscape characteristics, with natural land cover and preserved natural and semi-natural habitats, mainly floodplain forests along unregulated rivers;
- the adjacent areas are vastly transformed, which can be a threat for protection and landscape functioning;
- high prioritization rankings within PLAs than buffers;
- Soutok is like the two older PLAs regarding presence of natural habitats and their species;
- inside the PLAs, anthropogenic pressure on the landscape (including traffic intensity) is lower than in the 3km buffer and that anthropogenic pressure was more pronounced in the 3km buffer;
- the three areas serve as important links for migration routes of various animal species on a regional scale.

2. Materials and methods

We compared key landscape features in three PLAs and their buffers (Fig. 1) to show strengths and weaknesses of the landscape as well as opportunities and threats. We analyzed land cover changes, water stream change, anthropogenic pressures, associated landscape fragmentation, and functional connectivity. In addition, priorities regarding the values for each area were examined.

2.1 Study area

Litovelské Pomoraví mainly consists of persistent forests and meadows. The PLA was designated in 1990, covering 93.3 km^2 with a 248.6 km^2 buffer. This differs from other parts of the landscape along the Morava River with a larger portion of increasing arable land and settlements (Kiliánová et al. 2017). The Morava divides into many natural anastomosing channels, together with man-made channels (Máčka 2016). Veteran trees are crucial havens for biodiversity (Nakládal et al. 2022). The average annual flow of the Morava River in the Soutok PLA is around 20 m^3s^{-1} (ISVS CHMI.CZ).

Poodří PLA was designated in 1991, covering 81.5 km^2 with a 273.5 km^2 buffer, the average annual flow of the Odra River is 7 m^3s^{-1} (ISVS CHMI.CZ); close to Ostrava, it is an area formerly glaciated by a continental ice sheet. The Odra River flows through the flat terrain, where many branches originated. They have been used by human to build ponds and channels, but the river has remained relatively unaffected and meanders still exist (Hradecký et al. 2016;

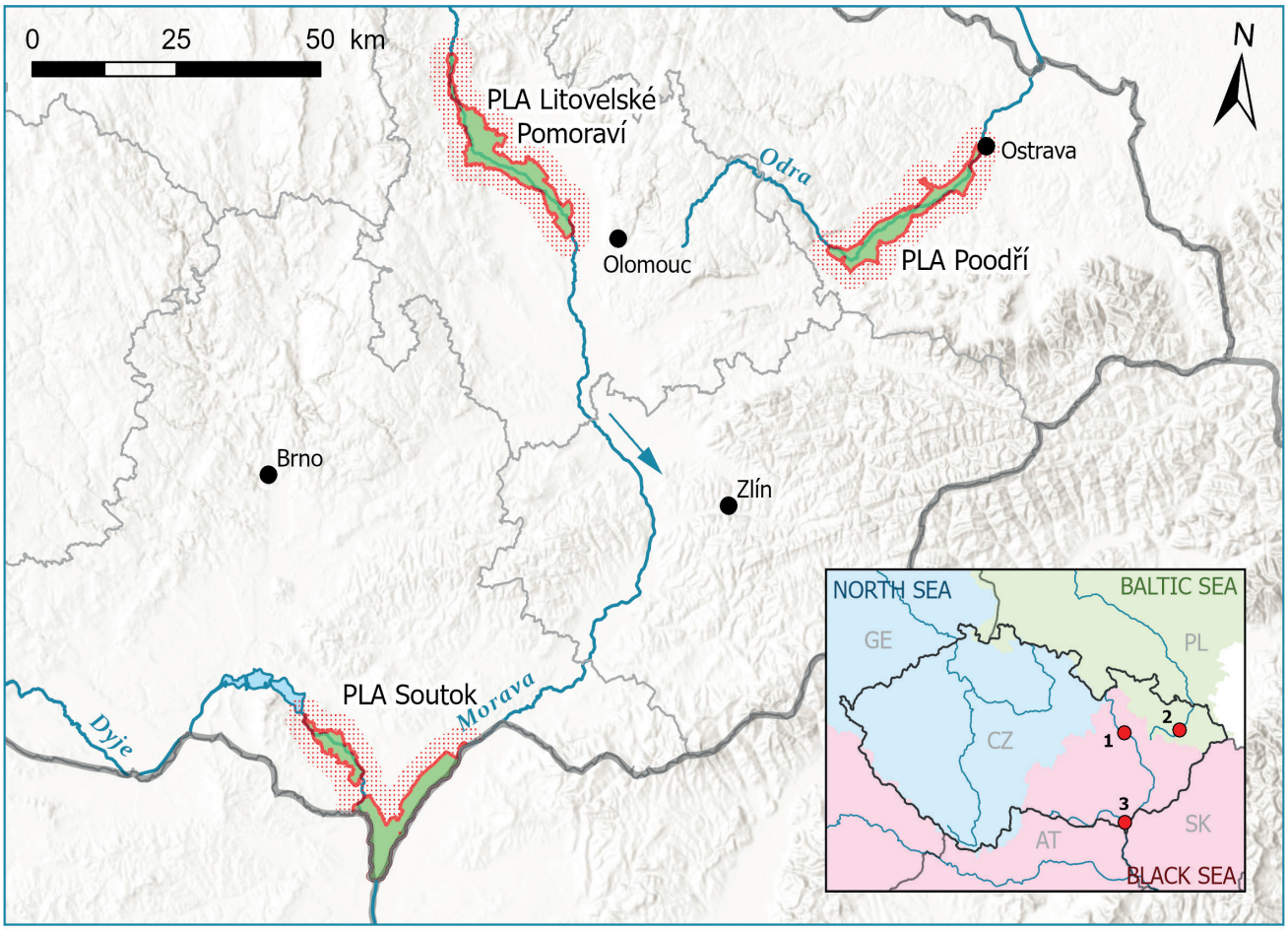

Fig. 1 Study area. (1) Litovelské Pomoraví, (2) Poodří, (3) Soutok PLAs and their buffers.

Połedniková et al. 2025). The area is less forested than other Czech PLAs (Janík et al. 2024a). Landscape changes are relatively dynamic, including non-forest woody vegetation as an important habitat for some species (Mácha et al. 2023).

Soutok consists mainly of floodplain forests and meadows (this new PLA covers 127 km^2, with a buffer in Czechia of 223.6 km^2). However, it is surrounded by an increasing share of arable land. Forestry has intensified alongside agriculture, threatening open woodlands and other valuable habitats (Miklín and Čížek 2014). The main water streams were affected by anthropogenic changes to the hydrological regimes, but some other streams have remained more natural (Miklín and Smolková 2011). The average annual flow of the main streams in the PLA Soutok is the largest of the three areas of interest, the Morava River 52 m^{3}s^{-1} and the Dyje River 34 m^{3}s^{-1} (ISVS CHMI.CZ).

2.2 Data

2.2.1 Land cover

Land cover data were processed manually by vectorization in ArcGIS 10.x (ESRI 2020) software. Using topographic maps and aerial imagery, we captured land cover in four periods for the three areas, including their buffers. Datasets cover the last seventy years (1950–2020).

The 1950s represent the beginning of modern nature conservation in Czechia, as well as large changes in landscape caused by agricultural collectivization. The dataset was based on 1:25,000 Czechoslovak military maps from 1952–1956 (General Staff of the Czechoslovak Army 1952–1956).

The 1990 dataset is a milestone for changes in political, economic, and social regimes; it is also a reference point because Litovelské Pomoraví PLA was designated in 1990 and Poodří in 1991. The dataset from this period was based on 1:25,000 Czechoslovak military maps from 1988–1995 (General Staff of the Czechoslovak Army 1988–1995).

The 2004 dataset represents EU accession and changes associated with agricultural policy and transposing other legislation into national law. Land cover data was vectorized from a 1:10,000 base map (Czech Office for Surveying, Mapping and Cadastre 2002–2006) and aerial imagery with a pixel size 0.5 m (Czech Office for Surveying, Mapping and Cadastre 2003–2005).

The last period is a contemporary dataset (2016 to 2020) based on aerial imagery with pixel size 0.2 m (Czech Office for Surveying and Cadastre 2016–2020)

Tab. 1 Land cover categories.

Land cover category	Description
Other area	Mining areas, dump sites, dams
Arable land	Arable fields, mosaics of fields and trees and small vineyards, fallow land
Permanent grassland	Meadows, pastures, steppes, wetlands
Garden and orchard	Intensive and extensive orchards, large gardens adjacent to built-up areas
Vineyard and hop field	Small and large scale, facility included
Forest	Forest, non-forest woody vegetation, mountain pine, shrubs, forest nurseries
Water body	Ponds, lakes, reservoirs, pools, flooded mining areas
Built-up area	Continuous and dispersed built-up areas, industrial, agricultural and military sites, cottages, cemeteries
Recreational area	Garden allotments, spa resorts, zoological gardens, golf courses, camps

and supported by LPIS (Land Parcel Information System – Soil registry; Ministry of Agriculture 2016–2020).

Land cover data were captured as polygons larger than 0.8 ha and wider than 40 m. This ensured the same level of generalization from sources of different spatial scale (1:10,000 to 1:25,000 topographic maps and aerial photographs with pixel sizes from 0.5 m to 0.2 m). Given the different sources that capture land cover types in different detail, and to make corresponding maps comparable, nine land cover categories were identified (Tab. 1).

2.2.2 Natural habitat mapping data

Natural habitat data were provided by the Nature Conservation Agency of the Czech Republic (©AOPK) as vector data for the whole of Czechia at 1:10,000. This dataset was developed during NATURA 2000 establishment and is continuously updated.

2.2.3 Water streams

Length of the water streams were analyzed from manually vectorized line spatial data based on maps of the second military survey from the 19th century (1836–1852) and the current Fundamental Base of Geographic Data of Czech Republic (ZABAGED®). It is expected that significant modifications of water streams began in 19th century and continued in the 20th century.

2.2.4 Anthropogenic pressure

Anthropogenic pressure is composed of structures such as built-up and recreational areas (camping sites, golf courses, sport fields, etc.) and communications (roads, dirt roads, and streets). Polygon structures are more detailed than within land cover. The minimum polygon size is 0.2 ha. It follows a similar temporal period as for land cover:

The 1960 dataset was created by vectorization from a 1:10,000 topographic map (Central Administration of Geodesy and Cartography 1957–1971) and aerial images from the 1950s.

The 1990 dataset is based on a 1:10,000 base map (Central Administration of Geodesy and Cartography 1986–1995).

The 2004 dataset is vectorized from a 1:10,000 base map (Czech Office for Surveying, Mapping and Cadastre 2002–2006) and aerial imagery with a pixel size 0.5 m (Czech Office for Surveying, Mapping and Cadastre 2003–2005).

The 2016–2020 dataset represents the current situation; it was obtained and edited from ZABAGED® and aerial imagery with a pixel size 0.2 m (Czech Office for Surveying, Mapping and Cadastre 2016–2020).

We also extracted buildable areas from current municipal spatial planning documents.

To analyze landscape fragmentation, we also used data on traffic intensity. This is expressed using annual average daily intensity measured during regular (usually every five years) National Transport Censuses provided by the Directorate of Roads and Motorways on all motorways, Class I and II roads, and selected Class III roads. For our study, results from 1950, 1990, 2005, and 2021 were used.

2.2.5 Landscape connectivity

Landscape connectivity analysis was built on previous research by Romportl et al. (2021), which created a set of habitat suitability models for the Czech environment for various protected animal species. Therefore, there was no need to prepare additional spatial data. In the map representation of landscape connectivity analysis, we used data on planned construction of the road and railway network and buildable areas.

2.2.6 Prioritization

Data about landscape quality can evaluate the PLAs and their buffers to highlight priorities for protection. We divided the data into four groups:

- Biodiversity – the inputs were habitat suitability models of animals selected by our experts and PLA administrations. Habitat suitability models were calculated from records on the National Database of Fauna-Flora Records [NDOP] (Nature Conservation Agency 2022a) and predictors characterizing landscape features (altitude, slope, precipitation, temperature, land cover, etc.). Predictors were selected individually for each species based on its requirements. Then, the MaxEnt approach was used (Phillips et al. 2006), which enables

habitat suitability modelling with presence-only data (Elith et al. 2011). MaxEnt is based on maximum entropy, which estimates the probability of species' distribution from occurrence data and environmental predictors (see selected species in Appendix 1). Habitat suitability models (HSM) were created by the MIAmaxent tools (Vollering et al. 2019; Romportl et al. 2021). Plants were represented by maps of richness of native and Red List species for grassland and forest vegetation modelled by Divíšek and Chytrý (2018).

- Natural qualities of the landscape are composed of seven individual features:
  - Geodiversity layer – based on abiotic factors of topography, climate, soil, and geology.
  - Habitat diversity – computed as the number of habitats in defined surroundings (cell of 10 × 10m and 500m buffer) from the Consolidated layer of ecosystems of the Czech Republic (Nature Conservation Agency 2013; Romportl et al. 2021).
  - Number of species – recorded in regular square net from NDOP (Nature Conservation Agency 2022a).
  - Quality of habitats – derived from the habitat mapping layer (Nature Conservation Agency 2022b).
  - Presence of habitats – from the habitat mapping layer (Nature Conservation Agency 2022b); less-represented habitats in Czechia were weighted more to better represent all habitats.
  - Length of edges – from the Consolidated layer of ecosystems of the Czech Republic (Nature Conservation Agency, 2013) to analyze landscape structure.
  - Natural forests and primeval forests layer (Vršska et al. 2023).
- Cultural qualities of landscape data are reflected by the map of potential presence of historical cultural landscapes (Šantrůčková et al. 2023). This map shows, in a 1 × 1 km grid, several types of historical small-scale cultural landscapes (extensive agriculture, forests, permanent grasslands, vineyards, hop fields, orchards, ponds, spas, mining, and religious landscapes). We extracted information on whether the cultural landscape was present in the current cell and how many landscapes were present.
- Anthropogenic transformation is scaled into nine classes, ranging from densely built-up areas to pristine forests, from the Consolidated layer of ecosystems of the Czech Republic (Nature Conservation Agency 2013; Romportl et al. 2021).

2.3 Methods

We compared the three areas and their buffers regarding land cover changes, changes in water stream length, natural habitat stability, landscape fragmentation and connectivity, and priorities for protection. This identified strengths, weaknesses, opportunities, and threats for these riverine landscapes.

2.3.1 Land cover

We analyzed changes and stability of land cover categories and landscape structure from 1950s to today for the areas and their buffers to evaluate differences between protected and non-protected landscapes and between the three areas.

2.3.2 Natural habitat assessment

Information about land cover changes was used to evaluate individual natural habitats and their formation groups in areas with different land use. The groups of natural habitats used in the analysis are as defined by Chytrý et al. (2010): streams and water bodies; wetlands and riverine vegetation; springs and mires; cliffs and boulder screes; secondary grasslands and heathlands; scrub and forests. Habitats heavily influenced or created by humans were not included. Polygons containing mosaics of different habitats were assigned to the dominant habitat type, provided it covered at least 51% of the polygon's area. If no single habitat type exceeded 51% of the area in a mosaic polygon, that polygon was excluded from the analysis.

2.3.3 Water streams

The density of water streams (km per km^2) and the index of change between the 19th century and today were calculated.

2.3.4 Anthropogenic pressure

The density of communications (roads, dirt roads, and streets) and the proportion of built-up, recreation, and buildable areas were counted for every time horizon. Differences between the areas and their protected and non-protected parts were then evaluated.

2.3.5 Landscape fragmentation

Selected anthropogenic structure data were merged into one layer of fragmentation geometry and the Effective Mesh Size (EMS; Jaeger 2000; Moser et al. 2007; Girvetz et al. 2008) was computed. Analysis consisted of fragmentation geometry, a mask of the selected areas, and a regular square grid (500 × 500 m).

In the first fragmentation geometry version (FGa), built-up areas and roads were merged with a buffer that expresses their estimated land area. The buffer radius corresponds to road network categories based on the following expert evaluation: motorway – 13 m; first class road – 8 m; second class road – 5 m; third class road – 4 m. The second version (FGb) again merged built-up areas and roads, but road buffers were expressed by traffic intensity with a conversion factor of 1 vehicle = 1 cm of buffer radius. Fragmentation geometry resulted in two versions (FGa and FGb) for the four milestones (1960, 1990, 2004, 2020).

The EMS method works on simple mathematical calculations of the size of the areas remaining after cutting fragmentation geometry from the layer of the interested area. These remaining areas are then intersected with a square grid, with resulting EMS calculated according to the formula (Girvetz et al. 2008):

$$m_{eff}^{CBC}(j) = \frac{1}{A_{tj}} \sum_{i=1}^{n} A_{ij} A_{ij}^{cmpl}$$

The resulting variable meffcbc (j) represents the EMS (in km^2) for the given unit (500 × 500 m square) where: n is total number of patches extending into one square; Atj total area of the square; Aij partial area of the patch that extends into the square; and Aijcmpl total area of the patch. The EMS values express, figuratively, the probability of mutual connection of two randomly located landscape points. Thus, the higher the EMS, the higher the connecting probability and, simultaneously, the lower the landscape fragmentation level.

2.3.6 Landscape connectivity

Landscape connectivity analysis was carried out for the whole country. From this, we prepared individual PLA maps. The analysis was based on the abovementioned HSM of protected species. From these HSM for dozens of different rare fauna species, seven functional animal groups were created (Tab. 2). Analysis was done for each functional group.

When analyzing landscape connectivity, we used least cost path modelling, where input data were resistance surface and the system of core areas. The resistance surface was created from the habitat model for each functional group by a simple mathematical operation (1 – habitat model); a larger value means greater resistance of the given species to movement through the landscape. Core areas were based on expertly determined parameters of habitat suitability and minimum area size.

Core areas were linked using Linkage Mapper Toolbox 3.0 (McRae and Kavanagh 2011). The resulting line network was expertly verified to ensure that modelled paths were not mis-defined (e.g. passing through built-up areas). A buffer zone was added to the edited line network, with which the connectivity raster was subsequently trimmed, as one of the outputs of the tool used. This step gave the migration corridors a changing riverbed that better matches the environmental conditions than simple lines. For clarity, the results for individual functional groups were combined according to prevailing and relevant environmental preference into forest, meadow, water (and wetland).

2.3.7 Prioritization

We utilized Zonation software, a conservation planning and prioritization tool, working with raster layers (Moilanen et al. 2005; Moilanen and Kujala 2006). All input data were transformed into a 100 × 100 m grid, a resolution corresponding with the most input layers and suitable for management planning. Zonation software works iteratively and hierarchically, removing cells from the landscape according to their priorities. We chose the algorithm of Additive benefit function, emphasizing richness and diversity and count average values of all inputs, which can represent a wider group of phenomena not included in the analysis (Lehtomäki and Moilanen 2013; Moilanen 2013; Moilanen et al. 2011).

Biodiversity data and natural qualities layers are then run separately. Biodiversity data were treated with weights for habitat suitability models from 1 to 5 according to how endangered a species is based on expert knowledge and the Red List for Czechia (2017; Appendix 1). Finally, aggregated outputs for animals and plants were given equal weight. Priorities for natural qualities were calculated separately with the same weight for each input.

To sum up, all four groups of data were run with the same weight, with final prioritization of the result.

3. Results

3.1 Land cover

Litovelské Pomoraví PLA is mostly forested, which increased during the study period. Before 1990 arable land increased while permanent grassland decreased; after 1990 (and PLA designation), the opposite processes began. Built up areas grew

Tab. 2 Parameters of landscape connectivity analysis used.

Functional groups	Parameters of landscape connectivity analysis		
	Minimum habitat suitability (%)	Minimum size of core area (ha)	Buffer zone of migration path (m)
Forest mollusks	40	1	500
Forest butterflies	50	5	1000
Wetland butterflies	40	5	1000
Open landscape amphibians	75	10	500
Forest birds	40	50	2500
Waterfowl and wetland birds	50	10	2500
Forest mammals	25	100	2500

throughout the whole period. The buffer is dominated by arable land, but coverage declined; there is less permanent grassland now than at the beginning, but it grew from 1990. Forest increased slightly and built-up areas hugely. The PLA and its buffer experienced increasing landscape fragmentation. Both parts remained relatively unchanged; the buffer has been predominantly used for agricultural and is more stable than the PLA. Most of the stable arable land areas within the PLA buffer are currently characterized by large fields. Remnants of small-scale arable land patterns, including former water bodies, are located mainly in the northern part of the buffer area. In the eastern part, the remnants of former water bodies are still visible, although most have been drained by several artificial watercourses.

Poodří shows two different regimes. Before 1990 (PLA designation), arable land grew, together with forest, water bodies, and built-up areas. After 1990, arable land decreased with ongoing forest expansion. Built-up areas and water bodies remained stable after 1990, while permanent grassland decreased and then increased. The buffer is dominated by arable land, but it decreased and built areas grew significantly. Forests steadily expanded and permanent grassland remained relatively stable – decreasing and then increasing again to the same level. We can see relatively contrasting landscapes. Permanent grassland and forests are increasing in the PLA with arable land decreasing; there is a stable share of waterbodies and built-up areas. The buffer has a large portion of arable land and built-up areas, with a stable share of permanent grassland and increasing forest area. Both parts experienced increasing landscape fragmentation; the buffer, with predominantly agriculture use, remained more stable than the PLA with more environmentally favorable changes. In the PLA buffer, traditional and continuously used agricultural land is currently dominated by larger plots, while in several municipalities, historical agricultural landscape structures have been preserved near built-up areas.

Soutok shows slightly different development. Arable land grew in the proposed PLA until 2004 (three Natura 2000 sites were established there in 2005) and then decrease between 2004 and today. Permanent grassland decreased during the whole period and built-up areas are negligible. The buffer is mainly arable land with a moderate reduction, and permanent grassland decreased too. The buffer is relatively diverse with increasing water bodies and built-up areas, plus gardens, orchards, and vineyards. Both the PLA and buffer experienced increasing landscape fragmentation. The PLA is slightly more stable, although both parts experienced relatively large change. Several areas with small plots of vineyards, fields, orchards and water bodies in the vicinity of the Soutok PLA preserve historically valuable agricultural landscape structures.

This analysis reveals that Litovelské Pomoraví and Soutok PLAs are continuously forested, whereas Poodří PLA has a larger portion of arable land, permanent grassland, and water bodies. The buffers are strongly agricultural in all cases with higher urbanization (Fig. 2).

3.2 Natural habitats

Land cover stability results were assessed in relation to the presence of natural habitats (Tab. 3). In Litovelské Pomoraví PLA, alluvial and oak-hornbeam forests dominate continuous forests. Alluvial forests are the most extensive habitats in the buffer, with two-thirds in continuously forested areas and one-third in areas that underwent land use changes. Meadows

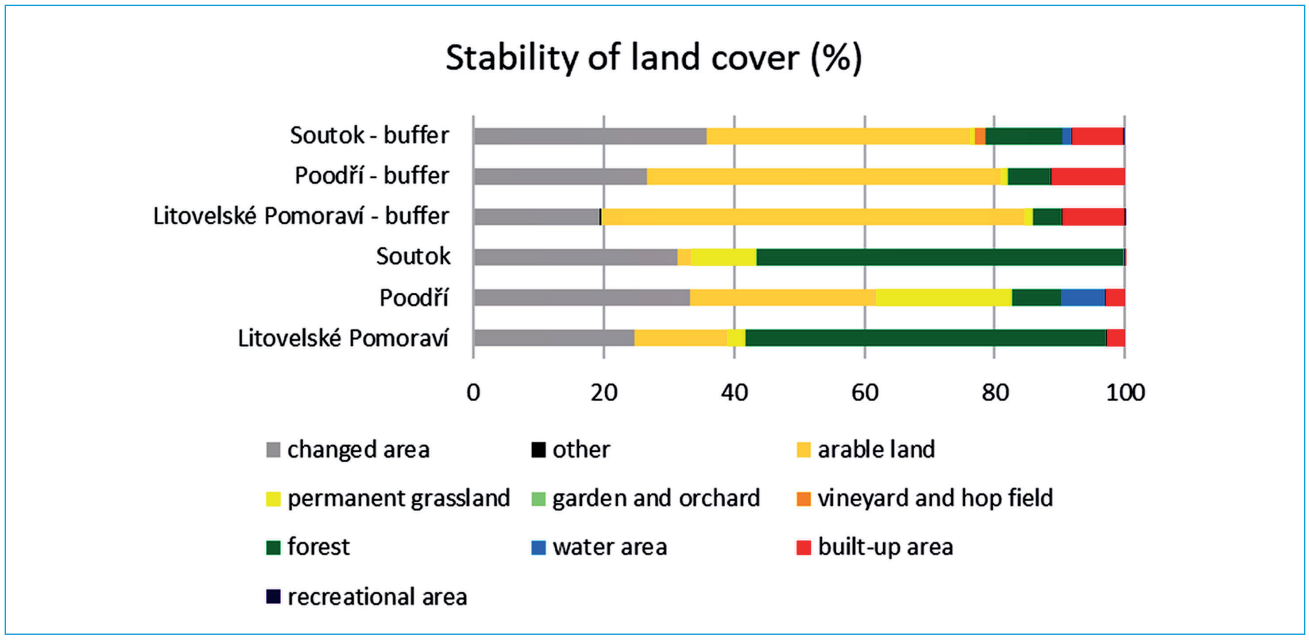

Fig. 2 Stable land cover categories in the PLAs and buffers for the whole study period (1950–2020).

and pastures are more prevalent in the buffer than the PLA, mainly present in areas where land cover has changed. The PLA was established to protect the river environment; therefore, macrophyte vegetation of water streams is present there. It is mostly found in unchanged areas, but one-quarter occurs in areas where land cover has changed.

Poodří PLA differs in that its most extensive habitats are meadows and pastures. Within the PLA, they prevail in unchanged areas, but they are also significantly present in areas where land cover has changed. Meadows and pastures are also important in the buffer, primarily in areas with land cover changes. The second most extensive habitats within the PLA are alluvial forests, found in both unchanged and changed areas. In contrast, oak-hornbeam forests dominate the buffer, where alluvial and beech forests are also significantly present. Within the PLA, habitats associated with the river environment are particularly important, including macrophyte vegetation of naturally eutrophic and mesotrophic still waters, macrophyte vegetation of water streams, and reed and tall-sedge beds. These habitats are predominantly found in unchanged areas but also occur in areas of land cover change.

Soutok is the most forested area, with alluvial forests as the dominant habitat, particularly within the PLA. These forests are primarily found in unchanged areas but have also developed in areas with land cover change. The buffer is significantly less forested, with oak-hornbeam forests present alongside alluvial forests in both changed and unchanged areas. Within the PLA, meadows and pastures, macrophyte vegetation of naturally eutrophic and mesotrophic still waters and reed and tall-sedge beds are also present. Notably, reed and tall-sedge beds are concentrated in the southern part of the PLA, at the confluence of the Morava and Dyje.

3.3 Water streams

The highest density is in Poodří PLA, which increased in the study period. Litovelské Pomoraví and Soutok PLAs had a slight decline. The PLAs and buffers together experienced a decrease, reflecting higher water stream regulation in the buffers (Tab. 4).

3.4 Anthropogenic pressure and Landscape fragmentation

The average EMS in Litovelské Pomoraví PLA, based on built-up area and road network (FGa), is currently 20.7 km^2. In 1960, it was 21.6 km^2, representing a 6% decrease in landscape fragmentation over time. The average EMS in the buffer is significantly lower, but this is largely due to methodological limitations (specifically, the fixed 3 km boundary). It is therefore essential to monitor the development of

Tab. 3 Natural habitat groups (in %) in the Protected Landscape Areas (PLA) and buffer zones (3 km surrounding the PLA). LC – Land cover (stable or changed during the whole study period 1950–2020).

Groups of habitats	Litovelské Pomoraví				Poodří				Soutok			
	PLA		Buffer		PLA		Buffer		PLA		Buffer	
	Plots with stable LC	Plots with changed LC	Plots with stable LC	Plots with changed LC	Plots with stable LC	Plots with changed LC	Plots with stable LC	Plots with changed LC	Plots with stable LC	Plots with changed LC	Plots with stable LC	Plots with changed LC
Streams and water bodies	0.90	0.36	0.01	0.02	4.88	1.13	0.03	0.08	2.00	1.19	0.16	0.37
Wetlands and riverine vegetation	0.13	0.12	0.01	0.09	0.71	0.73	0.02	0.04	1.44	0.40	0.11	0.39
Secondary grasslands and heathlands	1.00	1.81	0.46	0.59	12.37	5.69	0.38	0.67	4.30	1.50	0.25	0.38
Scrub	0.07	0.09	0.01	0.04	0.15	0.26	0.04	0.08	0.01	0.01	0.01	0.02
Forests	44.23	1.64	1.14	0.61	7.76	6.66	2.64	1.90	44.52	5.62	4.19	0.79
Total	*46.33*	*4.02*	*1.63*	*1.35*	*25.87*	*14.47*	*3.11*	*2.77*	*52.27*	*8.72*	4.72	1.95

Tab. 4 Length of water streams.

Period	1840		2020		Index of change
Area	Water streams (km)	Density (km /km^2)	Water streams (km)	Density (km /km^2)	2020/1840
CHKO Litovelské Pomoraví	307	2.87	286	2.67	0.93
CHKO Litovelské Pomoraví – including buffer	894	2.16	691	1.67	0.77
CHKO Poodří	269	3.32	335	4.13	1.24
CHKO Poodří – including buffer	698	1.96	681	1.92	0.98
CHKO Soutok	453	3.56	425	3.35	0.94
CHKO Soutok – including buffer	681	1.94	596	1.69	0.88

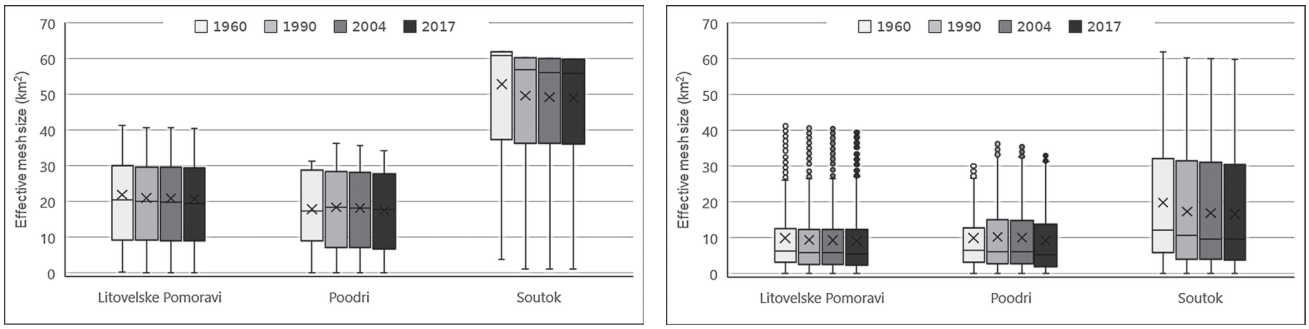

Fig. 3 Effective Mesh Size for built-up area and roads (FGa) in the PLAs (left) and buffers (right). The values should be compared relatively, with emphasis on trends over time. The absolute values in the buffers are influenced by the chosen methodology.

landscape fragmentation, as it has deteriorated by 8% since 1960, which is more than in the PLA itself. When traffic intensity (FGb) is included, the EMS decreases gradually with increasing traffic intensity; the EMS is now 3% lower in the PLA and 7% lower in the buffer. Increasing landscape fragmentation is primarily caused by the expanding built-up area and increasing road network density in both areas since the 1950s (Tab. 5). The built-up area is currently 3 times higher in the buffer than the PLA. While the

Tab. 5 Changes in anthropogenic structures in the PLAs and their buffers since the 1950s.

Study area	Period	Density of communications (km/km²)							
		Road network		Street network		Dirt-road network		Total	
		Buffer	PLA	Buffer	PLA	Buffer	PLA	Buffer	PLA
Litovelské Pomoraví	1960	1.04	0.33	1.48	0.28	3.71	5.54	6.23	6.15
	1990	1.15	0.40	1.49	0.34	2.30	4.93	4.94	5.67
	2004	1.23	0.41	1.56	0.38	2.51	4.84	5.30	5.63
	2017	1.26	0.45	1.71	0.47	2.43	4.68	5.40	5.60
		Buffer	PLA	Buffer	PLA	Buffer	PLA	Buffer	PLA
Poodří	1960	1.05	0.32	1.37	0.26	3.84	5.18	6.25	5.76
	1990	1.16	0.39	1.47	0.30	2.54	4.56	5.16	5.25
	2004	1.24	0.41	1.53	0.35	2.78	4.43	5.55	5.19
	2017	1.29	0.44	1.71	0.43	2.69	4.29	5.69	5.16
		Buffer	PLA	Buffer	PLA	Buffer	PLA	Buffer	PLA
Soutok	1960	0.72	0.11	0.90	0.03	3.95	3.60	5.58	3.75
	1990	0.87	0.15	1.01	0.03	3.46	3.55	5.34	3.74
	2004	0.88	0.15	1.06	0.03	2.85	2.87	4.79	3.06
	2017	0.88	0.17	1.63	0.01	2.81	3.44	5.32	3.62

Study area	Period	Proportion of recreational areas (%)		Proportion of built-up area (%)		Proportion of buildable area (%)	
		Buffer	PLA	Buffer	PLA	Buffer	PLA
Litovelské Pomoraví	1960	0.11	0.13	11.80	3.26	–	–
	1990	0.20	0.16	13.97	4.19	–	–
	2004	0.20	0.19	14.34	4.58	–	–
	2017	0.20	0.20	15.26	4.90	3.59	0.94
		Buffer	PLA	Buffer	PLA	Buffer	PLA
Poodří	1960	0.07	0.00	14.92	3.62	–	–
	1990	0.22	0.06	17.45	3.65	–	–
	2006	0.31	0.06	18.06	3.77	–	–
	2019	0.32	0.06	19.26	3.96	3.17	1.45
		Buffer	PLA	Buffer	PLA	Buffer	PLA
Soutok	1960	0.00	0.00	10.6	0.14	–	–
	1990	0.01	0.01	14.07	0.23	–	–
	2004	0.01	0.02	15.23	0.24	–	–
	2017	0.03	0.03	16.11	0.19	4.11	0.04

density of dirt roads has gradually declined, the overall density of all types of communications is comparable in both areas. Tab. 5 also shows that recreational areas in the PLA have increased steadily, whereas the buffer has remained stable since 1990s. Today, the proportion is the same in both areas (0.2%). Buildable area is nearly 4 times larger in the buffer than the PLA.

The current average EMS for built-up areas and roads (FGa) is 17.6 km^2 in Poodří PLA and 9.2 km^2 in the buffer. Like Litovelské Pomoraví, a gradual increase in landscape fragmentation can be observed – 1.3% in the PLA and 7.3% in the buffer compared to 1960. The influence of traffic intensity is particularly evident in the PLA, where the current average EMS (FGb) is 16.5 km^2 (8.2 km^2 in the buffer). Compared to 1960, this is a 7.7% and 17.5% deterioration in the PLA and buffer, respectively. This substantial difference in landscape fragmentation is largely due to the high proportion of built-up areas in the buffer, which increased from 15% in 1950s to nearly 20% today (Tab. 5). In contrast, the proportion in the PLA is 5 times lower, increasing by only 0.3% over the same period. In addition, road density has increased in the buffer but slightly decreased in the PLA. Street length has grown in both areas, although very minimally in the PLA. In contrast, dirt road density has declined in both areas and is now comparable. Like built-up area, the proportion of recreational areas in the PLA is 5 times lower than the buffer. While stable in the PLA since the 1990s, recreational areas in the buffer have expanded continuously. The proportion of buildable area in the PLA is more than 2 times lower than the buffer (Tab. 5).

In Soutok, the current average EMS for built-up areas and roads is 49 km^2 in the PLA, and 16.7 km^2 in the buffer. Compared to EMS values in Litovelské Pomoraví and Poodří PLAs, Soutok is 2–3 times higher, indicating a lower degree of landscape fragmentation (Fig. 3). Since 1960, the average EMS in the PLA has decreased by 7.4%, which is similar to the reduction observed in the other PLAs. However, the buffer experienced a 16.3% decrease, indicating a fragmentation rate twice as high as the PLA. This decline is likely due to the presence of larger unfragmented areas in Soutok PLA; thus, the split of these areas has a significant effect on overall fragmentation. Traffic intensity in the PLA is similar to that in the other PLAs and contributes only slightly to the degree of landscape fragmentation. Low fragmentation in the PLA can be attributed to its very low population density, reflected by the small proportion of built-up area (0.2%) which contrasts with its surroundings where it is 16% (Tab. 5). While road density has continuously increased in both areas, dirt road density has declined, except for a slight increase in the most recent period in the PLA. A substantial difference is also evident in the proportion of buildable area – 0.04% in the PLA and 4% in the buffer (Tab. 5).

3.5 Landscape connectivity

Litovelské Pomoraví PLA is an extensive complex of floodplain and lowland forests, representing a significant remnant of natural habitats within an otherwise intensively managed agricultural matrix. Although fragmented by the town of Litovel and its deforested surroundings, they remain a crucial element for forest connectivity and wetland habitat integrity in the broader region. The connectivity model identified several well-preserved and more extensive floodplain areas as important for amphibian populations. Migration corridors along watercourses are vital for dispersing these species. Similarly, for aquatic and wetland-dependent species, corridors along the Morava River constitute the most important landscape linkages.

Poodří PLA and its buffer exhibit low forest cover. Consequently, existing forest fragments are critical stepping stones for forest-dwelling faunal species in the transitional zone between the Western Carpathians and the Oder Mountains. However, the functioning of these ecological corridors is endangered by major anthropogenic barriers, namely the D1 motorway and the international railway line. For amphibians, migration pathways towards the south are particularly important. Here, the D48 motorway presents a fundamental barrier, as does, to some extent, the natural watershed dividing the Baltic and Black Sea drainage basins. Northward amphibian dispersal along the Oder River is conceivable. The PLA itself is a significant wetland complex. In this area, transportation infrastructure, coupled with numerous settlements and intensively cultivated agricultural land, constitutes major barriers that limit wetland habitat connectivity.

Soutok PLA also provides high-quality habitat for forest-dependent terrestrial fauna (Fig. 4); however, its connectivity is severely compromised. The entire central portion is fenced within Obora Soutok Game Reserve (the impact of this fence could not be incorporated into the landscape fragmentation analysis due to methodological constraints). The northeastern part of the PLA is isolated by the D2 motorway and the Brno–Bratislava railway corridor. Additional significant barriers include the town of Břeclav and its immediate urban periphery. This area also possesses high conservation value for amphibian populations. Numerous channels, pools, and coarse woody debris create valuable microhabitats, while the channels and floodplains themselves function as natural dispersal corridors. There are floodplain mounds (locally called 'hrúdy') – elevated, treeless remnants of aeolian sand dunes, dating from Pleistocene epochs prior to forest establishment, which have great ecological and biodiversity importance. These features support rare relict communities of organisms. Unfortunately, a significant portion of these unique habitats has already been degraded or lost due to conventional forestry practices.

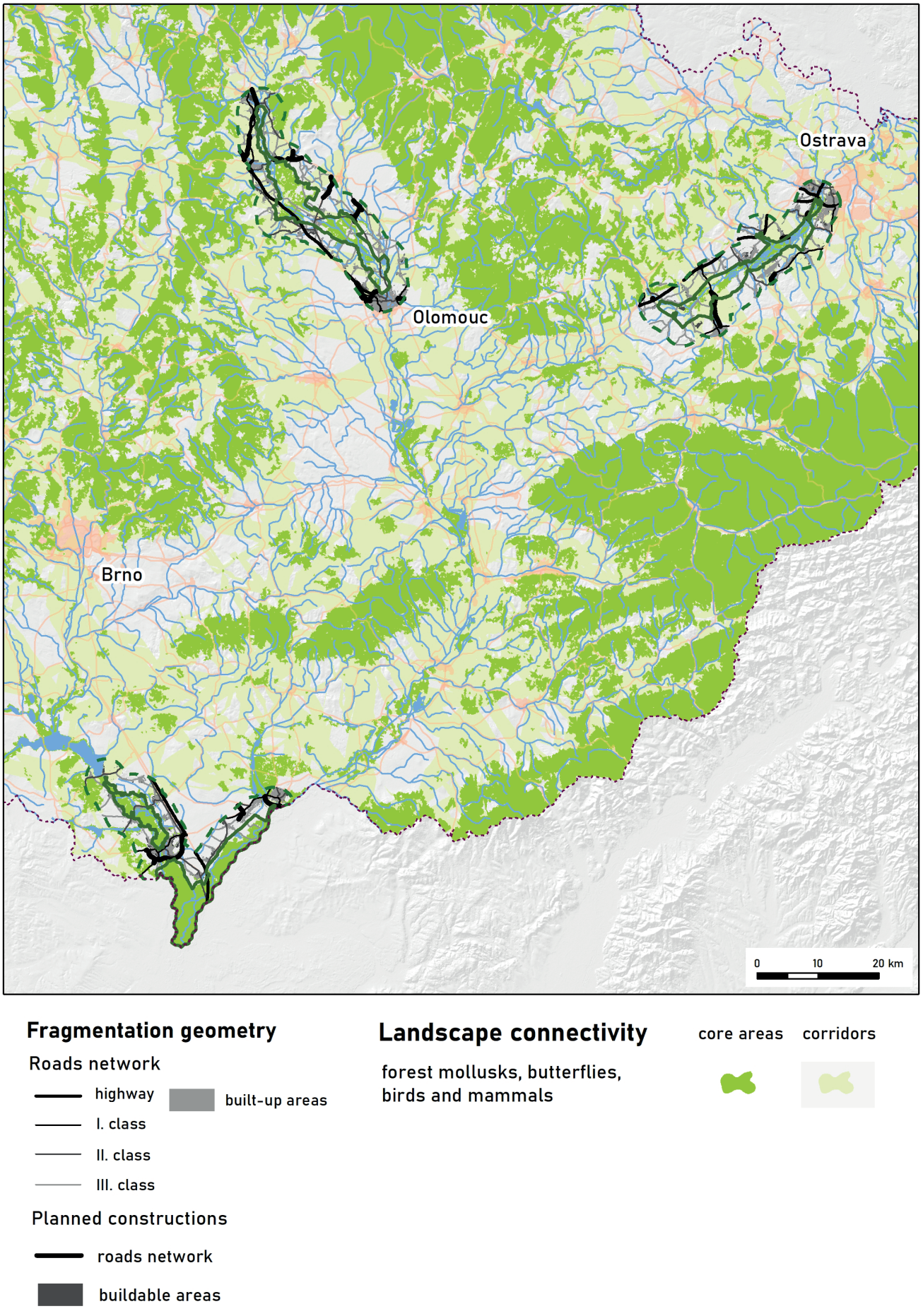

Fig. 4 Landscape connectivity of all three PLAs and buffers for forest habitat.

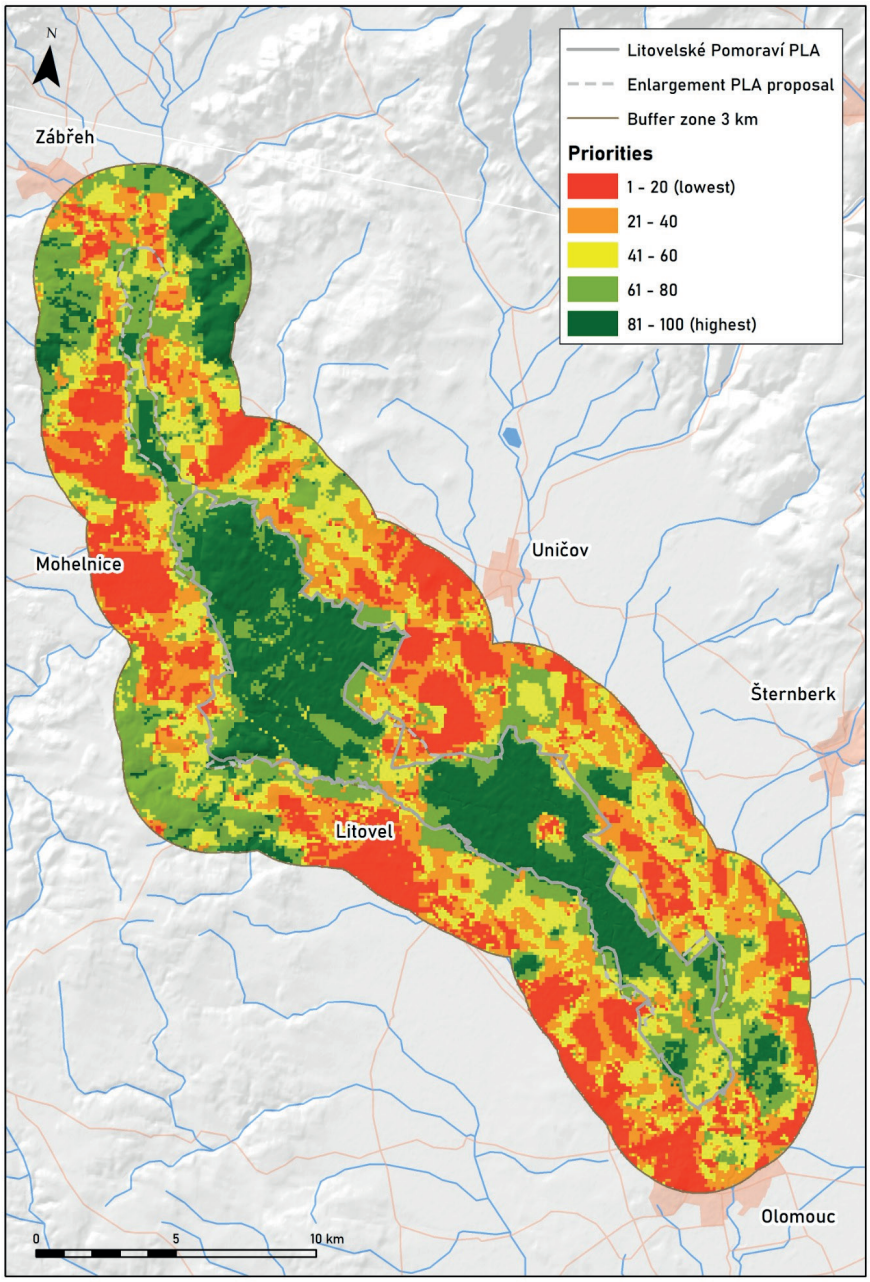
N
Litovelské Pomoraví PLA
Enlargement PLA proposal
Buffer zone 3 km
Priorities
1 - 20 (lowest)
21 - 40
41 - 60
61 - 80
81 - 100 (highest)
Zábřeh
Mohelnice
Uničov
Šternberk
Litovel
Olomouc
0
5
10 km

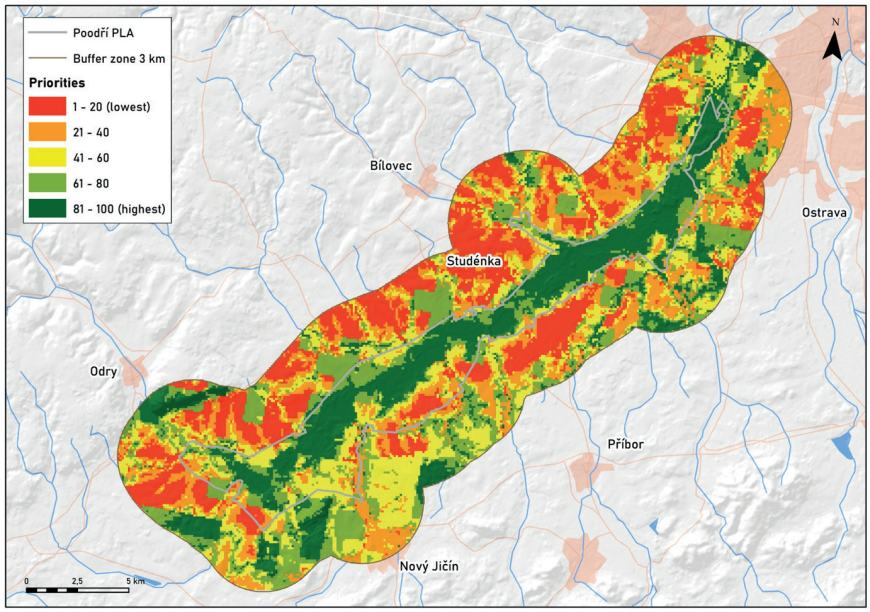
Poodří PLA
Buffer zone 3 km
Priorities
1 - 20 (lowest)
21 - 40
41 - 60
61 - 80
81 - 100 (highest)
N
Bílovec
Ostrava
Studénka
Odry
Příbor
Nový Jičín
0
2,5
5 km

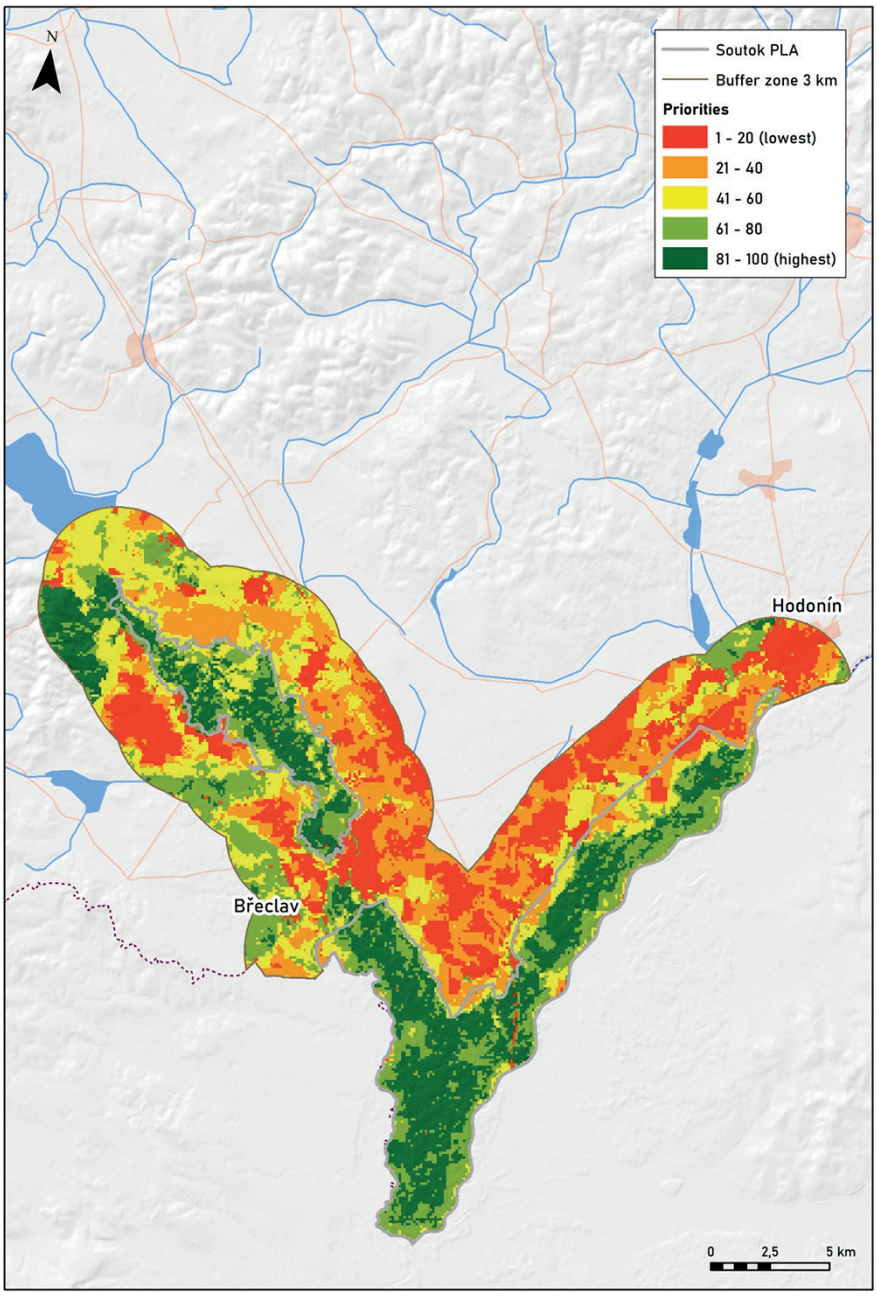

Fig. 5 Prioritization of three study areas – PLAs and 3km buffers.

3.6 Prioritization

In the study areas, priorities are concentrated especially on areas along the rivers. In Litovelské Pomoraví PLA, the core areas are in the south in the forested part, along the Morava River. If we consider the buffer, it has rather lower prioritization because of its intensively used landscape (agriculture and settlements); some areas along the river and forested areas are favorable. Similar priorities are found in Poodří PLA, with the values concentrated along the Odra River and associated ponds. The buffer is predominantly agriculture and settlements with intensively used infrastructure (motorways, railways, airport). Soutok has the highest priority in the core area with a dense network of water streams, but not along the borders and the largest rivers (Dyje and Morava) because of their regulation (an exception is the Dyje around Lednice, with high natural and cultural values). The surroundings are intensively agriculture, therefore there are no priorities, only around ponds and in forested areas and areas continuing into Pálava PLA (Fig. 5).

4. Discussion

The study areas are important parts of relatively large and persistent riverine landscapes within Morava, with similar features as well as differences (Tab. 6). Valuable nature conservation parts are concentrated along the rivers. Litovelské Pomoraví and Soutok are rather forested in contrast with Poodří, which is more open with prevalent meadows and a large share of

ponds although, since PLA designation, its ecosystem services have improved (Mácha et al. 2023; Pořednikova et al. 2025). However, landscape structure changes and management were negative for natural values in Soutok, so PLA designation may improve the situation (Miklín and Hradecký 2016). In the buffers, the analysis reveals intensification of land use along the Morava and Odra rivers, as elsewhere. Therefore, it is crucial to protect valuable forests with natural habitats. A positive trend of increasing permanent grassland is visible in the PLAs, despite the general decrease within the floodplain (Kiliánová et al. 2017). Land use intensification in the buffers is common for all three areas. Stability in arable land use and increased built-up areas cause limitations for landscape connectivity and potential threat of intensification of the land use within the protected areas as well.

The PLAs have a significant share of valuable natural and semi-natural habitats, providing evidence that they are an important component of both regional and global biodiversity conservation strategies (e.g. Jackson and Gaston 2008; Hoffmann 2022). Thus, they fulfil the fundamental role of protected areas, which is primarily to preserve a representative sample of biodiversity, especially rare and threatened features (typically habitats or species), and to isolate or buffer them from external pressures (Margules and Pressey 2000). In Litovelské Pomoraví and Soutok, natural habitats (mainly alluvial and oak-hornbeam forests) cover more than half of the PLAs. Macrophyte vegetation of still waters and water streams are important despite their relatively small areas. In Poodří, natural habitats cover less than half of the area, but there are significantly alluvial, oak-hornbeam, and beech forests, meadows and pastures, plus macrophyte vegetation of still waters and water streams. Soutok is comparable with the older PLAs and this newly designated PLA complements the Czech system of protected areas with its rare and endangered riverine landscapes.

Tab. 6 Results as a SWOT analysis for the study areas, individually and combined.

Study area	Strengths	Weaknesses	Opportunities	Threats
Litovelské Pomoraví	Stable forested PLA. Valuable natural habitats in unchanged areas (mainly alluvial and oak-hornbeam forests). Lengthening of water streams. Landscape connectivity along the river. Valuable parts of landscape along rivers.	Weak presence of natural habitats in buffer. Shortening of water streams. Increasing landscape fragmentation. Urban areas (Litovel, Olomouc), TEN-T railway, D35 motorway and agricultural intensive land use disrupt landscape connectivity.	Valuable natural habitats (mainly meadows and pastures but also macrophyte vegetation of water streams) in both changed and unchanged areas (potential for restoration).	Intensive land use and landscape fragmentation influencing the PLA and its connectivity from buffer, including potential buildable areas.
Poodří	Increasing share of natural and close-to-nature land cover categories. Valuable natural habitats in unchanged areas (mainly macrophyte vegetation connected with water streams and still water). Lengthening of water streams. Valuable parts of landscape along rivers. Valuable natural habitats of meadows and pastures.	Increasing landscape fragmentation. Urban areas (Ostrava), D1 motorway, TEN-T railway and agricultural intensive land use disrupt landscape connectivity.	Valuable natural habitats (mainly meadows and pastures but also forests) in both changed and unchanged areas (potential for restoration).	Intensive land use and landscape fragmentation influencing the PLA and its connectivity from buffer, including potential buildable areas. Railway to be upgraded to high-speed line.
Soutok	Stable forested PLA with minimal built-up areas. Valuable natural habitats in unchanged areas (mainly alluvial forests). Lower landscape fragmentation within PLA. Valuable parts of landscape along rivers.	Weak presence of natural habitats in PLA buffer. Shortening of water streams. Urban areas (Břeclav), TEN-T railway line, D2 motorway and fenced Game reserves disrupt landscape connectivity.	Relatively diverse and forested PLA's surrounding suitable for enhancing connectivity in the broader region.	Intensive land use of surroundings (arable land, built-up areas) and worsening of landscape connectivity due to potential future activities (e.g. buildable areas).
All	Valuable natural habitats in PLAs. Lower landscape fragmentation within PLAs. Valuable parts of landscape along rivers.	Weak presence of natural habitats in the PLA buffers. Urban areas, motorways, and agriculturally intensively used land in the buffers disrupting landscape connectivity and increasing landscape fragmentation. Lower quality of landscape in the buffers from the nature conservation point of view.	Valuable natural habitats in changed and unchanged areas (potential for restoration).	Intensive land use of surroundings (arable land, built-up areas) and worsening of landscape connectivity due to potential future activities (e.g. buildable areas).

Existing threats are motorways, which cross Soutok PLA (to a length of 4 km) and Litovelské Pomoraví PLA (5 km). They can have a negative impact on biodiversity, including habitat loss, barrier effect associated with landscape fragmentation, or disturbances such as noise, air and light pollution (e.g. Forman et al. 2003; Gimmi et al. 2011; Hlaváč et al. 2020). Litovelské Pomoraví PLA is the only PLA with a slightly higher density of communications compared with its buffer. Dirt road network density here is higher than the average value for all Czech PLAs – 4.13 km per km^2 (Janík et al. 2024b). Soutok PLA shows a lower density of dirt roads than the PLA average value, according to Janík et al. (2024b).

From the anthropogenic structure point of view, Soutok PLA has the lowest proportion of built-up and recreational areas. Nevertheless, the current proportion of built-up area in its buffer (16%) is very similar to Litovelské Pomoraví (15.3%) and Poodří (19.3%). Similar values for built-up areas around protected areas were published by de la Fuente et al. (2020) in European countries (e.g. Belgium 18.9%, the Netherlands 15.6%); however, they used a 10-km unprotected buffer at the country level. Furthermore, part of Soutok's buffer lies in neighboring countries whose effect was not taken into consideration. Conversely, opportunities to cross the rivers from Austria and Slovakia are limited, which reduces accessibility and intensity of anthropogenic activities within the Soutok PLA. Limited anthropogenic pressure in the western part of Soutok PLA is largely due to the strictly guarded border zone between 1950 and 1990 (part of the "Iron Curtain"). Densely built-up areas around protected areas can be seen as threat because it can be more problematic to acquire additional land for protected area extension (Turner et al. 2006). On the other hand, Jones et al. (2018) found that built-up structures in protected areas do not expand significantly with time. This was documented in both Poodří and Soutok PLAs. Recreational areas have a very low proportion in Soutok PLA and its buffer (both 0.03%) – lower than the other two PLAs and much lower than the average (0.19%) for Czech (Janík et al. 2024b).

5. Conclusions

The three selected PLAs are similar, and they protect rare landscapes of relatively non-regulated floodplain forests or meadows along anastomosing rivers in Czechia. We can see similar traits in all study areas; conversely some differences can be found as well, e.g. Poodří PLA with a lower portion of forest and higher share of water areas, namely ponds. In Litovelské Pomoraví and Poodří we reveal positive effects after designation as PLAs; therefore we can expect similar positive development for Soutok PLA. On the other hand, the contrast between PLAs and their surroundings is evident, which could be a threat for landscape connectivity due to increasing landscape fragmentation.

Acknowledgments

This work was funded by the Ministry of the Environment of the Czech Republic: Biological research and monitoring in Czech Republic – providing scientific support for Environment 2023–2027 (contract No. 0089/22/900), part D – Assessment of the potential for development of protected areas and assessment of landscape dynamics and connectivity. Transport Research Centre received financial support from the Ministry of Transport of the Czech Republic within the long-term conceptual development of research institutions (decision No. MD-8449/2021-730/145).

References

Czech National Council (1992): Act No. 114/1992 Coll., on Nature Conservation and Landscape Protection; Czech National Council: Prague, Czech Republic.

Chytrý, M., Kučera, T., Kočí, M., Grulich, V., Lustyk, P. (Eds.) (2010): Katalog biotopů České republiky [Habitat Catalogue of the Czech Republic]; Agentura ochrany přírody a krajiny ČR: Praha, Czech Republic.

Divíšek, J., Chytrý, M. (2018): High-resolution and large-extent mapping of plant species richness using vegetation-plot databases. Ecological Indicators 89, 840–851, https://doi.org/10.1016/j.ecolind.2017.11.005.

Elith, J., Phillips, S. J., Hastie, T., Dudík, M., Chee, Y. E., Yates, C. J. (2011): A statistical explanation of MaxEnt for ecologists. Diversity and Distributions 17(1), 43–57, https://doi.org/10.1111/j.1472-4642.2010.00725.x.

European Commission, Directorate-General for Environment, Sundseth, K. (2015): The EU birds and habitats directives – For nature and people in Europe. Available online: https://data.europa.eu/doi/10.2779/49288 (accessed on 8 July 2025).

European Commission, Directorate-General for Environment (2021): EU biodiversity strategy for 2030: bringing nature back into our lives. Available online: https://data.europa.eu/doi/10.2779/677548 (accessed on 8 July 2025).

Forman, R. T. T., Sperling, D., Bissonette, J. A., Clevenger, A. P., Cutshall, C. D., Dale, V. H., Fahrig, L., France, R., Goldman, C. R., Heanue, K., Jones, J. A., Swanson, F. J., Turrentine, T., Winter, T. C. (2003): Road Ecology. Science and Solutions; Island Press: Covelo, CA.

de la Fuente, B., Bertzky, B., Delli, G., Mandrici, A., Conti, M., Florczyk, A., Freire, S., Schiavina, M., Bastin, L., Dubois, G. (2020): Built-up areas within and around protected areas: Global patterns and 40-years trends. Global Ecology and Conservation 24: e01291, https://doi.org/10.1016/j.gecco.2020.e01291.

Gimmi, U., Schmidt, S. L., Hawbaker, T. J., Alcántara, C., Gafvert, U., Radeloff, V. C. (2011): Increasing development in the surrounding of U.S. National Park Service holdings jeopardizes park effectiveness. Journal

of Environmental Management 92(1), 229–239, https://doi.org/10.1016/j.jenvman.2010.09.006.
Girvetz, E. H., Thorne, J. H., Berry, A. M., Jaeger, J. A. G. (2008): Integration of landscape fragmentation analysis into regional planning: A statewide multi-scale case study from California, USA. Landscape and Urban Planning 86(3–4), 205–218, https://doi.org/10.1016/j.landurbplan.2008.02.007.
Grygar, T., Světlík, I., Lisá, L., Koptíková, L., Bajer, A., Wray, D. S., Ettler, V., Mihaljevič, M., Nováková, T., Koubová, M., Novák, J., Máčka, Z., Smetana, M. (2010): Geochemical tools for the stratigraphic correlation of floodplain deposits of the Morava River in Strážnické Pomoraví, Czech Republic from the last millennium. Catena 80(2), 106–121, https://doi.org/10.1016/j.catena.2009.09.005.
Hlaváč, V., Anděl, P., Pešout, P., Libosvár, T., Šikula, T., Bartonička, T., Dostál, I., Strnad, M., Uhlíková, J. (2020): Doprava a ochrana fauny v České republice. Metodika AOPK ČR; Agentura ochrany přírody a krajiny ČR: Praha, Czech Republic, 293 pp. [in Czech].
Hoffmann, S. (2022): Challenges and opportunities of area-based conservation in reaching biodiversity and sustainability goals. Biodiversity and Conservation 31, 325–352, https://doi.org/10.1007/s10531-021-02340-2.
Hradecký, J., Dušek, R., Velešík, M., Chudaničová, M., Škarpich, V., Jarošek, R., Lipina, J. (2016): Poodří – Landscape of Ponds and a Preserved Meander Belt of the Odra River. In Pánek, T., Hradecký, J. (Eds.), Landscapes and Landforms of the Czech Republic. World Geomorphological Landscapes; Springer: Cham, https://doi.org/10.1007/978-3-319-27537-6_26.
Jackson, S. F., Gaston, K. J. (2008): Land use change and the dependence of national priority species on protected areas. Global Change Biology 14(9), 2132–2138, https://doi.org/10.1111/j.1365-2486.2008.01628.x.
Jaeger, J. A. G. (2000): Landscape division, splitting index, and effective mesh size: new measures of landscape fragmentation. Landscape Ecology 15, 115–130, https://doi.org/10.1023/A:1008129329289.
Janík, T., Skokanová, H., Havlíček, M., Borovec, R., Romportl, D. (2024a): Landscape changes in Czech large protected areas 1950–2020: Two different landscapes types on the same path. Journal for Nature Conservation 81: 126705, https://doi.org/10.1016/j.jnc.2024.126705.
Janík, T., Zýka, V., Demková, K., Havlíček, M., Borovec, R., Lichová, A., Mrkvová, B., Romportl, D. (2024b): Anthropogenic pressure in Czech protected areas over the last 60 years: A concerning increase. Landscape and Urban Planning 250: 105146, https://doi.org/10.1016/j.landurbplan.2024.105146.
Jones, K. R., Venter, O., Fuller, J. R., Allan, J. R., Maxwell, S. L., Negret, P. J., Watson, J. E. (2018): One-third of global protected land is under intense human pressure. Science 360(6390), 788–791, https://doi.org/10.1126/science.aap9565.
Kilianová, H., Pechanec, V., Brus, J., Kirchner, K., Machar, I. (2017): Analysis of the development of land use in the Morava River floodplain, with special emphasis on the landscape matrix. Moravian Geographical Reports 25(1), 46–59, https://doi.org/10.1515/mgr-2017-0005.
Kubacka, M., Zywica, P., Subirós, J. V., Bródka, S., Macias, A. (2022): How do the surrounding areas of national parks work in the context of landscape fragmentation? A case study of 159 protected areas selected in 11 EU countries. Land Use Policy 113: 105910, https://doi.org/10.1016/j.landusepol.2021.105910.
Lehtomäki, J., Moilanen, A. (2013): Methods and workflow for spatial conservation prioritization using Zonation. Environmental Modelling & Software 47, 128–137, https://doi.org/10.1016/j.envsoft.2013.05.001.
Mácha, P., Červenka, R., Tlapáková, L. (2023): The challenges and possibilities in the reconstruction of non-forest woody vegetation: A case study of the hermit beetle microhabitat in the Poodří region, Czechia. Applied Geography 150: 102827, https://doi.org/10.1016/j.apgeog.2022.102827.
Máčka, Z. (2016): Litovelské Pomoraví – Landscape Around Anastomosing River Pattern of Morava. In Pánek, T., Hradecký, J. (Eds.), Landscapes and Landforms of the Czech Republic. World Geomorphological Landscapes; Springer: Cham, https://doi.org/10.1007/978-3-319-27537-6_23.
Margules, C. R., Pressey, R. L. (2000): Systematic conservation planning. Nature 405, 243–253, https://doi.org/10.1038/35012251.
McRae, B. H., Kavanagh, D. M. (2011): Linkage Mapper Connectivity Analysis Software. The Nature Conservancy: Seattle WA. Available online: https://circuitscape.org/linkagemapper (accessed on 8 July 2025).
Miklín, J., Čížek, L. (2014): Erasing a European biodiversity hot-spot: Open woodlands, veteran trees and mature forests succumb to forestry intensification, succession, and logging in a UNESCO Biosphere Reserve. Journal for Nature Conservation 22(1), 35–41, https://doi.org/10.1016/j.jnc.2013.08.002.
Miklín, J., Hradecký, J. (2016): Změny struktury krajiny v oblasti soutoku Moravy a Dyje. Geografie 121(3), 368–389.
Miklín, J., Smolková, V. (2011): Land use/land cover changes of the Pálava PLA and proposed Soutok PLA (Czech Republic) in 1841–2006. Moravian Geographical Reports 19(3), 15–28.
Mingarro, M., Lobo, J. M. (2023): European National Parks protect their surroundings but not everywhere: A study using land use/land cover dynamics derived from CORINE Land Cover data. Land Use Policy 124: 106434, https://doi.org/10.1016/j.landusepol.2022.106434.
Moilanen, A., Franco, A. M. A., Early, R. I., Fox, R., Wintle, B., Thomas, C. I. (2005): Prioritizing multiple-use landscapes for conservation: methods for large multi-species planning problems. Proceedings of the Royal Society B 272(1575), 1885–1891, https://doi.org/10.1098/rspb.2005.3164.
Moilanen, A., Kujala, H. (2006): Zonation spatial conservation planning framework and software v. 1.0, User manual; Edita: Helsinki, Finland, 126 pp.
Moilanen, A., Anderson, B. J., Eigenbrod, F., Heinemeyer, A., Roy, D. B., Gillings, S., Armsworth, P. R., Gaston, K. J., Thomas, C. D. (2011): Balancing alternative land uses in conservation prioritization. Ecological Applications 21(5), 1419–1426, https://doi.org/10.1890/10-1865.1.
Moilanen, A. (2013): Planning impact avoidance and biodiversity offsetting using software for spatial conservation prioritisation. Wildlife Research 40(2), 153–162, https://doi.org/10.1071/WR12083.
Montgomery, D. R., Wohl, E. E. (2003): Rivers and riverine landscapes. Developments in Quaternary Sciences 1,

221–246, https://doi.org/10.1016/S1571-0866(03)01011-X.
Moser, B., Jaeger, J. A. G., Tappeiner, U., Tasser, E., Eiselt, B. (2007): Modification of the effective mesh size for measuring landscape fragmentation to solve the boundary problem. Landscape Ecology 22, 447–459, https://doi.org/10.1007/s10980-006-9023-0.
Nakládal, O., Zumr, V., Remeš, J., Macháčová, M., Pešková, V. (2022): Heritage Trees as an Important Sanctuary for Saproxylic Beetles in the Central European Landscape: A Case Study from Litovelské Pomoraví, Czech Republic. Forests 13(7): 1128, https://doi.org/10.3390/f13071128.
Phillips, S. J., Anderson, R. P., Schapire, R. E. (2006): Maximum entropy modeling of species geographic distributions. Ecological Modelling 190(3–4), 231–259, https://doi.org/10.1016/j.ecolmodel.2005.03.026.
Połedniková, Z., Holušová, A., Vaverka, L., Galia, T. (2025): Effects of policy changes in the last 80 years on LU/LC and ecosystem services: A case study of the Odra River floodplain (Czech Republic): Moravian Geographical Reports 33(2), 91–105, https://doi.org/10.2478/mgr-2025-0007.
Romportl, D., Andreas, M., Chumanová, E., Janík, T., Mrkvová, B., Tichopádová, E., Vojta, J., Zýka, V. (2021): Metodika komplexního hodnocení druhové a habitatové diverzity v krajině ČR [Methodology for Comprehensive Assessment of Species and Habitat Diversity in the Landscape of the Czech Republic]; Výzkumný ústav pro krajinu, v. v. i.: Průhonice.
Šantrůčková, M., Vokoun, A., Skokanová, H., Vojta, J., Demková, K., Havlíček, M., Medková, L., Weber, M., Slach, T., Dostálek, J., Richter, P., Rozkošný, M., Fanta, V., Szabó, P. (2023): Území pravděpodobného výskytu historických kulturních krajin [The area of possible presence of historical cultural landscapes]; Výzkumný ústav pro krajinu, v. v. i.: Průhonice.
Tockner, K., Malard, F., Ward, J. V. (2000): An extension of the flood pulse concept. Hydrological processes 14(16–17), 2861–2883, https://doi.org/10.1002/1099-1085(200011/12)14:16/17%3C2861::AID-HYP124%3E3.0.CO;2-F.
Turner, W. R., Wilcove, D. S., Swain, H. M. (2006): Assessing the effectiveness of reserve acquisition programs in protecting rare and threatened species. Conservation Biology 20(6), 1657–1669, https://doi.org/10.1111/j.1523-1739.2006.00536.x.
Vollering, J., Halvorsen, R., Mazzoni, S. (2019): The MIAmaxent R package: Variable transformation and model selection for species distribution models. Ecology and Evolution 9(21), 12051–12068, https://doi.org/10.1002/ece3.5654.
Watson, J. E. M., Dudley, N., Segan, D. B., Hockings, M. (2014): The performance and potential of protected areas. Nature 515, 67–73, https://doi.org/10.1038/nature13947.

Data sources

Czech Office for Surveying, Mapping and Cadastre (ČÚZK): Raster Base Map of the Czech Republic 1:10 000 (2002–2006) [online]; ČÚZK: Prague. Available online: https://geoportal.cuzk.cz/(S(axzzppw0sacvxwlksyed41c5))/Default.aspx?mode=TextMeta&side=mapy_tiskZMSM&metadataID=CZ-CUZK-ZM10-T (accessed on 8 July 2025).
Czech Office for Surveying, Mapping and Cadastre (ČÚZK): Archival Orthophoto of the Czech Republic (2003–2005) [online database]; ČÚZK: Prague, ©2005 WMS service. Available online: https://geoportal.cuzk.cz/WMS_ORTOFOTO_ARCHIV/WMService.aspx (accessed on 8 July 2025).
Czech Office for Surveying, Mapping and Cadastre (ČÚZK): Archival Orthophoto of the Czech Republic (2016–2020) [online database]; ČÚZK: Prague, ©2020 WMS service. Available online: https://geoportal.cuzk.cz/WMS_ORTOFOTO_ARCHIV/WMService.aspx (accessed on 8 July 2025).
General Staff of the Czechoslovak Army and Central Administration of Geodesy and Cartography: Topographic maps of the Czechoslovakia in the system S-1952, scale 1:10 000 (1957–1971) [online database]; ČÚZK: Prague. Available online: https://geoportal.cuzk.cz/(S(3b1gkzfbsvxmbussczwsy2yi))/Default.aspx?mode=TextMeta&side=dSady_archiv&metadataID=CZ-CUZK-TMS52_10-R&head_tab=sekce-02-gp&menu=2908 (accessed on 8 July 2025).
Central Administration of Geodesy and Cartography: Base maps of Czechoslovakia, scale 1:10 000 (1986–1995).
General Staff of the Czechoslovak Army: Czechoslovak military topographic maps, scale 1:25 000 (1952–1956) [online]; ČÚZK: Prague. Available online: https://geoportal.cuzk.cz/(S(0csgh2l0tdj4lwobyer4sf3w))/Default.aspx?mode=TextMeta&side=dSady_archiv&metadataID=CZ-CUZK-TMS52_25-R&head_tab=sekce-02-gp&menu=2909 (accessed on 8 July 2025).
General Staff of the Czechoslovak Army: Czechoslovak military topographic maps, scale 1:25 000 (1988–1995); ČÚZK: Prague.
Ministry of Agriculture: Land Parcel Information System (2016–2020); Ministry of Agriculture: Prague. Available online: https://eagri.cz/public/app/lpisext/lpis/verejny2/plpis/ [online database] (accessed on 8 July 2025).
Nature Conservation Agency of the Czech Republic: Consolidated layer of ecosystems of the Czech Republic (2013); Nature Conservation Agency of the Czech Republic: Prague. Available online: https://data.nature.cz/ds/27 [online database] (accessed on 8 July 2025).
Nature Conservation Agency of the Czech Republic: Nálezová databáze ochrany přírody [National Database of Fauna-Flora Records] (2022a); Nature Conservation Agency of the Czech Republic: Prague. Available online: https://portal23.nature.cz/nd/ [online database] (accessed on 4 January 2022).
Nature Conservation Agency of the Czech Republic: Habitat mapping layers (2022b); Nature Conservation Agency of the Czech Republic: Prague. Available online: https://data.nature.cz/sds/7 [online database] (accessed on 4 January 2022).
Czech Hydrometeorological Institute: ISVS Evidence množství povrchových vod [Recording of surface water quantities] (2026); Czech Hydrometeorological Institute: Prague. Available online: https://isvs.chmi.cz/ords/f?p=11002:HOME:13429975927986 [online database] (accessed on 6 March 2026).
Vrška, T., Hort, L., Adam, D. (2023): Layer of natural forests; Landscape Research Institute: Brno. Available online: https://pralesy.cz/databanka-prirozenych-lesu [online database] (accessed on 6 February 2023).

Appendix 1

Group	Species	Red List	Weight	Litovelské Pomoraví	Poodří	Soutok
molluscs	*Cochlodina orthostoma*	NT	2			
molluscs	*Daudebardia brevipes*	VU	3			
molluscs	*Discus perspectivus*	NE	1			
molluscs	*Euconulus praticola*	NT	2			
molluscs	*Vertigo antivertigo*	NE	1			
butterflies	*Apatura ilia*	NE	1			
butterflies	*Arethusana arethusa*	EN	4			
butterflies	*Brenthis daphne*	NE	1			
butterflies	*Erebia medusa*	NT	2			
butterflies	*Euphydryas maturna*	CR	5			
butterflies	*Glaucopsyche alexis*	VU	3			
butterflies	*Hamearis lucina*	EN	4			
butterflies	*Hesperia comma*	VU	3			
butterflies	*Hipparchia fagi*	VU	3			
butterflies	*Hipparchia semele*	CR	5			
butterflies	*Limenitis camilla*	NT	2			
butterflies	*Lycaena alciphron*	VU	3			
butterflies	*Lycaena dispar*	NE	1			
butterflies	*Lycaena hippothoe*	NT	2			
butterflies	*Lycaena virgaureae*	NT	2			
butterflies	*Melitaea athalia*	NT	2			
butterflies	*Melitaea aurelia*	EN	4			
butterflies	*Melitaea cinxia*	VU	3			
butterflies	*Minois dryas*	VU	3			
butterflies	*Parnassius mnemosyne*	EN	4			
butterflies	*Phengaris arion*	EN	4			
butterflies	*Phengaris nausithous*	NT	2			
butterflies	*Phengaris teleius*	VU	3			
butterflies	*Plebejus argus*	NT	2			
butterflies	*Polyommatus bellargus*	VU	3			
butterflies	*Polyommatus coridon*	VU	3			
butterflies	*Polyommatus damon*	CR	5			
butterflies	*Polyommatus daphnis*	VU	3			
butterflies	*Polyommatus thersites*	VU	3			
butterflies	*Pseudophilotes vicrama*	CR	5			
butterflies	*Satyrium ilicis*	EN	4			
butterflies	*Satyrium w-album*	NT	2			
butterflies	*Zerynthia polyxena*	NT	2			
amphibians	*Bombina bombina*	EN	4			
amphibians	*Bufotes viridis*	EN	4			
amphibians	*Lissotriton vulgaris*	VU	3			
amphibians	*Pelobates fuscus*	NT	2			
amphibians	*Rana arvalis*	EN	4			
amphibians	*Rana dalmatina*	NT	2			

Group	Species	Red List	Weight	Litovelské Pomoraví	Poodří	Soutok
amphibians	*Triturus cristatus*	EN	4	■	■	
amphibians	*Triturus dobrogicus*	CR	5			■
reptiles	*Lacerta agilis*	VU	3		■	
reptiles	*Natrix natrix*	NT	2		■	
reptiles	*Zootoca vivipara*	NT	2		■	
birds	*Acrocephalus arundinaceus*	VU	3		■	
birds	*Actitis hypoleucos*	EN	4	■	■	
birds	*Alcedo atthis*	VU	3	■	■	■
birds	*Anas crecca*	CR	5		■	
birds	*Anas querquedula*	CR	5		■	
birds	*Aquila heliaca*	CR	5			■
birds	*Ardea alba*	NE	4		■	
birds	*Botaurus stellaris*	CR	5		■	
birds	*Bucephala clangula*	EN	4		■	
birds	*Ciconia ciconia*	NT	2		■	■
birds	*Columba oenas*	VU	3		■	
birds	*Crex crex*	VU	3		■	
birds	*Dendrocopos medius*	VU	3	■	■	■
birds	*Dendrocopos minor*	VU	3		■	
birds	*Falco cherrug*	CR	5			■
birds	*Ficedula albicollis*	NT	2	■	■	■
birds	*Gallinago gallinago*	EN	4		■	
birds	*Grus grus*	CR	5		■	
birds	*Haliaeetus albicilla*	EN	4		■	
birds	*Charadrius dubius*	VU	3	■	■	
birds	*Ixobrychus minutus*	CR	5		■	
birds	*Locustella luscinioides*	EN	4		■	
birds	*Luscinia svecica cyanecula*	EN	4		■	
birds	*Milvus migrans*	CR	5		■	■
birds	*Milvus milvus*	CR	5	■		■
birds	*Nycticorax nycticorax*	EN	4		■	
birds	*Pernis apivorus*	EN	4		■	■
birds	*Picus canus*	VU	3		■	■
birds	*Porzana parva*	CR	5		■	
birds	*Rallus aquaticus*	VU	3	■	■	
birds	*Remiz pendulinus*	VU	3		■	
birds	*Riparia riparia*	NT	2		■	
birds	*Saxicola rubetra*	LC	1		■	
birds	*Saxicola rubicola*	VU	3		■	
birds	*Sterna hirundo*	EN	4		■	
birds	*Tringa glareola*	NE	5		■	
birds	*Tringa ochropus*	EN	4		■	
birds	*Vanellus vanellus*	VU	3		■	
mammals	*Castor fiber*	LC	1	■	■	■
mammals	*Lutra lutra*	NT	2	■	■	■

The transformation of cartographic normality in tourist maps of the Teschen Beskids (1905–1947)

Jiří Kupka*

VSB – Technical University of Ostrava, Faculty of Mining and Geology, Department of Environmental Engineering, Czechia
* Corresponding author: jiri.kupka@vsb.cz

ABSTRACT
This article examines the transformation of cartographic normality in tourist maps of the Teschen Beskids between 1905 and 1947, a period marked by major political and institutional changes in Central Europe. Cartographic normality is understood as the set of conventions that determine which elements are treated as self-evident and which are explicitly explained within cartographic language. The analysis is based on a qualitative comparison of successive map editions, with particular attention to map legends and the categorization of tourist huts. The results identify three main phases. Before 1918, tourist huts appear as named but uncategorized elements within a landscape understood as a memory space. During the interwar period, cartographic normality shifts toward an explicitly articulated plurality, in which national and institutional affiliation becomes a systematically expressed category. Beginning in 1940, this model disintegrated through semantic reduction and subsequent homogenization, culminating in the complete removal of national distinctions in the 1947 edition. The article demonstrates that cartographic change cannot be interpreted solely as a reflection of political borders, but rather as a transformation of cartographic language through which political and institutional meanings are internalized and stabilized.

KEYWORDS
tourist cartography; cartographic normality; map legend; Teschen Beskids; historical geography

Received: 5 February 2026
Accepted: 5 May 2026
Published online: 20 May 2026

Kupka, J. (2026): The transformation of cartographic normality in tourist maps of the Teschen Beskids (1905–1947), AUC Geographica 61(2), 298–308
https://doi.org/10.14712/23361980.2026.9
© 2026 The Author. This is an open-access article distributed under the terms of the Creative Commons Attribution License (https://creativecommons.org/licenses/by/4.0).

1. Introduction

Tourist maps are commonly understood primarily as practical tools for spatial orientation. At the same time, they constitute an important historical source, as they not only record the physical configuration of the landscape but also reflect the ways in which space was interpreted, structured, and communicated at a given time. Historical tourist cartography has received increasing scholarly attention, including regional studies of mountain areas such as the Karkonosze (Woźniak 2005). More broadly, maps have been interpreted not as neutral mirrors of reality, but as socially conditioned representations shaped by selection and classification (Harley 1989).

In regions with a complex political development, such as Teschen Silesia (Hanslik 1907; Machatschek 1927), political and social transformations are not expressed in maps solely through changes in borders or toponymy. They also manifest themselves through subtler cartographic features that indicate what was considered relevant, self-evident, or worthy of explicit explanation in a given period. This study proceeds from the assumption that the map legend represents a key interpretative element through which such shifts can be traced.

Although historical cartography has paid considerable attention to the depiction of borders and place names, the role of map legends in shaping and stabilizing cartographic normality has remained relatively underexplored, particularly in the context of tourist maps.

In this paper, cartographic normality is understood as the set of information regarded at a given time as an obvious and necessary component of cartographic representation. It thus concerns the distinction between what a map leaves implicit and what it considers sufficiently significant to be explicitly articulated. Cartographic normality does not denote neutrality, but rather a historically contingent set of social and political conventions embedded in the cartographic language of a given period.

The aim of this paper is to examine the transformation of cartographic normality through a selected corpus of tourist maps depicting parts of the Teschen Beskids between 1905 and 1947 – a period marked by profound political ruptures. Particular attention is paid to the representation and categorization of tourist huts, whose changing treatment in map legends serves as a sensitive indicator of broader political, national, and institutional shifts.

Accordingly, the study addresses two interrelated questions: how did the categorization of tourist huts in map legends change across successive editions between 1905 and 1947, and what do these changes reveal about the ways political and institutional transformations became internalized into cartographic language?

2. Materials and methods

This study is based on a qualitative comparative analysis of tourist maps purposefully selected to represent key chronological and political phases between 1905 and 1947. This period was marked by profound political and institutional transformations in Central Europe. The analysed corpus consists of representative tourist cartographic works chosen to capture changes in cartographic conventions over time rather than to provide an exhaustive overview of regional tourist mapping.

With the exception of a reference map dated to around 1905, the analysis focuses primarily on maps published within the cartographic series of the Czechoslovak Tourist Club (Klub československých turistů, KČST) issued in Ostrava, together with a tourist map published by the Teschen district of the KČST, interpreted here as a direct predecessor of the later series. The internal continuity of this editorial line enables a detailed comparison of successive editions and the identification of gradual shifts in cartographic representation.

The upper temporal boundary of the analysed corpus is defined by the seventh and final edition of the series published in 1947, which concludes both the interwar and immediate post-war continuity of this type of tourist cartography. After 1948, the activities of the Czechoslovak Tourist Club were institutionally interrupted, resulting in the disappearance of a comparable editorial framework. The lower boundary is represented by a tourist map from the late Austro-Hungarian period, which serves as a reference point for the initial state of cartographic normality.

The Teschen Beskids are treated in this study as a historical-geographical region whose coherence cannot be reduced to later state borders. In addition to the analysed KČST/KČT map series, complementary primary sources in Czech, Polish, and German – including guidebooks and tourist maps (e.g. Herbatschek 1922; Galicz 1931; Mapa Beskidu = Beskidenkarte [early 1920s]), as well as materials issued by other associations such as Podhorská jednota Radhošť – were consulted in order to contextualize the broader multilingual and multi-institutional cartographic culture of the region. However, these materials are not analysed systematically.

The analysis focuses on tourist huts and related facilities, whose cartographic depiction and categorization provide a sensitive indicator of changing national, political, and institutional approaches. Particular attention is paid to map legends, symbols, and classificatory schemes, rather than to the quantitative expansion of tourist infrastructure. Although the network of tourist huts expanded considerably after 1920 (Polášková and Polášek 2009), this study does not pursue a quantitative assessment of this development.

The analytical procedure consisted of three consecutive steps. First, maps were selected according to chronological relevance, preservation status, and the possibility of comparison within one continuous editorial series. Second, each map was comparatively examined through four recurring analytical categories: legend structure, terminology, symbolization, and the categorization of tourist huts. Third, the observed changes over time were interpreted in relation to broader political and institutional transformations affecting the region.

2.1 Study area

Although the analysed maps cover a broader area including the Moravian-Silesian Beskids, the Javorníky Mountains, and the Vsetín Hills, the study concentrates on the region traditionally referred to as the Teschen Beskids. The term is used here not in a strict geomorphological sense, but as a historical-geographical concept corresponding to the area in which the analysed cartographic material was produced and used.

From a geomorphological perspective, the Teschen Beskids form part of the Western Beskids province and include sections of the Moravian-Silesian and Silesian Beskids, as well as the Jablunkov Furrow and Jablunkov Highlands (Sosna 2001; Bína 2012). Politically and historically, the region is characterised by a complex borderland position, which makes it particularly suitable for examining transformations of cartographic normality.

3. Phase I: The self-evident landscape without explanation (c. 1905)

The tourist map produced around 1905, entitled Spezialkarte der Beskiden für Touristen, represents the initial reference state for the observed development of cartographic normality. Tourist huts – among the earliest facilities of mountain tourism in the Teschen Beskids – are depicted and identified by specific names; however, they are not defined as a separate category in the map legend, nor are they differentiated according to national, linguistic, or institutional affiliation. This absence corresponds to a phase in which tourist huts were perceived as a self-evident component of the landscape rather than as objects requiring explicit cartographic explanation.

Typical examples include the Erzherzog Friedrich Schutzhaus on Javorový Mountain (1895) and the Erzherzogin Isabella Schutzhaus on Čantoryje Mountain, both established by the Beskidenverein. At the turn of the 20th century, this association functioned primarily as a regional tourist organisation operating within a multilingual social and cultural environment, without systematic national differentiation of tourist infrastructure.

Tourist initiatives associated with Czech and Moravian movements began to construct mountain huts in the Teschen Beskids only after 1918, following the political and institutional consolidation of the new state framework. It was this later organisational context that enabled the subsequent systematic cartographic categorization of tourist huts in map legends. In this sense, national classifications introduced in later maps reflect institutional plurality rather than retrospectively projected national ownership (Tab. 1).

The analysed map can be situated within the institutional and linguistic framework of the Habsburg monarchy, in which linguistic plurality functioned as a taken-for-granted element of public communication. Cartographic normality at this stage is characterized by an understanding of the landscape as a memory space, in which named objects serve as carriers of local continuity rather than as analytically classified entities.

At the same time, this period did not produce a single uniform cartographic model. Alongside professionally produced state and crown-land maps with supra-regional scope, Czech associational tourist maps also existed, typically employing simplified graphic conventions and omitting the naming of mountain huts. These differences do not reflect national hierarchy or value judgement, but rather distinct institutional purposes and conceptions of the role of maps within specific user contexts.

3.1 The c. 1905 edition (Austro-Hungarian period)

A representative example of this phase is the tourist map Spezialkarte der Beskiden für Touristen, issued around 1905 at a scale of 1:150,000 by the bookshop

Tab. 1 Institutional background of selected tourist associations underlying later national classifications of tourist huts in map legends (not direct national ownership).

Institutional framework	Association (Year founded)	First hut (Year opened)
Provincial associational framework (pre-1918)	Beskidenverein (1893)	Erzherzog Friedrich Schutzhaus (Javorový Mountain) (1895)
Polish associational framework (Teschen region)	Polskie Towarzystwo Turystyczne "Beskid" (1910)	Hut on Ropička Mountain (1913; destroyed by fire in 1918)
Czech-Moravian associational framework	Beskydská / Pobeskydská jednota slezská (1910)	Hut on Prašivá Mountain (1921)

Note: The associations listed do not represent exclusive or uniform operators of mountain huts. Prior to 1918, the Teschen Beskids and their wider surroundings were characterised by a parallel network of regional units, company-owned facilities, and tourist sections. In later map legends and summaries, this infrastructure was retrospectively classified along national lines or labelled as "private", reflecting subsequent cartographic and institutional reinterpretations rather than the original operational reality.

of Siegmund Stuks in Teschen, an Imperial and Royal Court and Chamber Bookseller. The map thus clearly belongs to the institutional framework of the Habsburg monarchy.

Although the map is not explicitly dated, its production can be determined with a high degree of probability on the basis of internal content indicators. The presence of the Isabellaschutzhaus on Čantoryje Mountain (opened in 1904), combined with the absence of the Frýdlant nad Ostravicí–Bílá railway line (constructed between 1906 and 1908), allows the map to be dated to around 1905.

The map depicts the entire Silesian Beskids as an internal space of a single state entity, in which political or administrative borders do not function as structuring elements of the cartographic image. Spatial organization is instead based on the territorial affiliation of the region to Silesia, prior to its later political and conceptual fragmentation.

It is characteristic that tourist huts are not defined in the legend as a separate cartographic category (Fig. 1). Although they are depicted and named in the map field, their significance is not further explained or systematically classified. This corresponds to the cartographic normality of the period, in which tourist huts were perceived as a self-evident component of the landscape rather than as objects requiring explicit interpretative framing.

The linguistic layer of the map is multilingual and reflects contemporary local usage. German and Slavic toponyms appear side by side without systematic differentiation or explanation in the legend. Linguistic plurality thus functions as a taken-for-granted element of the shared cultural space of the Habsburg

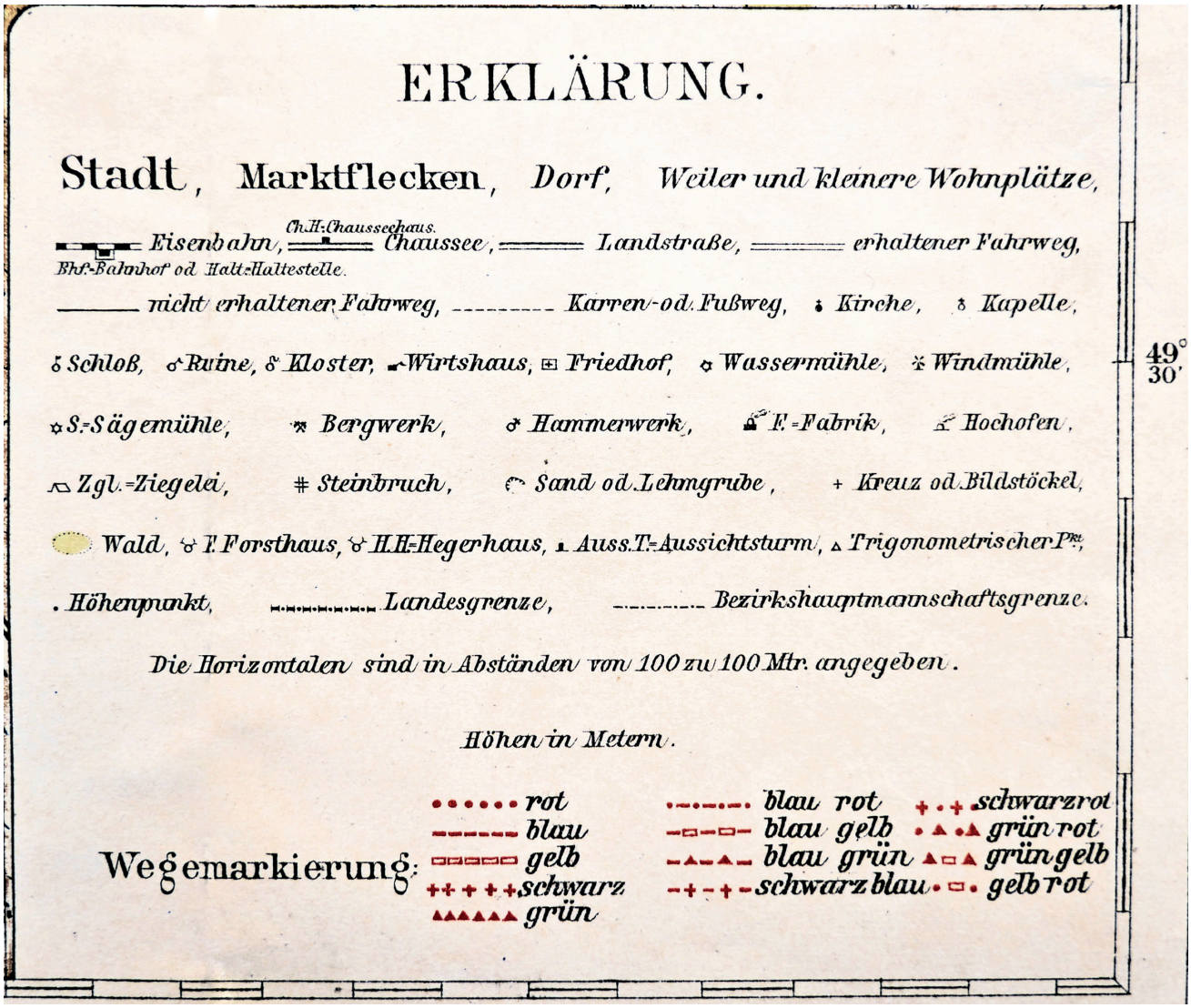

Fig. 1 Legend of the Spezialkarte der Beskiden für Touristen (c. 1905). The legend presents basic categories of settlement, transport infrastructure, land use, and economic features, yet does not define tourist huts as a distinct cartographic category. Although tourist huts are depicted and named in the map field, their presence is not thematised or explained in the legend. This absence reflects a form of cartographic normality in which tourist facilities are understood as self-evident elements of the landscape and function primarily as mnemonic reference points rather than as objects requiring explicit categorization.
Source: Author's private collection.

monarchy, preceding later national and institutional categorization.

4. Phase II: Named and structured plurality (1928–1938)

After 1918, most of the Teschen Beskids became part of Czechoslovakia, and tourist cartography – particularly the map series published by the Czechoslovak Tourist Club (Klub československých turistů, KČST) – began to articulate a new, standardized form of cartographic normality. Elements that had previously remained implicit or inconsistently expressed were now integrated into a unified and explicitly explained cartographic language.

In this phase, tourist huts cease to function merely as mnemonic components of the landscape and become instruments of its interpretation. Their institutional and national affiliation is newly treated as information that should be made explicit and graphically anchored in the map legend, rather than inferred from names or contextual knowledge.

4.1 The tourist map insert in the 1928 guidebook

The small tourist map included in the guidebook published by the Teschen District of the Czechoslovak Tourist Club in 1928 represents a transitional type of cartographic source. Unlike the later standalone map sheets, it is embedded within a pocket-format textual guide and does not yet function as an autonomous cartographic work. Instead, it takes the form of a schematic map (mapka), intended primarily as an auxiliary orientation aid.

Despite its simplified form, the map already displays an emerging logic of categorizing tourist facilities according to national affiliation (Fig. 2). The legend explicitly distinguishes Czech, German, Polish, and private huts, thereby anticipating the later standardized classificatory framework of the KČST map series.

An instructive comparison is provided by a contemporary postcard depicting the hut on Čantoryje Mountain (formerly Isabellaschutzhaus), whose reverse side lists the name of the object in Czech, German, and Polish. In the tourist map, however, the same object is

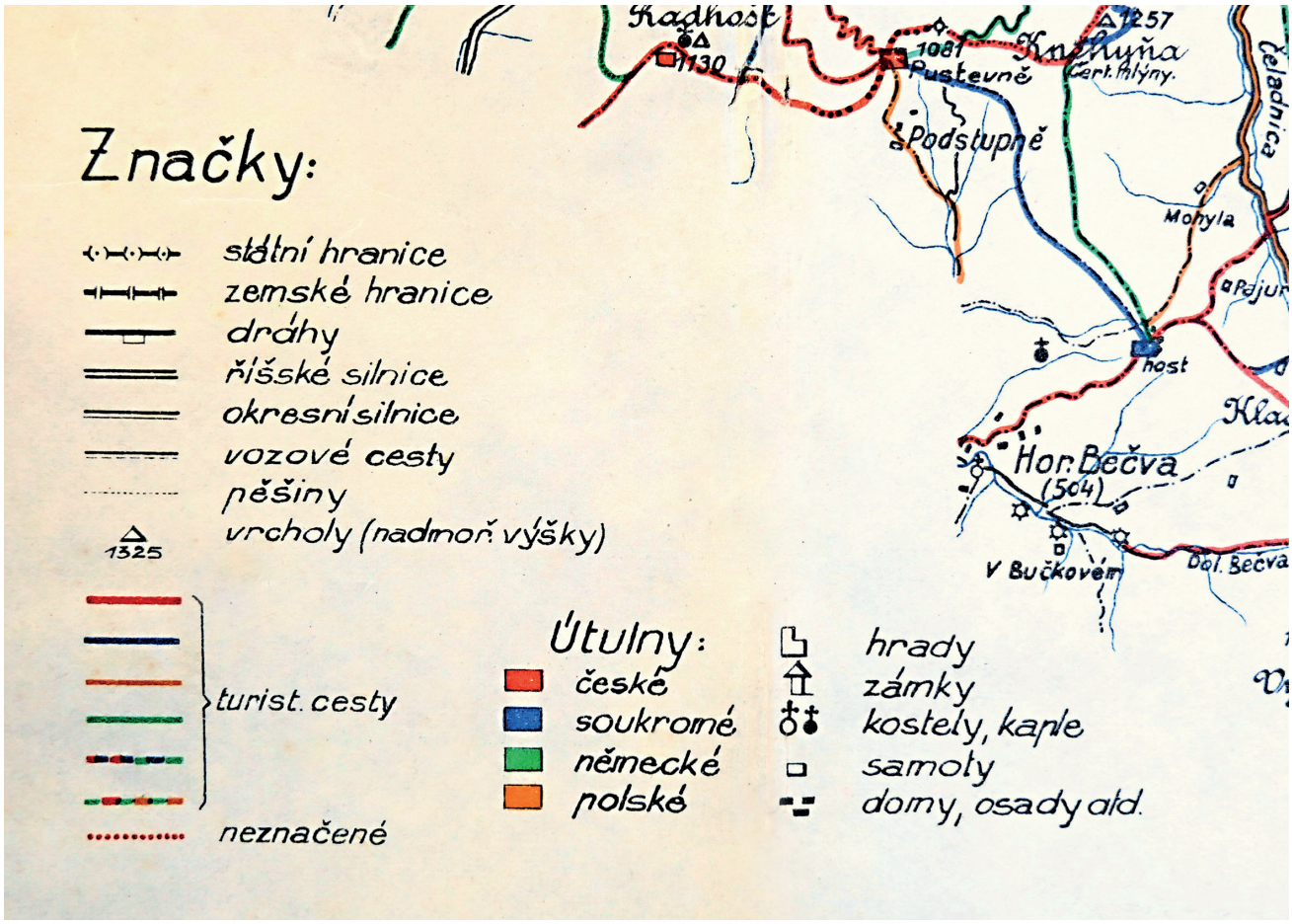

Fig. 2 Legend of the schematic tourist map included in the guidebook of the Teschen District of the Czechoslovak Tourist Club (1928). The legend introduces an emerging classificatory scheme that differentiates tourist huts according to national affiliation (Czech, German, Polish) and private ownership. Although still embedded in a guidebook and not conceived as an autonomous cartographic work, the map anticipates the standardized legend structure of the later KČST map series.
Source: Author's private collection.

Fig. 3 Postcard depicting the hut on Čantoryje Mountain (formerly Isabellaschutzhaus), probably before 1930. The reverse side lists the name of the object in Czech, German, and Polish, reflecting the continued multilingual use of the hut. In contrast, contemporary tourist maps of the Czechoslovak Tourist Club classify the same object exclusively as a German hut. This comparison highlights the discrepancy between lived linguistic plurality and its selective cartographic interpretation.
Source: Author's private collection.

classified exclusively as a German hut. This discrepancy demonstrates that cartographic classification does not necessarily reflect the plurality of linguistic or user practices, but rather the institutional framework within which the map was produced (Fig. 3).

Cartographic normality at this stage is clearly transitional. The national situation after 1918 had become sufficiently complex and salient that it could no longer remain uninterpreted even in tourist cartography. National affiliation thus begins to be explicitly articulated as a relevant cartographic category, although it does not yet form a fully stabilized editorial standard.

Differences in contemporary terminology further illustrate this transitional character. While the German Schutzhaus and Polish schronisko are etymologically equivalent, they cannot be unequivocally translated into the Czech term útulna, which initially functioned as a broad, non-differentiated designation. Only in the second half of the 1920s – particularly in connection with the normative activities of the Czechoslovak Tourist Club – did a more precise terminological system emerge (chata, útulna, ochranná útulna), as documented in contemporary tourist guides and editorial notes "at the time of printing" (Riegler 1928). In this study, terminology is therefore used contextually, with regard to contemporary cartographic and linguistic practice.

4.2 Standalone maps of the series (1929–1947)

The first standalone edition of the analysed map series, published by the Czechoslovak Tourist Club (KČST) and probably dating from around 1929, was produced within the stabilized framework of interwar Czechoslovakia. Its cartographic language is highly systematized, and the legend provides an explicit and unambiguous interpretation of spatial complexity. Tourist infrastructure is conceived not merely as a functional element, but as a meaning-bearing component of the landscape.

The legend presents a fully developed categorization of tourist huts according to national and institutional affiliation. Czech, German, Polish, and private huts are clearly distinguished, and the identity of each object is treated as a cartographically relevant form of information. This model remained largely stable throughout the subsequent editions of the 1930s.

The fifth edition, published in 1939, emerged in a period of rapid political and territorial change, yet largely preserves the established cartographic language and legend structure. Both the map field and the legend reveal a tension between the continuity of cartographic normality and the need to accommodate new political conditions.

Cartographic normality in this phase is characterized by explained plurality. The map does not merely record the presence of different actors in the landscape, but actively structures and interprets them through systematic naming and explicit legend-based categorization.

4.3 First standalone edition (undated, c. 1929)

The analysed map represents the earliest standalone edition of the examined series, published as Moravskoslezské Bezkydy – Hory Vsacké – Javorníky (c. 1929). Although no year of publication is stated, the map can be dated – on the basis of comparison with the second edition from 1931 and relevant cartographic and institutional features – to the late 1920s, probably shortly before that year.

It was published by the Pobezkydská District of the Czechoslovak Tourist Club in Moravian Ostrava, with cartographic processing associated with F. Karel and J. Pták. Its graphic design and legend structure correspond to the standardized conventions of interwar tourist cartography employed by the Club.

From the perspective of the present study, this edition is particularly significant for its fully developed and explicit categorization of tourist huts. The legend systematically distinguishes between private facilities and nationally defined huts – Czech, German, and Polish – treating national affiliation as a recognized and cartographically relevant form of information (Fig. 4A). Tourist huts thus function not merely as orientation points, but as carriers of cultural and identity-related meaning actively articulated through the map.

Together with its second, third, and fourth editions, this map constitutes a reference state of explained plurality, against which the later transformation observable from the fifth edition onward is comparatively assessed.

5. Phase III: Reduction of identity and functionalization of space (1940–1947)

Phase III marks a fundamental transformation of cartographic normality, in which the previously stabilized model of explained plurality begins to disintegrate. Although political changes after 1938 are reflected in the map image of the landscape, the decisive shift occurs primarily in the map legend and in the overall interpretative framework through which the landscape is represented.

In this phase, tourist maps gradually cease to function as instruments for articulating plurality and increasingly become tools for its reduction. The identity of tourist facilities is progressively stripped of its semantic dimension, and the cartographic representation of the landscape is reorganized around functional and administrative categories rather than explicitly articulated national or institutional distinctions.

5.1 The 1939 edition

The fifth revised edition of the map Moravskoslezské Beskydy – Javorníky – Vsacké Hory (1939) was produced in the immediate aftermath of the major

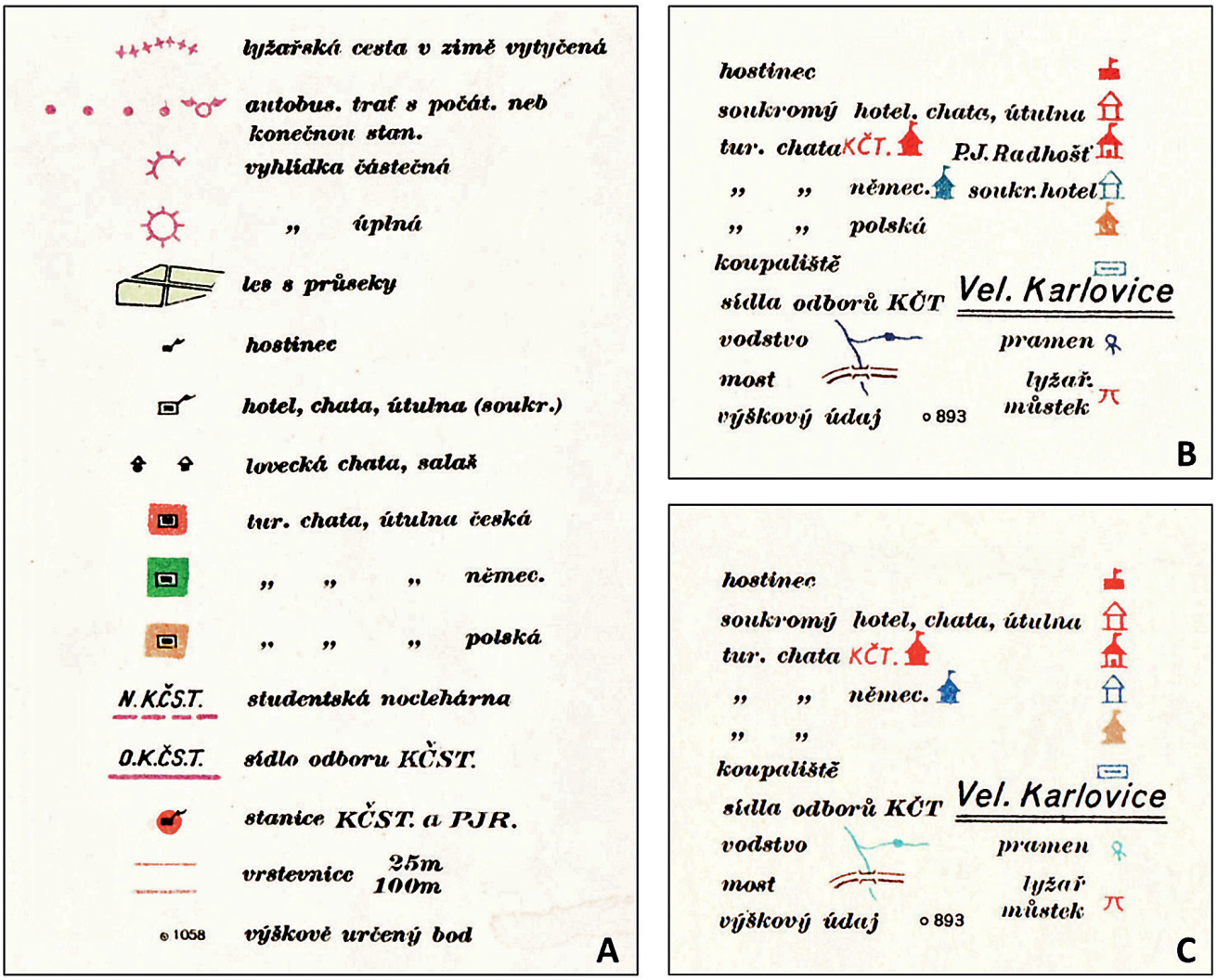

Fig. 4 Comparison of legend variants from successive editions of the KČST and KČT tourist map series produced under different political frameworks.
(A) First standalone edition of the series (c. 1929), issued in the stabilized interwar period.
(B) Fifth revised edition (1939), published after a major territorial reconfiguration of the region, yet still adhering to the established interwar system of legend-based national and institutional classification.
(C) Sixth revised edition (c. 1940), representing a further editorial revision under a newly consolidated political framework, in which selective categories are no longer explicitly explained in the legend.
The comparison illustrates the transformation of cartographic normality through changes in legend structure. While variants A and B maintain an articulated classification of tourist huts according to national and institutional affiliation, variant C marks a shift toward semantic reduction.
Source: Author's private collection.

political changes following the Munich Agreement. Despite this, its thematic legend and symbolic representation of tourist infrastructure largely preserve the cartographic normality established during the interwar period. The discrepancy between rapid political change and the relative stability of cartographic language makes this edition analytically significant.

It was published by the Pobeskydská branch of the Club of Czech Tourists, with cartographic processing by Jaroslav Pták. In the map field, newly established state boundaries are clearly depicted, and selected toponyms appear in modified linguistic forms.

From the perspective of the present study, this edition constitutes the culmination of pre-war cartographic normality. Both the map field and the legend continue to systematically distinguish tourist huts according to national and organizational affiliation. The legend explicitly retains categories of Czech, German, Polish, and private huts (Fig. 4B).

This categorization conveys semantic information about the plural structure of the tourist landscape, in which multiple organizations and traditions coexist. State boundaries, although present in the map image, do not yet function as the primary interpretative framework. Cartographic normality thus continues to operate as an articulated and explained plurality that has not yet undergone semantic reduction.

5.2 The 1940 edition

The sixth revised edition of the map Moravskoslezské Beskydy – Javorníky – Vsacké Hory (1940) marks

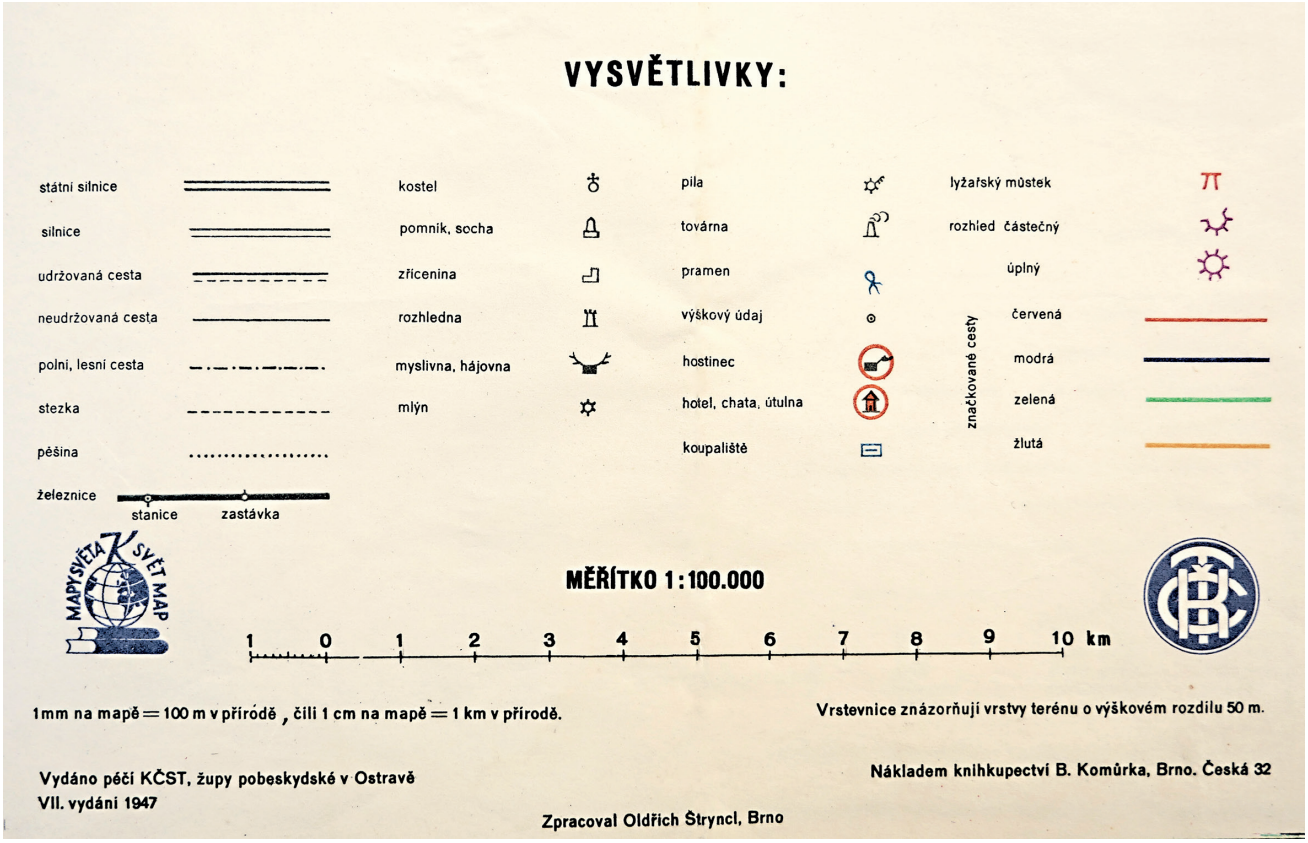

Fig. 5 Legend of the tourist map Beskydy, Javorníky, Vsacké Hory (seventh edition, 1947).
The legend employs a unified symbol for tourist huts and shelters, without any reference to national or institutional affiliation. This homogenization reflects the stabilization of a new cartographic normality in which the historically plural character of the region is no longer considered a relevant category of spatial representation.
Source: Author's private collection.

a transitional moment in the transformation of the analysed series. In contrast to the 1939 edition, the decisive change occurs not primarily in the map field, but in the conceptualization of the map legend.

Published by the Pobeskydská branch of the Club of Czech Tourists, with cartographic processing by Jaroslav Pták, the map gives increased prominence to newly established state borders, which begin to function as a primary organizing element of space.

A fundamental transformation takes place in the legend, where the category of Polish tourist huts is no longer explicitly listed, even though the corresponding symbols remain present in the map field (Fig. 4C). This does not constitute a physical erasure of objects from the map, but rather a form of semantic anonymization.

Cartographic normality thus shifts: national plurality is no longer treated as a recognized cartographic category, despite its continued presence in the landscape itself.

5.3 The 1947 edition

The final stage of the analysed series is represented by the seventh edition of the map Beskydy – Javorníky – Vsacké Hory (1947), published in Ostrava by the Club of Czechoslovak Tourists, Pobeskydská branch. It records the culmination of the transformation of cartographic normality within the post-war framework of Czechoslovakia. The linguistic layer of the map is fully unified, corresponding to broader post-war homogenizing tendencies in the territory.

In comparison with earlier editions, the analysed part of the map legend undergoes a fundamental transformation. National differentiation of tourist huts is no longer present – not only in the legend but also in the cartographic language associated with this category of objects (Fig. 5). Tourist huts and shelters are depicted using a single, uniform symbol, without any indication of former plurality.

This development does not represent a return to pre-war or pre-1918 cartographic neutrality. Rather, it marks the stabilization of a new cartographic normality in which the historically multi-layered character of the region is no longer treated as a relevant category of spatial representation.

6. Discussion: The transformation of cartographic normality

The analysis of tourist maps of the Teschen Beskids from the period 1905–1947 demonstrates that changes in cartographic normality cannot be interpreted

as a direct or mechanical consequence of shifts in state borders. More important than political ruptures themselves is the manner in which such changes were internalized into cartographic language and translated into the interpretative structure of the map. In this respect, the findings correspond with broader approaches in critical cartography that view maps as socially constructed representations rather than neutral mirrors of reality.

In the earliest phase, represented by the map from around 1905, plurality exists as an implicit and self-evident feature of the landscape. Tourist facilities are depicted and named, yet their identity is not systematically explained or categorized in the legend. This does not imply the absence of national or institutional identities, but rather that such distinctions were not yet considered cartographically relevant.

A fundamental shift occurs during the interwar period. After 1918, tourist cartography responded to the new institutional framework by expanding the legend and standardizing cartographic symbols. National and institutional affiliation became explicit and systematically articulated, giving rise to a phase of explained plurality in which the identity of objects was treated as meaningful information for the map user.

The editions from 1939 and 1940 mark a further transformation. While the map field reflects rapid political changes with considerable accuracy, the decisive shift takes place in the legend. In the 1940 edition, the explanatory reference to Polish tourist huts disappears, even though the symbols themselves remain present in the map field. This represents a key instance of semantic reduction: objects remain physically depicted, yet are deprived of explicit identity-related meaning. Whether this change resulted from deliberate editorial decisions or institutional constraints cannot be determined with certainty; what matters is the emergence of semantic silencing as a cartographic practice.

The post-war edition of 1947 carries this logic to its conclusion. National differentiation of tourist huts disappears, not as a return to pre-war neutrality, but as the stabilization of a new cartographic normality. The resulting political and national configuration of the landscape is presented as self-evident and no longer requires cartographic explanation. In this sense, the political dimension of the landscape does not vanish from the map; it becomes embedded in the taken-for-granted framework of representation.

The principal characteristics of the analysed maps and the transformations of cartographic normality across individual phases are summarized in Tab. 2.

Tab. 2 Overview of the analysed tourist maps of the Teschen Beskids and transformations of cartographic normality (1905–1947).

Year	Map title / series	Publisher	Editorial position	Political-historical context	Categorization of tourist huts in the legend	Character of cartographic normality
ca. 1905	Spezialkarte der Beskiden für Touristen	Private publisher	Pre-series reference map	Austro-Hungarian Monarchy	Tourist huts not defined as a separate legend category; huts named in the map field (e.g. Schutzhaus)	Implicit plurality; landscape as a memory space without explicit categorization
1928	Turistická mapa Bezkyd – map insert in a KČST tourist guide	KČST, Těšínská branch	Outside the main series	Interwar Czechoslovakia	Basic differentiation of huts; emerging concept of national categorization	Formation of categorization
ca. 1929	Moravskoslezské Bezkydy – Hory Vsacké – Javorníky	KČST, Pobezkydská branch	1st edition	Interwar Czechoslovakia (model established in 1929 and reproduced in subsequent editions)	Private, Czech, German, and Polish huts explicitly distinguished	Explicit and explained plurality (stabilized across editions 1–4)
1939	Moravskoslezské Beskydy – Javorníky – Vsacké Hory	KČT, Pobeskydská branch	5th edition	German Reich, Poland, and Protectorate of Bohemia and Moravia	Full set of national categories preserved	Plurality under political pressure
1940	Moravskoslezské Beskydy – Javorníky – Vsacké Hory	KČT, Pobeskydská branch	6th revised edition	German Reich and Protectorate of Bohemia and Moravia	Category of Polish huts removed from the legend; symbols remain in the map field	Selective semantic reduction
1947	Beskydy, Javorníky, Vsacké Hory	KČST/KČT, Pobeskydská branch	7th edition	Post-war Czechoslovakia	No national categorization of tourist huts	Homogenized cartographic normality

Note: The listed tourist associations do not represent exclusive or uniform operators of mountain huts. Before 1918, the Teschen Beskids and their wider surroundings were characterized by a parallel network of regional associations, corporate facilities, and tourist departments. In later tourist maps, this heterogeneous infrastructure was retrospectively nationalized through legend-based categorization or classified as private.

7. Conclusions

The analysis of tourist maps of the Teschen Beskids from the period 1905–1947 demonstrates that tourist cartography constitutes a valuable source for interpreting landscape. Political and social transformations are reflected in maps not only through changing borders or toponymy, but also through shifts in what is regarded as relevant, meaningful, and communicable within cartographic information.

A key analytical focus of this study is the map legend, where transformations of cartographic normality can be traced through the changing representation of tourist huts – from implicit plurality before 1918, through its systematic articulation during the interwar period, to its post-war semantic reduction. In this sense, maps do not merely mirror landscape change, but actively participate in stabilizing meaning and memory within specific historical contexts.

Processes sometimes interpreted as a depoliticization of cartographic representation may, in this case, be understood rather as a reconfiguration of politicization. Politics does not disappear from the map; instead, it becomes embedded in cartographic language and incorporated into an apparently self-evident framework of spatial interpretation.

The Teschen Beskids emerge as a particularly suitable model region for examining these dynamics. Their complex political history makes it possible to trace how the relationship between landscape, memory, and power was transformed in cartographic representation – from a memory-based space, through articulated plurality, to a homogenized political norm.

The transformation of cartographic normality also suggests that borders in maps need not be expressed solely as lines in physical space, but may also be constructed through categories treated as self-evident within cartographic language. The analytical approach presented here may therefore be applicable to other border regions of Central Europe and beyond.

References

Beskydy, Javorníky, Vsacké Hory [mapa, 1:100 000] (1947), 7. vyd.; Klub československých turistů, Pobeskydská župa: Ostrava.

Bína, J. (2012): Z nížin do hor. Geomorfologické jednotky České republiky; Academia: Praha, 343 p.

Bušek, B., Turoň, J. (1957): Těšínské Beskydy. Oblastní turistický průvodce 46; Sportovní a turistické nakladatelství: Praha, 132 p.

Galicz, J. (1931): Przewodnik po Beskidzie Śląskim, Cieszynie od Baraniej po Ostrawicę i Śląsku Cieszyńskim ze szczególnem uwzględnieniem miasta Cieszyna; Oddział Cieszyński Polskiego Towarzystwa Tatrzańskiego: Cieszyn, 256 p.

Hanslik, E. (1907): Kulturgrenze und Kulturzyklus in den polnischen Westbeskiden. Eine prinzipielle kulturgeographische Untersuchung; Justus Perthes: Gotha, 115 p.

Harley, J. B. (1989): Deconstructing the Map. Cartographica 26(2), 1–20, https://doi.org/10.3138/E635-7827-1757-9T53.

Herbatschek, A. (1922): Die tschechoslowakischen Beskiden und die Fatra. II. Band: Die Beskiden von Friedek bis Czacza und die Gebirgszüge von Czacza bis Rosenberg (Fatra); R. Papauschek: Mährisch-Ostrau, 164 p.

Machatschek, F. (1927): Landeskunde der Sudeten- und West-Karpatenländer; J. Engelhorns Verlag: Stuttgart, 440 p.

Mapa Beskidu = Beskidenkarte [mapa, 1:75 000] (ca. 1920); Sigmund Stuks: Cieszyn.

Moravskoslezské Beskydy – Javorníky – Vsacké Hory [mapa, 1:100 000] (ca. 1939), 5. přeprac. vyd.; Klub českých turistů, Pobeskydská župa: Moravská Ostrava.

Moravskoslezské Beskydy – Javorníky – Vsacké Hory [mapa, 1:100 000] (ca. 1940), 6. přeprac. vyd.; Klub českých turistů, Pobeskydská župa: Moravská Ostrava.

Moravskoslezské Bezkydy – Hory Vsacké – Javorníky [mapa, 1:100 000] (ca. 1929); Klub československých turistů.

Polášková, J., Polášek, J. (2009): Historie beskydské turistiky: Sto dvacet let organizované turistiky v Moravskoslezských Beskydech; Šmíra-Print: Ostrava, 253 p.

Riegler, K. (1928): Podrobný kapesní průvodce po Moravsko-Slezských Bezkydách s mapkou 1:150 000; Těšínská župa turistická KČST: Příbor, 395 p.

Sosna, W. (ed.) (2001): Śląsk Cieszyński: Środowisko naturalne, zarys dziejów, zarys kultury materialnej i duchowej; Macierz Ziemi Cieszyńskiej: Cieszyn, 419 p.

Spezialkarte der Beskiden für Touristen [mapa, 1:150 000] (ca. 1905); Siegmund Stuks: Teschen.

Woźniak, M. (2005): Niemieckie mapy turystyczne Karkonoszy do 1945 roku. Polski Przegląd Kartograficzny 37(2), 101–111.

Using georeferenced historical maps in support of archaeological research and urban planning

Giacomo Piazzini[1,*], Gabriele Bitelli[2], Giorgia Gatta[2]

[1] Ministry of Culture, Superintendency of Archaeology, Fine Arts and Landscape for the Provinces of Ancona and Pesaro-Urbino, Italy
[2] University of Bologna, Department of Civil, Chemical, Environmental and Materials Engineering (DICAM), Italy
* Corresponding author: giacomo.piazzini@cultura.gov.it

ABSTRACT

Historical cartography constitutes a rich source of information on ancient landscapes. When managed in digital form and accurately georeferenced, it becomes an invaluable tool for investigating the history and evolution of urban contexts. Within an archaeological framework, the multidisciplinary integration of georeferenced historical cartography and archaeological data in a Historical Geographic Information System (HGIS) offers significant advantages. One of the key strengths of historical cartography lies in its capacity to contextualise, within past environments, the archaeological evidence brought to light through investigations, thereby supporting archaeologists in identifying and interpreting elements of the ancient city. The present study aims to exemplify this application of historical maps, focusing on two recently investigated archaeological sites in Ancona, Italy. This city is characterised by a rich archaeological heritage, much of which remains buried and unexplored, resulting in a high likelihood of encountering archaeological assets during public or private works. The proposed methodology, applicable to a wide range of cases, proves to be valuable not only for enhancing archaeological knowledge of urban areas but also for supporting urban planning, urban regeneration, and risk management. Historical Geographic Information Systems, enriched with archaeological data, constitute essential tools for guiding urban development and selecting optimal locations for new structures and infrastructure.

KEYWORDS

archaeology; historical maps; geomatics; HGIS; urban planning

Received: 15 January 2026
Accepted: 17 May 2026
Published online: 29 May 2026

Piazzini, G., Bitelli, G., Gatta, G. (2026): Using georeferenced historical maps in support of archaeological research and urban planning. AUC Geographica 61(2), 309–321
https://doi.org/10.14712/23361980.2026.10
© 2026 The Authors. This is an open-access article distributed under the terms of the Creative Commons Attribution License (https://creativecommons.org/licenses/by/4.0).

1. Introduction

With ongoing urban growth and increasing land exploitation, comprehensive knowledge and monitoring of historical monuments, archaeological areas, and cultural heritage in general are fundamental requirements for cities. In this context, Geomatics plays an important role in detecting and monitoring heritage assets and remains, thereby facilitating more responsible urban development (Agapiou et al. 2015; Pappu et al. 2010; Roychowdhury et al. 2011).

To manage a territory effectively and plan its development, a thorough understanding of its history is essential. Among the various sources of historical knowledge, historical maps – now managed digitally through geomatic methods – are particularly valuable and effective where available. Cartographic heritage has a fundamental and universally recognised value, as it preserves historical and geographical data and often possesses artistic qualities. For these reasons, it must be preserved and made accessible, increasingly through digital means. The digital management and regeneration of ancient cartography represent valuable opportunities offered by Geomatics, which provides techniques not only to safeguard these precious documents from deterioration but also to enable innovative metric applications of the historical and geographical data they contain – applications that would not be possible using analogue media alone (Balletti 2000; Boutoura and Livieratos 2006; Bitelli et al. 2014; Livieratos 2006). Once digitised and appropriately processed, cartographic heritage becomes more accessible and usable, not only to experts (researchers, archivists, historians, archaeologists, technicians), but also to citizens, tourists, map enthusiasts, and the general public.

The metric regeneration of historical cartography is based on georeferencing, i.e., the process of assigning geographic coordinates to the digital image of an ancient document, usually within a modern reference system. A georeferenced digital map, therefore, possesses metric content and can be measured and directly compared with modern maps in a standard reference system. In this process, it must be considered that any map has a certain degree of error. This is especially true for historical cartography, which was produced using surveying methods and representation tools that were far less precise than those available today. Therefore, understanding the metric properties and assigning a reliability level to each map are essential for determining how accurately it represents a given area. An ancient map is invariably less precise than a modern one at the same scale, primarily due to errors arising from historical surveying techniques and instruments, the absence of rigorous geodetic-cartographic reference systems, and deformations of the map support material (Edney and Pedley 2019).

A particularly illustrative case is that of city maps, which began to appear in the sixteenth century. Initially, these were perspective representations with an oblique, non-zenithal viewpoint. From the eighteenth century onwards, higher viewpoints were gradually adopted, eventually becoming coincident with the zenith. By the mid-eighteenth century, zenithal maps had become the most common representations of cities and, due to their scientific and objective nature, the only accepted form in the nineteenth century. Eighteenth-century city maps are the first to provide reliable planimetric representations of urban areas and are fundamental sources for understanding the urban context of that period.

A valid and essential tool for reconstructing the history of cities and studying their evolution is the Geographic Information System (GIS) environment. Within a Historical GIS (HGIS), cartographic data from different historical periods, georeferenced within a common cartographic reference system, can be collected, managed, compared, and integrated with other data types (e.g., images, databases, texts), to perform change detection analyses or investigate specific topics across space and time. In recent years, numerous HGIS projects and studies have been developed, demonstrating the great potential of these tools for managing Cartographic Heritage (Balletti et al. 2020; Bitelli et al. 2019; Bitelli et al. 2016; Brovelli et al. 2016; Frazzica et al. 2015; Gatta et al. 2017; Gatta and Bitelli 2017; Gregory and Healey 2007; Larson 2003; Lundberg and Peterson 2005; Nobajas 2014; Schlichting 2008; Timár 2008; Wilson 2001). However, it is important to emphasise that only accurate georeferencing – often a challenging task, especially for very old maps – allows the extraction of quantitative data useful for further analyses, for example in urban archaeology or in support of future urban development.

1.1 Historical cartography and urban archaeology

The multidisciplinary integration of historical cartography and archaeological data offers significant benefits for historical and archaeological research. Historical cartography contains potentially unique data – otherwise lost or altered – regarding toponyms, natural features, buildings, and boundaries. Numerous studies have already highlighted the important contribution of historical maps to landscape archaeology (Green et al. 2019; Petrie et al. 2019; Cugno 2015; Dall'Aglio et al. 2002; Cambi and Terrenato 1994; Cataldo et al. 2005; Sperti et al. 2020).

However, the use of historical cartography in support of archaeological research does not always receive the attention it merits. This limited consideration is likely due to the dating of cartographic documents, which generally do not predate the sixteenth century. As a result, these sources are often associated with post-medieval archaeology, a field that still struggles to be regarded as equal to those related to other chronological periods. Evidence of this perspective, at least in Italy, is found in the frequent exclusion

of post-medieval data from archaeological maps (Milanese 2014; Augenti 2014).

In the specific case of urban archaeology, the object of study – the city – is often difficult to interpret. Human activities within a confined space have left overlapping traces, resulting in a highly complex stratification. It is precisely this difficulty in interpreting urban archaeological data that underscores the potential value of historical maps and the necessity of integrating them into research.

In addition to their relevance for the study of medieval and modern cities, historical maps can also aid in identifying elements of earlier urban phases, such as those from the Roman period. This is achievable by locating and describing features that have since disappeared but were still visible when the maps were produced, including natural elements and ancient structures.

For example, the project "Archeologia Urbana a Senigallia", conducted by the University of Bologna, made use of eighteenth-century maps originally produced to plan the diversion of the river that still flows into the city of Senigallia. Once georeferenced, these maps enabled the reconstruction of the river's course before the eighteenth-century modifications. The integration of this information within a GIS environment, together with extensive archaeological data, made it possible to hypothesise the course of the Roman city walls (De Donatis et al. 2012; Lepore et al. 2012).

Georeferencing a zenithal map of a city, particularly in the case of cadastral maps, enables the reconstruction of the historical urban layout with high geometric and dimensional accuracy. At a more detailed level, such georeferenced maps allow the contextualization of finds brought to light by archaeological investigations. The present research aims to demonstrate this latter type of application. By combining historical map processing techniques with archaeological data, this study attempts to facilitate meaningful integration between these sources.

The case study concerns the city of Ancona, Italy, where a rich archaeological heritage lies underground and remains largely unexplored (Piazzini 2017).

2. Materials

2.1 The city of Ancona and its historical cartography

Historiographical tradition dates the founding of Ancona to approximately 2,400 years ago. The port area and the historic city centre have constituted the core of urban life throughout this long period, without interruption (Fig. 1).

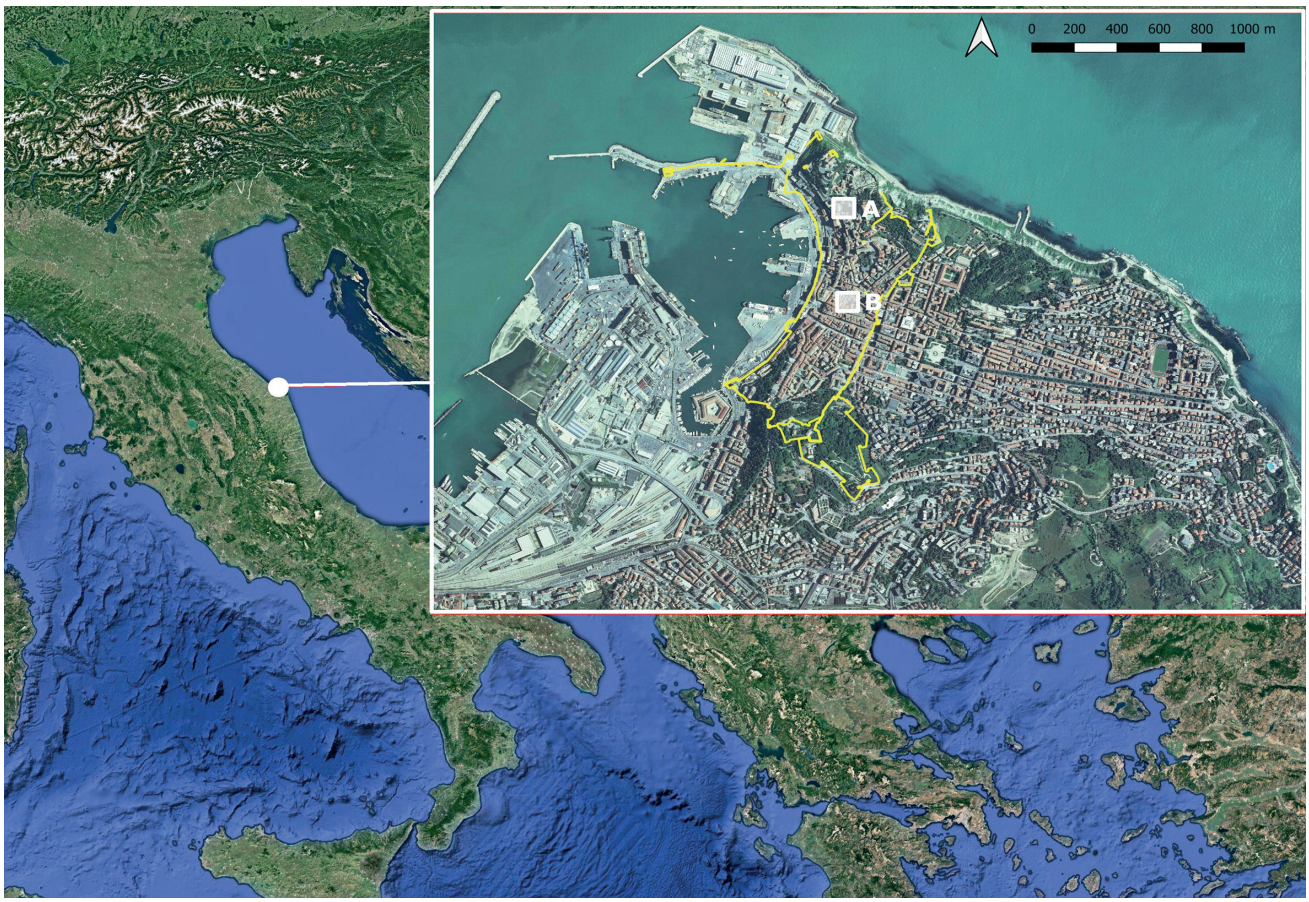

Fig. 1 Location of the city of Ancona (satellite photo from Google Earth) and fortifications – shown in yellow – that surrounded it in the early nineteenth century, with respect to the current city (1:2,000 scale orthophoto kindly provided by the Municipality of Ancona). The white box indicates the location of the two case studies: A (via Ferretti: 43.623464 N, 13.511098 E; Datum WGS 84) and B (via Buoncompagno: 43.619181 N,13.511452 E; Datum WGS 84).

Over the centuries, historical events and the city's evolving dynamics led to the near-total loss of ancient and early medieval archaeological evidence. From the tenth century onwards, a new urban layout gradually emerged. Despite the passage of time, large portions of the medieval city, together with its early modern expansions, remained visible at the beginning of the twentieth century. However, following urban renewal after the unification of Italy, the earthquakes of the twentieth century, and, above all, the bombings of the Second World War, most of the historic city – including the entire Port District – was destroyed. Several historical maps are available to scholars interested in the history of Ancona. In the present study, only maps with a zenithal view are considered.

The two oldest available maps date back to the sixteenth century. One is preserved at the State Archives of Turin; it is anonymous and undated. This map is currently under study, but, based on the buildings depicted, it is possible to propose a preliminary dating to the late 1560s–early 1570s. The second is a map of Ancona contained in the manuscript *Ms. 5463*, dated 1588 and held in the Vatican Apostolic Library in Rome.

No known cartographic documentation from the seventeenth century depicts the city of Ancona in a zenithal view. A similar situation exists for the eighteenth century, with only two known maps. The earliest, dated 1784, bears the signature of the architect Scipione Daretti. The second is the Plan de la Ville et du Port d'Ancone, included in M. de La Lande's Voyage en Italie (Tome Premier), published in 1786. Several graphic features suggest that the latter map derives from the former.

The nineteenth-century cartographic production of Ancona is both quantitatively and qualitatively significant. Two maps are particularly precise and detailed: the map of Ancona from the so-called Gregorian Cadastre (1813) and the *Topographical Map of the City of Ancona*, produced by the Department of Census of the Papal State in 1844. In 1852, the map *Plan der Stadt und Festung Ancona* was drawn up by the occupying Austrian authorities. Shortly afterwards, another map was published in Milan by Francesco Vallardi, likely dating from the 1870s.

The most recent urban developments before the Second World War are clearly visible in the 1937 map, the first to be produced from a photogrammetric aerial survey of the city.

2.2 Selected historical maps

Among the aforementioned maps, this study focuses on two documents that have provided the most

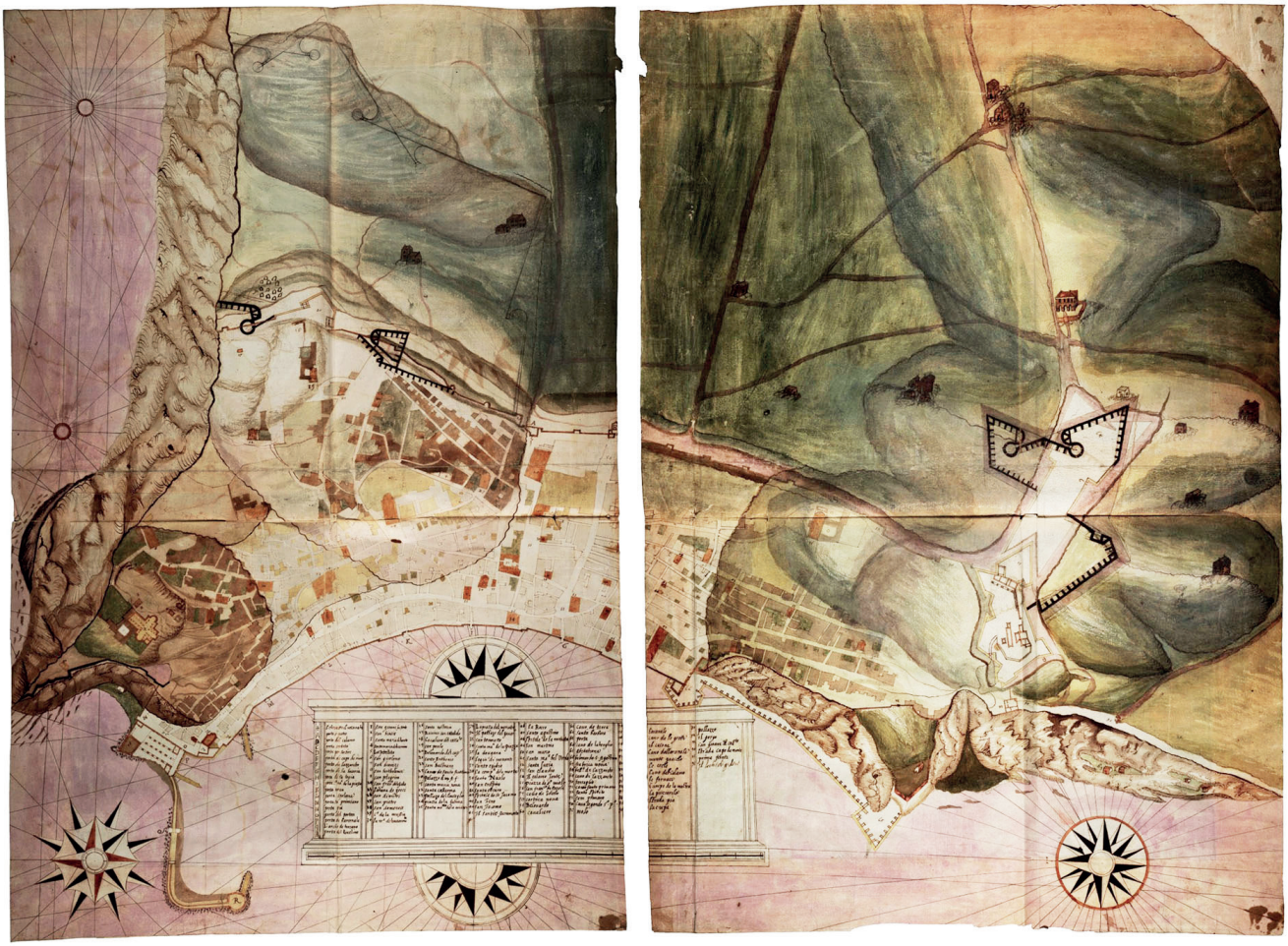

Fig. 2 Ancona: late 16th-century map in two parts.

significant insights for the research: the late sixteenth-century map and the Gregorian Cadastre (1813), selected to ensure an adequate chronological framework.

The first map is an anonymous sixteenth-century cartographic document (Fig. 2), which remains largely unknown in the scientific literature (see Menchetti 2007, fig. 5, p. 72, note 451). It is preserved in the State Archives of Turin (Collection "Architettura militare": Volume V, ff. 9v–10). The archive generally dates the map to the sixteenth century; however, based on an in-depth analysis currently underway, it is possible to estimate that it dates to the late 1560s–early 1570s.

The map measures 75 × 101 cm and was scanned by the State Archives of Turin at a resolution of 200 dpi; it is available at https://archiviodistatotorino.beniculturali.it/dbadd/visua.php?uad=189375.

There is no signature or dedication on the document; the only textual component is the legend, which consists of 96 numerical and 18 alphabetical references to public and religious buildings, as well as to the city's defensive structures. Courtyards, green spaces, and staircases are systematically represented. Despite the remarkable level of detail, the map is characterised by a significant degree of inaccuracy (mean error at check points: 8.6 m), which will be discussed in Section 3.1 (Tab. 1 and Fig. 7).

This is likely a "study" map, that is, a document used by architects to sketch their projects. Indeed, some ink drawings can be identified, representing fortification projects that were never realised. The map is composed of two sheets glued on a common support, unfortunately with the overlapping of one sheet on the other. For this reason, the two sheets were digitally separated. Once two distinct files were obtained, the sheets (Sheet A / Sheet B) were georeferenced independently. In the present case study, integration with archaeological data concerns Sheet A.

The second map, known as the Gregorian Cadastre, is a representation produced by the French administration in 1813, when Ancona was the capital of the Department of the Metauro in the Kingdom of Italy (Fig. 3).

The map measures 206 × 164 cm and was scanned by the State Archives of Rome at a resolution of 200 dpi. It is available at https://imagoarchiviodistatoroma.cultura.gov.it/Gregoriano/mappe.php.

Each cadastral parcel, identified by a number, is represented on the map by its perimeter and described in the cadastral registers by ownership, land use, and area (Fig. 4). The same applies to religious buildings, fortifications, and public spaces, which are indicated by alphabetical letters instead of numbers; urban gardens are systematically depicted

Fig. 3 Ancona: the Gregorian Cadastre, 1813.

in green. The map is drawn at a scale of 1:1,000. The representation includes only the land surface within the city walls at that time, while the description of the entire rural territory is provided on separate maps at a smaller scale.

2.3 Case studies

Two case studies are presented and discussed here as examples, referring to two significant archaeological areas. Both sites are located within the historic centre of Ancona. Investigations at these sites were conducted under the scientific direction of the *Soprintendenza Archeologia, Belle Arti e Paesaggio delle Marche*. The results of these investigations are still largely unpublished. At present, some of the findings from the Roman period have been briefly described in a publication concerning the urban development of Ancona in antiquity (Iacopini 2025a). As for the post-Roman archaeological evidence, only a preliminary excavation report has been published (Piazzini and Ciuccarelli 2022).

The first site is currently laid out as an open-air archaeological area, visible from outside a fence, and is situated along Via Ferretti, directly opposite the Archaeological Museum of the Marche Region. Archaeological investigations were conducted here between 2002 and 2004, when the area served as a car park. Immediately beneath the parking surface, the excavation revealed the pavement and several walls of a post-medieval building destroyed during the Second World War bombings (Fig. 5). After removing part of the pavement, the investigation proceeded into the underlying stratigraphic layers. These revealed remains of early medieval buildings, part of a late antique cemetery, sections of a colonnade, and a Roman-period road. The site is situated in an area of Ancona where many scholars have proposed the location of the Roman city's forum. For this reason, the discovery of the colonnade has led to the identification of the site as the "Roman forum of Ancona", a designation now widely used. The post-medieval building occupied the entire excavation area and extended beyond its limits. Numerous structural elements are associated with this building, including internal and perimeter walls, an entrance threshold, pillars, floors, drainage channels, a well, and a staircase leading to an underground cellar.

The second archaeological site is located in Via Buoncompagno. The remains discovered there are housed in the basement of the new wing of the Museum of the City of Ancona, owned by the municipality, and are visible through glass windows along the public street. The site was identified in 2001, during redevelopment works for the museum's expansion. Two main excavation campaigns were carried out in 2001

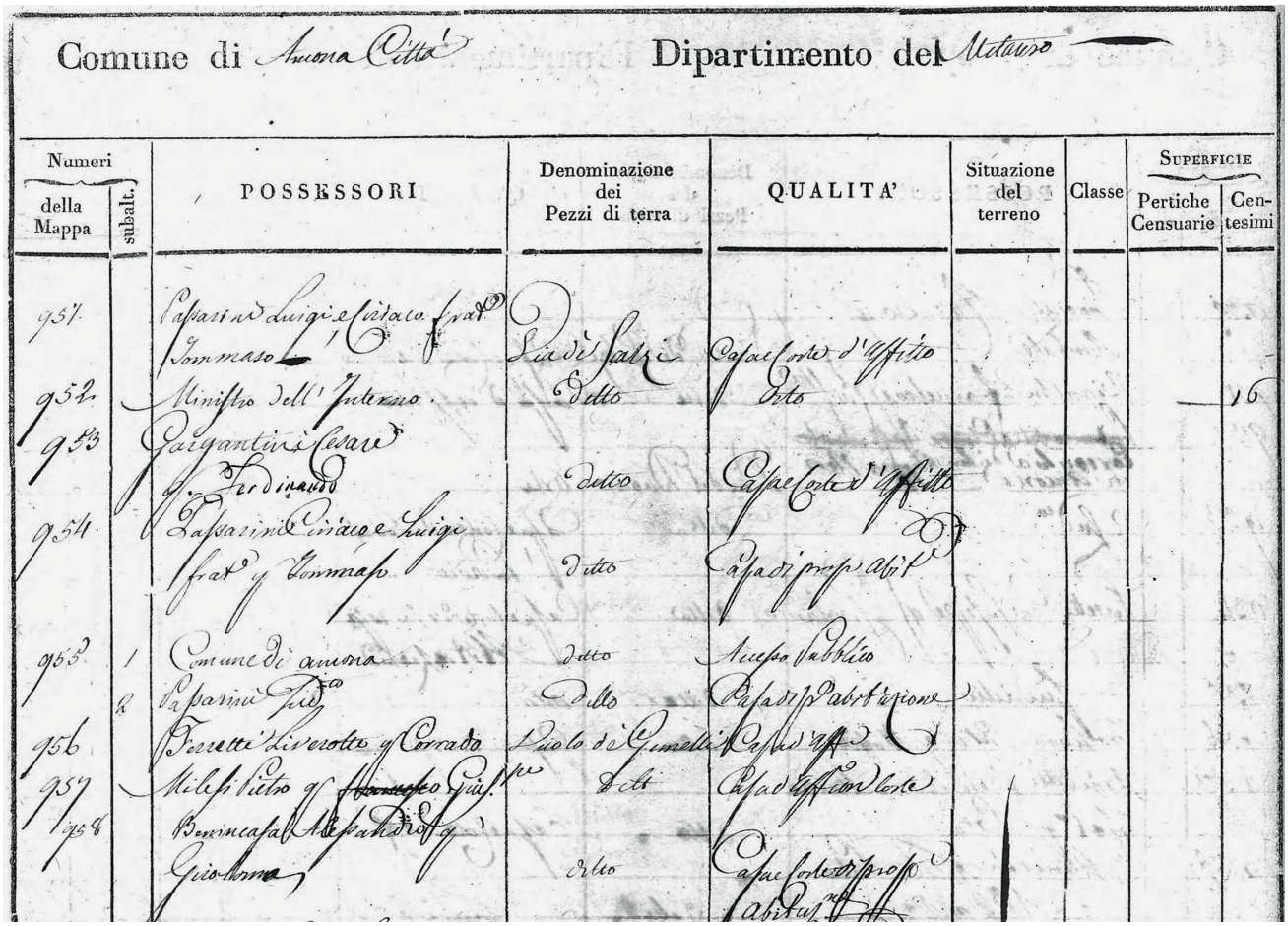

Fig. 4 An example of cadastral register, concerning the parcels of the site of Via Ferretti (Fig. 9).

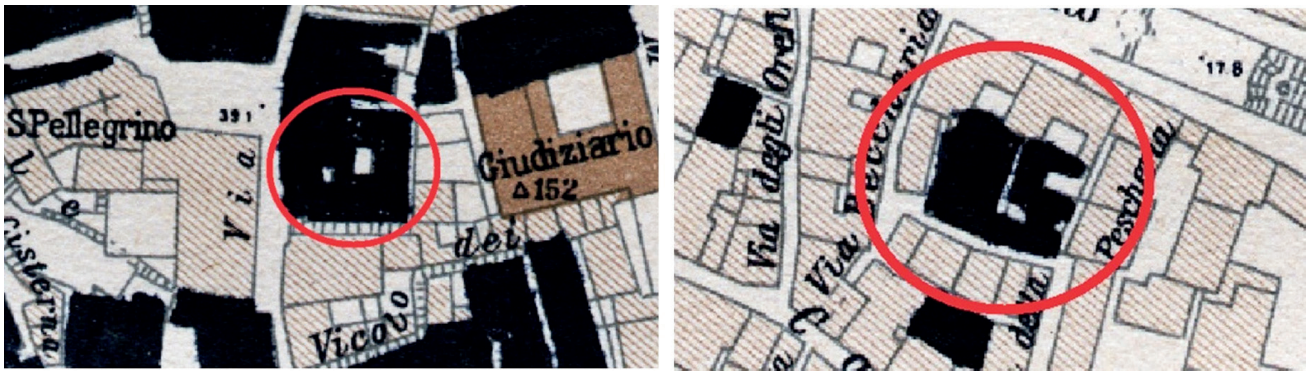

Fig. 5 Two details from the aerial-photogrammetric map of 1937, indicating (in black) the buildings struck by the bombings in 1943/44; the archaeological areas discussed in the text are highlighted by circles.

and 2009. The investigations revealed a stratigraphic sequence more than six metres deep, spanning from the Roman Republican period to the Modern Age. As for the earliest phase, only fragments of isolated walls were identified, whose function is difficult to determine. The phase, on the other hand, is better preserved and dates back to the Augustan Period. The walls of a *domus* were found, together with fragments of a mosaic floor. The early medieval layers are poorly preserved due to extensive later disturbances. For the late medieval and Modern Age phases, the excavations revealed a residential area of the city. For this phase, a building complex comprising at least seven rooms was identified. Outside the complex, the excavation uncovered a road, as well as the entrance threshold of another building. The structure remained in use over the centuries, undergoing minor modifications and renovations, until it was destroyed during the Second World War bombings (Fig. 5). A particularly noteworthy discovery is evidence of a fire that affected the entire area during the late medieval or early modern phase. This is indicated by a widespread layer of charcoal and ash (Fig. 6).

3. Methods

3.1 Georeferencing of historical maps

Georeferencing and the analysis of map deformations are based on the identification, in both historical and modern maps, of homologous points (Ground Control Points, GCPs) corresponding to features (primarily buildings, in the case of urban maps) that have remained unchanged over time and whose coordinates are known in the current cartographic reference

Fig. 6 Archaeological site of Via Buoncompagno: the layers of ash, coal, and rubble in the northern area, later used as a courtyard (photo SA AN 261480).

system. On the basis of these points – selected in large numbers and distributed as evenly as possible across the image – it is possible to calculate the parameters of the geometric transformation between the image coordinates of the historical map (in digital format) and the cartographic coordinates of the modern map. Using these parameters, during the resampling phase, cartographic coordinates are assigned to each pixel of the historical map.

The inevitable residuals observed for the GCPs are related both to the metric quality of the historical map and to the georeferencing process itself; therefore, they can be used as an indicator of map deformation. The spatial variation of these deformations can also be visualised directly on the map image using specialised software, based on the computation of local geometric transformations (Jenny and Hurni 2011).

In the present study, within a GIS environment, the two analysed maps were georeferenced in a modern reference system (UTM-ED50) using approximately one hundred Ground Control Points (GCPs), distributed as evenly as possible across the image. To facilitate the identification of GCPs between historical and modern maps (in this case, the digital Technical Map of the Municipality of Ancona), the georeferencing process was first performed on the more recent map (1813), using maps of intermediate age (from 1937 to 1844), then on maps of the eighteenth century, and finally on the late sixteenth-century map, using the same points whenever possible.

The selected points corresponded to building corners, which were verified to have remained unchanged over time. In addition to the GCPs, approximately twenty Check Points (CPs) were used for each map in order to obtain a more reliable estimation of the georeferencing residuals, as these points are not involved in the calculation of the transformation parameters. Table 1 presents the results of the residual analysis for both GCPs and CPs, obtained using second-order polynomial transformations.

Tab. 1 Statistical analysis on the georeferencing residuals using a 2nd order polynomial transformation.

	late 16th c. (Sheet A)		1813	
	GCPs	CPs	GCPs	CPs
Number of points	151	23	101	23
Mean error [m]	9.9	8.6	1.8	1.9
Standard deviation [m]	5.1	5.3	1.2	1.5
Root Mean Square error [m]	11.1	10.0	2.1	2.4

In Figure 7, the results of the map deformation analysis (based on the same GCPs used for georeferencing) are presented as obtained using the MapAnalyst software (Jenny and Hurni 2011). As expected, the variation in the scale factor is more limited in the nineteenth-century map, ranging from 1,040 to 1,070 (average 1,057) for the 1813 map, and from 1,850 to 2,200 (average 2,050) for the late sixteenth-century map.

3.2 Georeferencing and structuring of archaeological data

The graphical documentation produced during the archaeological campaigns conducted at the two sites was first digitized through scanning. As it had not been georeferenced at the time of the survey, it was necessary to perform this process using a set of clearly identifiable points recognised in the modern

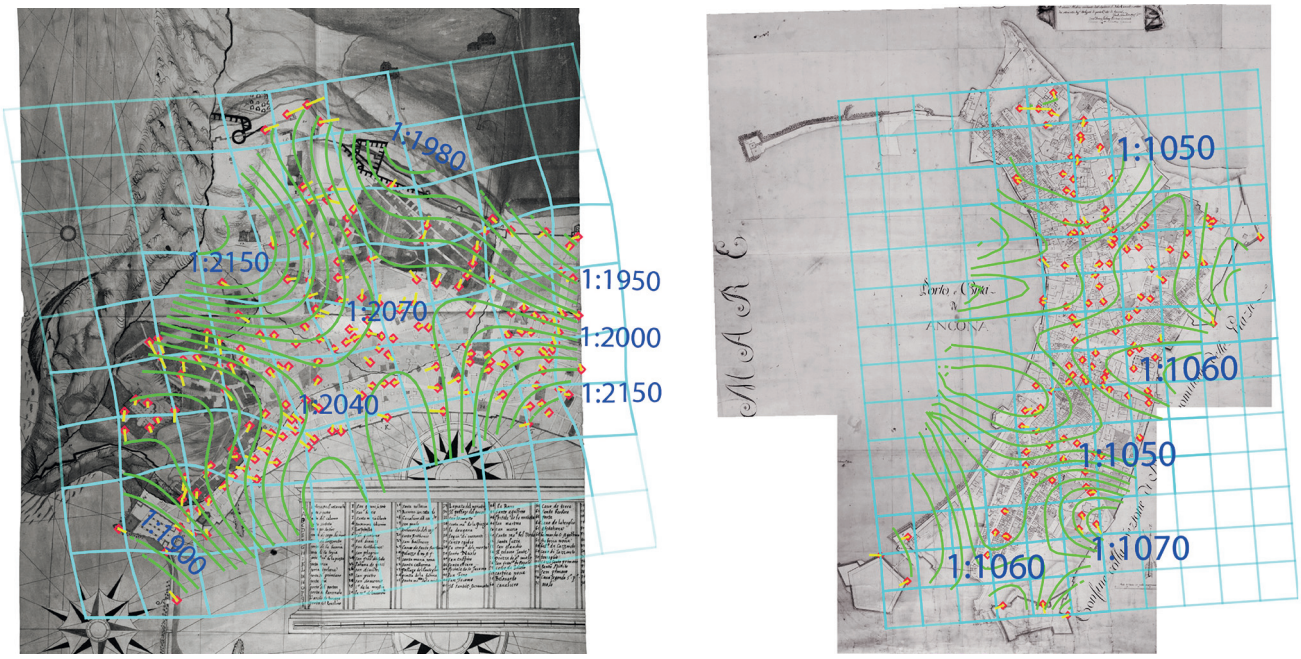

Fig. 7 Results from the analysis of deformations on the late sixteenth-century map (a) and the 1813 map (b): the cartographic grid with mesh = 100 m (exaggeration factor = 2 for the 1813 map) in light blue, the GCPs in red, the residual vectors in yellow (exaggeration factor = 2 for the late 16th century map and 5 for the 1813 map), the scale isolines in green (some values in blue).

cartography. For this purpose, certain cornerstones of the urban fabric surrounding the excavation areas were used. By matching these points with their homologous counterparts in the modern cartography, previously loaded into the GIS project, the plans were georeferenced using polynomial transformations.

This process enabled the subsequent vectorisation of the individual structures of interest. This phase required a careful analysis of the archaeological data and made it possible to organise the structures into different layers according to their chronological phases. Only structures dating to the late medieval or modern periods are likely to be identified in the historical maps.

4. Results and discussion

By superimposing the layers of the vectorised archaeological structures onto the two historical maps, it was possible to identify, in the latter, the late medieval and modern buildings uncovered during the excavations.

At both archaeological sites (Figs. 8–11), the overlap with the Gregorian Cadastre allows for the almost exact identification of several walls documented during the excavations. This enabled the distinction of perimeter walls, internal partitions, and boundary walls separating adjacent buildings among the structures identified.

Moreover, an important result for the interpretation of the excavation data was achieved: the reconstruction of the continuation of walls beyond the limits of the investigated areas. In the case of Via Buoncompagno, in particular, it is now possible to define the extent of the buildings identified through excavation beneath the current roadway and to assess the risk of encountering their remains during future works (e.g., the installation of underground utilities).

A further result is the possibility of assigning functional classifications and ownership information to modern buildings, based on the records attached to the cadastral documentation.

At both archaeological sites, the overlap between the two maps allows the recognition of the same buildings, which appear to have persisted over the centuries while undergoing specific modifications.

One example is the internal courtyard of the building identified in the Via Ferretti excavations. This courtyard presents a markedly different layout in the two maps. It can be inferred that its function as an internal courtyard remained unchanged, but that building modifications took place between the late sixteenth century and 1813.

Fig. 8 Archaeological site of Via Ferretti (for the localisation within Ancona, see figure 1, box A): detail of the superimposition of the late and post medieval findings on the current satellite view (left) and on the current digital Municipal Map 1:2,000 (right).

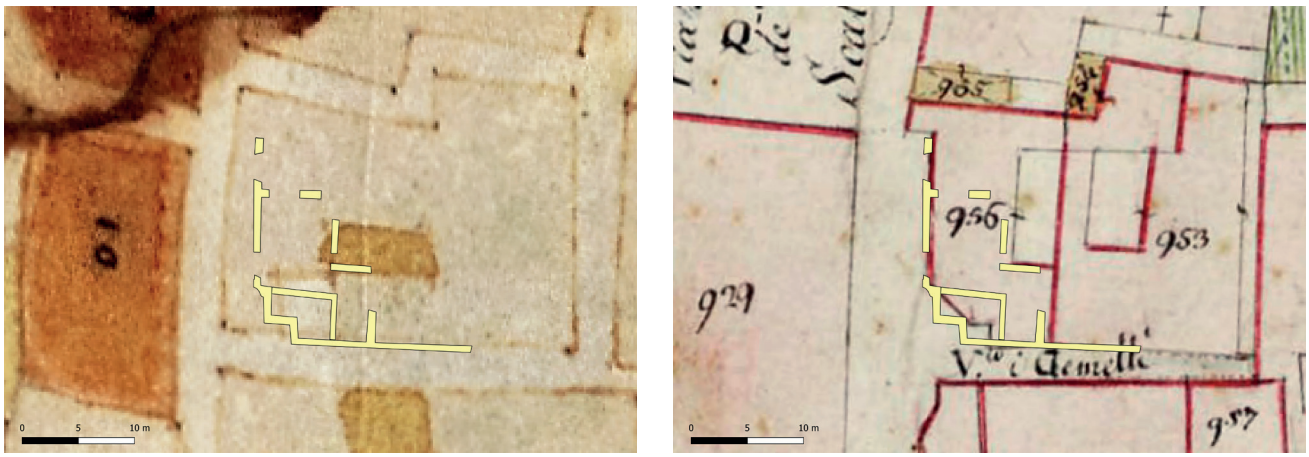

Fig. 9 Archaeological site of Via Ferretti: detail of the superimposition of the late and post-medieval findings on the late 16th century map (left) and on the map of 1813 (right).

Fig. 10 Archaeological area of Via Buoncompagno (for the localisation within Ancona, see figure 1, box B): detail of the superimposition of the late and post-medieval findings on the current satellite view (left) and on the current digital Municipal Map 1:2,000 (right).

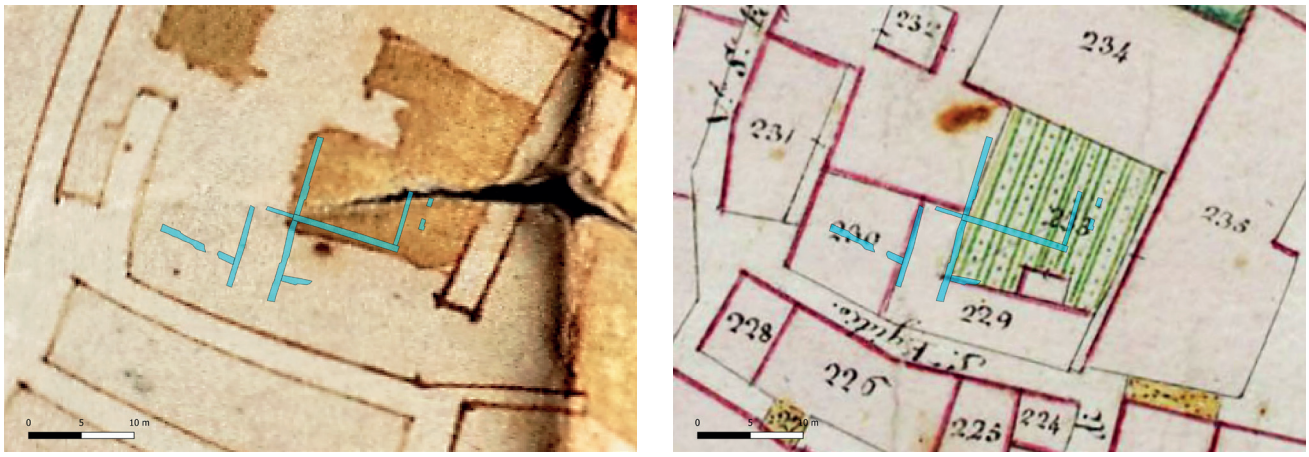

Fig. 11 Archaeological area of Via Buoncompagno: detail of the superimposition of the late and post medieval findings on the late sixteenth century map (left) and on the map of 1813 (right).

Another difference between the two maps concerning the Via Ferretti site relates to the configuration of the main façade. Written sources provide evidence of a renovation that likely set back the façade during the second half of the eighteenth century (Giochi and Mordenti 2005).

Concerning the Via Buoncompagno excavation, the superimposition of the two maps onto the archaeological plan reveals a discrepancy in the position of the southern boundary of the courtyard. This boundary corresponds to two different archaeological structures in the two maps. The southward shift may be attributed either to georeferencing residual errors associated with the sixteenth-century map or, alternatively, to the demolition of part of the building and the consequent expansion of the courtyard over the approximately two and a half centuries separating the two maps.

At the same site, the archaeological excavation revealed evidence of a major fire that affected the entire area. One of the damaged buildings, unlike the others, does not appear to have been subsequently restored. The debris was not removed, and the space was transformed into a courtyard. In this case, historical cartography proves useful for dating the fire. Indeed, this event must predate the creation of the late sixteenth-century map, as the courtyard is already clearly represented in it. The map therefore provides a *terminus ante quem* for the fire, most likely around 1567. The destruction identified during the excavation may thus be related to one of the most catastrophic events in the history of Ancona: the fire of 1348 (Pavia and Sori 1990).

5. Conclusions

The present study aimed to evaluate the contribution of historical cartography, once properly georeferenced, to the interpretation of archaeological evidence in an urban context.

The georeferencing of historical maps, when carried out accurately, enables their precise superimposition with both modern and archaeological cartography, allowing for rapid and effective comparison of spatial data. Working within an HGIS environment is particularly advantageous for this type of analysis, as it facilitates the visualisation of the spatial distribution of features represented in historical maps, as well as the detection and measurement of changes over time.

In the case of a city such as Ancona, characterised by a high density of pre-existing structures and a complex stratigraphic sequence, this approach proves particularly valuable. Through comparison with historical maps, it has been possible to assign precise qualitative and chronological attributes – previously unknown – to the archaeological structures analysed in this study.

The reconstruction of the spatial distribution of past urban features offers both cultural and practical benefits. From a research perspective, it contributes to a better understanding of the city's historical development and enhances the interpretation of archaeological data. From an urban planning perspective, the proposed method is highly effective for preservation and valorisation purposes. The ability to anticipate what may be uncovered during new interventions supports more informed planning decisions, improving both the protection of archaeological remains and their integration into urban regeneration processes.

The work presented here represents the initial stage of a broader research process aimed at developing a multifunctional tool. Further development in this direction would represent a significant advancement for cities such as Ancona, where the interpretation of archaeological data is hindered by their complexity and by the limited number of dedicated studies. It is worth noting that, in recent years, the methodology and HGIS project described here have already demonstrated their practical usefulness in Ancona, having been applied in the preparation of archaeological risk reports for various urban renewal projects (including squares, stairways, streets, buildings, and courtyards).

A recent project by the Soprintendenza Archeologia, Belle Arti e Paesaggio delle Marche and the University of Bologna enabled the mapping of all archaeological evidence currently known in the city of Ancona (Iacopini 2025b). This led to the creation and publication of the web-GIS "Archaeological Map of Ancona" (https://archeoancona.cultura.gov.it/). The data generated by this project have already been used for interpretative analyses of the pre-Roman and Roman city (Iacopini 2025a). However, the study of the city's subsequent evolution during the medieval and post-medieval periods, in light of these new data, remains to be completed. In this context, the use of georeferenced historical maps, following the methodology proposed here, appears both essential and highly promising.

Acknowledgements

This article is based on research conducted within the School of Specialization in Archaeological Heritage at the University of Bologna, and in particular on G. Piazzini's specialisation thesis in Surveying and Cartography, entitled "Digging into Maps: Digital Processing of Historical Maps for the Urban Archaeology of Ancona", supervised by the co-authors.

The authors would like to thank the Soprintendenza Archeologia, Belle Arti e Paesaggio delle Marche for providing access to unpublished data from the archaeological excavations cited in the text, and the State Archives of Rome and Turin for granting access to high-resolution digital copies of the historical maps used in this research.

References

Agapiou, A., Dimitrios, D. A., Vasiliki, L., Apostolos, S., Branka, C., Kyriacos, T., Diofantos, G. H. (2015): Impact of urban sprawl to cultural heritage monuments: The case study of Paphos area in Cyprus. Journal of Cultural Heritage 16(5), 671–680, https://doi.org/10.1016/j.culher.2014.12.006.

Augenti, A. (2014): Archeologia della città medievale. In Gelichi, S. (Ed.), Quarant'anni di Archeologia Medievale in Italia. La rivista, i temi, la teoria e i metodi; All'Insegna del Giglio: Firenze, Italy, pp. 173–182.

Balletti, C. (2000): Analytical and Quantitative Methods for the Analysis of the Geometrical Content of Historical Cartography. International Archives of Photogrammetry and Remote Sensing XXXIII(B5), 30–37. Available online: https://www.isprs.org/proceedings/xxxiii/congress/part5/30_XXXIII-part5.pdf (accessed on 20 September 2025).

Balletti, C., Galeazzo, L., Gottardi, C., Massaro, M., Vernier, P. (2020): From historical maps to digital technologies: the visualisation of the Venetian Ghetto's history. e-Perimetron 15(3), 155–167. Available online: http://www.e-perimetron.org/Vol_15_3/Balletti_et_al.pdf (accessed on 20 September 2025).

Bitelli, G., Bartolini, F., Gatta, G. (2016): HGIS and Archive Researches: A Tool for the Study of the Ancient Mill Channel of Cesena (Italy). The International Archives of the Photogrammetry, Remote Sensing and Spatial Information Sciences XLI-B5, 183–189, https://doi.org/10.5194/isprs-archives-XLI-B5-183-2016.

Bitelli, G., Cremonini, S., Gatta, G. (2014): Cartographic Heritage: Toward unconventional methods for quantitative analysis of pre-geodetic maps. Journal of Cultural Heritage 15(2), 183–195, https://doi.org/10.1016/j.culher.2013.04.003.

Bitelli, G., Gatta, G., Guccini, A. M., Zaffagnini, A. (2019): GIS and Geomatics for archive documentation of an architectural project: The case of the big Arc of entrance to the Vittorio Emanuele II Gallery of Milan, by Giuseppe Mengoni (1877). Journal of Cultural Heritage (38), 204–212, https://doi.org/10.1016/j.culher.2019.01.002.

Boutoura, C., Livieratos, E. (2006): Some fundamentals for the study of the geometry of early maps by comparative methods. e-Perimetron 1(1), 60–70. Available online: http://www.e-perimetron.org/Vol_1_1/Boutoura_Livieratos/1_1_Boutoura_Livieratos.pdf (accessed on 20 September 2025).

Brovelli, M. A., Kilsedar, C. E., Minghini, M., Oxoli, D. (2016): GIS-based analysis of a peculiar effect of urbanization: the case of the buried watercourses of Como (Italy).

Applied Geomatics 8, 91–105, https://doi.org/10.1007/s12518-016-0169-4.
Cambi, F., Terrenato, N. (1994): Introduzione all'archeologia dei paesaggi; Nuova Italia Scientifica: Roma, Italy, 313 p.
Cataldo, R., De Donno, A., De Nunzio, G., Leucci, G., Nuzzo, L., Siviero, S. (2005): Integrated methods for analysis of deterioration of cultural heritage the Crypt of Cattedrale di Otranto. Journal of Cultural Heritage 6(1), 29–38, https://doi.org/10.1016/j.culher.2004.05.004.
Cugno, S. A. (2015): Landscape archaeology and historical cartography: A contribution to the study of ancient and medieval settlement in Canicattini Bagni (Syracuse). In Benedetto, B., Farrugia, C., Romiti, B., Sipos, A. (Eds.), Cartography and Cadastral Maps. Visions from the Past, for a Vision of Our Future; Edizioni della Normale: Pisa, Italy, pp. 111–120.
Dall'Aglio, P. L., Di Cocco, I., Marchetti, G. (2002): La cartografia storica per la ricostruzione del paesaggio antico: Alcuni casi dell'Italia Padana. In Proceedings of the VI Conferenza Nazionale ASITA; Perugia, Italy, pp. 55–60.
De Donatis, M., Lepore, G., Susini, S., Silani, M., Boschi, F., Savelli, D. (2012): Sistemi informativi geografici e modellazione tridimensionale per la geo-archeologia a Senigallia: Nuove scoperte e nuove ipotesi. Rendiconti Online della Società Geologica Italiana 19, 16–19.
Edney, M. H., Sponberg Pedley, M. (2019): The History of Cartography. Volume 4: Cartography in the European Enlightenment; University of Chicago Press: Chicago and London, https://doi.org/10.7208/chicago/9780226339221.001.0001.
Frazzica, V., Galletti, F., Orciani, M. (2015): Gregoriano Cadastre: The Creation of a WebGIS from Historical Cartography through the Techniques of Classification of Satellite Images. e-Perimetron 10(2), 60–72. Available online: https://www.e-perimetron.org/Vol_10_2/Frazzica%20et%20al.pdf (accessed on 20 September 2025).
Gatta, G., Bitelli G. (2017): A historical GIS for the comparison of past and present views: Bologna, yesterday and today. e-Perimetron 12(3), 102–108. Available online: https://www.e-perimetron.org/Vol_12_3/Gatta_Bitelli.pdf (accessed on 2 November 2025).
Gatta, G., Arioti, E., Bitelli, G. (2017): Geomatics science applied to cartographic heritage and archive sources: A new way to explore the XIX century Gregorian Cadastre of Bologna (Italy), an ante-litteram 3D GIS. Journal of Cultural Heritage 23, 68–76, https://doi.org/10.1016/j.culher.2016.06.009.
Giochi, F. M., Mordenti, A. (2005): Civiltà anconitana. Vita quotidiana ad Ancona tra XVI e XVIII secolo: Palazzi, feste, modi di vestire, di arredare e di mangiare di una città adriatica; Il Lavoro Editoriale: Ancona, Italy, pp. 61–66.
Green, A. S., Orengo, H. A., Alam, A., Garcia-Molsosa, A., Green, L. M., Conesa, F., Ranjan, A., Singh, R. N., Petrie, C. A. (2019): Re-Discovering Ancient Landscapes: Archaeological Survey of Mound Features from Historical Maps in Northwest India and Implications for Investigating the Large-Scale Distribution of Cultural Heritage Sites in South Asia. Remote Sensing 11(18): 2089, https://doi.org/10.3390/rs11182089.
Gregory, I. N., Healey, R. G. (2007): Historical GIS: structuring, mapping and analysing geographies of the past. Progress in Human Geography 31(5), 638–653, https://doi.org/10.1177/0309132507081495.
Iacopini, E. (2025a): L'urbanistica di Ancona; Edizioni Quasar: Roma, Italy, 228 p., https://doi.org/10.48235/1219.
Iacopini, E. (2025b): The Archaeological Map of Ancona: new IT tools. Groma: Documenting Archaeology 9(1), 142–150, https://doi.org/10.32028/Groma-Issue-9-2024-3247.
Jenny, B., Hurni, L. (2011): Studying cartographic heritage: Analysis and visualization of geometric distortions. Computers & Graphics 35(2), 402–411, https://doi.org/10.1016/j.cag.2011.01.005.
Larson, R. R. (2003): Placing cultural events and documents in space and time. In Duckham, M., Goodchild, M. F., Worboys, M. (Eds.), Foundations of Geographic Information Science; Taylor & Francis: London, UK, pp. 223–239, https://doi.org/10.1201/9780203009543.ch12.
Lepore, G., Ciuccarelli, M. R., Assenti, G., Belfiori, F., Boschi, F., Carra, M. L., Casci Ceccacci, T., De Donatis, M., Maini, E., Ravaioli, E., Savelli, D., Silani, M., Visani, F. (2012): Progetto "Archeologia Urbana a Senigallia" I: le ricerche di Via Cavallotti. FOLD&R 248, 1–19.
Livieratos, E. (2006): On the Study of the Geometric Properties of Historical Cartographic Representations. Cartographica 41(2), 165–175, https://doi.org/10.3138/RM86-3872-8942-61P4.
Lundberg, C., Peterson, L. (2005): Land use history of central Luleå: a case study in the use of historical maps together with modern geographic municipal information. Applied GIS 1(3), 25.1–25.30, https://doi.org/10.2104/ag050025.
Menchetti, F. (2007): Note sui progetti di Francesco Paciotto per le fortificazioni e i lazzaretti di Ancona. In Viglino, M., Bruno, A. (Eds.), Gli ingegneri militari attivi nelle terre dei Savoia e nel Piemonte orientale (XVI–XVIII secolo); EDIFIR: Firenze, Italy, pp. 65–80.
Milanese, M. (2014): Dall'archeologia postclassica all'archeologia postmedievale. Temi e problemi, vecchie e nuove tendenze. In Gelichi, S. (Ed.), Quarant'anni di Archeologia Medievale in Italia. La rivista, i temi, la teoria e i metodi; All'Insegna del Giglio: Firenze, Italy, pp. 41–49.
Nobajas, A. (2014): Historical cartography as a tool to study urban change: the case of Garriga i Roca's quarterons. Treballs de la Societat Catalana de Geografia 77, 205–220.
Pavia, R., Sori, E. (1990): Le città nella storia d'Italia: Ancona; Laterza: Roma, Italy.
Pappu, S., Akhilesh, K., Ravindranath, S., Raj, U. (2010): Applications of satellite remote sensing for research and heritage management in Indian prehistory. Journal of Archaeological Science 37(9), 2316–2331, https://doi.org/10.1016/j.jas.2010.04.005.
Petrie, C. A., Orengo, H. A., Green, A. S., Walker, J. R., Garcia, A., Conesa, F., Knox, J. R., Singh, R. N. (2019): Mapping archaeology while mapping an empire: using historical maps to reconstruct ancient settlement landscapes in modern India and Pakistan. Geosciences 9(1), 11, https://doi.org/10.3390/geosciences9010011.

Piazzini, G. (2017): Digging into Maps: Digital Processing of Historical Maps for the Urban Archaeology of Ancona. Unpublished thesis, University of Bologna, School of Specialization in Archaeological Heritage, Bologna, Italy.

Piazzini, G., Ciuccarelli, M. R. (2022): Ancona. Archeologia urbana: i rinvenimenti postmedievali in Via Buoncompagno. Archeologia Postmedievale. Società, Ambiente, Produzione 26, 300–302.

Roychowdhury, K., Taubenböck, H., Jones, S. (2011): Delineating urban, suburban and rural areas using Landsat and DMSP-OLS night-time images. In Joint Urban Remote Sensing Event (JURSE 2011); Munich, Germany, pp. 33–36, https://doi.org/10.1109/JURSE.2011.5764712.

Schlichting, K. (2008): Historical GIS: new ways of doing history. Historical Methods 41(4), 191–196, https://doi.org/10.3200/HMTS.41.4.191-196.

Sperti, L., Cipriano, S., Paveggio, A., Delpozzo, E. (2020): Altinum: discovering a hidden municipium through GIS, historical research and new excavations. e-Perimetron 15(3), 114–129.

Timár, G., Székely, B., Molnár, G., Ferencz, C., Kern, A., Galambos, C., Gercsák, G., Zentai, L. (2008): Combination of historical maps and satellite images of the Banat region: re-appearance of an old wetland area. Global and Planetary Change 62(1–2), 29–38, https://doi.org/10.1016/j.gloplacha.2007.11.002.

Wilson, A. (2001): Sydney Timemap: Integrating Historical Resources Using Gis. Journal of the Association for History and Computing 13(1), 45–68, https://doi.org/10.3366/hac.2001.13.1.45.

Factors affecting school attendance in Buikwe district, Uganda

Jaromír Harmáček[1], Barbora Frličková[1], Eliška Škůrková[1], Jan Macháček[2], Martin Schlossarek[1,*]

[1] Palacký University, Department of Development and Environmental Studies, Czechia
[2] University of Ostrava, Department of Human Geography and Regional Development, Czechia
[*] Corresponding author: martin.schlossarek@upol.cz

ABSTRACT

Understanding the factors affecting school attendance is crucial for developing effective educational policies and interventions, particularly in regions with high absenteeism rates. This article focuses on explaining the factors affecting regular school attendance in the Buikwe district in Uganda. The primary data for this research were collected based on a questionnaire survey in three primary schools in the district. The sample included 480 participants, covering the period from February to September 2018. Using the Poisson regression technique, the analysis focused on factors affecting the pupils' number of absences per month (M = 1.54 days of absences, SD = 2.45 days). The results suggest that there are at least three factors with strong effects on the number of absences. First, it is clearly shown that children from female-led families have significantly lower absences. Second, children from incomplete families with one or both parents missing have significantly higher absences. And third, children receiving support through various sponsorship programs attend school more often. The results also confirm the trade-off between school attendance and paid child labor as well as the fact that education of parents (mothers) plays a role in school absenteeism of children.

KEYWORDS

school attendance; education; regression analysis; Buikwe; Uganda

Received: 10 November 2025
Accepted: 14 June 2026
Published online: 14 July 2026

Harmáček, J., Frličková, B., Škůrková, E., Macháček, J., Schlossarek, M. (2026): Factors affecting school attendance in Buikwe district, Uganda. AUC Geographica 61(2), 322–336
https://doi.org/10.14712/23361980.2026.11
© 2026 The Authors. This is an open-access article distributed under the terms of the Creative Commons Attribution License (https://creativecommons.org/licenses/by/4.0).

1. Introduction

Despite the key role of education as a prerequisite for development, 59 million children are not enrolled in schools – more than a half from Sub-Saharan Africa (UNESCO 2020). However, enrolment alone does not guarantee effective participation in education. Many children who are formally enrolled experience substantial absenteeism, which limits learning outcomes and the accumulation of human capital. In developing regions in particular, understanding the determinants of school attendance is crucial, as absenteeism may signal structural barriers such as economic constraints, household vulnerability, or limited access to school infrastructure. Identifying these factors is therefore essential for designing targeted interventions aimed at improving regular school participation and reducing the risk of dropout.

School absenteeism is shaped by a range of interrelated factors. Documented determinants include chronic illnesses and mental health conditions (Cook et al. 2017; Allen et al. 2018), characteristics of the school environment (Van Eck et al. 2017; Lenhoff and Pogodzinski 2018), and family-related factors such as inconsistent parenting or limited parental involvement (Sugrue et al. 2016). Economic disadvantage also represents a significant barrier to regular attendance, while limited peer engagement and certain individual characteristics may further exacerbate absenteeism (Allen et al. 2018; Gottfried and Kirksey 2017; Psyridou et al. 2024).

Persistent absenteeism is associated with lower academic performance and weaker long-term educational trajectories (Gottfried and Kirksey 2017; Gottfried 2019), as well as poorer social functioning (Gottfried 2014). Although various interventions have been developed and, in some cases, rigorously evaluated (Cook et al. 2017; Wang et al. 2017), most empirical evidence on the determinants and consequences of absenteeism originates from developed-country contexts.

This paper analyses the determinants of school absenteeism in the Buikwe District, Uganda. Using primary micro-level data, where the focus is on pupils of several local primary schools, it examines the association between living standards (captured through an asset index), socio-demographic characteristics, family background, and children's absenteeism, measured as the number of recorded absences. Additional factors, including distance to school, are also considered.

The main research question guiding this study is: which household-, socio-demographic, and contextual factors are associated with variation in school absenteeism in rural Uganda?

By focusing on absenteeism in rural Uganda, the study contributes empirical evidence from an under-researched setting, where most existing findings are derived from high-income countries. Rather than assuming universal determinants, it assesses whether commonly identified factors – such as economic disadvantage or family characteristics – also explain attendance patterns in this specific socio-economic context. The results therefore provide context-specific evidence relevant for understanding barriers to regular school participation.

The rest of the paper is organized as follows. The next section reviews the literature on determinants of school attendance. Section three presents the data and methodology. Section four reports the results, followed by a discussion. The final section concludes.

2. Literature review

The government of Uganda considers education as an essential human right and one of the basic tools to reduce poverty. It is guaranteed in the Constitution of the Republic of Uganda, more specifically in Articles 30 and 34. Uganda's formal educational system has been modified many times since independence. The Universal Primary Education (UPE) program, launched in 1997, represents Uganda's key policy initiative to provide free primary education and improve equitable access. It aims to reduce disparities and promote gender parity as part of broader poverty reduction and human development efforts (Bategeka and Okurut 2006; Harmáček et al. 2017).

The UPE program has also been implemented in Buikwe District, where the education system faces several challenges. The district has 647 schools (408 primary schools) (Buikwe.go.ug 2022), and about 84% of children aged 6–12 attend primary school (Uganda Bureau of Statistics 2017). Nevertheless, problems such as poor school performance, limited facilities, long travel distances to schools, and high dropout rates persist (Buikwe District Local Government 2015).

School attendance in Sub-Saharan Africa remains among the lowest globally. While over 99% of children are enrolled, only about 70% attend school regularly, highlighting the gap between enrollment and actual attendance (Roby et al. 2016; World Bank 2021). It is confirmed that school absenteeism is the main predisposition of dropout from school, and it is an important factor influencing the performance of pupils.

Socio-economic status strongly affects school attendance, with children from wealthier families attending school more regularly than those from poorer households (Roby et al. 2016; Saasa 2018; Zhang 2003). In many developing countries, education expenses remain a substantial burden for poor families, limiting children's access to schooling (UNICEF 2016).

In particular, extreme poverty may lead households to prioritize children's work over schooling to contribute to the family income (Cardoso and Verner 2006). In Uganda, poverty was found to be the main

obstacle to regular school attendance, even though primary education is free and mandatory (Namukwaya and Kibirige 2014). However, it's worth noting that some older research suggests that children from wealthier families might also miss school frequently, possibly due to different priorities placed on education (Devadoss and Foltz 1995).

Closely related to household poverty is children's nutrition, which may also affect school attendance. Many Ugandans do not consume enough calories daily, and a significant portion of school children go hungry during the school day (WFP 2021). Poor nutrition can lead to health problems, stunted growth, and hindered mental development, all of which can impact a child's ability to attend and perform well in school (De Muro and Burchi 2007; WFP 2006).

Household size may impact children's schooling as well. Research from Uganda by Nannyonjo (2007) suggests that smaller families tend to have children with higher test scores and better school attendance compared to larger families. This could be because in larger families, children may face more distractions from household responsibilities and receive less support from parents for their education. Additionally, larger families may require elder daughters to stay home for household chores or childcare, affecting their school attendance (Jayachandran 2002).

Women-led households tend to prioritize children's education more, leading to better school attendance (Ahiakpor and Swaray 2015; Ainsworth et al. 2002; Lloyd and Blanc 1996).

The death of parents, which is more common in poor contexts, can significantly impact a child's schooling. Orphans may face poorer school performance and attendance due to various reasons, including financial constraints and caregiving responsibilities (Yamano and Jayne 2005). Orphans often live with grandparents, who may prioritize household work over the child's education, leading to lower school attendance (Roby et al. 2014). Studies also suggest in this context that the presence of mothers is crucial for children's schooling, with children without their mother being more vulnerable (Tansel 1997; Ainsworth et al. 2002).

Support interventions, such as direct school support or sponsorship, can improve school attendance of orphaned pupils of various age categories (Cho et al. 2017). These interventions help mitigate barriers like school fees and lack of supplies, ensuring orphans have better access to education. Parents' education plays a crucial role in determining whether children attend primary school. Studies by Namukwaya and Kibirige (2014) and Pal (2004) suggest that parental education significantly influences children's enrollment and attendance. The research shows that higher levels of parental education are associated with more children attending school. Ahiakpor and Swaray (2015) found a positive connection between parental education and school attendance, particularly for girls. Saasa (2018) discovered in the Zambian setting that children (aged 6–14) living with a head of household who had attained primary education were more likely to attend school, with even higher attendance rates if the head of household had secondary or university education. Mothers' education seems to have a stronger impact than fathers' education (Ainsworth et al. 2002).

Household responsibilities and access to resources greatly affect school attendance. Families facing food insecurity may prioritize children working to support the household, hindering school attendance (De Muro and Burchi 2007). In Uganda, children's involvement in domestic work is a significant barrier to school enrollment and retention (Namukwaya and Kibirige 2014).

Child labor is another barrier to school attendance, particularly in sub-Saharan Africa, where a high number of children are engaged in work, preventing them from attending school (Cardoso and Verner 2006; Oryoie and Alwang 2018). As shown by Maligalig et al. (2010) for children aged 6–17, boys are more likely to choose work over school, while girls tend to focus on household chores and caregiving. Factors such as income, parental education, and government support influence the reduction of child labor and increase school attendance (Valero-Gil and Valero 2022).

The gender of children also plays a significant role in school attendance. In many developing countries girls face more obstacles to education than boys. However, education can empower girls and positively impact their families (Karabo and Natal 2013; Alika and Egbochuko 2009). Yet, cultural taboos and early marriages still affect girls' schooling, as found by Bhattarai et al. (2020) for girls of grades 8–10.

Health status of children significantly influences their school attendance and performance. In Uganda, youth living with HIV/AIDS often experience challenges like missing school, lower performance, and dropping out due to the stigma related to HIV/AIDS. Furthermore, various health conditions like epilepsy, parasitic infections, and malnutrition can also negatively affect school attendance and performance (Hassen and Beyene 2020; Jejaw et al. 2015). Additionally, Donnelly (2017) explored the relationship between physical fitness and school performance, and Barnes et al. (2020) highlighted how children and young people with inflammatory bowel disease attend school less than their healthy peers.

In terms of the distance to school, Nannyonjo (2007) found in the Ugandan context that (grade 6) pupils living near schools perform better than those living farther away. Children who live far from school are more likely to be late, spend more time walking to and from school, feel more tired, and have difficulty concentrating in class.

Low quality of school infrastructure, including suitable furniture, and the availability of educational resources like books, maps and charts (Burke and

Beegle 2004), or digital textbooks (Hermita et al. 2023) and equipment (Ma 2021) also negatively impact school attendance and educational performance of children.

Recently, several studies focused on the complex multidimensional factors of school attendance and performance. For example, Schreurs and Rundgren (2021) emphasized the significance of parents-related factors (such as their social, cultural, and economic backgrounds) in understanding children's elementary school attendance dynamics. Pezzulo et al. (2022) explored factors related to secondary school attendance in Tanzania and found associations between the attendance and age, parental education levels, household wealth, and the total number of children in a household.

3. Data and methods

3.1 Study area

Buikwe District is located in the Central Region of Uganda, east of Kampala, and is characterized by predominantly rural settlement patterns with several small urban centers. The local economy relies largely on smallholder agriculture and informal economic activities, reflecting relatively modest socio-economic conditions typical of many districts in rural Uganda. Dispersed settlements and uneven accessibility of educational infrastructure may result in longer travel distances to schools, which can represent an important constraint affecting pupils' regular school attendance.

3.2 Research design

The paper investigates factors affecting school attendance in the Buikwe District, Uganda. Using primary micro-level data of pupils of several local schools, the effects of various social, demographic and other attributes on pupils' absenteeism were examined. Given the nature of the dependent variable and the structure of the data, the random-effects Poisson model was employed in the analysis.

3.3 Sample

Three primary schools were purposively selected based on prior field engagement of one of the

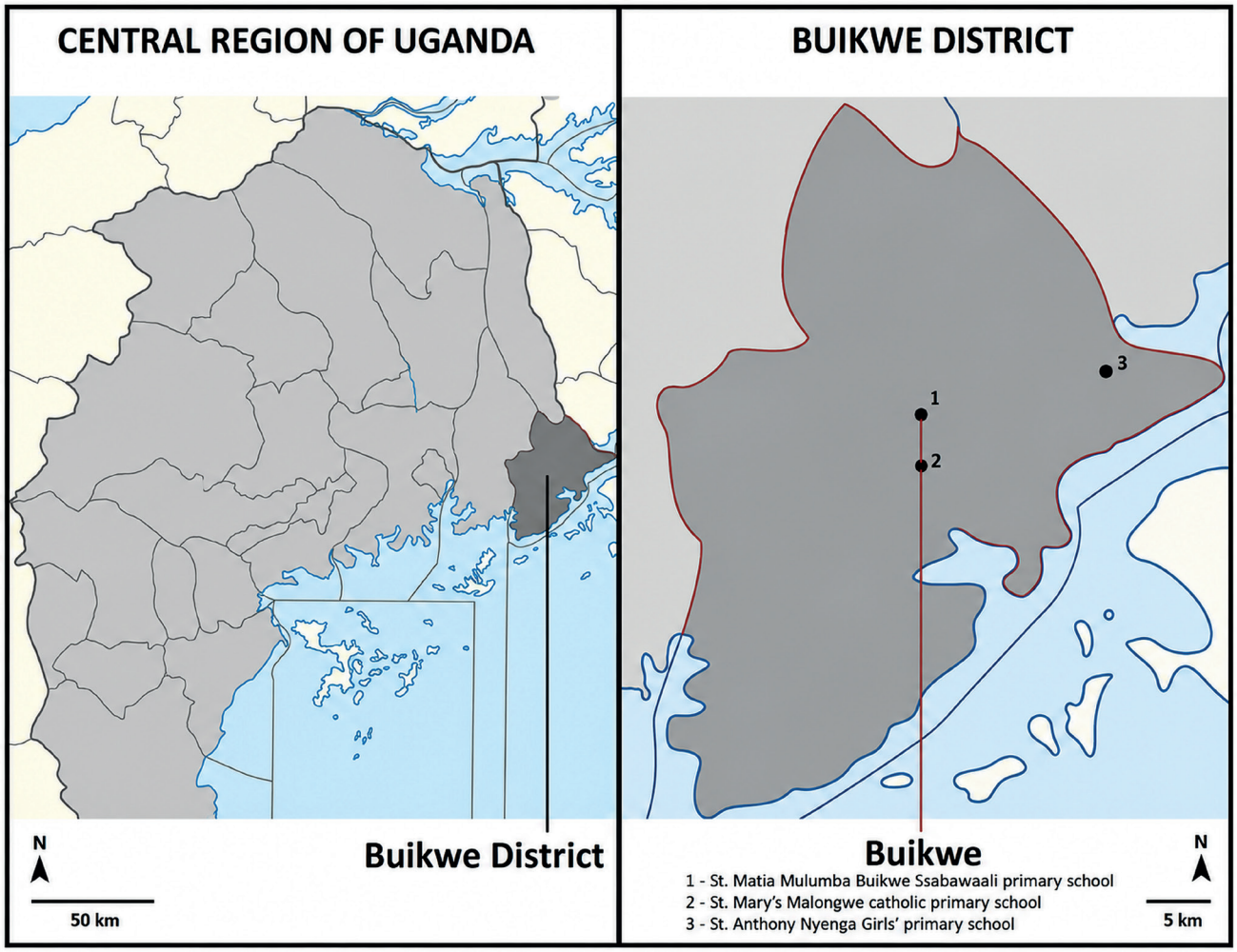

Fig. 1 Location of the survey area.

authors, which ensured established trust, familiarity with the institutional setting, and smooth administrative coordination necessary for conducting research with school-aged children: St. Matia Mulumba Buikwe Sabawaali Primary School, St. Mary's Malongwe Catholic Primary School, and St. Anthony Nyenga Girls Primary School.

Although the three schools were selected purposively and do not constitute a probability sample of schools in the region, the use of the regression analysis approach is appropriate for modelling within-sample variation. The inferential interpretation of the model is therefore restricted to the observed sample and does not assume random selection of schools from a broader population.

Within selected schools, all pupils enrolled in the fifth, sixth, and seventh grades (i.e., the final three grades) were considered eligible for participation. These grades were selected due to the assumed sufficient level of English proficiency required to understand the questionnaire, which was administered in English.

The study thus followed a census-based approach rather than a sampling procedure, aiming to include all pupils present on the day of data collection. The total number of pupils enrolled in the selected grades across the three schools during the second trimester of 2018 was 542 (221 in Grade 5, 194 in Grade 6, and 127 in Grade 7), based on official school registers.

On the day of the survey (including a follow-up data collection), 494 pupils were present (191 in Grade 5, 185 in Grade 6, and 118 in Grade 7), representing approximately 91% of all enrolled pupils. All present pupils completed the questionnaire (i.e., a 100% response rate among those present). During data cleaning, 14 questionnaires were excluded due to missing identifiers or empty responses. Therefore, the total number of observations included in the analysis is 480.

The school administration informed each parent about the survey, including its purpose and content. Considering that some parents were not literate and signing formal documents was a sensitive issue within the community, we decided, after consulting with the principals, not to request written consent. Nevertheless, every parent had the option to decline their child's participation. The research was conducted in full compliance with the Palacký University's ethical code of conduct and ethical standards for field research at the DEPARTMENT of Development and Environmental Studies, ensuring adherence to ethical standards, including respect for participants, informed consent, and the confidentiality of collected data.

No pupil was required to fill out the questionnaire, and they could have left the classroom at any time. They could have also skipped any question in the questionnaire if they wished to do so. This was stressed repeatedly during the data collection. After the data collection, the questionnaires were strictly anonymized.

3.4 Procedure

The underlying questionnaire was designed to examine various factors of school attendance of pupils in the selected primary schools in the Buikwe district, Uganda, and it consisted of eight parts:

1. Transport to school – how children commute to school.
2. Housework – what activities are children required to do at home (in terms of house chores, etc.).
3. Family – children's family situation, number of household members, whether the biological parents are alive, whether they are literate, and what is their highest educational attainment.
4. Housing – the type of housing and assets.
5. Food – children's eating habits.
6. Aid programs – whether children are supported through any assistance/aid program.
7. School – who sends the children to school every morning?
8. Personal information about children – gender, age, class, school, residence, etc.

The questionnaires were filled out collectively in classrooms, directly under supervision of one of the authors of the paper; all questions were read aloud slowly, so that the pupils were able to answer the same questions at the same time. The permissions to conduct the survey were requested from the school principals, and they were also urged to consult their decisions with the teaching staff.

Data for the dependent variable (number of pupils' daily absences per month) were collected from the schools' registers (used for daily registration of pupils).

3.5 Variables/Instruments

Our dependent variable indicates the number of days a pupil was absent in each calendar month, observed repeatedly for pupils in the three primary schools from February 2018 to September 2018. The resulting dataset comprises 3,522 pupil-by-month observations; monthly absences of individual pupils range from 0 to 20 days (M = 1.54 days, SD = 2.45 days).

In the presented analyses, in total 14 independent variables are used that can be grouped into four categories. The first category reflects basic characteristics of the pupil – *Age* (in years), and *Gender* – and it also includes the *Distance* between home residence and school. The underlying survey shows that at the three selected primary schools, there are 55 percent of girls and 45 percent of boys. The range of age at the fifth, sixth, and seventh grades is from nine years to 18 years. As for the *Distance* variable, it is converted into a dummy that equals 1 if the distance is higher

than the median distance (i.e., higher than 1.5 km). Distances from the schools range from 0.25 to 7 km, and more than 88.5 per cent of pupils walk to school. In accordance with previous findings (Nannyonjo 2007), the relationship between distance and absences is expected to be positive (higher distance is associated with higher absences).

The second group of variables captures the characteristics of the households in which a pupil lives. These variables are selected in line with previous research and studies (e.g., Ainsworth et al. 2002; Ahiakpor and Swaray 2015; Saasa 2018). The size of households is measured by the *Number of households members* while the variable *Younger siblings* captures the number of younger siblings of a pupil in that household. The *Orphan* variable shows whether a child is missing one or both parents. In the sample, 22.13 per cent of pupils lost at least one biological parent. Focusing on the education of parents, *Mothers with higher education* is a dummy variable that indicates whether the mother of a child has higher than primary education. In the data, 53.09 per cent of mothers have achieved education levels higher than primary. In line with the literature, the household size is expected to be positively related to absenteeism (Jayachandran 2002; Nannyonjo 2007), and the same is expected about orphanage (Yamano and Jayne 2005; Roby et al. 2014), while negative effects are anticipated about education of parents on absenteeism (better education of parents leads to lower absences, as in Ainsworth et al. 2002).

The *Asset index* is also classified into the second group of factors since it approximates the living standard of households. It consists of sub-indices that can be divided into two categories: house quality, and items ownership. While the former considers basic qualities of houses such as materials of walls, roof, access to the electricity, number of rooms etc., the latter accounts for ownership of various items (car, stove, bed, armchairs, freezer, phone, etc.) in households. The multiple correspondence analysis is used to determine the weights of sub-indicators. To make results more intuitive, the results are rescaled linearly in a manner that assigns zero points to households with the worst set of assets (i.e., they do not own any item on the list and characteristics of their house are always inferior) and 100 points to households with the best set of assets (i.e., households that own all items on the list and characteristics of their house are always superior), as in Němečková et al. (2020).[1] It is hypothesized that better living standards are associated with lower absences (similarly to, e.g., Roby et al. 2016; Saasa 2018; or Namukwaya and Kibirige 2014), although the opposite was found in the literature as well (Devadoss and Foltz 1996).

The third category of variables captures household decision-making in domains directly related to the child and schooling. Both variables were constructed from three questionnaire items: major household purchases, school choice/enrolment, and the child's everyday school attendance. In each domain, women received one point if at least one woman was involved in the decision, and men received one point if at least one man was involved; joint decision-making therefore gave one point to both. *Female-led household* indicates that women obtained a majority of points across these domains, while *Household head parent* indicates that the pupil's parent was among the person(s) with the highest number of decision-making points. These variables should be read as operational indicators of decision-making authority in the measured child- and schooling-related domains, not as formal measures of household headship or leadership in unmeasured areas of household life. In the sample, 82.95% of pupils lived in such households, and 49.46% lived in households classified as female-led. Following evidence on the role of mothers and women in children's schooling, lower absenteeism is expected among children from female-led households as defined here (Ainsworth et al. 2002).

The last group of variables reflects the social and economic conditions of pupils – how many different kinds of housework (e.g., fetching water, cooking, washing clothes, etc.) they need to carry out before going to school (*Work before school*), whether pupils do any paid work (*Employment*), whether they are supported or sponsored through any assistance program (*Sponsorship*), and whether they felt strong hunger or food shortage at least once a week (*Hunger*). For example, in the sample, over 55 percent of pupils do some paid work, and more than 18 percent are supported by some aid program.

In accordance with existing studies, it is hypothesized that house chores as well as paid work are associated with higher absenteeism (Namukwaya and Kibirige 2014; Teshome 2002; Cooper-Vince et al. 2017; Cardoso and Verner 2006). In contrast, less absences should be associated with better access to food and with the existence of support through aid programs (De Muro and Burchi 2007; Ainsworth et al. 2002).

The variables *Gender*, *Distance*, *Orphan*, *Mother with higher education*, *Female led household*, *Household head parent*, *Employment*, *Sponsorship*, and *Hunger* are dummy variables. Data for all independent variables were obtained from the questionnaire survey carried out at the three selected primary schools in the Buikwe district. The variables used in our analysis are summarized in Tab. 1.

1 After constructing the index, a sensitivity analysis is performed: specifically, an alternative asset index with equal weights of all indicators is calculated. A very high correlation between the original and alternative index (Pearson correlation coefficient is roughly 0.96) shows that the (normative) decision to create weights by MCA does not substantially change the picture of households' living standards presented by the asset index.

Tab. 1 Description of variables.

Variable name	Definition	Expected relationships to absenteeism
Dependent variable		
Number of absences	Number of absences per pupil per month (in days).	
Independent variables		
Group 1: Basic characteristics of pupils		
Age	Age in years.	unclear
Gender	Dummy variable that takes the value of 1 if the child is male, and 0 if the child is female.	unclear
Distance	Dummy variable that takes the value of 1 if the distance to school is higher than the median distance (1.5 km). It is equal to 0 otherwise.	positive
Group 2: Household characteristics		
Number of household members	Number of people within a household.	positive
Younger siblings	Number of younger siblings.	positive
Orphan	Dummy variable that takes the value of 1 if at least one parent is missing. It is equal to 0 otherwise.	positive
Mothers with higher education	Dummy variable that takes the value of 1 if the mother has higher than primary education. It is equal to 0 otherwise.	negative
Asset index	An index ranging from 0 to 100 measuring housing quality, and assets ownership (in a household).	negative
Group 3: Characteristics of the household head		
Female led household	Dummy variable coded as 1 if women had the majority decision-making role in three child- and schooling-related domains.	negative
Household head parent	Dummy variable coded as 1 if the pupil's parent was among the main decision-makers in the same three domains.	negative
Group 4: Social and economic conditions of pupils		
Work before school	The number of various types of housework the pupil needs to carry out before going to school	positive
Employment	Dummy variable that takes the value of 1 if the pupil does any paid work. It is equal to 0 otherwise.	positive
Sponsorship	Dummy variable that takes the value of 1 if the pupil is supported or sponsored through any assistance programs. It is equal to 0 otherwise.	negative
Hunger	Dummy variable that equals to 1 if the pupil felt strong hunger or food shortage at least once a week. It is equal to 0 otherwise.	positive

Source: Authors. Note: Positive expected relationship means that such a factor would increase the number of absences. Negative expected relationship means that the factor would reduce the number of absences.

3.6 Statistical analysis

The dependent variable captures the number of days absent per pupil per month in three primary schools, observed from February 2018 to September 2018. While this outcome varies over time (month by month), all independent variables are treated as time-invariant because they were measured only once in the survey. Accordingly, we assume that these characteristics remain constant over the observation window, although for some variables this assumption may be restrictive, as they could plausibly change even within several months.

The repeated monthly observations for each pupil motivate a panel-data modelling strategy. Given that the dependent variable is a count (monthly absence days), we employ Poisson regression as the standard approach for modelling count outcomes. Prior to estimation, we assess whether unobserved individual heterogeneity is present, indicating that a panel estimator is preferable to a pooled specification. The diagnostic results support a panel approach and, specifically, the use of a random-effects Poisson regression with heteroskedasticity-robust inference. A fixed-effects Poisson model is not suitable here because the explanatory variables are time-invariant and would therefore be absorbed by pupil fixed effects, preventing estimation of their coefficients.

In the random-effects Poisson model, the covariates are linked to the expected number of absence days per pupil-month. We include a pupil-specific random intercept to capture persistent unobserved differences between pupils (such as underlying health or household constraints), and to account for within-pupil dependence of observations across months. To absorb common seasonal patterns and systematic differences across schools, all specifications include month fixed effects and school fixed effects. We report pupil-clustered robust standard errors to allow for

Tab. 2 Absence structure by months and schools.

Month	Obs	Mean	St. Dev	Min	Max	Skewness	Zero abs.
February	367	2.58	3.72	0	17	2.00	40.0%
March	443	1.26	2.42	0	20	4.20	54.6%
April	442	0.63	1.68	0	19	5.43	73.1%
May	416	1.45	1.67	0	7	0.89	43.0%
June	414	1.42	2.28	0	16	2.94	47.3%
July	414	1.68	2.54	0	16	2.48	43.7%
August	336	1.56	2.44	0	14	2.42	49.1%
September	417	2.01	2.08	0	9	0.74	34.1%
School	**Obs**	**Mean**	**St.Dev**	**Min**	**Max**	**Skewness**	**Zero abs.**
Malongwe	971	1.51	2.33	0	17	2.76	46.9%
Nyenga	1060	1.27	2.37	0	20	3.27	57.6%
Ssabawaali	1218	1.81	2.59	0	19	2.55	41.8%

Source: Authors' calculations based on the survey data. Note: The last column reports the percentage of pupil-month observations with zero absences (no days absent), by month and by school.

within-pupil correlation across months and remaining distributional misspecification.

This approach rests on several standard assumptions. The model specifies the conditional mean of absences as a log-linear function of observed covariates, while the random intercept captures unobserved, time-invariant pupil characteristics. A key identifying assumption is that the unobserved pupil-specific propensity for absence is not systematically correlated with the included covariates. To reduce the scope for confounding, we include a broad set of controls as well as month and school fixed effects. In addition, because count data may exhibit overdispersion relative to the Poisson distribution, we rely on pupil-clustered robust standard errors and assess robustness to alternative variance assumptions. We estimated two alternative specifications, namely random-effects negative binomial regression and mixed-effects negative binomial model with a pupil-level random intercept. Both clearly supported the main random-effects Poisson model findings.

In terms of our estimation strategy, we perform four regression models in total, mostly with the same explanatory variables to test their statistical significance and the direction of their effects on the dependent variable. However, two variables – the *Asset Index* and *Mothers with higher education* – are excluded from some of the models because their inclusion significantly lowers the number of observations that enter the estimations (Appendix 1 and Appendix 2).

4. Results

In this section, we first present descriptive statistics for the dependent variable, showing how pupil absences vary across months and schools. We then summarize the independent variables included in the regression models. Finally, we report and describe the results of the regression analysis.

Tab. 2 summarizes the distribution of pupil absences (days absent per pupil per month) across the study period and by school. Absences vary markedly by month: the highest average is observed in February, after which mean absences drop sharply in March and reach their lowest level in April. From May onward, monthly means generally hover between about 1.4 and 1.7 days, with a moderate uptick again in September. Across all months, the minimum number of absences is zero, whereas the upper tail reflects occasional extreme absence spells, reaching 20 days in March and 19 days in April, which results in highly right-skewed distributions. Consistent with this pattern, the share of pupils with zero absence days in a given month varies markedly over time, ranging from 73.1% in April to 34.1% in September.

The lower panel of the table shows differences in absence levels across the three schools. Ssabawaali records the highest mean monthly absence, followed by Malongwe and Nyenga. While average differences are not large in absolute terms, the standard deviations are substantial relative to the means in all schools, pointing to considerable heterogeneity among pupils and months, with most observations at low absence levels but a small number of high-absence cases driving the upper tail (as also reflected in the values of skewness and percentages of zero absences).

Tab. 3 presents descriptive statistics for the explanatory variables included in the regression models. Sample sizes differ across variables due to item-level missingness in the survey. The covariates comprise both continuous measures and binary indicators, for which the reported means can be interpreted as sample proportions. The continuous variables exhibit considerable dispersion, most notably the asset index and household composition, indicating meaningful heterogeneity in socio-economic conditions within the study sample.

Tab. 3 Descriptive statistics of explanatory variables used in the regression.

Variable	Obs	Mean	St. Dev	Min	Max
Age	463	12.89	1.60	9	18
Gender (dummy)	480	0.45	0.50	0	1
Distance (dummy)	425	0.50	0.50	0	1
Number of household members	471	6.86	2.46	0	18
Female led household (dummy)	461	0.49	0.50	0	1
Household head parent (dummy)	475	0.83	0.38	0	1
Orphan (dummy)	461	0.22	0.42	0	1
Younger siblings	471	2.57	1.79	0	13
Mothers with higher education (dummy)	356	0.53	0.50	0	1
Employment (dummy)	467	0.55	0.50	0	1
Work before school	450	2.07	1.57	0	8
Sponsorship (dummy)	408	0.18	0.39	0	1
Hunger (dummy)	436	0.73	0.44	0	1
Asset index	361	34.87	17.05	0	100

Source: Authors' calculations based on the survey data. Note: All explanatory variables were measured only once in the survey. In the regressions, these values are assigned to each pupil's monthly observations and are therefore treated as time-invariant.

Tab. 4 shows the results of the four regression models that are estimated using the random-effects Poisson method with heteroskedasticity-robust standard errors clustered on pupils. The first model (1) excludes both variables that limit the number of observations (*Mothers with higher education*, and *Asset index*) entering the regression. Therefore, this model works with the highest number of observations (2,267). The second model (2) includes the *Asset index* while excluding the variable indicating higher education of mothers, resulting in 1,911 observations. Conversely, the third model (3) includes *Mothers with higher education* while excluding the *Asset index*, meaning that 1,665 observations enter the regression. And finally, the fourth model (4) includes both of these variables which limits the number of observations to 1,427.

Tab. 4 Regression model and results.

Dependent variable: Number of absences	Regression models			
Independent variables	(1)	(2)	(3)	(4)
Age	−0.079*** (0.030)	−0.069** (0.033)	−0.092*** (0.035)	−0.082* (0.037)
Gender (dummy)	0.238** (0.094)	0.325*** (0.102)	0.285*** (0.107)	0.362*** (0.112)
Distance (dummy)	0.081 (0.100)	0.150# (0.099)	0.115 (0.111)	0.170# (0.113)
Number of household members	−0.017 (0.026)	−0.023 (0.027)	−0.021 (0.027)	−0.027 (0.026)
Female led household (dummy)	−0.277*** (0.094)	−0.207** (0.101)	−0.410*** (0.109)	−0.356*** (0.117)
Household head parent (dummy)	0.056 (0.141)	0.104 (0.140)	0.089 (0.160)	0.214 (0.158)
Orphan (dummy)	0.376*** (0.127)	0.462*** (0.127)	0.556*** (0.152)	0.569*** (0.154)
Younger siblings	0.022 (0.033)	0.055* (0.033)	0.021 (0.037)	0.051# (0.035)
Mothers with higher education (dummy)			−0.188* (0.105)	−0.204* (0.111)
Employment (dummy)	0.178* (0.096)	0.195* (0.103)	0.184# (0.116)	0.212* (0.122)
Work before school	−0.051 (0.038)	−0.053 (0.039)	−0.092** (0.039)	−0.104*** (0.039)
Sponsorship (dummy)	−0.199# (0.139)	−0.234* (0.136)	−0.336** (0.150)	−0.312* (0.169)
Hunger (dummy)	0.010 (0.107)	−0.026 (0.111)	−0.021 (0.118)	−0.053 (0.121)
Asset index		0.005* (0.003)		0.007** (0.003)
Dummy variables for schools	Yes	yes	yes	yes
Dummy variables for months	Yes	yes	yes	yes
_const	1.658*** (0.428)	1.081** (0.485)	2.015*** (0.506)	1.315** (0.550)
Number of observations	2,267	1,911	1,665	1,427
Number of groups	321	270	242	207
Wald chi2	296.63***	261.49***	307.14***	276.48***

Source: Author's calculations. *** Significant at the 1% significance level. ** Significant at the 5% significance level. * Significant at the 10% significance level. # Significant at the 15% significance level. Robust standard errors are in parentheses.

Additionally, each model also contains two sets of dummy variables to control for the possible differences among the three schools, as well as to account for the possible effects of various months on school absences.

Generally, it can be concluded from Tab. 4 that the coefficients do not change much across the models, pointing to the same direction of effects in all significant cases. However, the statistical significance varies a bit among models which could also be influenced, to some extent, by the different number of observations entering the models.

The results in Tab. 4 show that *Age*, *Female led household*, *Mothers with high education*, *Work before school*, and *Sponsorship* have statistically significant and negative associations with absences at schools in the Buikwe district. This means that:

- older children have lower absences;
- children from female-led households have significantly lower absences;
- children of mothers with higher education (i.e., with higher than primary education) have lower absences, although this variable is significant only marginally;
- children who receive a sponsorship support have lower absences;
- children who must work more in the household in the morning (before school) have lower absences (although this may sound surprising it could mean that they have a better attitude to fulfilling their duties). It needs to be noted, however, that this variable is significant only in the models with lower number of observations.

Furthermore, the results presented in Tab. 4 also indicate that *Sex*, *Orphan*, *Asset index* and marginally *Distance*, *Employment*, and *Younger siblings* have statistically significant and positive associations with school absences, meaning that:

- boys have higher absences than girls;
- children from incomplete families (that lost one parent or both parents) have significantly higher absences;
- children that live farther away from schools have higher absences;
- children that have a paid employment miss classes more often;
- children who have (more) younger siblings in the household have higher absences (because they must look after them more often)
- children who come from households with more assets have higher absences. While this may seem as a surprising result, it may be that children from more wealthy households feel less motivated and pressured to attend school that frequently.

Variables *Number of households members*, *Household head parent*, and *Hunger* do not have statistically significant associations with absences from school even at the 15% level, as shown in Tab. 4.

The results suggest that there are at least three decisive factors of school absences in the Buikwe district. The first one is gender-related: girls have lower absences than boys, and children from households where women predominate in child- and schooling-related decision-making also have significantly lower absences. The second factor is the completeness of the pupils' families: children with both parents have significantly lower absences than children with at least one parent missing. And thirdly, sponsorship support of children seems to increase attendance in school, too. Apart from these three, there are other factors that seem to play a role in lowering absences of pupils, such as for example the education of mothers. The results also show that there are differences in absences among different schools and over different months under review.

5. Discussion

The main aim of this research is to examine factors associated with elementary school absenteeism in the Buikwe district, Uganda. The results indicate several factors significantly associated with absenteeism across all models: gender and age of the pupil, family environment, and sponsorship support. These findings should be interpreted as context-specific evidence from a predominantly rural Ugandan district, where school attendance is shaped by the interaction of household vulnerability, children's work responsibilities, access to support, and local livelihood conditions. The descriptive statistics also reveal substantial month-to-month variation in absences, suggesting that attendance in Buikwe is shaped not only by household characteristics but also by time-specific contextual conditions, such as the school calendar, household resource constraints, weather conditions, and seasonal labour needs.

The gender of the pupil is a frequently recognized factor that affects school attendance, often in a combination with other variables. The results suggest that girls exhibit lower absenteeism from elementary schools than boys. The presented finding, however, contradicts some other research such as Teshome (2002) or Ahiakpor and Swaray (2015) who indicated the opposite. In their case, girls are more involved in domestic work which leads to lower school attendance and performance. On the other hand, the results are more in line with Maligalig et al. (2010) who found that boys have more absences due to their involvement in paid work.

The results suggest that children from incomplete families (in which one or both parents are missing) have higher absenteeism than children from complete families. This finding is in accordance with Yamano and Jayne (2005) and Ainsworth et al. (2002) who show that orphanage has a detrimental effect on the households' incomes, which in turn leads to a lower

ability of households to pay school fees. Moreover, in poor households without one or two parents, children's time may be re-allocated from school to caregiving or work to compensate for the lost labour. Furthermore, if an orphan stays with its grandparents or other relatives (aunts, uncles), it is believed that their school attendance is also lower because of their higher involvement in household work due to discrimination (Roby et al. 2013; Roby et al. 2014).

In accordance with literature emphasizing the role of mothers and women in children's schooling (Ahiakpor and Swaray 2015; Ainsworth et al. 2002; Lloyd and Blanc 1996), we found that pupils from households classified as female-led have significantly fewer absences. As noted above, this variable refers to women's predominance in child- and schooling-related decision-making rather than to formal household headship. In the Buikwe context, this may indicate that women's stronger role in decisions about schooling and daily attendance is associated with closer monitoring of children's school participation. The findings also confirm to some extent that higher education of mothers is associated with lower absenteeism, as stated by previous research (Namukwaya and Kibirige 2014; Pal 2004; Ahiakpor and Swaray 2015; Saasa 2018; Ainsworth et al. 2002).

As shown by Ainsworth et al. (2002), children supported through aid programs attend school more, which is especially true for orphans (Cho et al. 2017). Our results are consistent with this finding, indicating that pupils receiving some sort of a sponsorship support have lower absenteeism. It needs to be emphasized however, that some of these programs may be conditional on regular school attendance. In other words, pupils are sent to school regularly (more often) so that their household stays eligible for the support.

On the other hand, only a weak effect was found for the *Younger siblings* variable – it holds merely marginally that a higher number of younger siblings increases the absences of pupils, as the literature would suggest. For example, Jayachandran (2002) found that especially in larger families, elder daughters may be required to stay at home more often (and be absent from school) to carry out household chores or care about their younger siblings. Similarly, according to Teshome (2002), girls' involvement in household chores and care for siblings can lead to poorer school performance.

We also show that if a child does household chores before school, the number of absences decreases. This result does not confirm the findings of the majority of previous research. For example, Namukwaya and Kibirige (2014) as well as De Muro and Burchi (2007) found that engagement in household work is one of the key reasons why children cannot attend school regularly. As hypothesized in this context, such children might be more active with better attitudes to work and duties and therefore miss classes less (which was also informally validated by some of the school principals). On the contrary, the trade-off between paid work and school attendance is confirmed: paid jobs of children tend to increase their absenteeism. This is in line with Cardoso and Verner (2006) who stated that child labour and regular school attendance were exclusive activities.

The relationship between the *Asset index* variable and school absenteeism is unexpectedly positive – children from families that are better off in terms of their asset ownership tend to have higher absences from school. Usually, this factor (as a proxy for better socioeconomic status or lower poverty) lowers the number of absences. According to Cardoso and Verner (2006), UNICEF (2016), and Namukwaya and Kibirige (2014), poverty was the most important barrier to attending school at all educational levels. However, Devadoss and Foltz (1996) found that financial support from parents may lead to a higher absenteeism since children from wealthier families may have a tendency to put less emphasis on education. For these reasons, such pupils may have more absences and worse grades compared to pupils from poorer families.

Our results do not provide enough evidence for the positive relationship between school absenteeism and household size. Such an association was identified in some previous papers, most importantly by Nannyonjo (2007), who suggests in a study from Uganda that children from smaller families tend to have better school attendance and test scores than children from larger families. A possible explanation is that individual children in larger families may receive less support for their education. The findings also provide only weak support for the association identified by Nannyonjo (2007) between longer distance to school and higher absenteeism.

Overall, the results suggest that absenteeism in Buikwe is not only a matter of individual or household characteristics, but also reflects the local context in which schooling takes place. In a rural setting where households often combine schooling with informal work, domestic responsibilities, and seasonal livelihood demands, factors such as child labour, sponsorship support, household decision-making, and distance to school may operate differently than in urban or high-income contexts. The findings should therefore not be read as universal determinants of absenteeism, but as evidence of how broader mechanisms identified in the literature materialize in a specific rural Ugandan setting.

6. Conclusion

The decision whether to attend school on a daily basis is influenced by a range of social, economic, personal, and institutional factors. This paper examined how selected factors relate to school absenteeism of pupils from three primary schools in the Buikwe district in south-eastern Uganda.

The results point to several factors that are significantly associated with pupils' absenteeism. In particular, family characteristics appear to play an important role. Pupils from households classified as female-led in terms of child- and schooling-related decision-making tend to have fewer absences, and children living with both parents show lower absenteeism compared to those from incomplete families. In addition, pupils receiving support through sponsorship programs are absent from school less frequently.

Other associations are also observed. Paid child labour is linked with higher absenteeism, suggesting a clear trade-off between work and school attendance. The educational level of mothers is another relevant factor, as pupils whose mothers have higher than primary education tend to miss school less often. Gender differences are also visible, with girls showing fewer absences than boys.

Some findings are less intuitive. Pupils who carry out household duties before school tend to have fewer absences. One possible explanation is that children who regularly perform household responsibilities may develop daily routines that also support regular school attendance. Another unexpected result concerns the assets ownership: pupils from relatively better-off households show slightly higher absenteeism. One possible interpretation is that children from wealthier households may place less emphasis on regular attendance, although this result should be interpreted with caution.

Several directions for further research emerge from this analysis. Future studies could examine additional contextual factors that may influence school attendance in rural Uganda, including cultural norms, teacher absenteeism, or school infrastructure. Longitudinal data could also provide a clearer picture of how family circumstances, sponsorship programs, and child labour affect attendance over time. Qualitative approaches, such as interviews with pupils and their families, could complement the quantitative results and offer deeper insight into the motivations and constraints affecting school participation.

The findings may also have practical relevance for educational policy and practice, although they should be interpreted as indicative rather than prescriptive. Programs supporting vulnerable households, initiatives encouraging parental involvement in education, or the continued expansion of sponsorship schemes may contribute to improving school attendance. At the same time, measures addressing child labour and raising awareness about the value of education within local communities may also play a role.

Finally, several limitations of this study should be acknowledged. The analysis is based on data from three purposively selected schools in the Buikwe district, which in fact limits the possibility to generalize the findings outside the sample. Additionally, although the survey instrument was piloted in the local context, it was not formally externally validated. Moreover, school registers, while useful, may contain inaccuracies that could influence some of the reported results.

Despite these limitations, the study provides empirical evidence on factors associated with school absenteeism in a specific rural Sub-Saharan African setting. The findings contribute to a better understanding of barriers to regular school attendance and may help inform future research as well as discussions on improving educational participation in similar contexts.

Acknowledgments

This work was supported by the Internal Grant Agency of the Faculty of Science, Palacký University Olomouc, under grant no. IGA_PrF_2021_018.

References

Ahiakpor, F., Swaray, R. (2015): Parental expectations and school enrollment decisions: Evidence from rural Ghana. Review of Development Economics 19(1), 132–142, https://doi.org/10.1111/rode.12122.

Ainsworth, M., Beegle, K., Koda, G. (2002): The impact of adult mortality on primary school enrolment in Northwestern Tanzania. Africa Region Human Development Working Paper Series; The World Bank, Human Development Sector, Africa Region: Washington, DC, USA.

Alika, I. H., Egbochuko, E. O. (2009): Drop out From School among Girls in Edo State: Implications for Counselling. Edo Journal of Counselling 2(2), 135–141, https://doi.org/10.4314/ejc.v2i2.60850.

Allen, C. W., Diamond-Myrsten, S., Rollins L. K. (2018): School Absenteeism in Children and Adolescents. American Family Physician 98(12), 738–744. Available online: https://www.aafp.org/pubs/afp/issues/2018/1215/p738.html#afp20181215p738-b1 (accessed on 13 March 2026).

Barnes, C., Ashton, J., Borca, F., Cullen, M., Walker, D., Beattie, R. (2020): Children and young people with inflammatory bowel disease attend less school than their healthy peers. Archives of Disease in Childhood 105(7), 671–676, https://doi.org/10.1136/archdischild-2019-317765.

Bategeka, L., Okurut, N. (2006): Universal Primary Education | Uganda. Policy Brief 10. London: Overseas Development Institute. Available online: https://cdn.odi.org/media/documents/4072.pdf (accessed on 13 March 2026).

Bhattarai, N., Bernasek, A., Pena, A. A. (2020): Factors Affecting School Attendance and Implications for Student Achievement by Gender in Nepal. Review of Political Economy 32(2), 259–282, https://doi.org/10.1080/09538259.2020.1769296.

Buikwe District Local Government (2015): District development plan (DDP II) 2015/16–2019/20. Buikwe District Local Government: Buikwe, Uganda. Available online: https://buikwe.go.ug/media/district-development-plan-ddp-ii-201516-201920 (accessed on 13 March 2026).

Buikwe.go.ug (2022): Education and Sports. Available online: https://buikwe.go.ug/dept/education-and-sports (accessed on 16 March 2026).

Burke, K., Beegle, K. (2004): Why Children Aren't Attending School: The Case of Northwestern Tanzania. Journal of African Economies 13(2), 333–355, https://doi.org/10.1093/jae/ejh011.

Cardoso, A. R., Verner, D. (2006): School Drop-Out and Push-Out Factors in Brazil: The Role of Early Parenthood, Child Labor, and Poverty. IZA Discussion Paper No. 2515; IZA: Bonn, https://doi.org/10.2139/ssrn.955862.

Cho, H., Ryberg, R. C., Hwang, K., Pearce, L. D., Iritani, J. I. (2017): A School Support Intervention and Educational Outcomes Among Orphaned Adolescents: Results of a Cluster Randomized Controlled Trial in Kenya. Prevention Science 18, 943–954, https://doi.org/10.1007/s11121-017-0817-x.

Cook, P. J., Dodge, K. A., Gifford, E. J., Schulting, A. B. (2017): A new program to prevent primary school absenteeism: Results of a pilot study in five schools. Children and Youth Services Review 82, 262–270, https://doi.org/10.1016/j.childyouth.2017.09.017.

Cooper-Vince, C. E., Kakuhikire, B., Vorechovska, D., McDonough, A. Q., Perkins, J., Venkataramani, A. S., Mushavi, R. C., Baguma, C., Ashaba, S., Bangsberg, D. R., Tsai, A. C. (2017): Household water insecurity, missed schooling, and the mediating role of caregiver depression in rural Uganda. Global Mental Health 4: e15, https://doi.org/10.1017/gmh.2017.14.

De Muro, P., Burchi, F. (2007): Education for rural people and food security: a cross-country analysis; Food and Agriculture Organization of the United Nations (FAO): Rome, Italy. Available online: https://openknowledge.fao.org/handle/20.500.14283/A1434E (accessed on 13 March 2026).

Devadoss, S., Foltz, J. (1996): Evaluation of Factors Influencing Student Class Attendance and Performance. American Journal of Agricultural Economics 78(3), 499–507, https://doi.org/10.2307/1243268.

Donnelly, J. A. (2017): The relationship between physical fitness and school performance. Journal of Social, Behavioral, and Health Sciences 11(1), 231–244, https://doi.org/10.5590/jsbhs.2017.11.1.16.

Duraisamy, P., Duraisamy, M. (1995): Determinants of Investment in Health of Boys and Girls: Evidence from Rural Households of Tamil Nadu, India. Indian Economic Review 30(1), 51–68. Available online: https://www.jstor.org/stable/24010453 (accessed on 15 March 2026).

Gottfried, M. A. (2014): Chronic Absenteeism and Its Effects on Students' Academic and Socioemotional Outcomes. Journal of Education for Students Placed at Risk 19(2), 53–75, https://doi.org/10.1080/10824669.2014.962696.

Gottfried, M. A. (2019): Chronic Absenteeism in the Classroom Context: Effects on Achievement. Urban Education 54(1), 3–31, https://doi.org/10.1177/0042085915618709.

Gottfried M. A., Kirksey, J. J. (2017): "When" Students Miss School: The Role of Timing of Absenteeism on Students' Test Performance. Educational Researcher 46(3), 119–130, https://doi.org/10.3102/0013189X17703945.

Hassen, O., Beyene, A. (2020): The effect of seizure on school attendance among children with epilepsy: a follow-up study at the pediatrics neurology clinic, Tikur Anbessa specialized hospital, Addis Ababa, Ethiopia. BMC Pediatr 20: 270, https://doi.org/10.1186/s12887-020-02149-y.

Harmáček, J., Syrovátka, M., Dušková, L. (2017): Pro-poor growth in East Africa. Quarterly Review of Economics and Finance 64, 82–93, https://doi.org/10.1016/j.qref.2016.07.002.

Hermita, N., Wijaya, T. T., Yusron, E., Abidin, Y., Alim, J. A., Putra, Z. H. (2023): Extending unified theory of acceptance and use of technology to understand the acceptance of digital textbook for elementary school in Indonesia. Frontiers in Education 8: 958800, https://doi.org/10.3389/feduc.2023.958800.

Jayachandran, U. (2002): Socio-Economic Determinants of School Attendance in India. Working Paper No. 103; Centre for Development Economics, Delhi School of Economics: Delhi, India. Available online: http://www.cdedse.org/pdf/work103.pdf (accessed on 12 March 2026).

Jejaw, A., Zemene, E., Alemu, Y., Mengistie, Z. (2015): High prevalence of Schistosoma mansoni and other intestinal parasites among elementary school children in Southwest Ethiopia: a cross-sectional study. BMC Public Health 15: 600, https://doi.org/10.1186/s12889-015-1952-6.

Karabo, M., Natal, A. (2013): Factors influencing high dropout rates of girl child from education: A case study of black women in North West Province, South Africa. Journal of Social Development in Africa 28(1), 111–138.

Lenhoff, S. W., Pogodzinski, B. (2018): School Organizational Effectiveness and Chronic Absenteeism: Implications for Accountability. Journal of Education for Students Placed at Risk 23(1–2), 153–169, https://doi.org/10.1080/10824669.2018.1434656.

Lloyd, B. C., Blanc, A. K. (1996): Children's Schooling in sub-Saharan Africa: The Role of Fathers, Mothers, and Others. Population and Development Review 22(2), 265–298, https://doi.org/10.2307/2137435.

Ma, J. K.-H. (2021): The digital divide at school and at home: a comparison between schools by socioeconomic level across 47 countries. International Journal of Comparative Sociology 62(2), 115–140, https://doi.org/10.1177/00207152211023540.

Maligalig, D., Caoli-Rodriguez, R. B., Martinez, A., Cuevas, S. (2010): Education Outcomes in the Philippines. ADB Economics Working Paper Series No. 199; Asian Development Bank: Manila, Philippines, https://doi.org/10.2139/ssrn.1611428.

Namukwaya, V. A., Kibirige, I. (2014): Factors Affecting Primary School Enrolment and Retention of Pupils in Kotido District, Uganda. Mediterranean Journal of Social Sciences 5(8), 354–363, https://doi.org/10.5901/mjss.2014.v5n8p423.

Nannyonjo, H. (2007): Education inputs in Uganda: an analysis of factors influencing learning achievement in grade six (English). World Bank working paper no. 98; World Bank: Washington, DC, USA, http://documents.worldbank.org/curated/en/445131468310730593.

Němečková, T., Harmáček, J., Schlossarek, M. (2020): Measuring the Middle Class in Africa – Income Versus Assets Approach. Afrika Spectrum 55(1), 3–32, https://doi.org/10.1177/0002039720916087.

Oryoie, A. R., Alwang, J. (2018): School attendance and economic shocks: Evidence from rural Zimbabwe. Development Southern Africa 35(6), 803–814, https://doi.org/10.1080/0376835X.2018.1496814.

Pal, S. (2004): Child schooling in Peru: Evidence from a sequential analysis of school progression. Journal of Population Economics 17, 657–680, https://doi.org/10.1007/s00148-004-0196-z.

Pezzulo, C., Alegana, V. A., Christensen, A., Bakari, O., Tatem, A. J. (2022): Understanding factors associated with attending secondary school in Tanzania using household survey data. PloS One 17(2): e0263734, https://doi.org/10.1371/journal.pone.0263734.

Psyridou, M., Prezja, F., Torppa, M., Lerkkanen, M., Poikkeus A., Vasalampi K. (2024): Machine learning predicts upper secondary education dropout as early as the end of primary school. Scientific Reports 14: 12956, https://doi.org/10.1038/s41598-024-63629-0.

Roby, J. L., Shaw, S. A., George, L. H. (2014): Perceived food and labor equity and school attendance among Ugandan children living in kin care. International Journal of Social Welfare 23(2), 205–214, https://doi.org/10.1111/ijsw.12051.

Roby, J. L., Erickson, L., Nagaishi, C. (2016): Education for children in sub-Saharan Africa: Predictors impacting school attendance. Children and Youth Services Review 64, 110–116, https://doi.org/10.1016/j.childyouth.2016.03.002.

Saasa, S. K. (2018): Education among Zambian children: linking head of household characteristics to school attendance. An International Interdisciplinary Journal for Research, Policy and Care 13(3), 239–246, https://doi.org/10.1080/17450128.2018.1456707.

Schreurs, Z. E. A., Chang Rundgren, S.-N. (2021): Neighborhood, Segregation, and School Choice. Multidisciplinary Journal of School Education 10(20), 111–133, https://doi.org/10.35765/mjse.2021.1020.06.

Sugrue, E. P., Zuel, T., LaLiberte, T. (2016): The Ecological Context of Chronic School Absenteeism in the Elementary Grades. Children & Schools 38(3), 137–145, https://doi.org/10.1093/cs/cdw020.

Tansel, A. (1997): Schooling Attainment, Parental Education, and Gender in Côte d'Ivoire and Ghana. Economic Development and Cultural Change 45(4), 825–856, https://doi.org/10.1086/452309.

Teshome, N. (2002): Low participation of female students in primary education: a case study of dropouts from the Amhara and Oromia Regional States in Ethiopia; UNESCO International Institute for Capacity Building in Africa (IICBA): Addis Ababa, Ethiopia.

Uganda Bureau of Statistics (2017): National population and housing census 2014 – area specific profile series: Buikwe District; Uganda Bureau of Statistics: Kampala, Uganda. Available online: https://www.ubos.org/wp-content/uploads/publications/2014CensusProfiles/BUIKWE.pdf (accessed on 9 March 2026).

UNDP (United Nations Development Programme) (2016): Human development report 2016: Human Development for Everyone; UNDP: New York. Available online: https://hdr.undp.org/content/human-development-report-2016 (accessed on 18 March 2026).

UNESCO (United Nations Educational, Scientific and Cultural Organization) (2020): Inclusion and Education: All Means All. Global Education Monitoring Report; UNESCO: Paris. Available online: https://unesdoc.unesco.org/ark:/48223/pf0000373718 (accessed on 18 March 2026).

UNICEF (United Nations Children's Fund) (2016): The State of the World's Children 2016: A Fair Chance for Every Child; UNICEF: New York. Available online: https://www.unicef.org/media/50076/file/UNICEF_SOWC_2016-ENG.pdf (accessed on 18 March 2026).

Valero-Gil, J., Valero, M. (2022): Why has there been a fall in child labour and an increase in school attendance in Mexico? Development Policy Review 40(6): e12611, https://doi.org/10.1111/dpr.12611.

Van Eck, K., Johnson, S. R., Bettencourt, A., Johnson, S. L. (2017): How school climate relates to chronic absence: A multi-level latent profile analysis. Journal of School Psychology 61, 89–102, http://dx.doi.org/10.1016/j.jsp.2016.10.001.

Wang, Z., Lapinski, M., Quilliam, E., Jaykus, L., Fraser, A. (2017): The effect of hand-hygiene interventions on infectious disease-associated absenteeism in elementary schools: A systematic literature review. American Journal of Infection Control 45(6), 682–689, https://doi.org/10.1016/j.ajic.2017.01.018.

World Food Programme (2006): World hunger series 2006: hunger and learning; World Food Programme: Rome, Italy. Available online: https://www.wfp.org/publications/world-hunger-series-2006-hunger-and-learning (accessed on 18 March 2026).

World Food Programme (2021): WFP Uganda country brief, September 2021. Available online: https://reliefweb.int/report/uganda/wfp-uganda-country-brief-september-2021 (accessed on 18 March 2026).

World Bank (2021): School enrollment, primary (% net). Available online: https://data.worldbank.org/indicator/SE.PRM.NENR?view=chart.

Yamano, T., Jayne, T. S. (2005): Working-Age Adult Mortality and Primary School Attendance in Rural Kenya. Economic Development and Cultural Change 53(3), 619–653, https://doi.org/10.1086/426463.

Zhang, M. (2003): Links Between School Absenteeism and Child Poverty. Pastoral Care in Education 21(1), 2–52, https://doi.org/10.1111/1468-0122.00249.

Appendix 1 Mixed-effects negative binomial regression.

Dependent variable: Number of absences	Regression models							
Independent variables	(1)		(2)		(3)		(4)	
Age	−0.083**	(0.036)	−0.071*	(0.039)	−0.098**	(0.04)	−0.08*	(0.043)
Gender (dummy)	0.228**	(0.108)	0.323***	(0.116)	0.255**	(0.121)	0.335***	(0.126)
Distance (dummy)	0.189#	(0.117)	0.226*	(0.119)	0.187#	(0.128)	0.227*	(0.13)
Number of household members	−0.017	(0.028)	−0.02	(0.03)	−0.016	(0.029)	−0.018	(0.029)
Female led household (dummy)	−0.248**	(0.106)	−0.173#	(0.112)	−0.391***	(0.115)	−0.329***	(0.122)
Household head parent (dummy)	0.183	(0.155)	0.178	(0.153)	0.164	(0.167)	0.248#	(0.167)
Orphan (dummy)	0.404***	(0.144)	0.479***	(0.146)	0.592***	(0.162)	0.582***	(0.164)
Younger siblings	0.023	(0.038)	0.055	(0.039)	0.019	(0.042)	0.046	(0.041)
Mothers with higher education (dummy)					−0.192*	(0.115)	−0.213*	(0.122)
Employment (dummy)	0.183*	(0.109)	0.183#	(0.119)	0.22*	(0.126)	0.229*	(0.135)
Work before school	−0.05	(0.044)	−0.05	(0.045)	−0.101**	(0.044)	−0.114**	(0.044)
Sponsorship (dummy)	−0.251#	(0.154)	−0.258#	(0.16)	−0.393**	(0.17)	−0.356*	(0.187)
Hunger (dummy)	0.017	(0.123)	0.002	(0.131)	−0.008	(0.136)	−0.014	(0.142)
Asset index			0.004	(0.003)			0.008**	(0.003)
Dummy variables for schools	Yes		yes		yes		yes	
Dummy variables for months	Yes		yes		yes		yes	
_const	1.293***	(0.501)	0.78	(0.568)	1.773***	(0.571)	0.987	(0.631)
Number of observations	2,267		1,911		1,665		1,427	
Number of groups	321		270		242		207	
Wald chi2	198.79***		174.96***		205.15***		178.36***	

Source: Author's calculations. *** Significant at the 1% significance level. ** Significant at the 5% significance level. * Significant at the 10% significance level. # Significant at the 15% significance level. Robust standard errors clustered on pupils are in parentheses.

Appendix 2 Random-effects negative binomial regression.

Dependent variable: Number of absences	Regression models							
Independent variables	(1)		(2)		(3)		(4)	
Age	−0.075***	(0.029)	−0.043	(0.032)	−0.07**	(0.033)	−0.04	(0.035)
Gender (dummy)	0.276***	(0.083)	0.309***	(0.09)	0.281***	(0.094)	0.325***	(0.098)
Distance (dummy)	0.116	(0.088)	0.099	(0.095)	0.085	(0.1)	0.073	(0.105)
Number of household members	−0.011	(0.023)	−0.003	(0.024)	−0.014	(0.025)	−0.007	(0.026)
Female led household (dummy)	−0.237***	(0.088)	−0.186*	(0.095)	−0.35***	(0.098)	−0.306***	(0.105)
Household head parent (dummy)	0.208*	(0.114)	0.158	(0.118)	0.143	(0.128)	0.146	(0.13)
Orphan (dummy)	0.0271***	(0.104)	0.296***	(0.109)	0.373***	(0.116)	0.354***	(0.122)
Younger siblings	0.019	(0.032)	0.026	(0.035)	0.016	(0.035)	0.028	(0.037)
Mothers with higher education (dummy)					−0.254***	(0.092)	−0.229**	(0.1)
Employment (dummy)	0.243***	(0.085)	0.227**	(0.092)	0.266***	(0.099)	0.257**	(0.106)
Work before school	−0.042	(0.031)	−0.045	(0.032)	−0.072**	(0.033)	−0.088***	(0.034)
Sponsorship (dummy)	−0.215*	(0.113)	−0.262**	(0.123)	−0.318**	(0.133)	−0.329**	(0.142)
Hunger (dummy)	0.138#	(0.093)	0.163#	(0.101)	0.045	(0.105)	0.09	(0.112)
Asset index			0.001	(0.003)			0.005*	(0.003)
Dummy variables for schools	Yes		yes		yes		yes	
Dummy variables for months	Yes		yes		yes		yes	
_const	0.618#	(0.417)	0.054	(0.486)	0.999**	(0.484)	0.245	(0.543)
Number of observations	2,267		1,911		1,665		1,427	
Number of groups	321		270		242		207	
Wald chi2	196.11***		162.65***		170.88***		143.88***	

Source: Author's calculations. *** Significant at the 1% significance level. ** Significant at the 5% significance level. * Significant at the 10% significance level. # Significant at the 15% significance level. Standard errors are in parentheses.